Faculté des Sciences & Techniques UMR CNRS 7566

U.F.R.S.T.M.P.
Ecole Doctorale
RP2E (Ressources, Produits, Procédés et Environnements)

Thèse

présentée pour l'obtention de titre de

Docteur de l'Université Henri Poincaré, Nancy-I

en Sciences de la Terre et de l'Univers

par

Vladimir LOBAEV

Mineralogical and petrogeochemical characteristics of the Mesoproterozoic Pasha – Ladoga volcanic - sedimentary basin and its basement (Baltic shield, Russia) Inferences on the genesis of unconformity related uranium deposits

Membres du jury:

Président	**M. Jacques LEROY**	Professeur, Université Henri Poincaré, Nancy
Rapporteurs	**M. Tapani RÄMÖ**	Professeur, Université d'Helsinki, Finland
	M. Maurice PAGEL	Professeur, Université d'Orsay Paris Sud
Directeur de thèse	**M. Michel CUNEY**	Directeur de Recherche, CNRS, UMR G2R, Nancy
Examinateurs	**M. Claude CAILLAT**	Ingénieur géologue, AREVA, Vélizy
	Mme Elena AFANASIEVA	Ingénieur géologue, VSEGEI, Saint-Pétersbourg, Russie

To Jane and Jack with love!

Table of content

Table of figures

Chapter I

Part 1.1.

Part 1.2.

Part 1.3.

Part 2.5

Chapter III

Chapter IV

List of tables

Remerciements

Ce travail entre dans le cadre d'une collaboration scientifique internationale entre le groupe **COGEMA** (Velizy, France), qui a financé entièrement ce projet, l'institut géologique **VSEGEI** (Saint-Pétersbourg, Russie), qui depuis déjà 7 années me compte parmi ses collaborateurs, ce pour quoi je lui suis infiniment reconnaissant, la société **CREGU** (Nancy, France) qui m'a employée pour mener à terme cette étude des gisements d'uranium de type discordance en Russie enfin l'**UMR G2R** au travers de laquelle j'ai pu bénéficier de toutes les possibilité accordées par **l'Université Henri Poincaré - Nancy 1**. Au terme de ce travail, je tiens à remercier celles et ceux qui ont participé de près ou de loin à la réalisation de ce projet, à la résolution de problèmes autres que scientifiques me permettant ainsi de m'occuper de mon affaire aimée - la géologie !

En premier lieu je veux exprimer ma reconnaissance immense à mon chef français - le Directeur de ma thèse **Michel CUNEY**, qui pendant trois années m'a aidé à développer mes connaissances dans la métallogénie de l'uranium, m'a forcé à croire en la possibilité de l'exécution de ce travail et a contribué à son achèvement fructueux. Je peux remercier la chance de m'avoir présenté un tel savant de la plus haute distinction, héros follement dévoué à la cause de la géologie et prêt à s'y engager sans réserve. **Michel** et sa femme **Liliane** sont devenus la première famille française, dans la maison de laquelle je suis entré et grâce à qui j'ai fait connaissance avec ce pays remarquable, la France, où vivent des gens admirables proches de nos cœurs russes. **Michel** et **Liliane**, merci pour votre hospitalité !

D'égale manière, je suis infiniment reconnaissant aux gens, qui m'ont amené vers cette voie - à **Youri MARIN,** le directeur de ma première thèse à l'Institut des Mines (alma mater), grâce à l'intervention de qui je me suis trouvé ici, et à **Vladimir TERENTIEV**, qui dirigeait mes études en Russie tout au début mais, malheureusement, n'a pas vécu jusqu'à leur fin.

Je veux exprimer ma gratitude à la direction de toutes les organisations scientifiques se rapportant à mon travail : à messieurs à **Jean-Claude CARISEY** (ancien directeur du service exploration des COGEMA), **Jacques LEROY** (le Directeur UMR G2R), **Michel CATHELINEAU** (le directeur CREGU) pour les possibilités accordées de réaliser ce travail sans complications.

Je remercie mes rapporteurs - le professeur de l'université d'Helsinki **Tapani RAMO** et le professeur de l'université d'Orsay - Paris XI **Maurice PAGEL** pour leur aimable accord de participer à l'évaluation de ma thèse. En outre je suis reconnaissant au professeur **RAMO** pour la remarquable semaine de travaux de terrain dans le nord du lac Ladoga.

Je veux aussi remercier tous les collaborateurs du groupe **COGEMA**, qui participaient directement ou indirectement à la réalisation du projet et, surtout :

Claude CAILLAT, qui a éprouvé avec moi toutes les difficultés de l'écriture de cette thèse, a pris part à tous nos travaux communs. Pour son amour infini de la Russie et de nous, les géologues russes, je lui exprime ma gratitude sincère;

Patrice BRUNETON, impressionnant par son érudition scientifique et sa passion de collectionneur;

Jean MONDY, Régis MATHIEU, Benoît MAGRINA, Philippe KISTER (*bonne chance, maintenant toi aussi à COGEMA!*).

Mon devoir sacré - l'expression de la reconnaissance à tous les collaborateurs de **VSEGEI**, qui se sont trouvés entraînés dans cette aventure de leur plein gré ou de fait. Je suis reconnaissant à tous les collaborateurs du département de la géologie du Précambrien VSEGEI et à son chef **Anver AKHMEDOV** qui m'ont envoyé, confiant dans le futur, travailler au département de la géologie de l'uranium. Je suis extraordinairement reconnaissant à tous les collaborateurs du service de la géologie des gisements d'uranium VSEGEI et son ancien (**Mikhaïl KHARLAMOV**) et actuel (**Youri MIRONOV**) directeur de m'avoir accordé tout le soutien possible et de bonnes relations. Ma reconnaissance spéciale à **Vitaly MIKHAÏLOV**, **Elena AFANASIEVA**, **Lyudmila BYLINSKAYA**, **Anatoly MOLCHANOV**, **Roman CHIPOV** pour leur soutien général et leur participation directe à d'autres études de terrain ou minéralogiques, ainsi que dans la discussion des résultats acquis.

Ma reconnaissance spéciale à **Sacha SHOURILOV**, pour son soutien inestimable en matière d'orientation dans les espaces inconnus, les cartes, les coupes, les couloirs et les bases géologiques de NEVSKGEO, à qui je souhaite bonne chance dans la réalisation de sa thèse également a Nancy avec Michel.

Je aussi remercie à **Youri POLEKHOVSKY** (maître de la minéralogie d'uranium, Université de Saint-Pétersbourg) pour son soutien général et sa participation directe à mes études minéralogiques, ainsi que dans la discussion des résultats acquis.

Je transmets mes salutations particulières aux collègues finlandais du Service Géologique de la Finlande et l'Université d'Helsinki : **Olli AIKAS**, **Jarmo KOHONEN**, **Arto LUTTINEN**, **Viveca LINDQVIST**.

Le cadre de la coopération scientifique a été large qu'il est difficile de n'oublier aucun des organismes y ayant contribué:

Tous les anciens et actuels **G2R**, **CREGU**, **UHP** (Service Commun) (Nancy, France) et, surtout : Bernard POTY (un immense merci à vous pour votre participation à mon destin), M. SCHUHMACHER et l'équipe des secrétaires : Marie-Odile, Laurence, Christine, Patrick LAGRANGE (merci à toi immense pour ta bonne relation), Roland MAIRET (Administrateur Magnifique), Marc BROUAND, Marc LESPINASSE, Cédric DEMEURIE, Alain COHLER, Laurent RICHARD (la Société Civile de l'Amitié russo-belge des amateurs de bière), Cédric CARPENTIER, Laurent DESINDES, Rémy CHEMILLAC, Grégoire ANDRE, Donatienne DEROME et vous tous qui m'avez soutenu pendant ma première année et m'avez appris beaucoup de choses, merci!

VSEGEI : Grégory TERENTIEV (l'as des gazelles), Anton ANTONOV (tu es très gentil!), Anna SALTYKOVA (les cafés, les mission de terrains, merci à toi, An !), Lyudmila SEMENOVA, Youri BOGDANOV, Rimma BRODSKAYA (les zircons sont votre passion), Vitaly CHATOV (le soin et la participation), Nicolas CHATKOV et André KHARLACHIN (pour d'agréables déjeuners communs et les discussions scientifiques)… si quelqu'un a été oublié - je demande d'inscrire le nom à cette liste indépendamment !

NEVSKGEO : Vladimir KOUCHNERENKO (vous avez été une histoire particulière dans ma vie!), Pavel CHARIKOV, Youri PETROV, Youri GROMOV et tous ceux que j'ai oublié ou dont je ne connais tout simplement pas le nom de famille.

NOVAYA LEKHTA : Tatiana REUS (pour sa bonté, compréhension et aptitude a toujours aider), Alexander PIMENOV, Yaroslava KUCHMET.

IGEM: Alexei ALECHINE (c'était marrant de travailler avec toi), Slava GOLOUBEV, Vassili VELICHKINE, Tatiana KRYLOVA - pour les relations fécondes.

Université de Moscou : Peter TIKHOMIROV - j'étais très-très content de te voir à Nancy le premier jour de mon séjour ici.

Le centre scientifique de Kola (Apatity) et **l'expédition de Kola** (Montchegorsk): Anatole SMOLINE (tu es le CONDUCTEUR), Antonina REMIZOVA - le praticien expérimentée.

L'Institut Des Mines (Saint-Pétersbourg): Galina CHNAY (pour les voies montrées).

Je voudrais aussi remercier **Alexandre VYSOTSKY** et **Lydie SHTEIN** de leur relation presque parentale avec moi. J'ai un très profond respect pour **Ivan VORONTSOV** – notre père et grand-père commun et grand praticien de la géologie. À mon premier professeur de géologie - **Lydie IVCHENKO** - merci immense.

Ici, en France, grâce au site de **Nella TSVETOVA** www.infrance.ru j'ai trouvé de nouvelles connaissances et de bons amis, la reconnaissance spéciale au maître **Boris KARPOV** et toi, **Maroucha** (mes salutations à **Jean**)! Merci immense à vous, les habitants de Nancy - **Roman** et **Tatiana**, je suis content de notre connaissance non-fortuite.

Pour vous, mes vieux et déjà bons **amis** presque éternels, je n'ai pas tant de mots que j'ai peur simplement qu'il n'y ait pas assez de place pour les exprimer sur le papier : **Simon** et **Nathalie**, **Aleks** et **Irinka**, **Svetka** et **Volker SIMONIS** (comme c'est superbe, que vous habitiez ainsi à côté de Nancy), **Denis**, **Choura et Leucha REMIZOV, Tatiana FROLOVA**, **Oxanka**, **Irinka** et **Stas**, **Michka** et **Tatiana, Gocha** et **Lena**, **Eugène GUREVICH**, **Vadik** et **Tatiana**, **Kostya TROTSKY**, **Yourik TSVETKOV**, **Grivady PAVLOV**, **Michael KAPINOS**, **Julie KURKOTOVA**, Herr **POLIATSKINE** et son épouse **Anna** (je ne suis pas arrivé jusqu'à vous, malheureusement) - merci à vous tous pour ce que vous êtes ! Je vous aime et vous suis terriblement reconnaissant de votre amitié avec notre famille ou pour une simple participation à ses affaires.

MAMAN et **PAPA** - je regrette que vous soyez ainsi loin, même de Saint-Pétersbourg, mais je suis sûr que vous êtes fiers de moi, merci à vous pour tout ! Tous **mes proches** merci à vous, venez chez nous, nous vous aimons!

Et, enfin, ceux, pour qui c'était fait : **JANE** et **JACK**! *JE VOUS AIME !* Vous êtes la partie la plus intime de ma vie! Je suis content que ces trois années difficiles dans notre vie, enfin finissent! A l'avenir de nouveaux essais nous attendent, mais c'est déjà une autre histoire! Merci à vous, mes chers!

Je suis reconnaissant à mon Destin pour tout...

P.S. Ma reconnaissance spéciale à tous les viticulteurs, fromagers boulangers français, brasseurs belges et confiseurs italiens.

Acknowledgments

This work has been carried out in the framework of the close scientific collaboration between the **COGEMA** company (Velizy, France) which completely financed this project, All-Russian Geological Institute (**VSEGEI**, Saint-Petersburg, Russia) which counts me as its employee since 7 years and I am very grateful to it, and the society **CREGU** (Nancy, France) which placed me in a job for these three, such difficult, years. The Mixed Unit of Scientific Research (**UMR G2R**), which comprises the CREGU and the University Henry Poincaré – Nancy I, a doctor of which I shall become in a near future, gave me a full access to all information and analytical resources. I am grateful to all the people, which participated in the realization of this project, promoted to solving of scientific, technical, bureaucratic and other problems, assisted (and not impeded) me in my lovely occupation – geology!!!

Firstly, I would like to express my heart full gratitude to my French chief – Director of my thesis **Michel CUNEY**, which in every way developed and strengthened my knowledge in uranium metallogeny during three years, forced me to believe in the possibility of fulfillment of this work and promoted in its successful completion. Michel and his wife Liliane became the first French family, which home I entered, from whom I got acquainted with this beautiful country – France, where such marvelous people, so close to our Russian hearts, live. **Michel** and **Liliane**, thank you for your hospitality!

In the same degree, I endlessly appreciate people who brought me on this way – **Yury MARIN**, the director of my first thesis in the Mining Institute (alma mater), with his happy touch I became here, and **Vladimir TERENTYEV**, who leaded my investigations from the Russian side at the beginning and who unfortunately didn't live to see their end.

I wish to express my gratitude to the administration of all the scientific organizations which are related to my work: Mr. **Jean-Claude CARISEY** (former Head of the Exploration Department, COGEMA), Mr. **Jacques LEROY** (Director of UMR G2R), Mr. **Michel CATHELINEAU** (Director of CREGU) for the providing me opportunities.

I am very grateful to my rapporteurs – Professor of the University of Helsinki **Tapani RAMO** and Professor of the Orsay University - Paris XI **Maurice PAGEL** for their kind

acceptation to participate to my thesis jury. Besides, I am also grateful to Professor **RAMO** for the excellent week during the joint field works in the Northern Ladoga district.

I want also to thank all colleagues from the COGEMA group, which directly or indirectly participated in my project realization, in particular:

Claude CAILLAT, which literally went through all the processes of the thesis writing, took part in all our joint field works. For his infinite love to Russia and for us, Russian geologists, I expressed him my sincere grateful;

Patrice BRUNETON, for his staggering scientific erudition and passion for collecting;

Jean MONDY, **Regis MATHIEU**, **Benoit MAGRINA**, **Philippe KISTER** (*good luck to you, you are in COGEMA now!*).

My sacred duty - to thank all colleagues from VSEGEI who *nolens volens* were engaged into this project. I am very grateful to *all the colleagues* from the Precambrian Geology Department of VSEGEI and its Head **Anver AKHMEDOV** because he keeps his confidence to me and gives me a chance to catch something like the better future. I am extremely grateful to *all the colleagues* from the Uranium Geology Department of VSEGEI and to its former (**Mikhail KHARLAMOV**) and present (**Yury MIRONOV**) administration for their support and kind relation. My especial regard is to **Vitaly MIKHAILOV**, **Elena AFANASYEVA**, **Lyudmila BYLINSKAYA**, **Anatoly MOLCHANOV**, **Roman SHIPOV** for their general support and participation in field works, mineralogical and other investigations as well as in the discussions.

My special gratitude to **Sasha SHURILOV**, who rendered me an assistance in keeping orientation in unknown spaces, maps, cross sections, corridors and camps of **NEVSKGEO**. I wish you good luck in the hard work of the thesis completion, but here in Nancy and also with Michel.

I am very grateful to **Yuri POLEKHOVSKY** (Master of the ore mineralogy of the Saint-Petersburg University) for his participation in my mineralogical investigations.

Individual thanks to Finnish colleagues from the Geological Survey of Finland and Helsinki University: **Olli AIKAS, Jarmo KOHONEN, Arto LUTTINEN** and **Viveca LINDQVIST.**

Frameworks of the scientific cooperation appeared to be so wide that it is difficult not to forget all who have not been mentioned yet:

All former and present staff of **G2R**, **CREGU**, **UHP** (Service Commun) (Nancy, France) and in particular: Bernard POTY (thank you so much for your participation in my fate), Mr. SCHUHMACHER and the secretary team: Marie Odile, Laurence, Christine, Patrick LAGRANGE (my hearty thanks to you), Roland MAIRET (Magnificent Administrator), Marc BROUAND, Marc LESPINASSE, Cedric DEMEURIE, Alain KOHLER, Laurent RICHARD (the Russian-Belgian Friendship Voluntary Society of the BEER LOVERS), Cedric CARPENTIER, Laurent DESINDES, Remy CHEMILLAC, Greg ANDRE, Donatienne DEROME - you greatly supported me during the first year and so on...

VSEGEI: Gregory TERENTYEV (True Ace of the ROAD), Anton ANTONOV (tu es très gentil !), Anna SALTYKOVA (coffee and field trips, thank you, An), Lyudmila SEMENOVA, Yury BOGDANOV, Rimma BRODSKAYA (Zircon is your real Passion), Vitaly SHATOV (for your care and participation), Nicolas SHATKOV and Andre KHARLASHIN (for the pleasant joint dinners and scientific discussions)… if I forgot someone – please insert your name into this Tablet by yourself!

NEVSKGEO: Vladimir KUSHNERENKO (you are a particular story in my life), Pavel SHARIKOV, Yury PETROV, Yury GROMOV and all who I didn't know or forgot on names.

NOVAYA LEKHTA: Tatiana REUS (for her kindness, comprehension and remarkable talent to help), Alexander PIMENOV, Yaroslava KUSHMET.

IGEM: Alexei ALESHIN – it was great to work with you, Slava GOLUBEV, Vasily VELICHKIN, Tatiana KRYLOVA – for productive contacts.

Moscow University: Peter TIKHOMIROV – I was very glad to meet you in Nancy on the first day of my stay here.

Kola Scientific Center (Apatity) and **Central Kola Expedition** (Monchegorsk): Anatole SMOLIN (you are the DRIVER), Antonina REMIZOVA (woman with Field Experience).

Mining Institute (Saint-Petersburg): Galina SHNAY (for demonstration of the route).

I would like also to thank **Alexander VYSOTSKY** and **Lydia SHTEIN** for their almost parental relation to me. My deepest respect to **Ivan VORONTSOV** – our common father and grandfather and great practical geologist. Many thanks to my first teacher in geology – **Lydia IVCHENKO**.

Here, in France, I have found many new good friends due to the internet site of **Nella TSVETOVA** www.infrance.ru, particular grateful to Maitre **Boris KARPOV** and you, Maroucha (best regards to **Jean**)! So many words to Nancy inhabitants – **Roman** and **Tatiana**.

I have so many words for you, my old kind (practically eternal) FRIENDS, that I am afraid there won't be enough space to express them on paper: **Simon** & **Nathalie**, **Aleks** & **Irinka**, **Svetka** & **Volker** (so great that you live nearby Nancy), **Denis**, **Shura** & **Lesha REMIZOV**, **Tatiana FROLOVA**, **Oksanka**, **Irinka** & **Stas**, **Mishka** & **Tatiana**, **Eugene GUREVICH**, **Gosha** & **Lena**, **Vadik** & **Tatiana**, **Kostya Mr. TROTSKY**, **Yurik TSVETKOV**, **Grivady PAVLOV**, **Michael KAPINOS, July KURKOTOVA, Kira VASILYEV**, sir **Polyatskin** with his wife **Ann** (I haven't reached you, unfortunately) – thank you for your existence ! I love you all very much and very grateful for you friendship with our family or just for the participation in its life.

MUMMY and **DADDY** – it's a pity that you are so far, even from Saint-Petersburg, but I am sure that you are proud of me, thank you for all! **Nice relatives** thank you for support, visit us please, we love you!

And, finally, those for which sake it was undertaken: **JANE** and **JACK**! I love you so much! You are the most fond part of my life! I am really glad that these three difficult years in our life are finishing at last! New tests wait for us in the future, where without them, it would be an another story! Thank you, my darling!

I thank my Destiny for all…

My special thanks to the French vine-makers, cheese-makers and bakers, Belgian brewers and Italian confectioners (for Tiramisu dessert).

Благодарности

Эта работа проводилась в рамках тесного научного сотрудничества между компанией **COGEMA** (Велизи, Франция), которая полностью финансировала данный проект, Всероссийским геологическим институтом (**ВСЕГЕИ**, Санкт-Петербург, Россия), который в течение уже 7 лет числит меня своим сотрудником (за что я ему бесконечно благодарен) и обществом **CREGU** (Нанси, Франция), которое трудоустроило меня на эти три, таких непростых для меня, года. Научно-исследовательское объединение (**UMR G2R**), в состав которого входят CREGU и университет Анри Пуанкаре – Нанси I, доктором которого мне и предстоит стать в ближайшем будущем, обеспечило полный доступ ко всем информационным и аналитическим ресурсам. Я благодарен всем людям, принявшим участие в реализации этого проекта, способствовавших разрешению научных, технических, бюрократических и прочих проблем, помогавших (или не мешавших) мне заниматься моим любимым делом – геологией!

В первую очередь я хочу выразить свою огромную благодарность моему французскому шефу – руководителю диссертации **Мишелю КЮНЕ,** который в течение трех лет всячески развивал и укреплял мои познания в области металлогении урана, помог поверить в возможность выполнения этой работы и способствовал ее успешному завершению. Я благодарен судьбе за возможность работать с таким человеком, преданным делу геологии и готовым отдать этому делу всего себя без остатка. **Мишель** и его жена **Лилиан** стали первой семьей, принявшей меня во Франции. Благодаря им я познакомился с этой прекрасной страной, с французами, так близкими русскому сердцу, и полюбил их. **Мишель** и **Лилиан**, спасибо Вашему теплому дому!

В равной степени, я бесконечно признателен людям, которые привели меня на этот путь – **Юрию Борисовичу МАРИНУ**, руководителю моей первой кандидатской диссертации в Горном институте (alma mater), с его легкой руки я и оказался здесь. **Владимиру Михайловичу ТЕРЕНТЬЕВУ**, который руководил моими исследованиями в самом начале и, к сожалению, не дожил до их окончания.

Я хочу выразить свою признательность руководителям всех имеющих отношение к моей работе научных организаций: господам **Жану-Клоду КАРИЗЕ** (бывшему руководителю отдела разработки месторождений COGEMA), **Жаку ЛЕРУА** (Директору UMR G2R), **Мишелю КАТЕЛИНО** (директору CREGU) за предоставленные возможности.

Я благодарю своих оппонентов – профессора университета Хельсинки **Тапани РАМО** и профессора университета Орсэ – Париж XI **Мориса ПАЖЕЛЯ** за их любезное согласие участвовать в рассмотрении моей диссертации. Кроме того, я благодарен профессору **РАМО** за замечательную неделю полевых работ в Северном Приладожье.

Я хочу также поблагодарить всех сотрудников группы **COGEMA**, которые прямо или косвенно участвовали в реализации проекта, и особенно:

Клода КАЙЯ, который буквально вместе со мной переживал все процессы написания диссертации, принимал участие во всех наших совместных полевых работах. За его бесконечную любовь к России и к нам, российским геологам, я выражаю свою искреннюю признательность;

Патриса БРЮНЕТОНА, за его потрясающую научную эрудицию и страсть к коллекционированию;

Жана МОНДИ, **Режиса МАТЬЕ**, **Бенуа МАГРИНА**, **Филиппа КИСТЕРА** (больших творческих удач - теперь ты тоже в КОЖЕМЕ!).

Моя священная обязанность – выразить благодарности тем сотрудникам ВСЕГЕИ, которые волей или неволей оказались вовлечены в мою работу. Я благодарен *всем сотрудникам* отдела геологии докембрия ВСЕГЕИ и его руководителю **Анверу Митхатовичу АХМЕДОВУ** за то, что он сохранил неизменным свое отношение ко мне и дал мне шанс поймать нечто, так похожее на удачу. Я чрезвычайно признателен *всем сотрудникам* отдела геологии урановых месторождений и радиоэкологии ВСЕГЕИ, и его бывшему (**Михаил Георгиевич ХАРЛАМОВ**) и нынешнему (**Юрий Борисович МИРОНОВ**) руководителям за всемерную поддержку и доброе отношение. Особая моя благодарность **Виталию Алексеевичу МИХАЙЛОВУ, Елене Николаевне**

АФАНАСЬЕВОЙ, Людмиле Васильевне БЫЛИНСКОЙ, Анатолию Васильевичу МОЛЧАНОВУ, Роману ШИПОВУ за их непосредственное участие в полевых, минералогических и прочих исследованиях, а также в обсуждении полученных результатов.

Моя особая благодарность **Саше ШУРИЛОВУ**, оказавшему бесценную поддержку при ориентировании в неизвестных пространствах, картах, разрезах, кулуарах, коридорах и геологических базах НЕВСКГЕО. С пожеланиями удачи в нелегком деле написания диссертации.

Я благодарен также **Юрию Степановичу ПОЛЕХОВСКОМУ** (Мэтру рудной минералогии Санкт-Петербургского государственного университета) за оказанную помощь в моих минералогических исследованиях и общих дискуссиях за чашкой чая.

Отдельный привет финским коллегам из Геологической Службы Финляндии и Университета Хельсинки: **Олли АЙКАС**, **Ярмо КОХОНЕН**, **Арто ЛАТТИНЕН**, **Вивека ЛИНДКВИСТ**.

Рамки научного сотрудничества оказались столь широки, что очень трудно не забыть всех тех, кто еще не был ни разу упомянут:

ВСЕМ бывшим и нынешним сотрудникам **G2R, CREGU, UHP** (Service Commun) (Нанси, Франция), и особенно: Бернар ПОТИ (спасибо Вам огромное за Ваше участие в моей судьбе), Мг. ШУМАШЕР и команда секретарей, Патрик ЛАГРАНЖ (сердечное спасибо за твое доброе отношение), Ролан МАЙРЕ (Administrateur Magnifique), Марк БРУАН, Марк ЛЕСПИНАСС, Седрик ДЕМЕРЬЕ, Алан КЕЛЕР, Лоран РИШАР (Добровольное общество любителей пива и русско-бельгийской дружбы), Седрик КАРПЕНТЬЕ, Лоран ДЕЗИНДЕС, Реми ШЕМИЙЯК, Грег АНДРЭ, Донатьен ДЕРОМ и все-все – вы меня здорово поддержали в мой первый год и многому научили, спасибо!

ВСЕГЕИ: Григорий ТЕРЕНТЬЕВ (настоящий ас - водитель), Антон АНТОНОВ (tu es très gentil!), Анна Салтыкова (кофе, незабываемые поля, спасибо тебе, Ань!), Людмила Риммовна СЕМЁНОВА, Юрий Борисович БОГДАНОВ, Римма Львовна БРОДСКАЯ (цирконы – Ваша страсть), Виталий Витальевич ШАТОВ (за заботу и участие), Николай ШАТКОВ и Андрей ХАРЛАШИН (за приятные совместные обеды и научные дискуссии)… если кого-нибудь забыл – просьба вписать свое имя в сии скрижали самостоятельно!

НЕВСКГЕОЛОГИЯ: Владимир Константинович КУШНЕРЕНКО (Вы – особая история в моей жизни), Павел Иванович ШАРИКОВ, Юрий Владимирович ПЕТРОВ, Юрий Андреевич ГРОМОВ и все-все-все, кого я просто зачастую не знал или забыл по имени-отчеству.

НОВАЯ ЛЕХТА: Татьяна Петровна РЕУС (за ее доброту, понимание и способность всегда приходить на помощь), Александр Федорович ПИМЕНОВ и Ярослава КУШМЕТ.

ИГЕМ: Алексей АЛЕШИН (это было здорово - работать с тобой вместе), Слава ГОЛУБЕВ, Василий Иванович ВЕЛИЧКИН, Татьяна КРЫЛОВА – за плодотворное общение.

МГУ: Петя ТИХОМИРОВ – я был очень рад увидеть тебя в Нанси в первый же день своего пребывания здесь, больших творческих удач тебе!

Кольский научный центр (Апатиты) и Центрально-Кольская экспедиция (Мончегорск): Толик СМОЛИН – штурмующий непроходимые дороги, Антонина Михайловна РЕМИЗОВА – опытный практик.

ГОРНЫЙ ИНСТИТУТ: Галина Константиновна ШНАЙ (спасибо за показанные Вами пути).

Я хотел бы также поблагодарить **Александра Анатольевича ВЫСОЦКОГО** и **Лидию Фрицевну ШТЕЙН** за их почти родительское ко мне отношение. Мой глубочайший респект **Ивану Николаевичу ВОРОНЦОВУ** – всеобщему папе и дедушке и замечательному геологу-практику. Моей первой учительнице геологии – **Лидии Викторовне ИВЧЕНКО** – огромное спасибо.

Здесь, во Франции, благодаря сайту **Неллы ЦВЕТОВОЙ** www.infrance.ru, я обрел новых хороших друзей и знакомых. Особая благодарность мэтру **Борису КАРПОВУ** и тебе, **Маруша** (большой привет **Жану**)! Спасибо огромное и вам, обитатели Нанси, **Роман** и **Татьяна**, я рад нашему, во многом не случайному, знакомству.

Для вас же, мои старые и добрые (уже почти вечные) **друзья**, у меня есть столько слов, что боюсь не хватит места, чтобы выразить их на бумаге: **Сенька** и **Наташка**, **Алекс** и **Иринка**, **Светка** и **Фолькер СИМОНИСЫ** (как здорово, что вы живете так рядом с Нанси), **Денис**, **Шура** и **Леша РЕМИЗОВЫ**, **Татьяна ФРОЛОВА**, **Оксанка**, **Иринка** и **Стас**, **Мишка** & **Татьяна**, **Гоша** и **Лена**, **Евгений Романович ГУРЕВИЧ**, **Вадик** и **Татьяна**, **Костя ТРОЦКИЙ**, **Юрик ЦВЕТКОВ**, **Гривадий ПАВЛОВ**, **Майкл КАПИНОС**, **Юлька КУРКОТОВА**, **Кира ВАСИЛЬЕВ**, сэр **Поляцкин** с супругой **Анной** (не доехал я до вас, к сожалению) – спасибо вам за то, что вы есть! Я всех вас люблю и благодарен вам за вашу дружбу с нашим семейством или за простое участие в ее делах.

МАМА И ПАПА – жаль, что вы так далеко, даже от Питера, но я уверен, что вы гордитесь мною, спасибо вам за всё! **Всем родственникам** – спасибо за поддержку, приезжайте к нам, мы вас любим!

И, наконец, те, ради кого всё это и было затеяно: **Янушкин и Яшечкин**! Я вас люблю! Вы - самая заветная часть моей жизни! Я рад, что эти три непростых года в нашей жизни заканчиваются! Впереди нас наверняка ждут новые испытания, куда же без них, но это уже другая история! Спасибо вам, мои хорошие!

Я благодарен своей Судьбе за всё…

ЗЫ: Моя особая благодарность французским виноделам, сыроварам, булочникам, бельгийским пивоварам и итальянским кондитерам (за исключительный по своим вкусовым качествам десерт Тирамизу).

Résume étendu

Dans la région du lac Ladoga (Carélie, Russe) un bassin volcano-sédimentaire intracontinental clastique s'est formé durant le mésoprotérozoïque. Le diamètre du bassin Pasha - Ladoga est actuellement de 150 km. La forme du bassin coïncide étroitement avec la rive du lac Ladoga (Carélie, Russe). Un gisement d'uranium associé à la discordance entre ce bassin et le socle archéen à paléoprotérozoïque a été découvert dans la zone Salmi au Nord Est du lac Ladoga.

Le socle cristallin de la partie Nord-Est du bassin Pasha - Ladoga est constituée de dômes granitiques-gneissiques archéens, renfermant déjà des granitiques potassiques. Ces domes sont entourés par des roches sédimentaires paléoprotérozoïques riches en carbonates, matière carbonée et sulfures, déposées en environnement de type de type plateforme épicontinentale et métamorphosées durant l'orogenèse svécofénienne dans le faciès amphibolite avec migmatisation naissante. Ces roches ont été transformées en gneiss à plagioclase-biotite, marbres, amphibolites et schistes à quartz-biotite-plagioclase-graphite et sulfures.

Au mésoprotérozoïque (Riphéen), de très grandes intrusions de granites rapakivi potassiques riches en uranium et thorium se sont mises en place dans la partie Sud-Est du bouclier fennoscandinave en liaison avec une phase d'extension. Le complexe granitique rapakivi de Salmi s'est mis en place dans la partie Nord du bassin Pasha – Ladoga ou se localise les minéralisations uranifères. A la différence des roches du socle archéennes-paléoprotérozoïque, les granites rapakivi ne subissent pas de métamorphisme, mais des processus hydrothermaux.

Après la mise en place de ces granites et une phase d'érosion de ce socle, l'activation de grandes structures orientées nord-ouest induit le développement d'une sédimentation rouge clastique en milieu continental dans un rift. De puissantes éruptions de basaltes continentaux alcalins (CFD) se mettent en place très rapidement après le début du remplissage du bassin sous forme de deux cycles principaux. La puissance du bassin a pu atteindre 3 à 4 km dans la région de Karku et peut être davantage si l'on tient compte des deux kilomètres de sédiments localisés sous le lac Ladoga.

La plupart des sédiments déposés sont riches en feldspath potassique, plagioclase, micas et en minéraux accessoires détritiques et sont donc très immatures. Cette caractéristique et la nature très anguleuse fréquente des grains de quartz et de feldspath détritiques indique une

altération pédogénétique très faible de l'arrière pays, un transport sur une distance relativement courte des sédiments et donc des conditions tectoniques très actives lors de la sédimentation, surprenantes pour une période typiquement anorogénique (200 Ma après la fin de l'orogenèse svécofennienne) et très différentes de celles ayant donné les grès très purs présentant une faible proportion de kaolinite et d'illite des bassins de l'Athabasca et de Kombolgie.

Comme dans le cas des districts fortement minéralisés de l'Athabasca, Canada et de Kombolgie, Australie, l'altération des zircons s'observe partout dans la zone Salmi aussi bien dans les roches du socle que dans les formations clastiques du bassin et indique la circulation de fluides diagénétiques suffisamment agressifs pour attaquer la structure des ces minéraux habituellement extrêmement réfractaires. Par contre la monazite est beaucoup moins altérées que dans le cas des districts de l'Athabasca et de Kombolgie indiquent une moindre agressivité des fluides. Les grains de zircon altérés s'observent aussi bien dans les échantillons carottés à proximité de la discordance sous le bassin que dans les affleurements éloignés de plusieurs dizaines de km de la limite d'extension présente du bassin. Les grains de zircons altérés montrent des structures internes très complexes, indiquant plusieurs cristallisations magmatiques et/ou plusieurs phases d'altérations, en particulier dans les granites rapakivi. L'altération se déroule par la substitution des éléments primaires de la structure des zircons (Zr, Si, Hf) par une variété d'éléments (Al, P, Ca, Fe, Y, Th, U), dont les abondances relatives varient d'un zircon à l'autre. Les zircons les moins altérés se trouvent dans les granites et les gneiss archéens avec remplacement de seulement 0,5 atomes sur un total de 33 (Zr, Si, Hf) par Al, P, Ca, Fe, Y et U. Les zircons altérés provenant des gneiss graphitiques et des schistes protérozoïques sont caractérisés par des substitutions atteignant jusqu'à 4 atomes de Ca, Al, Fe, Y, P, Th et U. Les zircons provenant des granites rapakivi présentent généralement des substitutions plus importantes (jusqu'à 8 atomes de Th, Al, Ca, Fe, Y et U), mais leur zonation primaire et leur idiomorphisme sont bien préservés à la différence des zircon primaires des zones de schistes. Les halos d'altérations et les veines abondantes sont fortement enrichies et uranium et thorium. La diminution de Zr+Si+Hf dans les parties altérées correspond également à une diminution dans la somme des oxydes, probablement causées par une métamictisation et une hydratation en relation avec des teneurs en uranium et thorium plus élevées et l'incorporation d'alumino-phosphate. Les taux de substitution dans la structure des zircons détritiques altérés provenant des grès de Pasha - Ladoga varient de 0,5 à 8 atomes sur

un total de 33 pour un zircon sain, comme cela a été observé dans les granites-gneiss, les schistes et les granites rapakivi.

Dans les roches altérées du socle du bassin d'Athabasca (Canada) le degré d'altération des monazites est généralement important, et une altération naissante est même observée dans des roches relativement fraîches. A l'inverse, les monazites qui sont particulièrement abondantes dans les schistes graphitiques de la région de Salmi, ne présentent d'évidence d'altération. Dans les granites rapakivi riphéens, la monazite n'existe pas et les phases minérales magmatiques porteuses de terres rares, Th, U, Zr et Y sont l'uranothorite, les carbonates de terres rares et l'allanite.

A la différence du bassin Athabasca, les grains de monazites ne sont pas uniquement observés en inclusions dans les quartz dans les grès de Pasha - Ladoga. Des reliquats de monazites (avec des évidences de figures de corrosion) sont abondants dans la matrice argileuse, associés aux oxydes de titane. Cela signifie que les monazites des grès de Pasha - Ladoga ont été légèrement corrodées, probablement par des fluides diagénétiques. Ce processus est courant dans les grès de l'Athabasca ou le P et les terres rares recristallisent ensembles avec l'aluminium et des quantités variables de Ca et de Sr pour former des alumino-phosphates-sulfates (APS) du groupe florencite-crandallite-goyazite. Dans les grès de Pasha - Ladoga, l'altération des monazites apparaît être plus limitée et il n'y a pas beaucoup de phases alumino-phosphatées. Le thorium, qui est un élément faiblement mobile, initialement essentiellement contenu dans les monazites, cristallise sous la forme de rare cristaux de thorite et/ou de microcristaux de silicates titanifères avec de très faibles concentrations en uranium et terres rares légères dans les grès de Pasha - Ladoga comme cela avait été déjà observé dans les grès protérozoïques du bassin de Franceville au Gabon hébergeant les gisements d'Oklo.

L'étude détaillée de l'altération des minéraux accessoires des roches du socle cristallin du bassin protérozoïque de Pasha - Ladoga indique que les lithologies du socle, incluant les granites rapakivi riphéens, ont été soumises à des altérations similaires à celles observées dans le socle et les grès du bassin Athabasca et de Kombolgie ainsi que dans les grès du bassin de Franceville au Gabon. Ces altérations sont en relation avec la percolation de fluides diagénétiques riches en calcium associée au lessivage de l'uranium contenu dans les lithologies sources et avec la formation des gisements d'uranium (Cuney et al., 2003). Par conséquent, l'altération observée dans la zone Pasha - Ladoga est probablement liée au même type d'événement.

Si des fluides diagénétiques de composition et de température semblables à ceux des bassins de l'Athabasca et de Kombolgie ont pu circuler dans le bassin et le socle de la région de Pasha Ladoga, cependant ceux-ci devaient avoir : (i) des pH plus alcalins du fait de l'abondance des feldspath dans le bassin, de l'importance des coulées basaltiques à la base de ce bassin et la cristallisation abondante de carbonates avec le minéralisation uranifère, (ii) des fO2 plus faibles du fait de la cristallisation de chlorites ferrifères dans les zones minéralisées au lieu des chlorites et tourmalines magnésiennes du bassin de l'Athabasca et de l'abondance de la pyrrhotite déposée avec les oxydes d'uranium, (iii) une sous saturation plus faible en silice ne conduisant qu'à une corrosion très limitée des grains de quartz détritiques des grès. Tous ces facteurs avec la moindre corrosion de la monazite dans le socle et dans le bassin représentent des conditions de libération de transport et de dépôt moins favorables pour l'uranium dans le bassin de Pasha Ladoga par rapport aux Bassin de l'Athabasca au Canada et celui de Kombolgie en Australie hébergeant les plus grands gisements d'uranium de type discordance.

Расширенное резюме

В мезопротерозое на территории Приладожья (Карелия, Россия), унаследовав положение палеопротерозойского Ладожского рифта, сформировался Пашско – Ладожский прогиб, выполненный вулканогенно-осадочными обломочными породами. Прогиб имеет близкую к изометричной форму диаметром около 150 км и примерно совпадает с береговой линией Ладожского озера. В северо-восточной части прогиба, в пределах Салминской площади, обнаружено урановое месторождение Карку, относимое по своим геологическим характеристикам к так называемым месторождениям «типа несогласия», наиболее яркими представителями которых являются ряд месторождений мезопротерозойских бассейнов Атабаска (Канада) и Комболджи (Австралия).

Важную роль в строении кристаллического фундамента Северного Приладожья играют архейские гранито-гнейсовые купола с малыми телами калиевых гранитоидов. Архейские купола обрамлены палеопротерозойскими супракрустальными сериями: преимущественно вулканогенной (с хемогенно-карбонатными осадками) и преимущественно терригенной. Супракрустальные породы в значительной степени обогащены кальцием, углеродистым веществом и сульфидами. Их формирование происходило в условиях платформенной эпиконтинентальной седиментации, в эпоху свекофеннского орогенеза эти породы претерпели сильный метаморфизм (вплоть до амфиболитовой фации) и мигматитизацию.

Отличительной особенностью Западного Приладожья является отсутствие пород архейского возраста и широкое развитие терригенных пород, претерпевших значительно более сильный метаморфизм гранулитовой фации.

Интрузивный палеопротерозойский магматизм наиболее интенсивно проявлен в Западном Приладожье и в переходной зоне между доменами. Ранне- и синорогенные интрузии норит-эндербитового и габбро-диоритового состава представлены, в основном, небольшими по размерам плутонами. Позднеорогенные интрузии калиевых гранитов, образующих крупные плутоны и в значительной степени обогащенные ураном и торием, напротив, играют значительную роль в геологическом строении района. Посторогенные интрузии повышенной щелочности характеризуются весьма пестрым составом и нередко обогащены также ураном, торием и редкоземельными элементами.

В мезопротерозое (раннем рифее) сразу после окончания процессов орогенеза в условиях аномально мощной континентальной коры в юго-восточной части Балтийского щита происходит становление громадных по масштабам проявления анортозит – рапакиви гранитных комплексов. В северо-восточной части Ладожского озера в это время формировались граниты рапакиви Салминского батолита, первично обогащенные ураном и редкими элементами.

В отличие от архейско-палеопротерозойских пород фундамента мезопротерозойские (рифейские) комплексы гранитов рапакиви не метаморфизованы. Вместе с тем, в них довольно интенсивно проявились процессы постмагматического гидротермального преобразования.

Сразу после становления гранитов рапакиви и кратковременного периода денудации фундамента происходит реактивация палеопротерозойских рифтообразующих разломов. На месте древнего Ладожского рифта начинается процесс заложения Пашско-Ладожского прогиба, сопровождающийся интенсивным отложением красноцветных обломочных пород и близ одновременными началу седиментации излияниями континентальных базальтов, тогда же происходит внедрение мощной межпластовой интрузии габбро-сиенитового состава – Валаамского силла. В результате интенсивного накопления осадков был сформирован прогиб с ориентировочной мощностью в 3- 4 километра, мощность сохранившихся осадков в акватории Ладожского озера в настоящее время превышает 2 км.

Большая часть красноцветных осадков в значительной степени обогащена полевыми шпатами, плагиоклазом, слюдами, акцессорными минералами и может быть охарактеризована как незрелая. Седиментация происходит в условиях чрезвычайной тектонической активности, незрелость осадков, а также угловатый размер обломков кварца свидетельствуют о недостаточно интенсивном процессе их переотложения, а также о переносе на очень небольшие расстояния в пределах бассейна. Все эти факторы и обусловили значительные отличия между песчаниками Пашско-Ладожского прогиба с песчаниками из аналогичных мезопротерозойских бассейнов Атабаски (Канада) и Комболджи (Австралия), которые характеризуются своей исключительной зрелостью (преимущественно кварцевые аренитты, содержащие лишь незначительные количества иллита и каолинита)

На территории Салминской площади Пашско – Ладожского прогиба как в породах фундамента, так и в песчаниках наблюдается процесс интенсивного изменения детритовых зерен циркона. По аналогии с районами крупнейших урановых

месторождений «типа несогласия» бассейнов Атабаска и Комболджи, это свидетельствует об активной циркуляции диагенетических растворов, исключительно агрессивных по отношению к обычно чрезвычайно устойчивому циркону. Напротив, акцессорный монацит изменен в значительно меньшей степени, чем в вышеуказанных бассейнах. Процесс изменения цирконов наблюдается как в образцах керна скважин у поверхности рифейского несогласия, так и на значительном расстоянии от несогласия, в обнажениях, находящихся на значительном удалении от Салминского прогиба. Сохранившиеся цирконы обнаруживают довольно сложную структуру, которая, по-видимому, является следствием неоднократной магматической кристаллизации и/или, также неоднократного гидротермального воздействия, что особенно сильно проявлено в цирконах гранитов рапакиви. Процесс изменения циркона характеризуется замещением элементов, первоначально формирующих структуру минерала (Zr, Si, Hf), другими элементами (Al, P, Ca, Fe, Y, Th, U), содержание которых может существенно меняться в различных зернах. Наименее измененные цирконы установлены в архейских гранито-гнейсах, где отношение замещаемых элементов к замещенным составляет 32,5/0.5 (из расчета атомного количества) или около 1,5 %. В измененных цирконах из протерозойских гранито-гнейсов и сланцев это доля замещающих элементов может достигать 12 %. Цирконы из гранитов рапакиви обычно обнаруживают более существенные изменения: доля атомов Th, Al, Ca, Fe, Y и U в некоторых кристаллах возрастает до 25 %. Вместе с тем, цирконы из гранитов рапакиви представлены идиоморфными зернами с хорошо сохранившейся кристаллизационной зональностью, в противоположность цирконам из сланцев, первичная кристаллизационная зональность которых сохраняется чрезвычайно редко. Измененные участки в цирконах (более темные в отраженных электронах), многочисленные микропрожилки заметно обогащены Th и U. С уменьшением суммарного содержания первоначально формирующих структуру минерала элементов (Zr, Si и Hf) и, соответственно, увеличением доли других элементов на участках изменения зерен, уменьшается и общая сумма. Это, скорее всего, связано с метамиктизацией и гидратацией цирконов в связи с высоким содержанием в них Th и U, а также присутствием в них микровключений Al-фосфата. Суммарная доля замещающих элементов в детритовых зернах циркона из песчаников Пашско-Ладожского прогиба обычно варьирует от 2 до 12 %, т. е. в том диапазоне изменений, отмечаемым в породах фундамента и гранитах рапакиви.

В породах фундамента бассейна Атабаска (Канада) степень изменения монацита варьирует в широком диапазоне. Даже в относительно свежих породах он обнаруживает некоторые признаки изменения. Напротив, монациты, обнаруженные в достаточном количестве в графит-биотитовых гнейсах и сланцах Салминской площади, не несут в себе практически никаких следов изменений. В гранитах рапакиви монацит встречается крайне редко, однако U, Th, Zr и REE содержатся в ураноторите, алланите и редкоземельных карбонатах.

В Пашско – Ладожских песчаниках, в отличие от песчаников Атабаски, монацит сохранился не только в виде включений кристаллов в детритовом кварце, но и в глинистой матрице в ассоциации с оксидами титана, где его реликты несут отчетливые следы изменений. Это означает, что монацит из Пашско - Ладожских песчаников подвергался воздействию агрессивных растворов в процессе диагенеза. Этот процесс широко развит в песчаниках бассейна Атабаска, когда в процессе переотложения фосфора и редких земель вместе с алюминием и различными количествами кальция и стронция происходит образование минералов группы флоренсита – гойязита и крандаллита (алюмофосфаты – сульфаты). В Пашско – Ладожских песчаниках степень изменения монацита значительно меньше, не столь широко развиты алюмофосфаты. Торий, который является слабо подвижным элементом, кристаллизуется в виде редких кристаллов торита и/или вместе с некоторым количеством урана и редких земель в микрокристаллах оксидов – силикатов титана. Аналогичный процесс достаточно хорошо проявлен в протерозойских песчаниках бассейна Франсевиль (Габон) на месторождении Окло.

Детальное изучение характера изменений акцессорных минералов в кристаллическом фундаменте мезопротерозойского Пашско-Ладожского прогиба позволило установить, что все литологические разновидности фундамента, включая рифейские граниты рапакиви, были подвержены изменениями, аналогичными тем, которые установлены в фундаменте и песчаниках бассейнов Атабаска, Комболджи и песчаниках бассейна Франсевиль. Эти изменения связаны с фильтрацией насыщенных кальцием диагенетических растворов, вызывающих выщелачивание урана из пород фундамента и формирование урановых месторождений. Следовательно, изменения, наблюдаемые в районе Паша-Ладога могут быть вызваны событиями аналогичного характера.

Таким образом, если диагенетические растворы, сходные по своему составу и температуре с бассейнами Атабаска и Комболджи, циркулировали в Пашско –

Ладожском прогибе, то в данном случае они характеризуются более щелочным составом раствора из-за обилия полевого шпата в составе песчаников. Значительное количество вулканических пород у основания прогиба обуславливает обилие карбоната приуроченного к урановорудной стадии. Более низкие значения фугитивности кислорода обуславливают появление железистого хлорита и пирротина в зонах минерализации, в отличие от магниевых хлорита и турмалина в бассейнах Атабаска и Комболджи. Значительно меньше, чем в упомянутых бассейнах, проявлены процессы окварцевания, а также последующего растворения кварца в песчаниках. Все эти факторы, а также слабое изменение детритового монацита в породах фундамента и песчаников и обуславливают, к сожалению, значительно менее благоприятные условия для формирования крупных месторождений урана, аналогичных месторождениям бассейнов Атабаски и Комболджи. Тем не менее, наличие широко проявленного процесса изменения цирконов позволяет предполагать обнаружение более значительных концентраций урана в породах фундамента, аналогично урановорудному району Аллигейтор Риверз в Австралии.

Résumé

Une étude minéralogique et géochimique du bassin volcano-sédimentaire clastique intracontinental mésoprotérozoique (Ripheen) de Pasha – Ladoga (Carélie, Russie) ainsi que des minéralisations uranifères associées et des lithologies du socle sous-jacent a été réalisée. Une comparaison avec d'autres districts fortement minéralises d'age et de lithologie comparables indique qui les sediments clastiques du bassin de Pasha – Ladoga sont nettement moins matures que ces de bassins fortement minéralises de l'Athabasca (Canada) et de Kombolgie (Australie). Toutefois, de circulations importantes de fluides ont été mises en evidence dans les roches métamorphiques de l'Archéen et du Paléoprotérozoique et les granites rapakivi, ainsi que dans les sediments clastiques sous-jacent de la région de Pasha – Ladoga ou le gisement d'uranium de type discordance de Karku ont été découverts. Ces circulations de fluides ont conduit a une alteration a l'échelle régional de zircon et, dans une moins de mesure, de monazite, ainsi qu'a la formation de chlorites ferrifères et de carbonates dans les zones minéralisées.

Mots clés : Uranium, Discordance, Grès, Bassin Mésoprotérozoique, Altérations hydrothermales, Zircon, Monazite

Abstract

The mineralogy and the geochemistry of the Mesoproterozoic (Riphean) Pasha-Ladoga volcanic - sedimentary intracontinental clastic basin (Russian Karelia), associated uranium mineralization and underlying basement lithologies have been characterized and compared with those of highly mineralized districts having similar age and lithologic associations. The clastic sediments appear much more immature than highly mineralized basins of the Athabasca (Canada) and Kombolgie (Northern Australia). However, large-scale fluid circulation has been evidenced in the Archean to Paleoproterozoic metamorphic rocks and Mesoproterozoic rapakivi granites of the basement and in the overlying clastic sediments of the Pasha - Ladoga area, where the Karku unconformity related uranium deposit has been discovered. These fluid circulations are related to zircon alteration and to a lesser degree to monazite at the regional scale and essentially with a Fe-chlorite and carbonate alteration assemblage produced in the mineralized districts.

Key words : Uranium, Unconformity related deposits, Sandstones, Mesoproterozoic basin, Hydrothermal alteration, Zircon, Monazite.

General introduction

Framework of thesis

Between 1971 and 1990 the contribution of nuclear energy to world electrical power rose from 2 to 17 % (Mining Journal, 18.09.1998). In the leading industrial countries, notably the European Union, United States and Japan, nuclear energy now accounts for 20 – 30 % of total electrical requirements and up to 78 % in France. Of the world's 438 commercial nuclear reactors, 31 were completed in the past few years and 32 more are under construction. The global share of nuclear-generated electricity could rise to 25 % by 2030 (National Post, 03.08.2004). In this case importance of the high-grade uranium deposits exploration and new deposits searching are very high now.

Uranium deposits may appear at each step of the geological cycle: from magmatic and fluid circulation in the deep continental crust to evapotranspiration at the ground surface (Cuney et al., 2003). World uranium resources are contained in some fourteen different deposit types, including the one giant Olympic Dam Mesoproterozoic breccia complex deposit in Australia (> 31 % of world resources), sandstone hosted (18 %, mostly in USA, Kazakhstan and Niger), surficial deposits (4 % mainly in Australia), large tonnage but low grade resources in Early Proterozoic conglomeratic deposits, and small percentages in volcanic, metasomatic, metamorphic, granite-hosted and vein-type deposits (World Uranium Mining; Nuclear Issues Briefing Paper 41, 2004). But only Mesoproterozoic unconformity-associated deposits (> 33 % of the world resources in Canada and Australia) represent the most significant high grade, low cost uranium resource currently being exploited on a world-wide basis (Jefferson et al., 2005; Thomas et al., 2000). Unconformity related uranium deposits from the Athabasca basin (Saskatchewan, Canada) represent the world largest and richest uranium ore bodies. With the development of the Sue, Midwest, McArthur and Cigar Lake deposits, the production of Canadian deposits is reached about 18,000 metric tons uranium by 2004 and will account for half of the world production by 2006.

The area of the Athabasca basin is more than 85, 000 square kilometers, yet 96 % of the known uranium resources of unconformity-related type in it are concentrated in less than 20 % of the area along the eastern margin of the basin. This presents a metallogenic challenge for any reasonable assessment of the potential of the remaining 80 % of the basin (Jefferson et al., 2005).

Uranium metal resources of the Kombolgie Basin are slightly more than 50 % of those in the Athabasca basin. Their ore tonnage is greater but their average grade is relatively low.

These deposits are confined an area of about 7500 square kilometers, known as the Alligator Rivers Uranium field. This field shows geological similarities with the eastern Athabasca basin (Jefferson et al., 2005).

On the last 10 – 15 years data have changed for some well-known deposits and some new deposits and perspective areas have come to light.

The area of the Mesoproterozoic Pasha – Ladoga volcanic-sedimentary basin (Baltic shield, Russia) is more than 70, 000 square kilometers. But this area almost completely covers by Ladoga Lake. The basin present only three extensions beyond the Ladoga Lake shore, which are completely covered by Quaternary (the first one) or Vendian - Paleozoic sediments (Kushnerenko & Pichugin, 2000; Novikov et al., 2001). There are also some similar Mesoproterozoic sedimentary basins in the Baltic shield in Finland, Sweden and Russia.

The Karku uranium deposit (North-eastern slope of the Pasha – Ladoga basin), from its geological characteristics can be also referred to unconformity-related uranium deposits. This deposit was discovered in 1989 through drilling during mapping of the southwest contact of the Salmi rapakivi granite pluton by Nevskgeology enterprise (Saint-Petersburg, Russia) (Sharpilo, 1991). Recent studies (Bruneton, 2001; Kushnerenko, Pichugin, 2000; Kushnerenko, Dolgushina, 2003; Ledeneva et al., 2000; Mikhailov, 2001, 2003; Novikov et al., 2001; Pichugin, 2000; Polikarpov, Molchanov, 2000; Shurilov et al., 2003; Velichkin et al., 2003) confirmed the first assumption about similarities with unconformity-related deposit characteristics of the Karku deposit, but also revealed some differences.

Objects of the study

The major objectives of the present study are to define the lithological, structural and metallogenic parameters controlling the genesis of the unconformity type uranium mineralization from the Karku deposit and the Northern Ladoga Lake districts and the whole Pasha – Ladoga basin. The data available on the two well-known districts with economic uranium mineralization of this type (Athabasca and Kombolgie basins) will be taken as a reference. The followings parameters, characteristic of the Athabasca and Kombolgie mineralized districts, have to be especially evaluated :

1. *Petrogeochemistry and mineralogy of the Archean - Paleoproterozoic basement formations*: importance of the Archean plutonic formations with respect to the Paleoproterozoic metasedimentary and plutonic formations from the different areas of the Pasha – Ladoga basin. Definition of their potentiality to represent an uranium

source (such as leucogranites or high-K calc-alkaline plutons) and/or their role as a trap (such as graphitic schist).

2. *Petrogeochemistry and mineralogy of the Mesoproterozoic anorthosite – rapakivi granite magmatism*: importance of the Mesoproterozoic huge anorthosite – rapakivi granite plutons intruded Archean – Paleoproterozoic basement with respect to their potentiality to represent an uranium source.
3. *Petrogeochemistry and mineralogy of the different parts of the Pasha – Ladoga volcanic – sedimentary basin*: degree of sandstone maturity, paragenetic succession for the ore and alteration minerals, provenance history of the basin.
4. *Occurrence of the regolith-type alteration in the Archean - Paleoproterozoic basement rocks and the Mesoproterozoic rapakivi granites below unconformity surface*: its origin and its possible role in the genesis of the uranium mineralization.
5. *Diagenesis and hydrothermal alteration in the Mesoproterozoic volcanic - sedimentary sequences and in the basement formations* : nature of the alterations in the sandstones and in the basement, determination of clay minerals.

Methodology

For the best understanding of the different objects of the present study a bibliographic synthesis of previous work (including geological maps in different scales) on the study area was compiled. Then, basement and sandstone lithologies were selected and sampled (regionally and in the vicinity of the uranium mineralization), from the unconformity (regolith), fresh and altered equivalents from drillings (from the drill store house of the Nevskgeology enterprise, Ulyanovka, Saint-Petersburg) and from outcrops. Surface samples were selected during field seasons (in 2003 – 2004) in the Ladoga Lake area, which were organized with financial support of COGEMA, CREGU (France) and University of Helsinki (Finland). The total amount of the selected samples by different rock types is listed in the Table 1.

Rock types	Outcrops samples	Drill core samples
Archean plutonic formations	20	10
Paleoproterozoic metasedimentary and plutonic formations	40	120
Mesoproterozoic rapakivi granites	30	60
Mesoproterozoic sedimentary rocks	10	220
Mesoproterozoic volcanic rocks	16	30
Total	116	440

Table 1. Total amount of selected samples from the Ladoga Lake district

The chemical composition of the Pasha – Ladoga sandstones, basalts and the basement rocks was determined on 194 samples using ICP-AES for major elements and ICP-MS for trace elements (CRPG, Nancy, France), following a procedure described by Govindaraju & Mevelle (1987). Interpretation of the chemical rock composition with main geochemical diagrams was acquired with "Lithogeochemistry" software - version 1.0 beta (COGEMA – CREGU, 2001, developer: Patrick Fratczak) and for triangle diagrams plotting "Trixel" plug-in version 1.0b for Windows™ Excel (University of Lausanne, Switzerland, developer: Julien Ferrer) was used.

Petrographic and mineralogical analysis of the rocks (297 polished thin sections and 6 polish sections) were observed through optical observation (transmitted and reflected light). Mineralogical and petrographical characteristics of accessory minerals (zircon, monazite), ore mineralization and associated alteration phases (chlorite, carbonate, clays) were observed in 40 polished thin sections through optical observation (transmitted and reflected light) and using Scanning Electron Microscopy (SEM) in Back-Scattered Electron Mode (BSEM).

BSEM images and semi-quantitative mineral analysis were performed with an Hitachi S2500 Kevex SEM equipped with an energy-dispersive spectrometer (EDS) at the "Service Commun d'analyse" of the Henri Poincaré University (Nancy, France) and with a CamScan MX 2500S SEM equipped with an energy-dispersive spectrometer INCA Energy 200 at the All-Russia Geological Research Institute (VSEGEI, Russia). The contrasts of grey on the BSEM images reflect the average atomic number (Z) of the phase: light grey corresponds to domains with high average atomic numbers, and darker grey to domains with low average atomic number.

Quantitative chemical composition of the main accessory minerals, uranium mineralization and alteration minerals from the Pasha – Ladoga sandstones, basalts and the surrounding basement rocks has been determined with a CAMECA SX-100 electron microprobe (EMP) at the "Service Commun d'analyse" of the Henri Poincaré University (Nancy, France). An electron beam focused over a surface of approximately 6 μm^2 was used. Analytical conditions for accessory minerals analysis were 20 nA, 20 kV for major elements and 100 nA, 30 kV for trace elements.

Nature of the clay minerals in the sandstones and the basement rocks were determined with XRD analysis and following normative calculation in 30 oriented thin sections and disoriented powders. Observation of the clay minerals textures, their morphology have been determined with a Jeol JSM5600 LV SEM with spectrometer RX in the University of Poitiers (France) by Mr. Romain Brunet within the framework of his Master degree.

The diffractograms of thin sections and disoriented powders were obtained with a diffractometer Philips Xpert Pro MPD (40 kV; 40 mA; l-1.54 Å) and detector X ' Celerator (RTMS technology) connected with a system of purchase X-Pert Data collector and processing X-Pert High Score (University of Poitiers). Diagrams of X-rays of thin sections were acquired between 2,5 and 30 °2 Θ (between 35Å and 3Å) and those of the powders which have been brought down since a way between 5 and 65 °2 Θ (between 17,65 Å and 1,5 Å).

Determination of the ages of the Mesoproterozoic basalts of the Salmi suite and gabbro-monzonites of the Valaam sill is in the process now in the University of Helsinki (Finland). The volcanic rocks will be dated using the conventional TIMS technique at the Geological Survey of Finland using baddeleyite fractions extracted from a considerable volume of rocks. Zircons will also be extracted from clastic sedimentary rocks and they will be analyzed using the NORDSIM ion microprobe in Stockholm for inheritance patterns.

Thesis structure

In *Chapter I,* presents a bibliographic synthesis of previous geological knowledge of the Ladoga Lake area (part 1.2) and from the typical unconformity related uranium deposits of the Athabasca basin (part 1.1). In part 1.3 used geochemical diagrams and definitions are presented. In part 1.4. the maps of the area with selected samples positions are given.

Chapter II concerns the geological characteristics of the basement: Archean – Paleoproterozoic rocks with the Mesoproterozoic anorthosite – rapakivi granites of the Salmi pluton.

Chapter III considers the main geological, mineralogical and petrogeochemical characteristics of the Pasha – Ladoga sedimentary basin (except the volcanics).

Chapter IV gives the characteristics of the Mesoproterozoic volcanic rocks of the Salmi suite and the Valaam sill.

Chapter V provides a synthesis of the data and a genetic model of uranium deposition for the Karku area uranium deposits. Comparison of favorable criteria for the occurrence of uranium mineralization with those of the two major unconformity type uranium deposit bearing districts are considered in the present work. Finally, conclusions and recommendations are proposed for following surveying and exploration.

Chapter I

Reviews and definitions

1.1. General characteristics of the typical unconformity-type deposits (on example of the Athabasca basin (Canada)

Unconformity-type uranium deposits are presently the most profitable uranium resources due to their exceptionally high grade and large tonnage. At least 17 unconformity-type uranium deposits were discovered in the Athabasca Basin (Northern Saskatchewan, Canada) (Fig. 1.1) since the discovery of the Rabbit Lake deposit in 1968 (Heine, 1986).

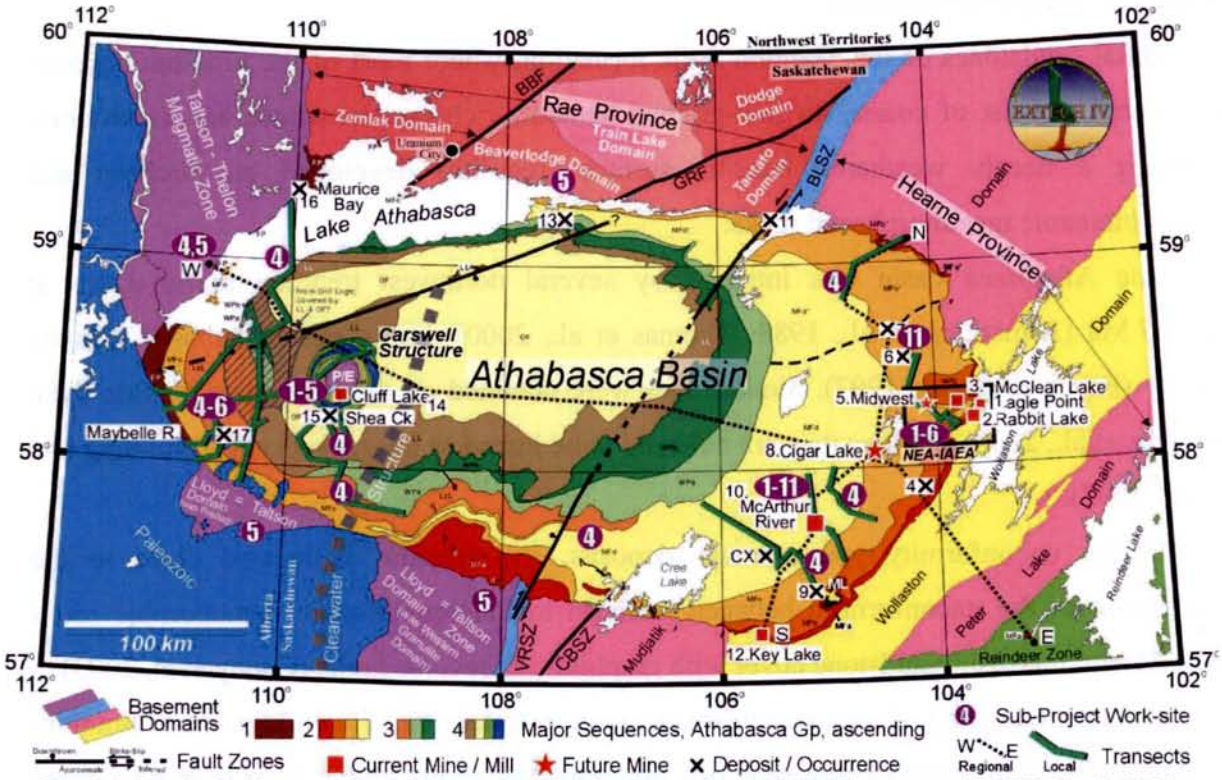

Fig. 1.1. Geological map of the Athabasca basin (after Ramaekers, 1990; Thomas et al., 2000; Card, 2001; Card and Pana, 2002 and Ramaekers et al., 2001).

Legend: FP = Fair Point, MFa through MFd = Manitou Falls, LzL = Lazenby Lake, WPa,b = Wolverine Point, LL = Locker Lake, OF = Otherside, WR = William River Subgroup (MF through OF), D = Douglas River, C = Carswell; d = diabase; ML = Moore Lakes gabbro complex; P/E = undivided Peter River / Earl River gneisses in the Carswell Structure; BBF = Black Bay Fault; BLSZ = Black Lake Shear Zone; GRF = Grease River Fault; VRSZ = Virgin River Shear Zone.

The Athabasca basin unconformable overlies a basement complex of Archean and Paleoproterozoic rocks. The basement rocks are separated into two distinct provinces by the northeast trending Snowbird Tectonic Zone (Hoffman, 1990). Both the Rae Province, to the West, and the Hearne Province, to the East, consist of Archean gneisses and Paleoproterozoic metasedimentary rocks and basic to acid plutons (Thomas et al., 2000). However, basement

rocks of the Hearne Province underwent extensive thermotectonic reworking during the Trans-Hudson Orogen (ca. 1820-1790 Ma.) (Thomas et al., 2000). Most of the unconformity-type uranium deposits are located in the Eastern part of the Athabasca Basin, in the vicinity of the graphite-rich Cable Bay shear zone that occur between the Mudjatik domain and the Wollaston domain.

Ramaekers (1980) proposed that the Athabasca basin (Fig. 1.1) was formed at 1.75-1.70 Ga as a series of NE-SW-oriented sub-basins controlled by major Mesoproterozoic faults rooted in underlying Paleoproterozoic metasedimentary rocks. The Mesoproterozoic thick sedimentary sequences, polycyclic, fluvial to marine quartz sandstones deposited in a continental margin environment.

Basal sandstones of the Manitou Falls formation, where most of the uranium deposits are located, consist of coarse- to fine-grained hematite-rich conglomerates and sandstones, overlying a deeply weathered lateritic surface (regolith) developed on Archean and Paleoproterozoic metamorphosed rocks.

The Athabasca basin was intruded by several northwest trending mafic dykes at ca.1227 Ma (Armstrong et al., 1988; Thomas et al., 2000) during post Athabasca tectonic activity (Fayek & Kyser, 1997). Similar ages were obtained on the McKenzie diabase dyke (Thomas et al., 2000) and thus they are believed to be linked to the same event (Cumming and Krstic, 1992).

In the unconformity-type uranium deposits, the uranium is located close to the intersection of the unconformity between Archean to Paleoproterozoic metamorphic rocks and a Mesoproterozoic sandstone cover with graphite-rich reverse faults (Cuney et al, 2003).

The understanding of the mechanisms leading to formation of such high-grade uranium ore at that time represents a major scientific problem. Numerous studies have been performed in the vicinity of the deposits in attempt to point out the processes that have lead to the formation of such uranium accumulations (Fayek and Kyser, 1997; Thomas et al., 2000).

Several processes, from supergene (Knipping, 1974) to hydrothermal (Little, 1974) have been proposed to explain the genesis of unconformity-type deposits. However, the most commonly accepted genetic model is diagenetic-hydrothermal. This model implies the mixing between oxidizing basinal brines with basement derived reducing fluids (Pagel, 1975; Hoeve and Sibbald, 1978; Pagel and Jaffrezic, 1977; Pagel et al., 1980; Wilson and Kyser, 1987; Kotzer and Kyser, 1995; Fayek and Kyser, 1997).

The pH, controlled by the kaolinite-illite paragenesis, was slightly acidic (ca. 4.5 at 200 °C), because of the lack of feldspar in highly mature quartzose sandstones or from its

alteration during diagenesis (Cuney et al., 2003). Early diagenetic brines from detrital quartz overgrowths are NaCl-rich and after interaction with the basement Ca-rich lithologies they became enriched in Ca (Derome et al., 2003). High Ca content in the mineralizing fluids is of major importance for accessory mineral alteration and for uranium mobilization as shown by: (i) incongruent dissolution of monazite with U-P-LREE leaching and new formation of a Th-U silicate with lower Th/U ratio; (ii) new formation of U-poor Ca-Se-REE hydrated Al-phosphates; (iii) Ca, REE, U, Al, P enrichment of zircon altered zones (Hecht & Cuney, 2000; Cuney et al., 2000). Favorable mixing occurs at temperatures of approximately 200 °C and results in precipitation of uranium at structural and physiochemical traps, developed near the sandstones – basement unconformity (Thomas et al., 2000). Zones of fluid mixing are characterized by well-developed alteration halos, containing illite, kaolinite, dravite, sudoite, euhedral quartz, and, locally, Ni-Co-As-Cu sulphides (Kotzer & Kyser, 1995).

Age dating of the Athabasca sediments indicates a main hydrothermal ore-related event occurred within the basin at 1500 Ma and was followed by further overprinting alteration and uranium remobilization events at approximately 900 Ma and 300 Ma (Fayek & Kyser, 1997).

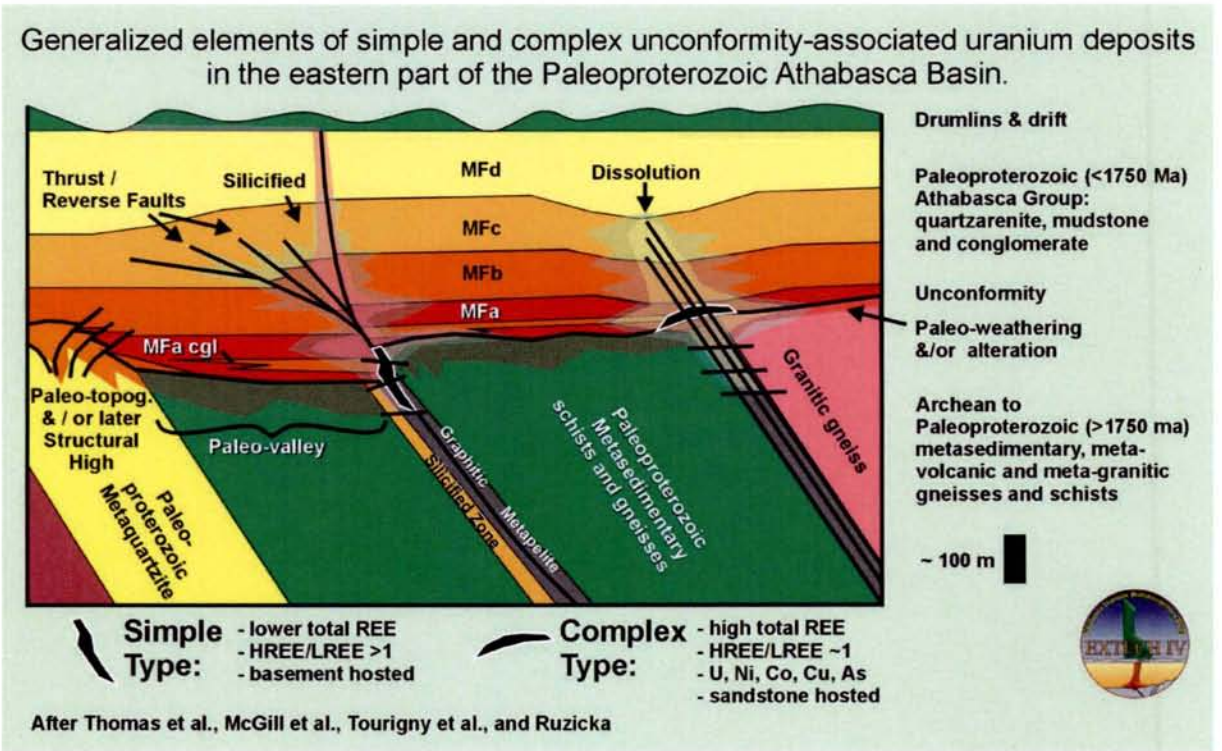

Fig 1.2. Generalized elements of unconformity-associated uranium deposits in the Paleoproterozoic Athabasca Basin. After Thomas et al. (2000), McGill et al. (1993), Tourigny et al. (2001), Ruzicka (1996) and current sub-project results in EXTECH IV, references listed in Jefferson et al. (2003).

These numerous studies have shown that two main types of deposits can be distinguished (Fig. 1.2). The fracture-controlled or "simple-type" deposits are frequently

hosted deep in the basement (down to 400 meters below the unconformity). The metal assemblage only consists of U and Cu. Simple type deposits present relatively low contents of REE. In contrast, polymetallic, or "complex-type" deposits typically occur within 25 – 50 meters of the basement – unconformity and are characterized by anomalous concentration of sulphides. They typically present a complex assemblage of Ni, Co, Cu, Pb, Zn, Mo and locally Au, Ag, Se and Pt group elements (Fayek and Kyser, 1997; Thomas et al., 2000).

1.2. Geology of the Riphean Pasha – Ladoga basin area (Baltic shield, Russia)

1.2.1. Geological setting of the Ladoga Lake area

The Ladoga Lake area is located in the south-eastern part of the Baltic shield in the north-western margin of the East-European platform.

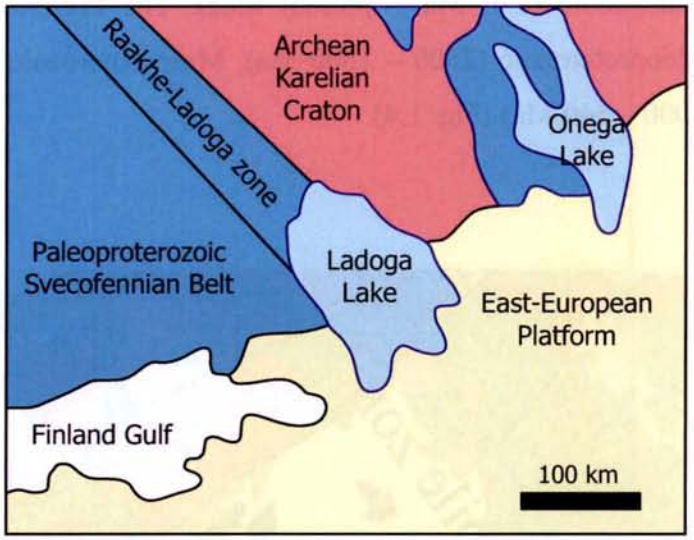

Fig. 1.3. Sketch geological map of the south-eastern part of the Baltic shield (from the Geological map of uranium mineralization of the Baltic shield (after Naumov et al, 2001)

The area includes two major tectonic elements: the *Karelian megablock*, cratonized in the Upper Archean and a Paleoproterozoic supracrustal belt formed during the Svecofennian orogeny. The Raakhe-Ladoga mobile zone (*Ladoga mobile zone* – its south-eastern part) represents the marginal part of the Paleoproterozoic Svecofennian belt adjoining the Karelian megablock (Fig.1.3).

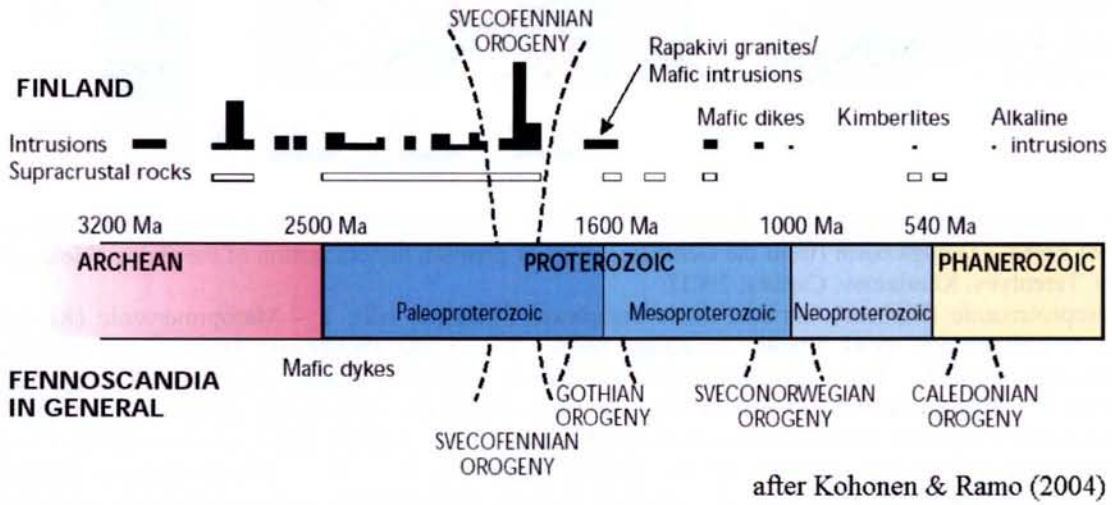

Fig. 1.4. Geological time scale with the igneous activity and the supracrustal rocks. Major orogenic events are also indicated (after Kohonen & Ramo, 2004)

To avoid confusion, the IUGS (2000) recommendations have been employed in this work. According to these recommendations, geological time scale for Baltic (Fennoscandian) shield is presented by Archean (3200 – 2500 Ma), Proterozoic (2500 – 540 Ma) and Phanerozoic (540 Ma – present time). The Proterozoic time was subdivided as follow: Paleoproterozoic (2500 – 1600 Ma), Mesoproterozoic (1600–1000 Ma) and Neoproterozoic (1000 – 540 Ma) (Fig. 1.4).

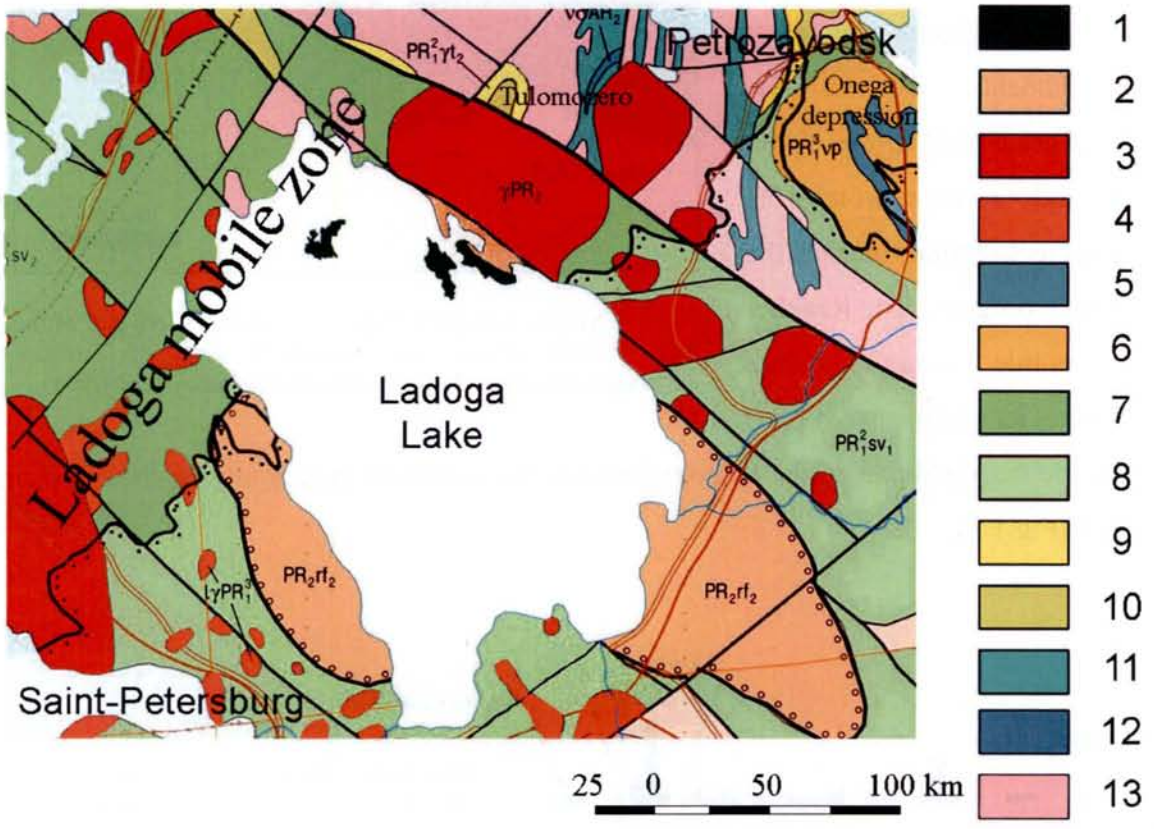

Fig. 1.5. Geological map of the Ladoga Lake area – Archean - Proterozoic basement with the Mesoproterozoic (Riphean) Pasha – Ladoga basin (from the Geological map of uranium mineralization of the Baltic shield, after Naumov, Terentyev, Kharlamov, Carisey, 2001)
1 – Mesoproterozoic (Riphean) intrusive basic complexes (Valaamo sill); 2 – Mesoproterozoic (Riphean) volcanic – sedimentary rocks (Pasha – Ladoga basin); 3 – Early Proterozoic leucogranite complexes (Kuznechensky, etc); 4 – Early Mesoproterozoic anorthosite - rapakivi granite complexes (Vyborg, Salmi batholiths); 5 – Paleoproterozoic (Vepsian) intrusive basic complexes (Rop-ruchey gabbro – dolerite); 6 – Paleoproterozoic (Vepsian) metavolcanics and metasediments; 7 - 8 – Archean granite-gneisses domes (7) and Paleoproterozoic schists and gneisses of the Kitelya series (8), 9 – 10 – Paleoproterozoic (Jatulian) metavolcanics and metasediments; 11 – 12 – Archean (Lopian) metavolcanics and metasediments (greenstone belts); 13 – Archean TTG complexes of the Karelian block.

Archean Karelian Craton

The Karelian Craton is located to the north-east from the Ladoga Lake district. It is composed of Middle Archean biotite, garnet-biotite, amphibole gneisses with amphibolite interlayers, yielding U-Pb zircon ages of 3.14 – 3.13 Ga, and tonalites, trondhjemites, granodiorites with U-Pb zircon ages of 3.17 – 3.14 Ga (Lobach-Zhuchenko et al, 1993). Late Archean (Lopian) volcanogenic and sedimentary-volcanogenic formations (so called - greenstone belts) metamorphosed into mica-quartz-feldspar schists and amphibolites (Fig. 1.5).

During the Paleoproterozoic (Fig. 1.6), the supracrustal formations of the Karelian Craton were covered by gently dipping Jatulian metavolcanic and metasedimentary rocks with insignificant degree of metamorphism. The whole Karelian megablock is divided by faults of various orders, which control the location of greenstone belts, linear fault-block systems, superimposed basins and depressions (Tulomozero, Onega).

Sariolian and Sumian rocks are not considered here because they are not widespread in the Paleoproterozoic sequence of this area.

The Tulomozero superimposed structure is composed of volcanogenic-carbonate shale and black shale sequences of Early Proterozoic Jatulian and Ludicovian ages (Fig. 1.5), which occurs to the south-western margin of the Karelian Craton.

Eastward, the major Onega basin (Fig. 1.5) covers the Archean basement. It is characterized by a complete section of Paleoproterozoic formations in the southeast Baltic Shield and by large amounts of carbonaceous sequences, including

MESOPROTEROZOIC(Riphean cover)

---------- ~ 1600 Ma --- unconformity

KALEVIAN and SVECOFENNIAN

---------- ~ 1950 Ma --- unconformity

LUDICOVIAN

---------- ~ 2080 Ma --- unconformity

Upper

JATULIAN ---- ~ 2150 Ma --- unconformity

Lower

---------- ~ 2300 Ma --- unconformity

SARIOLIAN

---------- ~ 2400 Ma --- unconformity

SUMIAN

---------- ~ 2500 Ma --- nonconformity

ARCHEAN BASEMENT

Fig. 1.6. Simplified time scale of the Paleoproterozoic supracrustal formations of the Baltic Shield (after Ojakangas et al (2001), ages are given after Heiskanen (1991, 1992), Karhu (1993) and Melezhik et al (1997).

schungites (Svetov et al, 1990). The Onega basin consists of Paleoproterozoic with the Jatulian (terrigenous-volcanogenic and carbonate - shale sequences) and Ludicovian (carbonate - black shale and ultrabasic and basic volcanogenic sequences) deposits. The carbonate – black shale sequences enclose numerous sills of diabases and dolerites and phyroclastic rocks, with an age of 2100-2000 Ma (Svetov et al, 1990).

The syncline-shaped Onega depression (Fig. 1.5) occurs to the south of the Onega basin. It is filled with Paleoproterozoic Kalevian (carbonaceous sandstones and siltstones) and Vepsian (sandstones, quartzite-sandstones and quartzites) sediments. Gabbros and gabbro-diabases of the Rop-Ruchey sill were emplaced ca. 1850 – 1750 Ma ago into the Vepsian quartzite-sandstones along the perimeter of the Onega depression (Svetov et al, 1990).

The Ladoga mobile zone

The Ladoga mobile zone belongs to the 50 - 150 km wide *Raakhe-Ladoga zone* located between the *Archean Karelian Craton* and the *Paleoproterozoic Svecofennian Belt (Domain)* (Fig. 1.5).

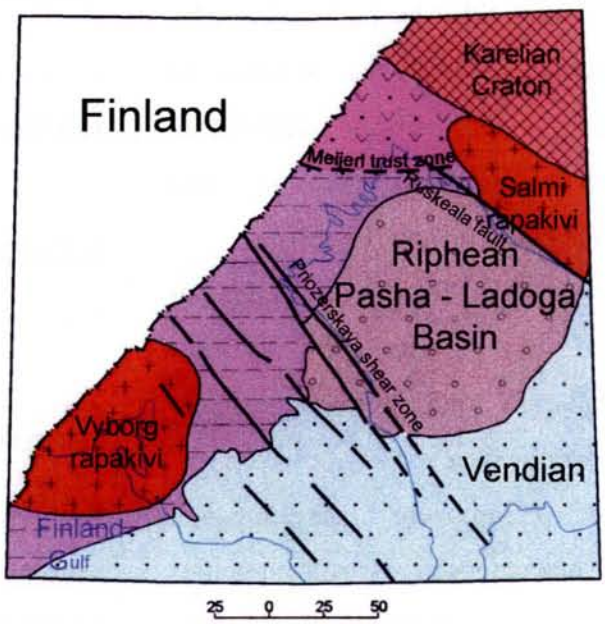

Fig. 1.7. Tectonic sketch map of the Ladoga mobile zone district (after unpublished Aphanasov, 1999)

The Ladoga mobile zone has been divided into two domains according to their geological characteristics: the *Northern Ladoga Domain* and the *Western (or Southern) Ladoga domain* (Shuldiner et al., 1997). The two domains are separated by the Meijeri thrust zone (Fig. 1.7) (Baltybaev et al., 1996).

The Northern Ladoga Domain represents a part of the Karelian Craton. Its structure is controlled by Archean granite-gneiss domes rimmed by intensely dislocated Paleoproterozoic supracrustal rocks including metapelites and metavolcanic rocks. This domain was intensively folded, fractured, metamorphosed, migmatized and subjected to magmatic and hydrothermal processes. Metamorphic grades are between greenschist – amphibolite facies.

The Western (Southern) Ladoga Domain belongs to the Svecofennian Belt, which is characterized by a strong metamorphism up to granulite facies. It is composed of an assemblage of metapelitic rocks of the Lakhdenpokh metamorphic series.

In the Northern Ladoga Domain the Paleoproterozoic rocks series have a thickness of 1 to 1.5 km. Two main lithostratigraphic units have been distinguished (Negrutsa, 1984; Koistinen et al, 1996): Pitkyaranta suite of the Ludikovian age and Impilakhti suite of the Kalevian age. There are three subhorizons in each unit: lower – transgressive, middle – transgressive – regressive and upper – regressive. Transgressive subhorizons comprise basal quartz conglomerates and mature quartzitic metasediments. Regressive subhorizons are dominantly presented by tuffs, tuffites and layered amphibolites. Both horizons have common features: carbonaceous matter enrichment (up to 5 %) and abundant sulphides dissemination.

In summary, during the Svecofennian orogeny the Paleoproterozoic rocks series underwent polyphase deformation and low- to intermediate-pressure, upper amphibolite (Northern Ladoga Domain) and granulite (Western Ladoga Domain) facies metamorphism, strong migmatization and intensive feldspar blastesis. Folding during this event produced northwest-elongated domes and basins. Granulitic gneisses of the Western Ladoga domain underwent also regional retrograde metamorphism to amphibolite and locally - epidote - amphibolite facies metamorphism (Shuldiner et al., 1997).

Ages of granitic migmatization in the Western Ladoga domain and tonalitic migmatization in the Northern Ladoga domain were recently studied by Baltybaev et al. (2002) who reported similar monazite ages of 1872 - 1869 Ma for leucosomes and their host gneisses in both the Western and the Northern domains. According to Baltybaev et al. (2002) both domains were affected by the same 1880 Ma metamorphism and the compositional variation observed in the migmatites resulted from compositional variation of their supracrustal protoliths.

Intrusive Paleoproterozoic magmatism of the Ladoga mobile zone

Intrusive magmatic series in the *Ladoga mobile zone* comprise granitoids and gabbroid complexes of various ages and represent up to 40% of the present surface (Fig. 1.8) (Saranchina, 1972; Svetov & Sviridenko, 1991). The oldest complexes include synorogenic norite-enderbite series and tonalite-granodiorite intrusions with associated gabbroic rocks. Conventional U-Pb zircon dating has produced an age of 1881±7 Ma for enderbite at Kurkijoki and 1878±4 Ma for diorite from the Lauvatsaari gabbro-diorite-tonalite intrusion

(Glebovitsky et al., 2001). These ages define the metamorphic culmination in the Northern domain and are in agreement with the ages of synorogenic tonalites and orthopyroxene-bearing granitoids that postdate the regional deformation in the south-eastern and central Finland (Huhma, 1986; Holtta, 1988; Ramo et al., 2001).

The transition to potassium-rich granites in the Northern domain is manifested by late- to post-orogenic intrusions where microcline granite represents the dominant rock type. The two major intrusions of this type in the Northern domain are the Tervus and the Puutsaari complexes (Konopelko & Eklund, 2003). In the Puutsaari island, the microcline granite is associated with significant amounts of potassium-rich mafic rocks and with rocks of tonalite - granodiorite series. The intrusions crosscut migmatites and are less deformed compared to the host rocks. Conventional U-Pb zircon dating of the Tervus microcline granite yielded an age of 1859±3 Ma (Glebovitsky et al., 2001).

However, some of the microcline granites in the Ladoga Lake area (Konopelko, 1997) were formed in a time interval between 1815 and 1790 Ma (Kuznechensky, Borodinsky, Lazurnensky, Lesogorsky plutons). According to Eklund et al. (1998) and Vaisanen et al. (2000), these young microcline granites were formed by anatectic melting of the crust triggered by heat provided by the emplacement of post-collisional shoshonitic intrusions ca. 1800 Ma ago.

The mantle-derived post-collisional alkali gabbroid – syenite (shoshonitic - after Eklund et al, 1998) intrusions (Elisenvaara, Oya-Yarvi, Vuoksa) represent the latest Svecofennian magmatic event in the region (Ladner, 1983; Khazov et al., 1993; Eklund et al., 1998; Konopelko et al., 1998). These rocks comprise a unique series extremely enriched in P, F, Ba, Sr and LREE, also moderately enriched in Th, U. The source of this shoshonitic association is considered to be a lithospheric mantle affected by carbonate metasomatism (Eklund et al., 1998). In the NW Ladoga Lake area the emplacement and mid-crustal fractionation of the shoshonitic lamprophyric melt was accompanied by crustal anatexis and produced significant volumes of granitoid rocks with variable compositions from anatectic S-type microcline granites to shoshonitic granites and syenites directly fractionated from the lamprophyric melt. A number of single grain $^{207}Pb/^{206}Pb$ zircon ages obtained by the evaporation method (Ivannikov, unpubl.; Konopelko, 1997) as well as conventional U - Pb zircon data (Shuldiner et al., 2000) and K-Ar amphibole ages (Konopelko, 1997) define an age interval of 1787 - 1809 Ma for the shoshonitic intrusions in this area. The intrusion at Elisenvaara, has been recently dated by conventional U - Pb zircon method at 1800±6 Ma (Vaasjoki, 2001, personal com.). However, a different range of $^{207}Pb/^{206}Pb$ apatite ages for the Elisenvaara intrusions

were given by Khazov et al (1993) at 1550 – 1430 Ma. This range of ages was also confirmed by Aphanasov (personal com.).

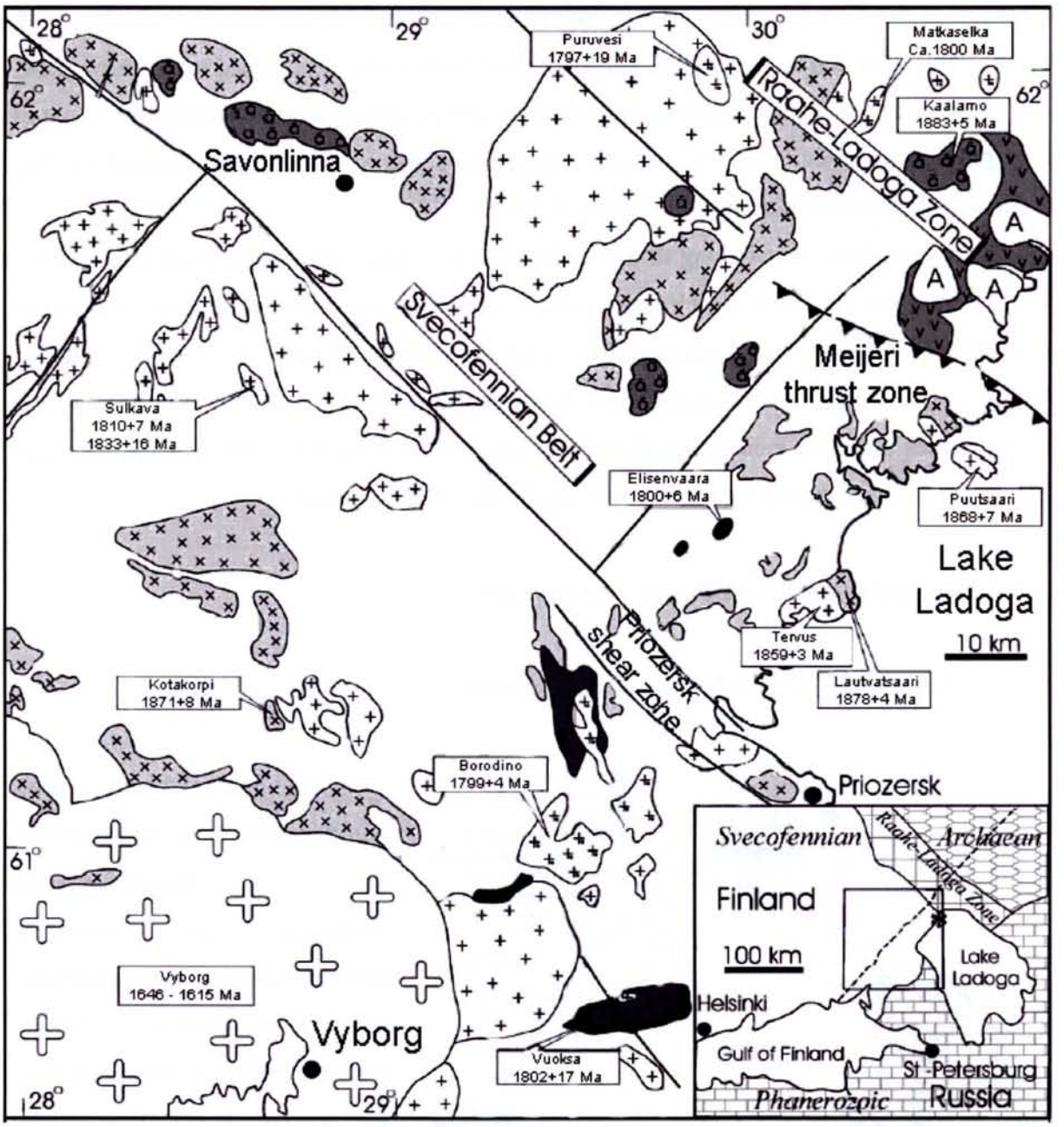

Fig. 1.8. Schematic geological map of the NW part of the Ladoga Lake region and south-eastern part of Finland from Koistinen & Saltykova (1999) and Konopelko (1997), available U-Pb zircon ages of intrusive rocks of the region are from Konopelko & Eklund (2003)

Mesoproterozoic anorthosites - rapakivi granite complexes of the Ladoga Lake area

The emplacement of the 1.65 – 1.54 Ga rapakivi granites was the latest major crustal increment to the Fennoscandian (Baltic) shield after the later Mesoproterozoic (Kohonen & Ramo, 2004). The rapakivi granites and associated basic rocks are typical anorogenic rocks and they sharply cut the surrounding Svecofennian and Archean orogenic formations. Most of these plutons show evidence of multiple intrusions, some of which have formed satellite stocks outside the main pluton (Laitakari et al, 1996).

Two main intrusions belong to the Ladoga Lake district: the Vyborg batholith with U-Pb ages of 1.645 to 1.625 Ga (Vaasjoki et al., 1991) on the western part and the Salmi batholith with Ulyalegi and Lodeinopolsky satellites with U-Pb ages of 1.547 to 1.530 Ga (Amelin et al., 1997), which related these intrusions to major EW (or NE-SW) lithospheric discontinuities implying incipient or aborted rifting. They will be described in detail below in Chapter II in concerning to the basement of the Pasha – Ladoga basin.

1.2.2. Geological setting of the Pasha – Ladoga basin

Mesoproterozoic (Riphean or Jotnian) sedimentation

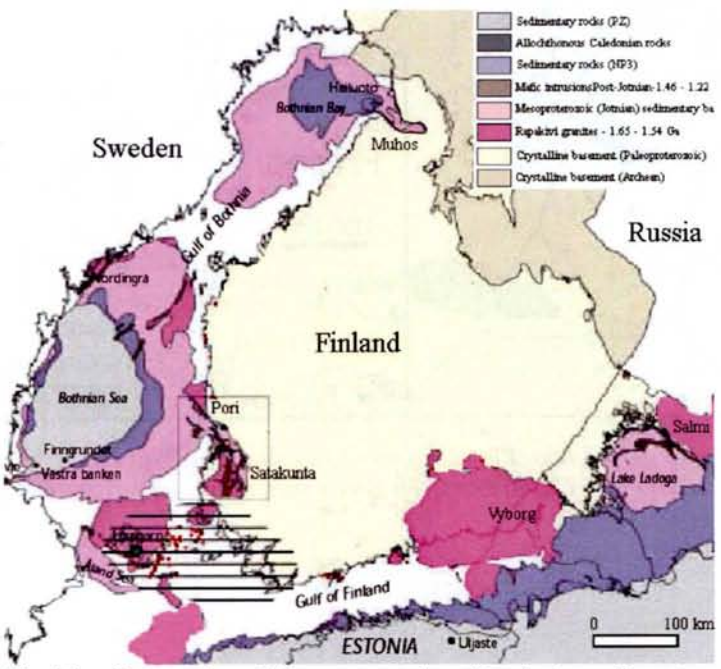

Fig.1.9. Present-day Mesoproterozoic (Jotnian) sedimentary basins and the rapakivi plutons on a simplified map of the Baltic Shield highlighting the Mesoproterozoic to Phanerozoic rock units (according to Koistinen et al., 2001 and Kohonen & Ramo, 2004)

The term "Jotnian" was introduced by Sederholm (1897) for unmetamorphosed sandstones and associated igneous rocks in the Precambrian of Fennoscandia, which corresponds to Mesoproterozoic age in the IUGS time scale (Riphean – in Russia). The Jotnian-type sediments, arkoses, siltstones, shales and conglomerates occur in several localities of the Baltic shield (Fig. 1.9).

These rocks occupy shallow basins, tectonic depressions or grabens bordered by fractures or fault zones, most of which are oriented NW – SE (Kohonen et al, 1993). Extensive diabase dykes and sills and, sometimes, coeval volcanic rocks may also occur.

Satakunta graben (Finland)

The Satakunta sandstones cover a northwest elongated, fault-bounded area covering about 1500 km^2 (Kohonen, 1993; Kohonen & Ramo, 2004). The maximum thickness of the Satakunta area may reach more than 1500 m. According to Winterhalter et al (1981), the Satakunta sandstone continues into the Bothnian Sea and links together the Mesoproterozoic sandstone areas of the Satakunta graben, Gävle valley and the Nordingrå area in Sweden (Fig. 1.9). The real extent of the submarine sandstones has been interpreted from seismic profiles. That interpretation has been confirmed by the presence of red arkosic sandstone in drillings (Winterhalter, 1972).

Muhos graben (Finland)

The Muhos sediments occupy a fault-bounded, SE-trending basin south of Oulu (Finland), extending ~50 km inland from the coast (Fig. 1.9). They are very poorly exposed. They have been correlated with the Muhos Formation, are were also observed in drillings at Hailuoto Island near the town of Oulu (Kohonen &Ramo, 2004). According to seismic data, a major part of the bottom of the Bothnian Bay is occupied by sedimentary rocks (Winterhalter et al., 1981). The extension of the Mesoproterozoic sediments in the Bothnian Gulf area has been summarized by Winterhalter (2000).

Pasha - Ladoga basin

The Pasha-Ladoga basin (Fig. 1.10) overlies Archean - Paleoproterozoic igneous and metamorphic rocks and the Mesoproterozoic (Early Riphean) Salmi rapakivi granites. The present extension of the Pasha – Ladoga basin is moderate (approximately 70 000 km^2). The Mesoproterozoic (Riphean) volcanic - sedimentary formations comprise graben-like basin with a thickness, which may locally be over 2000 m. The shape of the basin roughly coincides with the coastline of the Ladoga Lake (Amantov et al, 1991).

The NW-SE fault zones determine the shape of the Mesoproterozoic elongated graben-like structures. For example, the Ruskeala NW – SE master-fault is concordant with the boundary of the Salmi rapakivi granite intrusion in the NE and the Priozersk – Khiytola NW – SE shear-zone to the SW boundary of the Pasha – Ladoga graben-like basin (see Fig. 1.7).

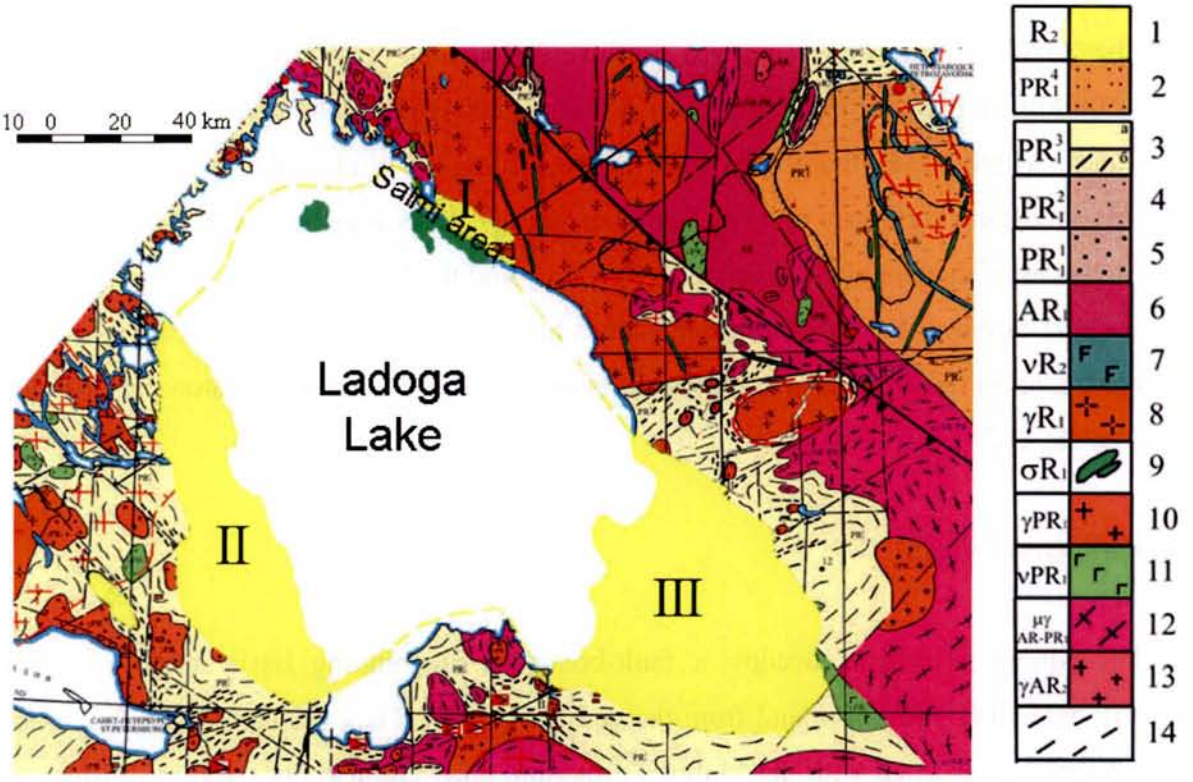

Fig.1.10. Geological map of the Ladoga Lake area (Mikhailov et al, 2002).
1 – Mesoproterozoic sandstones, basalts in the I – North-eastern (Salmi) area; II – Western (including Yablonevka) area; III – South-eastern (Pasha) area; 2 – 5. Paleoproterozoic metamorphic complexes: 2 - Vepsian conglomerates, shales; 3 - Kalevian-Ludicovian siltstones, schungite shales, diabases (a), biotite, biotite-amphibole and aluminiferous graphitic gneisses and shales (b); 4 - Jatulian conglomerates, quartzites; 5 - Sariolian polymictic conglomerates; 6 – Undivided Archean granites, gneisses, schists, amphibolites, migmatites; 7-9 – Magmatic complex of the epoch of the Riphean activity: 7 – Gabbro, gabbro-diabases; 8 – Rapakivi granites, anorthosites and associated rocks; 9 - Subvolcanic intrusions, sills and dykes of diabases, basalts; 10-11 – Late Svecofennian intrusions: 10 - Plagiogranites, anatectite-granites; 11 - Gabbro, gabbro-norites; 12 - Late Archean-Early Proterozoic gneiss granites; 13 - Late Archean plagiogranites; 14 – Areas of distribution of graphite-bearing gneisses and schists.

Apart from the main basin, which is mostly covered by the Ladoga Lake, there are also a few isolated occurrences of Mesoproterozoic (Riphean) rocks (Fig. 1.10), but also completely overlain by Vendian - Paleozoic or Quaternary sediments:

(i) to the North-East of the lake, in the *Salmi* area,

(ii) to the West, including the *Yablonevka* area, and

(iii) to the South-East, in the *Pasha* area.

The Pasha – Ladoga basin is filled with sedimentary and volcanic rocks, which are undeformed and unmetamorphosed. Cross sections through the basin show the differences in composition, structure and thickness of the lithologic units (Fig. 1.11). The stratigraphic succession from the bottom to the top as followed (Polikarpov & Molchanov, 2000; Kushnerenko & Pichugin, 2001; Mikhailov, 2001; Novikov et al., 2001) :

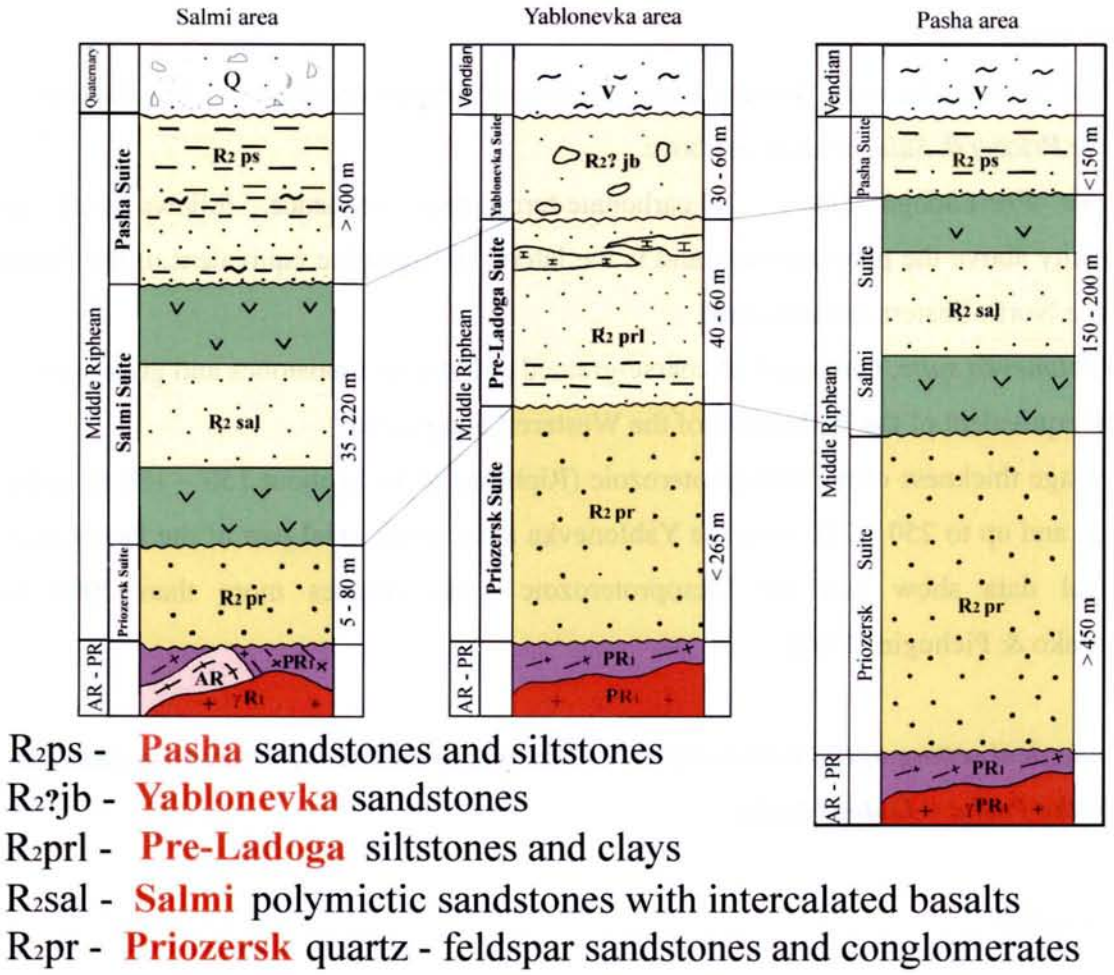

Fig. 1.11. Correlation scheme of the sections of the different part of the Pasha – Ladoga volcanic – sedimentary basin (adapted after Mikhailov et al, 2002).
1 – Archean granite-gneisses; 2 – Paleoproterozoic schists and gneisses; 3 – Paleoproterozoic K granites; 4 – Early Mesoproterozoic rapakivi granites; 5 – 11 - Mesoproterozoic sediments: 5 – Priozersk Suite (R_2pr): coarse-grained sandstones with gritstones and pebbled conglomerates; 6 – 7 – Pre-Ladoga Suite (R_2prl): 6 – fine-grained sandstones, siltstones and clays; 7 – lenses and interlayers of dolomites; 8 – Yablonevka Suite (R_2jb?): inequigranular sandstones with gravels and pebbles, tillite-like conglomerates; 9 – 10 – Salmi Suite (R_2sal): 9 - lavas of basalts, their lava breccias, mandelsteins; 10 – medium- fine-grained sandstones; 11 – Pasha Suite (R_2ps): sandstones, siltstones, tuff siltstones, carbonaceous clays; 12 – Late Mesoproterozoic (Vendian) (V) clays, sandstones

- *the Priozersk Suite* which represents the lower part of the succession, consists of a sequence of red coarse-grained sandstones with layers and interlayers of quartz and polymictic small-pebbled conglomerates;.

- *the Salmi suite* composed of sedimentary and volcanic rocks lies with a stratigraphic and structural unconformity on the rocks of the Priozersk suite; clasts of the Priozersk suite sandstones are observed in the basal layers of the Salminskaya suite;

- *the Pasha Suite* composed of sandstones and siltstones which only occur in the Salmi and Pasha areas.

In the Yablonevka area (Western Ladoga), the stratigraphic succession is as followed:

- *the Priozersk Suite*, similar as above,

- *the Pre-Ladoga Suite* - a carbonate-terrigenous sequence, follows with an unconformity above the previous suite and is the lateral stratigraphic equivalent of the Salmi Suite of the North-Eastern Ladoga area,

- *Yablonevka suite*, composed of coarse-grained polymictic sandstones and gritstones, is the lateral equivalent of the Pasha suite of the Western Ladoga area.

Average thickness of the Mesoproterozoic (Riphean) rocks is about 150 – 180 m in the Salmi area and up to 250 – 300 m in the Yablonevka area. In the axial part of the Pasha area, geophysical data show that the Mesoproterozoic rocks reaches more than 2000 m (Kushnerenko & Pichugin, 2001).

1.2.3. Geological setting of the Karku deposit as example of an unconformity-type uranium deposit in the Pasha – Ladoga basin

Salmi area

The *Salmi area* is situated on the eastern coast of Ladoga Lake, in the NE slope of the Pasha-Ladoga basin. It hosts the Karku unconformity-type deposit, which structural position is controlled by the Ruskeala deep fault zone and a north-eastern transformed fault. There are numerous meridional contracted dome-folded structures and a series of north-western, meridional and latitudinal faults. The deposit is confined to the Central Horst – uplifted zone of the Archean - Paleoproterozoic basement (Fig. 1.12).

In the area of the Karku deposit the basement occurs at a depth of 120 to 140 m and corresponds to a dome - shaped Archean granite – gneisses. The flanks of the dome and interdome synclines are filled with Paleoproterozoic migmatized and granitized amphibole-

biotite and biotite schists of the Pitkyaranta and Impilakhti suites, which contain horizons and lenses of graphite-bearing rocks. In the north-east, the dome-folded structures are cut by the Salmi rapakivi granites batholith, whose surface gently inclines south-eastward (Fig. 1.13).

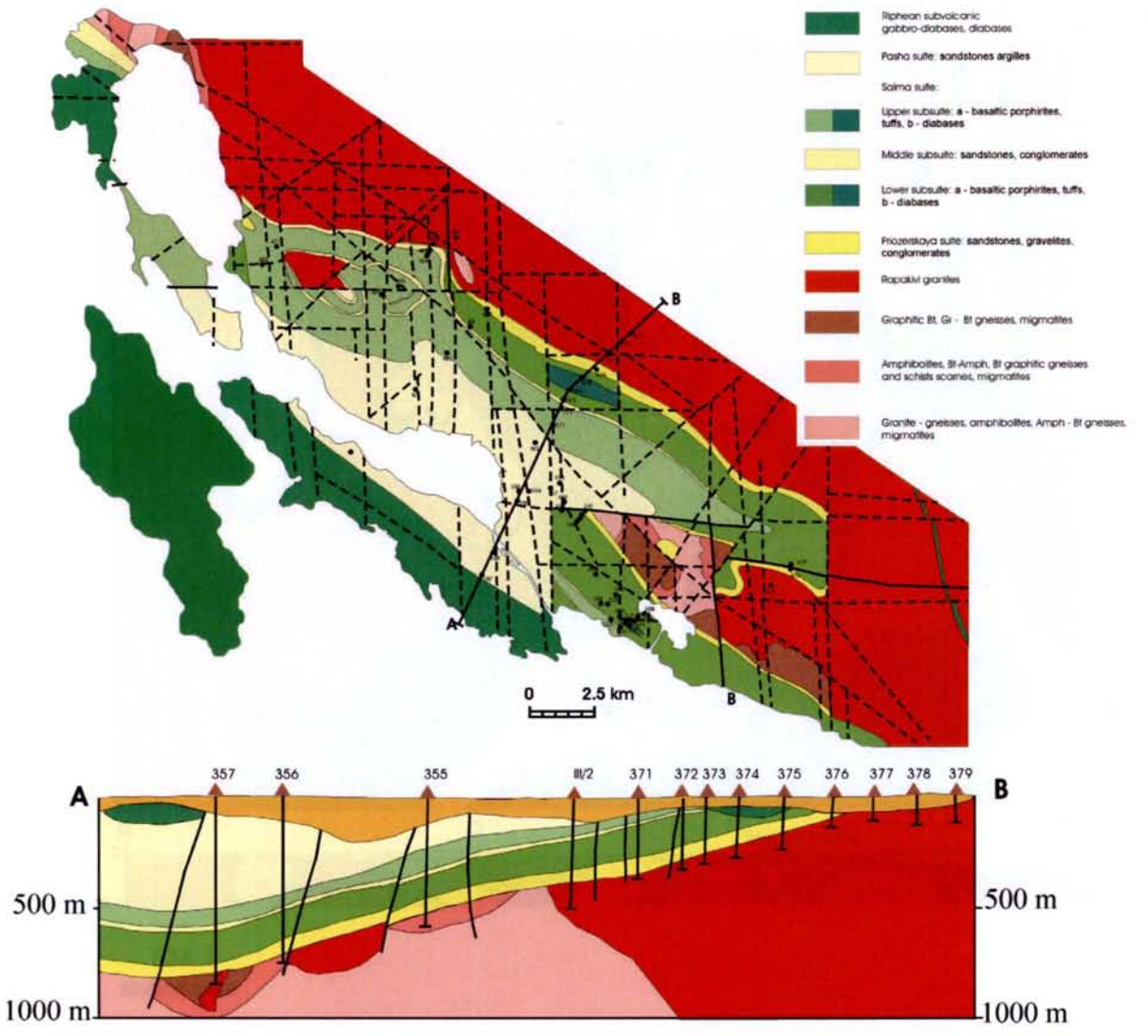

Fig. 1.12. Geological schematic map and section of the north – eastern part of the Ladoga Lake (Salmi area) (compiled by Mikhailov, 2002)

It has been proposed that supergene processes intensively altered the roof of the basement before the deposition of the sediments of the Pasha – Ladoga basin (Novikov et al, 2001). The thickness of the regolithized zone is up to 20 meters. Then, the volcanic-sedimentary Mesoproterozoic sequence forms a flat monocline dipping here to the southwest. Gentle folding and later tectonic dislocations complicate the monocline. Within the limits of the Salmi area the Mesoproterozoic volcanic-sedimentary sequence has a thickness of up to 800 m. However, within the limits of the Central Horst its section includes only the

lowermost Priozersk Suite (up to 40 m thick) and the lower volcanic Salmi Subsuite (up to 90 m thick). The total Mesoproterozoic thickness varies from 110 m to complete disappearance above some of the basement roof uplift.

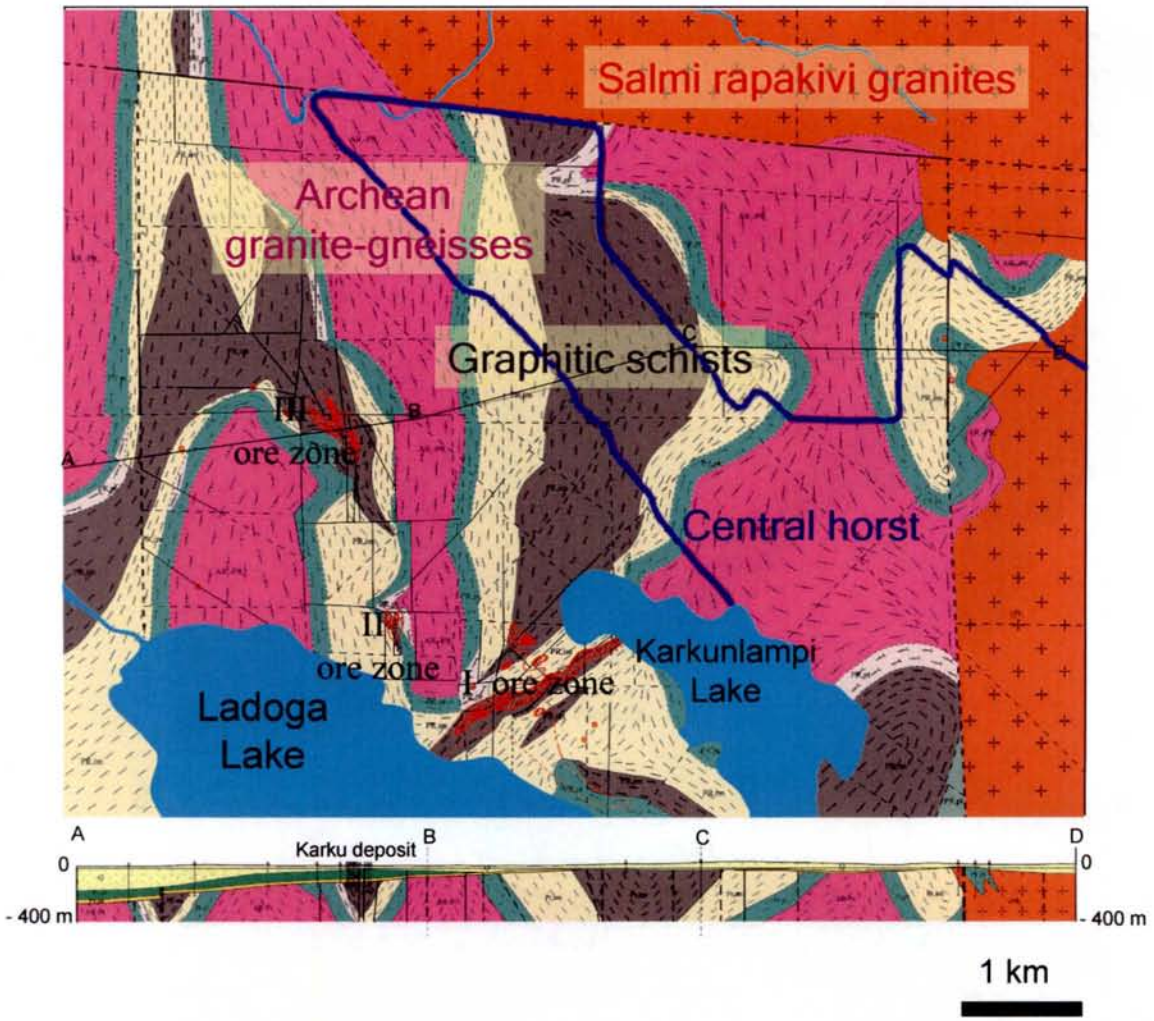

Fig. 1.13. Map of the basement rocks of the Karku deposit area with schematic geological section (compiled by Petrov, 2004)

Bedrock is everywhere covered by the Quaternary glacial moraine from 20 to 100 (and more) meters.

Structure of the Karku unconformity-type deposit

There are three main uranium ore bodies in the area (Fig. 1.13). All uranium ore bodies are located in the sandstones and conglomerates of the basal horizon of the Priozersk Suite. Besides some ore sections have been discovered within the weathering crust of the

basement, close to the unconformity. Some rare anomalic concentrations occur in fractures in the volcanic layers (Kushnerenko & Pichugin, 2000; Novikov et al., 2001; Shurilov et al., 2003).

The ore bodies have a complicated phacoidal-bed form (Fig. 1.14). They are traced along the strike for several hundred meters and have the width up to 80 meters. Thickness of the ore bodies is up to 10 meters, with content of uranium more then 300 ppm.

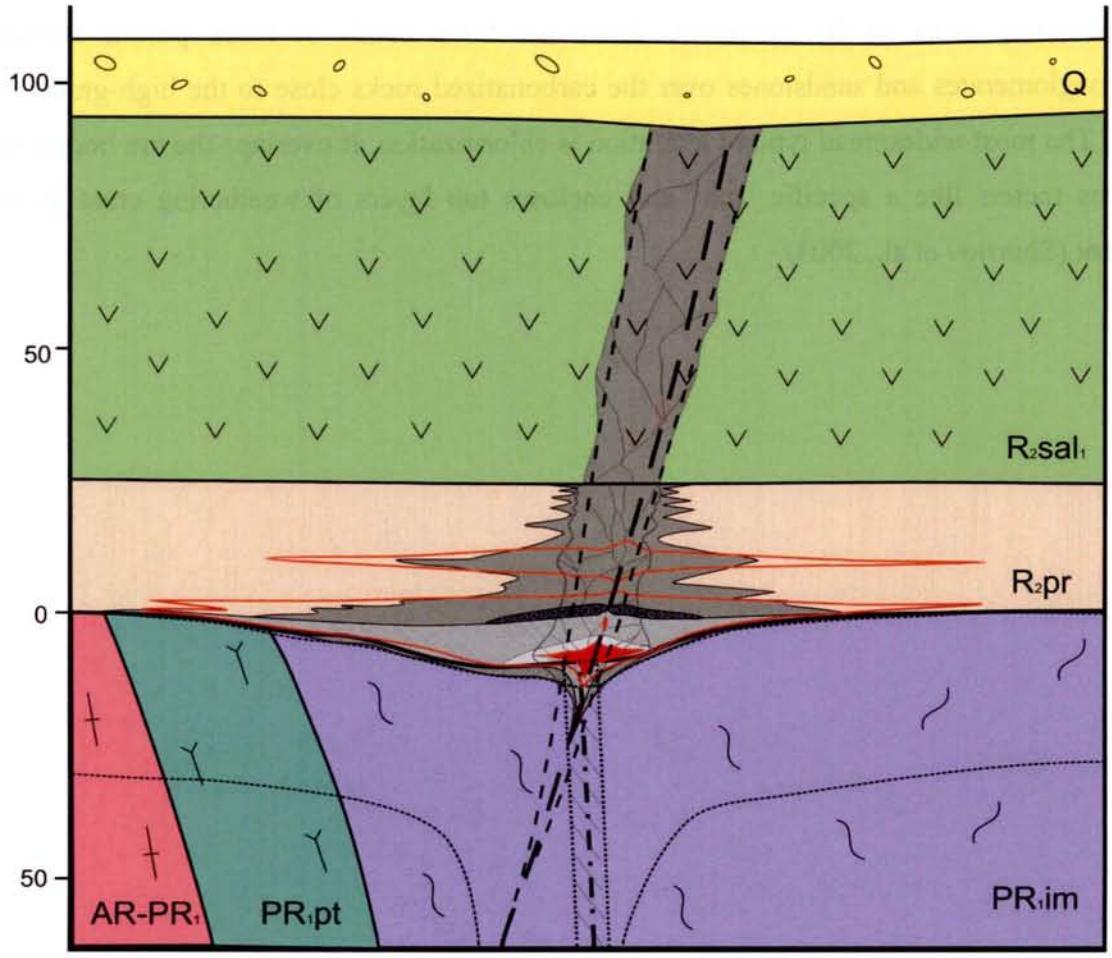

Fig. 1.14. Simplified geological section through the Karku deposit uranium ore body (compiled by Shurilov, 2003)
Legend: Q – Quaternary glacial deposits; R_2sal_1 – basalts of the lower volcanic subsuite of the Salmi suite; R_2pr – sandstones of the Priozersk suite; PR_1im – Paleoproterozoic biotite – graphite gneisses and schists of the Impilakhti suite; Pr_1pt – Paleoproterozoic amphibole – biotite - graphite gneisses and schists of the Pitkyaranta suite; AR – PR_1 – undivided Archean – Paleoproterozoic rocks; in grey tones – different zones of alteration; in red – high-grade uranium ores.

The third ore body contains more than 1 wt. % uranium and attain meter thickness. The highest uranium content is over 19 wt%. The estimated total resources of all ore bodies is

about 6 000 tons of uranium. The speculative resources are estimated to 40 - 50 kilotons of uranium. High content of zinc, lead, silver, molybdenum and some others elements are associated with the uranium ores (Kushnerenko et al., 2004).

The main characteristics of the Karku deposit are the following: the high-grade ore bodies are surrounded by an alteration zone with intense sulphidization, chloritization and carbonatization (Fig. 1.14). The altered zone has a heterogeneous constitution. The most productive horizon is mostly carbonatized and also rich in sulphides in the vicinity of the ore bodies. It occurs in the basal level of the Priozersk Suite and more rarely in the upper part of the weathering crust in the basement. There are thick bands of black porous leached microconglomerates and sandstones over the carbonatized rocks close to the high-grade ore bodies. The most widespread type of alteration is chloritization. It overlaps the ore bodies for a dozens meters like a specific "hat" and encloses top layers of weathering crust in the basement (Shurilov et al., 2003).

1.3.Tools for rock classification based on petrogeochemistry and mineralogy

This part deals with a review of classification diagrams chosen by the author as interpretation tools (geotectonic, mineralogical, geochemical...).

A short review on magmatic rock classifications seems necessary because of the great number of existing classifications and of their different objectives.

The TAS diagram (Total Alkali Silica; Le Bas et al., 1986)

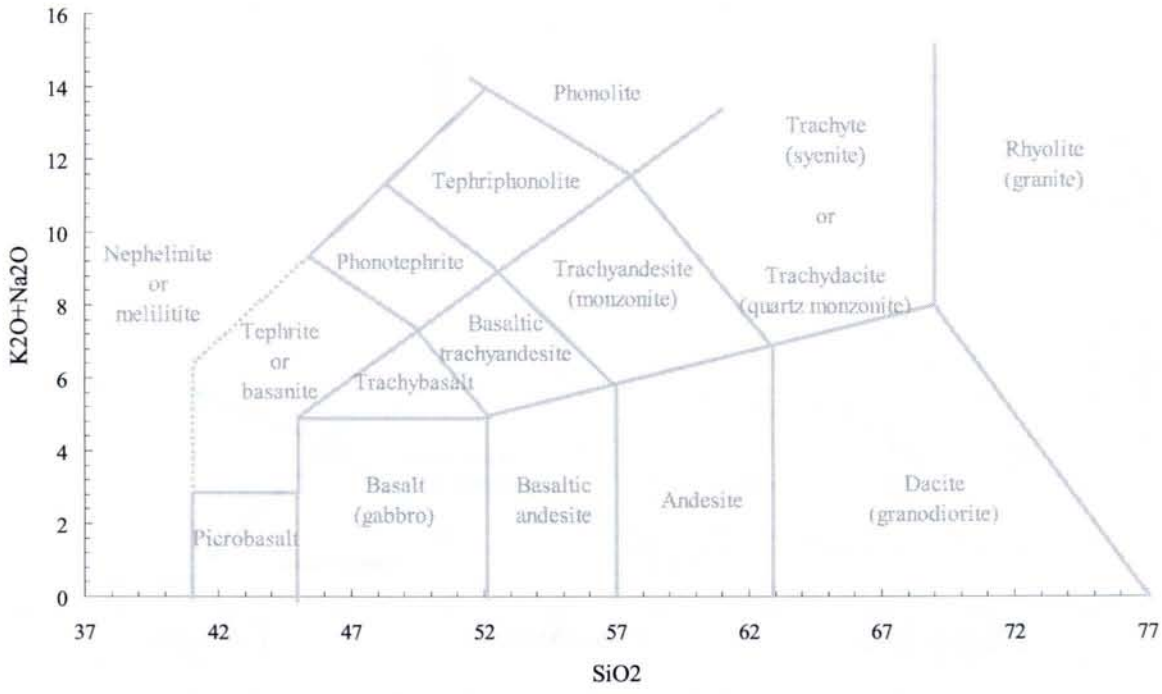

Fig. 1.15. SiO2 vs. $K_2O + Na_2O$ (TAS) diagram with the fields of different magmatic rocks (Le Bas et al, 1986)

This diagram representing the content of SiO_2 as a function of the sum of alkalies (Na_2O+K_2O) expressed as a percentage mass is the most usually used because it makes possible to represent the majority of the over-saturated silicate magmatic rocks and to apprehend their degree of evolution which generally follow the increase of content of SiO_2 and alkalies (Fig. 1.15). This diagram can be subdivided in two fields characterizing the tholeitic and calc-alkaline fields. It can be supplemented by the use of the K_2O/SiO_2 diagram to differentiate the magmatic series more specifically according to their enrichment in potassium.

The QP, AB and derivative QA diagrams (Debon et Le Fort, 1983, 1988)

These diagrams are chemical-mineralogical diagrams, in which the major elements are presented in millications. They make possible to specify the nomenclature of the rocks and to plot it within an evolutionary trend. In addition to the primary characteristics of the magmas, these diagrams also allow to determine quartz and feldspars fractionations and the various types of postmagmatic alterations.

Q-P diagram (Fig. 1.16)

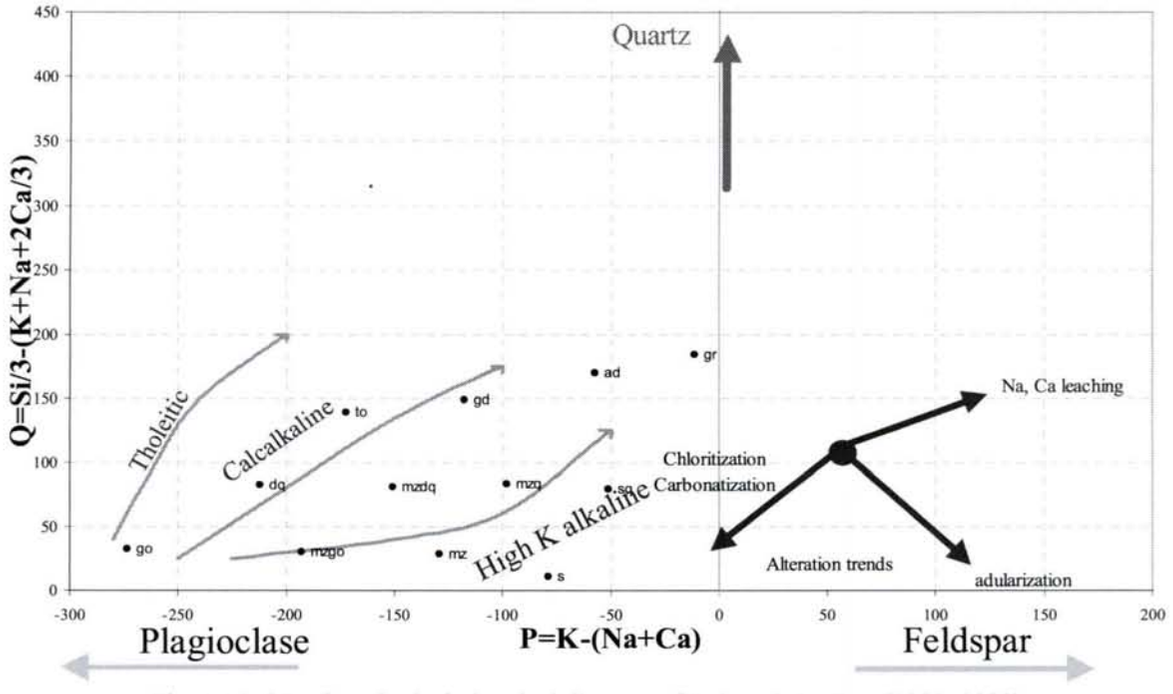

Fig. 1.16. QP mineralogical-chemical diagram of Debon & Le Fort (1983, 1988)
Each division of the grid corresponds to a rock type: **ad** – adamellite; **dq** – quartz diorite; **gd** – granodiorite; **go** – gabbro, diorite, anorthosite; **gr** – granite; **mz** – monzonite; **mzdq** – quartz monzodiorite; **mzgo** – monzogabbro; **mzq** – quartz monzonite; **s** – syenite; **sq** – quartz syenite; **to** – tonalite, trondhjemite. Typical trends of the different magmatic associations types are shown: tholeitic, calcalkaline, high K alkaline

Q-P diagram is a binary diagram, with Q = Si/3 - (K+Na+2Ca/3) in ordinate which represents the proportion quartz in the rock and P = K (Na + Ca) in abscissa which gives the relative proportion of feldspars, with potassic feldspar to the right diagram (P = 380) and plagioclase to the left (P = -380). The average compositions of the reference rocks defined a composition grid as well as the principal magmatic trends: tholeitic, calc-alkaline, high K alkaline and alkaline are represented. The effects of hydrothermal alterations (to clay minerals, chlorite, carbonates, albite, adular) also can be identified.

AB diagram (Fig. 1.17)

In the AB diagram the ordinate A = Al - (K+ Na + 2Ca) corresponds to alumina not incorporated into the feldspars (peraluminous index similar to normative corundum or A/CNK) and the abscissa B = (Fe+Mg +Ti) represents the amount of mafic minerals and is used as index of differentiation. This diagram makes possible to discriminate metaluminous from peraluminous magmatic rock associations. The composition fields of the major sediment groups are also reported

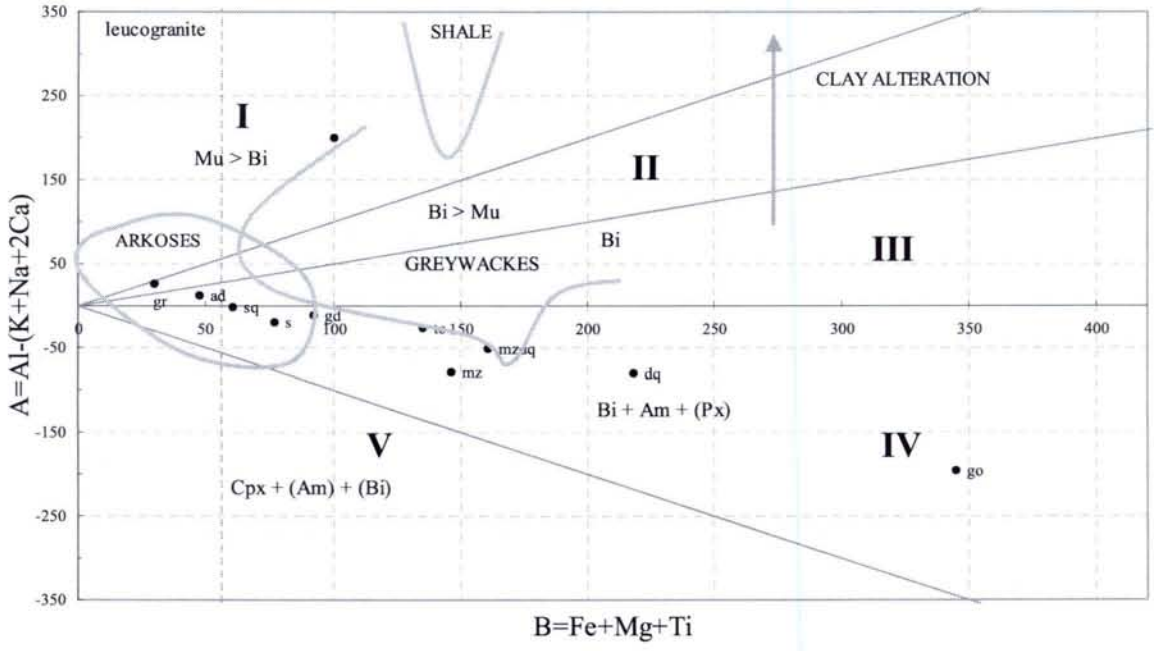

Fig. 1.17. AB mineralogical-chemical diagram (Debon and Le Fort, 1988)
Sectors, numbered from I to V, correspond to a specific mineralogical composition. I – III – sectors of peraluminous rocks with, respectively: I – muscovite > biotite (by volume); II – biotite > muscovite; III – biotite (usually alone, at times with a few amphibole); IV – V (without VI here) – sectors of metaluminous rocks with, respectively, IV – biotite + amphibole ± pyroxene; V – clinopyroxene ± amphibole ± biotite.
Each division of the grid corresponds to a rock type: see Fig. 1.16. Composition fields of sediments (shale and greywackes) are also represented with the clay alteration vector.

QA diagram (Fig. 1.18)

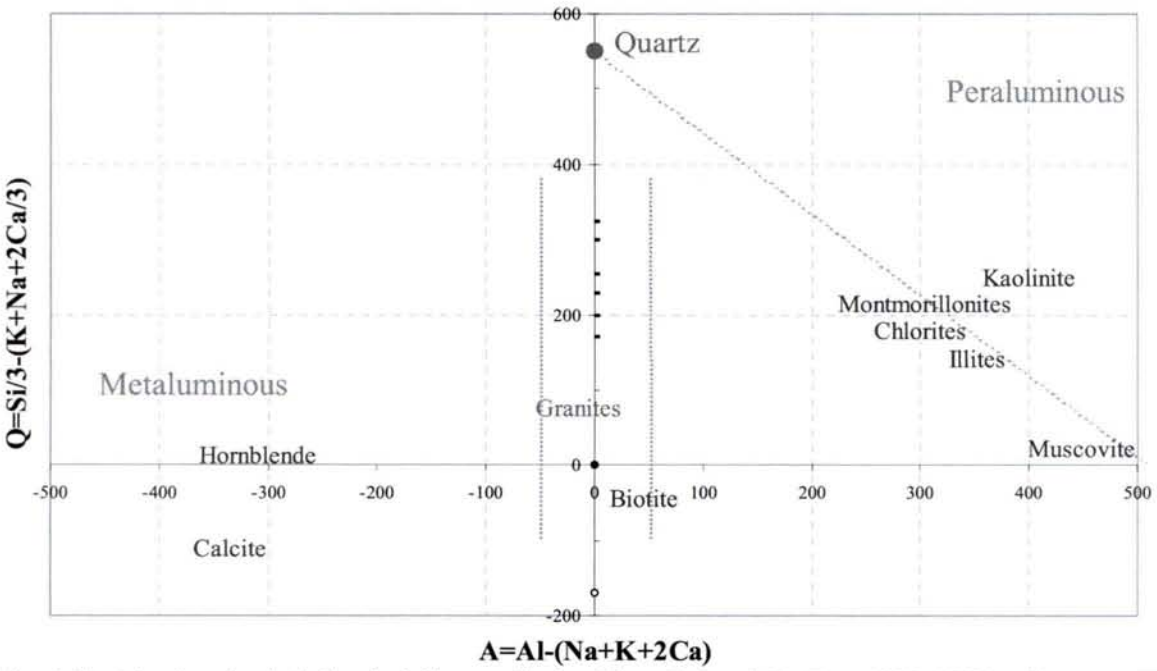

Fig. 1.18. QA mineralogical-chemical diagram (derived from Debon & Le Fort, 1983, 1988) with quartz, K feldspar, plagioclase and main alteration minerals plots

Q-A diagram is a binary diagram using the Q and A parameters from Debon & Le Fort (1983, 1988), where Q = Si/3 - (K+Na+2Ca/3) in ordinate which represents the proportion quartz in the rock and A in abscissa corresponds to the peraluminosity index. This diagram is useful to determine the relative proportion of minerals in clastic sedimentary rocks: quartz/feldspars/clay minerals/carbonates.

Metasedimentary rock origin diagrams (Moine & de la Roche, 1968)

The diagram (Al + Fe + Ti)/3 - Na versus (Al + Fe + Ti)/3 - K (Moine & de la Roche, 1968) allow first to distinguish former sedimentary (mainly positive values of the (Al + Fe + Ti)/3 - Na parameter) from magmatic rocks (mainly negative values of the (Al + Fe + Ti)/3 - Na parameter)(Fig. 1.19). To distinguish the greywackes and Ca-rich lithologies from the basalts which may be confused in this diagram, the interpretation of the data has to be coupled with the Al + Fe + Ti versus Ca + Mg diagram (all parameters calculated in millications, Moine & de la Roche, 1968) (Fig. 1.20).

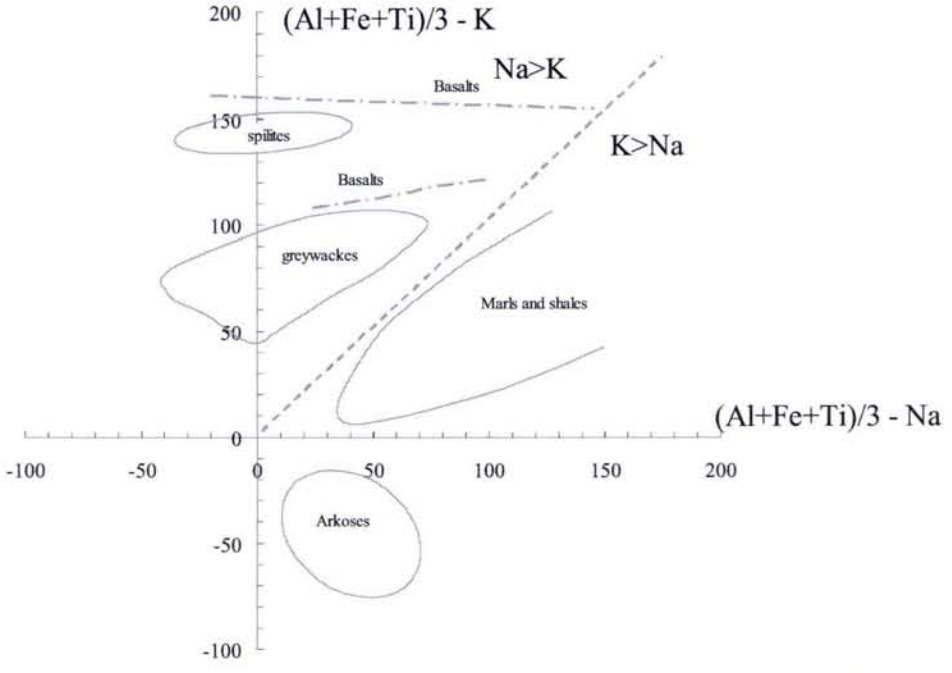

Fig. 1.19. (Al + Fe + Ti)/3 – Na vs. (Al + Fe + Ti)/3 - K diagram (Moine & de la Roche, 1968), it is useful for identifications of the initial protoliths of metasediments

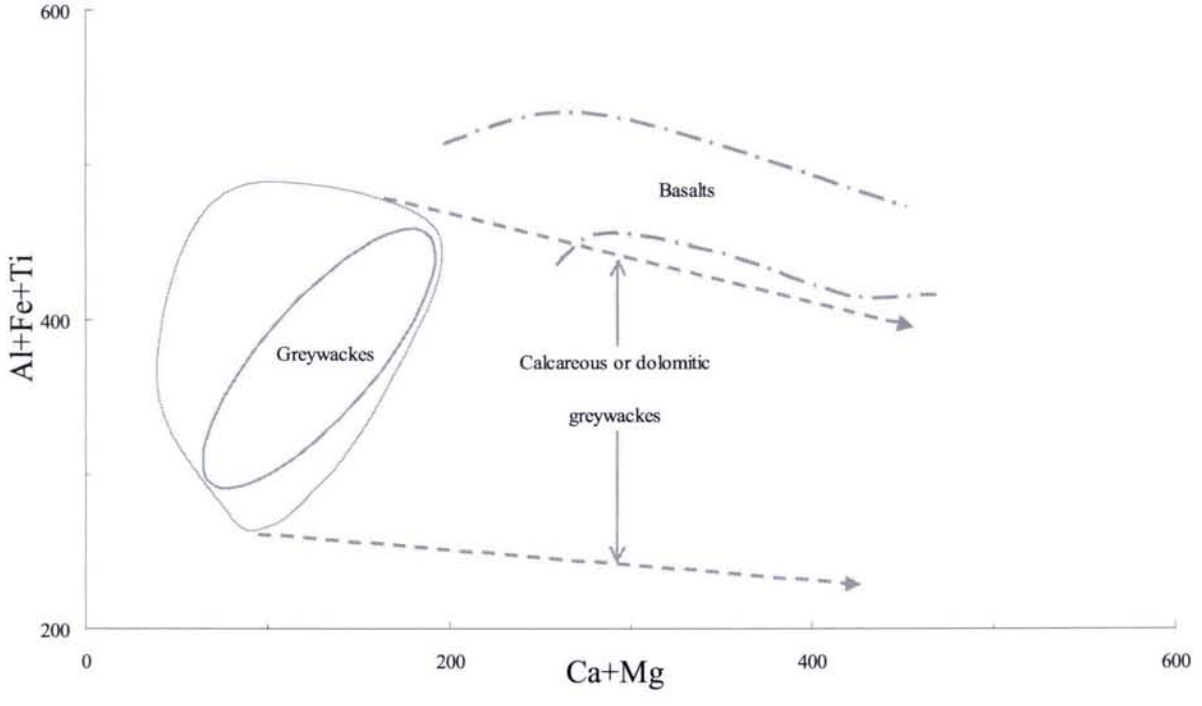

Fig. 1.20. Ca + Mg vs. Al + Fe + Ti diagram (Moine & de la Roche, 1968), to differentiate Ca-Mg rich greywackes from basalts

Trace elements spidergram

Trace element distribution can be represented in the is so-called spidergram or spider diagram (Sun, 1980), which let to classify geochemical data and to compare them to a reference composition generally the chondrites. There are a lot of different types of

spidergrams with different set of elements and order. In the present work Holm spidergram type (Holm, 1979), which are between of two well-known spidergram types after Pearce (1983) and Thompson (1988), was used with the following set of the trace elements (Fig. 1.21).

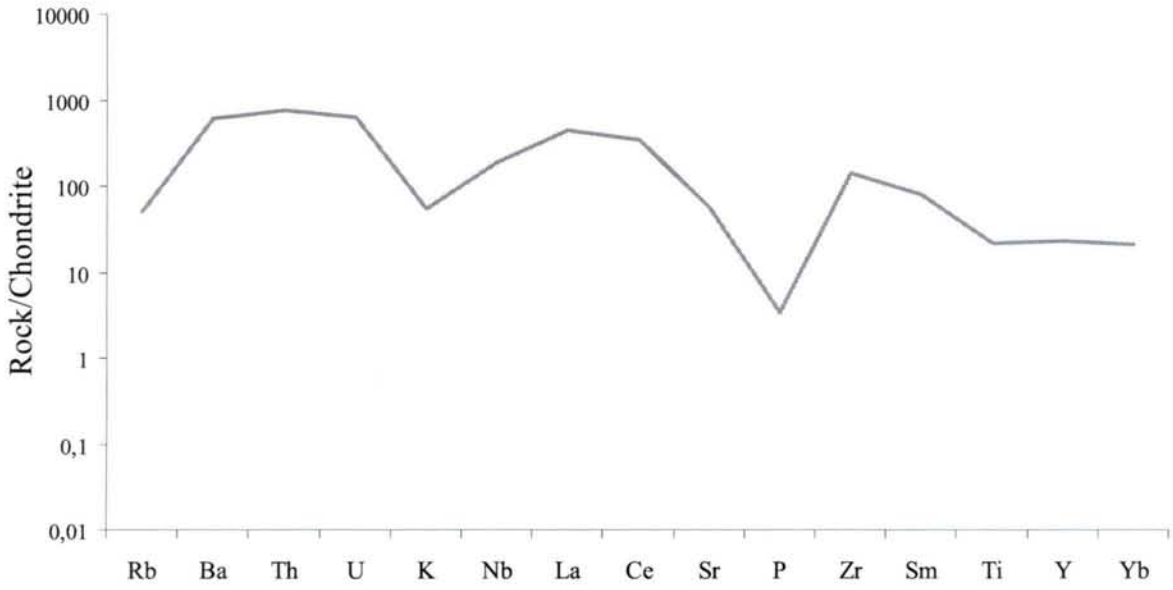

Fig. 1.21. Archean granite-gneiss in the spidergram type after Holm (1979) normalized to chondrite

1.4. DDH and sampled outcrop positions on maps of the Northern Ladoga Lake area

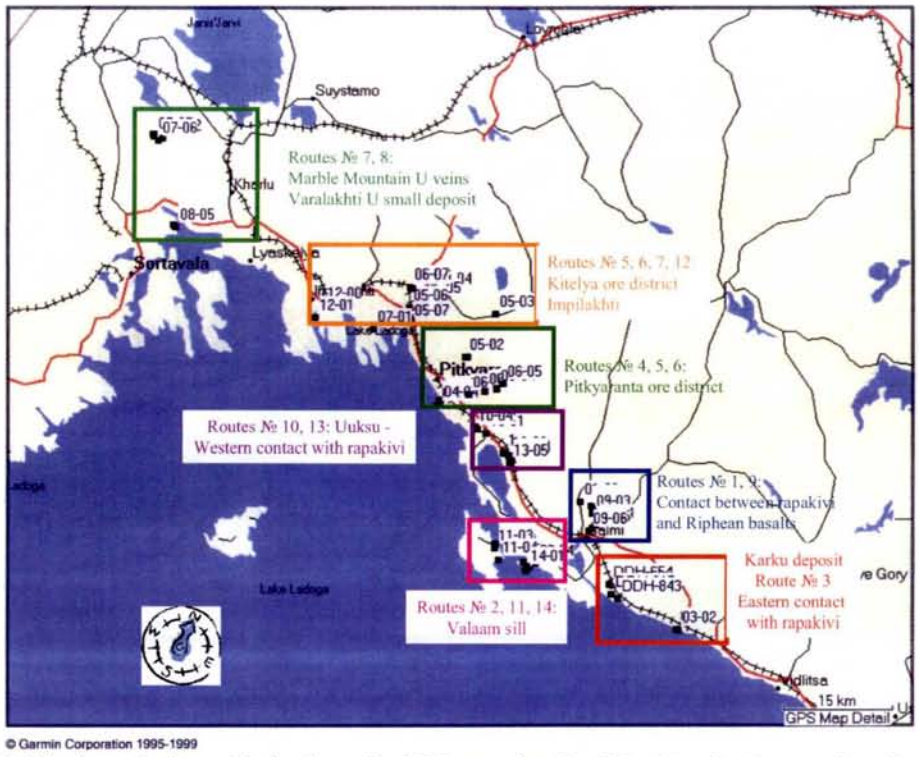

Fig. 1.22. Northern Ladoga district from the GPS map details of the Garmin Corporation. Scale 15 km. Field trip – 2003: routes and points, rectangle show following routs in detail below.

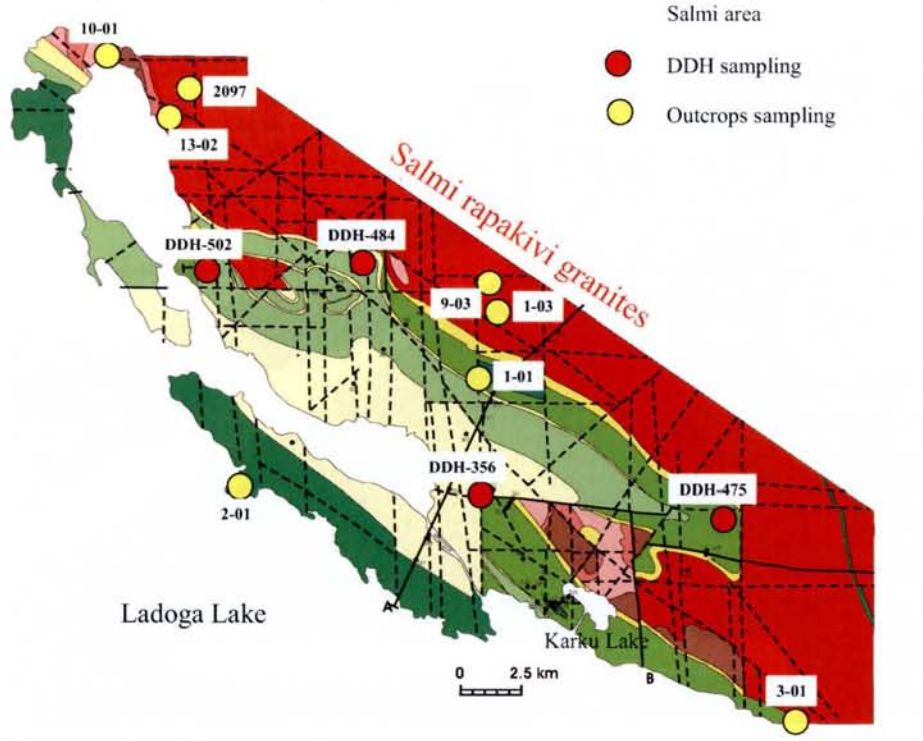

Fig. 1.23. Simplified map of the Salmi area (Northern Ladoga district), scale 2.5 km. Selected DDH and outcrops samples, which are described in the next chapters below

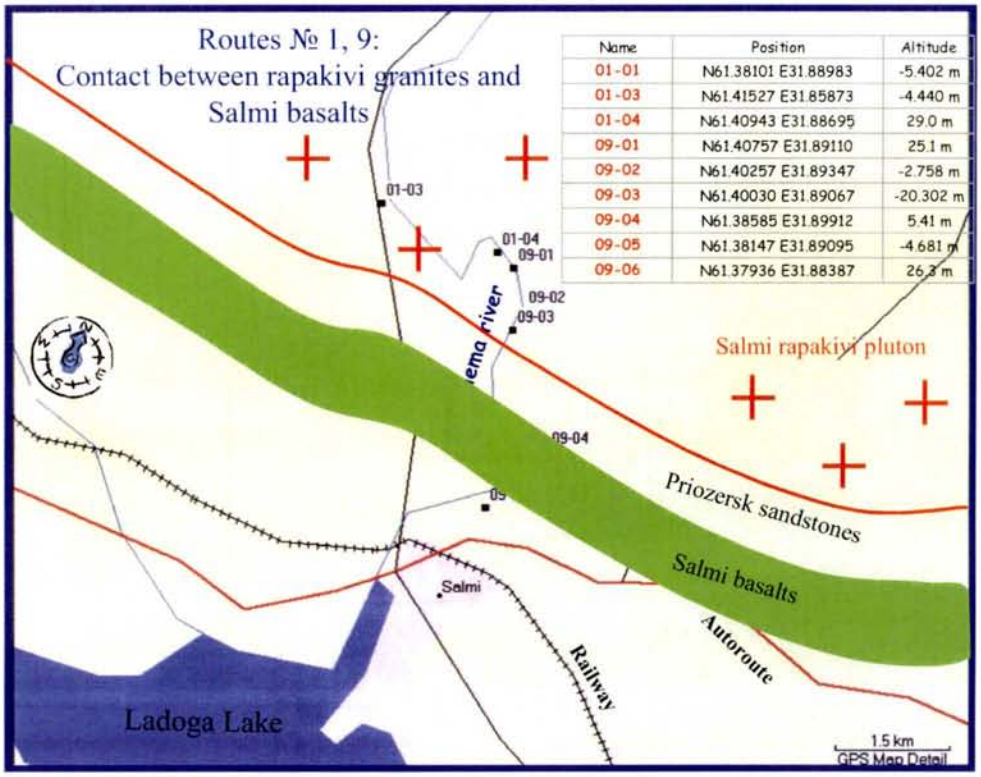

Name	Position	Altitude
01-01	N61.38101 E31.88983	-5.402 m
01-03	N61.41527 E31.85873	-4.440 m
01-04	N61.40943 E31.88695	29.0 m
09-01	N61.40757 E31.89110	25.1 m
09-02	N61.40257 E31.89347	-2.758 m
09-03	N61.40030 E31.89067	-20.302 m
09-04	N61.38585 E31.89912	5.41 m
09-05	N61.38147 E31.89095	-4.681 m
09-06	N61.37936 E31.88387	26.3 m

Fig. 1.24. Blue rectangle in the Fig. 1.22. Tulema river, Salmi village area, scale 1.5 km
The Pasha – Ladoga volcanics and sediments overlap the Salmi rapakivi granites
Selected GPS coordinates WGS-84 is listed in the table

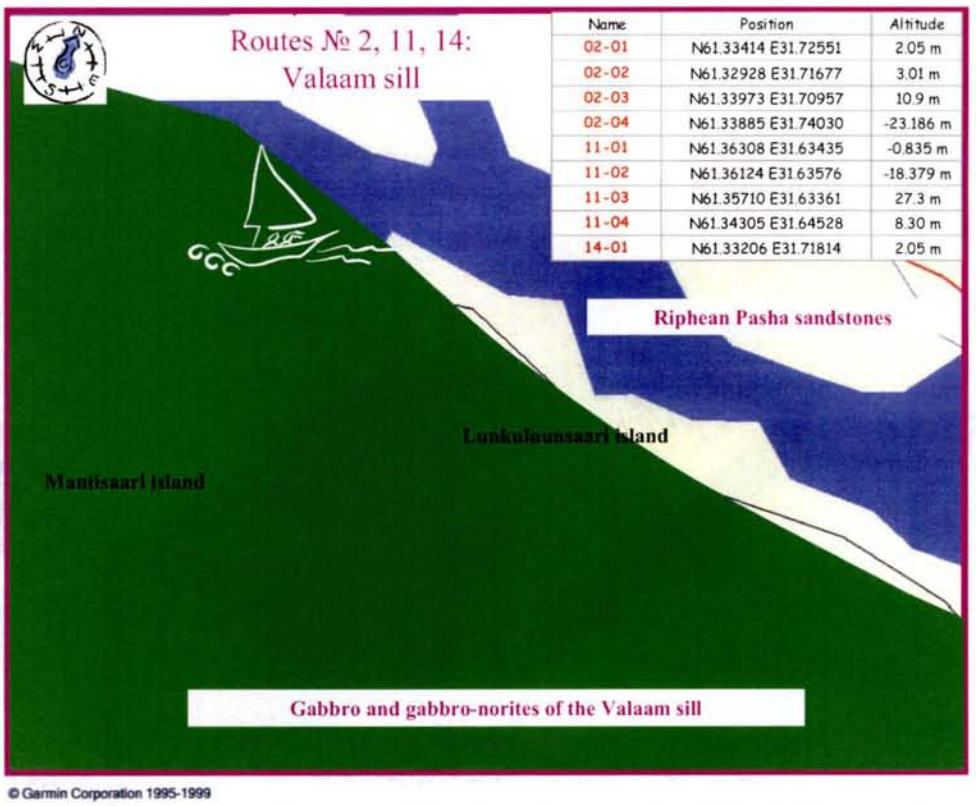

Name	Position	Altitude
02-01	N61.33414 E31.72551	2.05 m
02-02	N61.32928 E31.71677	3.01 m
02-03	N61.33973 E31.70957	10.9 m
02-04	N61.33885 E31.74030	-23.186 m
11-01	N61.36308 E31.63435	-0.835 m
11-02	N61.36124 E31.63576	-18.379 m
11-03	N61.35710 E31.63361	27.3 m
11-04	N61.34305 E31.64528	8.30 m
14-01	N61.33206 E31.71814	2.05 m

Fig. 1.25. Violet rectangle in the Fig. 1.22. Lunkkulunsaari and Mantsinsaari islands, scale 1.5 km
Selected GPS coordinates WGS-84 is listed in the table

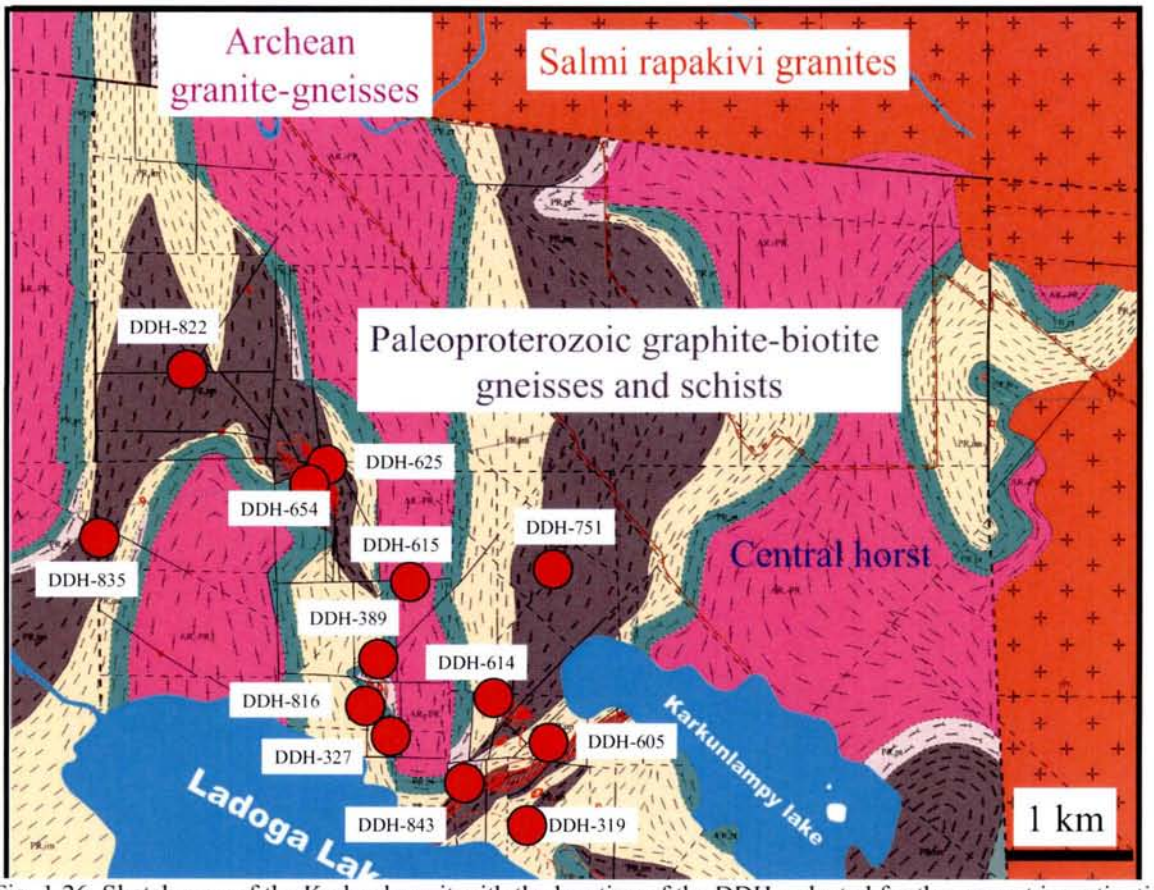

Fig. 1.26. Sketch map of the Karku deposit with the location of the DDH, selected for the present investigations.

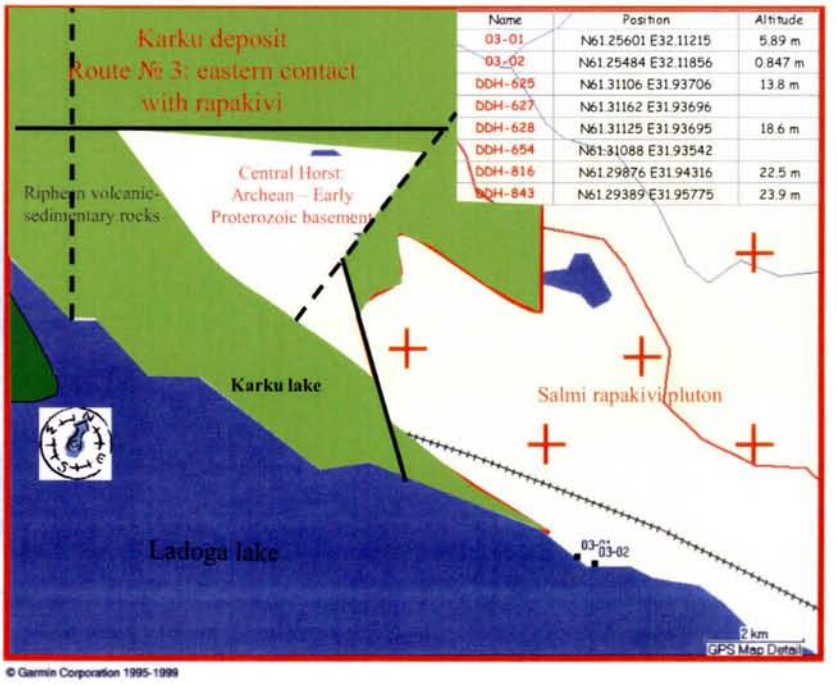

Name	Position	Altitude
03-01	N61.25601 E32.11215	5.89 m
03-02	N61.25484 E32.11856	0.847 m
DDH-625	N61.31106 E31.93706	13.8 m
DDH-627	N61.31162 E31.93696	
DDH-628	N61.31125 E31.93695	18.6 m
DDH-654	N61.31088 E31.93542	
DDH-816	N61.29876 E31.94316	22.5 m
DDH-843	N61.29389 E31.95775	23.9 m

Fig. 1.27. Red rectangle in the Fig. 1.22. Karku deposit area. Scale 2 km
Selected GPS coordinates WGS-84 of some DDH are listed in the table

Chapter II

The Ladoga Lake area basement formations

Part 2.1. Archean basement formations of the Northern Ladoga Domain

2.1.1. Geological setting

As shown by Trustedt (1907) and Eskola (1951) and confirmed by further investigations (Shurkin, 1958; Khazov, 1973), the main geological feature of the Pitkyaranta area is the occurrence of granite-gneiss domes, which are overlaid by biotite-amphibole schists, limestones and skarns of the Pitkyaranta suite.

Fig. 2.1. Ladoga Lake shore near Pitkyaranta town (Ristiniemi cape). Archean granite-gneisses of the Ristiniemi dome

Fig. 2.2. Ladoga Lake shore near Pitkyaranta town (Ristiniemi cape). The migmatitic granite-gneisses are characterized by their specific ptygmatic textures.

Physiographically the domes are remarkable by their greater elevation and ragged forms (Fig. 2.1), whereas the schist areas correspond to lowlands, largely covered by Quaternary sediments (Eskola, 1951). In the Northern Ladoga area there are about twenty domes covering a surface from 0.5 to 120 – 150 km^2 (Khazov, 1973). The domes are characterized by their inner structure (gneissic and migmatitic), whereas surrounding Paleoproterozoic rocks are schistose with planar textures (Fig. 2.2). Domes contacts in the generally steep (60 – 90°), sometimes showing a reverse dip (80 – 85°), rarely flat.

During the field studies of 2003, some of the dome structures (Uuksu, Hopunvaara - Lupikko, Pitkyaranta, Ristiniemi, Hunttila - Koirinoya) were revisited and sampled for the present study.

Grey and dark-grey oligoclase granite-gneisses are the most widespread rocks in the domes. They mainly consist of oligoclase (50 – 60 %), quartz (20 – 35 %), biotite (9 – 12 %). Alteration minerals are muscovite, sericite, chlorite, epidote and carbonate. Accessory minerals are titanite, apatite, allanite, zircon, tourmaline and different ore minerals (Fig. 2.3).

Fig. 2.3. Archean oligoclase granite-gneiss with pink microcline. Sample 10-01-01 (2003). Uuksu dome (Pitkyaranta area)

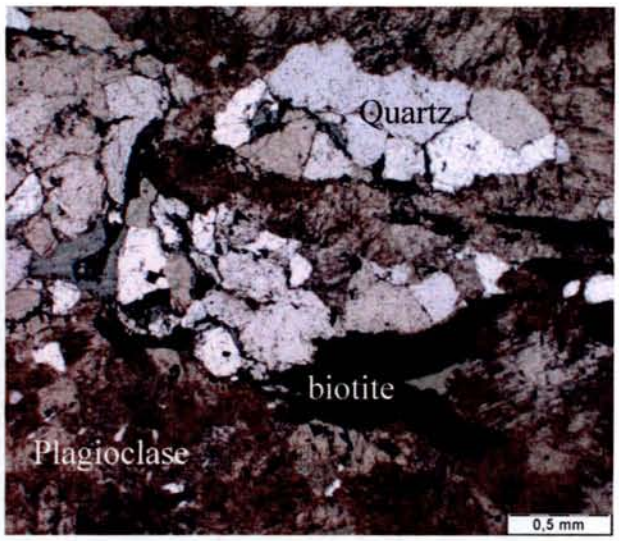

Fig. 2.4. Lepidogranoblastic texture of the Archean granite-gneisses in the Uuksu dome(sample 10-01-01, parallel nicols, Photomicrograph scale - 0.5 mm)

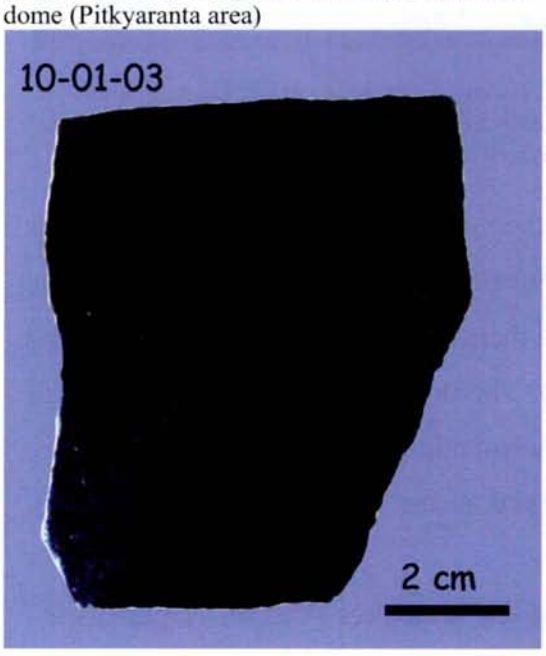

Fig. 2.5. Amphibolite from a small lense in the Archean granite-gneisses. Sample 10-01-03 (2003). Uuksu dome (Pitkyaranta area)

Fig. 2.6. Nematogranoblastic texture of the Archean amphibolites in the Uuksu dome (sample 10-01-03, parallel nicols, Photomicrograph scale 0.5 mm)

Gabbro-diabases and diabases and their metamorphosed varieties (gabbro-amphibolites and amphibolites) form bedded bodies in the granite-gneisses with sizes from 0.1 to 20 km^2. They are fine- to coarse-grained massive rocks (Fig. 2.5) and consist of hornblende (45 –

46 %), partially replacing pseudomorphically pyroxene, and albitic plagioclase (25 – 50 %). Alteration minerals are chlorite, epidote, biotite and carbonate which occur in a minor amounts. Accessories are represented by titanite, leucoxene, pyrite, chalcopyrite and ilmenite.

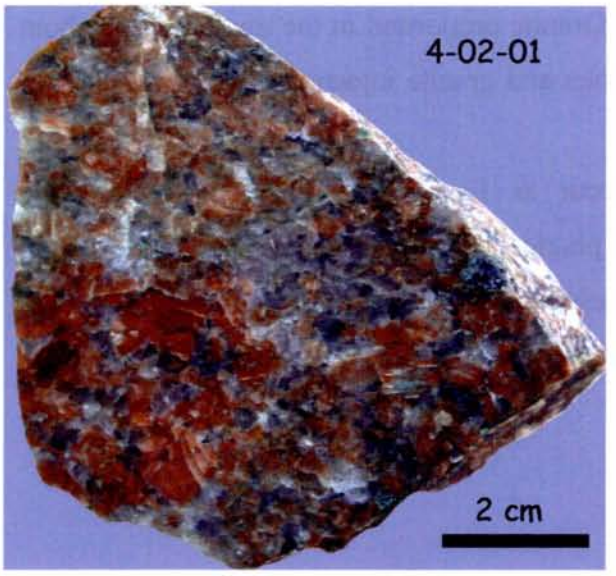

Fig. 2.7. Archean granite-gneiss migmatized in a contact with Paleoproterozoic schists. Sample 4-02-01 (2003). Ristiniemi dome (Pitkyaranta area)

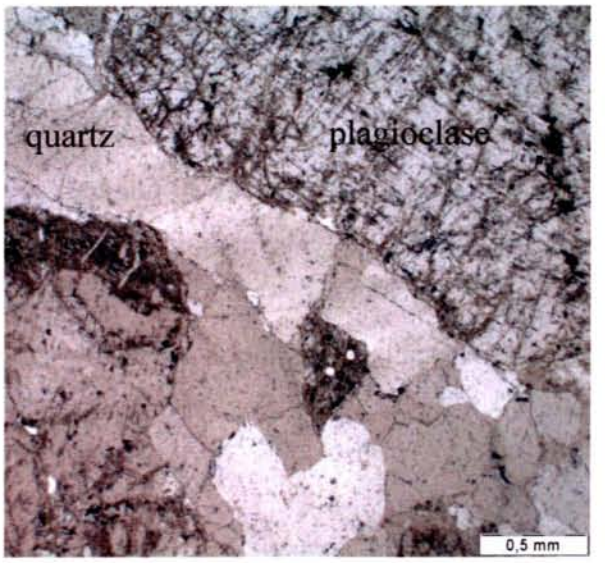

Fig. 2.8. Leucocratic migmatized granite-gneiss (sample 4-02-01, parallel nicols, photomicrograph scale 0.5 mm)

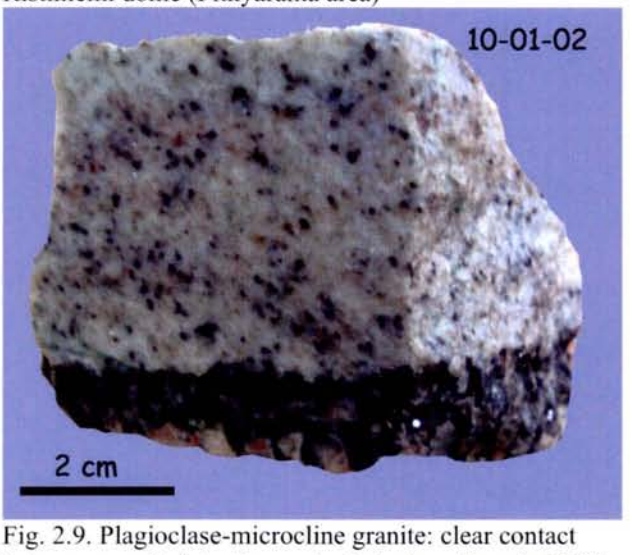

Fig. 2.9. Plagioclase-microcline granite: clear contact between granite injection and substratum. Sample 10-01-02 (2003). Uuksu dome (Pitkyaranta area)

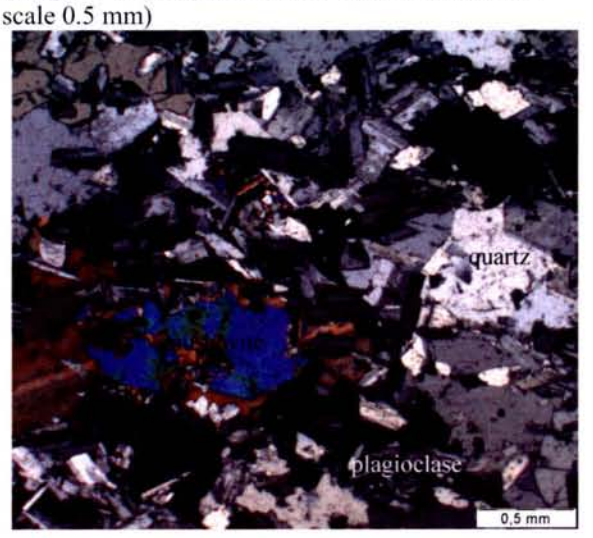

Fig. 2.10. Muscovite in the plagioclase-microcline granite (sample 10-02-01, crossed nicols, photomicrograph scale 0.5 mm)

Plagioclase – microcline granites occur both as large well-oriented bodies and small bed-like and lenticular-like bodies with abundant apophyses in the oligoclase granite-gneisses and amphibolites. These granites consist of oligoclase (30 – 50 %), microcline (20 – 45 wt. %), quartz (25 – 30 %) and biotite (5 – 10 %). Amphibole, pyroxene, garnet, epidote, ilmenite, hematite, titanite, zircon, apatite, rutile, pyrite, topaz, tourmaline, rare anatase, sporadically chalcopyrite, galena, molybdenite, allanite, scheelite and fergusonite have been observed in the heavy mineral fraction of the these granites (Shurkin, 1958).

Migmatites of plagioclase-microcline and microcline-plagioclase granites (Fig. 2.7) are widespread in the domes. They exhibit various forms: arterites, spotted and shadows migmatites. The thickness of the gneiss bands is up to 0.5 m and granite injections thickness varies from some centimeters to tens of meters. Granite proportion in the migmatites is about 50 – 70 %, rare 90 %. Contacts between gneisses and granite injections vary from clear to progressive (Fig. 2.9).

Petrographically shadows migmatites occur as fine-grained plagioclase-microcline granite-gneisses. They are mainly composed of plagioclase (30 – 70 %), microcline (1 – 45 %); quartz (15 – 25 %), biotite (up to 5 %). Accessories are zircon, apatite, allanite. Textures are mainly cataclastic, granoblastic and lepidogranoblastic.

2.1.2. Detrital mineralogy features

Zircon nature and alteration have been particularly studied in some samples of the Archean granite-gneisses (Table 2.1), to evaluate their potential role as an uranium source for the Karku ore deposit. Monazite grains were not observed in the studied samples.

Sample number	Location	Rock type	Zircon alteration phases	Monazite alteration phases	Other accessories	Zr, ppm	Th, ppm	U, ppm	ΣREE, ppm
10-01-01	Surface Pitkyaranta	Archean granite-gneisses	zircon	?	-	-	-	-	-

Table 2.1. Description, location, mineralogical occurrences and whole-rock composition of the Archean granite-gneisses of the Northern Ladoga area
Whole-rock trace elements composition for the sample 10-01-01 is not available

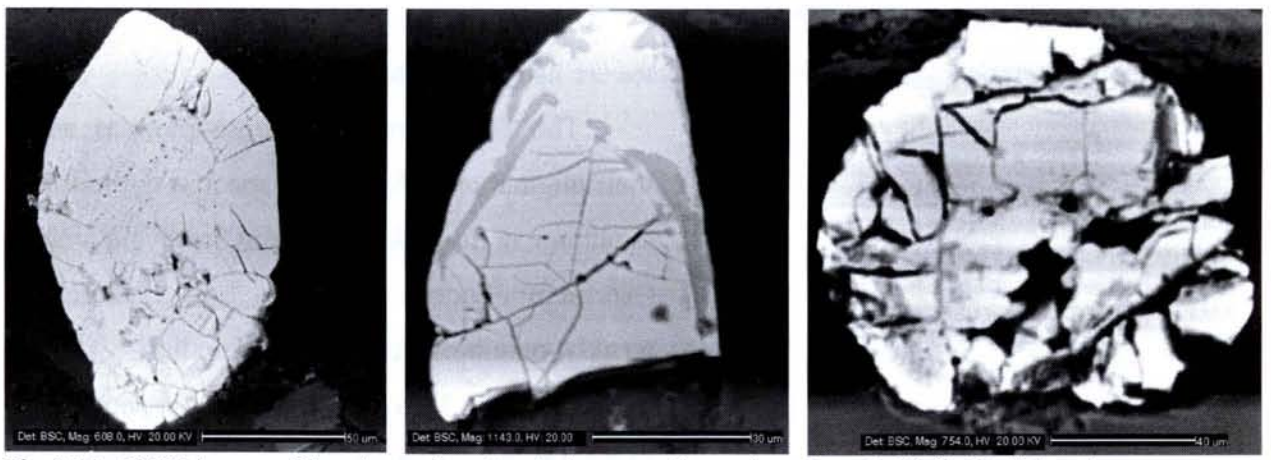

Fig. 2.11. BSEM images of the zircons from the Archean granite-gneisses (sample 10-01-01, Uuksu dome, Pitkyaranta area, photomicrograph scales: A – 50 μm; B – 30 μm; C – 40 μm

Idiomorphic crystals, slightly elongated, with well-developed bipyramid faces are observed in the Archean granite-gneisses (e.g.: sample 10-01-01). Primary zoning of crystals is visible. Microprobe analyses of these grains were not realized. Alteration in the studied zircon grains is not clearly visible. Some darker zones (in BSEM images) are observed at the margin of the grains. Archean granite-gneisses are primarily poor in radiogenic elements.

2.1.3. Alteration processes

The alteration processes in the Archean granite-gneisses in the vicinity of the unconformity surface within the limits of the Karku deposit has not been studied. New investigations in this direction have to be completed.

2.1.4. Petrogeochemistry of the Archean formations

Major and trace elements geochemistry has been studied both at the regional scale of the Northern Ladoga area (sampling from outcropping parts of the basement from Pitkyaranta, Impilakhti and Sortavala areas) and at the local drill hole scale in the Salmi and the Karku deposit areas. DDH and outcrops samples location is presented in Part 1.4.

Major and trace elements distribution in the Early Archean formations (i.e. granite-gneisses and amphibolites) of the Northern Ladoga area

Major and trace elements composition of the Early Archean rocks (mostly granite-gneisses and amphibolites) is listed in Annex Archean granite-gneisses (3 samples). The major element compositions of selected analyses are listed in the table 2.1.

	Archean formations			
	1	2	3	4
SiO_2	49.65	56.45	65.31	74.52
Al_2O_3	14.58	17.51	15.04	13.70
Fe_2O_3	13.63	10.67	5.63	2.34
MnO	0.21	0.00	0.06	0.01
MgO	7.16	4.75	0.91	0.35
CaO	10.73	9.28	2.45	1.00
Na_2O	2.20	4.06	3.49	4.40
K_2O	0.49	1.27	3.02	4.00
TiO_2	1.14	0.25	0.96	0.07
P_2O_5	0.08	0.00	0.42	0.02
PF	0.63	1.88	2.01	0.10
Total	100.50	106.12	99.30	100.51

Table 2.2. Major elements composition of the Archean rocks in the Northern Ladoga area: 1 – sample 5-07-01 – amphibolite; 2 – amphibolite – sample *5* from Shurkin (1958); 3 – sample 10-04-01 – granite-gneiss from the Uuksu dome (Pitkyaranta area); 4 – plagioclase-microcline granite – sample 3732 from Khazov (1973)

The Early Archean granite-gneisses and their migmatites, which form specific dome-like structures in the Pitkyaranta and Sortavala areas (Northern Ladoga district), are generally weakly peraluminous: from granodiorite (A = 30 for analysis 3) to granite (A = 6 for sample 4 in the Table 2.2) composition.

The SiO_2 content of the granite-gneisses and migmatites is generally high, K/Na ratios widely vary with an average value of about 1. In the SiO_2 versus $Na_2O + K_2O$ diagram (Fig. 2.12) most points plot into the granite field. Plagiogranites and granodiorites are rare and associated with feldspathic amphibolites. Some samples corresponding to orthoamphibolites (Shurkin, 1958), plot into the fields of picrobasalt, basalt (gabbro) and basaltic andesite.

The Archean gneisses correspond to a tonalite - granodiorite - adamellite – granite association according to the Q-P nomenclature diagram of Debon – Le Fort (1988), (Fig. 2.13), classical of the Archean Domains. Gabbro and syenite are also present. Most of these rocks are slightly peraluminous in the A-B diagram of Debon – Le Fort (1988), in due to the presence of minor amounts of muscovite (Fig. 2.14). In accordance with their biotite +

amphibole ± epidote mineralogy some of the Archean gneisses plot in the metaluminous field (sector IV of the diagram, Fig. 2.17).

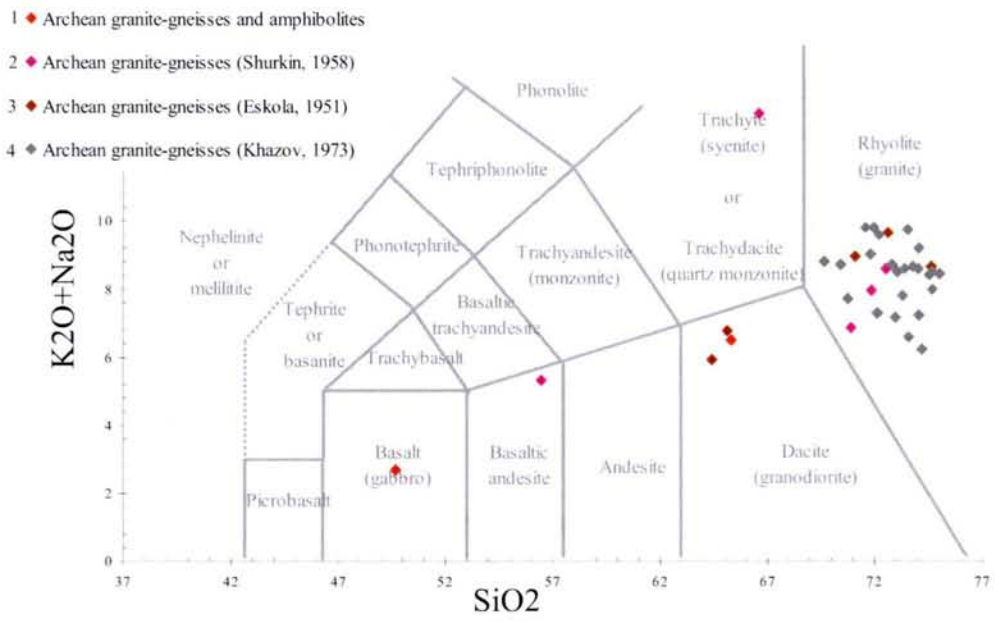

Fig. 2.12. Early Archean rocks from the dome structures of the Northern Ladoga area in the SiO_2 vs. $K_2O + Na_2O$ classification diagram.
1 - 4: chemical analysis data of the Archean granite-gneisses and amphibolites after 1) present work, 2) Shurkin, 1958; 3) Eskola, 1951; 4) Khazov, 1973.

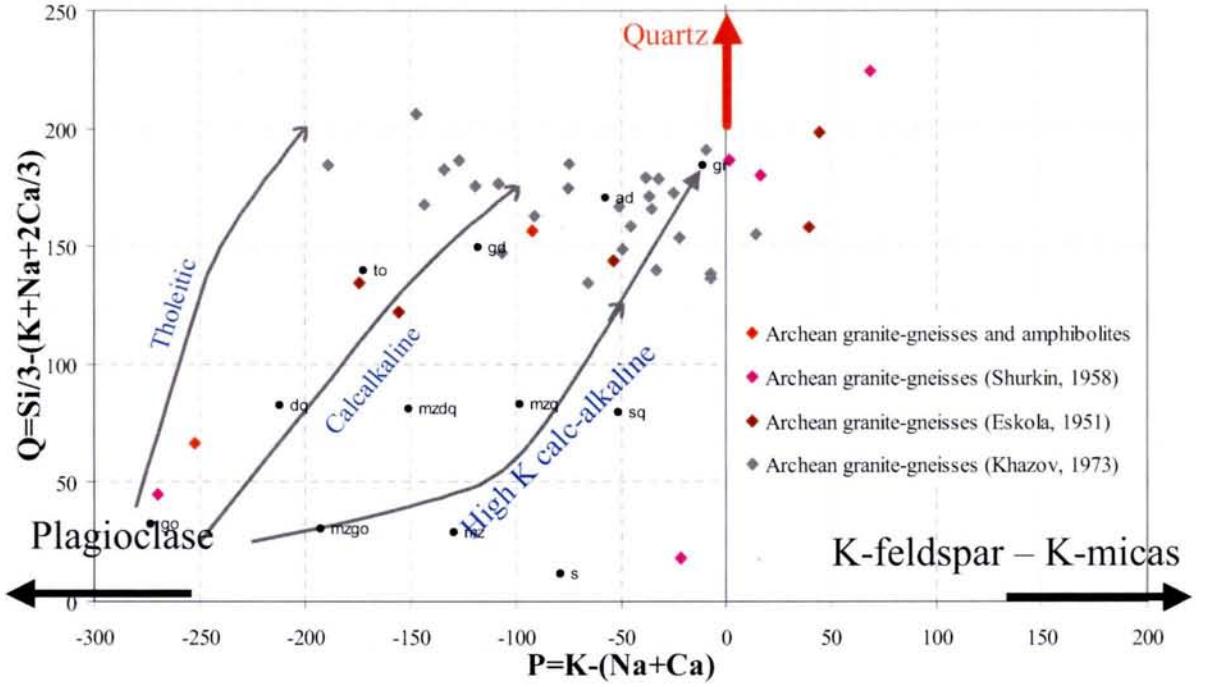

Fig. 2.13. The Early Archean rocks from the dome structures of the Northern Ladoga district in the Q-P diagram according to Debon and Le Fort (1988).
Each division of the grid corresponds to a rock type: **ad** – adamellite; **dq** – quartz diorite; **gd** – granodiorite; **go** – gabbro, diorite, anorthosite; **gr** – granite; **mz** – monzonite; **mzdq** – quartz monzodiorite; **mzgo** – monzogabbro; **mzq** – quartz monzonite; **s** – syenite; **sq** – quartz syenite; **to** – tonalite, trondhjemite. Typical trends of the different magmatic associations types are shown: tholeitic, calcalkaline, high K alkaline.
Symbols of legend: 1 - 4 as in Fig. 2.12

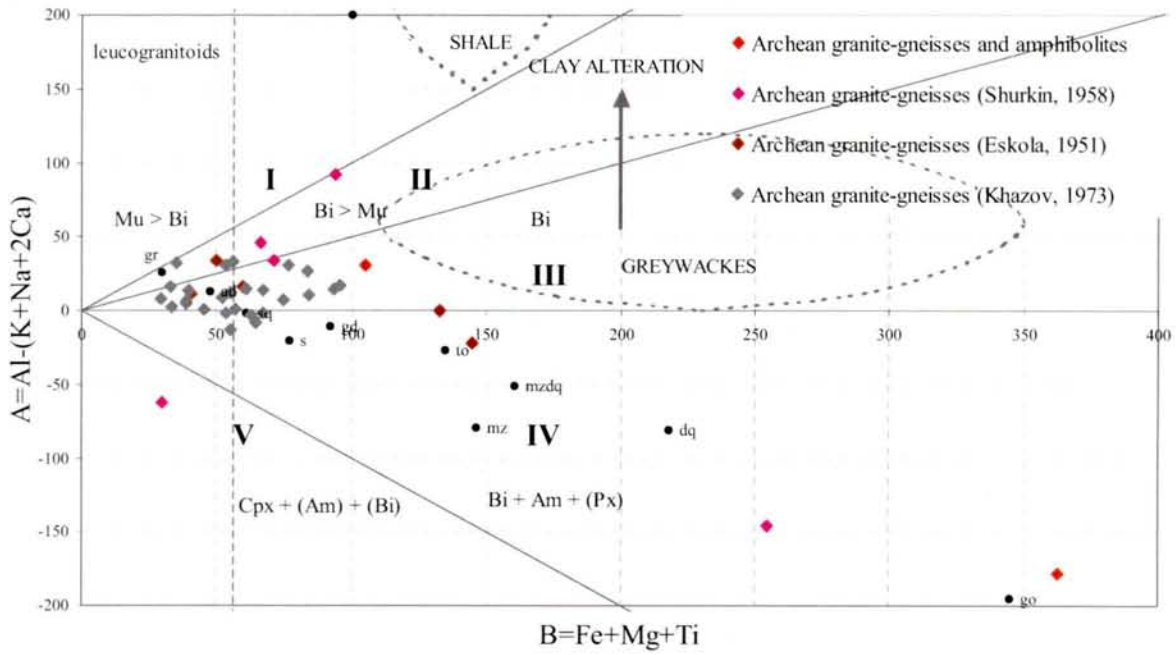

Fig. 2.14. Early Archean rocks from the dome structures of the Northern Ladoga district in the A-B characteristic mineral plot (Debon and Le Fort, 1988)
Sectors, numbered from I to V, correspond to a specific mineralogical composition. I – III – sectors of peraluminous rocks with, respectively: I – muscovite > biotite (by volume); II – biotite > muscovite; III – biotite (usually alone, at times with a few amphibole); IV – V (without VI here) – sectors of metaluminous rocks with, respectively, IV – biotite + amphibole ± pyroxene; V – clinopyroxene ± amphibole ± biotite.
Legend for the samples as in Fig. 2.12. Composition fields of sediments (shale and greywackes) are also represented with the clay alteration vector.
Symbols 1 - 4 as in Fig. 2.12.

Trace elements geochemistry of Archean rocks

The Archean rocks in the Salmi – Karku deposit and Pitkyaranta areas, have been analysed. Their compositions have been represented in chondrite-normalized spidergram (Fig. 2.15) and chondrite-normalized REE patterns diagram (Fig. 2.16).

The amphibolite (5-07-01) from the Koirinoya dome (Pitkyaranta area in the western contact of the Salmi batholith) is logically characterized by relatively low concentrations of all incompatible trace elements in comparison with granite-gneiss samples from the Uuksu dome and the Karku deposit (Central Horst). Th/U ratio is about 3.5. Its REE pattern is weakly fractionated with a REE abundance of 20 to 30 times the chondrites, typical of a former basalt.

Granite-gneiss from the Uuksu dome (10-04-01) are enriched in Ba, Th, Nb and Zr relative to the regolithized granite-gneiss from the Karku deposit area (see Annexe: DDH-615-109). U and Y contents are high and nearly the same (U = 5 ppm, Th/U ratio = 4.4). Rb and Sr concentrations are low (70 - 30 times the chondrites respectively. The REE patterns of

the two granite-gneisses exhibit some differences. The granite-gneiss from the Uuksu dome is characterized by a moderately fractionated REE pattern with Ce_N/Yb_N = 16 and a small Eu anomaly (Eu/Eu* = 0.74). On the contrary the Archean gneiss from the Karku deposit area exhibit a practically non-fractionated REE pattern (Ce_N/Yb_N = 2) with distinct Eu anomaly (Eu/Eu* = 0.65).

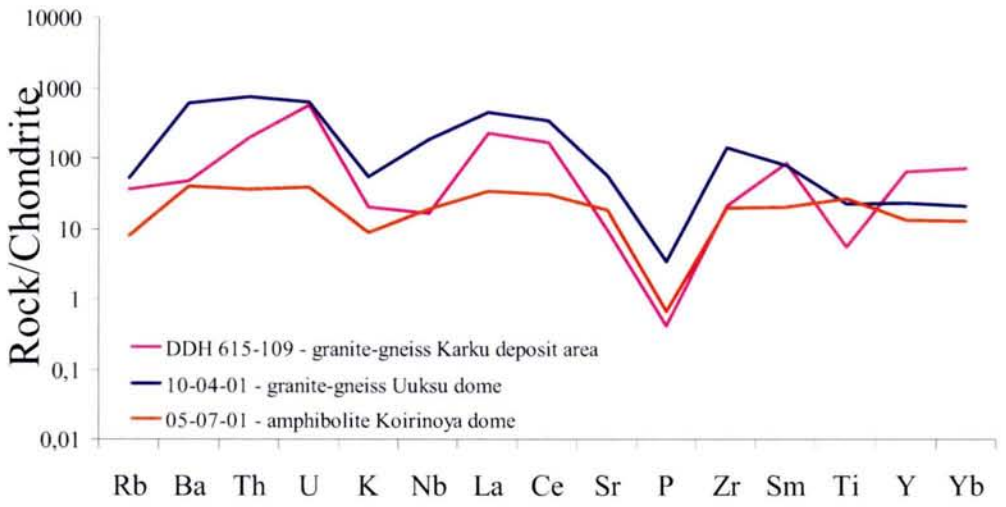

Fig. 2.15. Chondrite-normalized trace element patterns of the Early Archean rocks from the dome structures of the Pitkyaranta - Salmi - Karku deposit areas (Northern Ladoga district) (spidergram type after Holm (1979); chondrite composition after E. Anders and N. Grevesse: http://earthref.org/GERM/reservoirs/C1.htm)

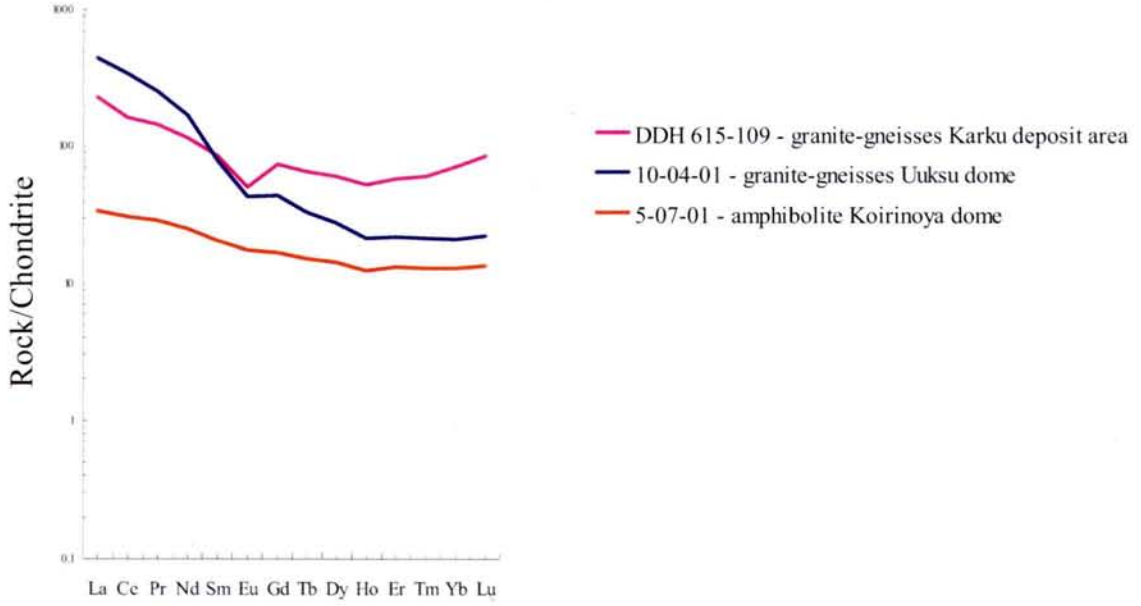

Fig. 2.16. Chondrite-normalized REE distribution patterns of the Early Archean rocks from the dome structures of the Pitkyaranta - Salmi - Karku deposit areas (Northern Ladoga district) (chondrite composition after Anders & Grevesse: http://earthref.org/GERM/reservoirs/C1.htm)

In conclusion the Archean rocks from the Northern Ladoga district appear globally rich in potassium relatively to the classical Archean TTG suites. The most potassic rocks indicate that a high-K magmatism probably enriched in U and Th already occurred during Archean in the area.

Part 2.2. Paleoproterozoic formations of the Northern Ladoga Domain

2.2.1. Geological setting

In the Sortavala and Pitkyaranta (and Salmi) districts, the Paleoproterozoic gneisses and schists mantle the Archean domes. In the Northern Ladoga district they distinctly belong to two formations: a lower one (with Ludikovian age), with predominantly amphibole-bearing schists and amphibolites, named the *Pitkyaranta suite* and an upper one (with Kalevian age), with predominantly biotite schists and gneisses, named the *Impilakhti suite* (Khazov, 1973; Negroutsa, 1984; Saltykova & Koistinen, 1996; Shurkin, 1958). Both suites comprise lenses of calc-silicate rocks (skarns), horizons of dolomitic rocks and schists. They are rich in sulphides (mostly pyrite) and graphite.

Pitkyaranta Suite

The lower member of the Paleoproterozoic Pitkyaranta suite form a 200 – 500 m thick zone around the Archean granite-gneisses dome. They comprise schistose fine to middle-grained dark-green amphibolites (with interstratified amphibole – biotite schists and layers of limestones and quartzites), which are frequently turned into skarns. The amphibolite rock structure is characterized by a schistosity a lineation and a rough cleavage.

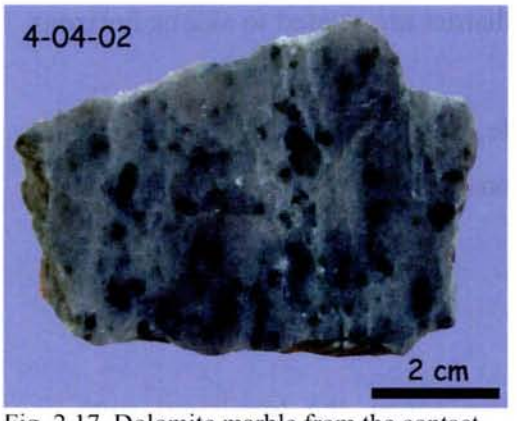

Fig. 2.17. Dolomite marble from the contact with Ristiniemi granite-gneiss dome. Sample 4-04-02 (2003). Pitkyaranta area

Fig. 2.18. U-rich marble from the uranium occurrence Marble Mountain (Ruskeala area). Sample 7-03-02 (2003)

Amphibole-biotite schists, amphibolites, quartzites and quartz-biotite schists belong to lower part of the Pitkyaranta sequence occurring in immediate contact with Archean granite-gneisses.

Amphibole schists are fine-grained clearly schistose rocks, and consist of hornblende (60 – 75 %), plagioclase (25 – 40 %), quartz (3 – 20 %), garnet and tremolite. Amphibolites consist of hornblende (30 – 40 %), biotite (up to 20 %), plagioclase (up to 50 %). Quartzites are fine- to middle-grained rocks. Quartz – biotite schists differ from quartzites by their high biotite content and their schistosity.

Carbonate rocks layers are widespread, but not abundant. They correspond to marbles, skarns (with amphibole, pyroxene, garnet) and limited layers of amphibolites and quartz-biotite schists.

Two types of marbles are present: dolomite-bearing (mostly in the south-eastern part of the Northern Ladoga area - Ristiniemi dome) (Fig. 2.17) and calcite-bearing (exclusively in the western part of the Northern Ladoga area – Ruskeala and Marble Mountain occurrences) (Fig. 2.18). Marble bed thickness varies from 1 to tens of meters. Non-altered marbles consist of 90 - 97 % of carbonate and minor amounts of tremolite (up to 40 %), phlogopite (up to 20 %), spinel, diopside (up to 15 %) and forsterite (generally serpentinized) (Khazov, 1973).

By their mineralogical composition and genesis the skarns are divided into magnesian (pre-ore and ore) and lime (hypomagnesian – post ore) types. Magnesian skarns consist of pyroxene (20 – 90 %), spinel (0 – 10 %), phlogopite (1 – 40 %), magnetite (0 – 80 %). Calcic skarns consist of garnet (0 – 90 %), vesuvianite (0 – 50 %), diopside – hedenbergite (0 – 80 %), magnetite (0- 80 %), associated with sphalerite, cassiterite, chalcopyrite, scheelite, pyrite etc. Most of the mineral deposits of the Pitkyaranta ore district are related to skarns horizons of the Pitkyaranta suite.

Contacts between carbonate rocks and amphibolite, amphibole-biotite schists present complex interbedding with abundant graphite impregnations.

Impilakhti Suite

The upper member of the Paleoproterozoic Kitelya series, the Impilakhti suite, is widespread and occupies extensive areas in the Northern Ladoga Domain. It is separated from the lower one by interbedded layers of amphibole-biotite and biotite schists. In the Kitelya area the Impilakhti rocks are essentially represented by coarse-flake biotitic schists with interlayers of quartz-biotite, garnet-biotite, quartz-sillimanite and graphite schists. In the

Pitkyaranta area biotite-quartz and quartz-biotite schists sometimes with graphite are the most common rocks. Interlayers of muscovite and sillimanite schists, quartzites and boudins of amphibole-biotite schists are also present. All these rocks are intensively migmatized (Shurkin, 1958).

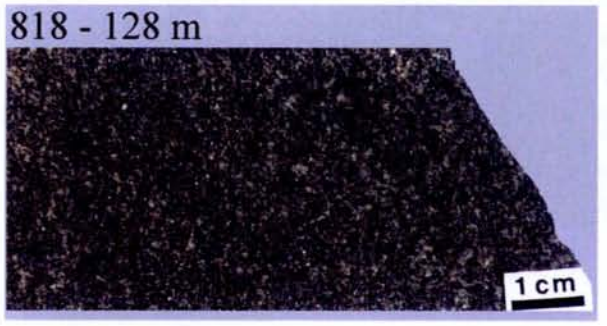

A. Quartz-plagioclase-biotite schist with abundant graphite. DDH-818-128 m (Karku deposit area, ore zone III)

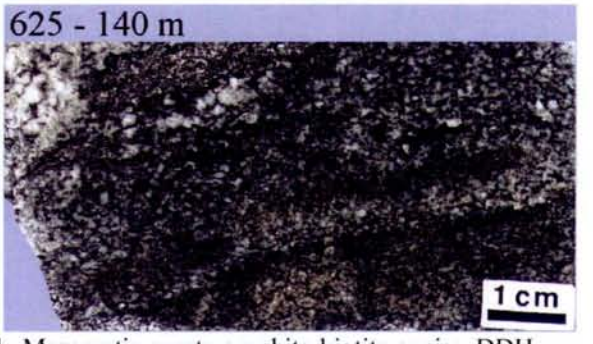

b. Mesocratic quartz-graphite-biotite gneiss. DDH-625-140 m (Karku deposit area, ore zone III)

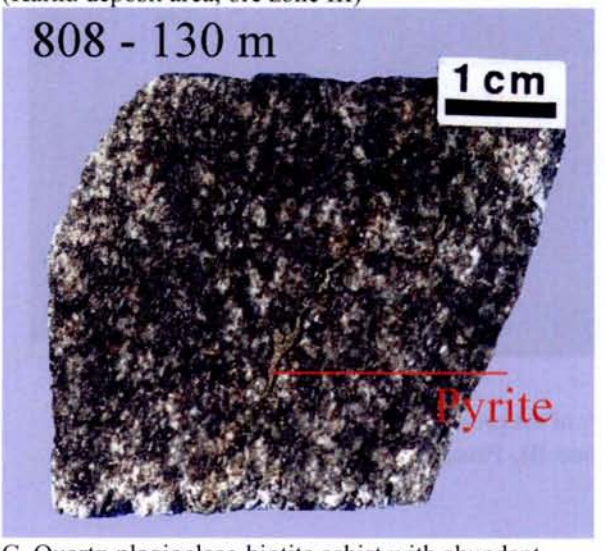

C. Quartz-plagioclase-biotite schist with abundant veins and impregnation of sulphides and graphite. DDH-808-130 m (Karku deposit area, ore zone III)

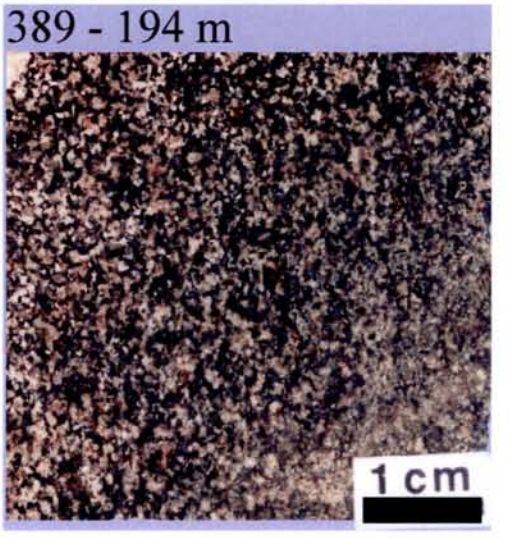

D. Quartz-feldspar-biotite gneiss. DDH-389-194 m (Karku deposit area, ore zone II)

Fig. 2.19. Paleoproterozoic gneisses and schists of the Salmi and Karku deposit areas

Biotite-quartz gneisses and schists are dark-brown-grey rocks, which consist of varied amounts of biotite (30 – 40 %) and quartz (25 – 30 %), plagioclase (5 – 15 %, in migmatized varieties – up to 50 %) and muscovite (10 – 12 %) are also present. Pyrite and pyrrhotite (1 - 3 %), graphite (1 - 2 %) are also widespread in these schists. Horizons of essentially graphitic schists are rare. Besides, different amounts of hornblende, microcline, garnet, magnetite, titanite, zircon, apatite, tourmaline, monazite are often present (Fig. 2.19).

In the vicinity of the pre-Riphean unconformity surface specific pegmatoidal "augen" gneisses are observed. They are generally altered in the regolith and composed of quartz,

relicts of biotite, rare feldspar and abundant chlorite and some interstratified minerals, which have replaced biotite (Fig. 2.20).

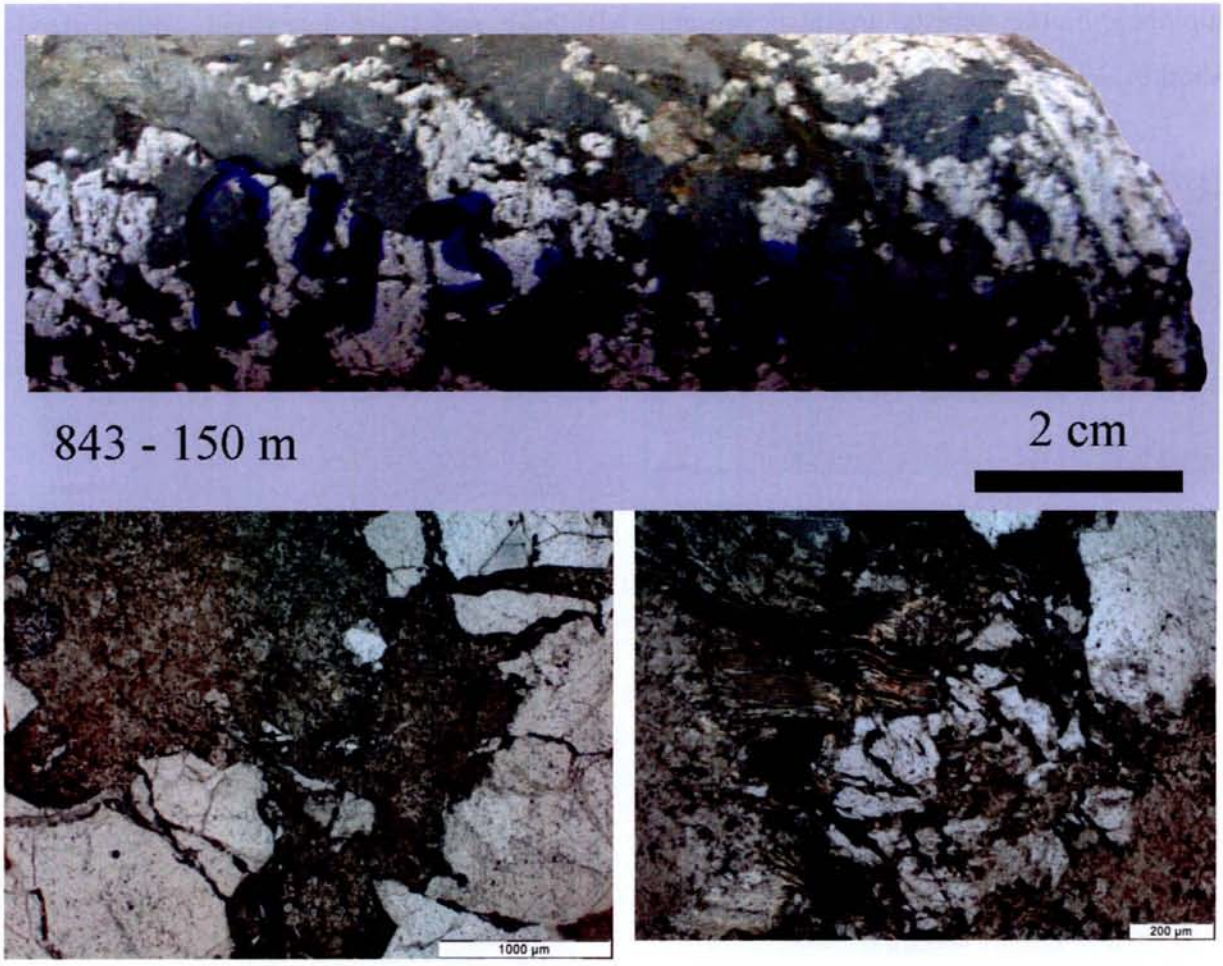

Fig. 2.20. Specific pegmatoidal "augen" gneiss in the vicinity of the pre-Riphean unconformity surface.
A: sample DDH-843 – 150 m (Karku deposit area, ore zone II), Photomicrograph scales: B - 1000µm, C – 200µm

2.2.2. Accessory mineralogy of the Paleoproterozoic basement formations

Sample number	DDH location	Rock type	Zircon alteration phases	Monazite alteration phases	Other accessories	Zr, ppm	Th, ppm	U, ppm	ΣREE, ppm
4-03-01	Surface Pitkyaranta	Graphitic schist	zircon	monazite	sulphides	177	12	3	176
627-149	DDH Karku III	Graphitic schist	zircon	monazite	sulphides (pyrite)	n.a.	n.a.	n.a.	n.a.
843-150	DDH Karku I	Regolithized graphitic schist	zircon	Th-monazite (≈20 wt. % of Th)	Ti oxides, sulphides	162	205	8	537

Table 2.3. Description, location, mineralogical occurrences and whole-rock composition of the Paleoproterozoic gneisses and schists of the Northern Ladoga Domain. Whole-rock trace elements composition for the sample DDH-627 – 149 is not available.

Zircon

Idiomorphic, slightly elongated, mainly prismatic grains with well-developed dipyramid faces are typical features of the zircon grains from the Paleoproterozoic graphitic schists. Primary zoning of crystals is generally invisible (Fig. 2.21).

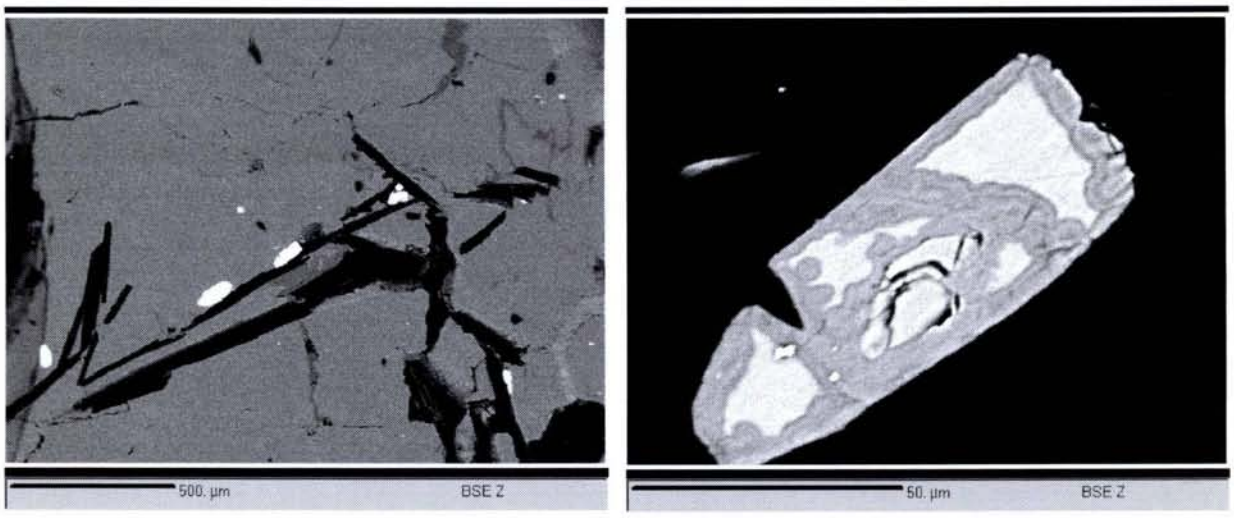

Fig. 2.21. BSEM images of a zircon grain in the Paleoproterozoic graphite-biotite gneisses (sample DDH-627-149, Karku deposit area). Photomicrograph scale: A – 500 µm, B – 50 µm

Altered zircon domains occur everywhere and without well define selectivity (though mainly developed at the margins of the grains). The altered zones have extremely different shapes. In average zircon in schists contains 61.85 ± 5.32 wt. % of ZrO_2, 29.78 ± 3.28 wt. % of SiO_2 and 1.42 ± 0.33 wt. % of HfO_2 (see Annex zircon). The brightest (in BSEM images) non-altered zircon domains correspond to classical zircon composition. The most altered zircon domain contains only 43.63 wt. % ZrO_2, 18.03 wt. % SiO_2, 0.82 wt. % of HfO_2. Hence,

substituted elements reach up to 9.58 wt. %. The altered zircon domains (the darkest in BSEM images) may contain up to 4.90 wt. % of ThO_2, 3.71 wt. % of Al_2O_3, 2.36 wt. % of CaO, 1.99 wt. % of Y_2O_3, 1.18 wt. % of U_2O_3 and 1.20 wt. % ΣREE (with HREE predominance).

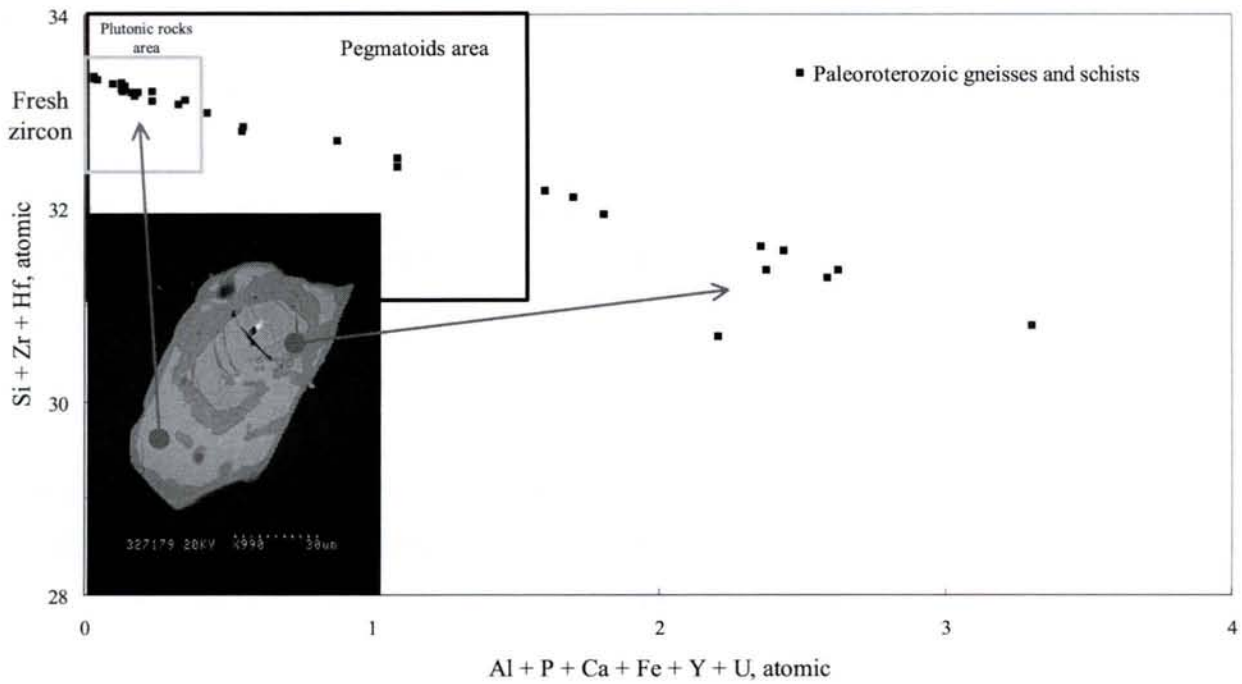

Fig. 2.22. Substitution of Zr + Hf + Si by Al + P + Ca + Fe + Y + U in zircons from the Paleoproterozoic schists

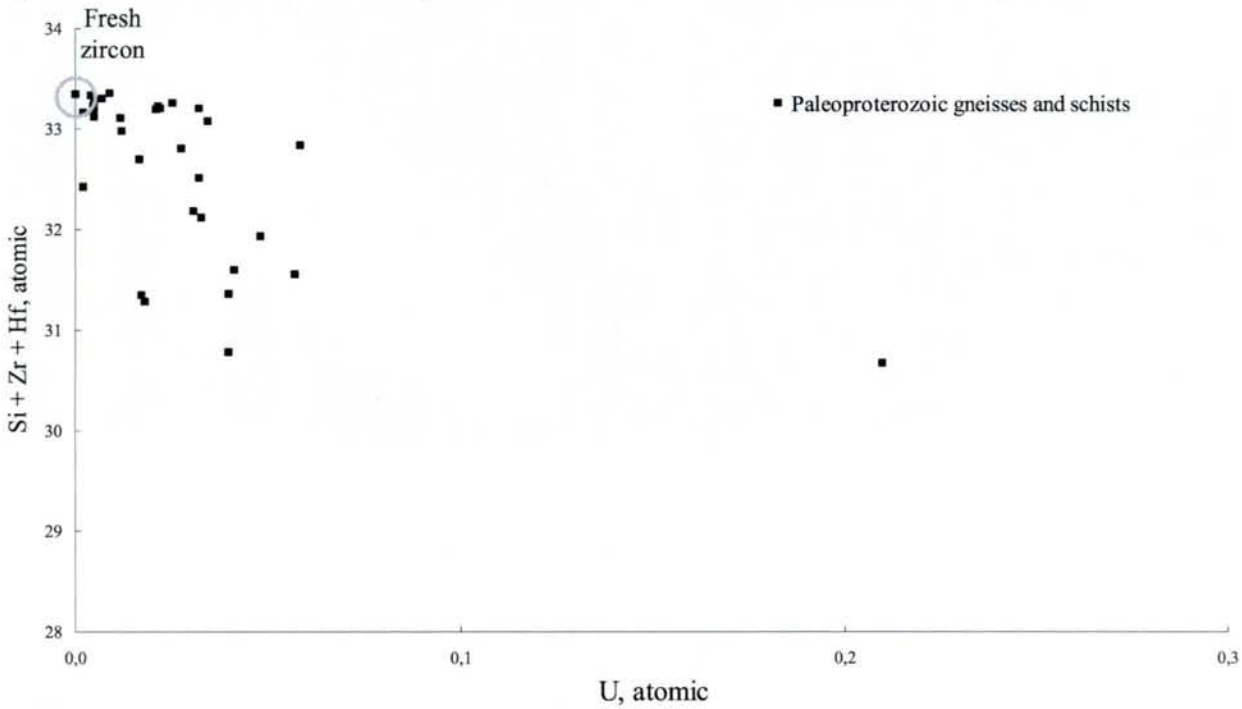

Fig. 2.23. Substitution of Zr + Hf + Si by U in zircons from the Paleoproterozoic schists

A maximum of 4 atoms among 33 in the zircon formula of graphitic schists are substituted by Ca, Al, Fe, Y, P, Th, U (Fig.2.22). Maximum uranium substitution is about 0.2 atoms for U content – 1.18 wt. % in this point (Fig. 2.23).

Monazite and associated monazite alteration

Monazite from graphitic schists is relatively abundant, typically isometric, well-rounded with poorly developed natural faces (Fig. 2.24).

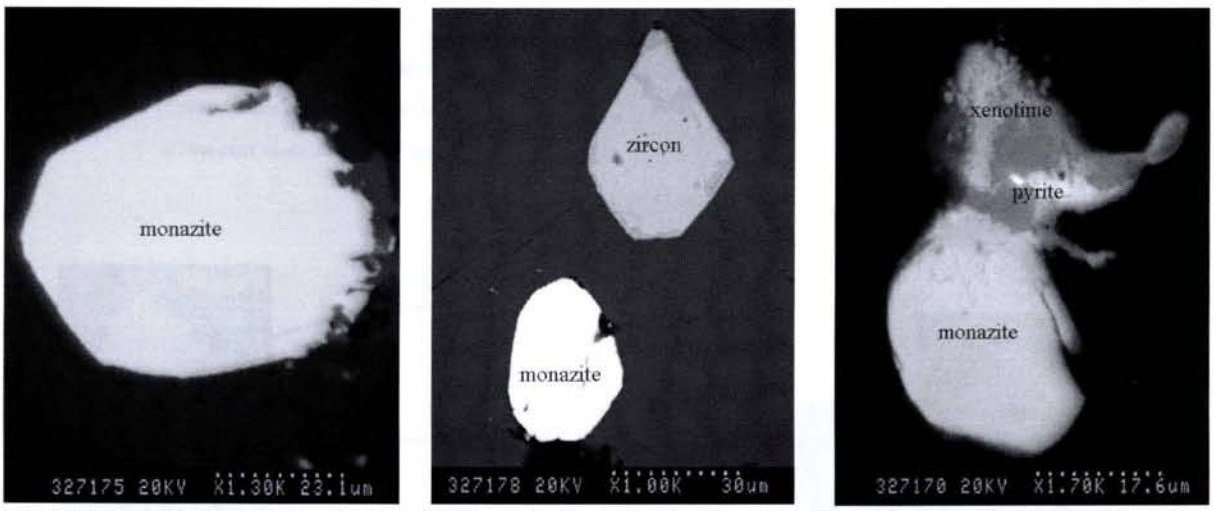

Fig. 2.24. BSEM images of detrital monazite grains from the Paleoproterozoic graphite-biotite gneisses (DDH-627-149, Karku deposit area). Photomicrograph scales: A – 23.1μm, B - 30μm, C – 17.6 μm

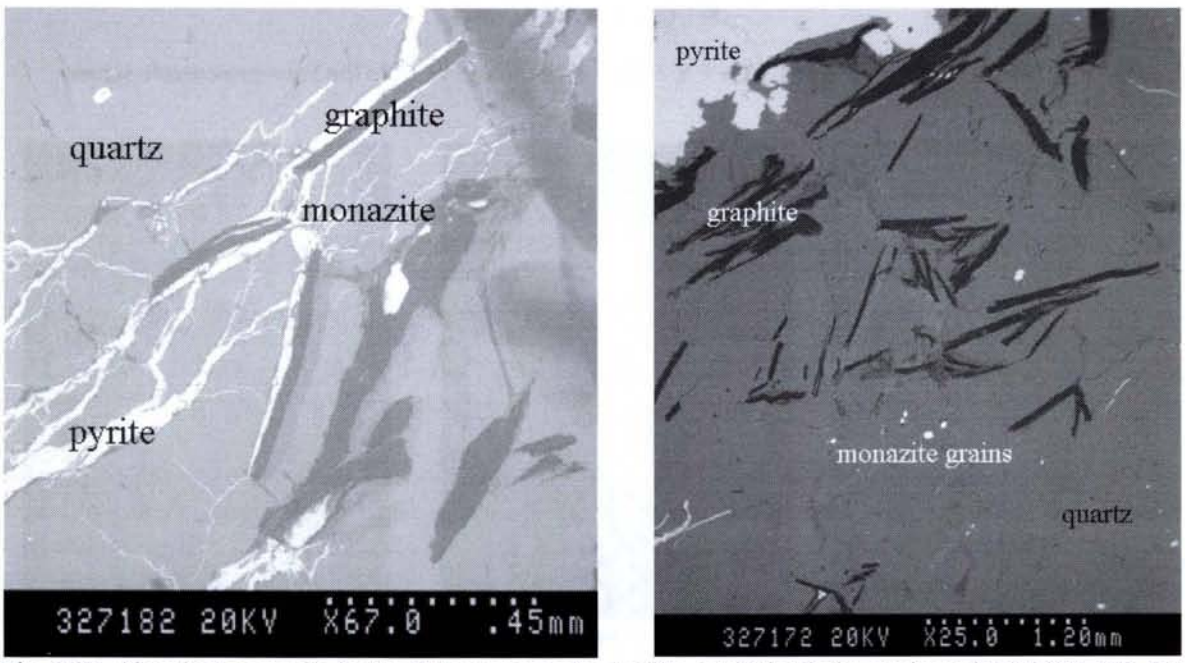

Fig. 2.25. Abundant monazite in the Paleoproterozoic graphite-sulphide-biotite gneisses (DDH-627-149, Karku deposit area) BSEM image photomicrograph scales: A – 45 mm, B – 1.2 mm

Fresh, non-altered grains have classical Ce-monazite composition, and in average contain 32.24 ± 5.52 wt. % of P_2O_5, 26.72 ± 3.37 wt. % of Ce_2O_3, 12.03 ± 2.06 wt. % of La_2O_3, 3.60 ± 1.21 wt. % of ThO_2 (see Annex monazite). Mostly included in quartz grains, quite often – close to graphite flakes within sulphide veins together with pyrite, zircon and xenotime (Fig. 2.25). Alteration of monazite is quite rare. Monazite can be associated with xenotime and pyrite (Fig. 2.24-C).

Maximum P – LREE substitution is only 3 atoms of Si, Ca and Y. There are no substitution of Al, Fe, Th and U in these relatively fresh graphitic schists (Fig. 2.26).

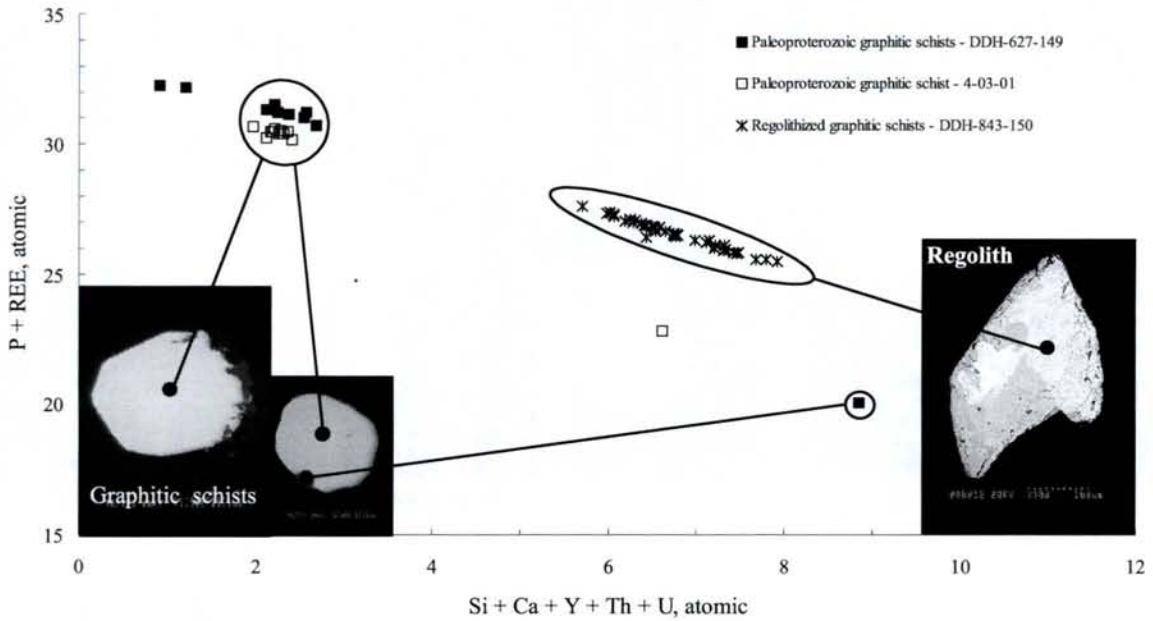

Fig. 2.26. Substitution of P + REE by Si + Ca + Y + Th + U in monazites from the Paleoproterozoic schists

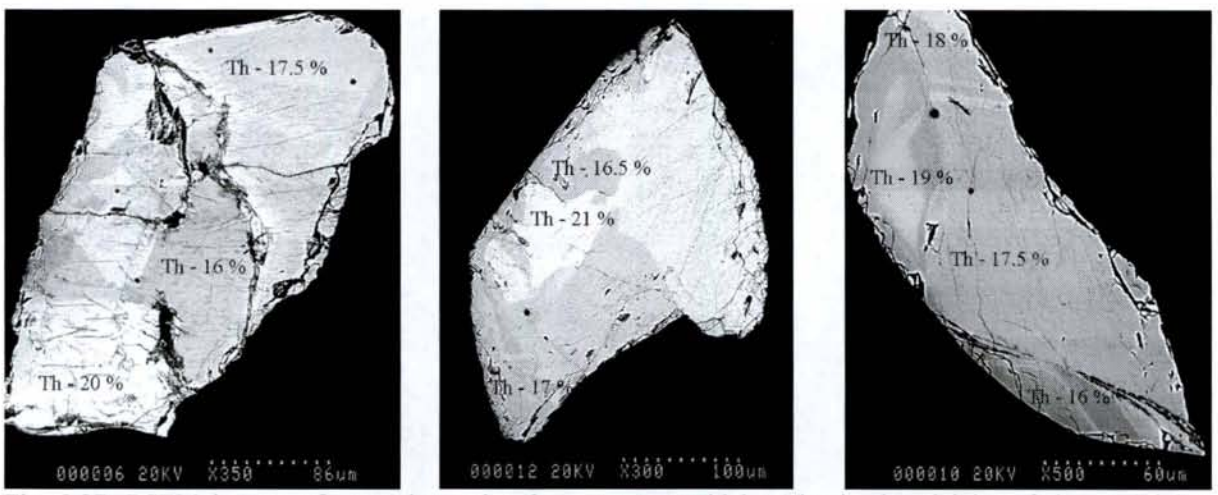

Fig. 2.27. BSEM images of monazite grains from a pegmatoidal gneiss in the vicinity of the pre-Riphean unconformity surface (DDH-843-150 m, Karku deposit area, ore zone II). Photomicrograph scales: A – 86 μm, B – 100 μm, C – 60 μm

Monazite from the "augen" pegmatoid in the vicinity of the Pre-Riphean unconformity surface is very rich in Th (18.58 ± 1.61 wt. % ThO_2, Annex monazite). Phospohorus contents vary from 32.24 to 24.61 wt. % P_2O_5, whereas silica increases up to 3.39 wt. % (Fig. 2.27). Maximum P – LREE substitution in these monazite grains is up to 7,5 atoms with Th (3,4 atoms), Si, Ca and Y (Fig. 2.26).

We have no evidence of monazite alteration in the Paleoproterozoic graphite-biotite and biotite gneisses and schists. In the vicinity of the regolith zone, the Th-rich monazite shows a patchy distribution of the domains with varying Th contents, including «intergrowth-like» pattern (as described by Zhu & O'Nions, 1999). The high Th content of the monazites from the regolithized Paleoproterozoic gneisses and schists is a primary feature. Such high Th contents are observed in monazite from high grade metamorphic rocks, because the average Th-content in monazite increases with the temperature if Th is available in the rock (Overstreet, 1967). This rock is particularly enriched in Th (205 ppm). Such Th-rich pegmatoids, rich in monazite are also quite common in the basement of the Athabasca basin (Brouand and Cuney, person. com.).

Whole-rock Zr, LREE and Th gneisses geochemistry concerning to mineralogical aspect

Zr in the Paleoproterozoic gneisses and schists is mainly contained in zircon. Y is relatively enriched in the altered parts of zircon grains and in xenotime, which sometimes occurs at the margin of monazite grains (Fig. 2.24c). Non-altered zircon contains less than 0.1 wt. % Y. The altered part may contain up to 3 - 4 wt.% Y (exchange $Zr^{4+} \leftrightarrow Y^{3+}$). The Zr/Y ratio is an indicator of the degree of zircon alteration in Proterozoic clastic basins: in fresh zircons this ratio is higher than 100 (Fig. 2.28), while altered zircons are typically characterized by Zr/Y ratios between 100 and 20 (Kister, 2003). The Paleoproterozoic gneisses and schists of the Karku area present Zr/Y ratios ranging from 20 to 1, much lower than the ones recorded in the Athabasca basin, indicating a stronger mobility of yttrium during zircon alteration in the Karku area.

Average Th/U ratio of intrusive rocks is close to 4. The metasedimentary Paleoproterozoic gneisses and schists of the Karku area (Fig. 2.29) have Th/U ratios mainly ranging from 10 to 1, most of them present U-enrichment with Th/U lower than 2, some are strongly enriched in U, with Th/U ratios down to 0.01 or more. Some of these samples rich in uranium are however located away from the mineralized zones and thus indicate that the Paleoproterozoic gneisses and schists of the Karku area were initially enriched in uranium.

The sample the richest in Th, corresponding to the pegmatoid, have the highest Th/U ratio (Th/U ≈ 10), which may indicate an uranium loss.

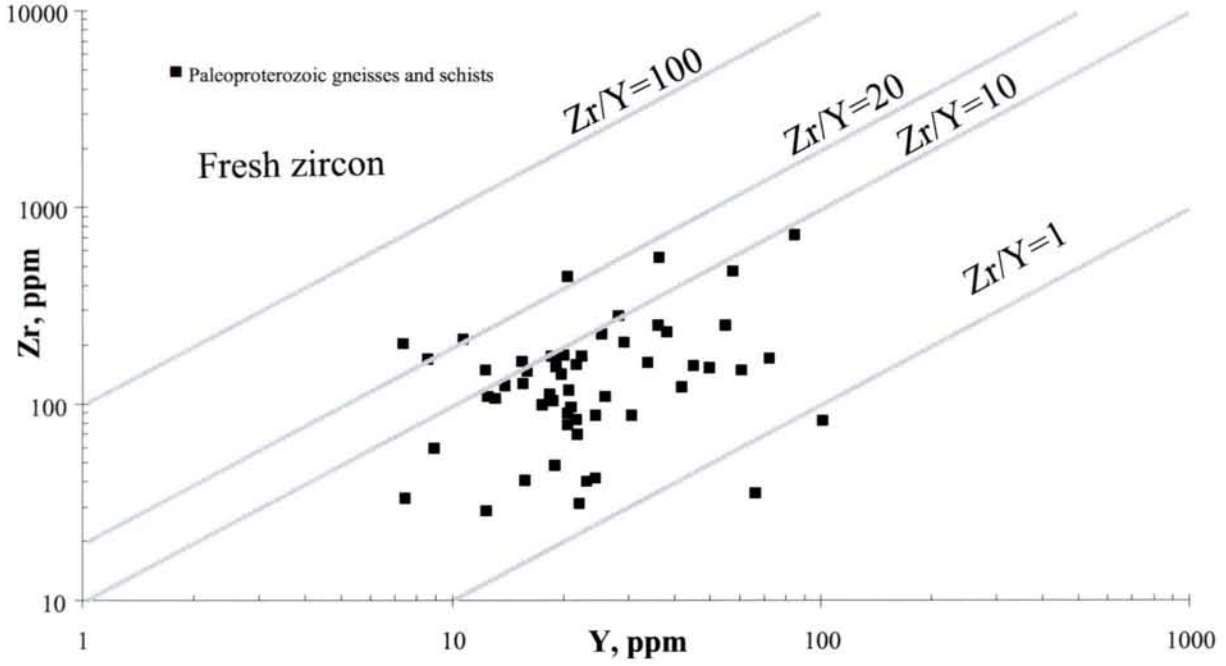

Fig. 2.28. Y vs. Zr diagram for the Paleoproterozoic gneisses and schists

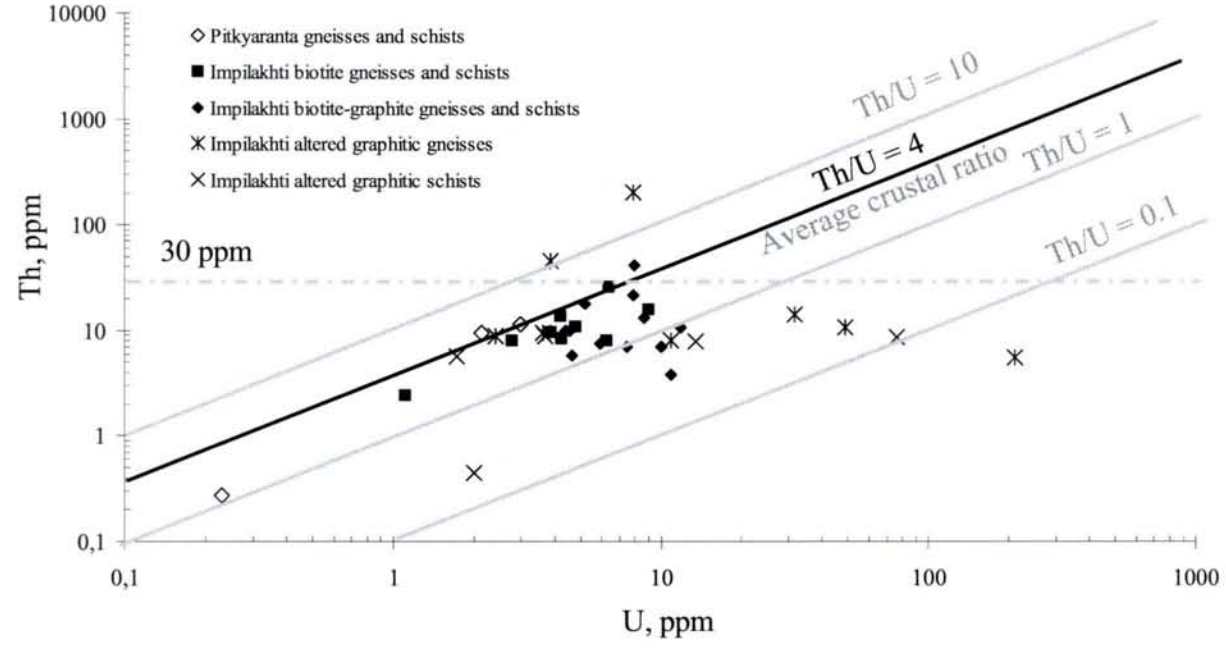

Fig. 2.29. Th vs. U diagram for the Paleoproterozoic gneisses and schists

Th is also well correlated with light rare-earth elements (LREE), because these elements are mainly hosted in the same mineral, monazite. La can be chosen as an indicator of the LREE behavior. Archean and Proterozoic quartzites and shales all over the world have similar Th/La ratios between 0.2 and 0.4 (Cuney et al., 2000; Mathieu et al., 2001). In the Th/La

diagram (Fig. 2.30) most Paleoproterozoic gneisses and schists from the Northern Ladoga Domain have Th/La ratio series ranging from 0.4 to 0.2. About 20% of the samples have Th/La higher than 0.4 indicating a depletion in LREE. Only one sample with Th/La lower than 0.2 indicating a slight LREE enrichment.

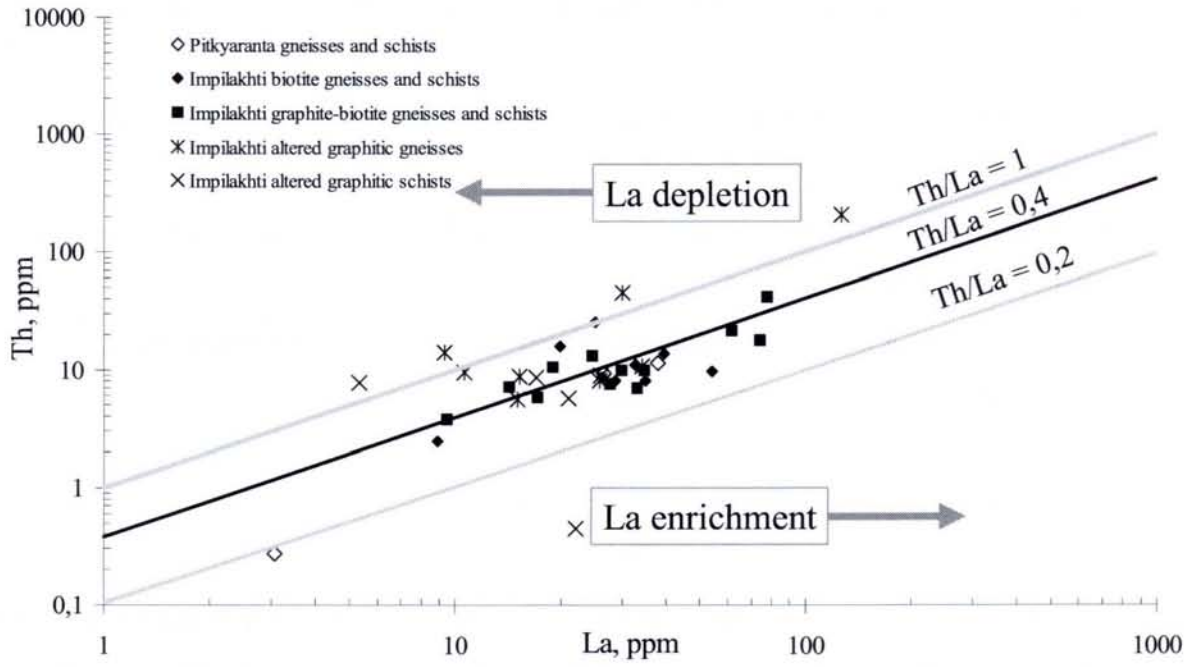

Fig. 2.30. Th vs. La diagram for the Paleoproterozoic gneisses and schists. The Th/La field represent the field for the sediments

2.2.3. Alteration processes in the Paleoproterozoic basement formations

On the basis of petrographic observations and mineral paragenesis, three main alteration stages have been distinguished in the Paleoproterozoic basement formations in the vicinity of the Riphean clastic sediments of the Pasha – Ladoga basin (Salmi area) (Bylinskaya et al., 2004; Lobaev et al., 2003; Novikov et al., 2001; Shurilov et al., 2003; Velichkin et al., 2001):

(i) Retrograde metamorphic alteration, associated with the late stage of the Svecofennian orogeny;

(ii) Regolithic alteration interpreted as representing of a pre – Pasha - Ladoga paleoweathering profile;

(iii) Hydrothermal alteration, which is related to the uranium mineralization processes and extends up into the Pasha – Ladoga sandstones.

(i) Retrograde metamorphic alteration

In the Kitelya – Pitkyaranta zone retrograde metamorphic alteration is widespread. The rocks were first metamorphosed to the upper *amphibolite* facies at medium pressure, reaching partial melting. Cordierite appears spatially associated with the development of potassium feldspar (microclinization). Later, a staurolite-bearing paragenesis formed during *epidote – amphibolite* facies metamorphism (Koistinen et al., 1996).

The typical paragenesis of the schists is plagioclase (An_{15-25}) + biotite + muscovite + quartz replaced by the low-temperature association of sericite + chlorite + rare carbonate. Fresh cordierite is relatively rare and often replaced by finely crystalline flaky muscovite or phlogopite or fibrolite – sillimanite. The plagioclase – biotite paragenesis is replaced by the muscovite + garnet + quartz + fibrolite paragenesis. At the contacts with quartz grains, garnet flattened along the schistosity, and staurolite cutting the schistosity appears.

Studies of garnet and biotite from the Paleoproterozoic schists (Baltybaev et al., 1996) has indicated two-stages of metamorphism. The first stage (T = 600 – 650 °C; P = 5 kbar) was in the conditions of the amphibolite facies, the second (T = 460 – 560 °C; T = 2.2 – 3.7 kbar) was in the conditions of the epidote-amphibolite facies.

(ii) "Regolithic" alteration stage

Just under the Athabasca sediments the basement, an alteration profile called "regolith", is developed in the uppermost basement rocks through the whole Athabasca basin and has been attributed by some authors to "paleoweathering" (Hoeve & Sibbald, 1978; McDonald, 1980, 1985, Bruneton, 1993). However, Cuney (2003) from the similarity of the clay mineral paragenesis observed in the basement and the absence of Ce-anomaly typical of laterites proposed that the alteration profile may result from the alteration of the basement by the diagenetic fluids. The regolith thickness may reach up to 40 – 50 m. Macroscopically, it shows four zones characterized by different colours, which are from bottom to top: (1) green; (2) transitional green – red; (3) red and (4) orange, ochre to white a "bleached zone". The thickness of the bleached zone (0.1 – 1 m) is larger near the uranium deposits.

In the first three zones the primary metamorphic or granitic textures of the rocks are preserved. At the top, in the bleached zone rock textures are partially or totally destroyed. Fe- and Mg-chlorite, sudoite and illite are present in the first two zones. In the third red zone, kaolinite is the predominant mineral with hematite and illite (Pagel, 1991; Bruneton, 1993). The transitional green-red zone is a basin-wide redox boundary separating oxidized Athabasca red-bed sandstones above the unconformity from reduced basement rocks below (Hoeve & Quirt, 1984). Differences in the thickness of the regolith are primarily due to variations in the basement rock types (McDonald, 1985), i.e. quartz-feldspathic gneisses and calc-silicate rocks are more deeply weathered than graphitic rocks.

In the Ladoga Lake area this phenomenon was also observed regionally. The alteration profile in the graphite-biotite gneisses and schists is widespread and its thickness varies from 1 – 5 to 20 – 30 m. Along the faults, the thickness of the alteration profile may reach 40 – 90 m. Three alteration zones have been identified in the Ladoga Lake area profiles (Fig. 2.34) which are from bottom to top: (1) slightly altered mostly green zone; (2) kaolinite – chlorite – hydromica green zone and (3) kaolinite - hematite red zone (Novikov et al, 2001).

Alteration process begins with illitization of plagioclase and chloritization of biotite in the green zone. In the upper part of the profile, the granite, gneisses and schists are partially to totally replaced by kaolinite and illite. In basic rocks interstratified illite-chlorite and brownish illite-smectite clay minerals appear. Bleached zone has not been distinctly observed, but only some colour variations from whitish to brownish are described.

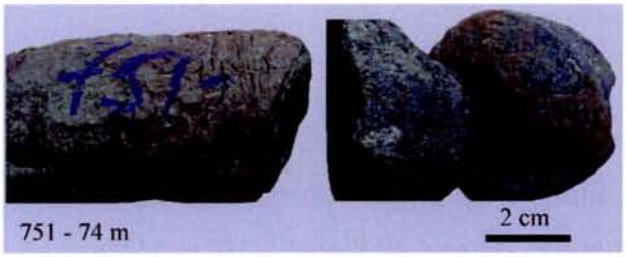

A – red zone: hematized, partially disintegrated gneiss DDH-751-74 m

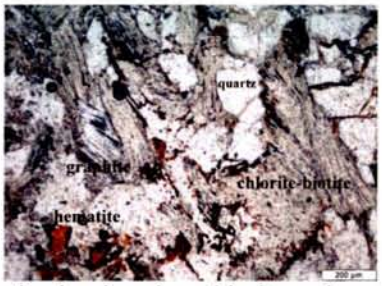

B – hematite developed on chlorite-carbonate matrix (DDH-751-74 m), parallel nicols, scale 200 μm

C – red-green transition zone: intensively chloritized and hematized gneiss DDH-751-75 m

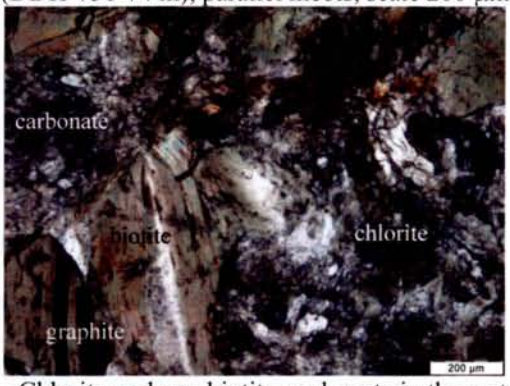

D – Chlorite replaces biotite, carbonate in the matrix (DDH-751-75 m), parallel nicols, scale 200 μm

E – green zone: predominant chlorite alteration with carbonate in sulphidic biotite gneiss DDH-751-85 m

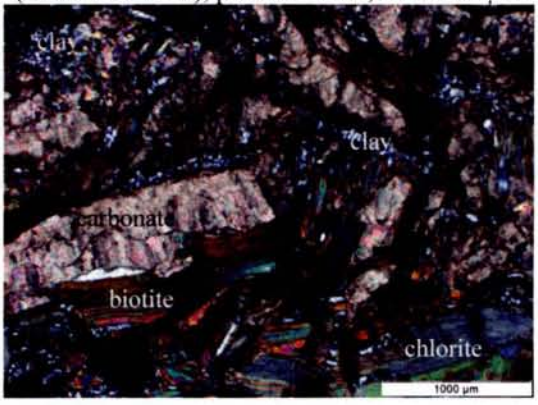

F – Carbonate totally replaces plagioclase, chlorite develops on biotite, different clay minerals are also present (DDH-751-85), crossed nicols, scale 1000μm

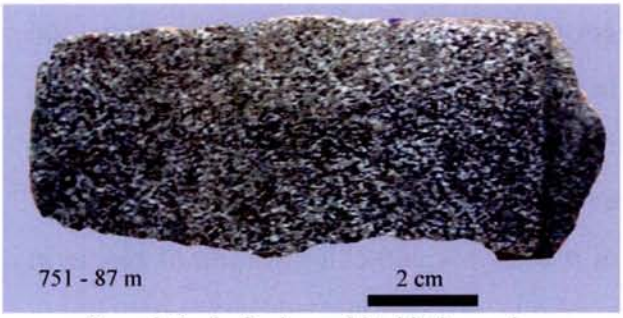

G – relatively fresh graphite-biotite gneiss DDH-751-87 m

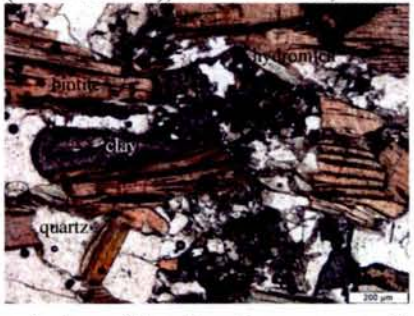

H – beginning of the alteration process with clay minerals - illite formation (DDH-751-87 m), parallel nicols, scale - 200 μm

Fig. 2.31. Typical alteration profile in the graphite-biotite gneisses and schists (DDH-751, Karku deposit area)

As the type of clay minerals observed in the alteration profile at the top of the basement below the Pasha – Ladoga basin scale are similar to those observed in the overlying

sediments, it appear that the syn-diagenetic alteration processes have also strongly affected the underlying basement formations, as observed in the Athabasca regolith profile. It is not totally excluded that a paleoweathering may have existed, but it has been strongly overprinted by the syn- and post-diagenetic alteration. Carbonates are frequently present in the green and red zones (usually 0 – 5 wt. % of CaO, sometimes up to 26 wt. % in DDH-751-75 m), at variance with what is observed in the Athabasca, but are typical of the ore stage at Karku.

(iii) Hydrothermal alteration stage

The syn-ore hydrothermal alteration stage may have locally totally obliterated earlier metamorphic retrograde and syn-diagenetic alteration in the Archean – Paleoproterozoic formations of the basement.

The syn-ore hydrothermal alteration event in the basement is accompanied by partial dissolution or pseudomorphical replacement of the rock-forming minerals of the Paleoproterozoic gneisses and schists (plagioclase, K-feldspar, quartz, biotite) by neoformed chlorite, interstratified clay minerals and carbonates. Uranium mineralization (pitchblende and coffinite accompanying by different sulphides) is also observed in the upper part of the basement formations in the vicinity of the unconformity surface.

Analysis number	625-140	625-157	319-193
SiO_2	29.33	35.64	25.42
Al_2O_3	21.38	23.00	21.47
MgO	17.87	16.30	13.04
FeO	18.30	11.05	26.81
TiO_2	0.08	0.38	0.03
MnO	0.21	0.23	1.25
CaO	0.12	0.36	0.04
Na_2O	0.01	1.67	0.02
K_2O	0.39	0.04	0.01
Total	**87.67**	**88.66**	**88.08**
Si	3.02	3.13	2.61
Al^{IV}	0.98	0.87	1.39
Al^{VI}	1.62	1.62	1.20
Mg	2.74	2.87	1.99
Fe^{2+}	1.57	1.00	2.29
Ti	0.01	0.03	0.00
Mn	0.02	0.02	0.11
Total VI	**5.96**	**5.54**	**5.60**
Ca	0.01	0.04	0.00
Na	0.00	0.33	0.00
K	0.05	0.01	0.00
Fe/(Fe+Mg)	**0.36**	**0.26**	**0.54**
Points number	22	10	18

Table 2.4. Chemical composition of chlorites from slightly mineralized basement formations

Chloritization of the Archean – Paleoproterozoic basement is a prolonged superimposed process of alteration, which starts from the retrograde metamorphic stage, continues during the diagenetic alteration of the Pasha – Ladoga clastic sediments and finally during the hydrothermal ore stage.

Thus, the chloritization process is widespread and characterized by the formation of different types of chlorites and interstratified chlorite-smectites (Bylinskaya et al, 2004). Green to dark-green Mg-Fe chlorite (ripidolite) is typical of the graphitic gneisses in the vicinity of the unconformity surface away from mineralized zones (DDH-319-193 m - Fig.

2.32, Fig. 2.33). Dark-green Fe-Mg chlorite (chamosite - pycnochlorite) is observed in the vicinity of the unconformity surface within the ore zone III of the Karku deposit (DDH-625-140 m – Fig. 2.32, Fig. 2.35). Fe-Mg chlorite (pycnochlorite - delessite) is observed in the ore zone III of the Karku deposit (about 20 m from the unconformity surface) (Fig. 2.32, 2.36). Chemical compositions of chlorites from DDH-625 and DDH-319 (Karku deposit area) (for DDH location see Fig. 1.26) were analyzed by electron microprobe at the Henri Poincaré University (Table 2.4) and their structural formula were calculated (Table 2.5).

Sample number	Structural formula of chlorite	Distance to unconformity surface
625-140 m	$(Mg_{2.74}\ Fe_{1.57}\ Mn_{0.02}\ Al_{1.62})(Si_{3.02}\ Al_{0.98})\ O_{10}(OH)_8$ - pycnochlorite	8 m
625-157 m	$(Mg_{2.87}\ Fe\ Mn_{0.02}\ Al_{1.62})(Si_{3.13}\ Al_{0.87})\ O_{10}(OH)_8$ - delessite	25 m
319-193 m	$(Mg_{1.99}\ Fe_{2.29}\ Mn_{0.11}\ Al_{1.20})(Si_{2.61}\ Al_{1.39})\ O_{10}(OH)_8$ - ripidolite	Graphitic gneiss

Table 2.5. Structural formula of chlorites from the mineralized (Karku deposit area, ore zone III - DDH-625) and slightly mineralized (Karku deposit area, ore zone I - DDH-319) Paleoproterozoic basement formations

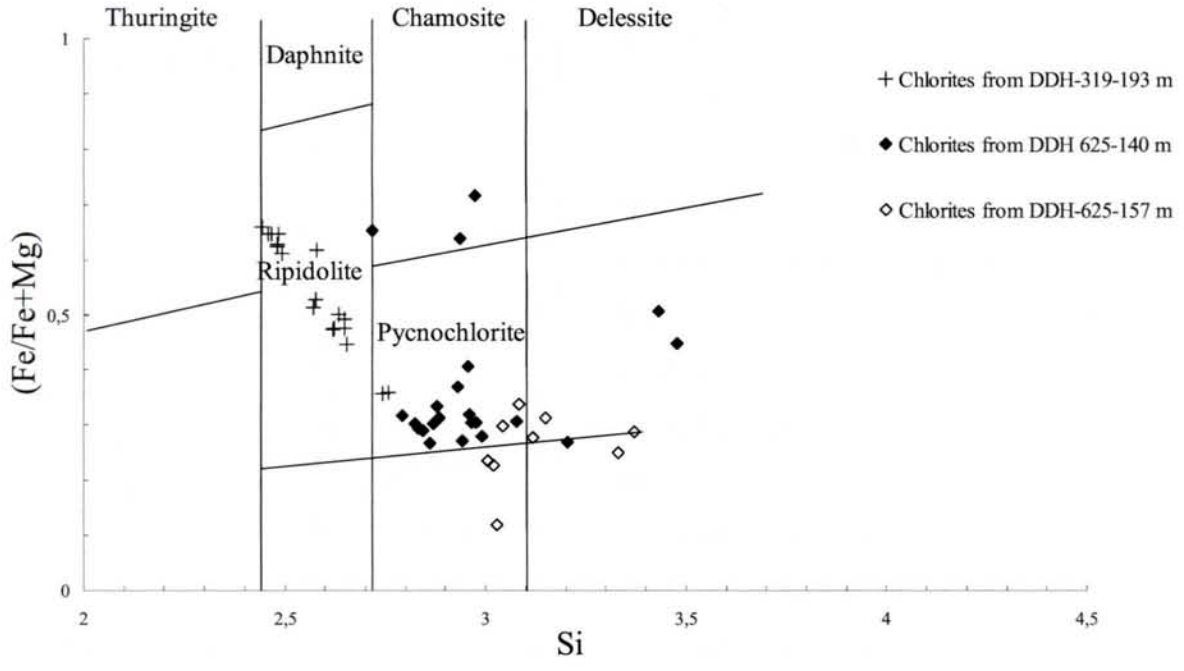

Fig. 2.32. Chlorites from the Paleoproterozoic graphitic gneisses and schists of the Karku deposit area (present work) in the classification chlorite composition diagram

Mg-Fe chlorite (ripidolite) in the weakly altered graphitic gneiss from the deepest part of the drill hole (DDH-319-194 m) has the highest Fe/(Fe+Mg) ratio (0,54) and highest Al-content in the tetrahedral sites (Al_{IV} =1.4) (Fig. 2.34). High Al content in the tetrahedral sites

of chlorite can correspond to high formation temperature: more than 300 °C (Nieva & Cathelineau, 1985) and may correspond to retromorphic chlorite.

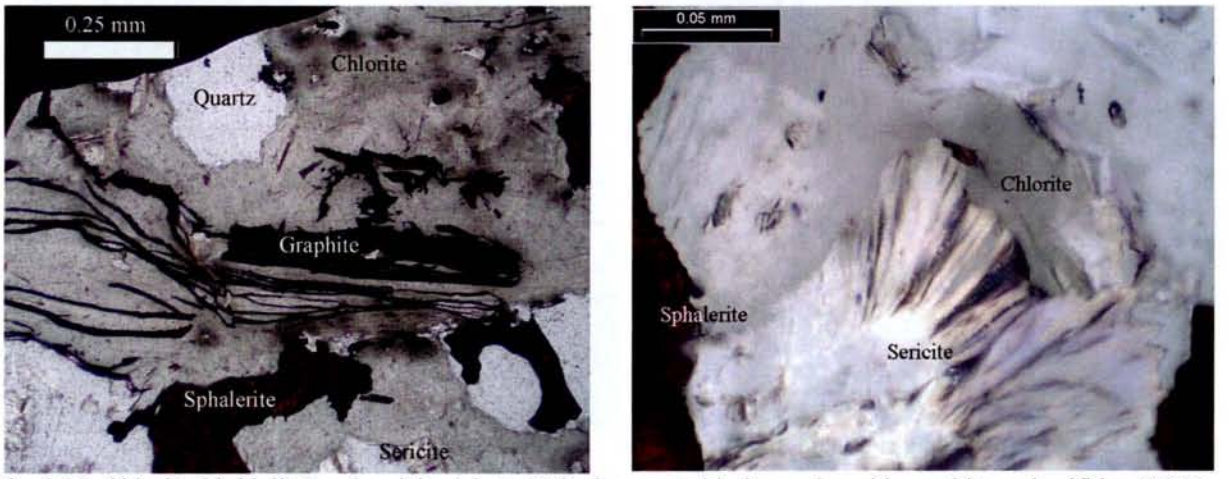

Fig. 2.33. Chlorite (ripidolite) and sericite (photo B) in the quartz-biotite gneiss with graphite and sulfides (DDH-319 – 193 m, Karku deposit area, ore zone I). Microphotograph scale : A - 0.25 mm ; B – 0.05 mm

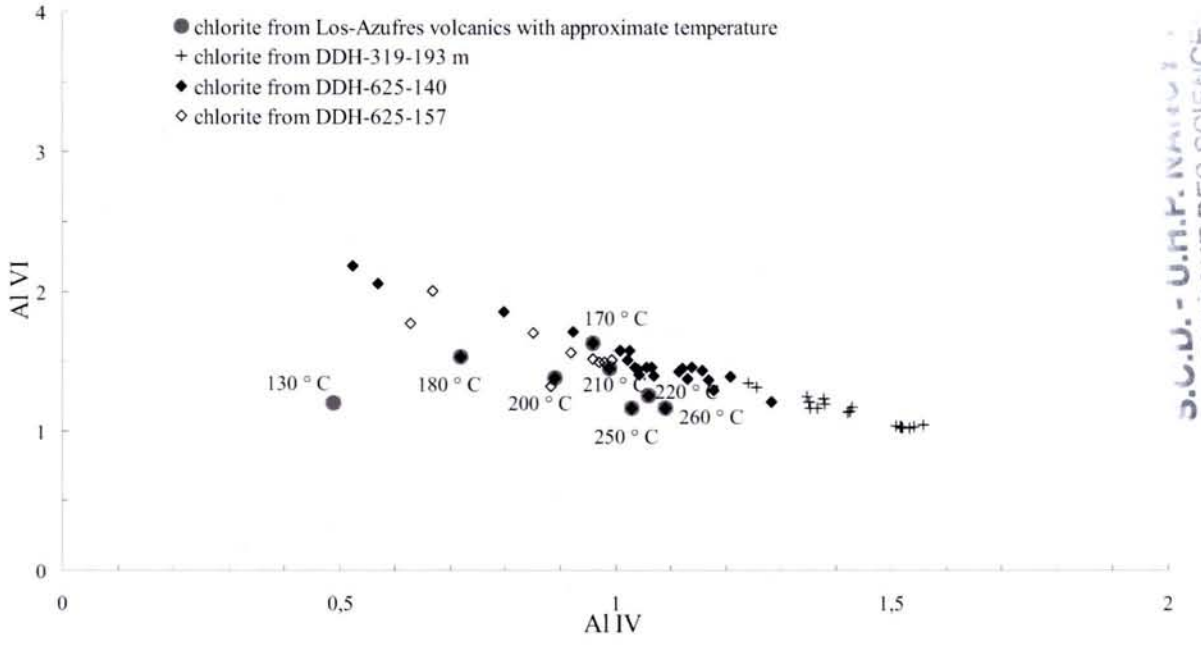

Fig. 2.34. Chlorites from the Paleoproterozoic gneisses and schists in the diagram Al_{IV} vs. Al_{VI} (chlorite formation geothermometer – after Cathelineau & Nieva, 1985)

The average chlorite from graphitic schists in the ore zone III of the Karku deposit area (intermediate depth - DDH-625-157 m) and the average chlorite from the graphitic gneiss just below the unconformity (DDH-625-140 m) have the lowest Fe/(Fe+Mg) ratios (0.26 and 0.36 correspondingly) and lower Al-content in the tetrahedral sites (Al_{IV} = 0.87 and 0.98

correspondingly) corresponding to low formation temperatures – from about 100°C to 200 - 240°C respectively (Fig. 2.34).

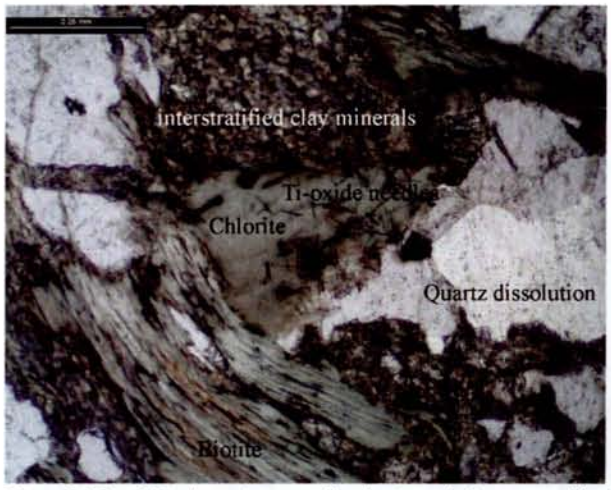

Fig. 2.35. Chlorite (pycnochlorite) and interstratified minerals neoformation, accompanied by quartz dissolution and biotite alteration (DDH-625-140 m, Karku deposit, ore zone III) Microphotograph scale - 0.25 mm

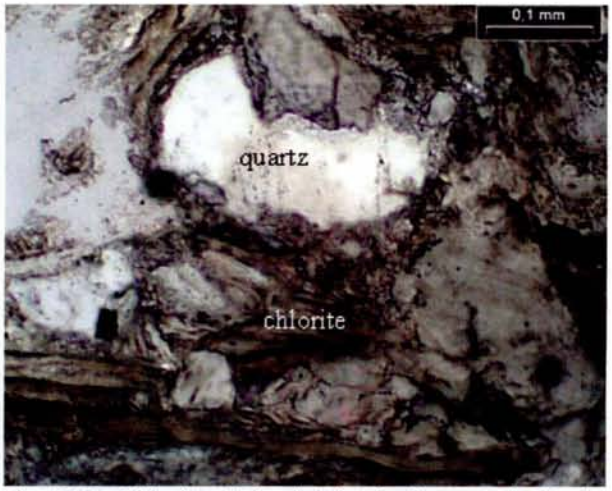

Fig. 2.36. Chlorite (delessite) in the leucocratic biotite gneiss (DDH-625-157 m, Karku deposit, ore zone III) Microphotograph scale - 0.1 mm

2.2.4. Petrogeochemistry of the Paleoproterozoic basement formations

Major elements distribution

Major and trace elements composition of the Paleoproterozoic gneisses and schists including amphibolitic, biotitic, graphitic and sulphidic varieties is listed in the Annex Paleoproterozoic. The major element compositions of selected slightly altered samples are listed in the table 2.6. DDH and outcrops samples location is presented in Part 1.4.

Reference group	1	2	3	4	5
Sample number	4-03-01	319-193	816-225	306-100	843-250
SiO_2	65.10	52.25	67.70	59.05	59.63
Al_2O_3	15.14	18.13	10.45	15.98	13.69
Fe_2O_3	6.53	10.00	6.37	7.24	6.27
MnO	0.07	0.08	0.12	0.09	0.06
MgO	2.16	5.44	2.60	4.99	5.60
CaO	1.67	2.41	1.49	2.82	2.62
Na_2O	3.34	3.70	0.91	3.10	2.63
K_2O	2.83	3.78	2.26	2.62	3.39
TiO_2	0.64	0.85	0.39	0.75	0.68
P_2O_5	0.14	0.14	0.06	0.12	0.10
PF	1.76	2.76	5.88	3.26	4.12
Total	99.38	99.53	98.23	100.01	98.79

Table 2.6. Major elements composition of selected slightly altered analysis of the Paleoproterozoic rocks of the Northern Ladoga Domain. Reference groups are correspond to: 1 - Pitkyaranta biotite-amphibole schist; 2 - 3 - Impilakhti biotite gneisses and schists; 4 - 5 - Impilakhti graphite-biotite gneisses and schists

The Paleoproterozoic gneisses and schists have a composition with highly variable quartz, feldspar, carbonate and calc-silicate contents. They are generally migmatized to various extend. In the vicinity of the contact with the Salmi rapakivi batholith, skarns and pegmatites are widespread. Close to the Riphean volcanic-terrigenous cover all these rocks are strongly altered. The major element composition of selected fresh samples are listed in the table 2.7.

Reference group	1	2	3	4	5
Sample number	306-90	835-245	843-150	654-151	751-80
SiO_2	68.46	45.08	68.69	60.07	62.72
Al_2O_3	11.78	22.55	14.00	13.13	10.66
Fe_2O_3	9.94	15.33	8.49	8.73	10.82
MnO	0.06	0.08	0.05	0.08	0.08
MgO	1.89	2.89	1.26	3.22	6.13
CaO	0.66	1.41	0.00	1.41	0.17
Na_2O	0.22	0.19	0.00	0.33	0.26
K_2O	3.01	4.35	1.16	2.07	1.45
TiO_2	0.12	1.12	0.48	0.47	0.56
P_2O_5	0.00	0.72	0.05	0.14	0.11
PF	4.10	6.19	4.85	10.82	7.40
Total	100.24	99.91	99.03	100.47	100.36

Table 2.7. Major elements composition of selected altered analysis of the Paleoproterozoic rocks of the Northern Ladoga Domain in the Karku deposit area. Reference groups are correspond to: 1 - Impilakhti regolithized graphite-biotite gneiss (ore zone I); 2 - Impilakhti regolithized graphite-biotite gneiss; 3- Impilakhti regolithized "augen" graphite-biotite gneiss (ore zone I); 4 - Impilakhti regolithized graphite-biotite schist (ore zone III); 5 – Impilakhti regolithized graphite-biotite schist

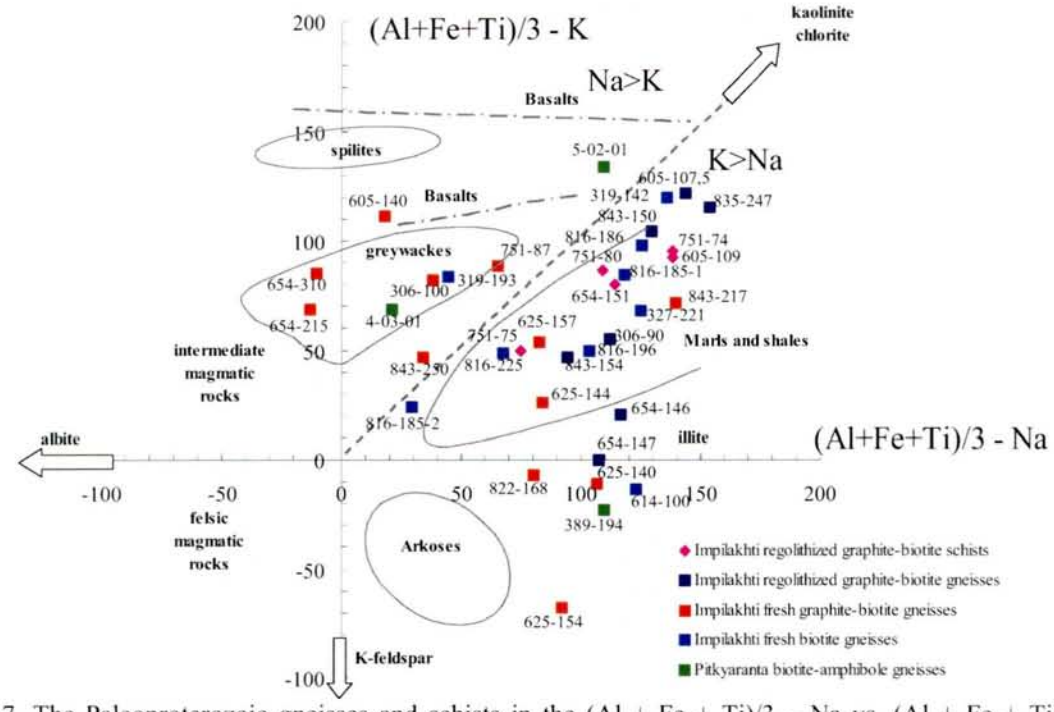

Fig. 2.37. The Paleoproterozoic gneisses and schists in the (Al + Fe + Ti)/3 – Na vs. (Al + Fe + Ti)/3 - K diagram (Moine & de la Roche, 1968), to identify the initial protoliths of metasediments

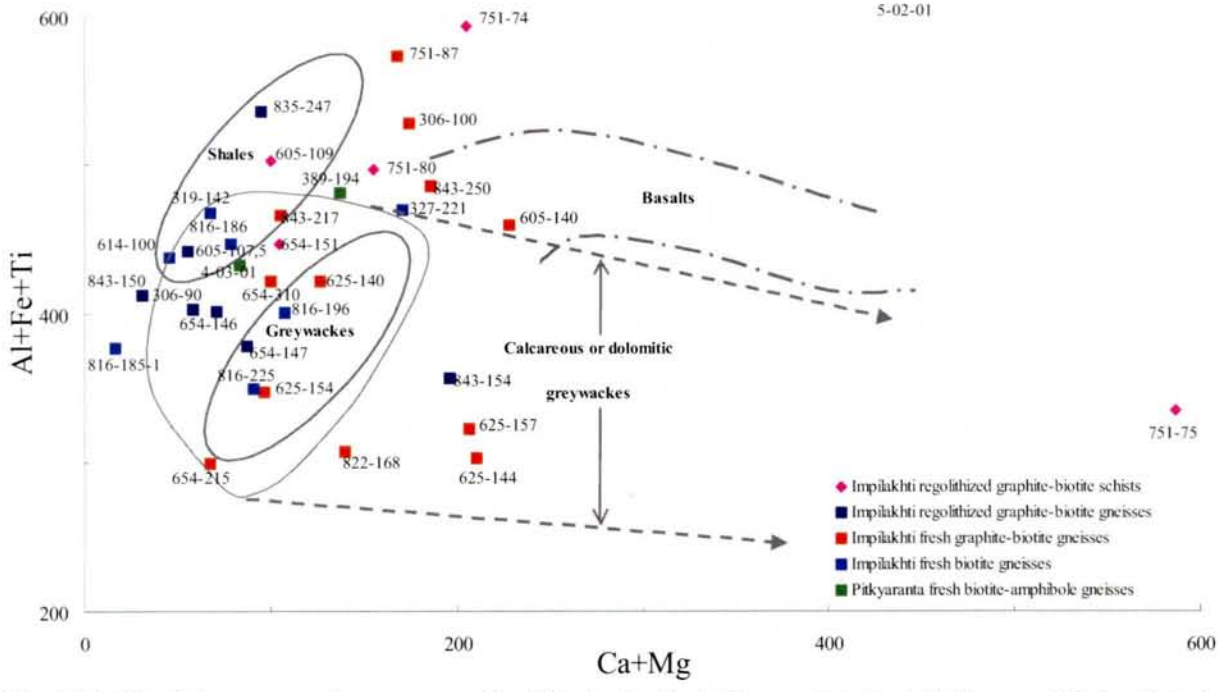

Fig. 2.38. The Paleoproterozoic gneisses and schists in the Ca + Mg vs. Al + Fe + Ti diagram (Moine & de la Roche, 1968), to differentiate Ca-Mg rich greywackes from basalts

Five main varieties of Paleoproterozoic rocks depending on their prevalent rock forming minerals, schistosity and alteration degree have been distinguished:

(i) Four groups, belonging to the Impilakhti Suite subdivided into

- slightly altered graphite-biotite schists;

- slightly altered mainly biotite gneisses;
- regolithized graphite-biotite schists;
- regolithized graphite-biotite gneisses;

(ii) One, belonging to the Pitkyaranta biotite-amphibole gneisses and schists.

The diagram (Al + Fe + Ti)/3 - Na versus (Al + Fe + Ti)/3 - K (Moine & de la Roche, 1968) allow first to distinguish sedimentary (mainly positive values of the (Al + Fe + Ti)/3 - Na parameter) from magmatic rocks (mainly negative values of the (Al + Fe + Ti)/3 - Na parameter)(Fig. 2.37). To distinguish the greywackes and Ca-rich lithologies from the basalts which may be confused in this diagram, the interpretation of the data has to be coupled with the Al + Fe + Ti versus Ca + Mg diagram (all parameters calculated in millications, Moine and de la Roche, 1968) (Fig. 2.38).

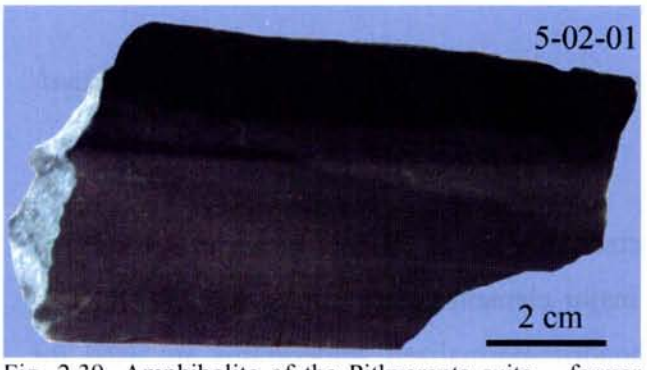

Fig. 2.39. Amphibolite of the Pitkyaranta suite – former metavolcanic rock

Fig. 2.40. Quartz-feldspar gneiss with carbonates of the Impilakhti suite – former arkose

Most of the samples are located in the sedimentary field in accordance with the lithological characteristics of the samples in the field. The samples located the closest to the origin correspond to the quartz richest samples (quartz is located at the origin in the diagram). Three main group of samples can be distinguished in these diagrams:

- former greywackes (with Na > K) in the (Al + Fe + Ti)/3 - Na vs. (Al + Fe + Ti)/3 - K diagram (Fig. 2.37), two of them (5-02-01 – Pitkyaranta suite (Fig. 2.39) and DDH-605-140 – Impilakhti graphite-biotite gneiss) may eventually correspond to former basalts in the Al + Fe + Ti vs. Ca + Mg diagram (Fig. 2.38), but have element patterns have to be considered to control such an origin (especially REE) because the two samples richer in Ca + Mg plot just at the limit between the basalt and greywackes field. The other Ca + Mg rich samples correspond to calcareous greywackes.

- former shales and marls (K > Na) (the main part of the samples) representing a mixture between quartz and clays (mainly kaolinite and/or chlorite).
- illite-rich shale plotting on the positive part of the (Al + Fe + Ti)/3 - Na axis.

The less altered Impilakhti graphitic gneisses present wide range of composition spreading all over the different sedimentary field from relatively basic greywackes to very potassic shales or even arkoses (one sample - DDH-625-154 (Fig. 2.40)), plotting in the lower right part of the diagram, is very rich in K-feldspar (former meta-arkose).

The Pitkyaranta biotite-amphibole gneiss (sample 4-03-01) plots in the greywacke field, the Pitkyaranta quartz-feldspar-biotite gneiss (DDH-389-194 – Fig. 2.19-D) in the illitic shale field.

The Impilakhti regolithized gneisses and schists (DDH-654-146, 654-147) plot in the shale field because alteration tend to remove preferentially sodium and thus create a relative enrichment in alumina corresponding to the development of abundant clay minerals.

Trace elements distribution in the vicinity of a contact between Paleoproterozoic regolithized and Riphean clastic sediments

In the petrochemical diagrams all selected samples of Paleoproterozoic schists and gneisses are characterized by highly variable major element compositions. For the study of the primary distribution of trace elements chondrite-normalized spidergrams are used for slightly altered amphibole-biotite gneisses of the Pitkyaranta suite (Fig. 2.41) and for slightly altered biotite gneisses of the Impilakhti suite (Fig. 2.42). Their spidergram patterns are relatively similar, but in the biotite gneisses of the Impilakhti suite – are more constant.

They are characterized by U contents of about 3 – 5 ppm and not exceeding 9 ppm (DDH-327-221), Th value is about 8 – 15 ppm (up to 25 ppm in DDH-614-100), Rb - 100 ppm (maximum 170 ppm), Ba – 50 – 80 ppm, in feldspars-rich lithologies – up to 1000 ppm , Sr values vary from 9 to 280 ppm, Nb - 2 - 14 ppm, Zr – 33 - 280 ppm, La - 8 - 54 ppm, Ce - 18 - 90 ppm, Sm - 2 - 7 ppm, Yb - 1 - 3 ppm and Y - 7 - 28 ppm.

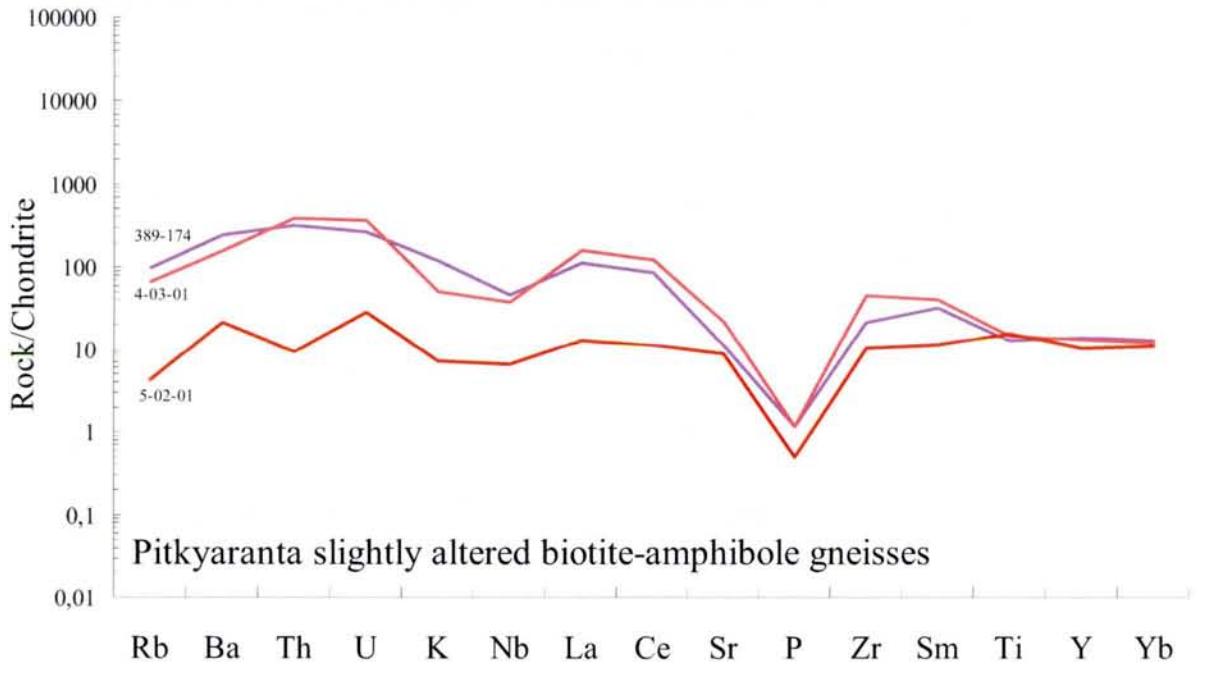

Fig. 2.41. Chondrite-normalized trace element patterns of the slightly altered Pitkyaranta gneisses in the Karku deposit and Salmi – Pitkyaranta areas (Northern Ladoga district) (spidergram type after Holm (1979); chondrite composition after E. Anders and N. Grevesse: http://earthref.org/GERM/reservoirs/C1.htm)

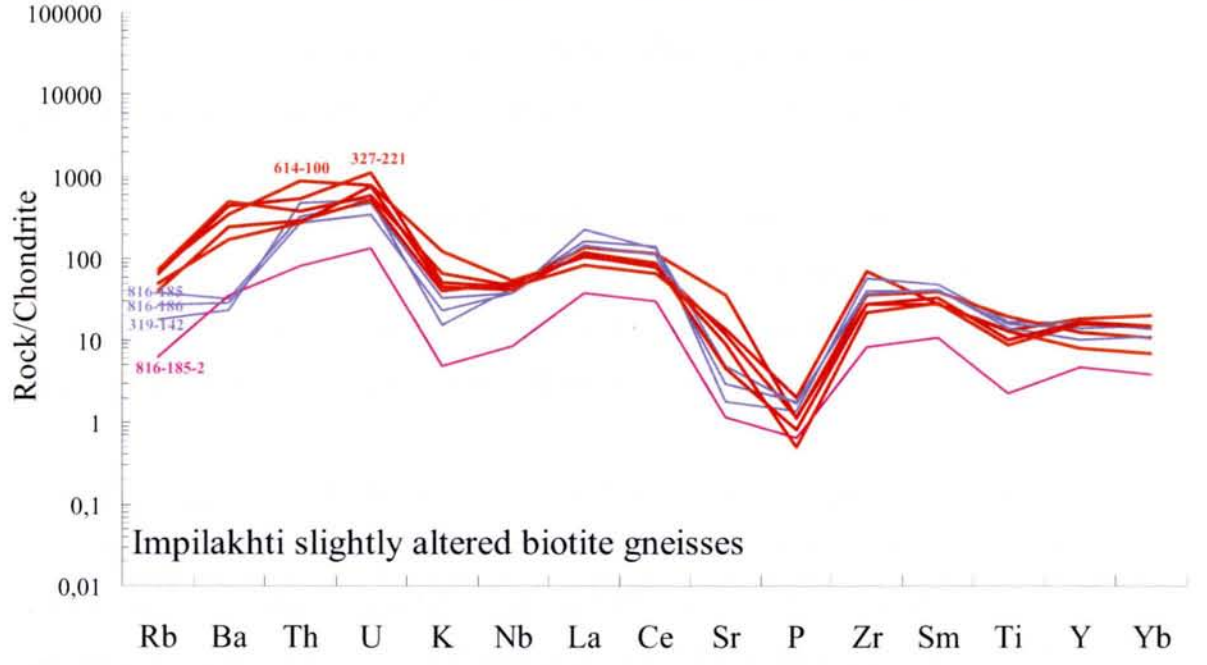

Fig. 2.42. Chondrite-normalized trace element patterns of the slightly altered Impilakhti gneisses in the Karku deposit and Salmi – Pitkyaranta areas (Northern Ladoga district) (spidergram type after Holm (1979); chondrite composition after E. Anders and N. Grevesse: http://earthref.org/GERM/reservoirs/C1.htm)

For a better interpretation all samples were divided into different groups according to their origin: shales and greywackes the most abundant, basalts and arkoses more scarce.

To compared altered former *shale* lithologies (see Fig. 2.37 – 2.38) relatively fresh former shale lithologies were selected from the Impilakhti biotite gneisses. A mean of the

"former shale" (816-185-1, 816-186, 816-196, 816-225, 319-142) was calculated (Table 2.8) for normalization (spidergram type after Holm (1979)):

ppm	Rb	Ba	Th	U	K	Nb	La	Ce	Sr	P	Zr	Sm	Ti	Y	Yb
shale	80	234	10	4	1.8	11	37	67	37	0.15	145	6	0.6	23	2

Table 2.8. Trace element values calculated for Mean of "former shale" sample

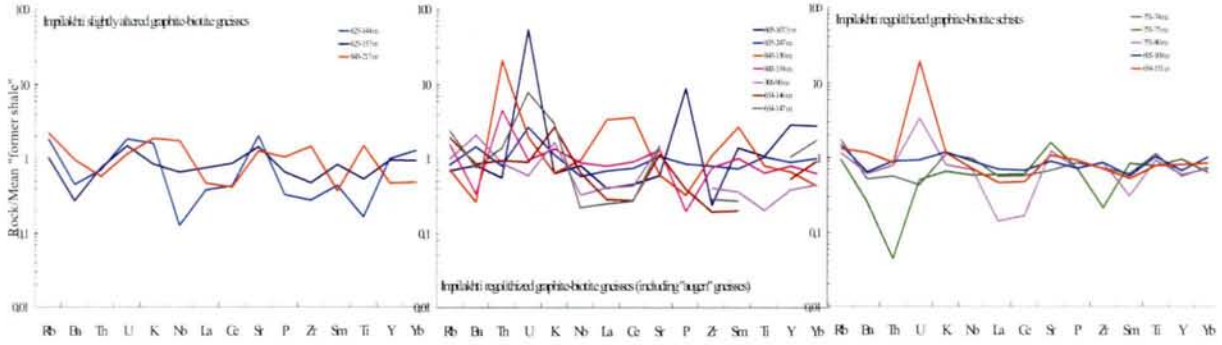

Fig. 2.43. Mean "former shale"-normalized trace element patterns of the Impilakhti graphite-biotite gneisses and schists in the Karku deposit area (Northern Ladoga district) (spidergram type after Holm (1979):
1 – slightly altered gneisses; 2 – regolithized gneisses; 3 – regolithized schists.

By comparison with the "average former shale" (slightly altered biotite gneisses of the Impilakhti suite), graphite-biotite gneisses are characterized by a similar distribution of trace elements:

- a slight enrichment is observed for U (graphite-bearing lithologies in 1.5 - 2 times richer in U than biotite gneisses), K_2O and Sr;

- a slight depletion is observed for Ba and Zr, Nb with 0.5 to 2 average "former shale;

- nearly the same distribution is observed for Rb, P_2O_5, TiO_2, Th, Y and LREE and Yb (Fig. 2.43-A).

Strong variations in the trace element distribution are observed in the regolithized graphite-biotite gneisses (mostly in "augen" gneisses). In the vicinity of the unconformity surface (ore zone I - DDH-843-150 m – red line in Fig. 2.43-B) in comparison to the gneiss, which are in 4 meters below (DDH-843-154 m – rose line in Fig. 2.43-B) strong Th (200 ppm to 45) and LREE (520 ppm to 130) enrichment is observed, but this is related to a local Th-rich pegmatoid injection which can be really compared with the graphite-biotite gneiss. Also for the "augen" gneisses, but in the ore zone III moderate U enrichment is observed.

In the regolithized graphite-biotite schists variations in the trace element distribution are not significant. Th, LREE and Zr depletion in DDH-751 is observed in the vicinity of the unconformity surface and U enrichment - in DDH-654-151 m (Fig. 2.43-C).

For comparison with altered former *greywacke* lithologies (see Fig. 2.37 – 2.38) some relatively fresh former greywacke lithologies were selected from the slightly altered Impilakhti graphite-biotite gneisses. The average for a "former greywacke" sample (654-215, 654-310) was calculated (Table 2.9) for normalization (spidergram type after Holm (1979)):

ppm	Rb	Ba	Th	U	K	Nb	La	Ce	Sr	P	Zr	Sm	Ti	Y	Yb
greywacke	92	290	17	**8**	1,4	12	43	88	121	0,1	119	8	0,2	40	4

Table 2.9. Trace element values calculated for Average "former greywacke" sample

In comparison to the "average former greywacke" and slightly altered graphite-biotite gneisses of the Impilakhti suite (DDH-654-215, 654-310), altered graphite-biotite gneisses are characterized by no significant variations in the trace elements distribution which may result from the initial heterogeneities of the metasediments (Fig. 2.44). Only U content in DDH-654-151 reaches value of 10 "former greywackes", all other elements are varied within the 0.2 – 5 values of "former greywackes".

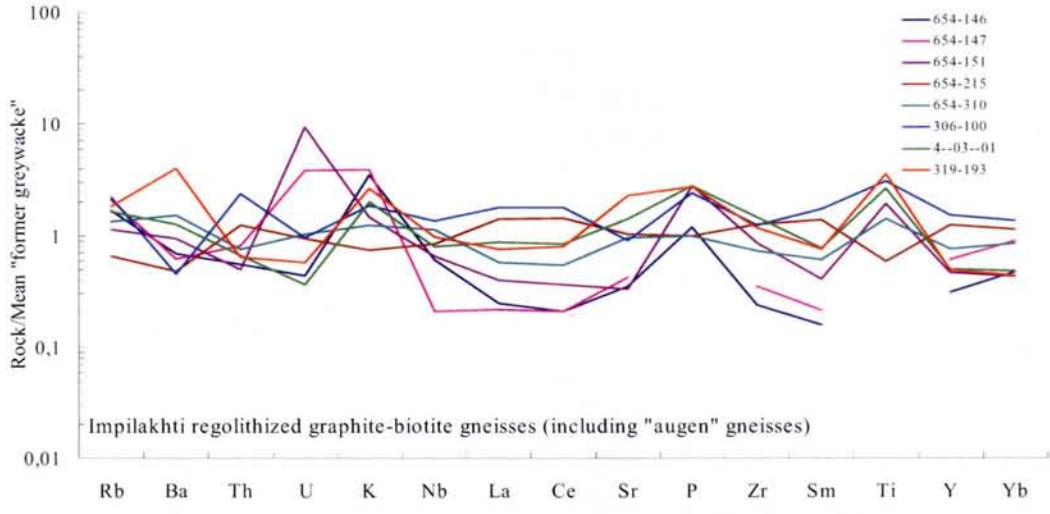

Fig. 2.44. Average "former greywacke"-normalized trace element patterns of the Impilakhti gneisses and schists of the Karku deposit area (Northern Ladoga district) (spidergram type after Holm (1979)

For a better understanding of the trace element distribution with depth and alteration degree the geochemical information has been also examined according to the depth position of the samples in the drill holes in the vicinity of the Pre-Riphean unconformity surface also with mean "former shale"-normalized and "former greywacke"-normalized spidergrams (Fig. 2.45). DDH-654 (ore zone III), DDH-843 (ore zone I) and DDH-751 (in the vicinity of the Karku deposit) (For DDH location see Fig. 1.26).

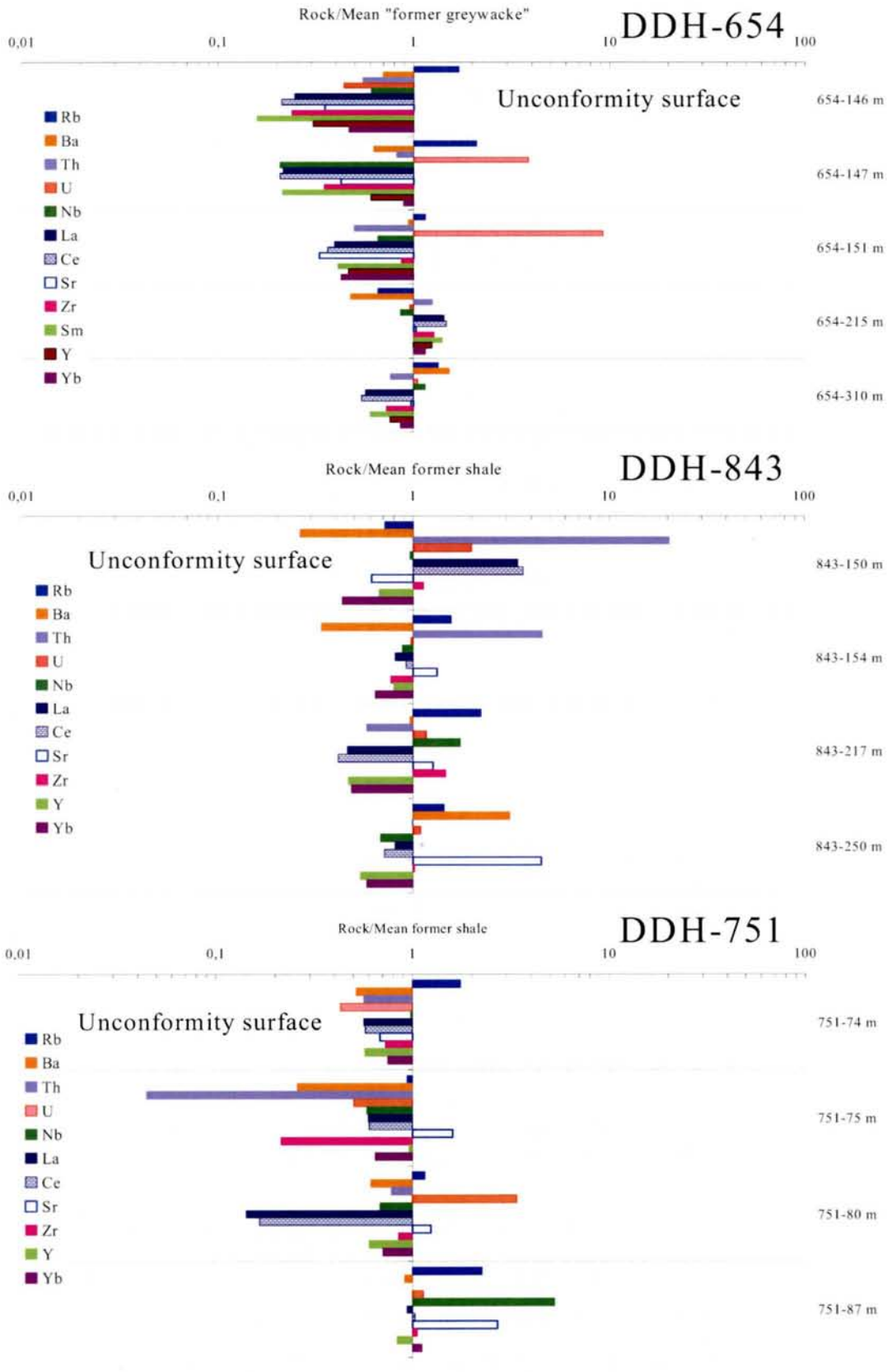

Fig. 2.45. Trace element distribution in the Paleoproterozoic gneisses and schists in concerning to the DDH position and depth of the samples

In DDH-654 (ore zone III) trace elements distribution was compared with Mean of "former greywackes". With depth it varies slightly: Rb is slightly depleted, Ba, Sr, Nb, LREE, Y and Yb are slightly enriched, Th content varies very slightly. U content increases from the unconformity surface (0.45 of former greywacke value) up to 5 meters from the unconformity (10 times to former greywacke value) and then with depth its content decreases up to 1 of former greywacke.

In *DDH – 843* (ore zone I) together with U, Th and LREE contents decrease with depth significantly: at 1 meters from the unconformity surface a strong Th (about 200 ppm) and moderate LREE enrichment is observed and in the fresh rocks with depth Th content is about 5 - 9 ppm. With depth Ba, Sr enrichment is observed.

In DDH-751 (within the limits of the Karku deposit area) former shale lithologies' trace element distribution with depth are studied: in the regolithized rocks strong depletion of Th and moderate of all other elements within 2 meters from the unconformity are observed. With depth Nb, Rb and Sr contents increase. In 6 meters from the unconformity maximum U (14 ppm) is observed.

Rare-Earth elements distribution

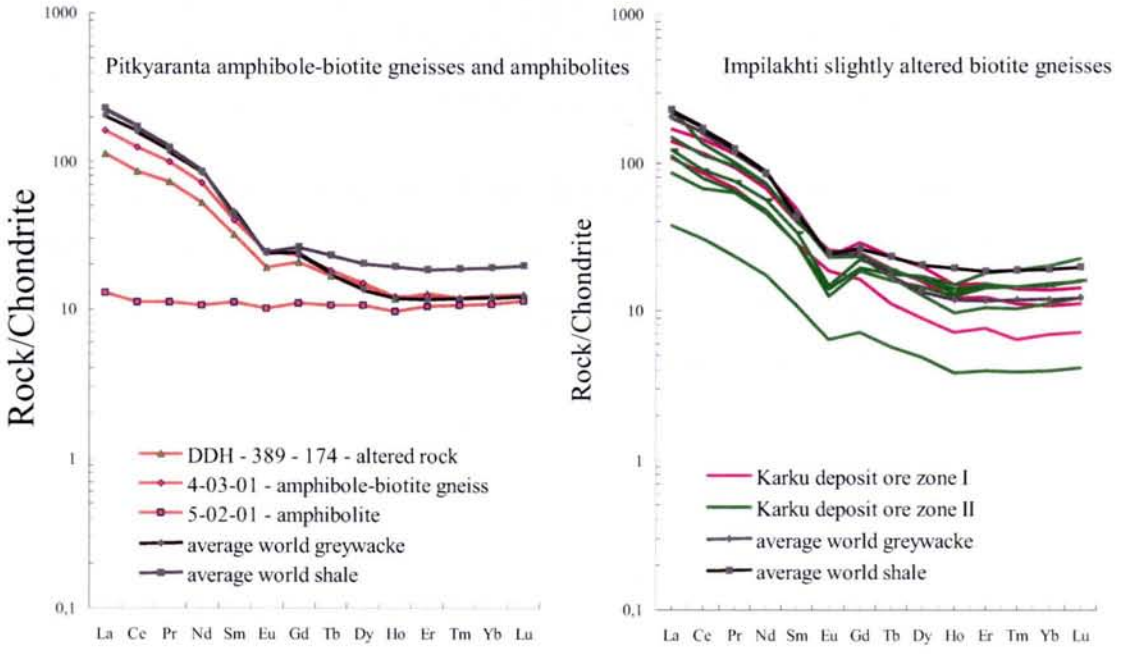

Fig. 2.46 Chondrite-normalized REE patterns of the Pitkyaranta amphibole-biotite gneisses and amphibolites and the Impilakhti slightly altered biotite gneisses of the Pitkyaranta - Salmi - Karku deposit areas (Northern Ladoga district) (spidergram type after Holm (1979); chondrite composition after E. Anders and N. Grevesse: http://earthref.org/GERM/reservoirs/C1.htm)

At first rare-earth elements (REE) distribution and total REE contents in the Paleoproterozoic rocks are studied in the relatively fresh – slightly altered lithologies. Total REE contents are similar in the slightly altered Impilakhti biotite gneisses and in the Pitkyaranta amphibole-biotite gneisses (ΣREE = 140 – 160 ppm).

The Pitkyaranta amphibole-biotite gneisses (Fig. 2.46-A) have smoothly fractionated REE patterns ($(Ce/Yb)_N$ = 7 – 10) with no significant Eu anomaly (Eu/Eu* = 0.75 - 0.80). The slightly altered Impilakhti biotite gneisses (Fig. 2.46-B) have more variably fractionated REE patterns ($(Ce/Yb)_N$ = 3 - 12) and distinctly revealed Eu anomaly (Eu/Eu* = 0.7 on average).

Same as for trace elements distribution the Paleoproterozoic gneisses and schists were divided in two groups by their former origin: shales and greywackes as the most representative in the analyzed data set (see Fig. 2.37 – 2.38).

For comparison with altered former *shale* and *greywacke* lithologies some relatively fresh former shale lithologies were selected from the Impilakhti biotite gneisses and some slightly altered greywacke lithologies were selected from the Impilakhti graphite-biotite gneisses. Mean of "former shale" sample (816-185-1, 816-186, 816-196, 816-225, 319-142) and mean of "former greywacke" sample (654-215, 654-310) were calculated (Table 2.9) for normalization (spidergram type after Holm (1979)):

ppm	La	Ce	Pr	Nd	Sm	Eu	Gd	Tb	Dy	Ho	Er	Tm	Yb	Lu
shale	36.63	67.43	8.08	30.08	5.66	1.10	4.54	0.68	3.92	0.76	2.19	0.33	2.27	0.36
greywacke	43.12	88.08	10.46	38.36	7.69	0.84	6.54	1.09	6.62	1.31	3.77	0.60	4.02	0.61

Table 2.10. REE values calculated for Mean of "former shale" and "former greywacke" samples

Compared to the non-altered rocks, the regolithized gneisses and schists (Fig. 2.47) are depleted in total REE. Only one sample (843-150) in the vicinity of the unconformity surface is characterized by a strong REE fractionation with enrichment in LREE ($(Ce/Yb)_N$ = 75) and strong Eu negative anomaly (Eu/Eu* = 0.2).

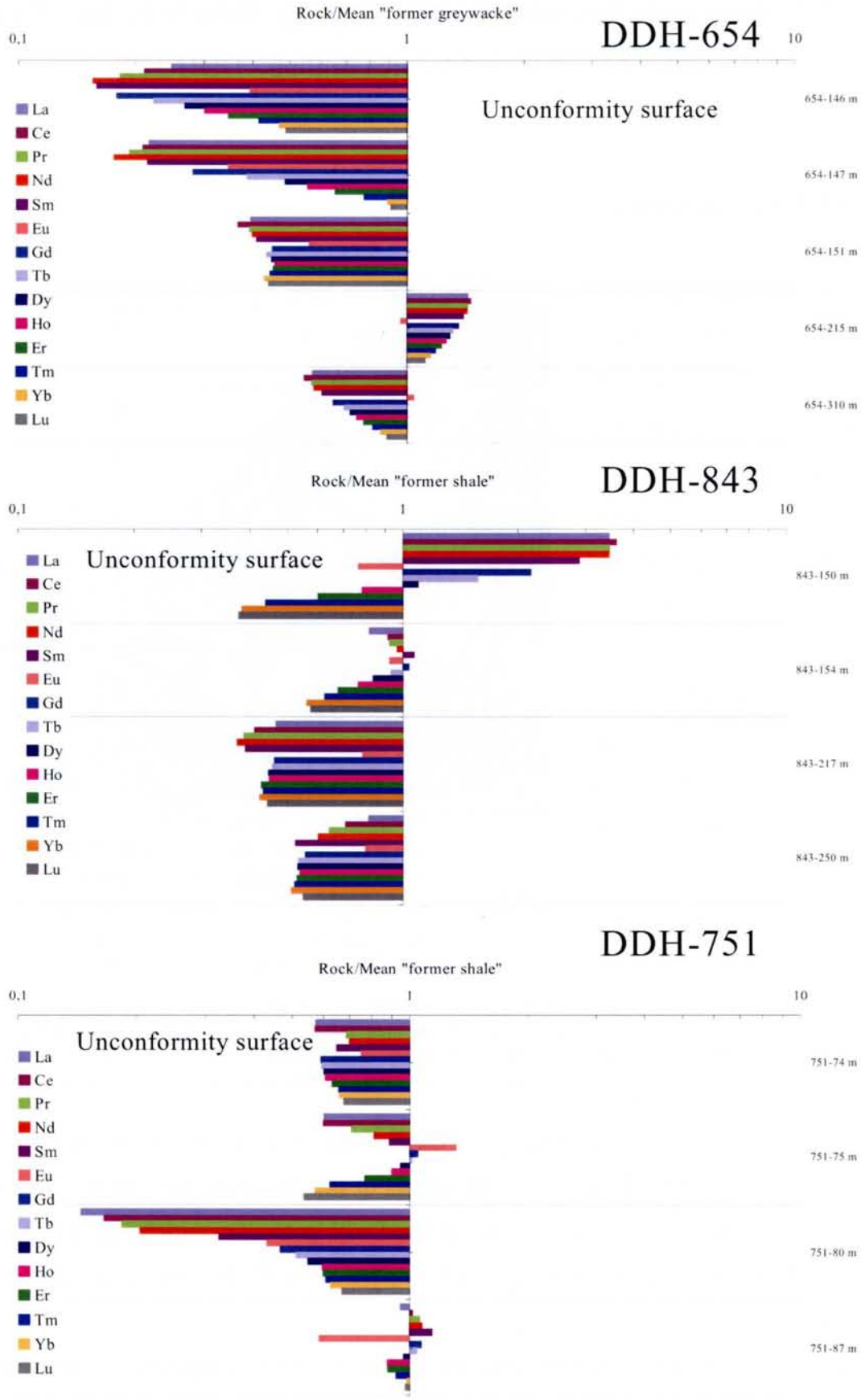

Fig. 2.47. REE distribution in the Paleoproterozoic gneisses and schists in concerning to the DDH position and depth of the samples

Part 3. Paleoproterozoic basement formations of the Western Pasha – Ladoga basin area (on example of the Yablonevka area drilling - DDH-103)

2.3.1. Geological setting

Crystalline basement of the Western Pasha – Ladoga basin area is represented by Paleoproterozoic metamorphic and intrusive rocks (Chapter 1.2), which are completely overlaid by the Mesoproterozoic (Riphean) and Late Mesoproterozoic (Vendian) clastic sediments.

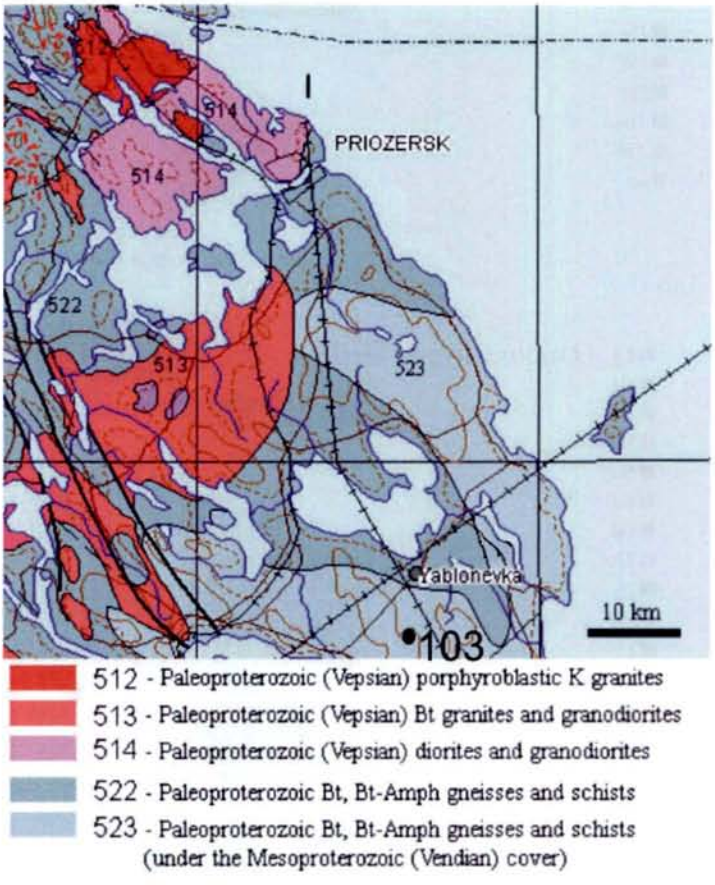

Fig. 2.48. Geological map of the basement of the Western Pasha – Ladoga basin area (after Geological map of the pre-Middle Riphean formations of the Pasha – Ladoga area (Petrov, Caillat, Naumov, 2004)). DDH-103 position is shown in the map

The Paleoproterozoic (Kalevian and Ludikovian undivided) rocks of the Priozersk metamorphic complex are represented by biotite, biotite-amphibole gneisses and schists with cordierite, garnet and sillimanite strongly metamorphosed in granulite facies, which are interpreted usually as the high-temperature analogues of the Paleoproterozoic terrigenous series in the Northern Ladoga Domain. The gneisses and schists of the Priozersk metamorphic complex are usually potassic metapelites, strongly migmatized with potassium enrichment. (Baltybaev et al., 2000). Retrograde metamorphism is very important for the Paleoproterozoic rocks of the Priozersk zone.

The metamorphic rocks of this zone are various by their composition, but garnet is presented in the most associations. Typical paragenesis are presented by:

(i) garnet + biotite + plagioclase ± K feldspar ± quartz;

(ii) garnet ± cordierite + sillimanite + biotite + plagioclase ± K feldspar ± quartz (± spinel);

(iii) garnet + orthopyroxene + biotite + plagioclase ± K feldspar ± quartz.

Intrusive magmatism of this zone is widespread and represented by early and syn-orogenic I-type norite-enderbite and gabbro-diorite-tonalite complexes, late-orogenic S-type potassium granite complexes and post-orogenic mixed-composition mostly alkaline complexes (Shuldiner et al., 1995).

DDH-103 petrographic description

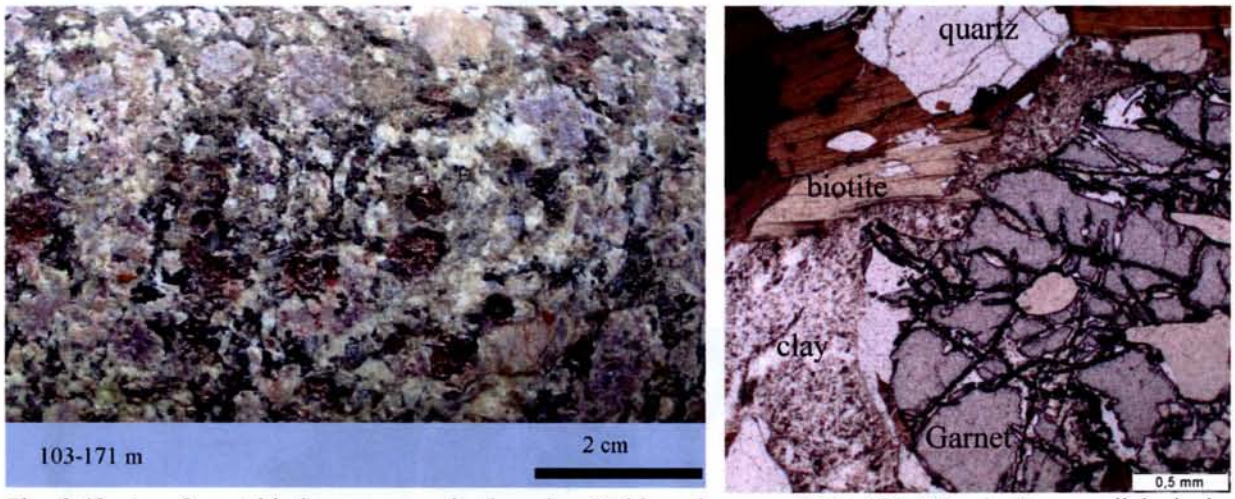

Fig. 2.49. A - Garnet-biotite coarse-grained gneiss (Yablonevka area, DDH-103-171 m); B – parallel nicols, microphotograph scale – 0.5 mm

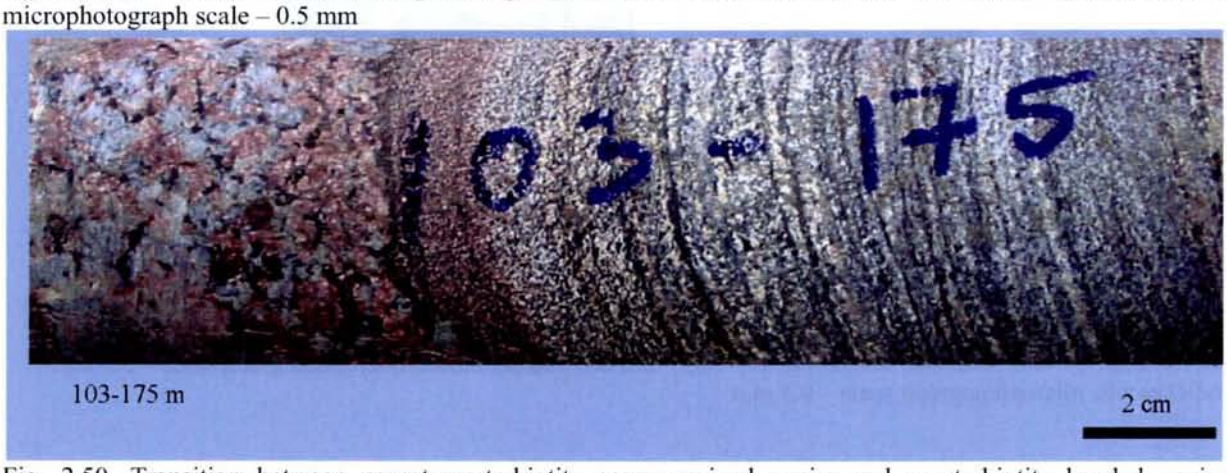

Fig. 2.50. Transition between garnet-quartz-biotite coarse-grained gneiss and quartz-biotite banded gneiss (Yablonevka area, DDH-103-175 m)

The fresh garnet-quartz-biotite gneisses in the DDH-103 (Fig. 2.49 – 2.50) is composed of garnet (20 - 40 %), biotite (20 % in leucosomes and up to 40 % in mesosome), quartz (20 – 30 %) and plagioclase - oligoclase (15 – 25 %). Accessory minerals are rare, mostly ilmenite or different sulphides. The "regolith" profile is also observed in the DDH-103 (Fig. 2.51 –

2.52) and is represented by moderate illitization and sericitization of feldspars and hematization. In the vicinity of the unconformity more hematized and chloritized gneisses are observed. At 6 meters from the unconformity there is a zone of intensive kaolinization and sericitization.

Fig. 2.51. Regolithized quartz-biotite feldspar gneiss in the vicinity of the unconformity surface (Yablonevka area, DDH-103-157 m)

Fig. 2.52. Slightly regolithized quartz-biotite feldspar gneiss at 5 meters from the unconformity surface (Yablonevka area, DDH-103-162 m)

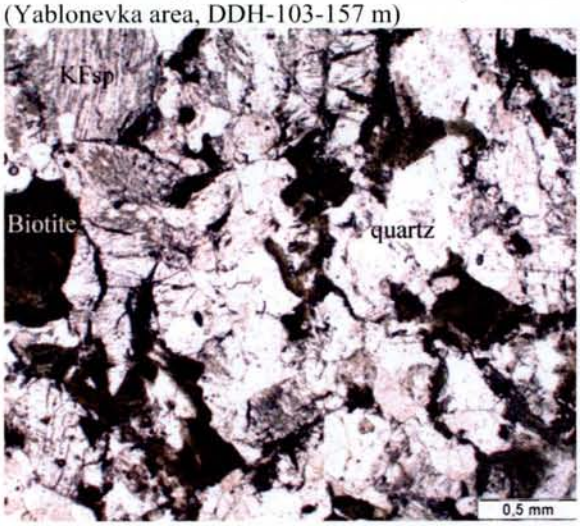

Fig. 2.53. Kaolinization of K feldspar and chloritization of biotite in the vicinity of the unconformity surface (sample DDH-103-157 m), parallel nicols, microphotograph scale – 0.5 mm

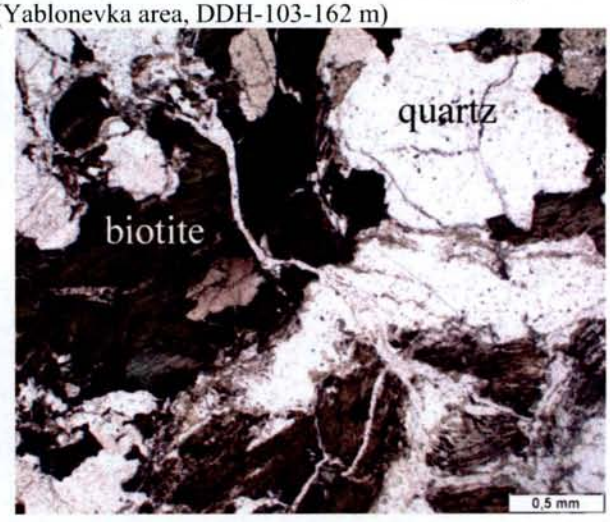

Fig. 2.54. Chloritization of biotite and hematization in the vicinity of the unconformity surface (sample DDH-103-156 m), parallel nicols, microphotograph scale – 0.5 mm

2.3.2. Petrogeochemistry of the basement formations

The geochemistry of major and trace elements has been studied for the samples from drill core DDH-103. Major and trace element composition of the Paleoproterozoic basement rocks is listed in Annex Yablonevka basement rocks. The major element compositions of these rocks are also listed in the Table 2.11.

Reference	1	2	3	4
DDH	103-156 m	103-157 m	103-171 m	103-176 m
SiO_2	60.24	58.25	61.76	63.63
Al_2O_3	15.83	17.22	17.35	16.87
Fe_2O_3	9.86	8.91	7.26	4.85
MnO	0.03	0.00	0.04	0.09
MgO	2.52	2.85	2.81	2.35
CaO	0.19	0.00	0.46	0.84
Na_2O	0.00	0.24	0.20	0.00
K_2O	4.88	7.29	3.36	5.32
TiO_2	0.89	0.86	0.95	0.55
P_2O_5	0.16	0.08	0.26	0.20
PF	5.16	4.09	5.48	5.09
Total	**99.76**	**99.79**	**99.93**	**99.79**

Table 2.11. Major element composition of the Paleoproterozoic basement rocks of the Western (Yablonevka) Pasha – Ladoga basin area – DDH-103: 1 - 2 - slightly altered quartz – feldspar-biotite gneisses; 3 - 4 – quartz-garnet-biotite gneiss. DDH number and depth of the samples are listed.

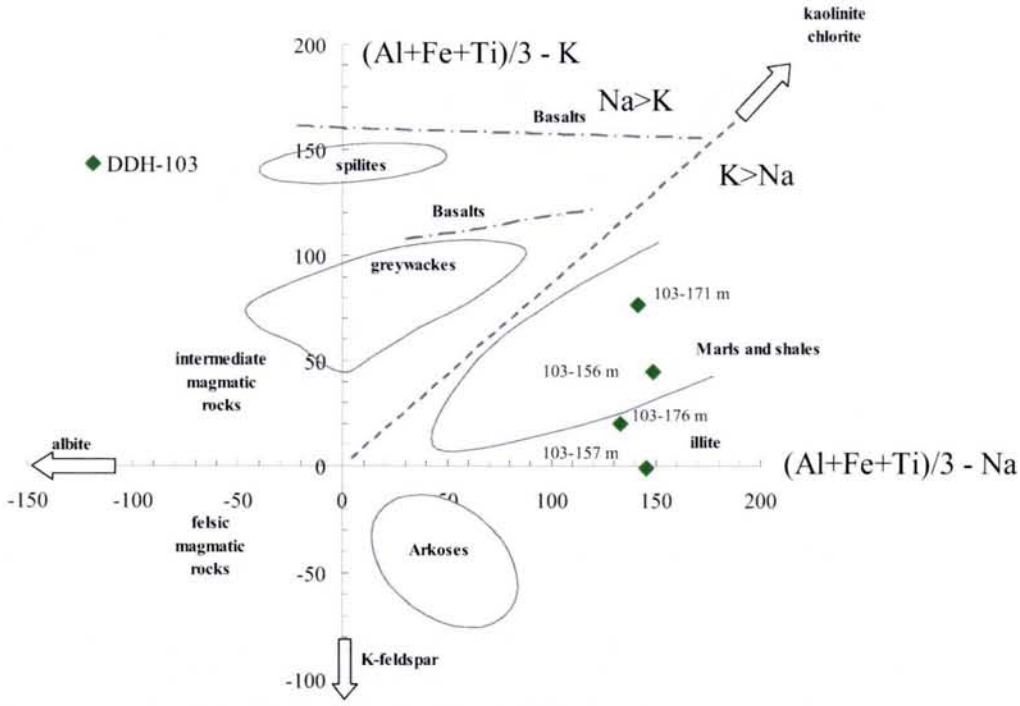

Fig. 2.55. The Paleoproterozoic gneisses of the Western (Yablonevka) Pasha – Ladoga basin area in the (Al + Fe + Ti)/3 – Na vs. (Al + Fe + Ti)/3 - K diagram (Moine & de la Roche, 1968) – DDH-103

The Paleoproterozoic gneisses from the DDH-103 (Yablonevka area) are peraluminous with relatively high SiO_2 and Al_2O_3 contents. Fe_2O_3 content is also high due to the intensive

processes of hematization in the vicinity of the pre-Riphean unconformity surface. MgO is about 2.5 – 3 wt % on average. They are also relatively rich in potassium. Loss on ignition remains moderate in the slightly altered gneisses.

In the diagram (Al + Fe + Ti)/3 - Na versus (Al + Fe + Ti)/3 - K (Moine & de la Roche, 1968) these rocks plot between the shale field and illite (Fig. 2.55). Therefore they correspond to allow to former illite-rich pelitic rocks.

Trace elements distribution of the Paleoproterozoic basement rocks of the Western (Yablonevka – DDH-103) Pasha – Ladoga basin area have been represented in chondrite-normalized spidergram (Fig. 2.56) and chondrite-normalized REE patterns diagram (Fig. 2.57).

The Paleoproterozoic gneisses from DDH-103 are characterized by a strong enrichment in all incompatible elements and especially in U and Th near the vicinity of the unconformity surface (7 and 42 ppm correspondingly), but also 16 meters below (6 and 45 ppm correspondingly).

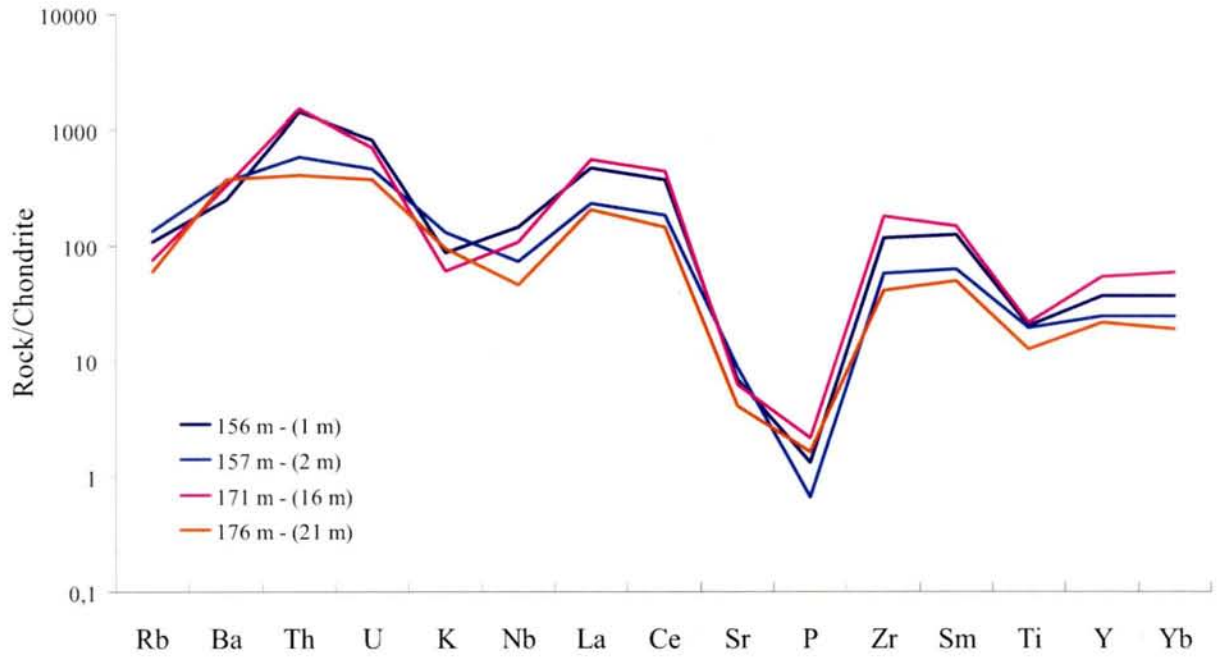

Fig. 2.56. Chondrite-normalized trace element patterns of the Paleoproterozoic basement formations of the Western (Yablonevka) Pasha – Ladoga basin area – DDH-103 (spidergram type after Holm (1979); chondrite composition after E. Anders and N. Grevesse: http://earthref.org/GERM/reservoirs/C1.htm)
In the brackets – distances to the unconformity surface are listed

The Paleoproterozoic gneisses (Fig. 2.57) of DDH-103 have highly fractionated REE patterns ($(Ce/Yb)_N$ = 7.5 - 10) and distinct Eu anomaly in the vicinity of the unconformity and 16 meters below (Eu/Eu* = 0.26 - 0.28) but becoming weak for two other samples (Eu/Eu* = 0.5 – 0.7). A slight depletion of intermediate HREE is observed in samples DDH-103-156 m and 171 m but id not clear for the two others.

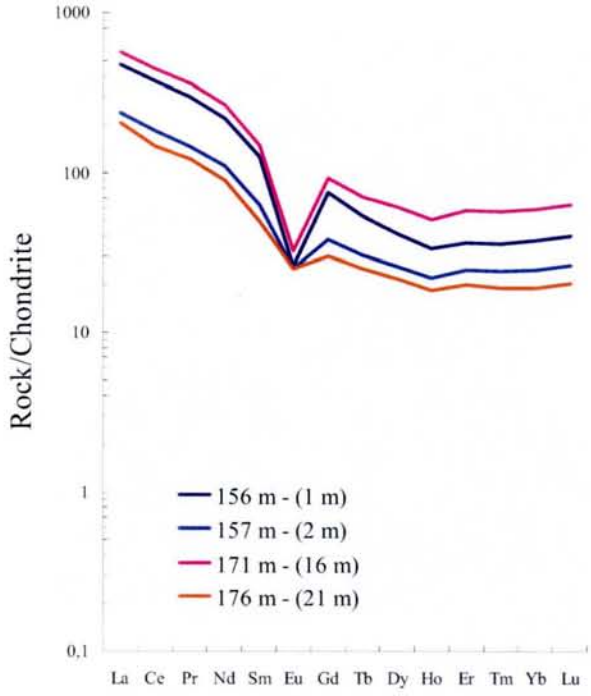

Fig. 2.57. Chondrite-normalized REE distribution patterns of the Paleoproterozoic basement formations of the Western (Yablonevka) Pasha – Ladoga basin area – DDH-103 (chondrite composition after Anders & Grevesse: http://earthref.org/GERM/reservoirs/C1.htm). In the brackets – distances to unconformity surface

Part 4. Paleoproterozoic basement formations of the South-Eastern Pasha – Ladoga basin area (on example of the drill cores – DDH-11, 14)

2.4.1. Geological setting

Crystalline basement of the South-Eastern area of the Pasha – Ladoga basin is represented by Archean – Paleoproterozoic rocks (Fig. 2.58). The Archean granite-gneisses, granites, plagiogranites, migmatites belong to dome structures, which are overlaid by the Paleoproterozoic (Kalevian – Ludikovian) biotite, biotite-amphibole gneisses and schists, minor garnet-cordierite-biotite, amphibole and biotite-amphibole gneisses. The Paleoproterozoic gneisses and schists are usually graphite-bearing. The Archean – Paleoproterozoic rocks were metamorphosed to the *amphibolite* facies at medium pressure and migmatized to a variable degree. In the south-eastern part of the area Late Paleoproterozoic plagio-microcline porphyroblastic granites are widespread. In the northern part of the area the Mesoproterozoic rapakivi granites (Ulyalegi and Lodeinopolsky satellites of the Salmi batholith – see Part 5 of this Chapter) were emplaced, intruding all rock types.

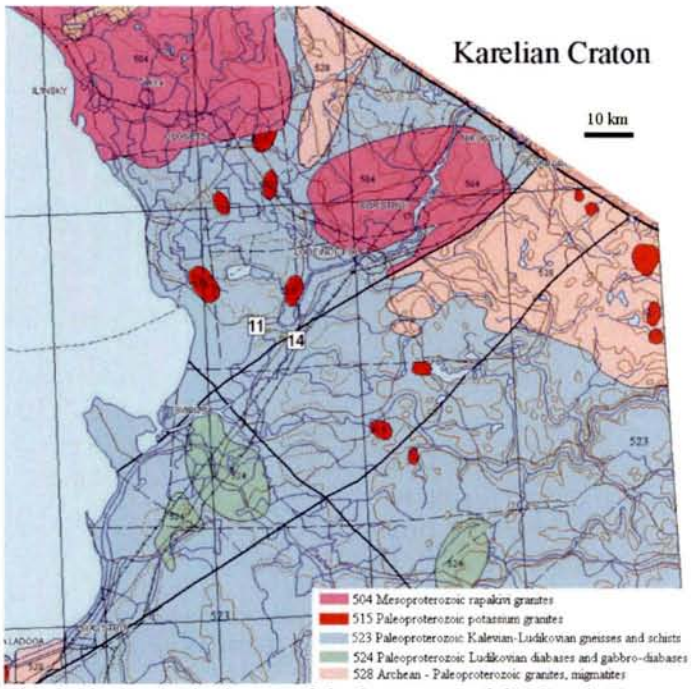

Fig. 2.58. Geological map of the basement of the South-Eastern Pasha – Ladoga basin area (after Geological map of the pre-Middle Riphean formations of the Pasha – Ladoga area in a scale 1 : 500 000 (Petrov, Caillat, Naumov, 2004).
DDH-11 and DDH-14 positions are shown in the map

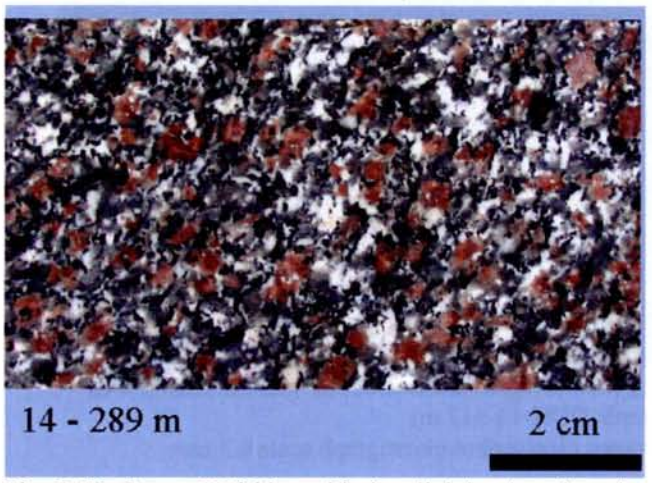

Fig. 2.59. Quartz-K feldspar-biotite slightly altered gneiss (Pasha area – DDH-14-289 m)

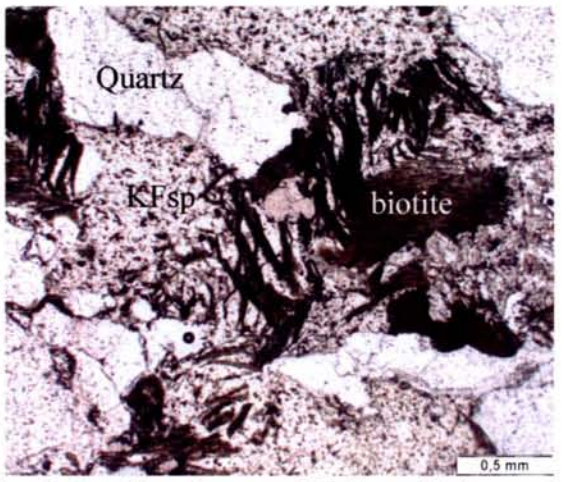

Fig. 2.60. Altered quartz-K Feldspar-biotite gneiss (sample DDH-14-289 m)
Parallel nicols, photomicrograph scale 0.1 mm

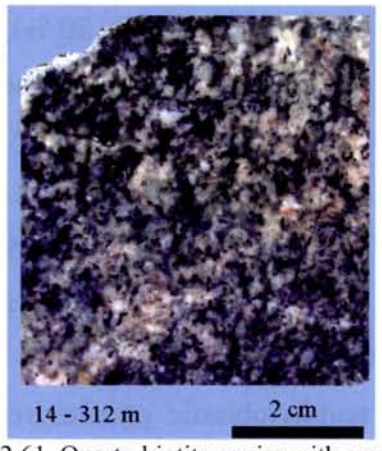

Fig. 2.61. Quartz-biotite gneiss with graphite (Pasha area - sample DDH-14-312 m)

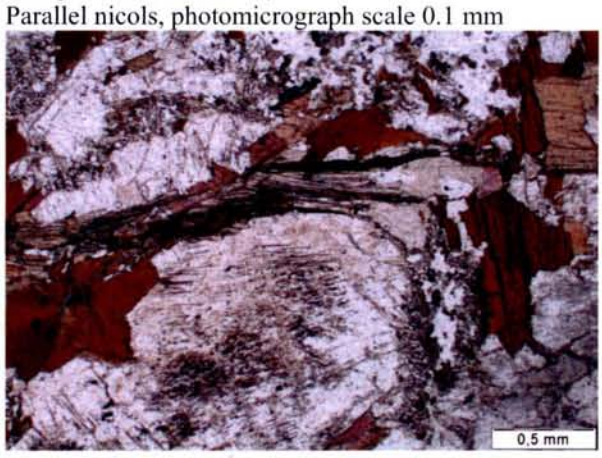

Fig. 2.62. Quartz-feldspar-biotite gneiss with graphite (sample DDH-11-283 m), parallel nicols, photomicrograph scale 0.5 mm

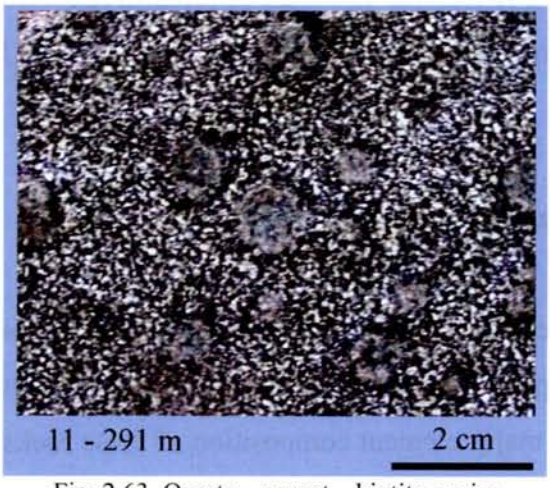

Fig. 2.63. Quartz – garnet – biotite gneiss (Pasha area - sample DDH-11-291 m)

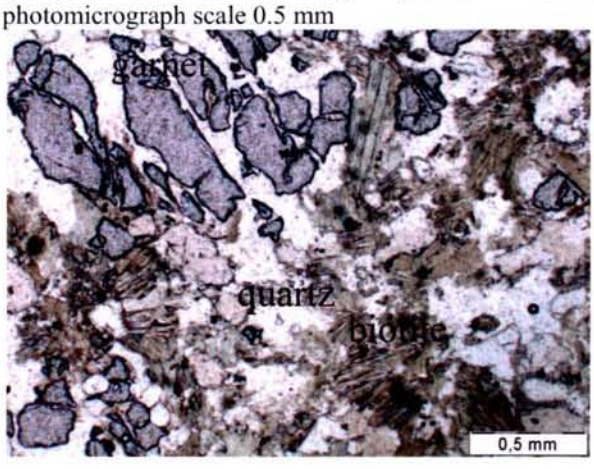

Fig. 2.64. Quartz – garnet – biotite gneiss (DDH-11-291 m), parallel nicols, photomicrograph scale 0.5 mm

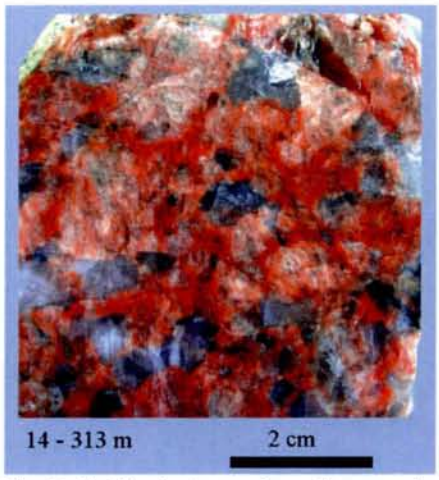

Fig. 2.65. Plagioclase-microcline granite (Pasha area – sample DDH-14-313 m)

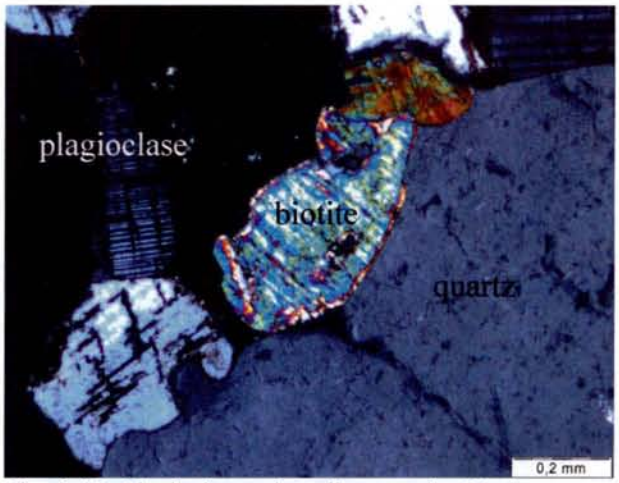

Fig. 2.66. Plagioclase-microcline granite (Pasha area – sample DDH-14-313 m)
Crossed nicols, photomicrograph scale 0.2 mm

Quartz-K feldspar-biotite and quartz-biotite gneisses sometimes with graphite (Fig. 2.59 – 2.62) are widespread rocks, which consist of quartz (40 %), K feldspar (10 – 20 %), biotite (15 – 25 %), plagioclase (10 %). Accessory minerals are graphite, zircon and hematite. Quartz-garnet-biotite gneisses are also present (Fig. 2.63 – 2.64). Alteration "regolith" profile is also widespread and is mostly represented by 10 – 30 m thick hematized gneisses. Kaolinite is also a typical alteration mineral. An alteration zone of intensive hematization (0.5 – 2 m thick) is a characteristic feature of this area and is usually observed in the vicinity of the pre-Riphean unconformity surface (Mikhailov et al., 2000; Pichugin, 2000).

The Late Paleoproterozoic plagioclase-microcline porphyroblastic granites represent abundant small bodies within the Paleoproterozoic gneisses and schists (Fig. 2.65 - 2.66). Red-rose granites consist of plagioclase (30 – 40 %), K feldspar (20 – 25 %), quartz (20 – 25 %) and biotite (5 %). Accessory minerals are zircon, allanite. They are usually enriched in U (5 – 8 ppm) (Mikhailov et al., 2000).

2.4.2. Petrogeochemistry of the basement formations

The geochemistry of major and trace elements has been studied in two drill cores (DDH-11, DDH-14). Major and trace element composition of the Paleoproterozoic basement rocks is listed in Annex Pasha basement rocks. The major element composition of these rocks is also listed in the Table 2.12.

The Paleoproterozoic gneisses are generally peraluminous felsic rocks with high SiO_2 and Al_2O_3 contents. The analyzed Paleoproterozoic granite is extremely rich in silica (79.5 wt. %) and sodium (6.7 wt. % - normative albite) and leucocratic (normative biotite is absent).

In the diagram (Al + Fe + Ti)/3 - Na versus (Al + Fe + Ti)/3 - K (Moine & de la Roche, 1968) which allow to distinguish sedimentary from magmatic rocks (Fig. 2.67) and in the Al + Fe + Ti versus Ca + Mg diagram (Fig. 2.68), most samples are located in the sedimentary field (except one granite sample) and three main groups can be distinguished:

- DDH-11: all samples plot in the field of former shales (with K > Na) in the (Al + Fe + Ti)/3 - Na vs. (Al + Fe + Ti)/3 - K diagram (Fig. 2.67);
- DDH-14 most samples correspond to former greywackes (with Na > K) in the (Al + Fe + Ti)/3 - Na vs. (Al + Fe + Ti)/3 - K diagram (Fig. 2.67), sample DDH-14-289 (altered gneiss from the unconformity surface) also can correspond to the former greywacke;
- Plagioclase-microcline granite from the DDH-14 is an acidic magmatic rock.

Reference	1	2	3	4	5	6	7	8	9	10
DDH	11-269-2	11-270	11-281	11-283	11-287	11-291	14-289	14-301	14-312	14-313
SiO_2	61.55	62.46	64.93	61.00	75.06	58.76	70.19	67.08	69.93	79.41
Al_2O_3	16.21	17.13	8.01	15.03	14.11	16.84	17.22	14.90	15.19	12.63
Fe_2O_3	10.04	8.34	4.49	7.96	0.85	9.28	2.71	4.97	2.87	0.00
MnO	0.04	0.00	0.59	0.11	0.00	0.06	0.00	0.06	0.00	0.00
MgO	2.64	2.18	4.80	4.10	0.66	4.19	0.37	2.49	0.82	0.00
CaO	0.00	0.16	5.04	0.76	0.47	0.34	0.00	3.64	1.65	0.00
Na_2O	0.00	0.00	0.00	0.26	0.15	0.18	0.16	1.92	3.49	6.66
K_2O	4.10	2.34	1.99	5.69	1.18	4.42	4.04	2.05	4.60	0.80
TiO_2	0.70	0.77	0.56	0.67	1.03	0.87	0.28	0.55	0.37	0.00
P_2O_5	0.10	0.18	0.06	0.10	0.31	0.11	0.2	0.22	0.15	0.06
PF	4.35	5.70	9.30	4.22	6.01	4.81	4.63	1.95	0.88	0.15
Total	**99.73**	**99.25**	**99.77**	**99.90**	**99.83**	**99.86**	**99.8**	**99.83**	**99.95**	**99.71**

Table 2.12. Major element composition of the Paleoproterozoic basement rocks of the South-Eastern Pasha – Ladoga basin area: 1 - 5 - quartz – feldspar-biotite gneisses with graphite; 6 – quartz-garnet-biotite gneiss; 7 – 9 – quartz-feldspar-biotite gneisses; 10 – plagioclase-microcline granite. DDH number and depth of the samples are listed.

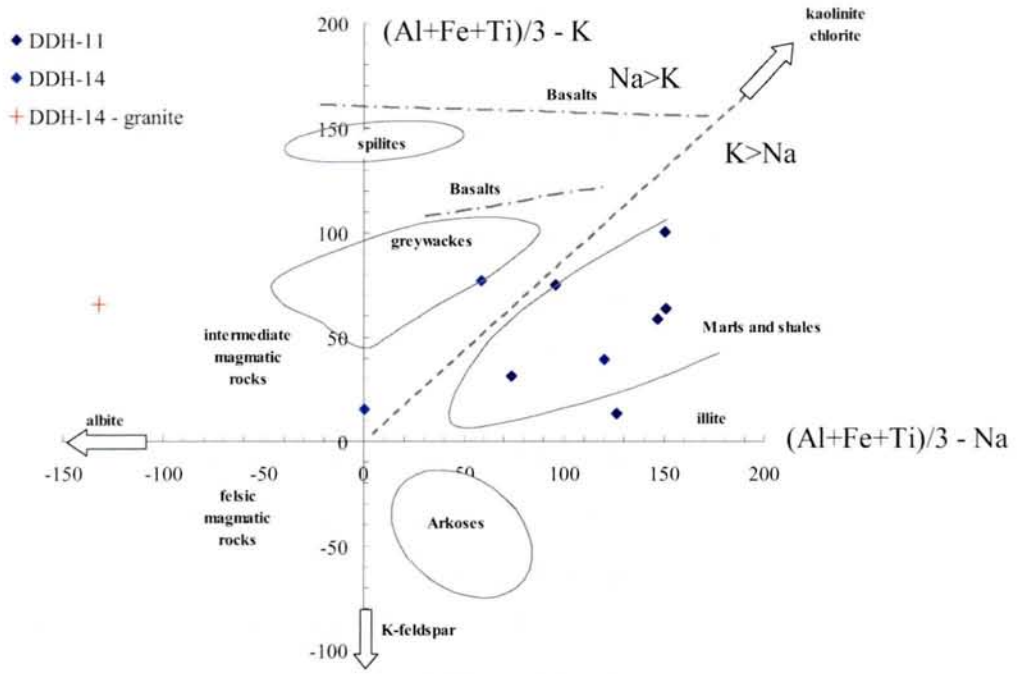

Fig. 2.67. The Paleoproterozoic gneisses of the Southern Pasha – Ladoga basin area in the (Al + Fe + Ti)/3 – Na vs. (Al + Fe + Ti)/3 - K diagram (Moine & de la Roche, 1968)

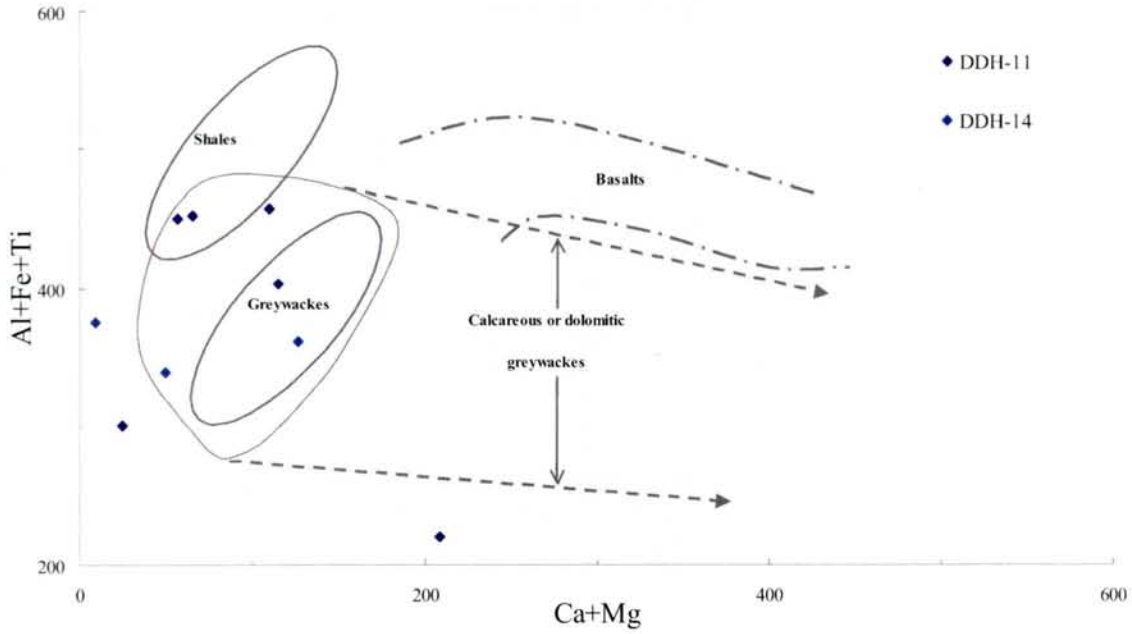

Fig. 2.68. The Paleoproterozoic gneisses of the Southern Pasha – Ladoga basin area in the (Ca + Mg) vs. (Al + Fe + Ti) diagram (Moine & de la Roche, 1968)

Trace elements distribution of the Paleoproterozoic basement rocks of the South-Eastern Pasha – Ladoga basin area have been represented in chondrite-normalized spidergrams (Fig. 2.69 – 2.70) and chondrite-normalized REE patterns diagram (Fig. 2.71).

Trace elements composition of the Paleoproterozoic gneisses in DDH-11 and DDH-14 are characterized by an extreme enrichment in all incompatible elements with relatively high U - 3 – 7 ppm, moderate Th - 4 – 20 ppm, high Rb (80 - 260 ppm), Ba (100 – 1300 ppm) and Sr (20 - 200 ppm), accessory minerals are mostly represented by zircon and possibly xenotime (Zr = 100 - 450 ppm, Y = 8 - 55 ppm, Nb = 7 - 18 ppm).

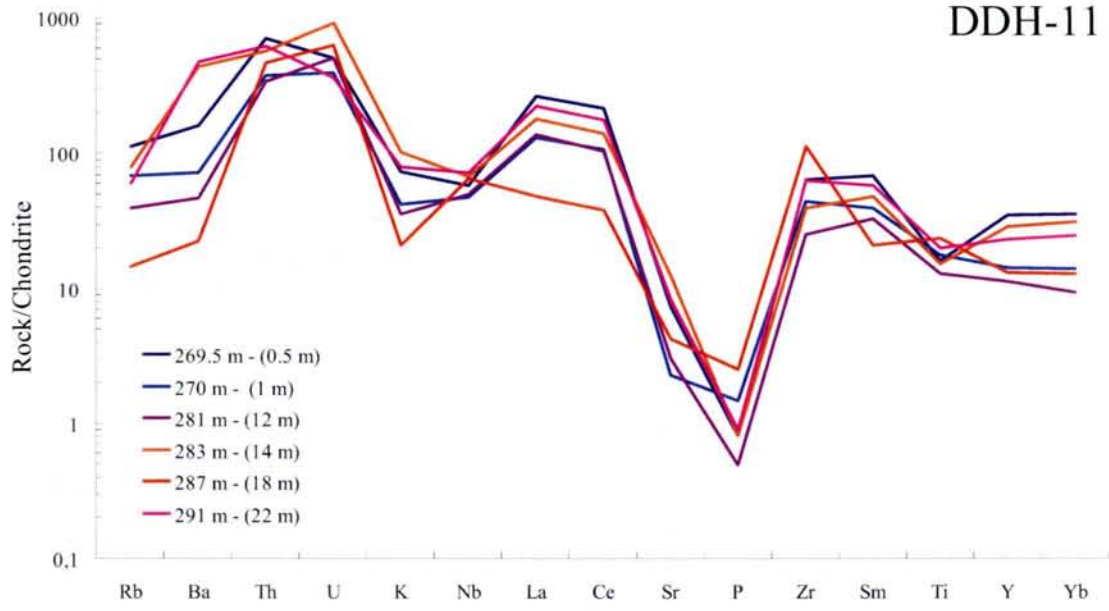

Fig. 2.69. Chondrite-normalized trace element patterns of the Paleoproterozoic basement formations of the South-Eastern Pasha – Ladoga basin area – DDH-11 (spidergram type after Holm (1979); chondrite composition after E. Anders and N. Grevesse: http://earthref.org/GERM/reservoirs/C1.htm)

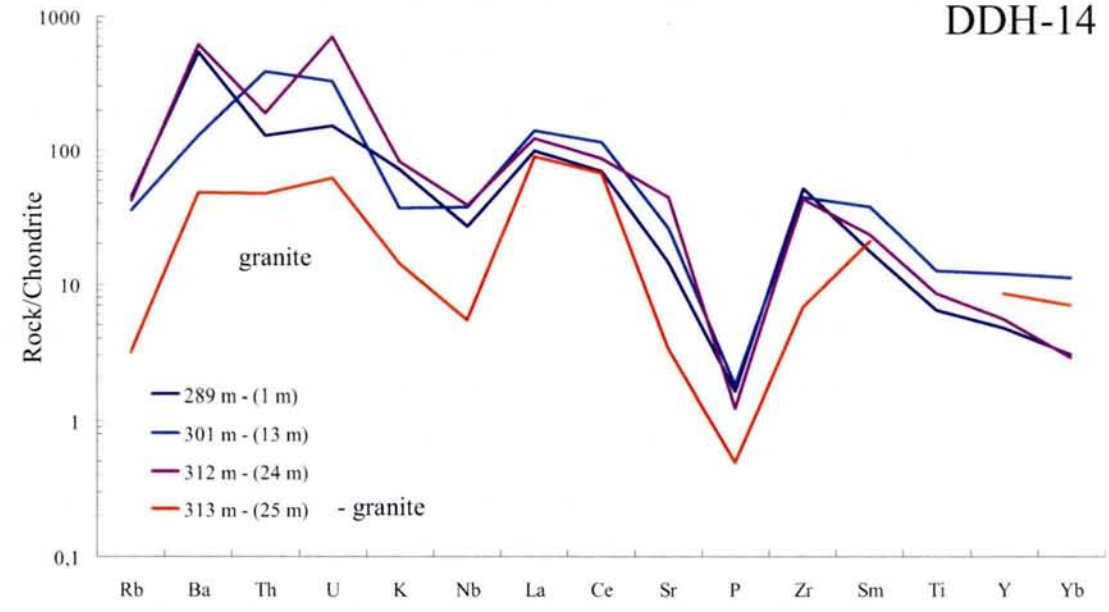

Fig. 2.70. Chondrite-normalized trace element patterns of the Paleoproterozoic basement formations of the South-Eastern Pasha – Ladoga basin area – DDH-14 (spidergram type after Holm (1979); chondrite composition after E. Anders and N. Grevesse: http://earthref.org/GERM/reservoirs/C1.htm)

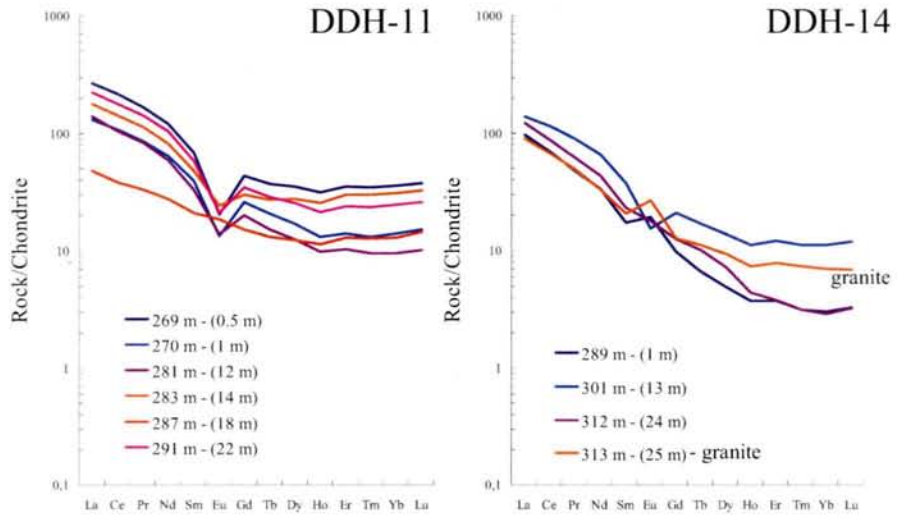

Fig. 2.71. Chondrite-normalized REE distribution patterns of the Paleoproterozoic basement formations of the South-Eastern Pasha – Ladoga basin area – DDH-11 and DDH-14 (chondrite composition after Anders & Grevesse: http://earthref.org/GERM/reservoirs/C1.htm). In the brackets – distance to unconformity surface

The Paleoproterozoic plagioclase-microcline granite is surprisingly not rich in U (0.45 ppm) and Th (1.4 ppm) and in all other analyzed trace elements.

The Paleoproterozoic gneisses (Fig. 2.71-A) in the DDH-11 have distinctly fractionated REE patterns ($(Ce/Yb)_N$ = 6-7) and distinct Eu anomaly (Eu/Eu* = 0.4 - 0.5) (except sample 11-287, which is characterized by no Eu anomaly).

The Paleoproterozoic gneisses (Fig. 2.71-B) in the DDH-14 have well-fractionated REE patterns ($(Ce/Yb)_N$ = 10 - 30). Eu anomaly is different in all samples : in the vicinity of the unconformity surface and in the granite it has positive value (Eu/Eu* = 1.5 – 1.7); in 13 meters from the unconformity surface it does not exist (Eu/Eu* = 1); at a depth of 24 meters from the unconformity, immediately above the granite sample the Eu anomaly is distinctly negative (Eu/Eu* = 0.6).

For a better understanding of the trace elements (Fig. 2.72) and rare-earth elements (Fig. 2.73) distribution with depth and their alteration degree the gneiss geochemistry was examined according to their depth position in the drill holes in the vicinity of the Pre-Riphean unconformity surface and compared with average "former shale" (Table 2.8) – as done also for the Paleoproterozoic gneisses and schists of the Salmi area.

In DDH-11 (Fig. 2.72-A) trace elements distribution was compared with the average of "former shale". In the vicinity of the unconformity surface we have enrichments in Rb, Ba, Th, LREE, Y and Yb and depletion in Ba and Sr. Maximum U content is observed at 14 meters from the unconformity. With depth Rb is slightly depleted, whereas Ba, Sr, Nb are slightly enriched.

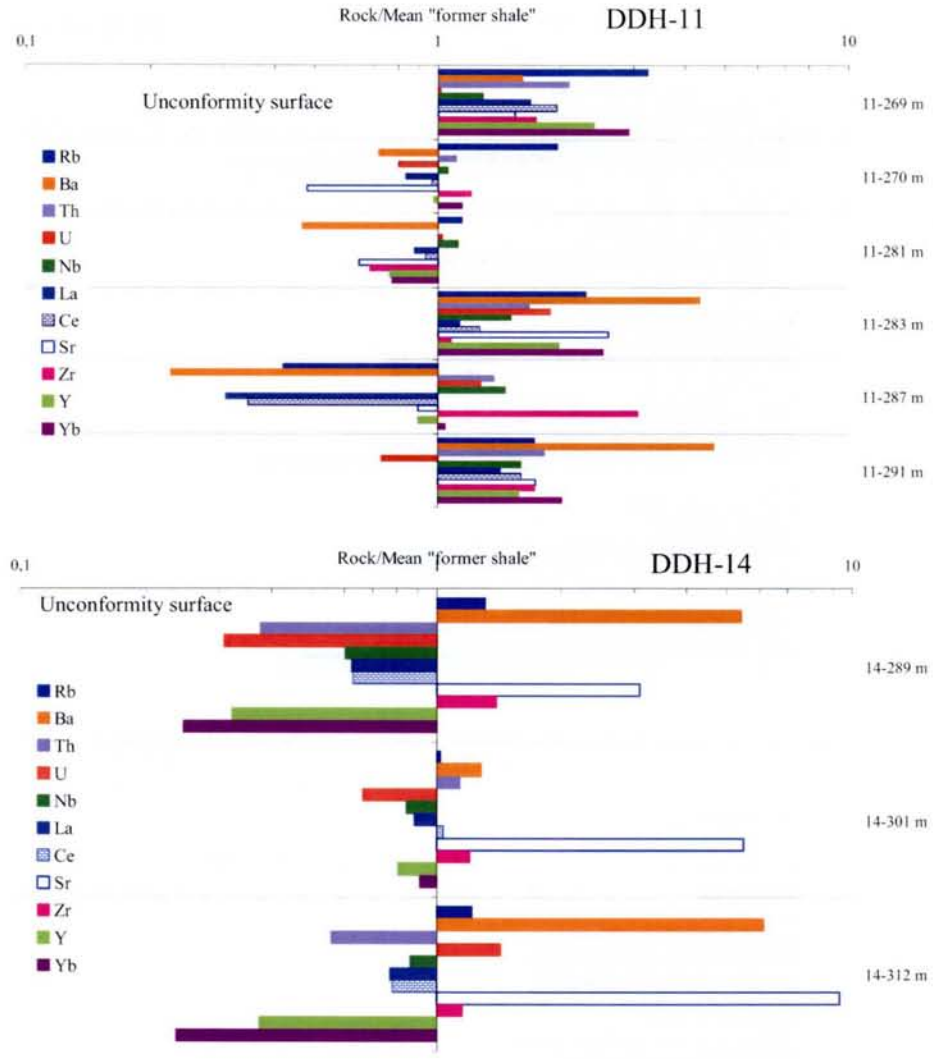

Fig. 2.72. Trace element distribution in the Paleoproterozoic gneisses of the South-Eastern Pasha – Ladoga basin area according to the drill hole and their depth

In DDH-14 (Fig. 2.72-B), close to the unconformity surface Rb, Sr, Ba, are relatively enriched, at a moderate depth they are depleted and at a distance of 23 meters from the unconformity they have the same values or are slightly enriched. Th, LREE, Y and Yb are have the same values as the average shale, but Ba and Sr are depleted. Near the unconformity and at depth Th, LREE, Y and Yb are depleted and have their maximum at a moderate depth (DDH-14-301 m). Maximum U content is observed at 23 meters from the unconformity.

REE distribution with depth is shown in Fig. 2.73. There is no significant variation in REE distribution with depth for both analyzed drill holes.

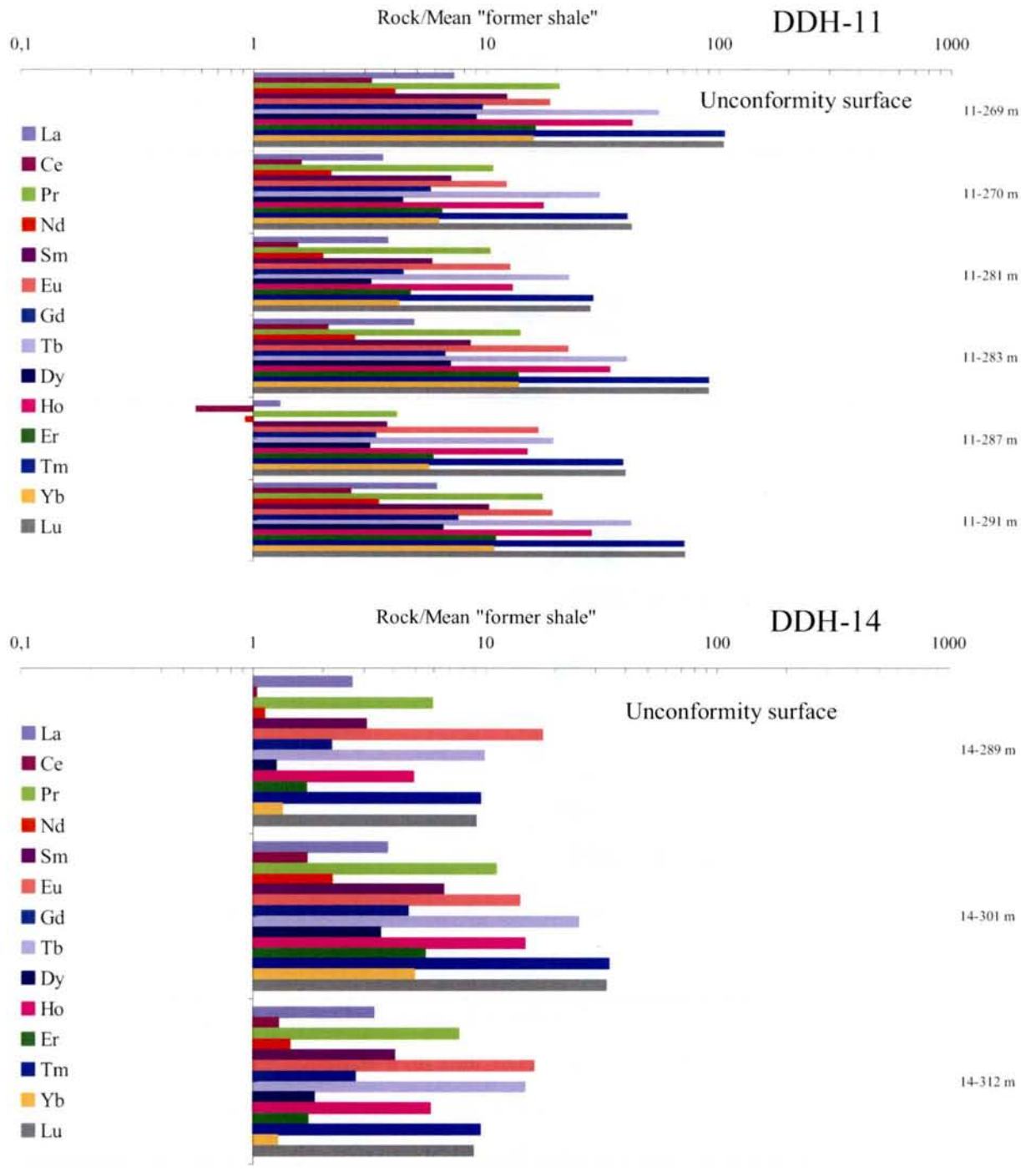

Fig. 2.73. REE distribution in the Paleoproterozoic gneisses of the South-Eastern Pasha – Ladoga basin area in concerning to their DDH position and depth of the samples

Part 5. Early Mesoproterozoic anorthosite – rapakivi granite magmatism: the Salmi pluton

2.5.1. Geological setting

The emplacement of the classic 1.65 – 1.54 Ga rapakivi granites was the last major crustal increment to the Fennoscandian (Baltic) shield during Mesoproterozoic (Kohonen & Ramo, 2004) (Fig. 2.72). The rapakivi granites and associated basic rocks are typical anorogenic rocks and they sharply cut the surrounding Svecokarelian and Archean orogenic formations. Most of the plutons show multiple intrusions, some of which form satellite stocks outside the main pluton (Laitakari et al, 1996).

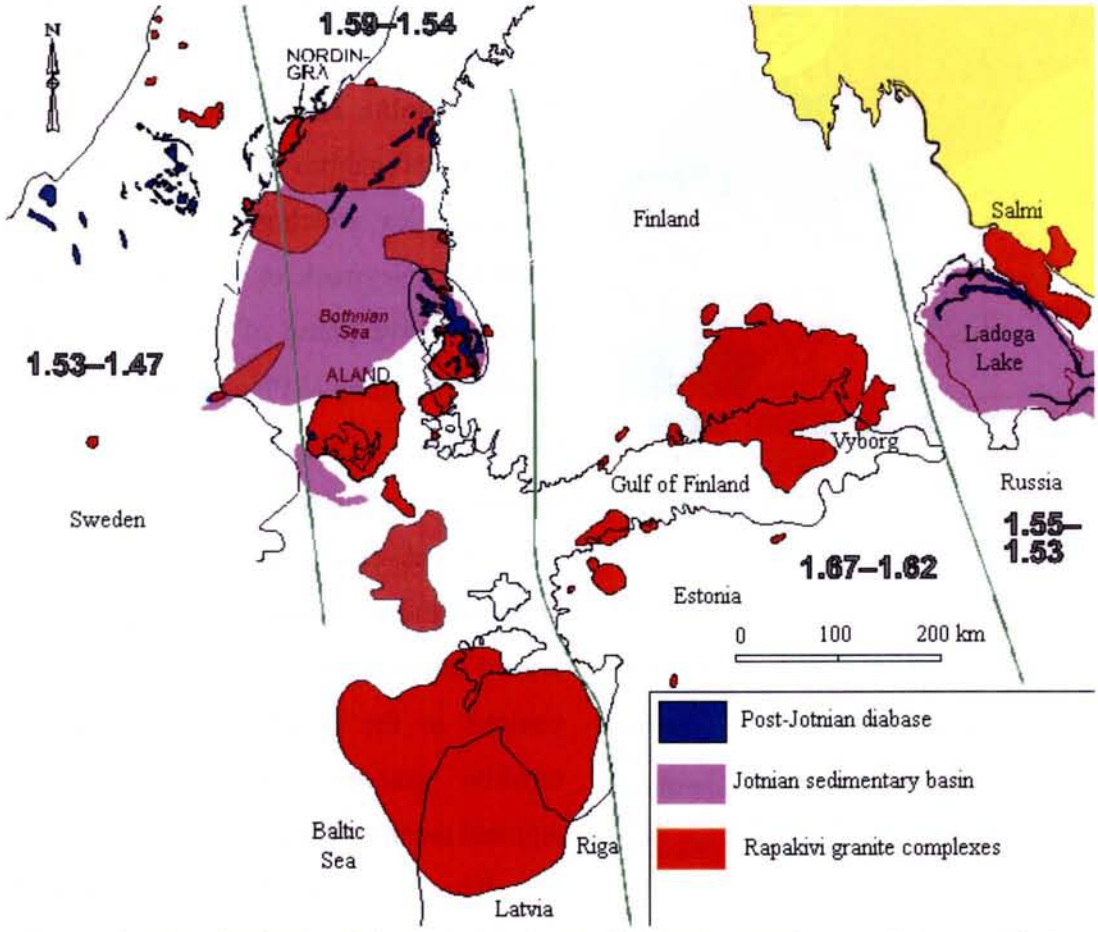

Fig. 2.72. Map showing distribution of the 1.67–1.47 Ga rapakivi granite complexes, mid-Proterozoic (Jotnian or Riphean; 1.4–1.3 Ga) sedimentary basins, and mafic (Post-Jotnian) dikes and sills in southern Finland and adjacent Sweden and Russia. Thin green lines delineate different age groups of rapakivi granites (ages denoted in Ga). Postjotnian mafic magmatism is dated at 1.27–1.26 Ga in south-western Finland (Suominen, 1991), but is clearly older (circa 1.46 Ga) in the Lake Ladoga basin in Russian Karelia (after Rämö et al., 2001)

Two main rapakivi intrusions belong to the Ladoga Lake district: the Vyborg batholith with U-Pb ages of 1.645 to 1.625 Ga (Vaasjoki et al., 1991) on the western part and Salmi batholith with Ulyalegi and Lodeinopolsky satellites with U-Pb ages of 1.547 to 1.530 Ga (Neymark et al., 1994, Amelin et al., 1997).

For the first time P. Eskola described the Salmi batholith in 1930 (Eskola, 1930) and later was the object of detailed studies by L. Sviridenko (1968).

Salmi batholith and enclosing Archean-Paleoproterozoic basement

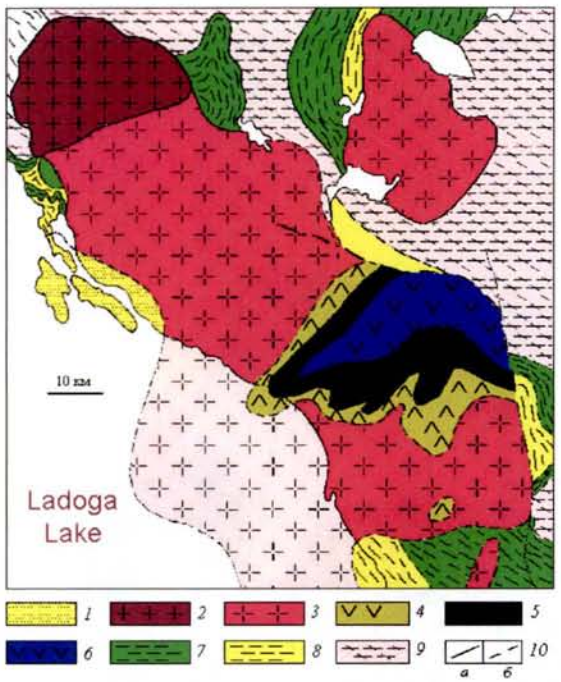

Fig. 2.73. Geological map of the Salmi rapakivi batholith and Ulyalegi satellite area (after Sharkov, 1999)

1 - Mesoproterozoic Salmi volcanic-sedimentary suite; 2 - rose even-grained biotite granites; 3 – rose amphibole-biotite rapakivi granite of the main phase; 4 - grey rapakivi granites and diorites; 5 - monzonites and quartz monzonites; 6 - gabbro-norites - anorthosites and norites; 7 - 8 - Late Paleoproterozoic volcanic-sedimentary formations: 7 – Paleoproterozoic (Jatulian) formations of the Karelian Craton, 8 - Svecofennian formations of the Kitelya series; 9 - Archean tonalite-gneisses; 10 - boundaries: a - traceable, b - probable.

Boundaries in the southern part of the batholith are after geophysical and drilling investigations (Bantova et al., 1975). Dotted line shows western continuation of the batholith under water level of the Ladoga Lake from geophysical investigations (Berkovsky, pers com. 1975 to Sharkov)

In Russian Karelia, the Salmi rapakivi granite – anorthosite batholith (and its Ulyalegi and Lodeinopolsky satellites) is the youngest rapakivi pluton in the Ladoga Lake area (Fig. 2.73). The emplacement of the Salmi batholith started about 1560 Ma with intrusion of gabbro and anorthosite of the early complex, which gives U - Pb ages about 1560 Ma (Neymark et al., 1994). Then, the main intrusive phase of the Salmi batholith has been dated by U-Pb ages at 1539 ± 11 Ma (Suominen, 1991) and 1543 ± 8 Ma (Neymark et al., 1994).

It was emplaced in an upthrust zone between the Paleoproterozoic and Archean crustal domains, intruding all rock types. In contrast to the basement rocks, the Salmi rapakivi granites did not undergo any regional metamorphism.

The Salmi batholith is well exposed in its northern part, but the Mesoproterozoic (Riphean) volcanic-terrigenous rocks of the Pasha – Ladoga graben, overlie its southwestern part. Also, all the southern part

of the pluton with Lodeinopolsky satellite is overlaid by quaternary sediments and only geophysical and rare drilling investigations gave some information about pluton structure.

The Salmi batholith is about 125 km long in NE-SW direction. According to gravity and magnetic geophysical data, the Salmi batholith corresponds to a shallow sheet-like body with a thickness of about 10 km in its central part (Velikoslavinsky, 1978). Geophysical investigations (Berkovsky, pers. com. 1975 to Sharkov) indicate that the western part of the batholith continues under the water level of the Ladoga Lake (Fig. 2.73).

The pluton is zoned. The southern non-exposed part consists of anorthosites, gabbros, and monzonites – syenites of the early intrusive phase. The northern exposed part consists of different granite types intruded in the following order:

(i) biotite – hornblende ovoidal granite;

(ii) biotite-amphibole ovoidal granite with fine-grained matrix;

(iii) even-grained biotite granite;

(iv) ovoidal porphyritic biotite granite with fine-grained matrix (Sviridenko, 1994).

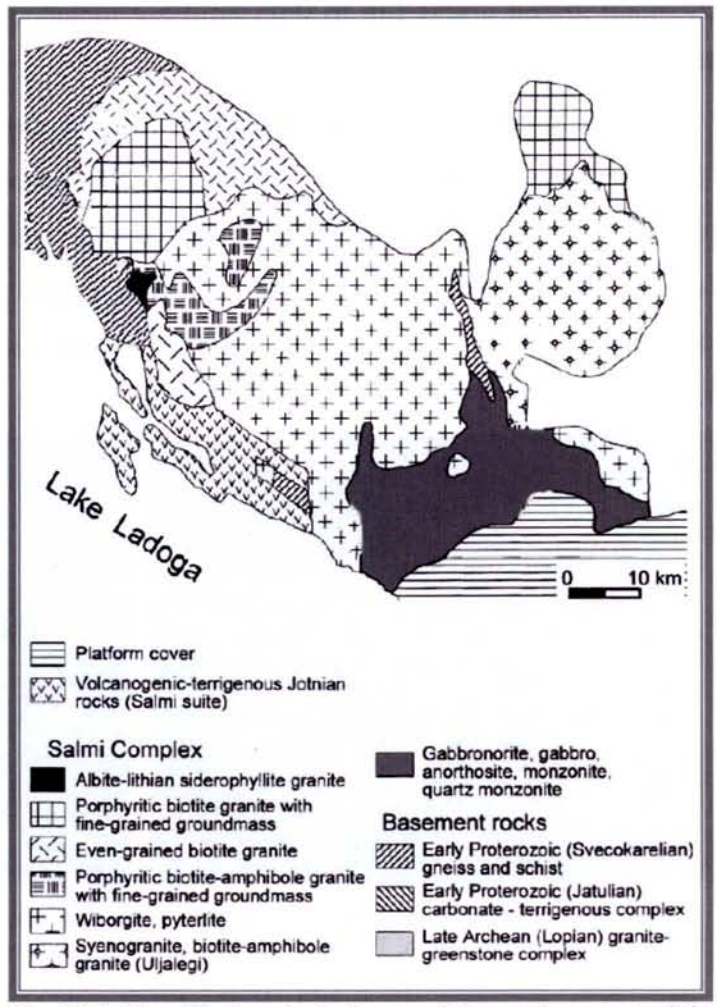

Fig. 2.74. Simplified geological map of the northern part of the Salmi anorthosite – rapakivi granite complex (after Amelin et al, 1997).

The latest phase corresponds to lithium - fluorine topaz - bearing leucocratic granites emplaces as dikes and small bodies. Globally the pluton structure can be interpreted as rough layered zoning, where gabbros and anorthosites are the lower member and inequigranular biotite and topaz-bearing granites are the upper members of magmatic differentiation (Sharkov, 1999).

Among the variety of structural types of granites, two major ones were recognized: ovoidal biotite – hornblende rapakivi granites (vyborgite, pyterlite and porphyritic) and non-ovoidal essentially biotitic granite (equigranular or inequigranular), Sviridenko, (1994).

2.5.2. Petrographic description of main rock types

Typical gabbro-norite of the early phase of the Salmi pluton is a medium-grained dark-grey rock, which consists of plagioclase (An_{40-60}) – 50 – 55 %, clinopyroxene and orthopyroxene – 20 – 25 %, orthoclase - 10 %, biotite - 2 %, quartz – 1 – 2 %, apatite, ilmenite and titanomagnetite. Plagioclase forms tabular crystals sometimes with orthoclase-antiperthite. Orthoclase-microperthite is located in interstitial phase together with quartz. Very small zircon grains (up to 0.05 mm) are included in plagioclase (after Amelin et al., 1997).

Grey medium- to coarse-grained monzonite is composed of plagioclase (An_{35-55}) – 25 – 30 %, orthoclase-microperthite – 50 – 55 %, clinopyroxene + orthopyroxene – 8 – 10 %, quartz – 3 – 5 %. Accessory minerals are apatite and zircon. Apatite is associated with pyroxene. Elongated crystals of zircon (up to 0.4 mm) are interstitial and located between feldspar grains. Myrmekites are located on the boundaries between plagioclase and orthoclase (after Amelin et al., 1997).

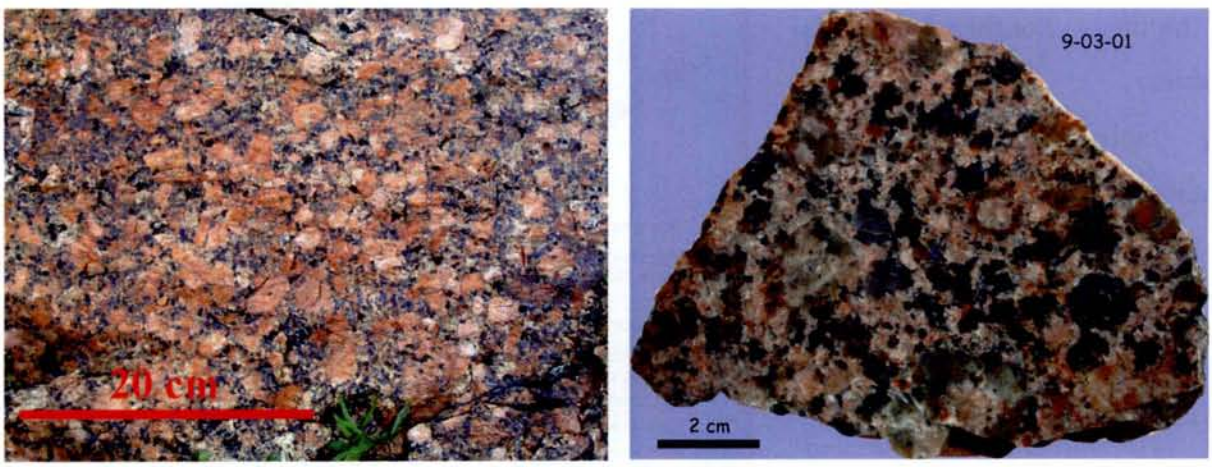

Fig. 2.74. Ovoidal coarse-grained biotite-amphibole rapakivi granite of the main phase of the Salmi pluton (south-western part of the pluton, Tulema river bank near hydroelectric power station). Sample 9-03-01 (2003)

Ovoidal biotite-amphibole rapakivi granite with plagioclase mantle on K-feldspar ovoids (vyborgite – term after Sviridenko (1968)) presents main the most widespread intrusive phase. Sample 9-03-01 (south-western part of the Salmi complex) was collected from an outcrop on the bank of river Tulema about 10 km from the village of Salmi (Fig. 2.74). This is a porphyritic pink granite with K-feldspar ovoids ranging in size from 2 to 4 cm with a medium-grained groundmass consisting of orthoclase, plagioclase An_{15-27}, quartz, biotite, amphibole. Accessory minerals are fluorite, zircon, apatite and ore minerals.

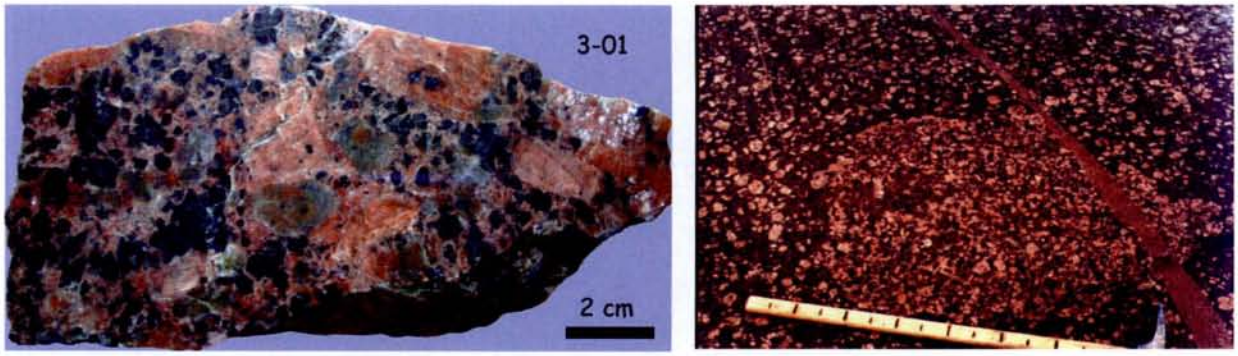

Fig. 2.75. Non-ovoidal coarse-grained amphibole-biotite rapakivi granite of the main phase of the Salmi pluton (southern part of the pluton, Ladoga Lake shore near Pogran-Kondushi village). Sample 3-01(2003)

Ovoidal biotite-amphibole rapakivi granite, but with rare or without plagioclase mantle on K-feldspar ovoids (pyterlite – term after Sviridenko (1968)), was collected in the southern part of the Salmi pluton (Ladoga Lake shore near Pogran-Kondushi village) (Fig. 2.75). Pink porphyritic amphibole-biotite granites with coarse-grained groundmass consist of microcline-perthite, plagioclase (An_{17-20}), quartz, biotite, amphibole. Accessory minerals are zircon, apatite and fluorite.

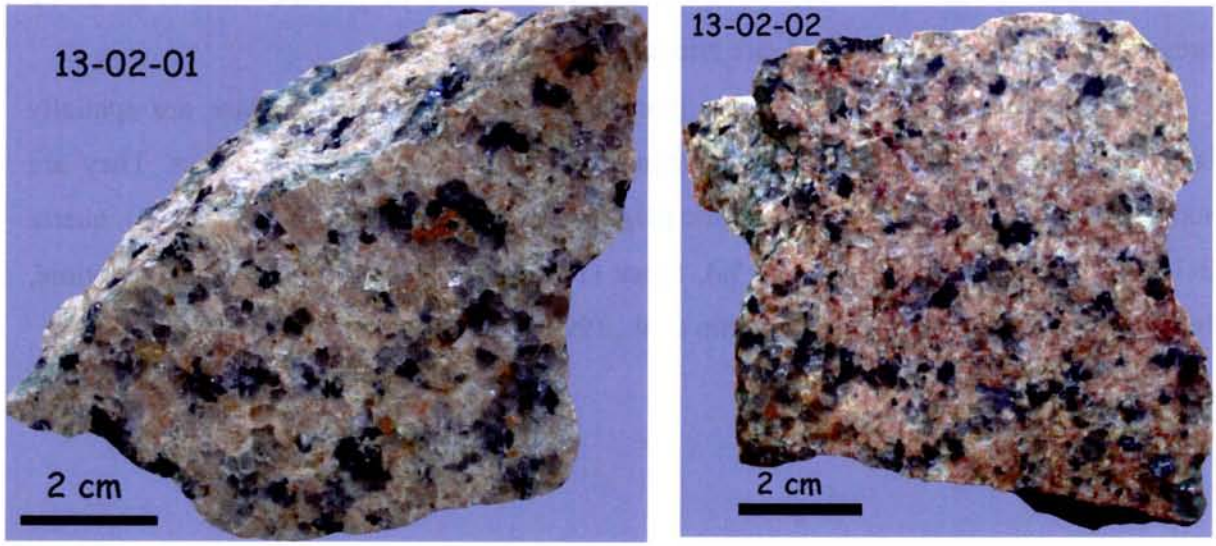

Fig. 2.76. Even-grained biotite granite from the south-western part of the Salmi pluton (Satulinoya river near Uuksu village) Sample 13-02-01 and 13-02-02 (more altered) (2003)

The light-rose to light-red even medium grained biotite granite, is a relatively widespread rock in the south-western part of the Salmi pluton. They consist of orthoclase-perthite, plagioclase An $_{18-23}$, quartz and biotite. Accessory minerals are zircon and fluorite (Fig. 2.76).

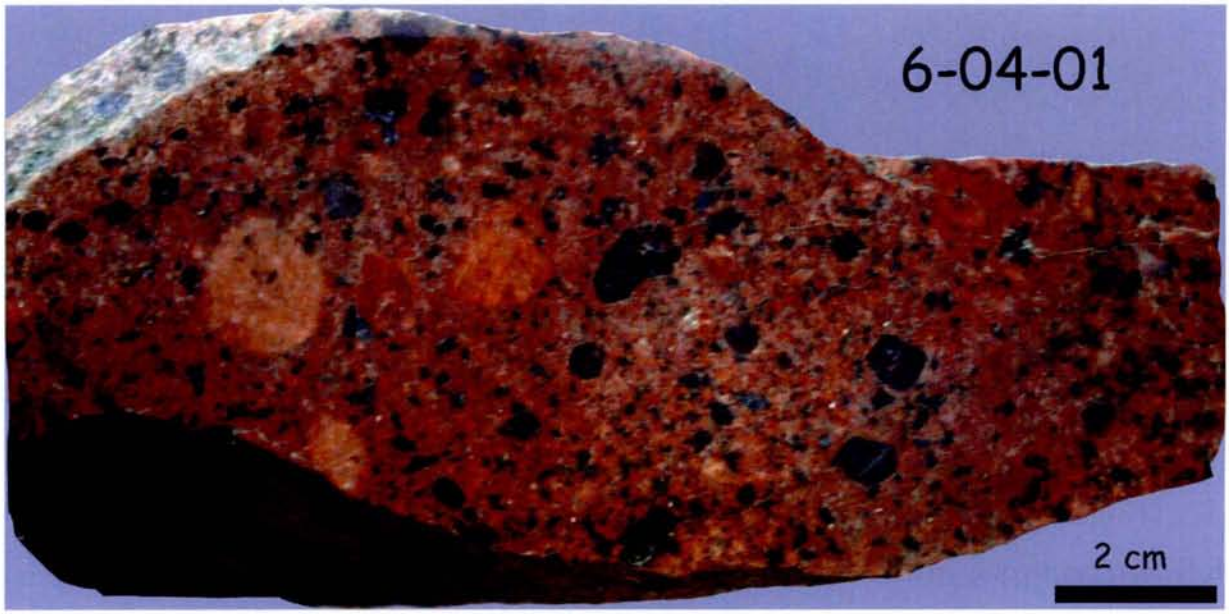

Fig. 2.77. Porphyritic pink biotite granites with K-feldspar ovoids and a fine-grained groundmass from the western contact of the Salmi pluton with Archean domes (Lupikko dome). Sample 6-04-01 (2003)

Porphyritic pink biotite granites with K-feldspar ovoids and a fine-grained groundmass are composed of orthoclase-perthite (about 40 %), plagioclase (An_{5-18}) (about 30 %), quartz (25-30 %) and biotite (1-3 %). Some of the ovoids have plagioclase rims (Fig. 2.77). Accessories are mainly fluorite and rare zircon.

The lithium-fluorine topaz-bearing granites of the late intrusive phase are spatially related to the porphyritic ovoidal biotite granites with fine-grained groundmass. They are composed of 40 % of predominantly albitic plagioclase (An_{5-18}), microcline (23-25 %), quartz (32-34 %), lithian siderophyllite (2-4 %), topaz (1-2 %). Accessory minerals are xenotime, columbite and rare monazite (after Amelin et al., 1997 and Poutiainen & Sherbakova, 1998).

2.5.3. Alteration processes in the rapakivi granites of the Salmi pluton

During their emplacement the rapakivi granites of the Salmi pluton have produced important transformation in surrounding Archean – Paleoproterozoic rocks. A contact metamorphism halo (some meters to some ten meters) is well observed in the surrounding rocks (Sviridenko, 1968). During the emplacement of the fluorine-lithium granite widespread albitization and greisenization processes also take place.

But more important for the present work, are the alteration processes which may have had an influence of the genesis of the uranium mineralization at Karku. These are:

(i) alteration, which takes place before Pasha – Ladoga basin sedimentation, when the rapakivi granites were weathered which may correspond to the so-called regolith zone,

(ii) diagenetic alteration, which takes place after the sedimentation of the Pasha – Ladoga basin,

(iii) hydrothermal alteration occurring during and after ore deposition.

Fig. 2.78. Salmi rapakivi granites along the Tulema river near a contact with the Mesoproterozoic Pasha – Ladoga volcanic-sedimentary sequences. Sight from the hydroelectric power station dam on the Tulema river

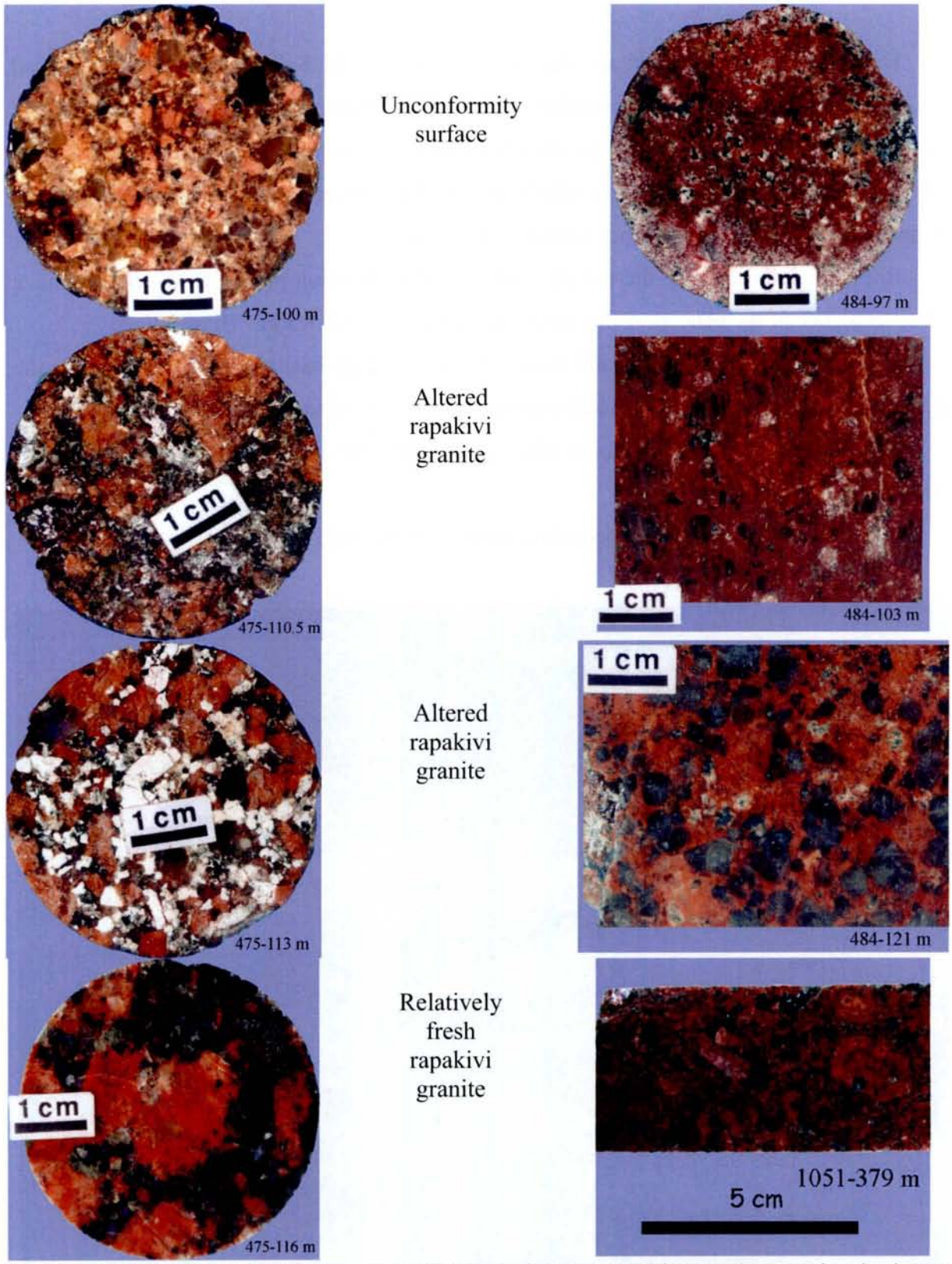

Fig. 2.79. Regolithic profiles developed on a rapakivi granite in DDH-475 and DDH-484 (DDH location in Part 1.4). Fresh varieties in DDH-484 are absent, the closest freshest sample to DDH-484 sample 1051-379 m is used for comparison along the section.

The Mesoproterozoic Priozersk conglomerates and the Salmi basalts overlie the Salmi rapakivi batholith over its western part along the northeastern shore of the Ladoga Lake.

In the vicinity of the Salmi village along the Tulema River it is possible to observe on outcrops and boulders the contact between the Salmi biotite – amphibole rapakivi granites of the main phase and the Salmi basalts (Fig. 2.78).

(i) Regolith alteration

The alteration, which may have taken place before the Pasha – Ladoga basin sedimentation, is observed in the DDH-475 (Salmi area – see for DDH location Fig. 1.23). It corresponds to the so-called regolith zone, analogues to that described for the Paleoproterozoic gneisses and schists above in the Part 2.2.3.

The alteration mostly consist of intensive kaolinization and sericitization of the rapakivi granites. In the vicinity of the unconformity surface (upper left part of the Fig. 2.79) sample 475-100 m in fact is a sedimentary rock (gritstone) with abundant detrital quartz and feldspar grains, but macroscopically it looks like normal rapakivi granite. 10 meters below a very similar rock, but corresponding to slightly altered (chlorite + kaolinite) rapakivi granite, occurs (sample 475-110 m). The fresh coarse-grained amphibole-biotite rapakivi granite (sample 475-116 m) appears 16 meters below the unconformity. This type of alteration can be produced by intensive paleoweathering processes, when the granites were altered "in situ" to form eluvial deposits.

(ii) Diagenetic alteration

The alteration, which can take place during and immediately after the sedimentation of the Pasha – Ladoga basin, is observed in the DDH-484 (right part of the Fig. 2.79). In the Salmi area diagenetic alteration is revealed in partial obliteration of the granite textures. Intensive hematization and kaolinization in these granites can be a result of the paleoweathering processes, but the newly formed idiomorphic quartz, interstratified clay-minerals neoformation (Fig. 2.80) can be related to the processes of the diagenetic alteration occurring in the overlapping Pasha – Ladoga sandstones.

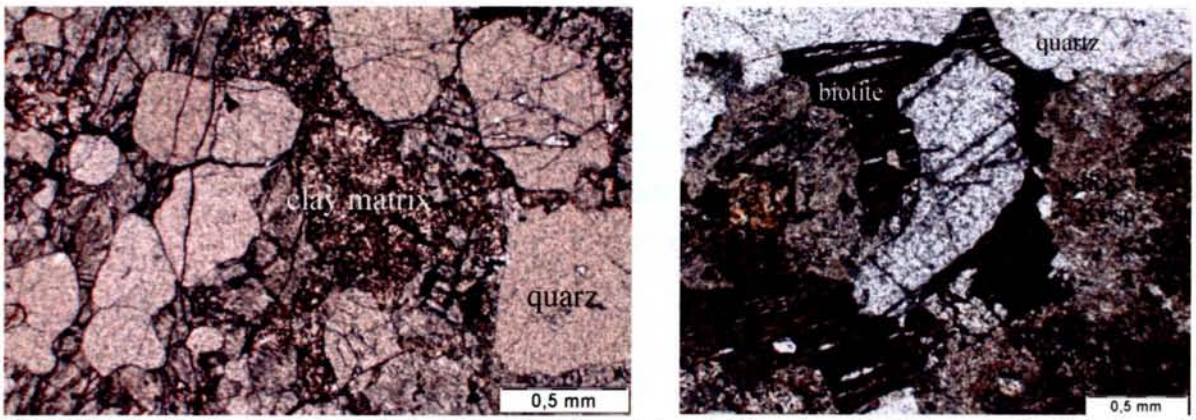

Fig. 2.80. A: Newly formed quartz in clay minerals matrix, which replace K-feldspar in the Salmi rapakivi granites (sample DDH-484-121 m), parallel nicols, photomicrograph scale – 0.5 mm;
B - Newly formed or fragment of quartz and biotite flakes in the clay matrix (sample DDH-484-103 m), parallel nicols, photomicrograph scale – 0.5 mm

(iii) Hydrothermal alteration occurring during and after ore deposition

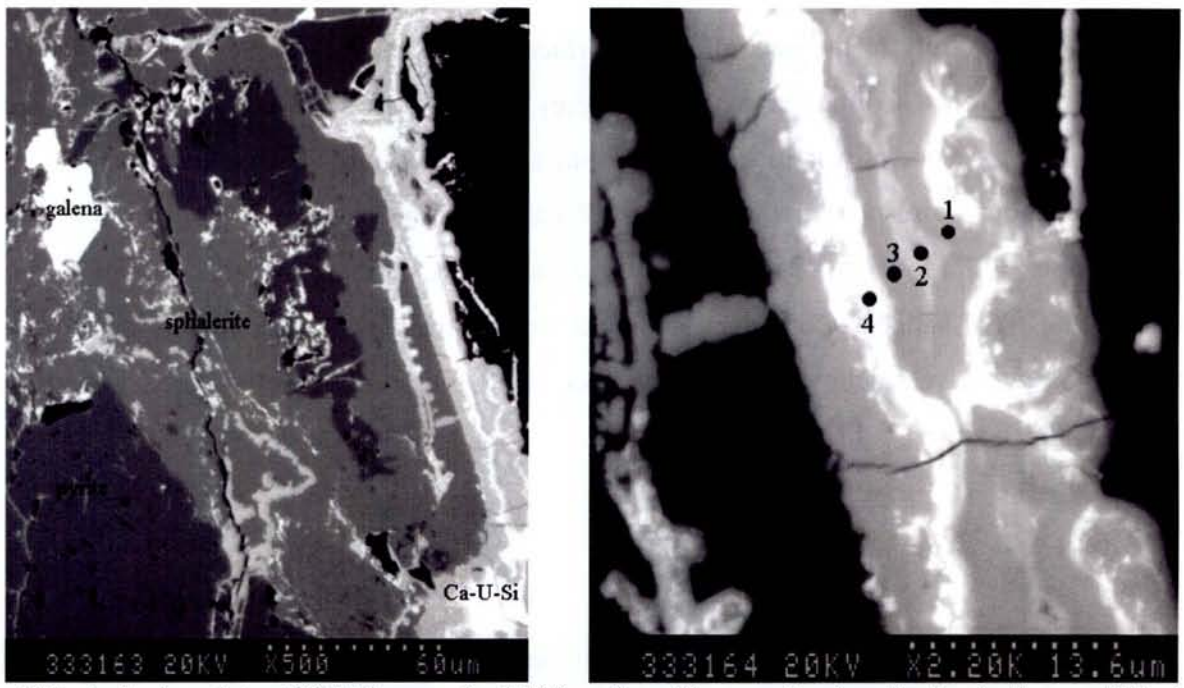

Fig. 2.81. Left microphoto: BSEM image of sulphidic veins with some U-mineralization in the regolithized rapakivi granites (sample DDH-333-140 m), photomicrograph scale 60 μm;
Right microphoto: detail of the sulphidic vein with uranium minerals), microphotograph scale – 13.6 μm

Wt. % / Point	UO_2	PbO	SiO_2	TiO_2	CaO	P_2O_5	SO_3	Y_2O_3	Total
1	70.28	0.05	9.93	0.18	3.47	0.92	0.04	1.53	86.40
2	57.44	0.32	15.26	0.08	2.65	1.36	0.08	2.60	79.79
3	57.31	0.00	14.95	0.10	2.88	1.32	0.11	2.27	78.94
4	72.11	0.00	7.81	0.13	3.52	0.82	0.07	0.85	85.31

Table 2.13. Chemical composition of the uranium minerals in the altered rapakivi granites (points in Fig. 2.81-B) (sample DDH-333-140 m – Karku deposit area) (CAMECA SX-100 electron microprobe (EMP) analyses, Public Analysis Service of the Henri Poincaré University (Nancy, France)

Hydrothermal alteration processes, which take place during and after uranium deposition in the sandstones, also affect the rapakivi granites. They appear as intensive chloritization and carbonatization of the granites. Uranium mineralization in the regolithized rapakivi granites occurs as Si-Ca-Y-rich pitchblende and Y-P-rich coffinite (Table 2.13), which appears in sulphidic (pyrite, galena, sphalerite) veins, cutting rapakivi granites in the vicinity of the mineralized zones of the sandstone (Fig. 2.81). The lead content of the uranium minerals is extremely low suggesting either an open system with lead loss or a very recent mineralization.

2.5.4. Accessory mineralogy of the rapakivi granites

Sample's number	DDH location	Rock type	Zircon's alteration phases	Monazites alteration phases	Other accessories	Zr, ppm	Th, ppm	U, ppm	ΣREE, ppm
3-01	Pogran-Kondushi	Rapakivi granite	zircon	-	apatite	300	22	5	540
5-04-01	Kitelya	Even-grained biotite granite	zircon	-	xenotime, thorite, other REE minerals	n.a.	n.a.	n.a.	n.a.
6-04-01	Pitkyaranta	Porphyritic ovoidal	zircon	-	xenotime, allanite	n.a.	n.a.	n.a.	n.a.
13-02	Satulinoya river	Even-grained biotite granite	zircon	-		138	51	5	300
2097	Uuksu river	Even-grained biotite granite	zircon	-		206	33	6	315
484-97 m	DDH Salmi area	Regolithized rapakivi granite	zircon with xenotime overgrowths	-	-	480	25	4	840

Table 2.14. Description, location, mineralogical occurrences and whole-rock composition of the Mesoproterozoic (Riphean) rapakivi granites of the Salmi batholith. Whole-rock trace elements composition for the samples 5-04-01 and 6-04-01 are not available.

Zircon and associated zircon alteration

Euhedral, prismatic, zircon grains have been observed in the Mesoproterozoic (Riphean) Salmi rapakivi granites (Fig. 2.82). Sometimes poorly developed faces of the dipyramid or strongly elongated crystals can be observed (Fig. 2.83). Primary crystal zoning is well developed (Fig. 2.84).

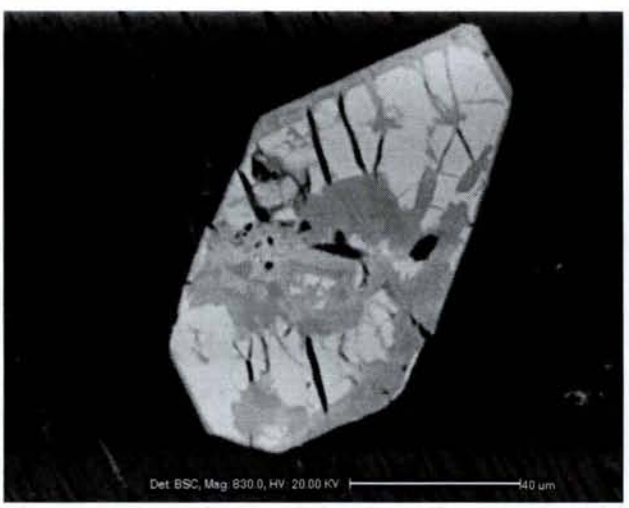

Fig. 2.82. BSEM image of the zircon from non-ovoidal biotite-amphibole granite (sample 3-01, Ladoga Lake shore near Pogran-Kondushi village)
Photomicrograph scale = 40 μm

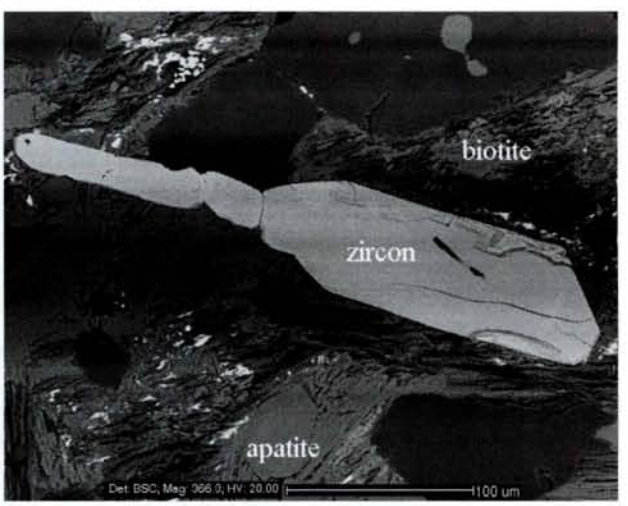

Fig. 2.83. BSEM image of zircon grains from the ovoidal biotite-amphibole coarse-grained rapakivi (sample 9-03-01, Tulema river)
Photomicrograph scale = 100 μm

Zircon alteration is mainly developed from edges to core of the crystals. On average zircons from the rapakivi granites are more altered, than zircon from the graphitic schists. They contain 55.50 ± 9.45 wt. % ZrO_2, 27.46 ± 4.92 wt. % SiO_2 and 1.49 ± 0.44 wt. % HfO_2, in average. Other substituted elements reach up to 9.23 wt. % (Annex zircon).

The most altered zircon domain contains down to 29.70 wt. % ZrO_2 and 16.85 wt. % SiO_2, with substituted elements reaching up to 34.09 wt. % (Annex zircon), including up to 10.05 wt. % Y_2O_3 and 5.52 wt. % P_2O_5, when neoformed xenotime develops in epitaxis at the margin of altered zircon (Fig.2.85). The darker (in BSEM image) altered zircon domains may also contain up to 4.14 wt. % ThO_2, 3.52 wt. % Al_2O_3, 2.78 wt. % CaO, 2.28 wt. % FeO, 0.64 wt. % U_3O_8, 5.48 wt. % ΣREE (with HREE predominance). Maximum water content in particularly metamictized zircon grains may reach up to 18.42 wt. %.

Maximum 8 (without some anomalous points) from 33 atoms of zircon formula can be substituted by Y, P, Th, Al, Ca, Fe, U (Fig. 2.87). Maximum 6.5 from 33 atoms is substituted by Y + P (xenotime neoformation) (Fig. 2.86). U maximum substitution reaches only 0.1 atoms of Zr + Si + Hf (Fig. 2.88), and the substitution does not increase proportionally with the increase of the other substituting elements.

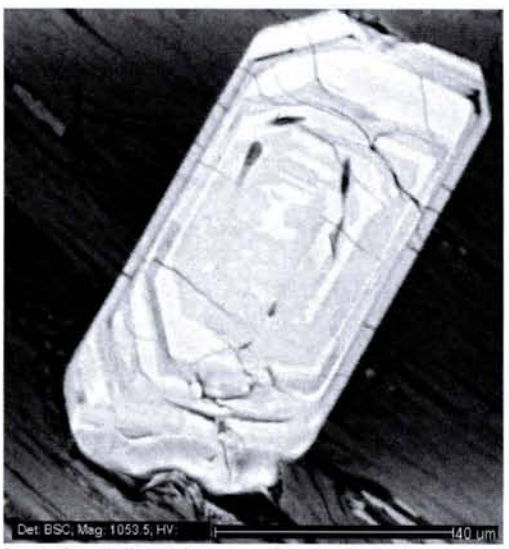

Fig. 2.84. BSEM image of a detrital zircon grain with well-developed primary crystal zoning (sample 6-04-01, Pitkyaranta area)
Photomicrograph scale - 40µm

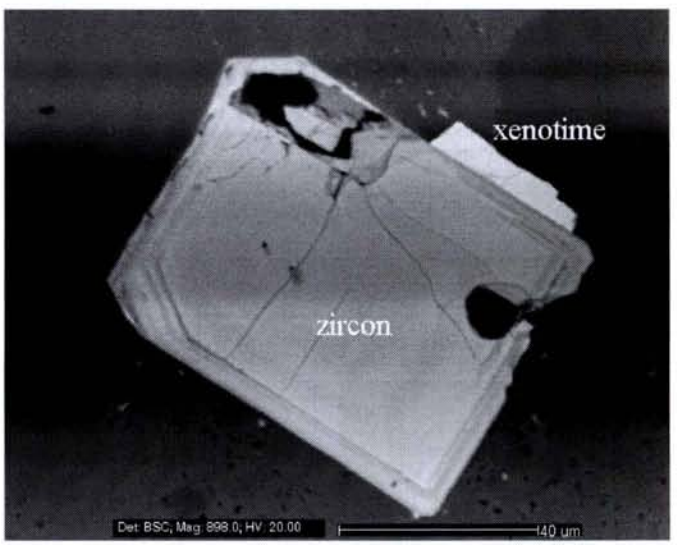

Fig. 2.85. BSEM image of a detrital zircon grain with neoformed xenotime (sample 6-04-01, Pitkyaranta area). Photomicrograph scale – 40 µm

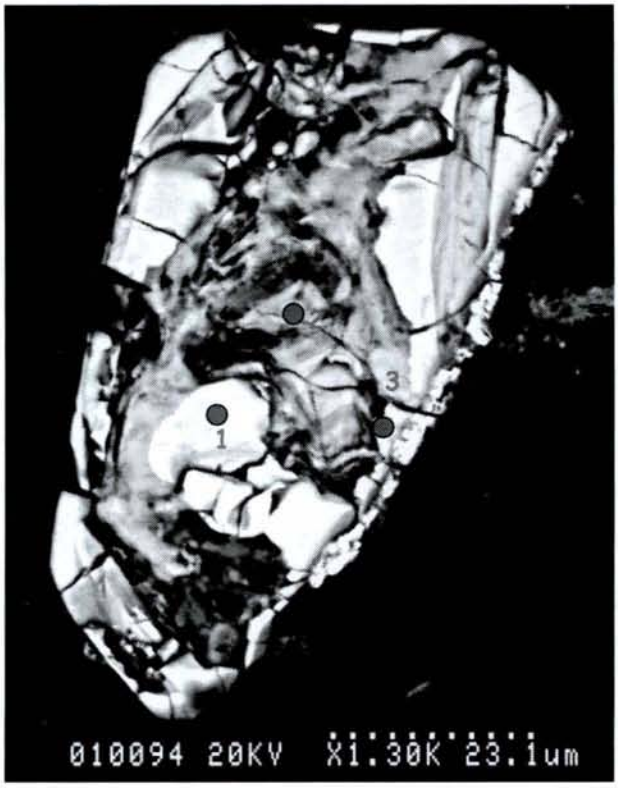

	1	2	3
Comment	484-97-6	484-97-6	484-97-6
SiO2	33,62	25,83	8,82
ZrO2	68,16	49,90	11,11
HfO2	1,66	1,06	0,40
Al2O3	0,03	1,18	0,47
P2O5	0,04	2,20	21,26
CaO	0,01	1,84	2,03
PbO	0,00	0,01	0,00
FeO	0,15	1,21	0,85
Y2O3	0,00	7,45	29,26
Ce2O3	0,02	0,24	0,21
Nd2O3	0,04	0,16	0,51
SmO	0,00	0,20	0,59
Gd2O3	0,00	0,41	2,14
Yb2O3	0,02	0,88	1,88
ThO2	0,01	0,31	0,41
U2O3	0,05	0,09	0,10
Total	103,81	92,98	80,04

Fig. 2.86. BSEM image and chemical composition of a zircon grain from regolithized rapakivi granites and neoformed xenotime, which develops in epitaxis at the margin of the altered zircon (sample DDH-484-97, Salmi area). Photomicrograph scale – 23.1μm

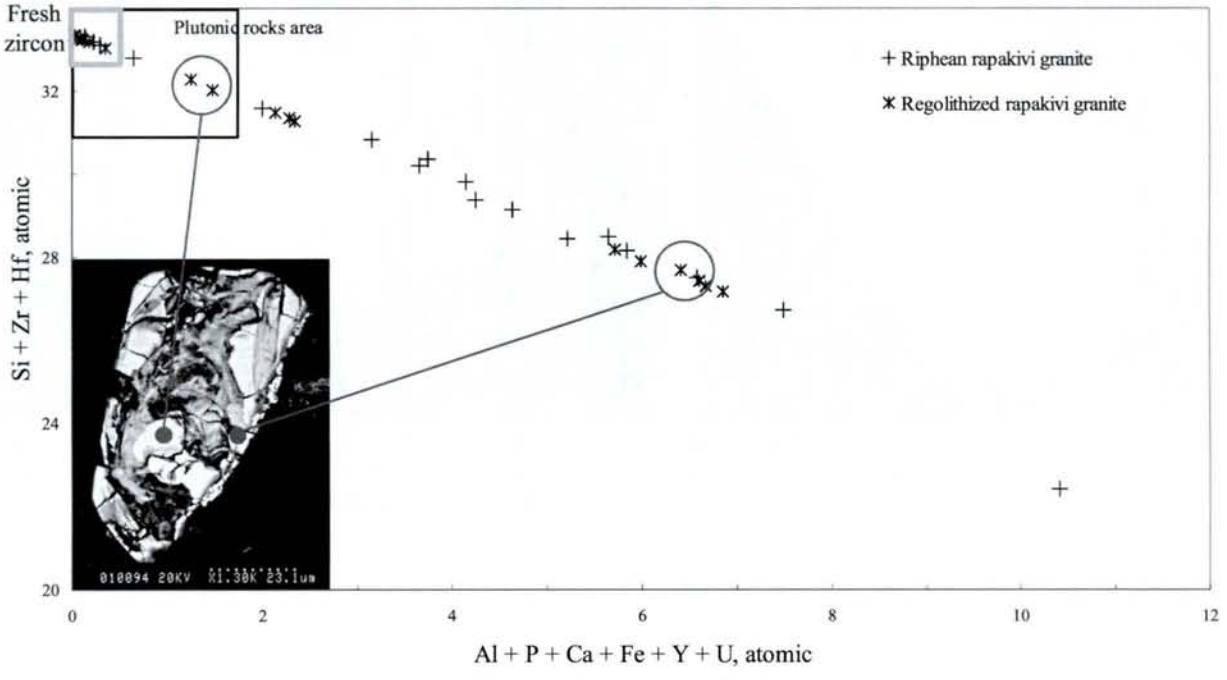

Fig. 2.87. Substitution of Zr + Hf + Si by Al + P + Ca + Fe + Y + U in zircons from the Salmi rapakivi granites

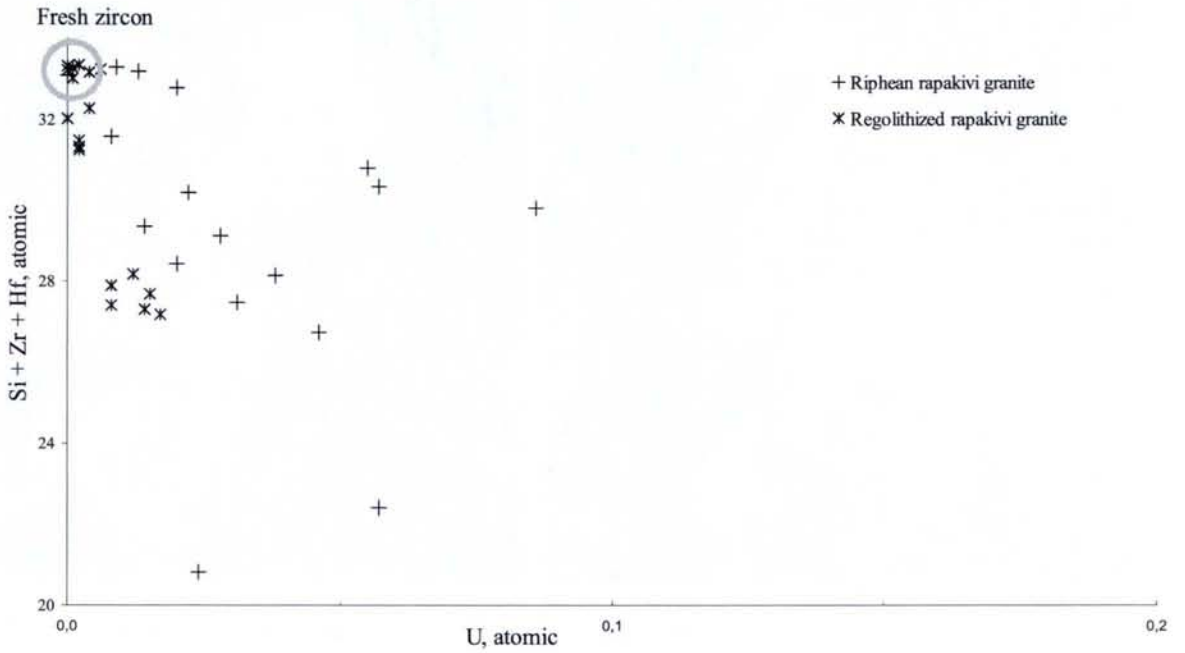

Fig. 2.88. Substitution of Zr + Hf + Si by U in zircons from the Salmi rapakivi granites

Monazite and other REE minerals

Brownish-yellow tabular monazite is a very uncommon accessory mineral in the rapakivi granites of the Salmi pluton. It was discovered only in non-ovoidal rapakivi granites near the contact with Archean granite-gneisses domes (Sviridenko, 1968).

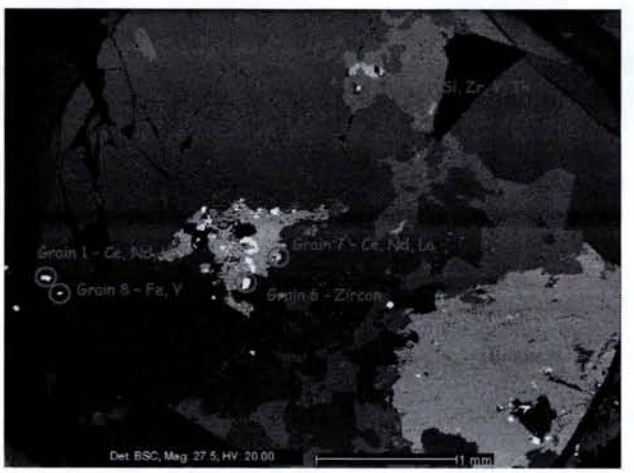

Fig. 2.89. Abundant REE-bearing accessory minerals included in biotite in the even-grained biotite granite (sample 5-04-01, Pitkyaranta area). BSEM image, photomicrograph scale – 1 mm

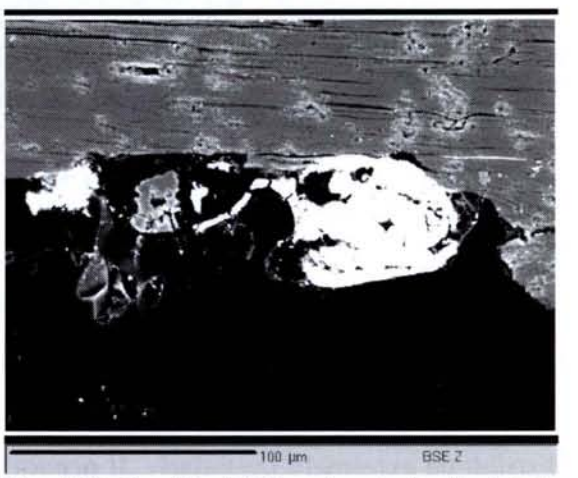

Fig. 2.90. Possible REE carbonate in the biotite grain (sample 5-04-01, Pitkyaranta area). Grain 1 in Fig. 2.89, BSEM image, photomicrograph scale – 100 µm

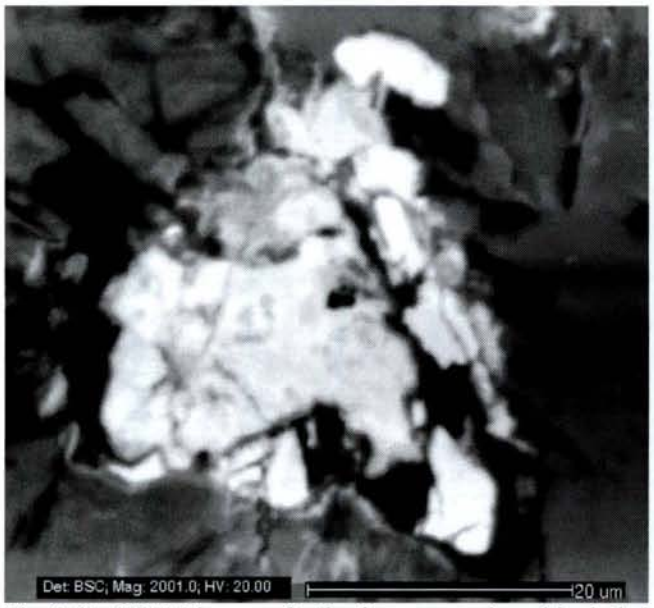

Fig. 2.91. BSEM image of a thorite-group mineral included in biotite (sample 5-04-01, Pitkyaranta area). Grain 4 in Fig. 2.85. Photomicrograph scale = 20 μm

Fig. 2.92. BSEM image of allanite twins in the porphyritic rapakivi granite (sample 6-04-01, Pitkyaranta area). Photomicrograph scale = 100 μm

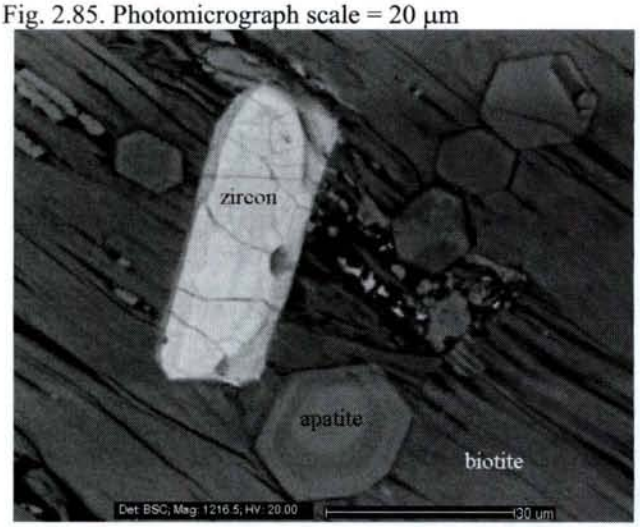

Fig. 2.93. BSEM image of the altered zircon and zoned apatite crystals in the porphyritic rapakivi granite (sample 6-04-01, Pitkyaranta area). Photomicrograph scale – 30 μm

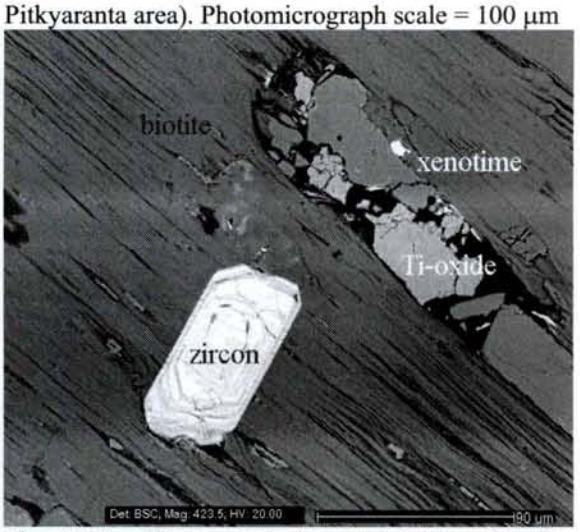

Fig. 2.94. Zircon, xenotime, Ti-oxide in the porphyritic rapakivi granite (sample 6-04-01, Pitkyaranta area).Photomicrograph scale – 90 μm

Other REE bearing accessory minerals were observed (Fig. 2.89) in some samples: REE carbonates (Fig. 2.90), thorite-group minerals (Fig. 2.91) and Zr – Fe – Y – Th silicates.

Fluorite is the prevalent accessory mineral in the non-ovoidal rapakivi granites, but is distributed extremely irregularly. It occurs between the rock-forming minerals and is enriched in yttrium.

Long-prismatic and twinned crystals of allanite (orthite) are relatively common in all varieties of granite (most common in the non-ovoidal rapakivi). Non-altered allanite is characterized by brownish dark-green to bottle-green colour, but in the most of cases allanite is metamict (Fig. 2.92).

Accessory apatite, Ti-oxides (ilmenite, rutile) and magnetite are widespread in the rapakivi granites, xenotime is less common (Fig. 2.93 – 2.94).

Whole-rock Zr, LREE and Th granites geochemistry

Zr in the rapakivi granites is mainly contained in zircon, but also in some another REE-Zr-Th-bearing minerals.

Y is mainly contained in fluorite (Sviridenko, 1968) but is also enriched in altered parts of zircon grains and neoformed xenotime, which sometimes occurs at the margin of monazite grains (Fig. 2.85 – 2.86).

Non-altered zircon contains less than 0.1 wt. % Y. The altered part may contain up to 29 wt.% Y_2O_3 (exchange $Zr^{4+} \leftrightarrow Y^{4+}$) but representing more probably intergrowths with xenotime. The Zr/Y ratio is an indicator of the degree of zircon alteration: in fresh zircons this ratio exceeds 100 (Fig. 2.95), while altered zircons are typically characterized by Zr/Y ratios between 100 and 20. In the Zr-Y diagram the Early Riphean rapakivi granites of the Salmi pluton have Zr/Y ratios ranging from 20 to 1, according to the intensity of zircon alteration, but this trend may be due also to the presence of other Y-rich phases in these granites (such as Y-fluorite).

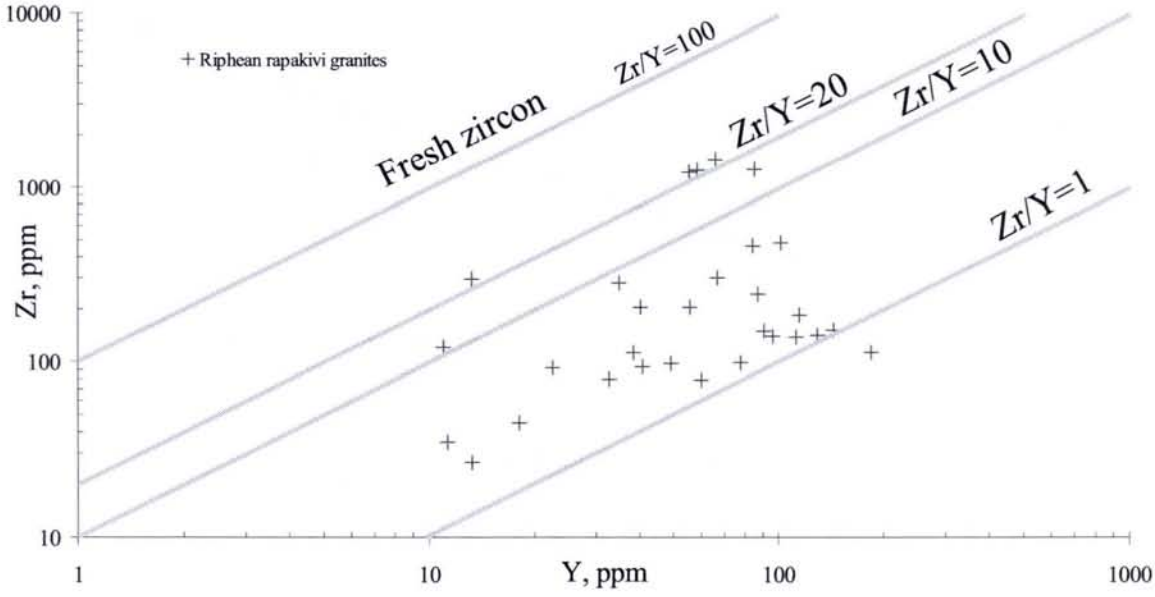

Fig. 2.95. Mesoproterozoic Salmi rapakivi granite in the whole-rock chemical composition Y vs. Zr diagram

Average Th/U ratio of the main types of intrusive rocks is close to 4. On the diagram (Fig. 2.96) most rapakivi granites analyzed in the present work have Th/U ratios ranging from

4 to 1, most of them are strongly enriched in U have Th/U ratios lower than 1. Whole-rock Th contents are high and frequently slightly exceeds 30 ppm.

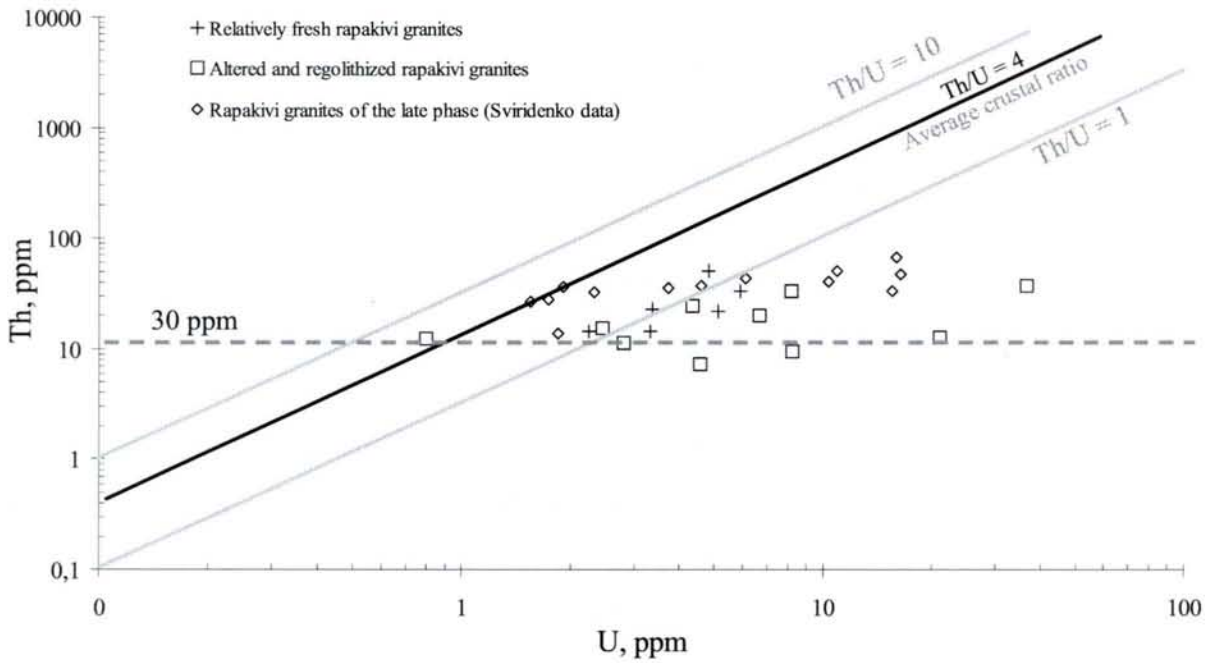

Fig. 2.96. Mesoproterozoic Salmi rapakivi granite in the U vs. Th diagram

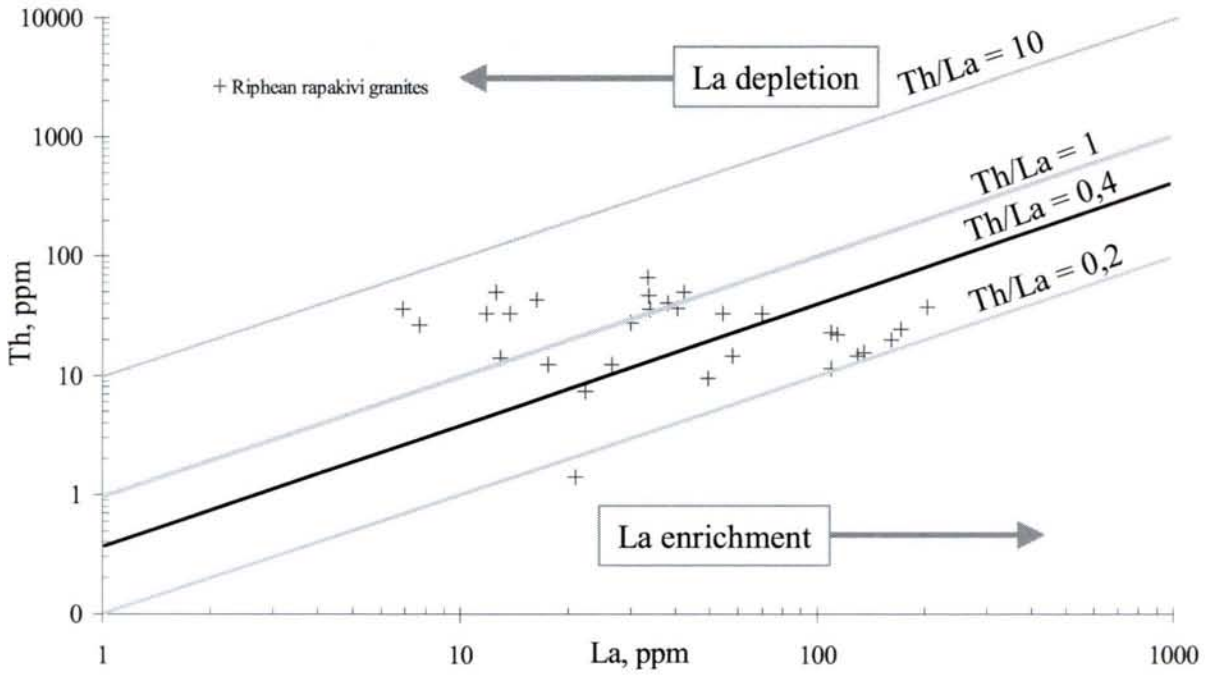

Fig. 2.97. Mesoproterozoic Salmi rapakivi granite in La vs. Th diagram

Th does not show any correlation with the light rare-earth elements (LREE) which present a very large range of concentration variations. La has been chosen as an indicator of the LREE behavior. On the diagram (Fig. 2.97) most of Salmi rapakivi granites have relatively high Th/La ratio ranging from 10 to 0.2.

2.5.5. Petrogeochemistry of the Salmi rapakivi granites

Major elements distribution

Major elements composition of the main types of the Salmi rapakivi granites is listed in Table 2.15. Complete data of major and trace element composition of the Salmi rapakivi granites from the Salmi area is listed in Annex rapakivi granite. DDH and outcrops samples location is presented in Part 1.4.

The granites of the Salmi batholith are essentially leucogranites rich in potassium feldspar and characterized by high contents of SiO_2, K_2O, Fe_2O_3, F and low abundances of TiO_2, Al_2O_3, MgO, CaO and P_2O_5 (Amelin et al., 1991, Ramo, 1991, Sviridenko, 1994).

The SiO_2 content is variable for the different intrusive phases of the Salmi pluton (except early basic phase): from 64.08 in adamellite to 67.12 - 75.65 wt. % in non-ovoidal rapakivi granites of the main phase, and finally from 74.04 to 75.86 wt. % in even-grained and porphyritic biotite granites of the late phases (Velikoslavinsky, 1978).

	Adamellite	Ovoidal biotite-amphibole granite		Ovoidal biotite granite	Even-grained biotite granite		Porphyritic biotite granite	
SiO_2	64.08	67.12	71.15	75.65	74.04	75.86	74.13	75.68
Al_2O_3	14.94	14.66	13.28	11.57	12.35	11.75	11.73	11.98
Fe_2O_3	7.03	5.18	3.75	2.9	2.87	2.44	2.6	2.35
MnO	0.07	0.05	0.05	0.05	0.04	0.04	0.09	0.06
MgO	0.6	0.49	0.28	0.22	0.18	0.14	0.21	0.15
CaO	3.36	1.52	1.06	0.62	0.86	0.77	0.73	0.33
Na_2O	2.76	2.89	2.94	2.82	3.26	3.15	3.76	4.01
K_2O	4.59	5.85	5.62	4.99	5.12	4.91	5.22	4.9
TiO_2	0.9	0.39	0.32	0.24	0.21	0.13	0.25	0.14
P_2O_5	0.13	0.17	0.1	0.12	0.04	0.06	0.09	0.08
Total	98.46	98.32	98.55	99.18	98.97	99.25	98.81	99.68

Table 2.15. Average major element composition of the main rock types of the Salmi pluton (after Velikoslavinsky, 1978)

In a SiO_2 versus $Na_2O + K_2O$ diagram (Fig. 2.98) the average sample (Velikoslavinsky data, 1978) from the early phase plot in the quartz monzonite field. Three samples of the main plutonic phase plot between the quartz monzonite and the granite fields. They belong to the biotite-amphibole rapakivi granites ovoidal and non-ovoidal. Samples corresponding to the late phases of the pluton, which are even-grained and porphyritic biotite granites, plot only in the granite field.

In general the Salmi rapakivi granites are characterized by high alkali contents ($Na_2O + K_2O$ = 7 to 9 wt. %). Characteristic features of the pluton are high K and K/Na for the granites

of the main phase, and moderate enrichment of Na in the late phases in relation with higher fluorine content of the melt.

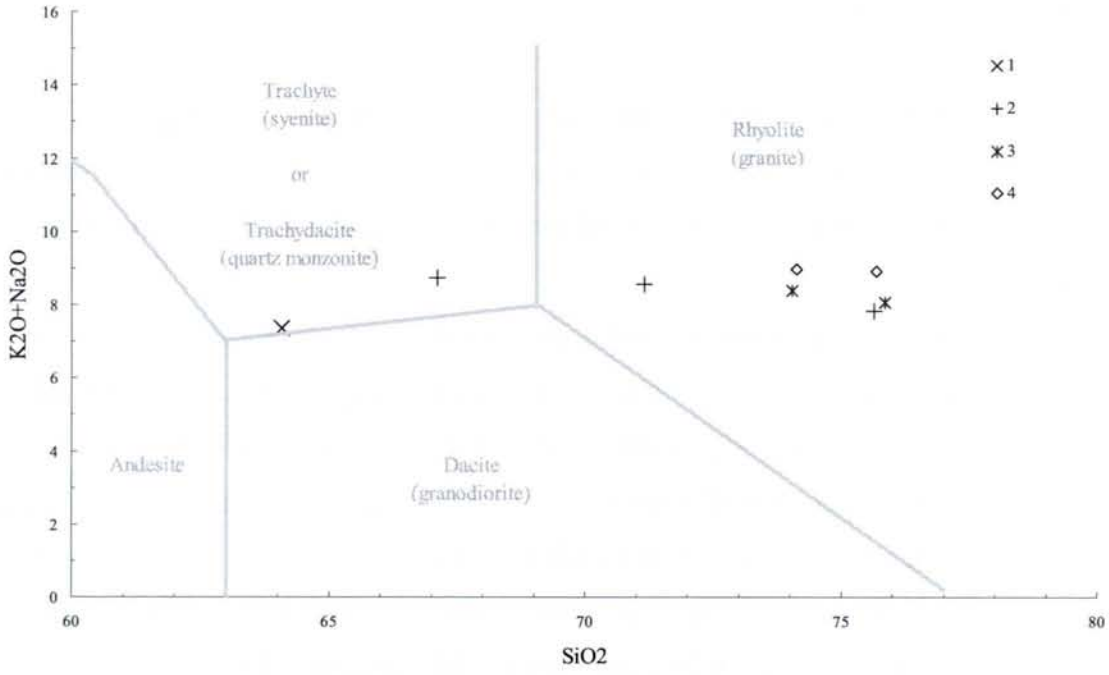

Fig. 2.98. The Salmi rapakivi granites in the SiO_2 vs. $K_2O + Na_2O$ classification diagram
1 - 4 - average composition of the different phases of the Salmi batholith after Velikoslavinsky (1978): 1 – early phase I – adamellite (n = 7); 2 – main phase II – ovoidal rapakivi (three different samples with n = 4, 51 and 13); 3 – late phase III – even-grained rapakivi (n = 20 and 13); 4 – late phase IV – porphyritic granites (n = 3 and 4)

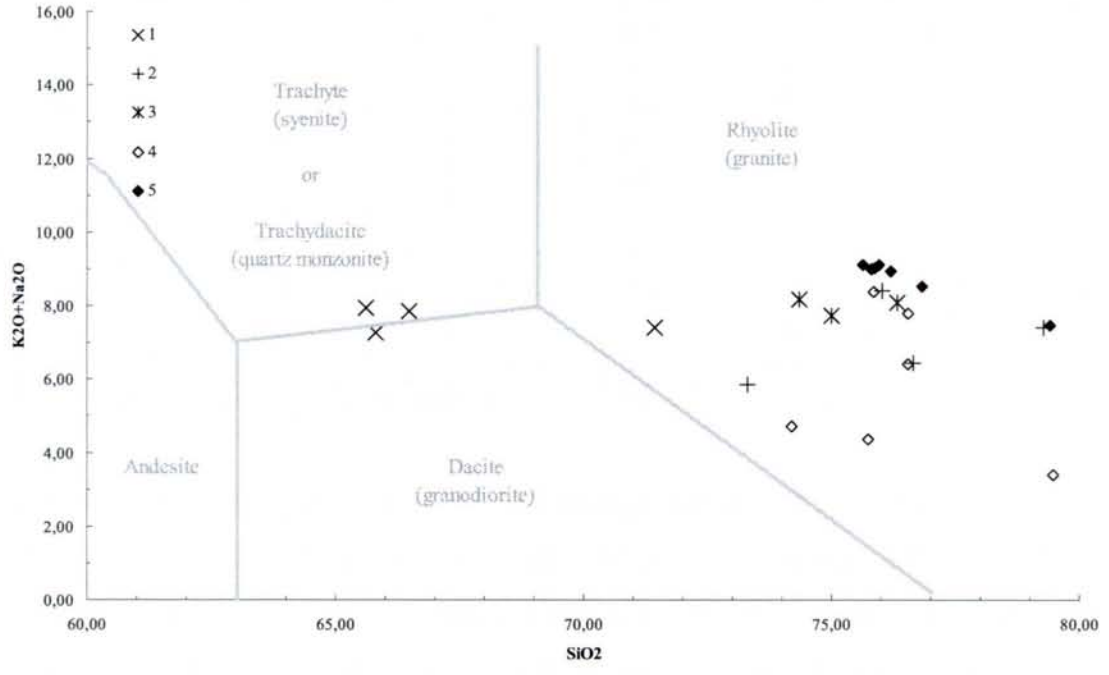

Fig. 2.99. The Salmi rapakivi granites from the south-western part of the Salmi pluton (Pitkyaranta and Salmi area) in the SiO_2 vs. $K_2O + Na_2O$ classification diagram.
1 – DDH - 475 - ovoidal amphibole-biotite granites including regolithized varieties; 2 – DDH – 484 (and DDH - 1051) - regolithized ovoidal granites; 3 – ovoidal and even-grained granites from the outcrops in the Salmi area; 4 - 5 – late phases of the Salmi granites in a contact with Archean granite-gneisses (Sviridenko sampling):
4 – DDH – 412; 5 – DDH - 139

The rapakivi granites sampled in the drillings below the Mesoproterozoic volcanic-sedimentary sequence or in the outcrops within the Salmi area were also plotted into the SiO_2 versus $Na_2O + K_2O$ diagram (Fig. 2.99):

(i) DDH-475 – drill samples from the eastern part of the Salmi area correspond to compositions at the limit between fields of quartz monzonite and granodiorite for three samples and for all other samples to granites.

(ii) DDH-484 – drill samples from the northern part of the Salmi area, in spite of the fact that they correspond to ovoidal biotite-amphibole granites (quartz monzonite or granodiorite fields I the diagram), because of their alteration (Fig. 2.79) plot in the granite field.

(iii) Outcrops – the Salmi non-altered non-ovoidal biotite-amphibole (Fig. 2.75 – sample 3-01) and even-grained biotite (Fig. 2.76 – samples 13-02 and 2097) rapakivi granites sampled in the outcrops within the Salmi area plot into the granite field.

(iv) Sviridenko sampling – corresponding to even-grained granites from a drilling located at the western contact of the Salmi pluton with Archean domes, correspond to average even-grained granites in Fig. 2.98.

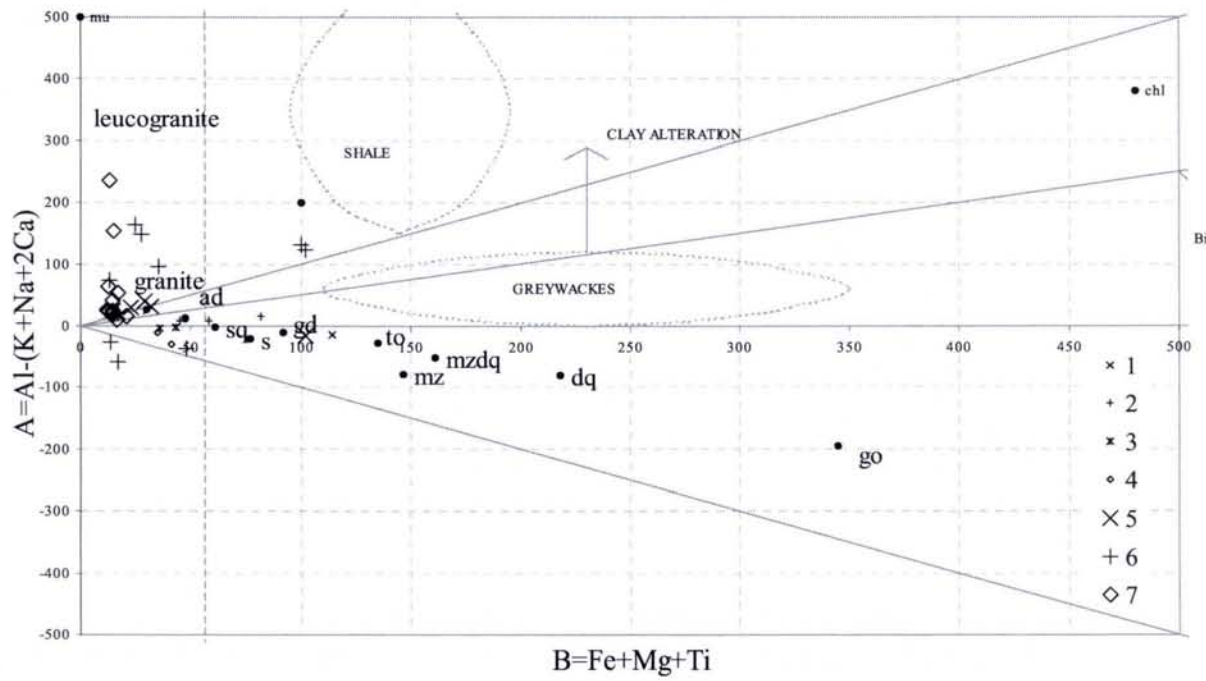

Fig. 2.100. The Salmi rapakivi granites in the B vs. A diagram according to Debon and Le Fort (1983, 1988)
Symbols: Average composition of the different phases 1 - 4 as in Fig. 2.98, 5 – fresh rapakivi granite from the Salmi and Pitkyaranta area; 6 – altered and regolithized rapakivi granite from the drilling in the Karku deposit area; 7 – late phase granites from the drilling in a contact with Archean granite-gneisses domes (Sviridenko data)

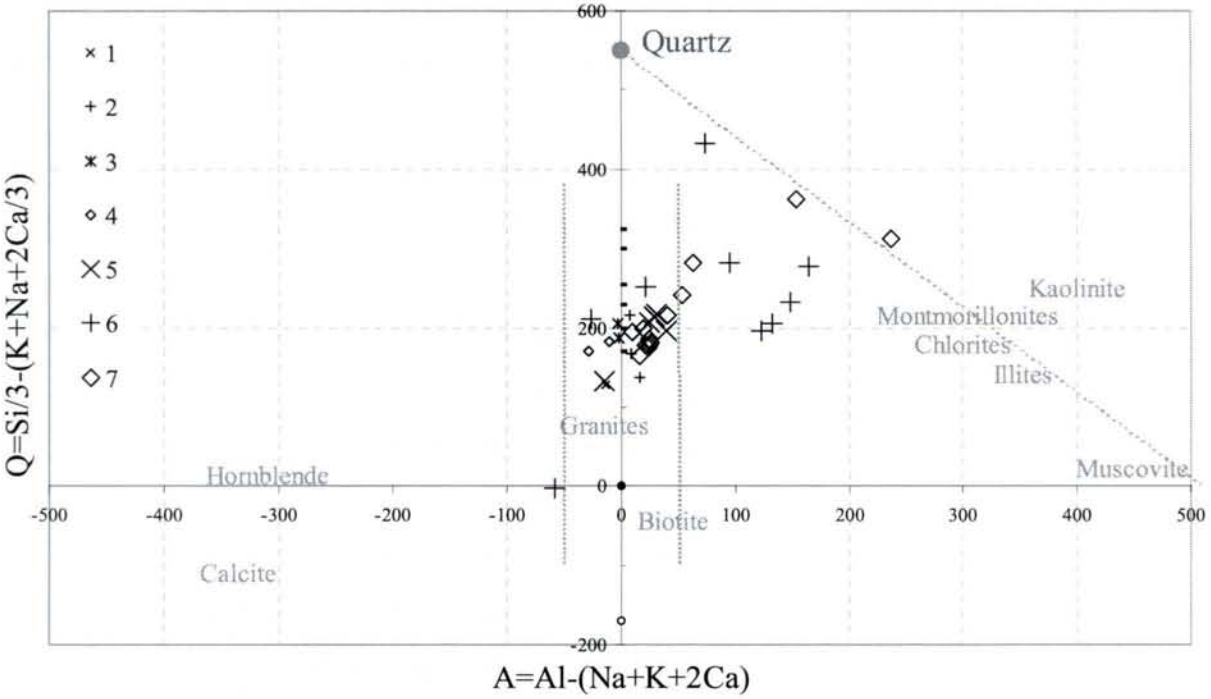

Fig. 2.101. The Salmi rapakivi granites in the A vs. Q diagram according to Debon and Le Fort (1983, 1988) Symbols 1 - 5 as in Fig. 2.100.

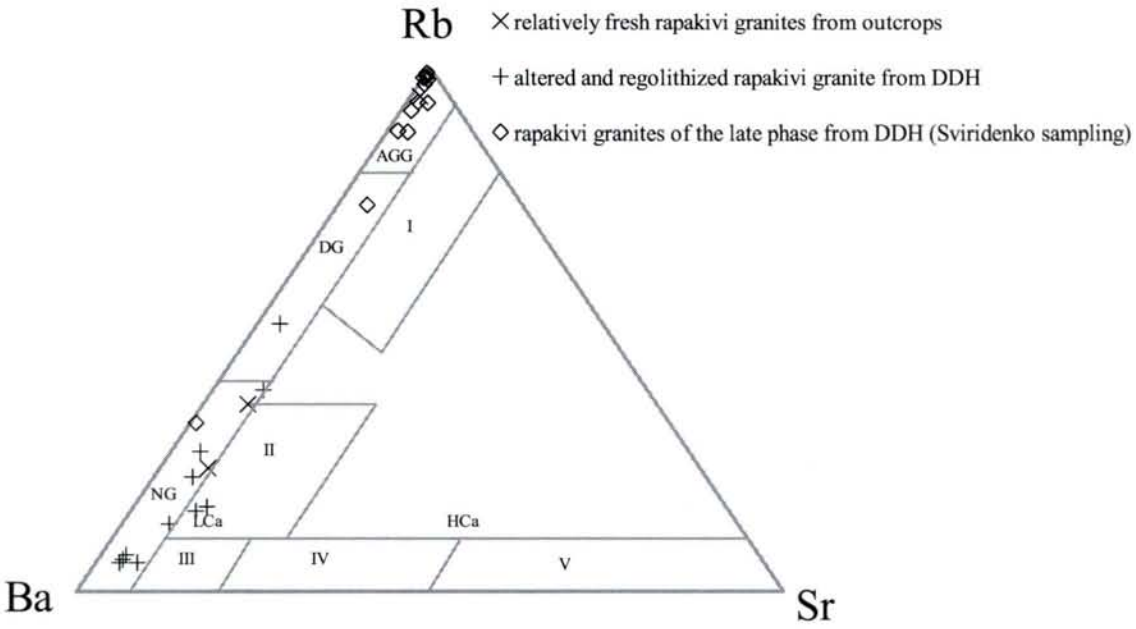

Fig. 2.102. Salmi rapakivi granites in the Ba–Sr–Rb diagram (Kleeman & Twist, 1989).
Fields: I – granites with associated Sn, W, Mo mineralization; AGG – albitized and greisenized granites; DG – differentiated granites; NG – normal granites; II – anomalous granites; III - granodiorites; IV – quartz diorites; V – diorites; LCa – low-calcium granite; HCa – high-calcium granite.

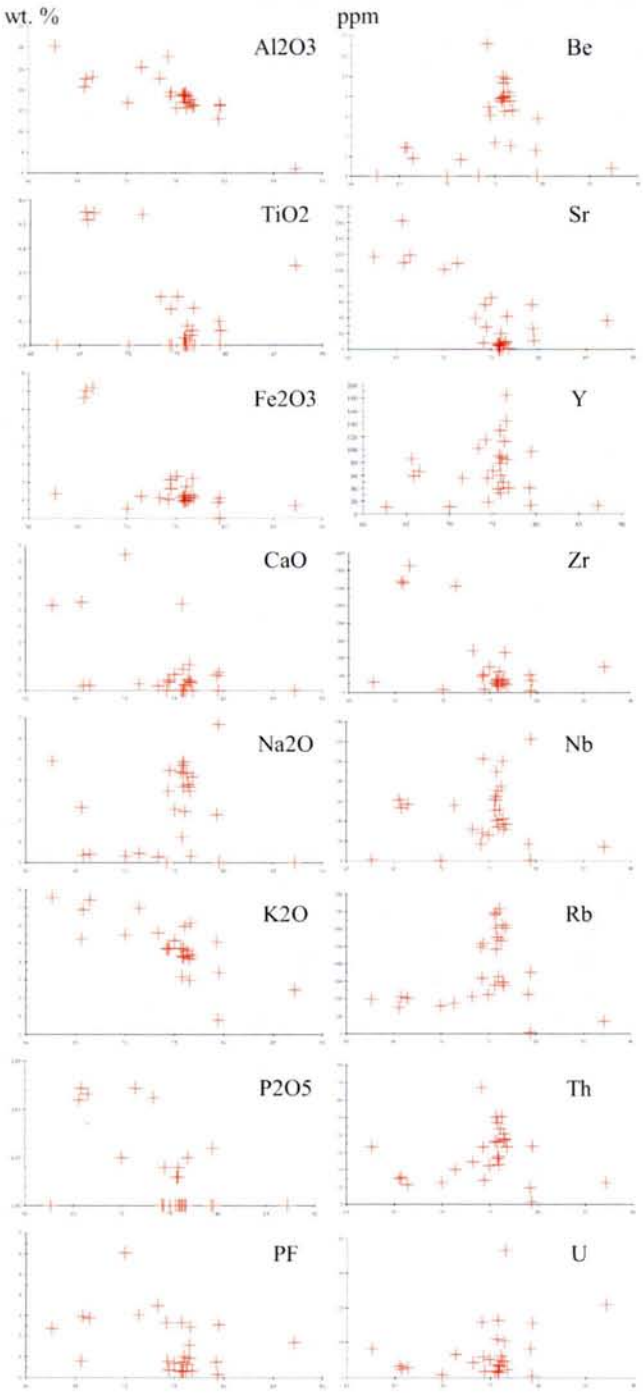

Fig. 2.103. Major and trace element contents plot versus silica content in the Salmi rapakivi granites

Salmi rapakivi granites are metaluminous to slightly peraluminous granites as the Phanerozoic subalkaline A-type granites (Ramo, 1991).

In the A-B diagram of Debon – Le Fort (1983, 1988) (Fig. 2.100) the average compositions of the different phases (Velikoslavinsky, 1978) lie close A = 0 line, but is metaluminous. Relatively fresh rapakivi granites from the surface and two from the drilling (DDH-475-116 and DDH-1051-379 – Fig. 2.79) are slightly peraluminous. Altered and regolithized drilling samples from the Salmi batholith located below the Riphean basin are distinctly peraluminous (high A values) indicating clay alteration of feldspars (Fig. 2.101). The same evolution is observed in the Q-A diagram, where the clay amounts increase with increasing quartz content (Fig. 2.101).

In the Rb-Ba-Sr diagram (Fig. 2.102) the Salmi rapakivi granites range from "normal granites" to "strongly differentiated granites". The Salmi rapakivi granites present two types of trends : (i) one representing a normal fractionation trend with decreasing Ti, Fe, Ca, K, Zr, Sr, Ba contents with increasing silica content whereas incompatible trace elements content does not vary significantly, (ii) a special evolution which for a relatively constant silica content presents a strong increase in incompatible elements such as Be, Sn, Rb, Th, U, Rb, Ga, Zr, Hf, and REE, which may be related to a fractionation from a fluid phase.

As the similar Mesoproterozoic anorthosite-rapakivi granites of the Baltic shield (Vyborg, Riga batholiths) the rapakivi granites of the Salmi batholith show chemical characteristics of subalkaline A-type granites and within-plate granites (Ramo & Haapala, 1985). They show an evolutionary trend from fayalite-biotite-hornblende granite via biotite-(hornblende) granite to topaz-bearing microcline-albite granite.

Trace elements distribution of the rapakivi below the Mesoproterozoic sequences

No geochemical investigations have been previously made on the rapakivi granites located presently below by the Mesoproterozoic (Riphean) volcanic-sedimentary sequences in the Salmi – Pitkyaranta area, or which are presently outcropping, but which may have been covered before the erosion by the Mesoproterozoic sediments.

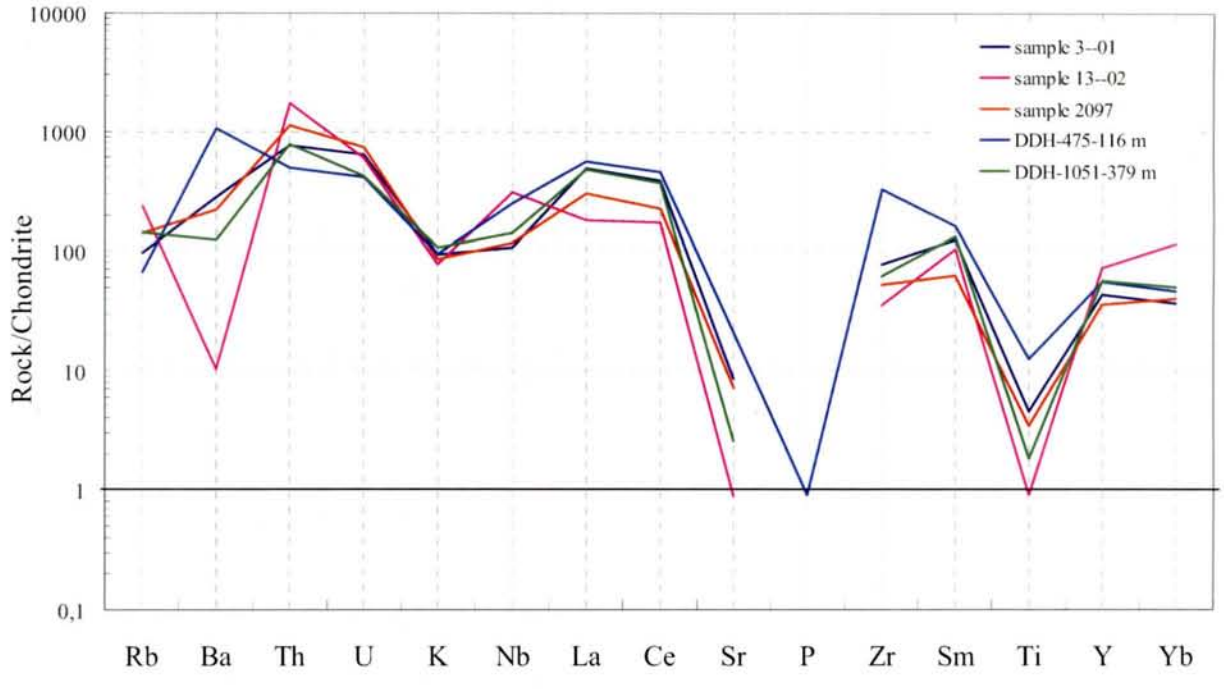

Fig. 2.104. Chondrite-normalized trace element patterns of the relatively fresh granites of the Salmi batholith from the outcrops and drilling in the Salmi area (spidergram type after Holm (1979); (chondrite composition after E. Anders and N. Grevesse: http://earthref.org/GERM/reservoirs/C1.htm)

For the study of the primary distribution of trace elements and REE, chondrite-normalized spidergrams are used for relatively fresh rapakivi granites of the Salmi batholith from the outcrops and drilling in the Salmi area (Fig. 2.104). Trace elements composition of the relatively fresh granites, located below the Mesoproterozoic sediments, is similar to that

described above for average rapakivi granites of the different phases and small variations depends from slightly variable differentiation degree of the different granites.

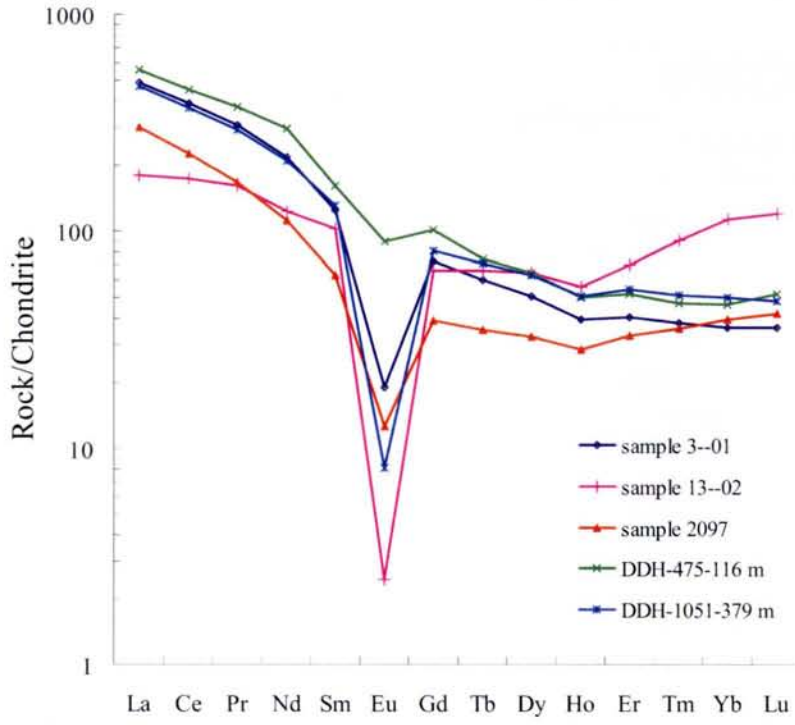

Fig. 105. Chondrite-normalized REE distribution patterns of the relatively fresh granites of the Salmi batholith from the outcrops and drillings in the Salmi area (chondrite composition after Supplemental data for chondrite (Anders & Grevesse: http://earthref.org/GERM/reservoirs/C1.htm)

The rare-earth elements (REE) distribution of the Mesoproterozoic rapakivi granites from the relatively fresh rocks from the outcrops and drillings in the Salmi area is presented in Fig. 2.105. Total REE content in the granites is high and vary from 660 ppm in the slightly altered drilling sample DDH-475-116 m, 500 - 530 ppm (in granites from outcrops), down to 300 ppm in the late phase granites (samples 13-02 and 2097).

The relatively fresh rapakivi granite (Fig. 2.105) are characterized by well-fractionated REE patterns ($(Ce/Yb)_N = 5 - 10$) with an important Eu anomaly ($Eu/Eu^* = 0.2$) for the fresh biotite-amphibole granite of the main phase (sample 3-01) and a very smooth anomaly ($Eu/Eu^* = 0.7$) in the slightly altered biotite-amphibole granite (sample DDH-475-116 m). For the granite of the late phases an extremely strong Eu anomaly ($Eu/Eu^* = 0.02 - 0.25$) is typical.

For a better understanding of the some major, trace and rare-earth elements distribution with depth and alteration degree the data are now examined according to their depth position in the drill holes in the vicinity of the Pre-Riphean unconformity surface and were normalized

to the average "fresh rapakivi"-granite (Fig. 2.106) for DDH-475 and DDH-484 (see Fig. 2.79) from the Salmi area.

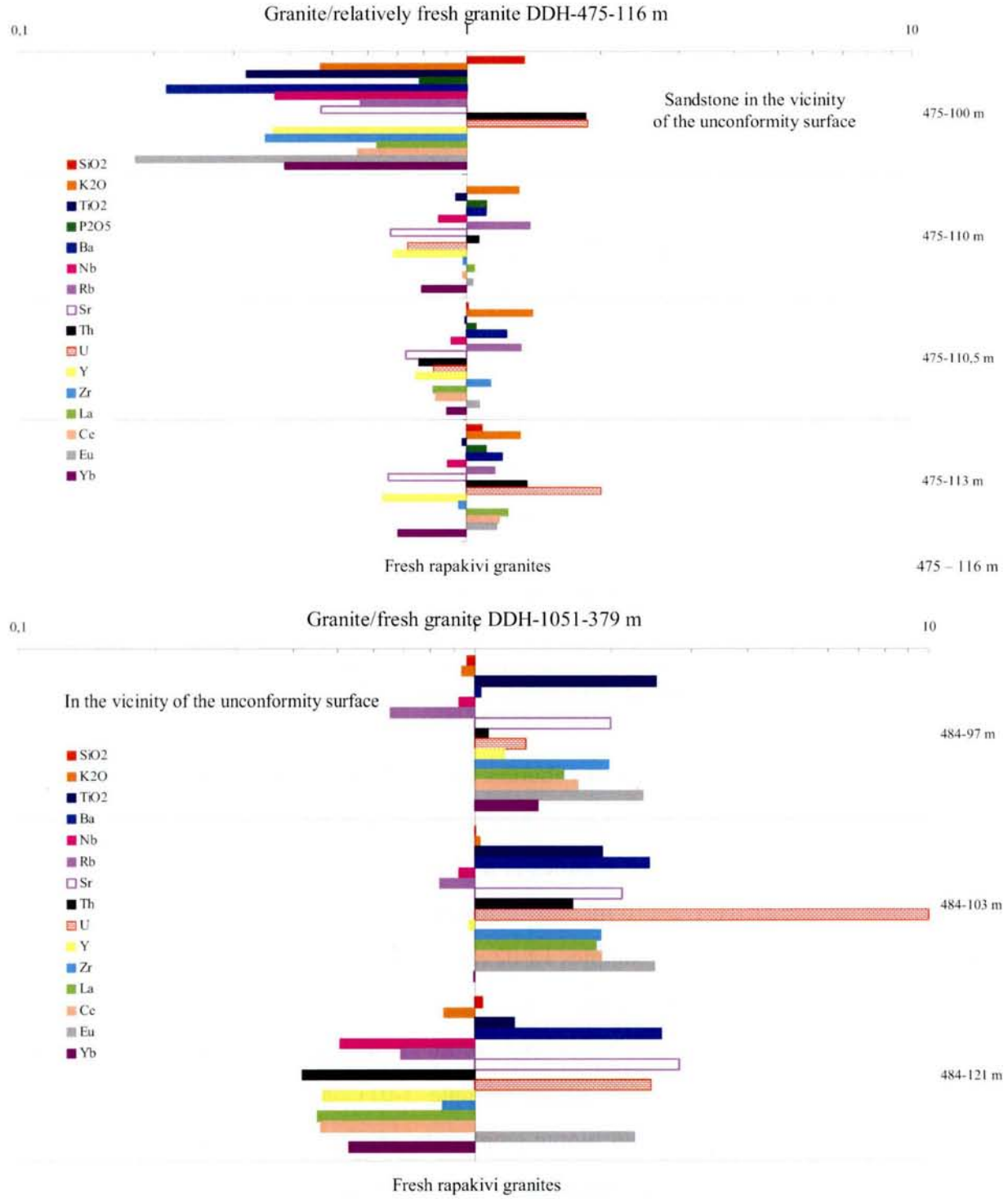

Fig. 2.106. Major, trace and rare-earth elements distribution in the Mesoproterozoic rapakivi granites located below the Mesoproterozoic Pasha – Ladoga basin in concerning to their distance to the unconformity surface.
A - granites from DDH-475 to the fresh granite (DDH-475-116 m) normalization diagram; B – granites from DDH-484 to the fresh granite spatially closed (DDH-1051-379 m) normalization

In DDH-475 (Fig. 2.106-A) the variations of chemical composition along the profile do not exceed about 30% for most elements relatively to the fresh rapakivi granite from the deepest part of the drill hole. No systematic variation is observed along the profile. The samples mainly present an enrichment in K and Rb , and to a lesser extend Ba corresponding to the illitic alteration. Most other element are constant or moderately depleted. Y and HREE are the most depleted elements. The two upper regolithized granites are depleted in U, but the lowermost sample (the freshest one) is significantly enriched in uranium.

In the DDH-484 more significant variations in major and trace elements distribution are observed (Fig. 2.106-B). The two upper regolithized granites are enriched in most elements which may result from a volume loss due to the leaching of alkalies and Ca from the granite or difference of composition between the real protolith and the chosen one. At the contrary the lowermost sample is enriched in most elements excepted Ba, Sr and U. This probably result from the appearance of an other less fractionated granite facies at depth as indicated by the much lower contents in elements relatively immobile during most alteration processes such as Th, Nb, Zr.

Uranium is strongly enriched in all the samples of DDH-484 and especially more strongly at -103 m. Contrary to the observations along the preceding regolith profile Rb and to a lesser extend K are depleted in the regolithized samples.

Conclusions for chapter II

The Ladoga mobile zone which represents a part of the Raahe – Ladoga fault-thrust zone, is located at the margin of the Archean Karelian craton and belongs to the Paleoproterozoic Svecofennian Domain. The petrological, mineralogical and geochemical studies have led to the characterization of the following features:

(i) The Archean domes are mainly composed of gneissic orthoderived rocks, which correspond to a tonalite - granodiorite - adamellite – granite association. The average U content in tonalites is about 0.5 ppm, Th – 4 ppm, in potassium granites – U content is about 2 ppm, Th – 7 ppm.

(ii) The Paleoproterozoic formations correspond to strongly metamorphosed and migmatized metavolcanic and metasedimentary sequences. The metasediments typically correspond to epicontinental platform lithologies corresponding to former black shales, carbonated and silicoclastic rocks. Graphite and sulfides resulting from the metamorphism of these sediments have been remobilized during retrograde metamorphism and contact metamorphism related to the emplacement of the rapakivi granites. The average U content in these gneisses and schists is about 4 – 5 ppm, Th – 7 – 8 ppm.

(iii) Several generation of Paleoproterozoic syn-orogenic potassium-rich granite complexes enriched in Th (up to 28 ppm in leucocratic porphyroblastic granites) and U (up to 6.4 ppm in two-mica leucogranites) have been emplaced in this zone, but are very abundant in the Western Domain.

(iv) the emplacement of the Vyborg and Salmi huge rapakivi intrusions provide an additional potential uranium rich source in the area (U content in the rapakivi granites vary from 3.6 in the ovoidal biotite-amphibole granites to 7.6 ppm in the fine-grained leucogranites, Th vary from 20 to 32 ppm correspondingly).

An regolithic profile occurs at the top of the basement developed in the schists and in the granites just below the Mesoproterozoic sandstones. In the gneiss and schist lithologies it presents by a red hematite - kaolinite zone followed by a green Fe-chlorite – kaolinite – illite zone as in the Athabasca and Kombolgie basins. In the rapakivi granites the regolithic profile presents especially by a red hematite – kaolinite quartz-rich zone.

It is still debatable if this alteration was related to a paleoweathering prior to the Mesoproterozoic sedimentation or to an alteration of the basement by the basinal diagenetic fluids. However, the present alteration paragenesis is very similar to the alteration observed in the sandstone indicating a least a strong overprinting of a presumed paleoweathering profile.

Monazite and zircon have been used as indicators of uranium leaching and uranium mineralized fluid circulation correspondingly, were especially studied in the investigated basement rock types. Monazite alteration of the basement was not discovered in the Ladoga Lake area on the contrary to the well revealed alteration of monazite in the Athabasca and Kombolgie basement rock lithologies.

Contrary to monazite, clear evidences of zircon alteration were observed in all basement rocks of the Ladoga Lake area, even in outcropping domains up to 20 km outside the present extension of the Pasha – Ladoga basin. The different types of zircon from the different basement lithologies are characterized by moderate to strong enrichment of Al, P, Ca, Fe, Y, U and sometime Th in the zircon formula. Compared to the Athabasca basin, zircon alteration in the Pasha Ladoga basin area is characterized by larger amounts of Y and the presence of significant Th substituted in the structure.

In the vicinity of the unconformity surface all basement rocks were strongly altered during diagenesis and hydrothermal alteration of the Pasha – Ladoga volcanic-sedimentary formations. They are characterized by the strong variations in their chemical composition, especially within so-called paleoregolith profile. Some regolithized gneisses and schists in the vicinity of the unconformity surface present a slightly negative Ce anomaly. This slightly negative Ce anomaly may represent an indication of a paleolateritic alteration, which is highly oxidizing enough to oxidized cerium from the trivalent to quadrivalent valence. In the rapakivi granites, this Ce negative anomaly was not found, they are mostly richer in REE than gneisses and schists. Eu anomaly is less important in the regolithized rocks than in the fresh granites.

The most altered Paleoproterozoic rocks are moderately enriched in U and chalcophile association elements and are usually depleted in Th and LREE, but in some profiles strong enrichment in Th and LREE together with moderate enrichment in U and intermediate HREE in the altered pegmatoidal graphitic gneisses have been observed.

Chapter III

Riphean sedimentary sequences of the Pasha – Ladoga basin

Part 3.1. Geology and petrography of the sandstones

3.1.1. Geological setting

In the Ladoga Lake region (Russian Karelia) during Mesoproterozoic the Pasha-Ladoga complex volcanic - sedimentary basin was formed. Riphean volcanic – sedimentary formations were deposited in graben-like basin. The maximum present thickness exceed 2000 m according to Amantov et al. (1996). The present extension of the Pasha – Ladoga basin is moderate (approximately 70 000 km^2), and its shape roughly coincides with the coastline of the Ladoga Lake (Russian Karelia). The basin present three extensions beyond the Ladoga Lake shore: (i) North-Eastern (Salmi), (ii) Western (including Yablonevka) and (iii) South-Eastern (Pasha) areas, which are completely covered by Quaternary (the first one) or Vendian - Paleozoic sediments (Kushnerenko & Pichugin, 2000; Novikov et al., 2001).

The cross section through the Pasha – Ladoga basin and the stratigraphic succession for each isolated area of the basin were given above (Chapter 1.2), detail lithological and petrographical description will listed below. DDH and outcrops samples location is presented in Part 1.4.

3.1.2. Composition and provenance of the Riphean Pasha – Ladoga basin succession

Lithology, petrography and mineralogy of the Pasha – Ladoga succession has been described in unpublished reports of Sevzapgeology (Sharpilo et al, 1991) Nevskgeo (Polikarpov, 1993), VSEGEI (Amantov, 1989; Mikhailov, 2001), VIMS (Ledeneva, 1990), IGEM (Velichkin et al, 2001) and MGGA (Ignatov, 2000) as well as in published papers (Kushnerenko and Pichugin, 2000; Ledeneva, 2000; Lobaev et al, 2003; Mikhailov, 2001, 2003; Novikov et al, 2001; Shurilov et al. 2003; Velichkin et al., 2003).

Priozersk Suite

The composition and the structure of the Priozersk suite are rather monotonous over the territory of the Pasha-Ladoga Basin (Fig. 3.1). The thickness of the Priozersk suite varies from 20 to 80 m in the Salmi area, may reach 265 m in the Yablonevka area and from 452 m

at the margin and up to 1500 – 1600 m in the axial part of the Pasha area (Kushnerenko & Pichugin, 2001). The Priozersk suite section is the most completely studied in the Pasha area (southern part of the basin), where it is intersected by a deep drilling (DDH-2 see for location Fig. 2.58) from - 457 to - 909 m. This drilling did not reach the base of the suite.

The sandstones of the suite lie gently on the Archean – Paleoproterozoic basement rocks above a well-developed alteration profile. They are not affected by any metamorphic process and have a massive structure, sometimes with cross-beds. Beds of coarse-grained sandstones and small pebble-conglomerates occur at the base of the suite. Rare claystones intercalations occur along with sandstones and gritstones horizons.

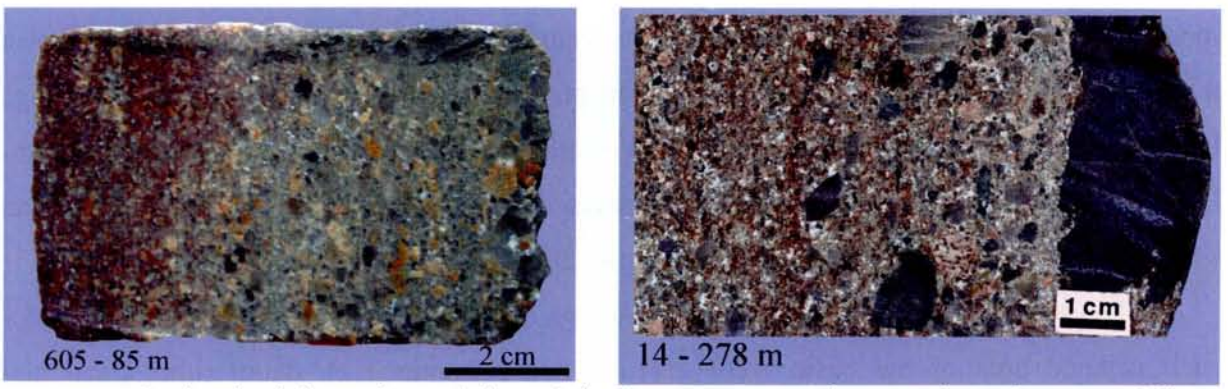

A - coarse-grained polymictic sandstone (gritstone) in the Salmi area (sample DDH-605- 85 m, Karku deposit, ore zone I)

B - quartz conglomerate layer in quartz-feldspar gritstone in the Pasha area (sample DDH-14-278 m)

Fig. 3.1. Priozersk suite sediments in the different parts of the Pasha – Ladoga basin

Most of the Priozersk suite sandstones present highly immature mineralogical characteristics and reflect correspondingly the composition of the subjacent basement rocks. The sandstones consist of polymict quartz – feldspar (arkosic) conglomerates and coarse to medium-grained sandstones with 70-90 % of clastic material. Rocks are mainly massive, sometimes stratified horizontally or with crossbeddings, with various intensity of pink to red, also grey and violet colours. Brown spots and banding sometimes occur (Fig. 3.2). The layers are gently dipping (5 to 15° to SW direction).

Detrital minerals are represented predominantly by quartz (50-70 %), abundant K-feldspar (10-30 %), minor plagioclase (up to 5 %), biotite and rare muscovite (2-5 %). Basement rock clasts (up to 5 %) are also very common. The shape of the quartz grains varies from angular and elongated to well rounded and isometric (Fig. 3.3). Grain size varies from 0.2-0.3 mm up to 3-5 mm in sandstones and gritstones (5-20 mm in basal conglomerates). Roundness of the grains increases from the bottom to the top of the Priozersk suite.

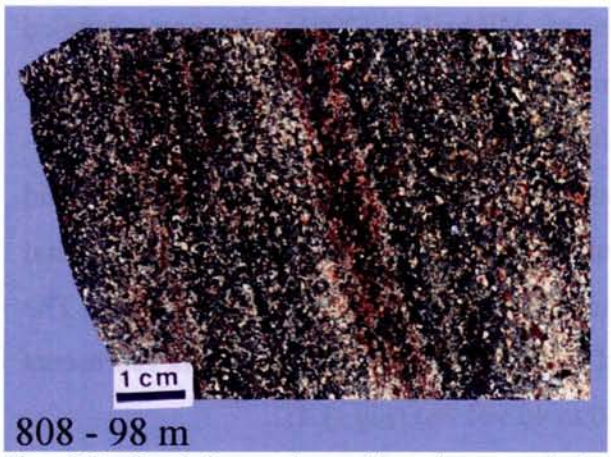

Fig. 3.2. Banded grey-brownish gritstone of the Priozersk suite (sample DDH-808-98 m)

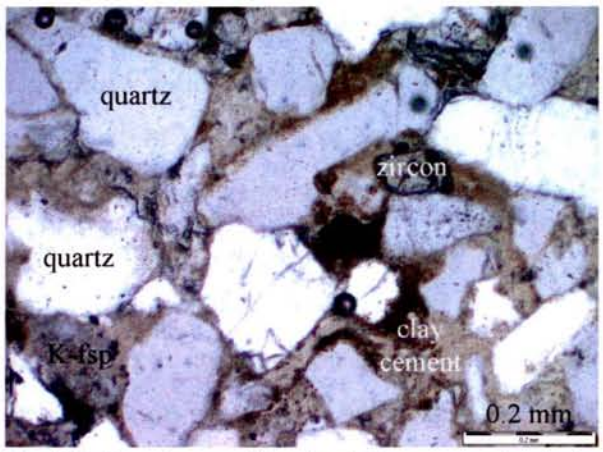

Fig. 3.3. Roughness of the detrital quartz grains in the Priozersk sandstones (sample DDH-389-174 m), parallel nicols, scale 0.2 mm

Detrital accessory minerals are predominantly represented by zircon, abundant Ti oxides (mostly rutile) and rare monazite, apatite, garnet and xenotime.

The primary cement consists predominantly of kaolinite and smectite. The matrix represents 5 to 10 vol. % of the rock (up to 15 – 20 vol. %).

Salmi Suite

In the Salmi and Pasha areas, the Priozersk suite is overlapped by the volcanic – sedimentary association of the Salmi suite with a structural unconformity.

In the Salmi area, the Salmi suite, reaches a total thickness of 50 to 220 m and is characterized by three subsuites (Mikhailov et al, 2001):

(i) The Lower volcanic subsuite (up to 140 m thick) represented by aphyric basalts with lenses and interlayers of poikilophytic diabases;

(ii) The Intermediate clastic subsuite ((22 to 30 m thick) consisting of light grey to light brown, middle to coarse grained quartz – feldspar and polymictic sandstones;

(iii) The Upper volcanic subsuite (7 to 76 m thick) composed of amygdaloidal basalts, lava breccias and tuffs. The volcanic rocks are mostly aphyric or microporphyritic with a hyaline to holocrystalline groundmass. The amygdales are filled with carbonate, chlorite, quartz and sometimes iron hydroxides. The most dominant type is an olivine-plagioclase-clinopyroxene basalt.

In other interpretation the Lower Volcanic Subsuite belongs to the top of the Priozersk suite (Kushnerenko & Pichugin, 2001; Novikov et al., 2001), but in the present work I will

remain consistent with the first interpretation of Mikhailov (2001). A more detailed description of the volcanic subsuites will be given below in the Chapter IV.

From the base to the top of the suite a sedimentation rhythm is well observed: coarse-grained polymictic sandstones - greywackes change to medium-to small-grained arkoses and finally to quartz-feldspar fine-grained sandstones. The Salmi suite sandstones detrital minerals are mainly quartz and K-feldspar, abundant volcanic clasts, minor plagioclase. The predominant cement composition is composed of carbonate and clays. The matrix represents 15 to 25 vol. % of the rock (exceptionally up to 30 to 40 vol. %) (Fig. 3.4).

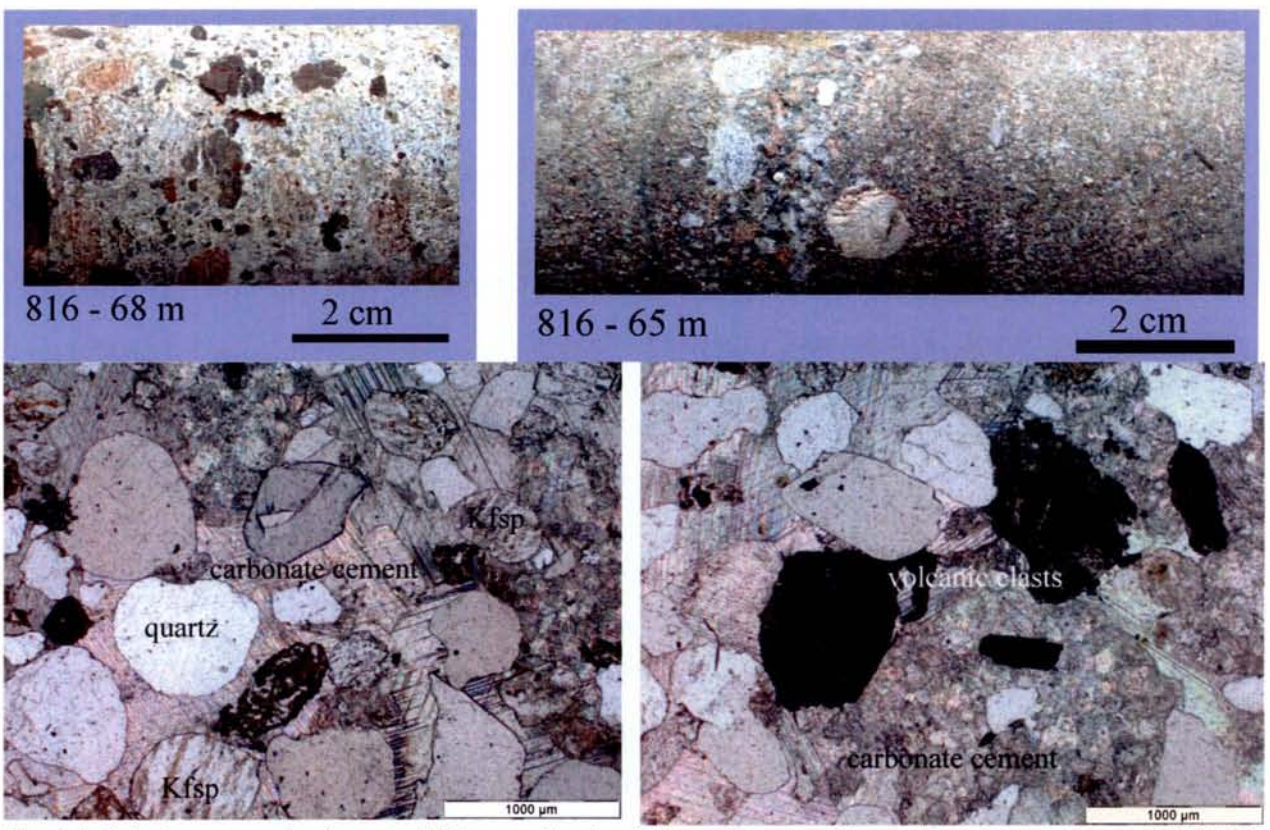

Fig. 3.4. Salmi coarse-grained quartz-feldspar and polymictic sandstones with conglomerate interlayers (DDH-816, A – B: interval 65 – 68 m, Salmi area). Photomicrography of sample 816-68 m: C and D – parallel nicols, scale 1000 µm

Pre-Ladoga suite

In the Yablonevka area (Western Ladoga), the Pre-Ladoga suite stratigraphically corresponds to the Salmi Suite in the Salmi and Pasha areas.

Sandstones and conglomerates of the Priozersk suite are overlapped by sandstones, siltstones and clays, sometimes with a carbonate cement, limestones and dolomites of the Pre-Ladoga suite. The thickness of the Pre-Ladoga suite varies from 40 to 60 m.

The detrital material (40 – 50 vol. % of the rock) of the Pre-Ladoga sandstones (Fig. 3.5 – 3.7) are presented by quartz (up to 60 % of detrital material), K feldspar (15 – 25 %) and plagioclase (15 – 20 %), biotite is also observed in biotite-rich layers and interlayers (up to 50 vol. %) The primary red-bed hematized sandstones are usually bleached (hematite is replaced by interstratified illite-smectite minerals). The clay matrix represents 50 to 60 vol. % of the rock. A carbonate cement is often recorded in the sandstones. Accessory minerals are usually represented by zircon and Ti oxides.

Rare layers and lenses of dolomitic stromatolite-like nodulous and microcavernous rocks with the presence of terrigenous material are also found (DDH-103-137 m – Fig. 3.8) within an essentially siltstone-sandstone sequence .

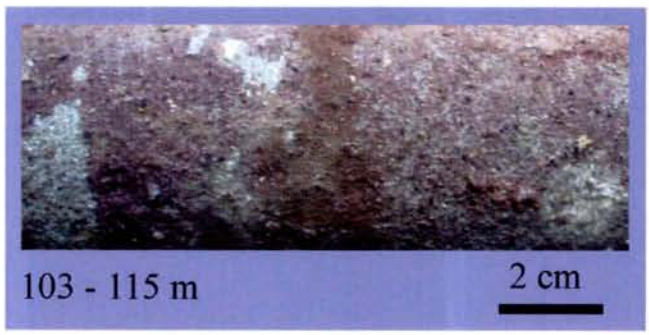

Fig. 3.5. Red-bed sandstone of the Pre-Ladoga suite with bleached parts (sample DDH-103-115 m, Yablonevka area)

Fig. 3.6. Pre-Ladoga fine-grained sandstone with small pebbles of quartz and clays (sample DDH-103-136 m, Yablonevka area)

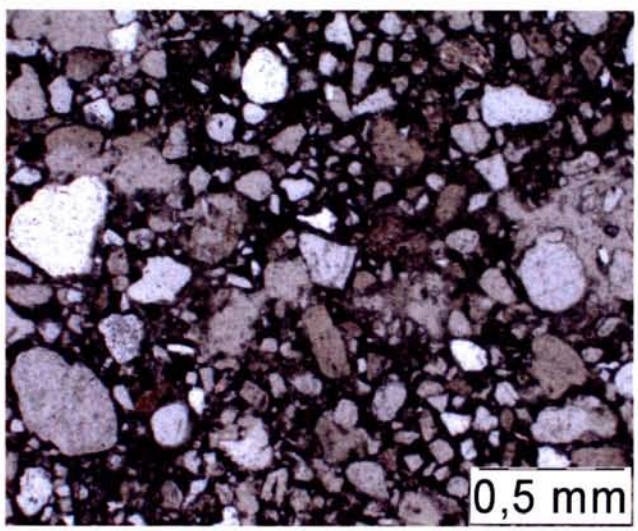

Fig. 3.7. Pre-Ladoga fine-grained sandstone with small pebbles of quartz and clays (sample DDH-103-136 m, Yablonevka area)
Parallel nicols; photomicrograph scale – 0.5 mm

Fig. 3.8. Stromatolite-like dolomitic rocks within the essentially clastic sequences (sample DDH-103-137 m, Yablonevka area)

Pasha suite

In the Salmi and Pasha areas, the Middle Riphean deposits section is covered by the siltstone-sandstone-clays sequence of the Pasha suite. The composition of terrigenous sediments of the suite differs in these areas.

In the Salmi area the Pasha suite is represented by fine-pebbled quartz conglomerates at the bottom and polymictic siltstones, clays, fine-grained sandstones in the upper part of the sequence. The thickness of the suite is over 250 meters (Fig. 3.9).

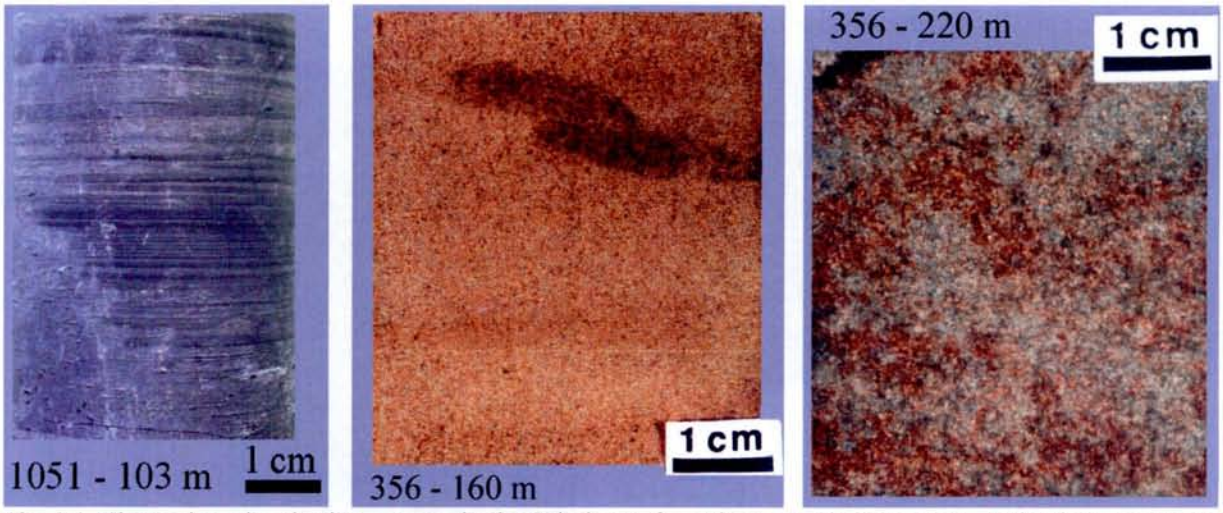

Fig. 3.9. The Pasha suite clastic sequence in the Salmi area from the top to the bottom: a – polymictic sandstone (sample DDH-1051-103 m); b – fine-grained sandstone (sample DDH-356-160 m); c – sandstone (sample DDH-356-220 m)

The Pasha area suite, is mostly characterized by coarse-grained sediments: well-rounded quartz – feldspar conglomerates, gritstones and sandstones (Fig. 3.10). The thickness of the suite reaches up to 150 m. In this area, the Pasha suite is covered by the Vendian sedimentary rocks of the Gdov horizon (not studied here).

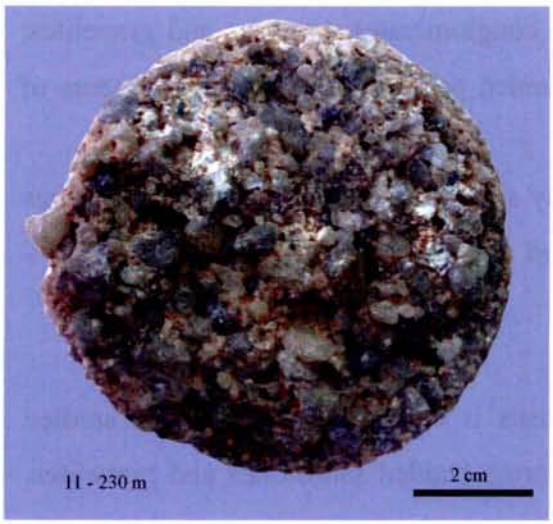

Fig. 3.10. Quartz-feldspar small-pebbled conglomerate of the Pasha suite (sample DDH-11-230 m, Pasha area)

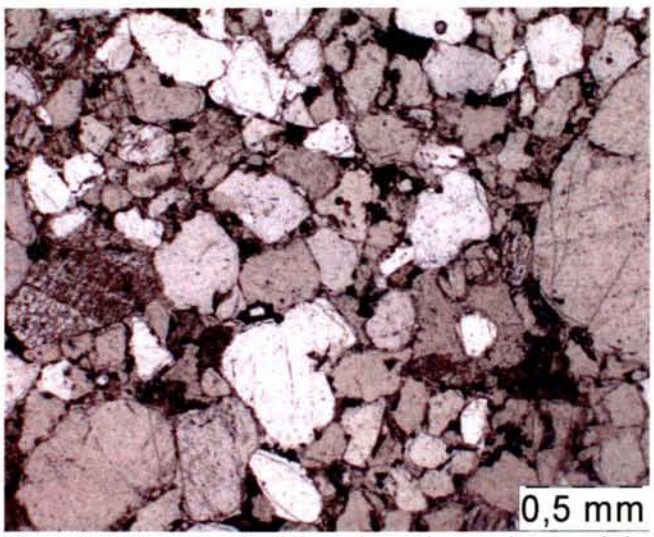

Fig. 3.11. Coarse-grained inequigranular sandstone of the Pasha suite (sample DDH-11-237 m, Pasha area), parallel nicols, photomicrograph scale 0.5 mm

Yablonevka suite

The Yablonevka suite (5 to 55 m thick) is the final member of the Pasha – Ladoga volcanic – sedimentary group in the Yablonevka area, which can be stratigraphically correlated with the Pasha suite. It consists of coarse-grained polymictic sandstones, gravelites and till-like sediments (red–brown clay sediments with coarse pebbles of quartzites, gneisses and volcanic rocks). The Yablonevka sandstones correspond to very badly sorted rocks with a very low degree of lithification and enrichment in iron oxides.

3.1.3. Lithogenetic types of the Pasha – Ladoga Mesoproterozoic (Riphean) sequence

The most stratigraphically complete Mesoproterozoic (Riphean) sections are observed in the DDH-101, 103 and 104 in the Yablonevka area (Fig. 2.48) (Ignatov et al, 2000).

A series of lithologic associations, characteristic of continental deposits, are evidenced by their petrographic characteristics with eluvial, deluvial-proluvial, polygenic subaerial, deltaic (alluvial-proluvial) and lake deposit types.

Eluvial deposits are widely distributed directly on the basement rocks and include soft and friable (regolithized) granite-gneisses, schists and granites, which is composed essentially of hydromica with relicts of quartz and feldspars.

Deluvial-proluvial deposits correspond to two types of rocks:

(i) Mostly red colour badly sorted polymictic conglomerates, breccias and gravelites, cemented by fine- and medium angular to rounded pebbles and angular fragments of quartz and metamorphic rocks.

(ii) Dark – cherry coloured mudstones and clay siltstones, interlayered with gravelites and breccias. In mudstones impurity, non sorted quartz - feldspars grains may occur – which is typical of basal Riphean strata.

The association of the alluvial-proluvial deposits is clearly observed in the studied sections. It corresponds to red-coloured well sorted cross-bedded sandstones and gravelites. They mostly consist of typical coarse - middle and fine-grained arkosic and quartz-feldspathic sandstones with large diagonal, middle wedge-like, cross wave-like and fine cross wave-like laminations. Laminations and flaminations are emphasized by the distribution of biotite and frequently hematite. In coarse-grained sandstones large cross wave-like lamination is frequently emphasized by the distribution of feldspar and quartz gravels.

The main common features of the Mesoproterozoic (Riphean) formations (Kayryak, 1979, Konopleva, 1979, Konopleva, Tikhomirova, 1979; Ignatov et al, 2000) are:

(i) The presence of large sedimentologic rhythms corresponding to terrigenous rocks with coarse detrital fragments at the base and fine detrital fragments above. In stratigraphically complete sections it goes up to true change of petrographic composition of the rocks – from greywackes at the base progressively replaced by arkosic rocks upwards, grading to quartz – feldspar and oligomictic quartzose sandstones at the top.

(ii) The presence of tuffs of the basic volcanics covers which occur in the median part of the Riphean sequence and which are considered as marking horizons.

3.1.4. Stratigraphy of the Mesoproterozoic Formations below the Ladoga Lake

Lithology and stratigraphy of the Mesoproterozoic (Riphean) Formations below the Ladoga Lake has been described in Amantov et al, (1989, 1990, 1991, 1992, 1993, 1996). The rock units have been defined from their seismic properties and correlated with the geology of the adjacent shore areas and outcrops from the bottom of the lake. Some lithological varieties are also known from glacial boulders and a few drill cores performed on the lake (Amantov et al, 1989).

According to Amantov data (mainly based on seismic observations) the whole Mesoproterozoic (Riphean or Jotnian) sequence can be divided into four main units (Fig. 3.12). The lowermost unit belongs to Lower – Middle Riphean; the two following units to Middle Riphean mainly, while the youngest one is attributed to Middle Riphean mainly or eventually Lower Vendian (Amantov, 1992, 1993).

The basal conglomerate of *unit 1* covers the crystalline basement. Layers of fine-grained sandstones and siltstones are subordinate. The maximum total thickness of the unit is about 1000 m.

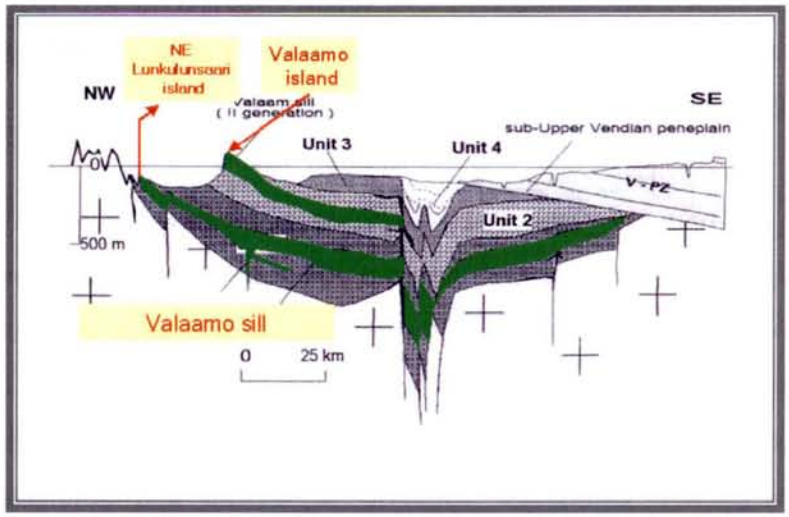

Fig. 3.12. Cross section of the Lake Ladoga basin based on seismic reflection studies as reported by Amantov et al (1996).
Two major mafic sill sequences and 4 sedimentary units are discerned

Unit 2 has been traced everywhere and overlay unit 1 without evident unconformity but with a distinct seismic boundary (Amantov, 1992; 1993). The unit is characterized by dark-coloured laminated siltstones. The layer thickness increases downwards, where also sandstone layers appear. The total thickness of the unit is about 500 m. This unit probably corresponds to the upper part of the Salmi suite, but there are limited evidences for this conclusion.

Unit 3, about 400 m thick, is mostly a seismic subdivision. Lithological composition is as yet unknown, but by its position may correspond to the sediments of the Pasha Suite.

Finally, *unit 4* does not correspond to any horizons known in the sub-surface Mesoproterozoic (Riphean) sequences. This unit is connected with a new phase of tectonic activity, starting with emplacement of magma of the same age as Valaam sill. The associated sequence overlies older Mesoproterozoic (Riphean) sequences with obvious unconformity. The upper part of the unit has probably Upper Riphean to Lower Vendian age. *Unit 4* represents the youngest known infilling of the Pasha – Ladoga graben – syncline, with a total thickness of about 600 – 700 m. After peneplation, the mature tableland was covered by Upper Vendian sediments of the Valday series (Amantov, 1993).

Part 3.2. Alteration processes in the Mesoproterozoic Pasha - Ladoga sandstones during diagenesis and hydrothermal activity

On the basis of petrographic observations and mineral paragenesis, three main alteration stages have been distinguished in the Mesoproterozoic (Riphean) clastic sediments of the Pasha – Ladoga basin (Salmi area) (Bylinskaya et al., 2004; Lobaev et al., 2003; Novikov et al., 2001; Shurilov et al., 2003; Velichkin et al., 2001):

1) *Regional diagenetic re-equilibration processes* at the scale of the whole Pasha – Ladoga basin. The regional diagenetic features are well expressed in selected samples from the *Salmi*, *Yablonevka* and *Pasha* areas, which have not been significantly affected by subsequent alterations. The diagenetic event is multistage and mainly consists in the quartz overgrowths over detrital quartz crystals, hematization, recrystallization and transformation of coarse-grained authigenic kaolinite to dickite and authigenic smectite by illite with neoformation of interstratified illite-smectite;

2) *Syn- to late-ore local hydrothermal alteration processes* at the scale of the *Salmi* area, where the *Karku* uranium deposit is located, close to the unconformity surface. The hydrothermal alteration event is also multistage and is characterized by partial quartz dissolution, chloritization, carbonatization, sulphidization and uranium mineralization;

3) *Post-ore retrograde diagenetic processes* occurring locally in the Karku deposit area. Post-ore processes are represented by secondary hematization and sandstone bleaching with secondary kaolinization, probably related to the infiltration of meteoric fluids.

3.2.1. Regional diagenetic re-equilibrations processes

Quartz dissolution and silicification

The processes of quartz dissolution under pressure at the grain contacts led to the development of epitaxic quartz overgrowths around the detrital grains and around which hematite, chlorite crystals and clays are trapped. This process is particularly observed in the middle and partly at the top of the Priozersk Suite, where variably hematized arkoses occur. The primary contour of the quartz crystals is underlined by inclusions of cement minerals difficult to identify and by chlorite and hematite (Fig. 3.14).

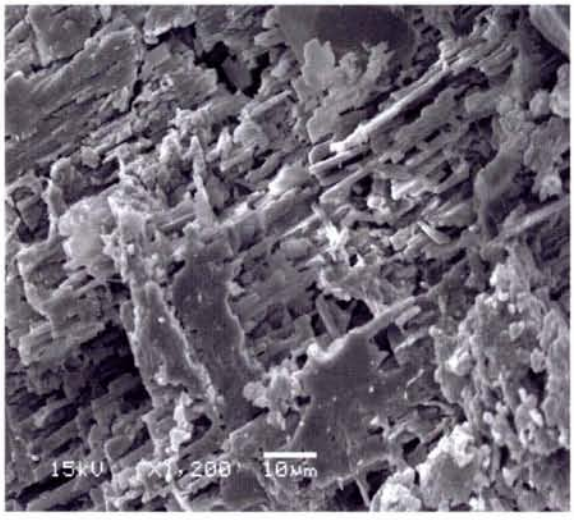

Fig. 3.13. Process of the partial dissolution of K feldspar in the Priozersk sandstones. BSEM image: DDH-654-117 m, line scale 10 µm (photo from Brunet, 2004).

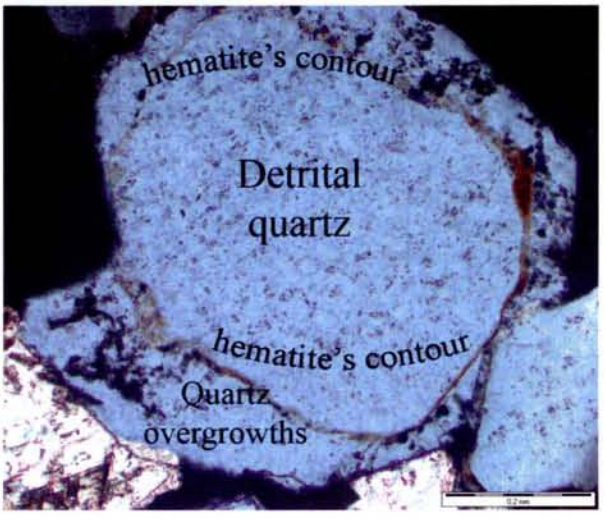

Fig. 3.14. Detrital grains of quartz with diagenetic overgrowths in the basal sandstones of the Priozersk suite. Photomicrograph: DDH - 625 - 127 m. Parallel nicols, line scale – 0,2 mm.

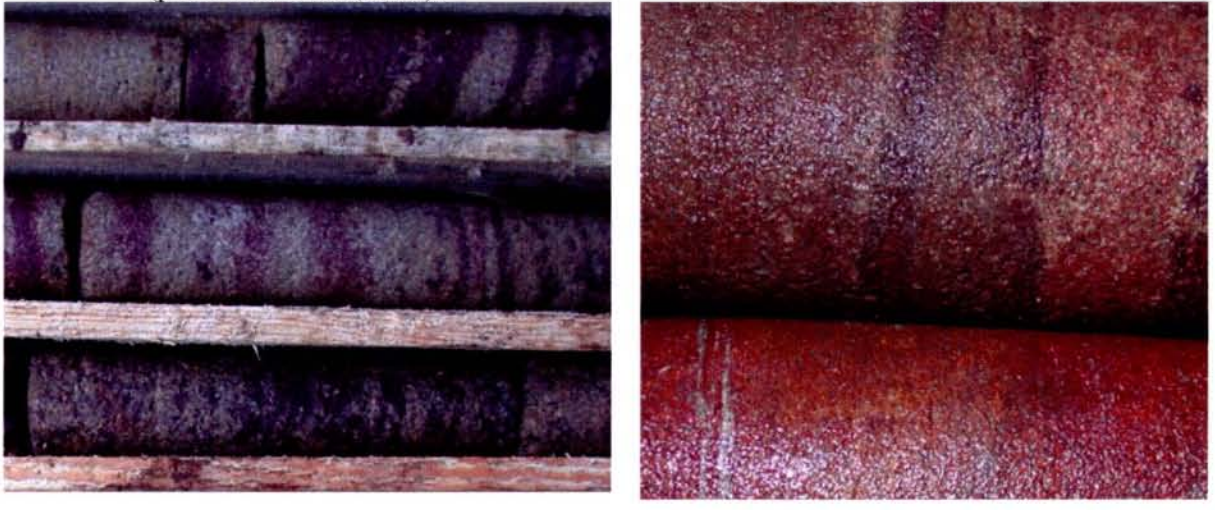

Fig. 3.15. Relics of the diagenetic hematization in the Priozersk sandstones - dark purple hematite bands (photo 1), overprinted by secondary hematization corresponding to bright red rose hematite (photo 2). DDH-861 (Salmi area).

Diagenetic hematite has a red purple colour or appears as red grey bands parallel to the stratification, contrary to the secondary alteration, which has a rose to light red colour appearing in bands cutting the previous hematite banding (Fig. 3.15).

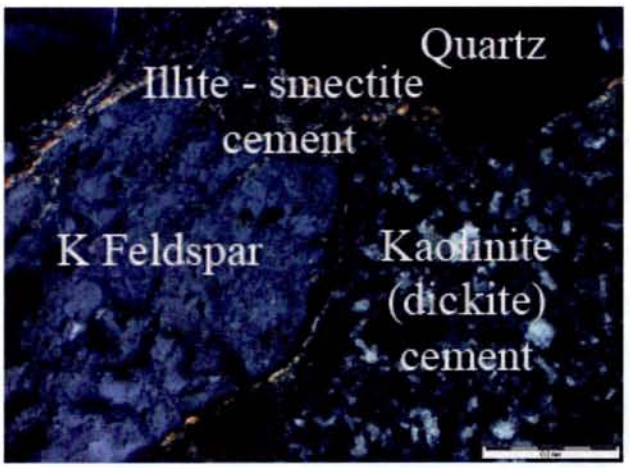

Fig. 3.16. Kaolinite (dickite) and illite – smectite cement is in the sandstones from the upper part of the Priozersk suite (Salmi area). Photomicrography: DDH- 625 - 113 m, Crossed nicols, line scale – 0.2 mm

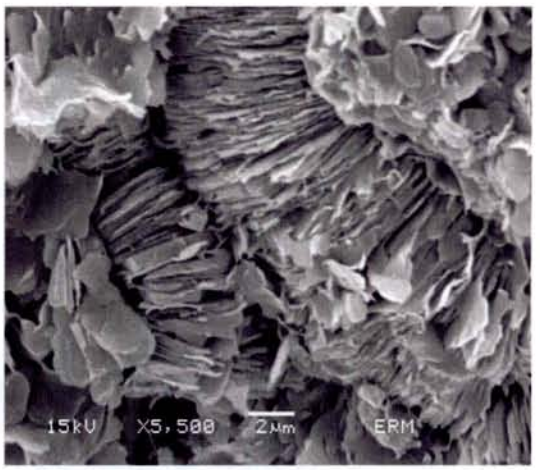

Fig. 3.17. Vermicular kaolinite with intercalated pseudomorphs of dickite (thick booklets) in the sandstones of the Priozersk suite (Salmi area). BSEM image: DDH-816-179, line scale 2 µm (photo from Brunet (2004)

Kaolinite – dickite associations

In Figure 3.17 the pseudomorphic replacement of the coarse-grained booklets of kaolinite by dickite is observed. Partial dissolution of kaolinite (locally on the margin of the booklets) may occur locally. The relative proportions of kaolinite (vermicular and booklet morphology) and dickite (subhedral to euhedral hexagonal morphology) polymorphs is about 40 - 30 % and 60 – 70 % respectively (Fig. 3.18, 3.19).

Detailed X-ray diffractometry (XRD) studies of disoriented powder samples by Brunet (2004) allow the distinction of the different kaolinite polymorphs: peak at 2.34 Å for kaolinite and 2.32 Å - for dickite. Kaolinite is also characterized by the presence of a double peak at 4.12 and 4.17 Å and dickite – by single peak at 4.13 Å. In most cases, kaolinite (or dickite) infrared spectra display dominant free water 1900 nm absorption peak and/or minor asymmetry in the 1400 nm absorption peak, which can not be explained by the presence of intergranular water. These features may indicate the presence of minor amounts of smectite clays in the kaolinite (dickite) structure.

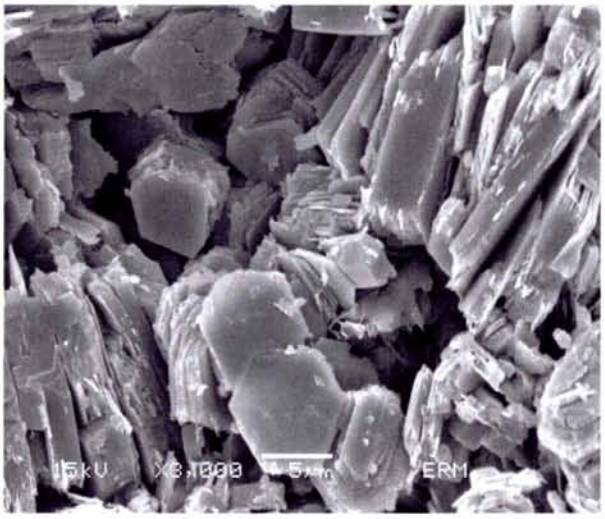

Fig. 3.18. Thin booklets of kaolinite with intercalated thick booklets of dickite in the sandstones of the Priozeskaya Suite of the Pasha area. SEM image: DDH-11-255, line scale 5 μm (photo from Brunet (2004)

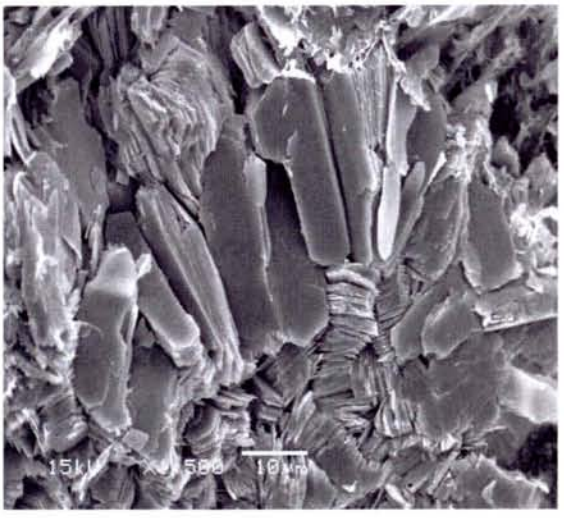

Fig. 3.19. Elongation and thickening of kaolin group minerals by *c* axis during kaolinite – dickite transition in the Priozerskaya sandstones of the Pasha area. SEM image: DDH-11-255, line scale 10 μm (photo from Brunet (2004)

Illite – smectite structure ordering

Ordering of the smectite structure is characterized by the formation of interstratified I/S minerals (Fig. 3.20, 3.21). Progressive conversion of smectite to illite is controlled by the temperature evolution and burial depth. Absence of pure illite confirms that the temperature or depth were not sufficient for the formation of this mineral.

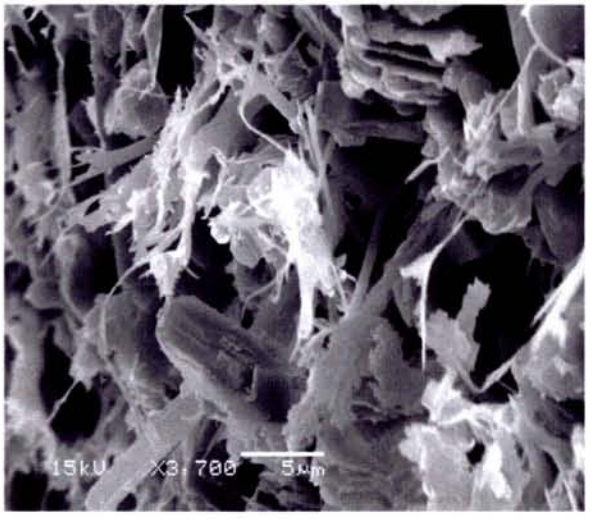

Fig. 3.20. Fibrous elongated crystals of I/S minerals in the Priozersk sandstones (Pasha area). BSEM image: DDH-11-255, line scale 5 μm (photo from Brunet (2004)

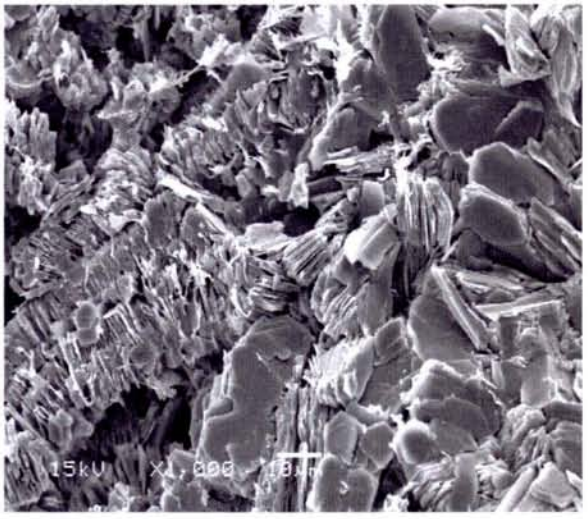

Fig. 3.21. Appearance of fibrous I/S minerals on the margins of vermicular crystals of kaolinite in the Priozersk sandstones (Pasha area). BSEM image: DDH-11-255, line scale 10 μm (photo from Brunet (2004)

XRD investigations by Brunet (2004) show a single peak, varying from 10.2 Å to 14.35 Å, depending on the illite proportion, and provide evidences for the existence of two distinct types of interstratified minerals: a first predominant one - with 60 – 65 % of illite and a second minor one – with 80 % of illite.

The chemical composition of the I/S minerals was determined by subtracting the theoretical formula of illite - $[Si_{3.3}Al_{0.7}]O_{10}Al_{1.8}R^{2+}{}_{0.2}(OH)_2K_{0.9}$ (Meunier, 1989) to the I/S composition assuming that the potassium was exclusively in the illite structure as:

$[Si_{3.46}Al_{0.7}]O_{10}Al_{1.81}Fe_{0.13}Mg_{0.08}(OH)_2K_{0.6}Ca_{0.05}Na_{0.01}$ taking a proportion of illite component of 67.6 % (Brunet, 2004).

Sandstone clay composition in the whole Pasha - Ladoga basin

The relative proportions of the detrital minerals in of the Pasha – Ladoga sandstones can be also globally deduced from the geochemical data for 45 analyzed samples using the Q-A (Debon and Le Fort, 1988 modified) and in the ternary classification diagram (Fig. 3.22 and 3.23).

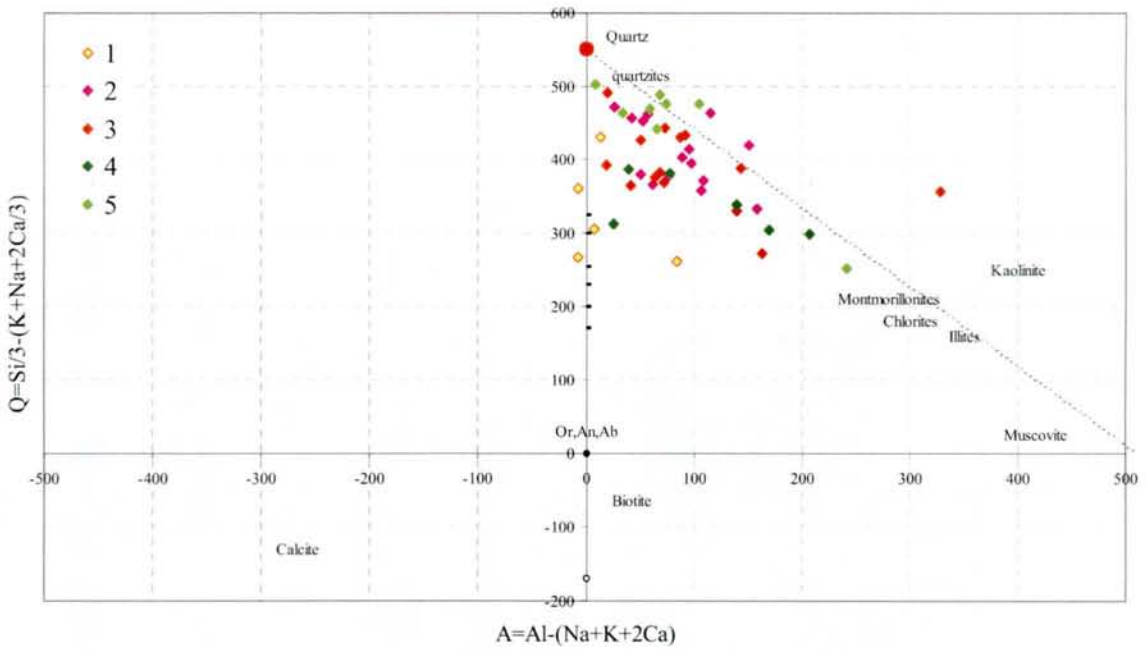

Fig. 3.22. Clay composition of the sandstones from the Pasha - Ladoga basin in the Q-A diagram (parameters Q and A after Debon and Le Fort,1988).
Legend: 1 – Salmi and Pasha sandstones (Salmi area); 2 – non-mineralized (U < 4 ppm) Priozersk sandstones (Salmi area); 3 - slightly mineralized (4 < U < 15 ppm) Priozersk sandstones (Salmi area); 4 – non-mineralized sandstones (Yablonevka area, Western Ladoga); 5 – non-mineralized sandstones (Pasha area, SE Ladoga).

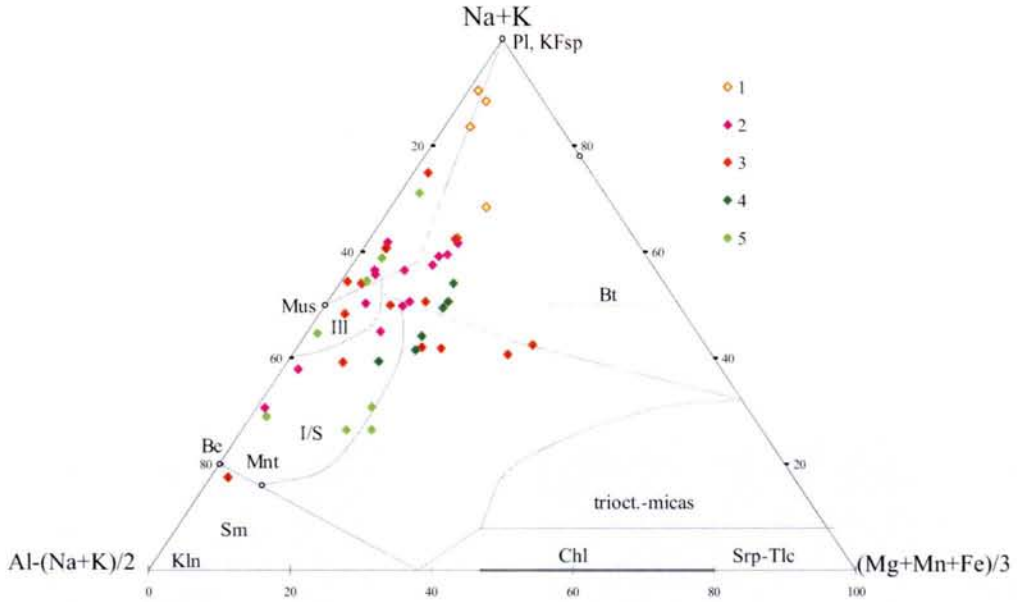

Fig. 3.23. Mineral composition of the Pasha – Ladoga basin sandstones in the ternary clay diagram. Legend: as in Fig. 3.22.

The sandstones of the Salmi and Pasha suites from the Salmi area are essentially composed of quartz and feldspar because they plot along the Q axis (with A ≈ 0) (Fig. 3.22). In the triangular diagram these sandstones appear rich in K-feldspar and/or plagioclase with small amounts of illite/muscovite and/or kaolinite, and/or chlorite (Fig. 3.23).

Non-mineralized (U < 4 ppm) and slightly mineralized (4 < U < 15 ppm) Priozersk sandstones and conglomerates of the Salmi area, in the Q-A diagram (Fig. 3.22) correspond to a mixture of quartz and clay minerals with variable amounts of K-feldspar and/or plagioclase. In the ternary clays diagram (Fig. 3.23) their composition plot between the kaolinite/illite – feldspars side and the chlorite field. They are globally richer in clay minerals relative to feldspars with kaolinite, illite, chlorite and possibly interstratified minerals (but cannot be discriminated here), some of them are characterized by high proportions of chlorite.

Non-mineralized sandstones from the single DDH of the Yablonevka area present highly variable proportions of feldspars and clay minerals (Fig. 3.22), mostly consisting of interstratified minerals (illite-chlorite, illite-smectite mixtures) (Fig. 3.23).

On the contrary non-mineralized sandstones from two DDH of the Pasha area are characterized by their maturity relative to other sandstones of the Pasha – Ladoga basin with a large proportion of quartz relative to feldspars and clay minerals (Fig. 3.22). The proportion of feldspar to clay is highly variable but most of the samples are clay-rich with I/S illite-smectite – kaolinite mixtures (Fig. 3.23).

3.2.2. Syn to late-ore alteration processes

The syn-ore hydrothermal alteration event is accompanied by significant dissolution of the diagenetic minerals (kaolin minerals, hematite and quartz), neoformation of Fe-Mg chlorite (chamosite) and Mn-enriched calcite and subsequent intensive sulphidization (pyrite, pyrrhotite, Cd-sphalerite, galena, chalcopyrite etc). Uranium mineralization: pitchblende, coffinite formed as a later alteration product of U oxides and U-Ti-Si oxides.

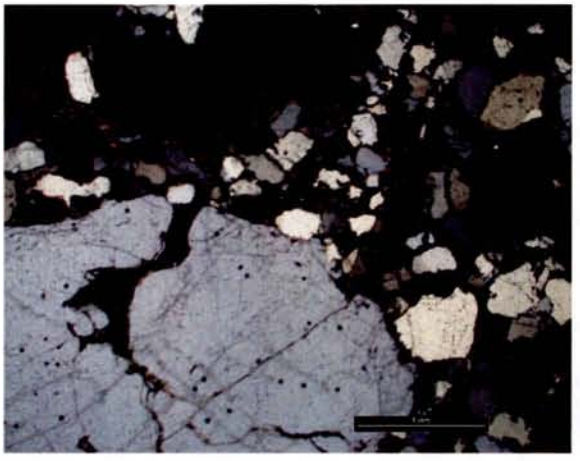

Fig. 3.24. Detrital corroded grains of quartz in the basal conglomerates of the Priozersk suite. Photomicrograph: DDH - 356 - 475 m Crossed nicols, line scale – 1 mm.

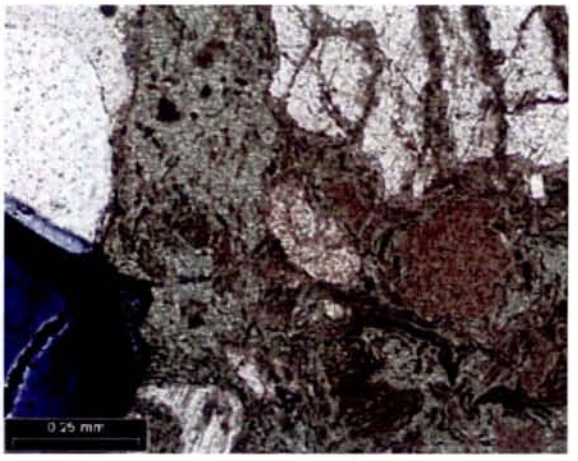

Fig. 3.25. Partial dissolution of quartz during chloritization process in the slightly mineralized sandstones of the Priozersk suite. Photomicrograph: DDH - 625 - 110 m, Parallel nicols, line scale – 0.25 mm.

This process begins with partial quartz dissolution creating open space for the deposition of other minerals. The presence of corroded quartz grains wrapped by chlorite and carbonate indicates filling of open spaces during and/or closely after the quartz removal (Fig. 3.24, 3.25).

Syn-ore chloritization

Chloritization of the cement is the most prolonged process of alteration, which starts already during the diagenetic stage and becomes very intensive and widespread during the hydrothermal stage. Different chlorite generations were formed. At the diagenetic stage minor amounts of chlorite (clinochlore) occur mostly between the detrital quartz grains.

	Karku deposit area			Shea Creek area			
Analysis number	625-110	625-128	625-134	sudoite	Fe-chlorite 1	Fe-chlorite 2	Fe-chlorite 3
SiO_2	27,23	24,65	29,80	36.77	23.34	29.00	34.77
Al_2O_3	20,86	19,98	18,34	33.36	12.10	16.35	18.62
MgO	5,43	3,30	8,49	11.38	3.07	2.77	2.79
FeO	33,69	37,32	30,51	1.41	31.37	32.42	28.66
TiO_2	0,01	0,01	0,23	-	-	0.11	-
MnO	0,43	0,44	1,01	-	-	-	-
CaO	0,14	0,71	0,57	-	0.18	0.19	0.33
Na_2O	0,16	0,04	0,09	-	-	-	-
K_2O	0,02	0,02	0,07	1.18	0.11	0.37	0.51
Total	**87,97**	**86,47**	**89,09**	**84.19**	**70.52**	**81.81**	**85.69**
Si	2,80	2,57	3,02	3.40	3.30	3.40	3.71
Al^{IV}	1,20	1,43	0,98	0.60	0.70	0.60	0.29
Al^{VI}	1,32	1,04	1,21	3.00	1.31	1.66	2.05
Mg	0,83	0,51	1,28	1.57	0.64	0.48	0.44
Fe^{2+}	2,89	3,25	2,58	0.11	3.71	3.18	2.56
Ti	0,00	0,00	0,02	-	-	0.01	-
Mn	0,04	0,04	0,09	-	-	-	-
Total ^{VI}	**5,08**	**4,84**	**5,18**	**4.68**	**5.66**	**5.43**	**5.05**
Ca	0,02	0,08	0,06	-	0.03	0.02	0.04
Na	0,03	0,01	0,02	-	-	-	-
K	0,00	0,00	0,01	0.14	0.02	0.06	0.07
Fe/(Fe+Mg)	**0,78**	**0,86**	**0,67**	**0.07**	**0.85**	**0.87**	**0.85**
Points number	23	22	7	SHE 66-675.5	SHE 79-709.1	SHE 16-696.8	SHE 16-696.8

Table 3.1. Average chemical composition of chlorites from the mineralized Priozersk sandstones (DDH-625) (third ore zone of the Karku deposit)(present work compared with average chlorites from the mineralized Shea-Creek sandstones (Athabasca, Canada) (Lorilleux, 2001).

In the lower part of the Priozerskaya sandstones (mostly in the third ore zone of the Karku deposit area) diagenetic Fe-chlorite (chamosite) is completely replaced as well as the relicts of detrital mica. Dark-green to black-green spherical chlorite is neoformed and widespread in non- to slightly-mineralized Priozerskaya sandstones and conglomerates. Dirty-green to black Fe-(Mg) chlorite is typical for mineralized zones in the vicinity of the unconformity surface (Fig. 3.26).

Sample number	Structural formula of chlorite	Distance to unconformity
654-117 m	$(Fe_{3.23}\ Mg_{1.02}\ K_{0.01}\ Na_{0.01}\ Al_{1.49})\ [Si_{2.96}\ Al_{1.04}]\ O_{10}\ (OH)_8$	28 m
625-110 m	$(Fe_{2.89}\ Mg_{0.83}\ Mn_{0.04}\ Al_{1.32})\ [Si_{2.80}\ Al_{1.20}]\ O_{10}\ (OH)_8$	24 m
625-128 m	$(Fe_{3.25}\ Mg_{0.50}\ Mn_{0.04}\ Al_{1.03})\ [Si_{2.57}\ Al_{1.43}]\ O_{10}\ (OH)_8$	6 m
625-134 m	$(Fe_{2.58}\ Mg_{1.28}\ Mn_{0.09}\ Al_{1.21})\ [Si_{3.02}\ Al_{0.98}]\ O_{10}\ (OH)_8$	0 m
816-161 m (dark zone)	$(Fe_{2.95}\ Mg_{0.98}\ K_{0.03}\ Ca_{0.02}\ Mn_{0.02}\ Al_{1.64})\ [Si_{3.10}\ Al_{0.90}]\ O_{10}\ (OH)_8$	23 m
816-161 m (light zone)	$(Fe_{3.38}\ Mg_{0.80}\ K_{0.01}\ Ca_{0.02}\ Mn_{0.02}\ Al_{1.52})\ [Si_{2.96}\ Al_{1.04}]\ O_{10}\ (OH)_8$	23 m

Table 3.2. Structural formula of chlorites from the mineralized III ore zone (DDH-625, DDH-654) and slightly mineralized II ore zone (DDH-816) in the Priozersk sandstones

Chemical composition of chlorites was also determined and given in Table 3.1. Chemical chlorite formula was calculated on the data from DDH-625 (present work), DDH-654, DDH-816 (Brunet, 2004) and are listed in Table 3.2.

They mostly correspond to trioctaedric ferriferous chlorites of the chamosite group (Fig. 3.27, 3.28). Sometimes interstratified chlorite-smectite and nontronites varieties have been also described (Velichkin, 2001). In contrast to the chlorites from mineralized sandstones of the Shea-Creek area (as well as in the whole Athabasca basin) Mg-chlorite (sudoite) is the prevalent clay mineral, which is associated to uranium mineralization and Fe-chlorites are mostly formed during late mineralization events (Lorilleux, 2001) whereas in the Karku deposit Fe-chlorites are associated with the main mineralization event (Fig. 3.28).

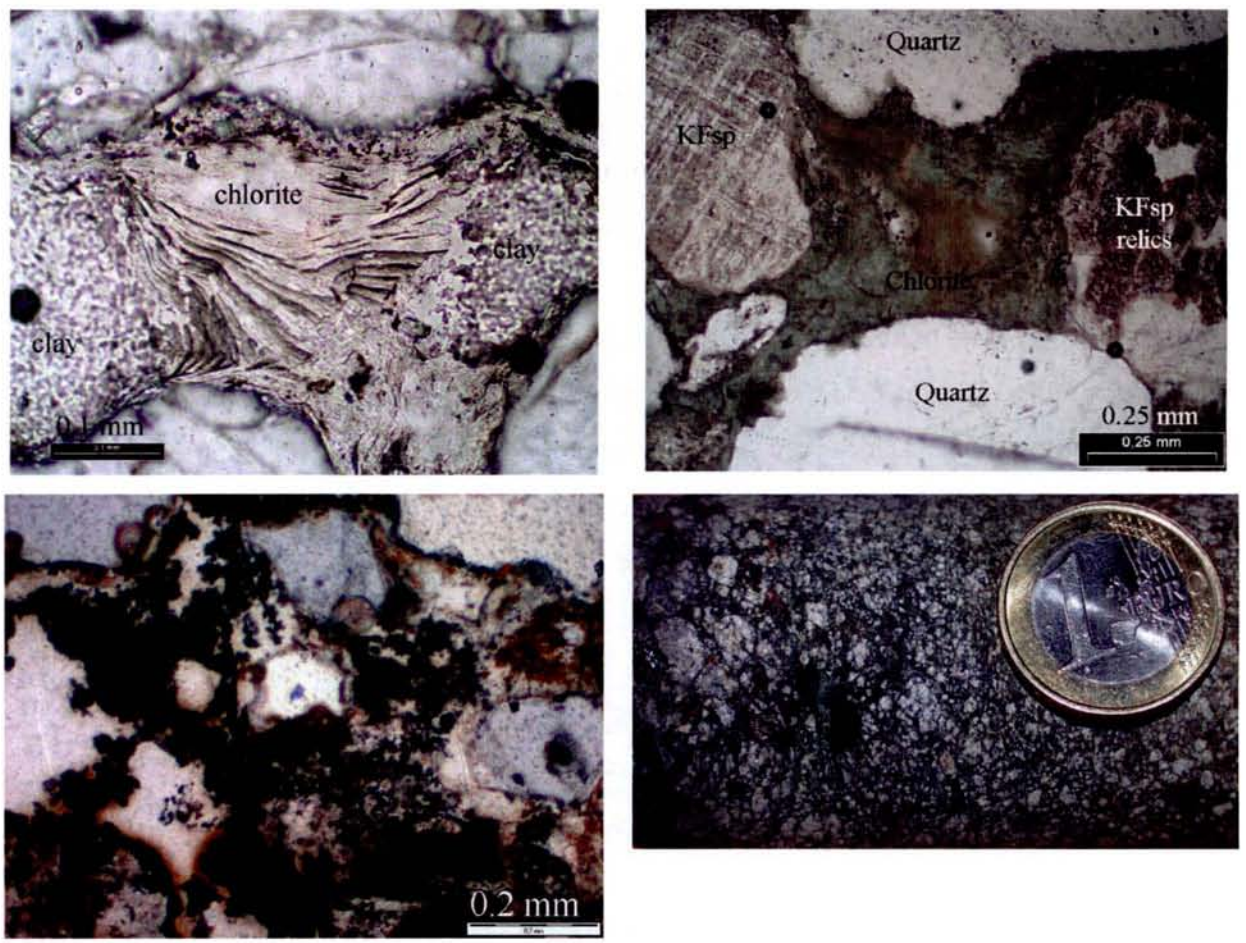

Fig. 3.26. *a*: light-green chlorite, which partially replace the clay cement, in non-mineralized gravelites of the Priozersk suite (Salmi area, DDH-356-475 m), line scale = 0.1 mm, parallel nicols;
b: dark-green chlorite totally replacing the clay cement, in the slightly mineralized sandstones of the Priozersk suite (III ore zone of the Karku deposit, DDH-625-110 m), line scale = 0.25 mm, parallel nicols;
c: dirty-green-black chlorite in the strongly mineralized Priozersk sandstones of the Karku deposit ore zone I, (DDH-605-107), line scale = 0.2 mm, parallel nicols;
d: dirty-dark green chlorite in the strongly mineralized Priozersk sandstones of the Karku deposit ore zone III (DDH-671), scale = 1 euro coin.

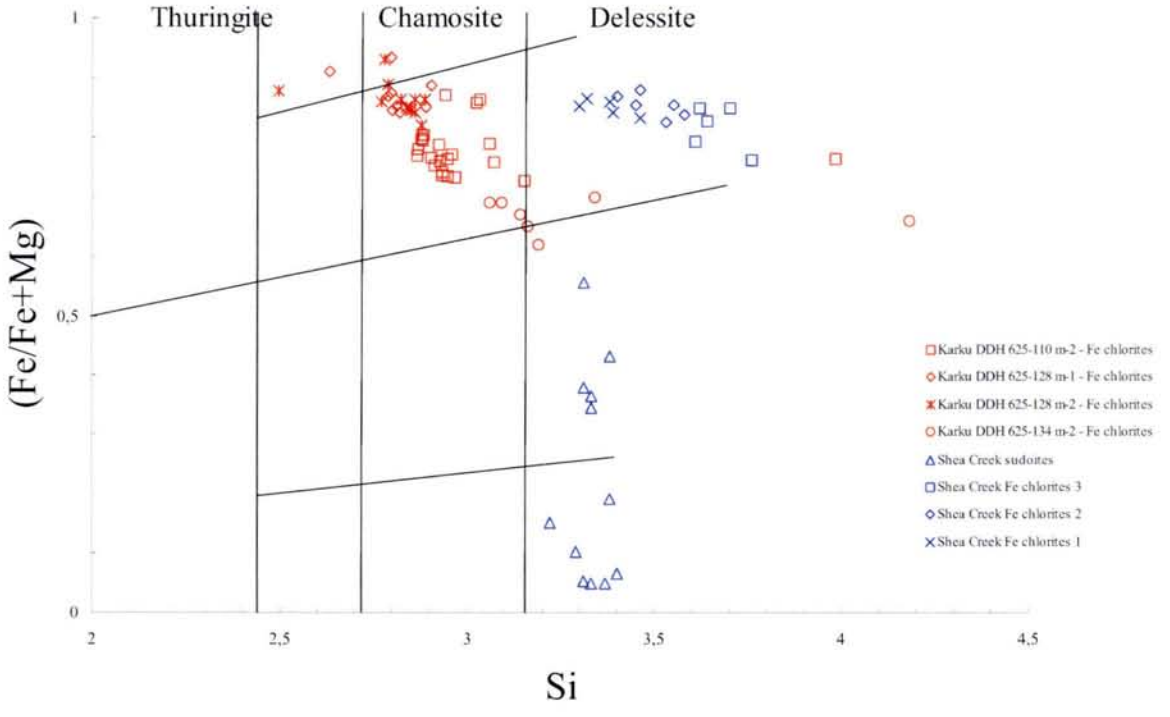

Fig.3.27. Composition of the chlorites from the Karku deposit (present work) compared to those of Shea Creek (Lorilleux, 2001) in the classification diagram of chlorite composition.

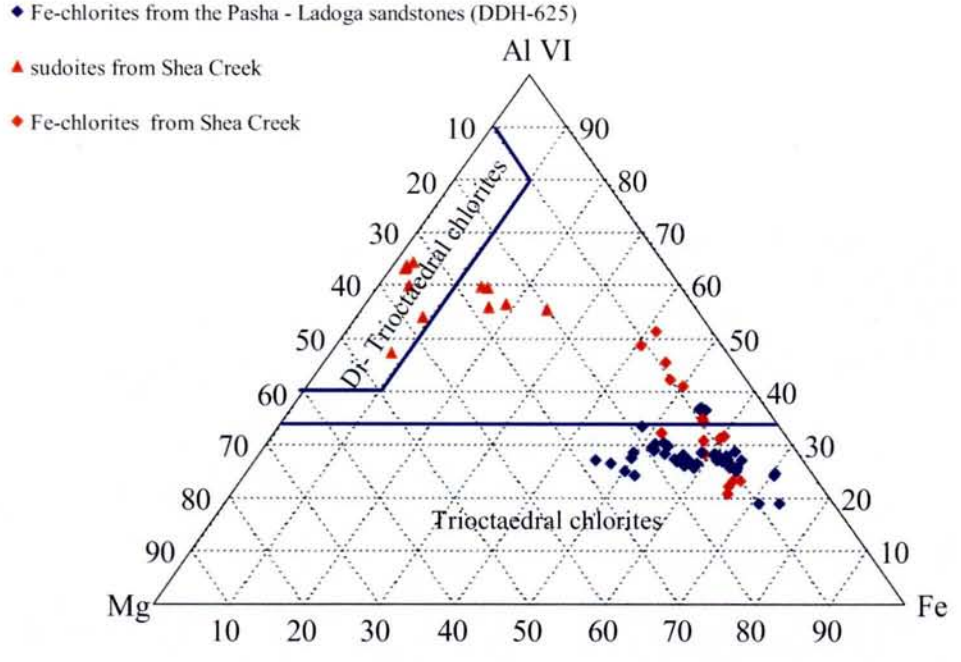

Fig. 3.28. Composition of the chlorites from the Karku deposit (Salmi area) and Shea Creek chlorites represented in a Al^{VI}-Mg-Fe ternary diagram. Fe-rich chlorites are trioctahedral whereas Mg-rich chlorites (sudoites from Shea Creek area, Athabasca basin) are close to the sudoite field (Lorilleux, 2001)

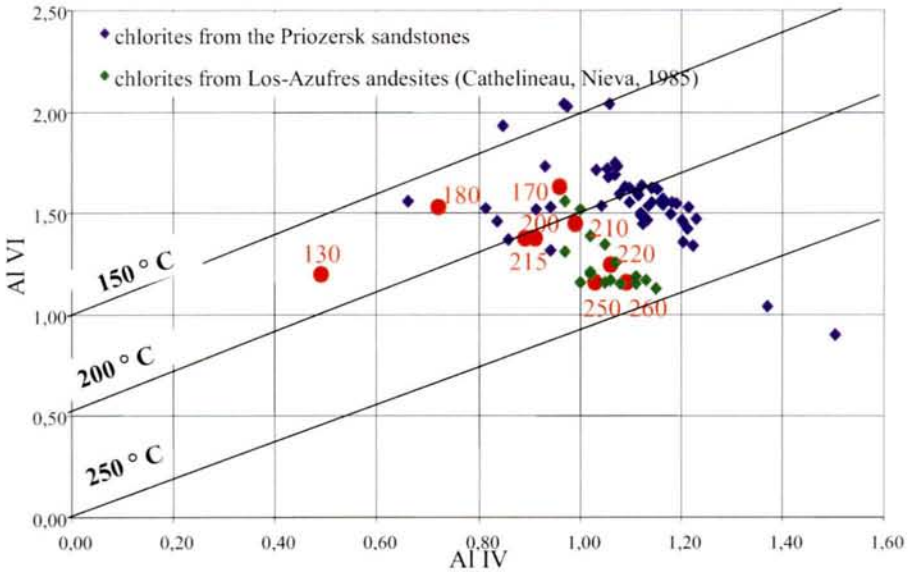

Fig. 3.29 Chlorite from the Priozersk sandstones in the Al ^{IV} – Al ^{VI} diagram compared with chlorites from the Los-Azufres andesites and approximate temperatures of the process according to Cathelineau and Nieva (1985)

Chlorites of the Los Azufres geothermal field were plotted in the Al ^{IV} vs Al^{VI} diagram with their estimated temperatures (Cathelineau and Nieva, 1985). The isotherms defined by Los Azufres data were used to estimate a temperature of crystallization of the chamosites from the Karku deposit. Most of them are comprised between 180 and 220 °C (Fig. 3.29).

Syn-ore carbonatization

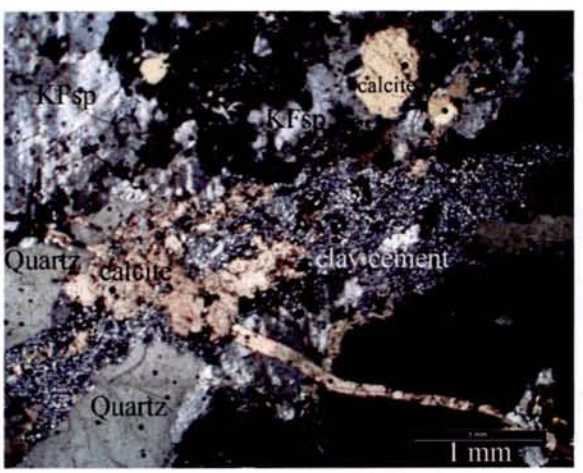

Fig. 3.30. Carbonatization stage in the Priozersk sandstones: developed in the clay cement and as calcite vein (DDH-389-189 m). Crossed nicols, line scale – 1 mm

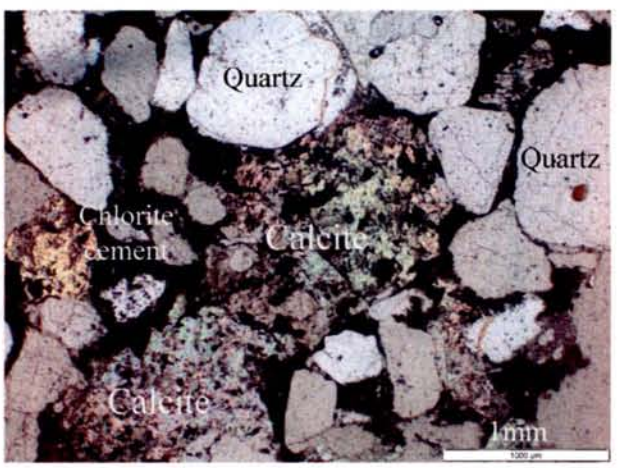

Fig. 3.31. Alteration processes in the mineralized Priozersk sandstones: chlorite - calcite cement around detrital quartz with overgrowths. Sample DDH-654-143 m. Parallel nicols, line scale – 1 mm

Carbonatization especially occurs in the lower part of the Priozersk sandstones in the first ore zone of the Karku deposit. It corresponds to post-ore calcite veins up to several centimetres thick (Fig. 3.30). Carbonates are *Mn-calcite*, occurring in the cement as poikilitic, basal and porous textures, and *siderite*, occurring as lozenge-shaped crystals or rosette druses. Chemical composition of *calcites* from DDH-625 is listed in Table 3.3.

DDH-625-134 m	CaO	FeO	MnO	MgO	BaO	SiO_2	Al_2O_3	Na_2O	K_2O	TiO_2	F_2O	Total
Point 1	58.62	0.16	0.61	0.13	0.00	0.38	0.14	0.02	0.02	0.44	0.20	60.71
Point 2	59.75	0.26	0.56	0.09	0.00	0.29	0.11	0.00	0.01	0.46	0.00	61.53
Point 14	53.40	0.52	2.12	0.15	0.00	0.01	0.01	0.32	0.00	2.20	0.00	58.90
Point 15	51.29	0.34	0.86	0.05	0.10	0.13	0.08	0.00	0.00	5.86	0.08	58.95
Point 21	56.54	0.29	0.94	0.08	0.04	0.00	0.01	0.01	0.01	1.25	0.02	59.22
Point 23	54.37	0.13	1.18	0.03	0.07	0.06	0.00	0.16	0.00	4.07	0.06	60.41

Table 3.3. Chemical composition of calcites from the mineralized Priozersk sandstones (DDH-625-134 m)

At the beginning carbonatization takes place only in the cement within the kaolinite-hydromica matrix. Simultaneously dark-green-brown chlorite and pyrite are formed. At the end of the main mineralization event calcite and chlorite totally replace the clay cement and all feldspar crystals and lithoclasts, and crosscut the quartz grains (Fig. 3.31). Siderite is also associated with U-minerals and form monomineralic aggregates and veins, also cutting U-minerals.

Global sandstone composition in the Karku deposit (Salmi area)

The global mineral composition of the mineralized sandstones of the Karku deposit area has been also determined using the Q-A diagram (after Debon and Le Fort, 1988) and the ternary classification diagram.

Mineralized sandstones of the Karku deposit area appear relatively rich in quartz with a relatively constant proportion of clay minerals. The trend developed into the metaluminous field ($A < 0$), correspond to increasing proportions of calcite (Fig. 3.32). The most mineralized samples have the most negative A value (the highest calcite content), which confirm the previous petrographical and mineralogical observations.

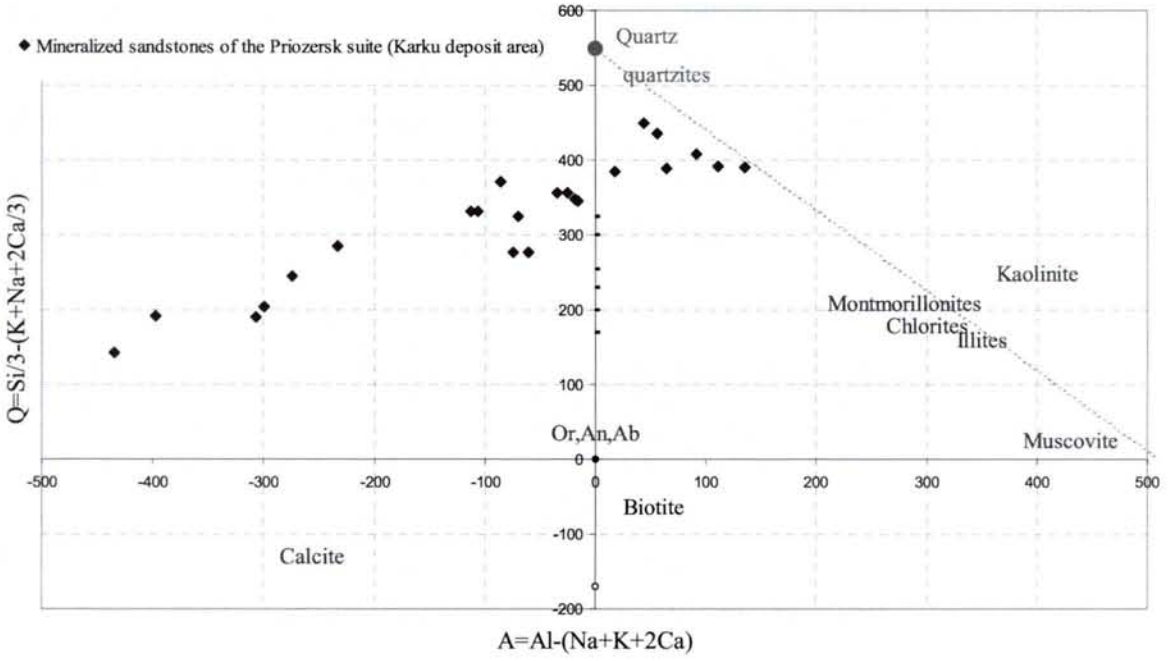

Fig. 3.32. Mineralized sandstones from the Karku deposit area plotted in the Q-A diagram (derived from parameters Q and A of Debon and Le Fort (1988)).

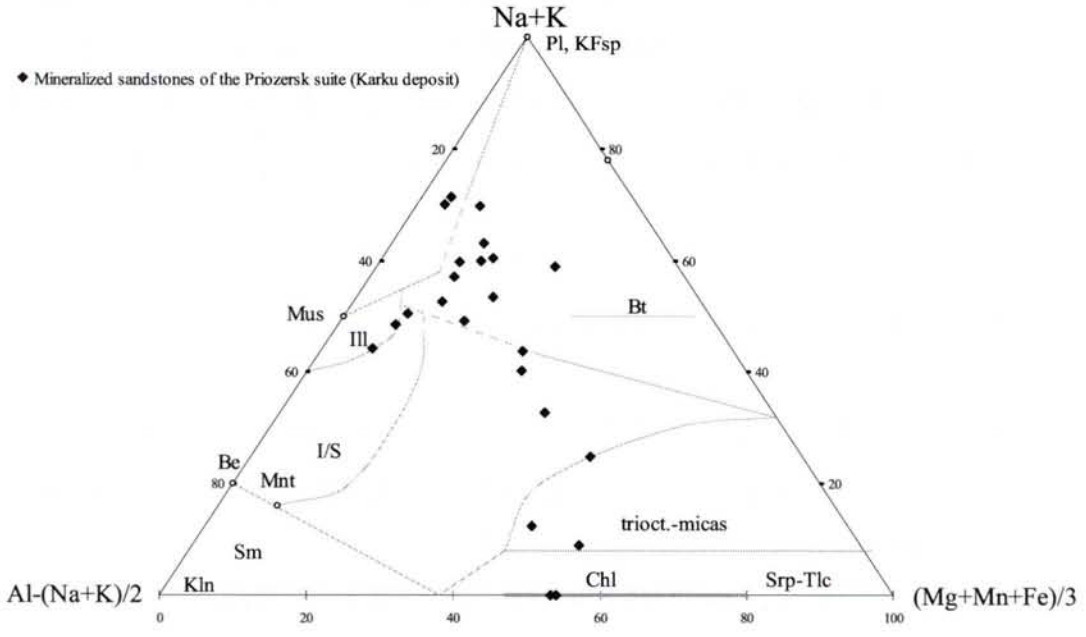

Fig. 3.33. Clay composition of the mineralized sandstones from the Karku deposit area plotted in the ternary K+Na – Al-(Na+K)/2 – (Mg+Mn+Fe)/3 diagram.

In the triangular diagram (Fig. 3.33) the mineralized sandstones define a major trend between a feldspar-illite-kaolinite pole and the chlorite field. Some samples (DDH-625: interval 110 - 134 m) are largely dominated by chlorite. A smaller trend (DDH-822: interval 143 - 157 m) is directed towards I/S illite-chlorites, illite-smectites.

Ore mineralization event

During the ore stage in the Karku deposit several types of mineral associations were observed (Bylinskaya et al., 2004):

(i) chlorite-dominant uranium mineralization (ore zone III of the Karku deposit);

(ii) carbonate-dominant uranium mineralization (ore zone I of the Karku deposit);

(iii) vein type uranium mineralization in the basement rock and in basalts (described in the corresponding chapters II and IV respectively).

These mineral associations may overlap each other in the same ore zone or may appear independently (Novikov et al., 2001).

i) Chlorite-dominant association

The chlorite – uranium association is widespread in the third ore zone of the Karku deposit (see Fig. 1.11 for ore zone position) and corresponds to the high-grade ores.

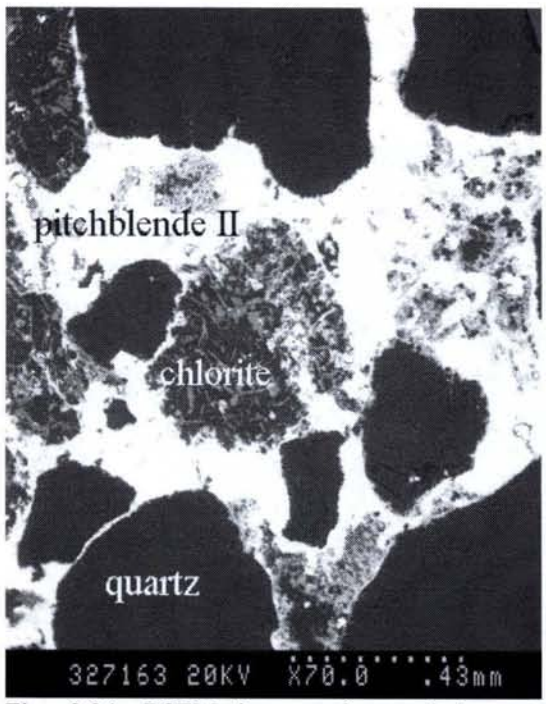

Fig. 3.34. BSEM image of corroded quartz crystals in a cement composed of *pitchblende II* and chlorite with sulphides. Sample DDH-671-132 m (Karku deposit area, ore zone III), photomicrograph scale = 43 mm

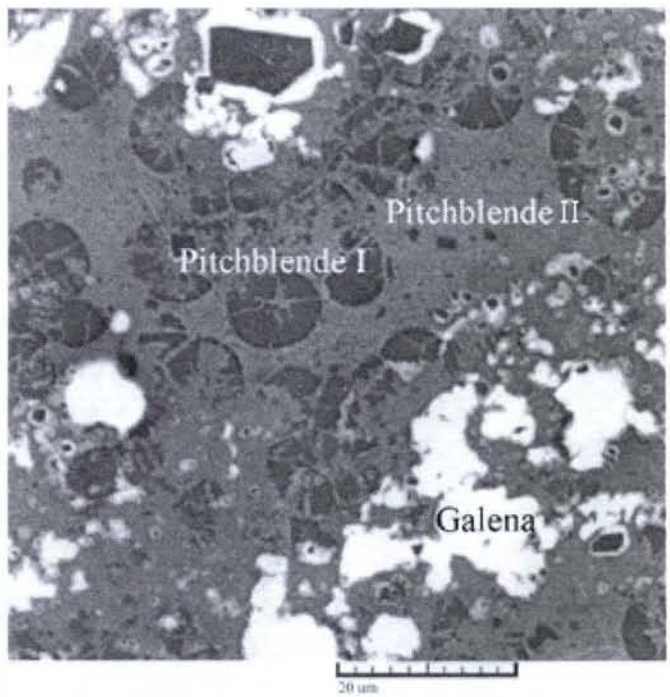

Fig. 3.35. Relicts of the *pitchblende I* spherolites in *pitchblende II.* Sample DDH-680/125 (Karku deposit area, ore zone III), photomicrograph in reflected light, scale = 20 μm (Bylinskaya et al, 2004)

The uranium mineralization is located in the Priozersk sandstones and is associated with carbonate and chlorite in the cement. The detrital quartz grains are corroded (Fig. 3.34). The

uranium mineralization is represented by two generations of pitchblende, individual crystals of prismatic coffinite and different Ti-U-Si phases. Chemical composition of the uranium minerals is listed in the Table 3.4.

Relicts of more reflective *pitchblende I* are observed as separated spherolites in *pitchblende II* (Fig. 3.35). The *pitchblende II* (less reflective) is the dominant mineral in the high-grade ores.

Pitchblende I and II differ mainly by their SiO_2 and PbO contents (*pitchblende I* - 1.5 - 3.5 wt. % SiO2, 9.7 wt% PbO, *pitchblende II* – 6 - 9 wt. % SiO2, 5.2 wt% PbO). Besides inclusions of sulfides - pyrrhotite, sphalerite, galena, molybdenite, loellingite only occur in *pitchblende II*.

Wt. %	SiO_2	TiO_2	FeO	MnO	CaO	UO_2	PbO	SO_3
Pitchblende I (5 analysis)	4.40±0.70	0.17±0.01	2.15±0.07	1.61±0.20	2.91±0.18	77.91±4.60	9.67±5.25	1.82±0.07
Pitchblende II (7 analysis)	7.98±1.15	0.49±0.02	1.92±0.02	1.42±0.60	2.32±0.08	78.72±4.10	5.24±4.80	1.08±0.68
Coffinite (5 analysis)	14.77±4.80	2.37±0.01	1.20±0.80	0.50±0.06	4.11±1.44	53.27±3.50	1.10±0.65	0.87±2.50

Table 3.4. Chemical composition of the main uranium minerals of the Karku deposit area (unpublished data from Polekhovsky)

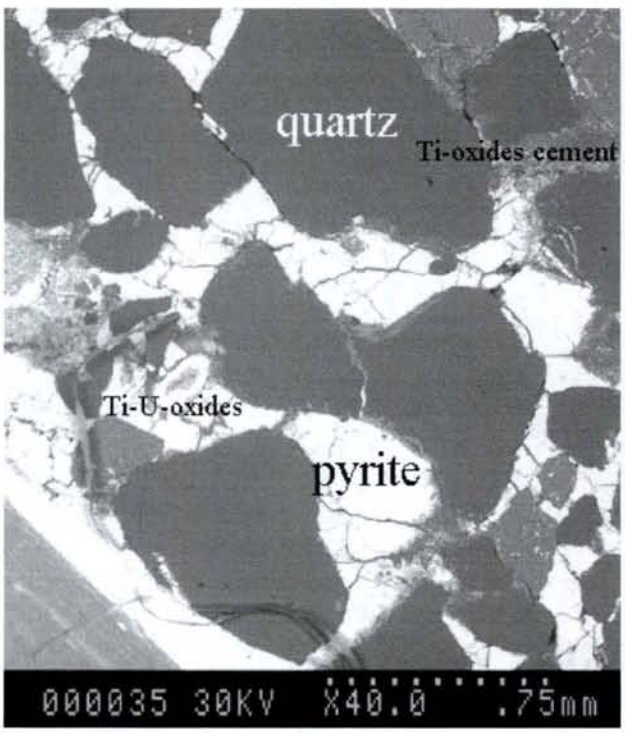

Fig. 3.36. Abundant pyrite as a cement in slightly mineralized Priozersk sandstones – sample DDH-680-125 m (Karku deposit area, ore zone III)
BSEM image photomicrograph, scale 75 mm

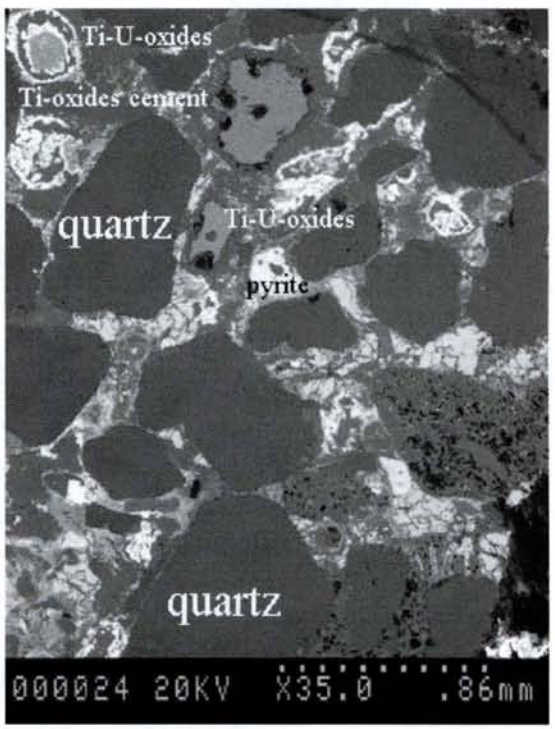

Fig. 3.37. Pyrite and Ti-U-oxides in a Ti-oxide cement of the mineralized Priozersk sandstones – sample DDH-680-125 m (Karku deposit area, ore zone III)
BSEM image photomicrograph, scale 86 mm

Pyrrhotite - the most widespread sulfide in the high-grade ores forms prismatic and needle-like crystals and sometimes cement aggregate. It contains 57 wt. % Fe, 42 wt % S, 0.06 wt. % Co, 0.04 wt. %Ni.

Pyrite is rather widely distributed in the non-mineralized or slightly mineralized Priozersk sandstones (Fig. 3.36). In rich ores (U > 3.0 wt. %) pyrite content is much less abundant than pyrrhotite. In the ore bodies microcrystalline pyrite is characterized by tear-shaped and globular forms. Its composition is following: 46.6 wt. % Fe, 53.3 wt. % S, 0.05 wt. % Co, 0.03 wt. % Ni, 0.02 wt. % Cu.

Mineralized zones in the sandstones sometimes contain porous melnikovite. This mineral is enriched in Ni (2.25 wt. %), Co (0.2 wt. %), Cu (0.68 wt. %).

In the cement of the mineralized sandstones cryptocrystalline aggregates of [Ti, (Th, U, Ca, Fe, Zr)] oxides (Fig. 3.37), which are also associated with rounded Ti-U oxides (detrital brannerite?) (Fig. 3.38) and recrystallized Ti-oxides grains coated with a coffinite/carbonate succession (Fig. 3.39) with UO_2 content up to 75 %, often occur. Locally, cryptocrystalline aggregates may correspond zirkelite (Ti, Zr, Ca, Fe ± Mg, U, Th ± REE)$_3O_5$ according to an unpublished report (Reyx, 2000).

Fig. 3.38. BSEM image of a Ti-U oxide (detrital brannerite ?) in the mineralized Priozersk sandstones – (DDH-680-125 m (Karku deposit area, ore zone III). Photomicrograph scale = 150 µm

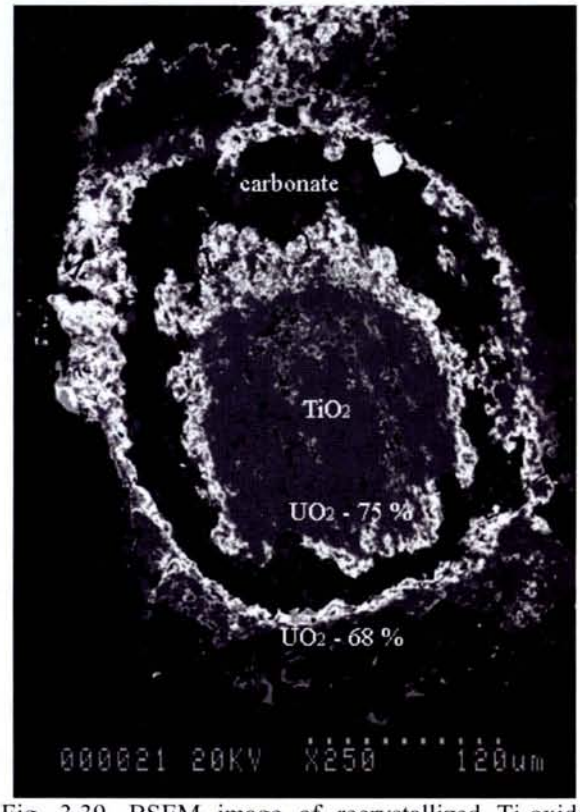

Fig. 3.39. BSEM image of recrystallized Ti-oxide grain coated by layers of carbonate and coffinite (DDH-680-125 m) (Karku deposit area, ore zone III). Photomicrograph scale = 120 µm

ii) Calcite-dominant association

The calcite – uranium association is widespread in the first ore zone of the Karku deposit both in the basement rocks and in the sedimentary cover (see Fig. 1.11 for ore zone position) and well developed in the second and third ore zones.

The degree of carbonatization varies from partial to complete replacement of the clay cement. The carbonate is calcite. Uranium mineralization in the sandstones is represented by pitchblende associated with calcite – coffinite. Sulphide mineralization is also widespread and represented by pyrite, sphalerite, galena (Fig. 3.40), molybdenite, gersdorphite, ferrosilite, Ni-Co arsenides (Fig. 3.42), Pb sulphoselenide. Stromeyrite – Cu-Ag sulphide was also found. Rare inclusions of the solid bitumen are found in the carbonatized mineralized sandstones (Bylinskaya et al., 2004). Needles of pyrrhotite in the carbonate – coffinite cement are also observed (Fig. 3.41).

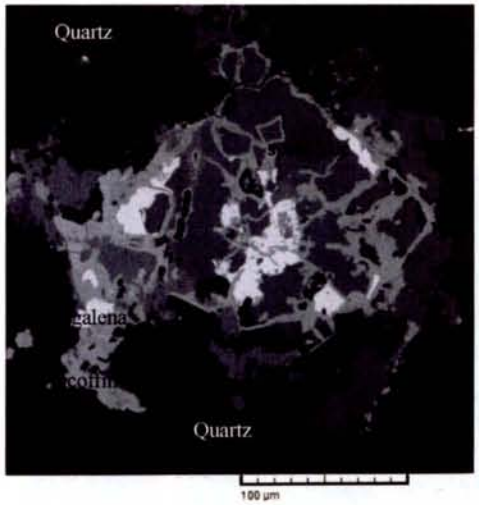

Fig. 3.40. Sulphides associated with coffinite in the cement of the sandstones (DDH-680/125, Karku deposit, ore zone III). BSEM image, photomicrograph scale = 100 µm

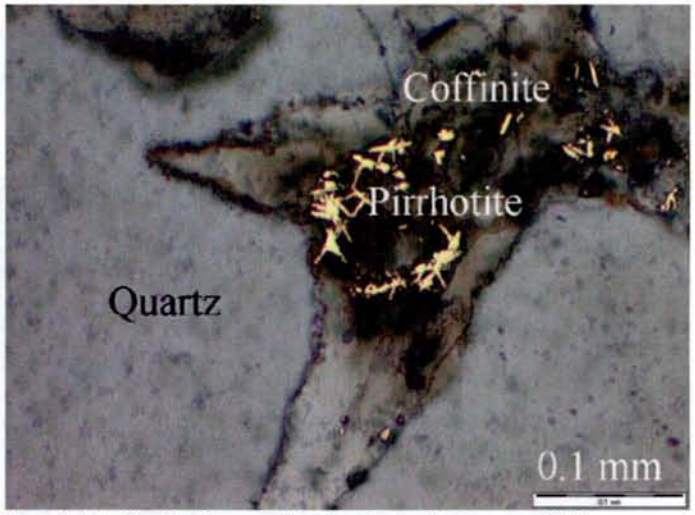

Fig. 3.41. Pyrrhotite needles in the carbonate-coffinite cement (DDH-605-107, Karku deposit area, ore zone I) Parallel nicols, scale = 0.1 mm

Pyrite is replaced by coffinite from the outside and on the inside and characterized by irregular corroded forms (Fig. 3.43.). Sphalerite crystals are often coated by coffinite and pitchblende.

Coffinite forms thin microveinlets, spotty aggregates, coating on pitchblende. Sometimes zoned coffinite form fine-grained prismatic crystals or nodular masses with collomorph structure. Its colour is commonly brown and yellow – brown in transmitted light and light - grey to dark-grey in reflected light.

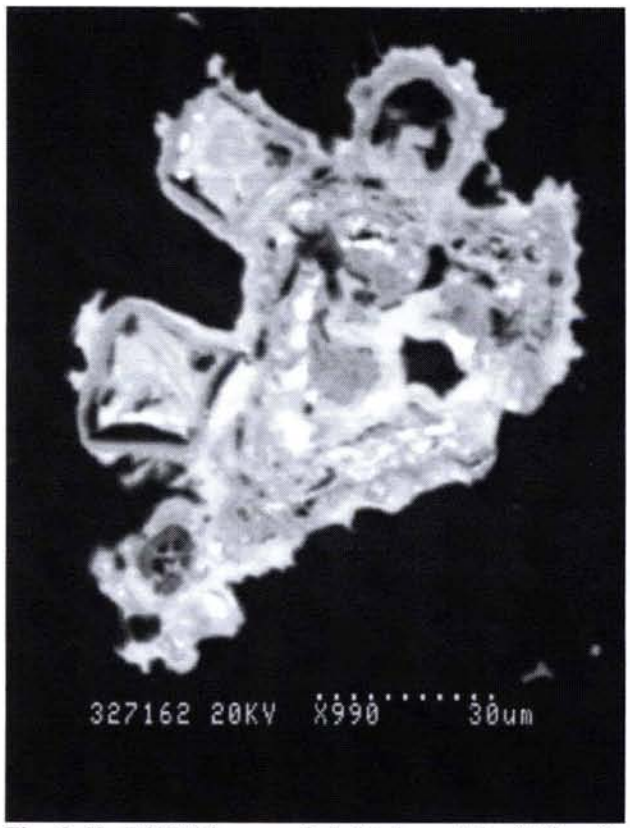

Fig. 3.42. BSEM image of skeletal crystal of Ni – Co arsenides (DDH-384-144, Karku deposit area, ore zone I), photomicrograph scale = 30 μm

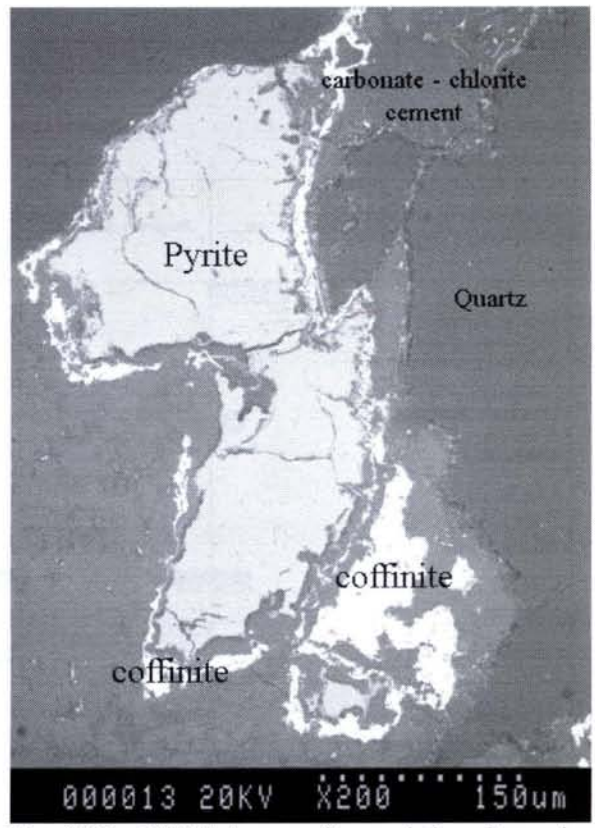

Fig. 3.43. BSEM image of corroded pyrite grains coated by coffinite in a carbonate-chlorite cement of the Priozersk mineralized sandstones (DDH-680-125, Karku deposit area, ore zone III), photomicrograph scale = 150 μm

(iii)Post-mineralization retrograde diagenesis

The post ore retrograde diagenesis mainly consists of local low temperature hematitization (hematite, limonite, leucoxene) along reactivated fractures and microfaults and kaolinite developed on the chlorite cement of the sandstones as rather large fan-like crystal. The hematization in the Mesoproterozoic (Riphean) time could be a multiple process (Ignatov, 2000) (Fig. 3.15).

Late limonitization and leucoxene formation were accompanied by leaching and redeposition of uranium with formation of the secondary uranium mineralization. These processes may have taken place after the Neoproterozoic and during Mesozoic and Cenozoic, to form an alteration halo around the mineralization zones (Ignatov, 2000).

(iv) Sequence of events

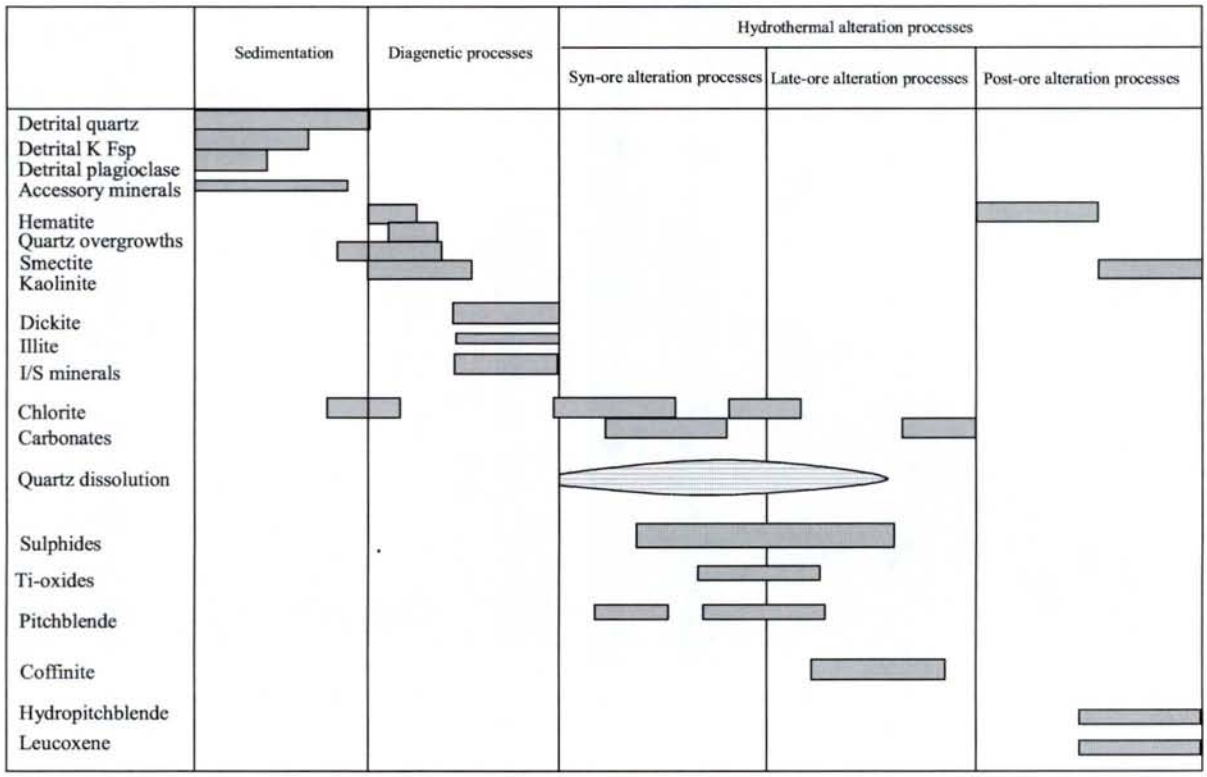

The paragensis is a compilation of Petrov, Kushnerenko (Nevskgeology); Bylinskaya, Mikhailov (VSEGEI); Velichkin (IGEM, Moscow), Polekhovsky, Shurilov (Saint-Petersburg University), Ignatov (MGGA, Moscow) conceptions

Fig. 3.44. Mineral paragenesis established in the Priozersk sandstones of the Karku deposit area. The diagram represents successively sandstone deposition, diagenesis and hydrothermal stages of uranium mineralization.

Stage 1: Sedimentation of the quartz, quartz - feldspar and arkosic sandstones with primary clay (kaolinite - smectite) cement and accessory zircon, Ti-oxides (with possible brannerite) and rare monazite, first hematization;

Stage 2: Diagenetic alteration –quartz overgrowths, kaolinite-dickite and smectite-I/S minerals-illite recristallizations;

Stage 3: Syn-ore hydrothermal alteration - development Mg-Fe chlorite and Mn calcite;

Stage 4: Sulphidization of cement and consequent formation of the pitchblende;

Stage 5: Coffinite and Ti-U-Si phase formation;

Stage 6: Supergene kaolinitization and late hematitization.

Part 3.3. Detrital accessory mineralogy of the Priozersk sandstones (Salmi area)

Sample number	Surface/DDH position (area)	Rock type (sandstones – distance to unconformity	Zircon alteration phases	Monazite alteration phases	Other accessories	Zr, ppm	Th, ppm	U, ppm	ΣREE, ppm
822-145	DDH Salmi	Priozersk sandstone (15 m)	Zircon +	monazite vein	-	183	6	3	83
822-155	DDH Salmi	Priozersk sandstone (5 m)	Zircon +	monazite	-	n.a.	n.a.	n.a.	n.a.
605-92	DDH Karku I	Priozersk sandstone (15 m)	Zircon +	relics of monazite	Ti oxides	753	26	12	285
605-93	DDH Karku I	Priozersk sandstone (14 m)	Zircon +	-	-	405	39	18	230
605-107	DDH Karku I	Priozersk sandstone (0 m)	Zircon +	-	pitchblende, coffinite	1097	1040	3615	467
389-163	DDH Karku II	Priozersk sandstone (26 m)	Zircon +	-	-	678	28	3	260
389-174	DDH Karku II	Priozersk sandstone (15 m)	Zircon +	single grain of monazite	-	1052	30	6	364
615-99	DDH Karku II	Priozersk sandstone (10 m)	Zircon +	monazite with thorite phase	coffinite (?)	954	47	215	351
816-167	DDH Karku II	Priozersk sandstone (18 m)	Zircon +	monazite	Ti oxides	1482	67	11	483
625-128	DDH Karku III	Priozersk sandstone (12 m)	Zircon +	-	-	334	8	19	134
627-127	DDH Karku III	Priozersk sandstone (about 0 m)	Zircon +	-	pyrite and apatite in zircons	n.a.	n.a.	n.a.	n.a.
654-117	DDH Karku III	Priozersk sandstone (28 m)	Zircon +	monazite altered	-	799	30	2	224
654-145	DDH Karku III	Priozersk sandstone (0 m)	Zircon +	monazite	pitchblende, coffinite	554	15	1210	103

Table 3.5. Description, location, mineralogical occurrences and whole-rock composition for selected trace elements of the Priozersk sandstones from the Karku deposit (Salmi area). Whole-rock trace elements composition for the samples DDH-822-155 and DDH-627-127 are not available

As described above typical accessory detrital minerals in the sandstones (here – the Priozersk sandstones from the Karku deposit and Salmi areas) are zircon and Fe-Ti-oxides (rutile, ilmenite, brannerite) and pyrite. Ta-Nb minerals, apatite, cassiterite, xenotime, monazite are less common. During denudation processes detrital accessory minerals from the different basement rocks were concentrated in the alluvial deposits in the form of natural placer type layers. In the third ore zone of the Karku deposit, heavy mineral layers mainly consist of zircon grains and Fe-Ti-U-oxides (Fig. 3.45).

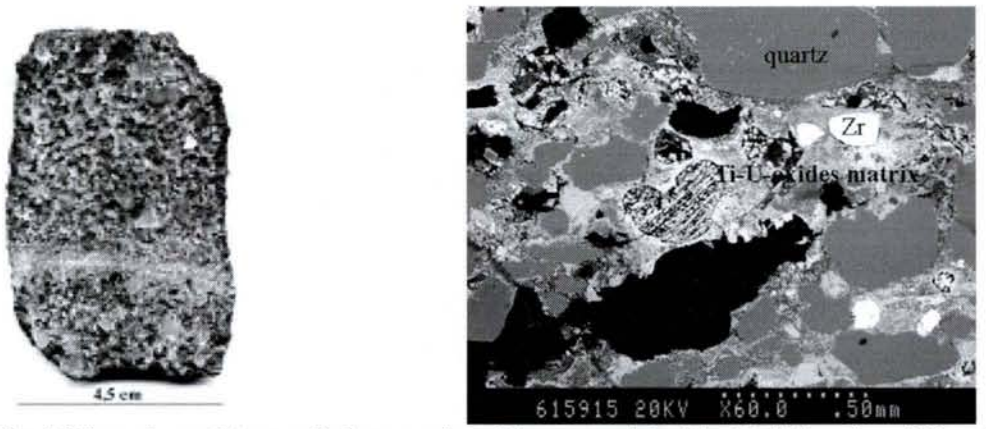

Fig. 3.45. Mineralized Priozersk sandstone with heavy mineral layer – enriched in detrital grains of Ti oxides with U and zircons (sample DDH – 627 – 127 m). Photograph scale = 4.5 cm; BSEM image scale = 50 mm

3.3.1. Zircons and zircon alteration

Detrital zircon grains from the Priozersk sandstones can be divided into four groups from their possible source rocks (Fig. 3.46):

(i) zircons derived from the Archean granite-gneisses, quite fresh grains without any evidence of alteration, most likely primary poor in radiogenic elements;

(ii) zircons from the Paleoproterozoic gneisses and schists, which are mostly idiomorphic, slightly elongated, mainly prismatic, with well developed dipyramid faces, primary zoning is invisible;

(iii) zircons from the Early Riphean rapakivi granites, which are idiomorphic, mainly of prismatic shape, poorly advanced faces of the dipyramid are also typical, primary crystal zoning is well developed everywhere;

(iv) elongated zircons, which are not observed in the studied basement rocks samples, idiomorphic elongated grains (200 - 800 μm) , without any evidence of alteration or very slight alteration, primary zoning is well developed.

The chemical compositions of the zircon crystals are listed in the Annex zircon.

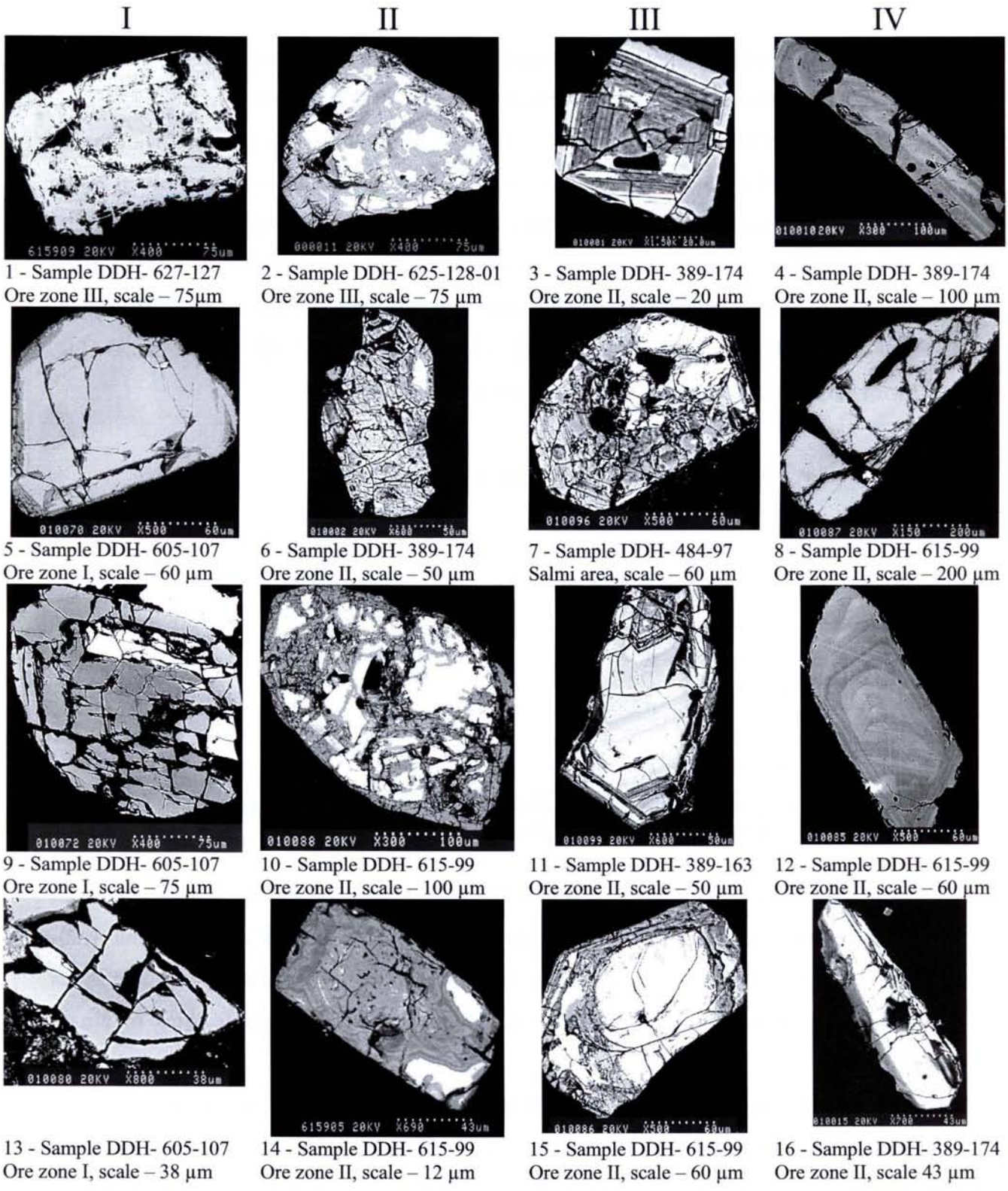

1 - Sample DDH- 627-127
Ore zone III, scale – 75μm

2 - Sample DDH- 625-128-01
Ore zone III, scale – 75 μm

3 - Sample DDH- 389-174
Ore zone II, scale – 20 μm

4 - Sample DDH- 389-174
Ore zone II, scale – 100 μm

5 - Sample DDH- 605-107
Ore zone I, scale – 60 μm

6 - Sample DDH- 389-174
Ore zone II, scale – 50 μm

7 - Sample DDH- 484-97
Salmi area, scale – 60 μm

8 - Sample DDH- 615-99
Ore zone II, scale – 200 μm

9 - Sample DDH- 605-107
Ore zone I, scale – 75 μm

10 - Sample DDH- 615-99
Ore zone II, scale – 100 μm

11 - Sample DDH- 389-163
Ore zone II, scale – 50 μm

12 - Sample DDH- 615-99
Ore zone II, scale – 60 μm

13 - Sample DDH- 605-107
Ore zone I, scale – 38 μm

14 - Sample DDH- 615-99
Ore zone II, scale – 12 μm

15 - Sample DDH- 615-99
Ore zone II, scale – 60 μm

16 - Sample DDH- 389-174
Ore zone II, scale 43 μm

Fig. 3.46. BSEM images of variably altered zircon grains from the Priozersk sandstones (Salmi area and Karku deposit)

(i) Zircons derived from the Archean granite-gneisses

Non- or very slightly altered zircon detrital grains, possibly derived from the Archean granite-gneisses, correspond to classical zircon composition. They usually contain 65 - 67 wt. % ZrO_2, 31 – 32 wt. % SiO_2 and 1 – 2 wt. % HfO_2. Only slight enrichments in Y is observed (photo 1) (up to 1.4 wt. % of Y_2O_3 at the marginal part), in Fe, Ca, Al, Y and LREE in the marginal part of a grain (photo 5) with about 1 – 1.4 wt. % of Al_2O_3, Fe_2O_3, CaO up to a total of about 6 wt. %. U and Th enrichments are moderate in spite of the fact that some of the grains occur in strongly mineralized samples (photo 9, 13) with U content - up to 3615 ppm. The Y, Fe, Ca and Al substitution to Zr – Hf – Si does not exceed 0.5 atoms over 33 (Fig. 3.52) with very small amounts of water in its structure (less than 2 wt. %).

(ii) Zircons from the Paleoproterozoic gneisses and schists

Fig. 3.51	Photo 2	Photo 6	Photo 10	Photo 14
ZrO_2	53	**47**	58	53
SiO_2	27	**23**	27	26
Al_2O_3	2	2	2	2
Fe_2O_3	1	**1.5**	0.5	2
CaO	2.5	3	**4**	3.5
P_2O_5	0.5	0.5	0.5	0.5
Y_2O_3	1	**5**	3	**4**
REE_2O_3	1	3	3	3
ThO_2	0.5	2.5	**3**	1
UO_2	0.5	0.5	**1.5**	0.5
Total	90	**89**	94	90

Table 3.6. Average composition of the dark domains (wt. %) in the detrital zircon grains, which are possible derived from the Paleoproterozoic gneisses and schists

Alteration similar to the one observed in the zircons from the Paleoproterozoic gneisses and schists have been identified. Altered domains are common and occur without well-defined selectivity (though mainly occurring on the margins of the grains). The altered zones have extremely different shapes, but may also follow crystallographic features of zircon (photo 10).

The lighter domains of zircon grains in BSEM images correspond to non-altered zircon composition and contain 65 - 66 wt. % of ZrO_2, 31 - 33 wt. % of SiO_2, 1 - 2 wt. % of HfO_2 and only up to 0.15 – 0.40 wt. % of Y_2O_3 (Fig. 3.46 - photo 10, 14). The altered darker domains in BSEM images are characterized by strong and variable enrichments in Y, Ca, Al, Fe, REE, P, Th and U (Table 3.6):

Zircons from the Priozersk sandstones, possibly derived from the Paleoproterozoic gneisses and schists are characterized by a substitution of up to 5 atoms of Al, Ca, Y, REE, Fe, Th and U in the Zr – Hf – Si structure (Fig. 3.47). U contribution into the zircon structure substitution varies from 0.2 and up to 0.8 atoms (contamination with U-minerals may locally be possible for the highest values) (Fig. 3.48).

(iii) Zircons from the Early Riphean rapakivi granites

Alteration is also well developed in zircon grains attributed to the Rapakivi granites. Altered dark domains occur mostly at the marginal part of the grains with alternating brighter and darker domains and with a well-defined selectivity to the primary crystal zoning. Zircons cores are usually preserved (except photo 3).

The brighter domains correspond to non-altered zircon composition and contain only 65 - 66 wt. % of ZrO_2, 32 - 33 wt. % of SiO_2 and 1 - 2 wt. % of HfO_2 (Fig. 346 - photo 15). The altered darker domains are also characterized by a strong and variable enrichment in Y, Ca, Al, Fe and REE (Table 3.7):

Fig. 3.51	Photo 3	Photo 7	Photo 11	Photo 15
ZrO_2	58	61	61	**54**
SiO_2	29	**25**	29	27
Al_2O_3	**1.5**	0.5	0.5	1
Fe_2O_3	0.5	0.5	**1**	**1**
CaO	**2**	1	1	**2**
P_2O_5	0.2	**0.5**	0.2	0.4
Y_2O_3	2	**3**	1.5	2
REE_2O_3	**2**	0.5	1	1.5
ThO_2	0.2	0.1	0.4	**0.9**
UO_2	0.2	-	0.1	**0.3**
Total	97	95	97	**90**

Table 3.7. Average composition of the dark domains (wt. %) in the detrital zircon grains, which are possible derived from the Salmi rapakivi granites

Zircons from the Priozersk sandstones possibly derived from the Salmi rapakivi granites, are characterized by a substitution of up to 6 atoms of Ca, Y, Al, REE, Fe and P in the Zr – Hf – Si structure (Fig. 3.47). U contribution into the zircon structure substitution is about 0.1 atoms (Fig. 3.48).

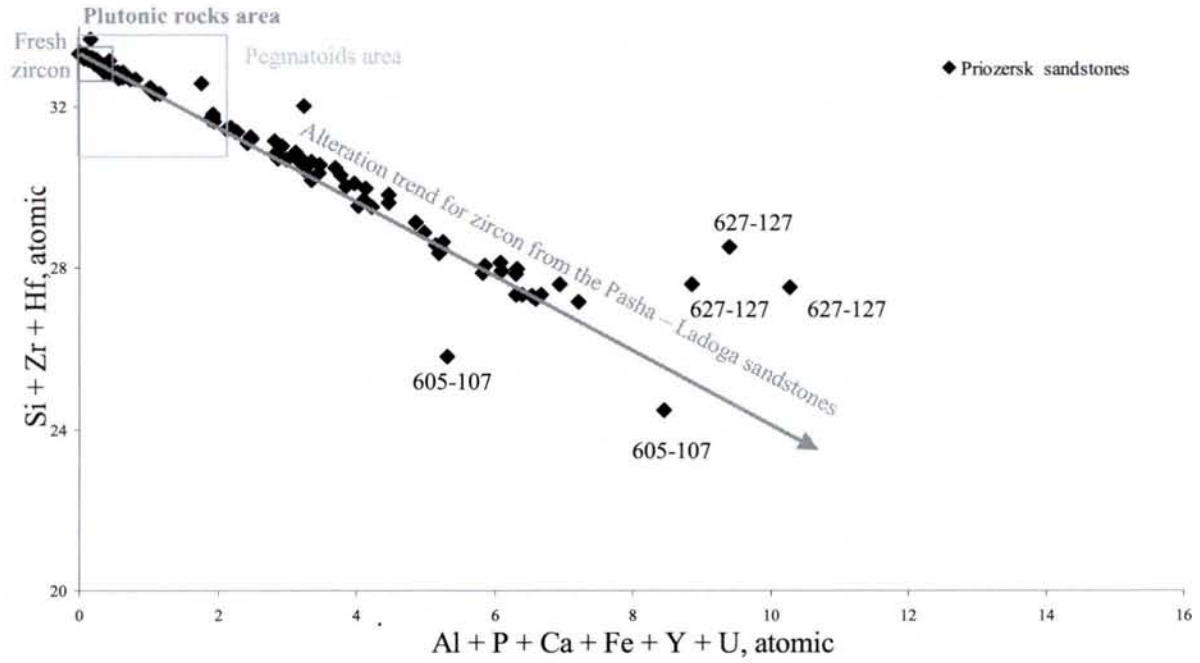

Fig. 3.47. Substitution of Zr + Hf + Si by Al + P + Ca + Fe + Y + U in zircons from the Priozersk sandstones

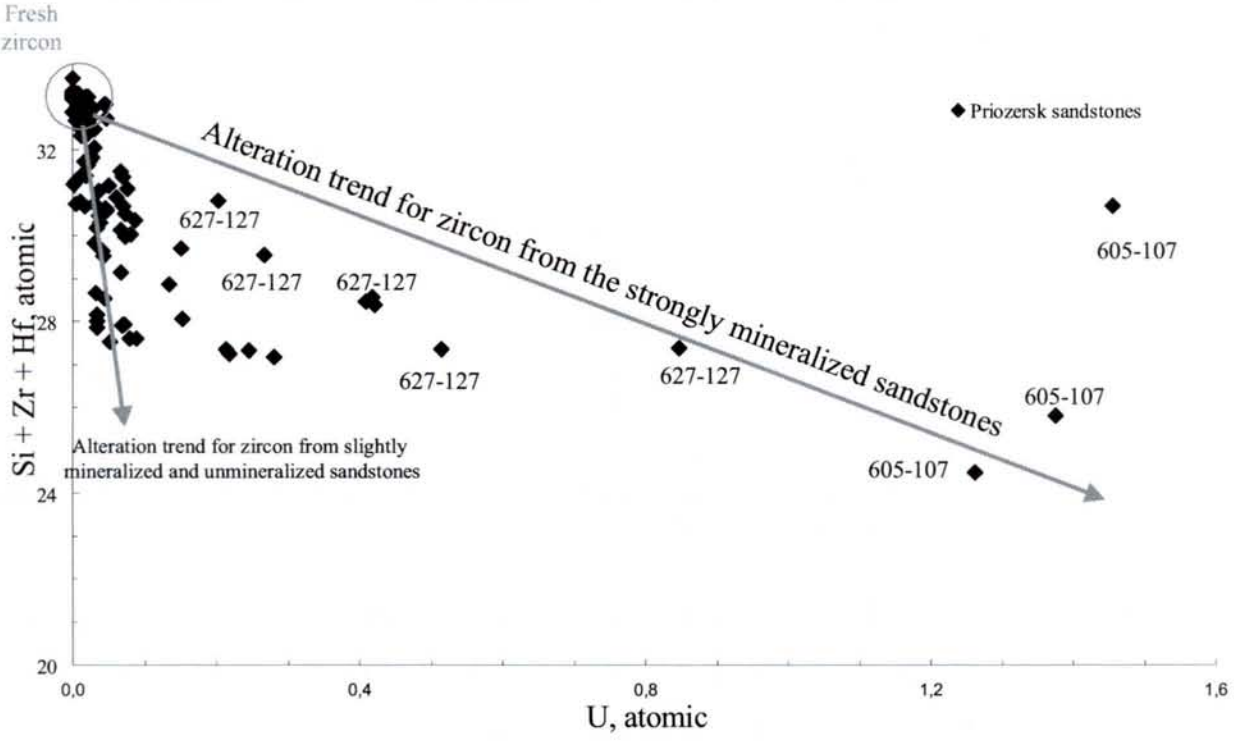

Fig. 3.48. Substitution of Zr + Hf + Si by only U in zircons from the Priozersk sandstones

(iv) Elongated zircons

The characteristic feature of this type of zircons with well developed crystal zoning is the absence of any alteration evidence. They contain 66 - 67 wt. % ZrO_2, 32 – 33 wt. % SiO_2 and about 1 wt. % HfO_2. Only a slight enrichment in P (up to 0.2 wt. % P_2O_5) and in Y and Fe (up to 0.15 wt. % Y_2O_3 and Fe_2O_3) is observed in the darker domains. These zircons are characterized by only 0.1 – 0.3 atoms of Zr – Hf – Si substituted by P, Y and Fe (Fig. 3.47).

Conclusions: The degree of substitution of the primary elements of the zircon structure (Zr, Si, Hf) by a variety of elements (Al, P, Ca, Fe, Y, Th, U) in the detrital grains from the Priozersk sandstones (Salmi area, Karku deposit) varies from 0.5 to 8 atoms, like in the observed host granite-gneisses, schists and rapakivi granites (Fig. 3.47). Uranium contribution in the substitution value (except for some contamination cases in strongly mineralized sandstones) is no more than 0.2 atoms of the zircon structure (Fig. 3.48).

3.3.2. Monazite and associated monazite alteration

In the Priozersk sandstones (Salmi and Karku deposit areas) preserved detrital monazite crystals are common unlike as in the Athabasca basin where it is only preserved when included in detrital quartz grains (Hecht & Cuney, 2000). Detrital monazite crystals are relatively widespread in the cement (chloritic and sulphidic) of the Priozersk sandstones (Fig. 3.49).

Single idiomorphic crystals with well developed natural faces, only partially dissolved are observed in the chloritic cement of non-mineralized (U content = 2.5 ppm) Priozersk sandstones (DDH-654-117 m - top of the sequence in the ore zone III of the Karku deposit area) (Fig. 3.49-A). The brighter crystal core contains 26 - 28 wt. % P_2O_5, 24 - 25 wt. % Ce_2O_3, 12 - 14 wt. % La_2O_3, 9 - 11 wt. % Nd_2O_3, 4.4 – 4.7 wt. % ThO_2 and 0.3 – 0.5 wt. % UO_2. Darker crystal margins are depleted in Th and U. It may correspond to monazite domains recrystallized at lower temperature, because Th and U incorporation in the monazite structure decease with the temperature (Overstreet, 1967). At the margin contribution of Th, U, Ca, Si and Fe, which are substituted P – LREE in the monazite structure, reaches 5 atoms (Fig. 3.54).

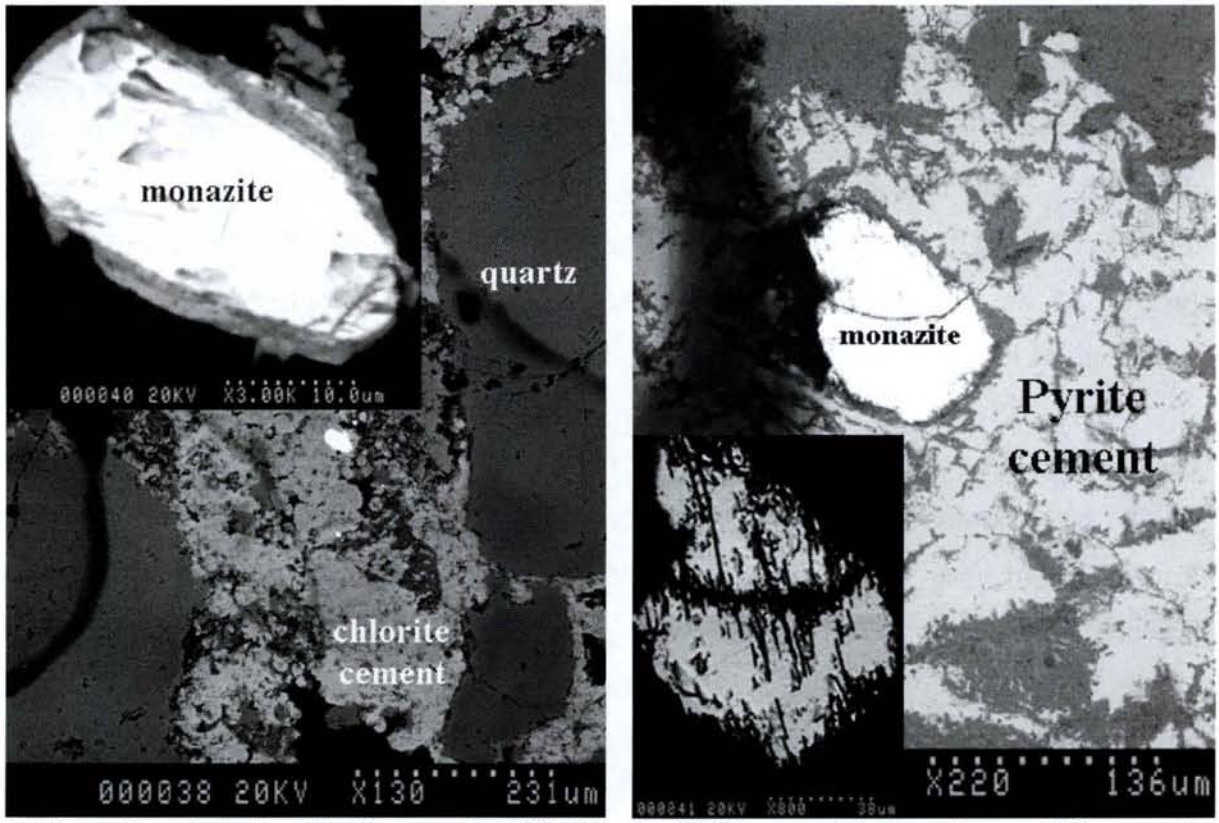

A: Monazite grain in the chloritic cement DDH-654-117 m. Photomicrograph scales: 10 & 231 μm

B: Slightly corroded monazite crystal in a pyritic cement with relics of chloritic cement (DDH-654-145 m). Photomicrograph scales: 38 and 136 μm

Fig. 3.49. BSEM images of preserved detrital monazite grains in the cement of the Priozersk sandstones (DDH-654, ore zone III)

Rare corroded monazite crystals are observed in the sulphidic cement of strongly mineralized Priozersk sandstones (U content = 1210 ppm) (at the bottom of the sequence in the same drill hole (DDH-654-145 m) in the vicinity of the unconformity surface (Fig. 3.49-B). These crystals contain 28 - 30 wt. % P_2O_5, 31 - 32 wt. % Ce_2O_3, 18 - 20 wt. % La_2O_3, 9 - 11 wt. % Nd_2O_3, 2.8 – 3.7 wt. % ThO_2 and a maximum of 0.07 wt. % UO_2.

Rare Ce-monazite crystals occur with detrital zircons in the chlorite matrix of the non-mineralized Priozersk sandstones (Fig. 3.50). Chemical composition of these monazites is mostly similar to the monazite described above, and is given in Annex monazite.

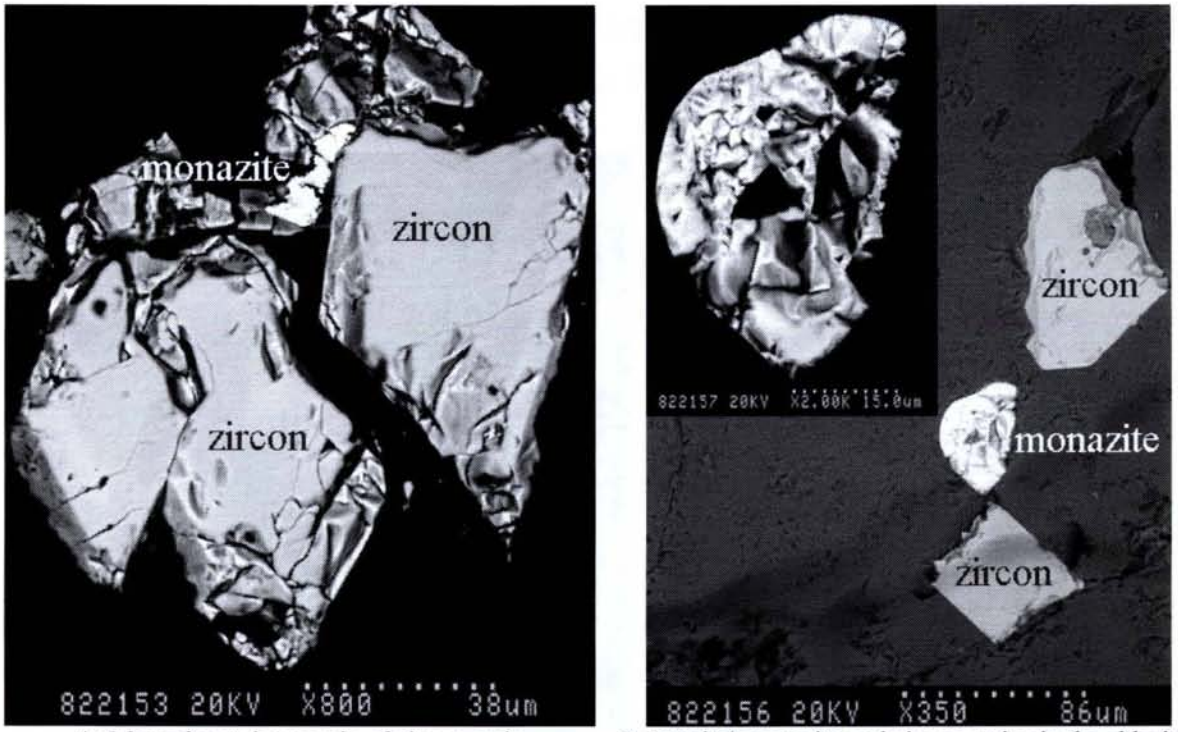

A: Monazite at the margin of zircon grain
Photomicrograph scale = 38 μm

B: Detrital monazite and zircon grains in the chloritic cement of the sandstones
Photomicrograph scales = 15 and 86 μm

Fig. 3.50. BSEM images of monazite from non-mineralized Priozersk sandstones (DDH-822-155 m – Karku deposit area)

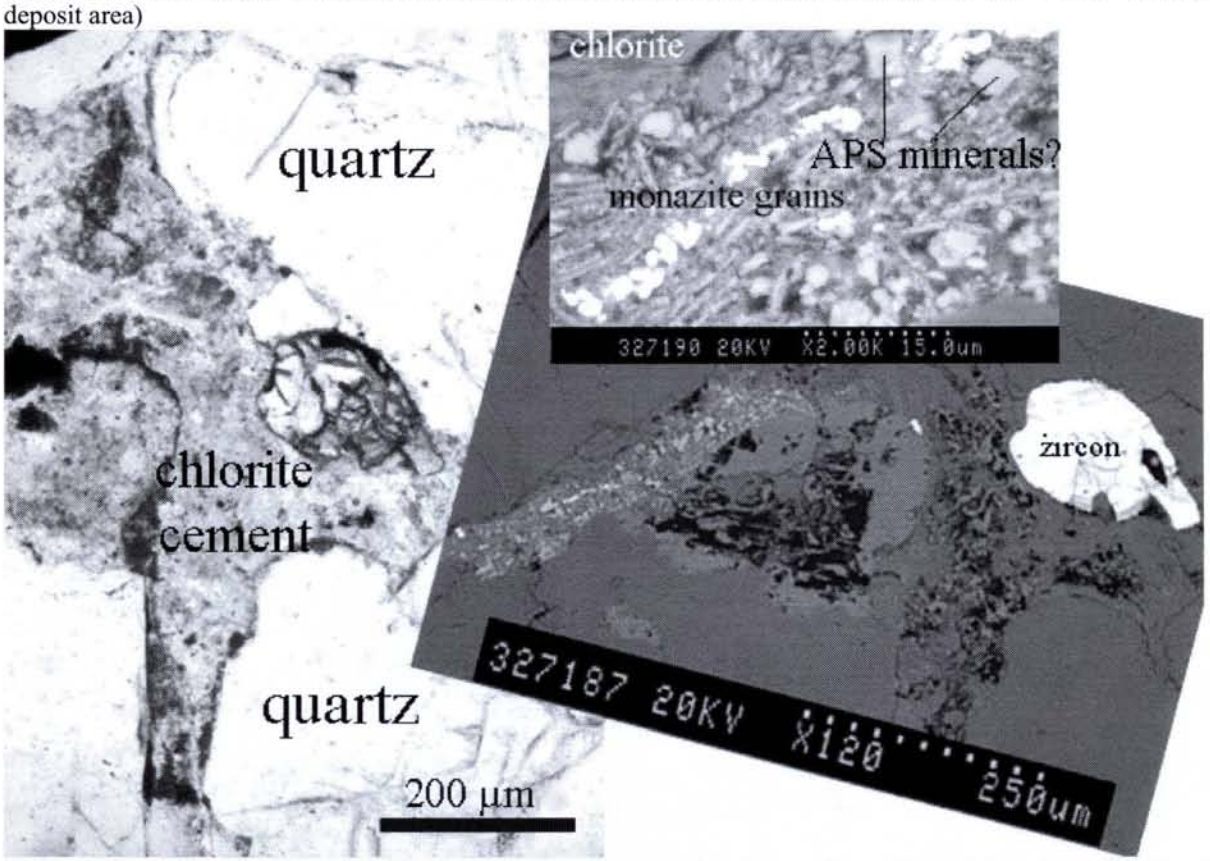

Fig. 3.51. Transmitted light and BSEM images of monazite grain relicts with possible Al phosphates (APS) of crandallite-goyazite-florencite group in a chloritic cement of the non-mineralized sandstones (DDH-822-145 m – Karku deposit area). Photomicrograph scales: 200, 250 and 15 μm

Relicts of monazite (with corrosion figures) are abundant in the clay matrix associated with chlorite (Fig. 3.51) and Ti-oxides (Fig. 3.52).

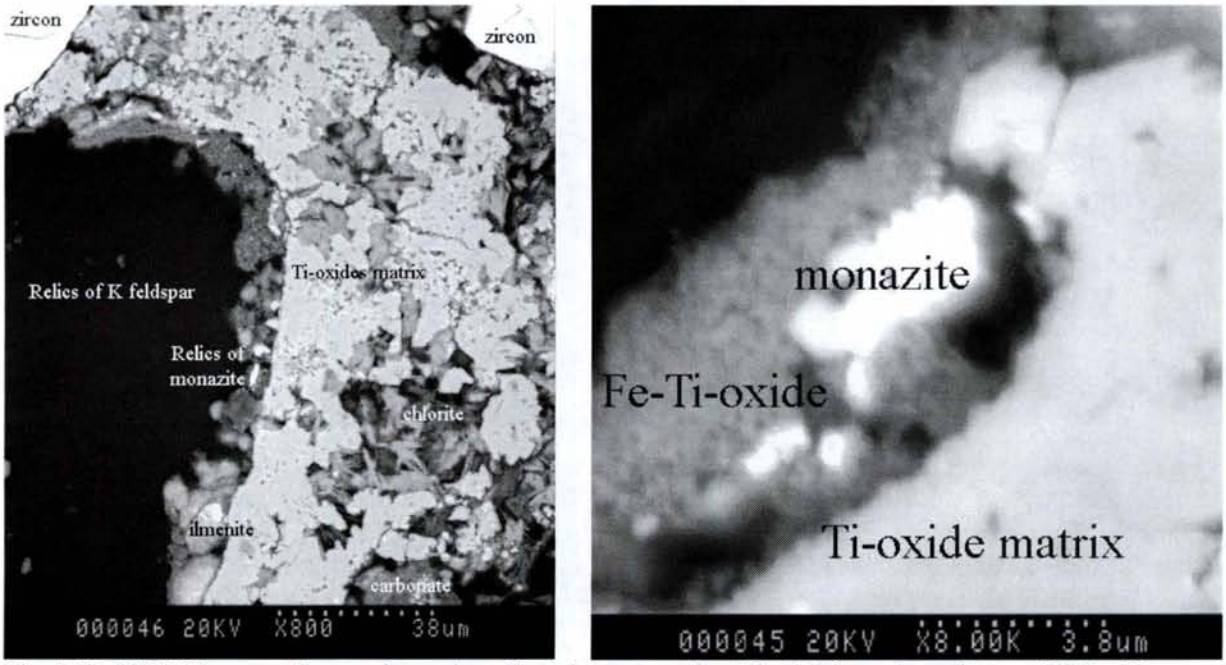

Fig. 3.52. BSEM images of monazite grains relicts from non-mineralized Priozersk sandstones (605 – 92 m, ore zone I of the Karku deposit). Photomicrograph scales: A – 38 μm; B – 3.8 μm

In conclusion, monazite from the Priozersk sandstones in the Salmi area of the Pasha – Ladoga basin has been slightly corroded probably by the diagenetic fluids. This process is much more widespread in the Athabasca sandstones (Hecht & Cuney, 2000), where P and LREE recrystallize together with Al and variable amounts of Ca and Sr to form Al-phosphates-sulphates (APS) of the florencite-crandallite-goyazite group. Only single observation of possible APS minerals is presented in the Priozersk sandstones (Fig. 3.51).

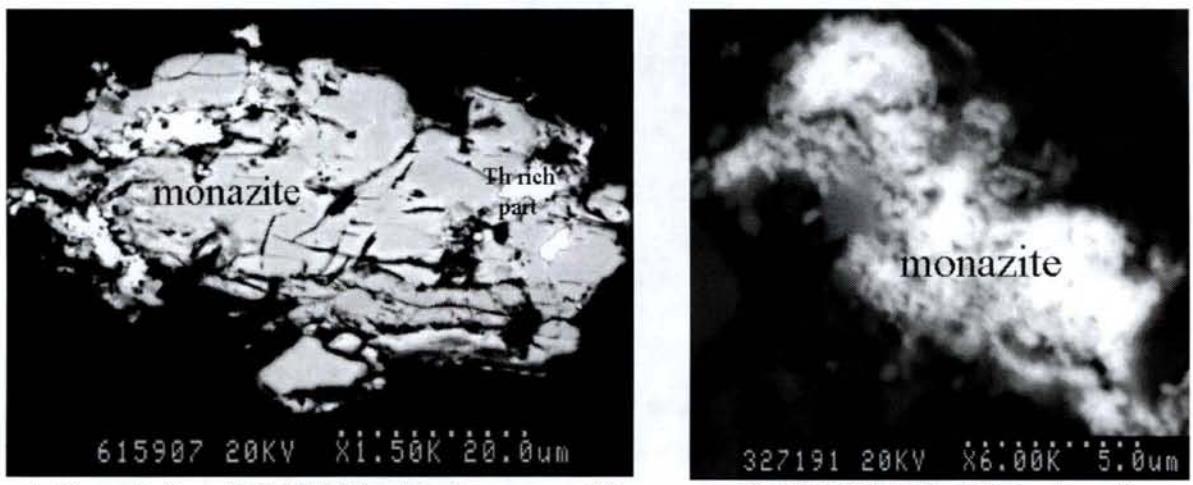

A: Monazite from DDH-615-99 m (Karku, ore zone II) Photomicrograph scale - 20 μm

B: DDH-822-145 m (Karku deposit) Photomicrograph scale - 5 μm

Fig. 3.53. BSEM images of monazite (the brighter part of the crystals is enriched in Th)

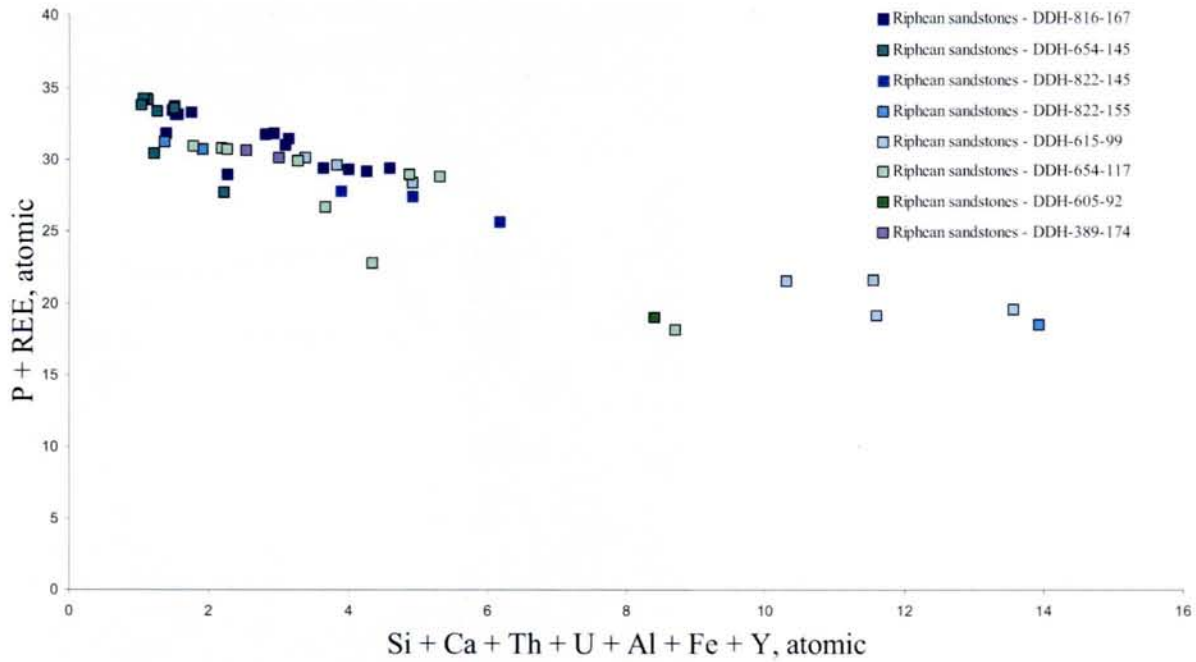

Fig. 3.54. Substitution of P + REE by Si + Ca + Th + U + Al + Fe + Y in detrital monazites from the Priozersk sandstones

In the Priozersk sandstones, monazite alteration is limited and only minor amounts of Al-phosphate are observed. Th is a weakly mobile element, initially essentially contained in the monazite crystal. Locally, it crystallizes as rare newly formed thorite crystals (Fig. 3.53) or microcrystalline phase with very low concentrations of U and LREE in the Priozersk sandstones as already observed in the Lower Proterozoic sandstones of the Franceville basin (Mathieu et al., 2001).

3.3.3. Whole-rock Zr, LREE and Th geochemistry

For a better understanding of the alteration processes of the accessory minerals at the scale of the Pasha – Ladoga basin area and adjacent basement rocks, the behavior of Zr, REE and Th has been studied from the whole-rock trace element analyses.

Zr in the Pasha – Ladoga sandstones (on the example of the Salmi and Karku deposit areas) is mainly hosted by detrital zircons.

Y is enriched both in the altered parts of zircon grains and in xenotime, which frequently occurs at the margin of zircon grains (Fig. 3.55). Non-altered zircon contains less than 0.1 wt. % Y. The altered part may contain up to 3 - 6 wt.% Y (exchange $Zr^{4+} \leftrightarrow Y^{4+}$). The Zr/Y ratio is an indicator of the degree of zircon alteration: in fresh zircons this ratio exceeds 100 (Fig. 3.56), while altered zircons are typically characterized by Zr/Y ratios between 100 and 20. In the Zr – Y diagram the Pasha - Ladoga sandstones show Zr/Y ratios ranging from 70 to 1, according to the intensity of their zircon alteration. It is interesting to note, that some fresh zircon from the sandstones have relatively higher Zr/Y ratio (up to 70) than the ones from Paleoproterozoic gneisses and schists and Salmi rapakivi granites. It means that contribution of the Early Archean granite-gneisses as source for the Pasha – Ladoga basin sediments is also important.

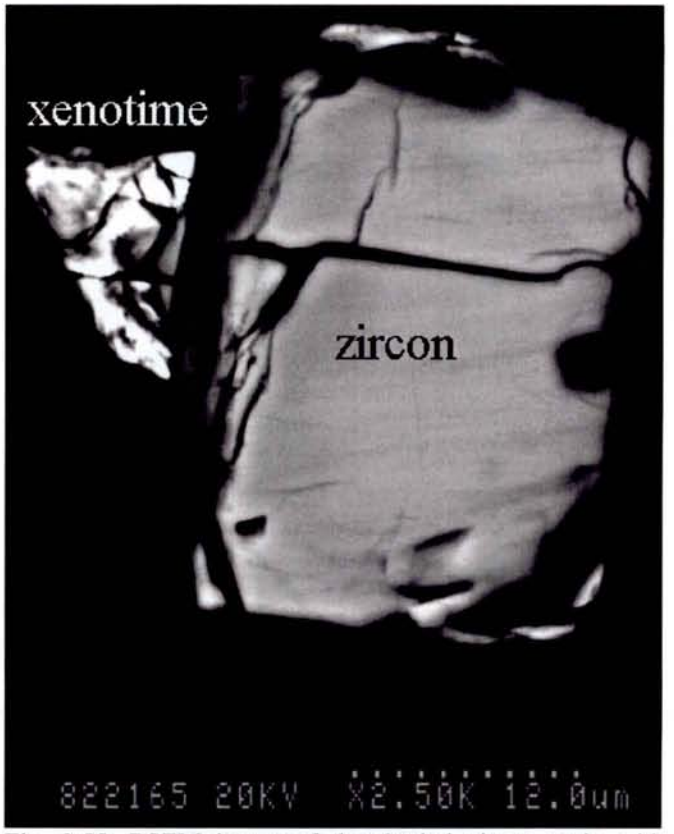

Fig. 3.55. BSEM image of the detrital zircon grain with xenotime, which occurs at the margin of zircon (sample DDH- 822-155, Karku deposit) in the Priozersk sandstone Photomicrograph scale 12 μm

The average Th/U ratio of the main types of intrusive rocks is close to 4. On the diagram (Fig. 3.57) only one sample is characterized by Th/U ratio more than 4 (with a Th content of about 40 ppm). A number of Pasha – Ladoga sandstones have Th/U ratios ranging from 4 to 1 and only two of them with Th content more than 30 ppm. Most sandstones are strongly enriched in U and have a very low Th/U ratio, lower than 1. The lowest ratios correspond to U enrichment during the mineralizing processes. The intermediate ratios may correspond to a primary feature of such immature sandstones.

Th is generally well correlated with light rare-earth elements (LREE), because mainly located in monazite, and La can be chosen as an indicator of the LREE behavior. The Archean and Proterozoic quartzites and shales all over the world have similar Th/La ratios between 0.2 and 0.4 (Mathieu et al., 2001). On the diagram (Fig. 3.58) most Pasha – Ladoga sandstones

have Th/La ratio series ranging from 1 to 0.2, with only a few higher than 1, indicating a slight leaching of the LREE, but less important than in the Athabasca sandstone.

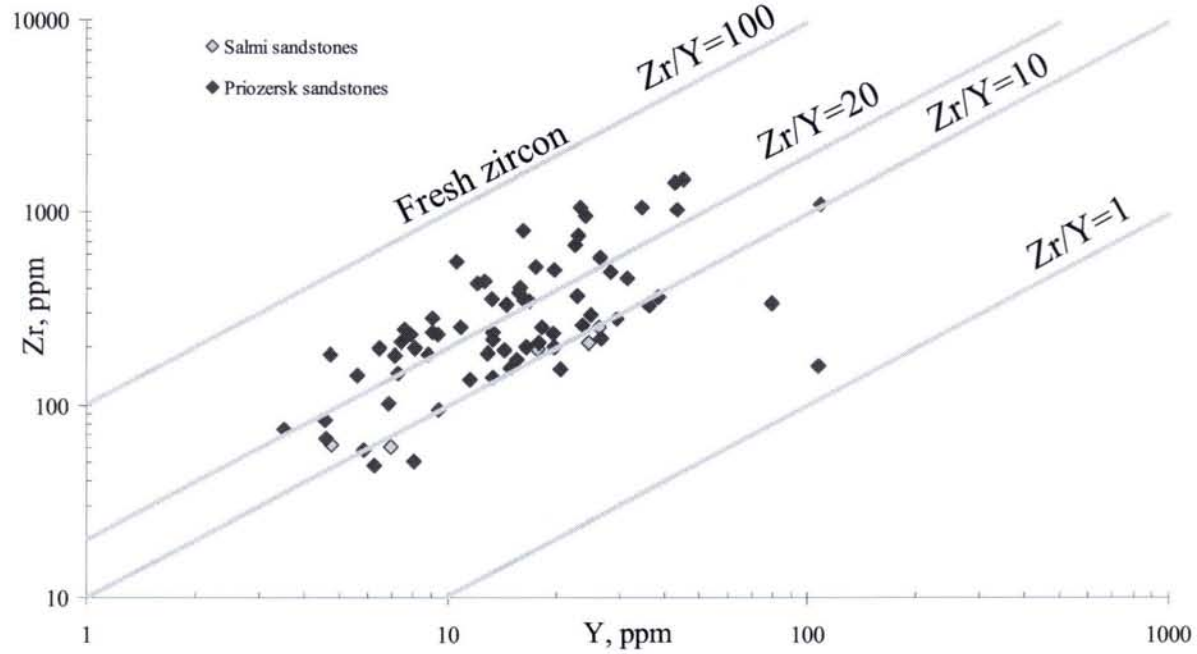

Fig. 3.56. Priozersk and Salmi suites sandstones of the Pasha – Ladoga basin in a Y vs. Zr diagram

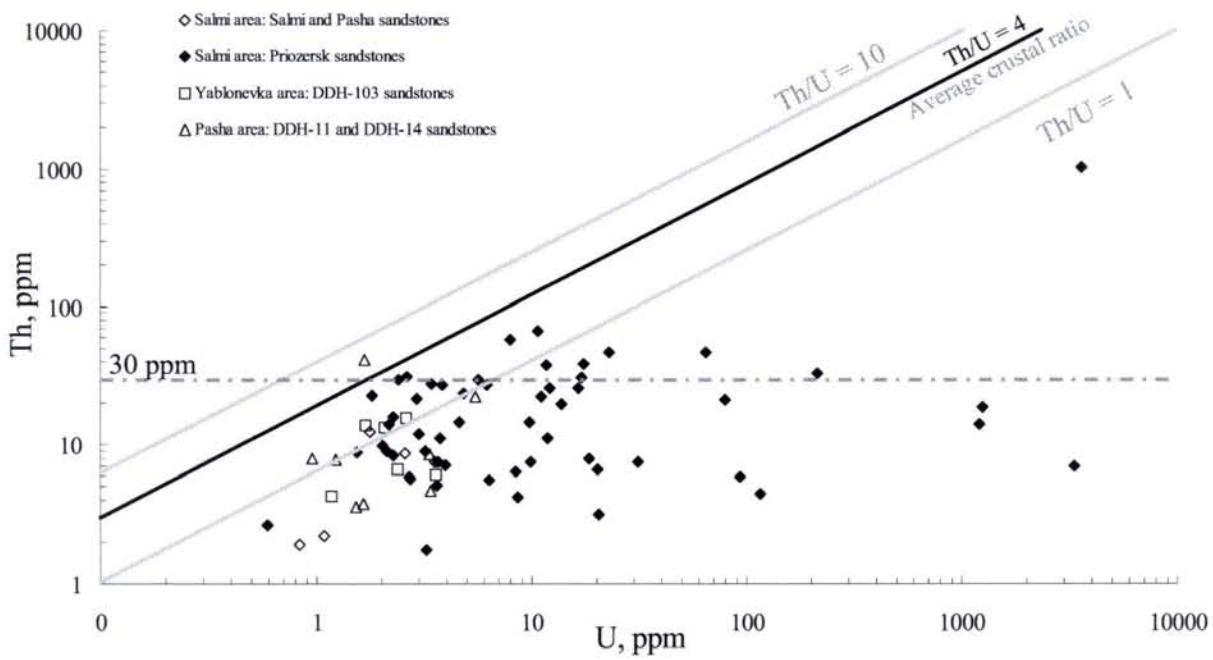

Fig. 3.57. Priozersk and Salmi suites sandstones of the Salmi, Yablonevka and Pasha areas of the Pasha – Ladoga basin in a U vs. Th diagram

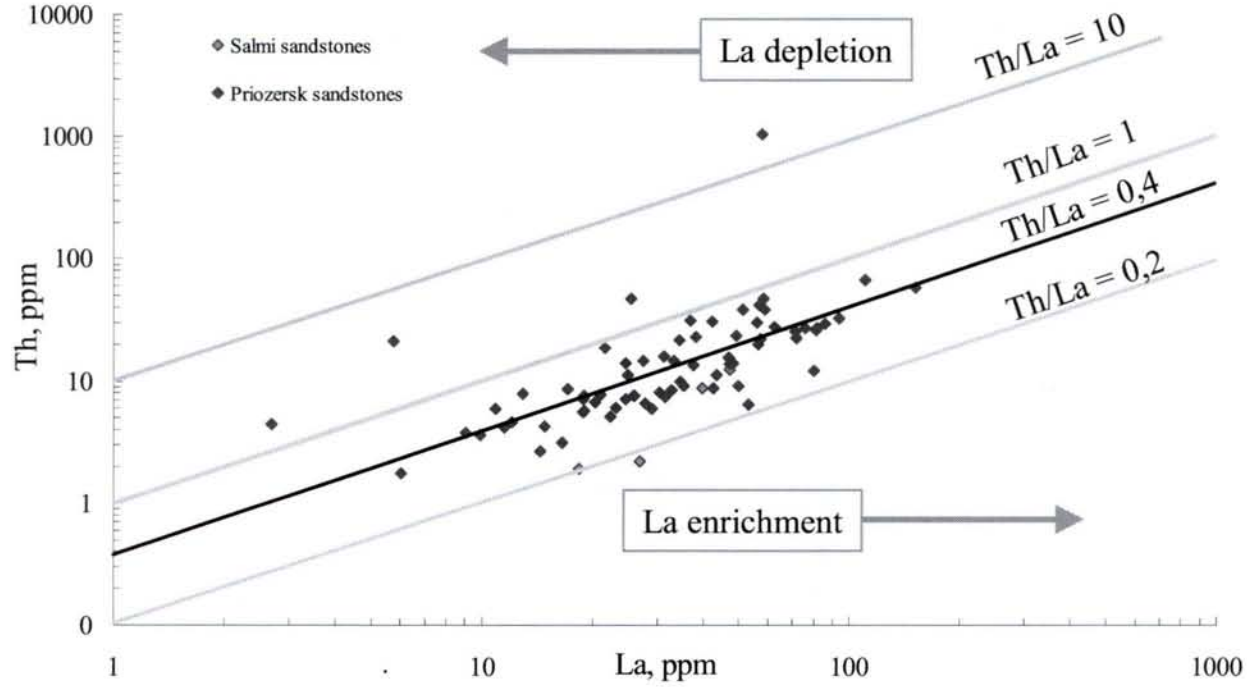

Fig. 3.58. Priozersk and Salmi suites sandstones of the Pasha – Ladoga basin in the La vs. Th diagram

Part 3.4. Petrogeochemistry of the Pasha – Ladoga Basin sedimentary sequences

The geochemistry of major and trace elements has been studied both at the scale of the Riphean Pasha – Ladoga sandstones mostly within the Salmi (and Karku deposit) and also within Yablonevka and Pasha areas. The similar geological situation of the Mesoproterozoic Athabasca (Canada) and Pasha – Ladoga (Russian Karelia) basins (Polikarpov and Molchanov, 2000; Novikov et al. 2001; Lobaev et al. 2002) allows us to formulate some important questions and to try to answer them using available petrogeochemical data. The main questions include:

1. What elements still reflect the detrital contribution in the sediments?
2. What elements are associated with the mineralizing processes?

3.4.1. Major element distribution

Major elements composition of the Pasha – Ladoga sandstones compared to the Satakunta sandstones (Finland), Shea-Creek sandstones (Athabasca basin, Canada) and from the Jabiluka decline (Australia) is listed in Table 3.8. Full chemical analysis data of major and trace element composition of the Pasha – Ladoga sandstones are listed in the Annex Sandstones. DDH and outcrops samples location is presented in Part 1.4.

Average composition	Pasha – Ladoga sandstones	Satakunta sandstones	Shea-Creek sandstones	Jabiluka sandstones
SiO_2	81.33 ± 10.53	81.74 ± 9.22	96.95 ± 3.02	93.43 ± 4.86
Al_2O_3	7.65 ± 3.20	8.93 ± 3.80	1.31 ± 1.44	2.65 ± 2.11
Fe_2O_3	2.19 ± 1.79	1.32 ± 1.77	0.46 ± 1.03	0.51 ± 0.67
MnO	0.03 ± 0.07	0.10 ± 0.04	0.00	0.00
MgO	0.38 ± 0.53	0.79 ± 0.82	0.08 ± 0.27	0.69 ± 1.17
CaO	1.52 ± 4.93	1.01 ± 0.77	0.00 ± 0.10	0.03 ± 0.11
Na_2O	0.41 ± 0.82	1.69 ± 1.38	0.00	0.00
K_2O	2.57 ± 1.04	3.26 ± 0.63	0.21 ± 0.35	0.65 ± 0.64
TiO_2	0.34 ±0.29	0.24 ± 0.26	0.05 ± 0.07	0.03 ± 0.05
P_2O_5	0.07 ± 0.11	0.11 ± 0.07	0.01 ± 0.03	0.03 ± 0.07
PF	3.19 ± 3.82	1.44 ± 1.11	0.55 ± 0.65	1.78 ± 1.64
Total	**99.68 ± 0.36**	**99.70 ± 0.41**	**99.71 ±0.08**	**99.80 ± 0.12**
n	**29**	**13**	**155**	**37**

Table 3.8. Major element data of the Pasha – Ladoga Basin (Russia), Satakunta (Finland), Shea-Creek zone (Athabasca basin, Canada) and Jabiluka deposit (Australia) sandstones (Cuney & Brouand, unpublished data)

The SiO_2 content (mainly reflecting the abundance of quartz) varies from 41.3 wt. % (Pasha siltstones) to 95.2 wt. % (Pasha quartz arenites) with an average value of 81,33 wt. % SiO_2. The average Priozersk coarse-grained arkosic sandstone contains about 75 – 80 wt. % of SiO_2. It correlates with the Average Arkose of Pettijohn (1981) with 77.1 wt % of SiO_2. The samples with lower SiO_2 content (40 – 60 wt. %) correspond to the Pasha siltstones or to the lower part of the Salmi sandstones immediately above the Salmi lower basalt layer. The Pasha quartz arenites by their high SiO_2 contents are close to the mature sandstones from the Shea-Creek zone (Athabasca basin, Canada) and the Jabiluka decline (Australia). The average Shea-Creek zone quartzose sandstone contains 97 wt.% of SiO_2 (80 to 99.6 wt. %). The average Jabiluka sandstone contains 93.4 wt.% of SiO_2 (81.1 to 99.3 wt. %).

The Al_2O_3 (2.1 to 16.3 wt. %, average = 7.6 wt. %) and K_2O (0.4 to 4.8 wt. %, average 2.6 wt. %) contents which mainly reflect total K-feldspar and clay mineral contents of the sandstones present a wide scatter of the values. Clay composition diagrams of the Pasha – Ladoga sandstones from the different parts of the basin were given above (Fig. 3.22, 3.23). Slightly higher values of Al_2O_3 are observed in the Satakunta sandstones. It means that the Satakunta sandstones on average are richer in feldspars and clay minerals. The Average Arkose of Pettijohn (1981) shows a slightly higher value of Al_2O_3 (8.7 wt %) but the same K_2O (2.8 wt.%) content. For comparison, average Shea-Creek quartzose sandstone contains only 2.3 wt. % of Al_2O_3 and 0.2 wt.% K_2O reflecting its very high maturity. High maturity is also typical of the Jabiluka sandstones with only 2.7 and 0.7 wt. % of Al_2O_3 and K_2O respectively.

The CaO and MnO values (normative Mn–calcite) are generally quite low. CaO contents of the Pasha Ladoga sandstones varies from traces to 3.7 wt. % and MnO contents from traces to 0.2 wt. %. Only two samples (DDH-816-68 m and DDH-1051-134 m) belonging to the basal part of the intermediate Salmi sandstones, which lies immediately above the Salmi lower basalt layer and contains abundant volcanic clasts are strongly enriched in CaO (up to 27 wt. %) and MnO. Most Ignition Loss values for the sandstones vary from 0.4 to 5 % (average 2.3 wt.%), only the most Ca and Mn enriched samples have I.L. values from 12 to 21 wt.% because of the carbonate ion. The lower amount of carbonate is observed in the Satakunta sandstones. Carbonates are rare in the Shea-Creek and the Jabiluka sandstones. Only traces of CaO and MnO are generally observed in these occurrences with anomal content up to 1.3 wt.% of CaO, 0.06 wt. % of MnO, 0.5 wt.% of PF in Shea Creek, and anomal content up to 0.5 wt.% of CaO, 1.8 wt. % of PF in Jabiluka.

TiO_2 and P_2O_5 contents in the sandstones correspond to Ti oxides (rutile, anatase) and phosphates (apatite, monazite, xenotime, Ca-Al-phosphates). Average TiO_2 content in Pasha Ladoga sandstones is 0.3 wt % and the average P_2O_5 content is 0.1 wt %. Average TiO_2 (0.24 wt. %) in Satakunta sandstones is slightly lower than the Pasha – Ladoga, but average P_2O_5 (0.11 wt. %) is slightly higher. Average TiO_2 (0.05 wt. %) and P_2O_5 (0.01 wt. %) contents in the Shea Creek zone are also lower. Average TiO_2 content in Jabiluka sandstones is also low with 0.03 wt % and average P_2O_5 with 0.03 wt %.

Fe_2O_3 content (normative chlorite and Fe oxides) in the Pasha Ladoga sandstone varies from 0.2 to 7.4 wt. % according to initial rock composition and intensity of chloritization processes. Smaller values are observed in the Satakunta sandstones (0.2 – 2.5 wt. %) which are only weakly chloritized (Ibrahim, 2004). The average Fe_2O_3 value (2.2 wt. %) corresponds to the Average Arkose of Pettijohn (1981). The average Fe_2O_3 value in the Shea-Creek and the Jabiluka sandstones are much lower (0.5 wt %) accordingly to their more mature character.

Major element composition analysis of the four sedimentary basins show that two types of sediments can be distinguished: (i) the Pasha – Ladoga and the Satakunta sediments, both very immature, and (ii) the highly mature Shea-Creek and Jabiluka sediments.

3.4.2. Trace element distribution

Trace elements	Earth crust Clarke concentration* ppm	Pasha – Ladoga sandstones, ppm	Satakunta sandstones, ppm	Shea-Creek sandstones, ppm	Jabiluka sandstones, ppm
As	*1*	*2*	*2*	*0.6*	*1*
Ba	*x0*	***423***	***429***	*12*	*12*
Be	*0.x*	*1*	*3*	*0*	*0.5*
Bi	-	*0.1*	*0.3*	*0.2*	*0*
Cd	*0.0x*	*0.5*	*0.4*	*0*	*0*
Co	*0.3*	*4*	*3*	*0.2*	*1*
Cr	*35*	*16*	*24*	*6*	*4*
Cs	*0.x*	*2*	*2.5*	*0*	*0.2*
Cu	*x*	*8*	*31*	*1*	*1*
Ga	*12*	*11*	*11*	*2*	*5*
Ge	*0.8*	*1*	*1*	*1*	*1*
Hf	*3.9*	*8*	*3*	*3*	*2*
In	*0.0x*	*0*	*0.1*	*0*	*0*
Mo	*0.2*	*0.5*	*0*	*0.2*	*0*
Nb	*0.0x*	*17*	*6*	*1*	*1*
Ni	*2*	*8*	*17*	*1*	*3*
Pb	*7*	*27*	*16*	*3*	*2*
Rb	*60*	***83***	***126***	*2*	*10*
Sb	*0.0x*	*0.1*	*0.2*	*0.1*	*0.1*
Sn	*0.x*	*3*	*2*	*0.1*	*1*
Sr	*20*	*59*	*91*	*73*	*28*
Ta	*0.0x*	*1*	*1*	*0.1*	*0.2*
Th	*1.7*	***13***	***14***	*3*	*9*
U	*0.45*	***3***	***4***	*1*	*1*
V	*20*	*29*	*23*	*5*	*4*
W	*1.6*	*1*	*0.5*	*0.2*	*1*
Y	*40*	***17***	***15***	*6*	*3*
Zn	*16*	*71*	*27*	*0.6*	*0.5*
Zr	*220*	***311***	*130*	*123*	*87*
La	*30*	***38***	*28*	*11*	*20*
Ce	*92*	***70***	*57*	*23*	*39*
Pr	*8.8*	*8*	*7*	*2*	*4*
Nd	*37*	*26*	*24*	*8*	*14*
Sm	*10*	*4*	*5*	*1*	*2*
Eu	*1.6*	*1*	*0.6*	*0.2*	*0.4*
Gd	*10*	*3*	*4*	*1*	*1*
Tb	*1.6*	*0.5*	*0.5*	*0.2*	*0.1*
Dy	*7.2*	*3*	*3*	*1*	*1*
Ho	*2*	*0.5*	*0.5*	*0.2*	*0.1*
Er	*4*	*2*	*1*	*0.5*	*0.3*
Tm	*0.3*	*0.3*	*0.2*	*0.1*	*0.1*
Yb	*4*	*2*	*1.2*	*0.5*	*0.3*
Lu	*1.2*	*0.1*	*0.2*	*0.1*	*0.1*

Table 3.9. Trace and Rare Earth element average contents in the Pasha – Ladoga (Russia), Shea-Creek (Athabasca basin, Canada) and Jabiluka (Pine-Creek geosyncline, Australia) sandstones.
**Turekian K., Wedepohl K. Distribution of the elements in some major units of the Earth's crust. Bull. of the Geol. Soc. of America. 196,. 72- 2 : 175 – 192; For some elements, only order of magnitude are given, indicated by the symbol x*

Trace element average composition of the sandstones from Pasha – Ladoga and Satakunta (Finland), Shea-Creek (Athabasca basin, Canada) and Jabiluka (Australia) are listed

in Table 3.9. Clarke concentrations (Turekian & Wedepohl, 1961) are also listed in this table for comparison.

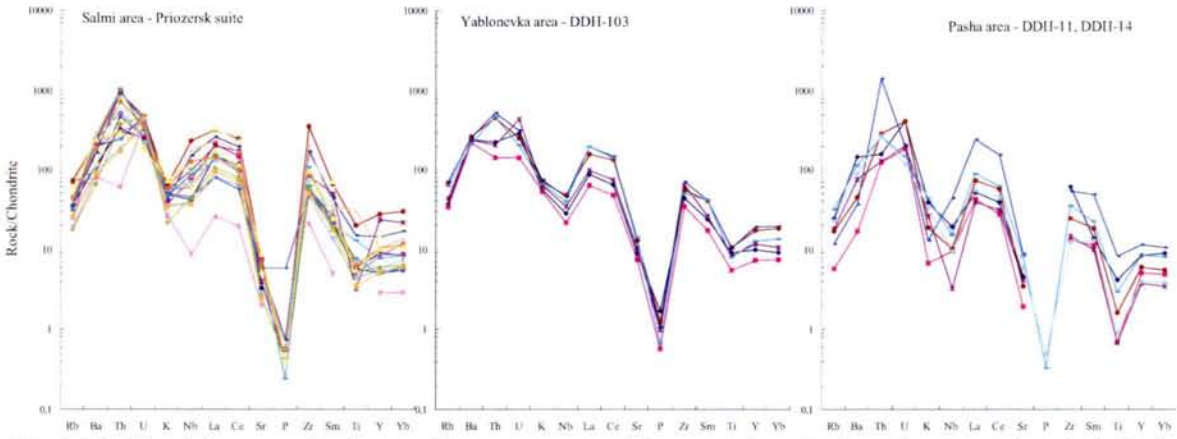

Fig. 3.59. Chondrite-normalized trace element patterns of the non-mineralized sandstones of the whole Pasha – Ladoga basin from Salmi, Western (exclusively Yablonevka) and Pasha areas (spidergram type after Holm (1979); chondrite composition after E. Anders and N. Grevesse: http://earthref.org/GERM/reservoirs/C1.htm)

Trace element distributions in the non-mineralized sandstones of the different parts of the Pasha – Ladoga basin are represented in the chondrite-normalized spidergrams (Fig. 3.59). There only minor differences between the Priozersk non-mineralized sandstones from the Salmi, Yablonevka and Pasha areas. In comparison with Clarke concentrations in the Earth Crust they are strongly enriched in Ba, Sr, Nb, Ta, Th, U and moderately enriched in Rb, Zr, Hf, Cd, Zn, Mo, Ni, Sn, Be, and Pb.

The characteristic feature of the non-mineralized sandstones from the different parts of the basin is the high abundance of the lithophile element association: U - Th - Ti - Zr - Y - LREE, which can be related to the detrital accessory minerals composition of the sandstones inherited from the basement rocks.

Average sandstones from Satakunta (Finland), Shea-Creek (Athabasca basin, Canada) and Jabiluka (Pine-Creek geosyncline, Australia) have been also reported in similar spidergrams (Fig. 3.60). The clear-cut distinction is observed in the left part of the diagrams, with strong Rb and Ba enrichments in the Pasha – Ladoga and Satakunta sandstones reflecting the abundance of feldspars. Th, U, K and Nb are also enriched in the Pasha – Ladoga and Satakunta sandstones. The non-mineralized sandstones from the Athabasca basin are depleted in most elements including U compared to the two other basins.

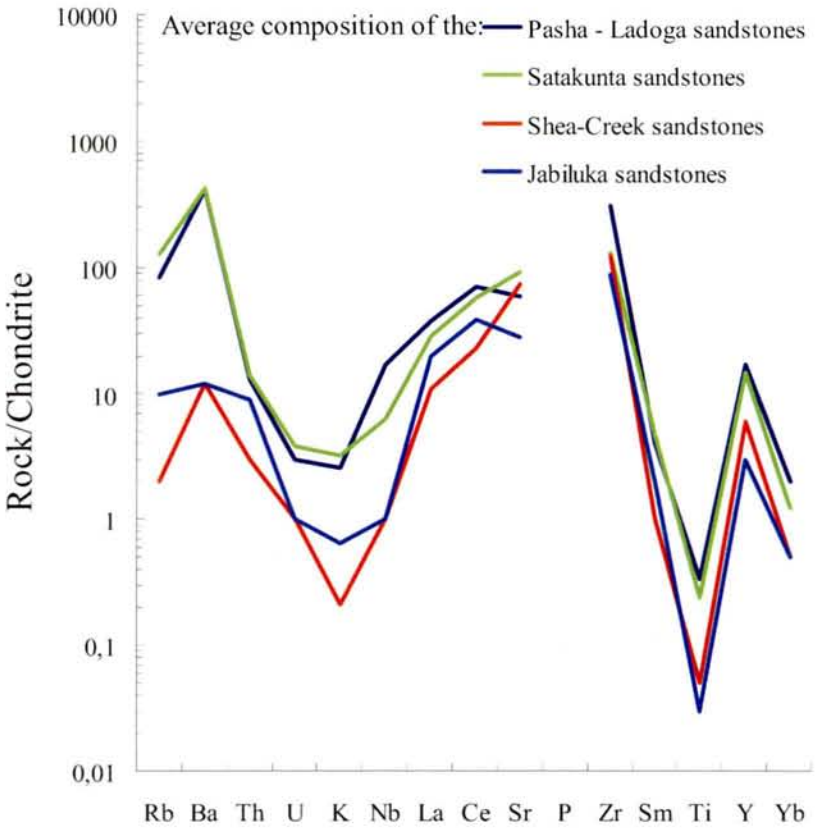

Fig. 3.60. Chondrite-normalized trace element patterns of the average non-mineralized sandstones from the Pasha – Ladoga, Satakunta, Shea-Creek and Jabiluka basins (spidergram type after Holm (1979); chondrite composition after E. Anders and N. Grevesse: http://earthref.org/GERM/reservoirs/C1.htm

Trace element distribution in the mineralized sandstones of the Salmi and the Karku deposit area have some specific features. The chondrite-normalized spidergrams patterns of the non-mineralized (less than 4 ppm of U), slightly mineralized (less than 9 ppm of U) and mineralized (more than 9 ppm of U) are represented in Fig. 3.61. There is no major variation between non-mineralized and slightly mineralized sandstones. But in the mineralized sandstones, strong depletion in Rb, Ba and Sr is observed in relation with the alteration of the detrital feldspars. Uranium is logically high in the mineralized sandstones, but Th is not correlatively enriched. The characteristic feature of the mineralized sandstones from the Karku deposit area is the development of a chalcophile association: U - Mo - Zn - Pb - Cu, which has to be related to the chlorite - carbonate - sulphide hydrothermal alteration processes.

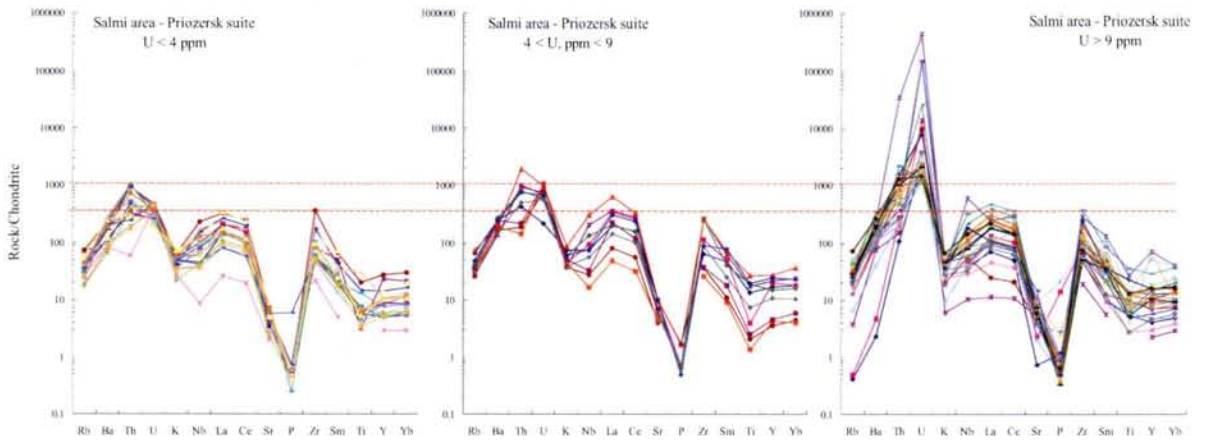

Fig. 3.61. Chondrite-normalized trace element patterns of the Priozersk sandstones of Salmi and Karku deposit areas: (i) non-mineralized < 4 ppm U; (ii) slightly mineralized 4 < U < 9 ppm; (iii) mineralized > 9 ppm U. Spidergram type after Holm (1979); chondrite composition after E. Anders and N. Grevesse: http://earthref.org/GERM/reservoirs/C1.htm)

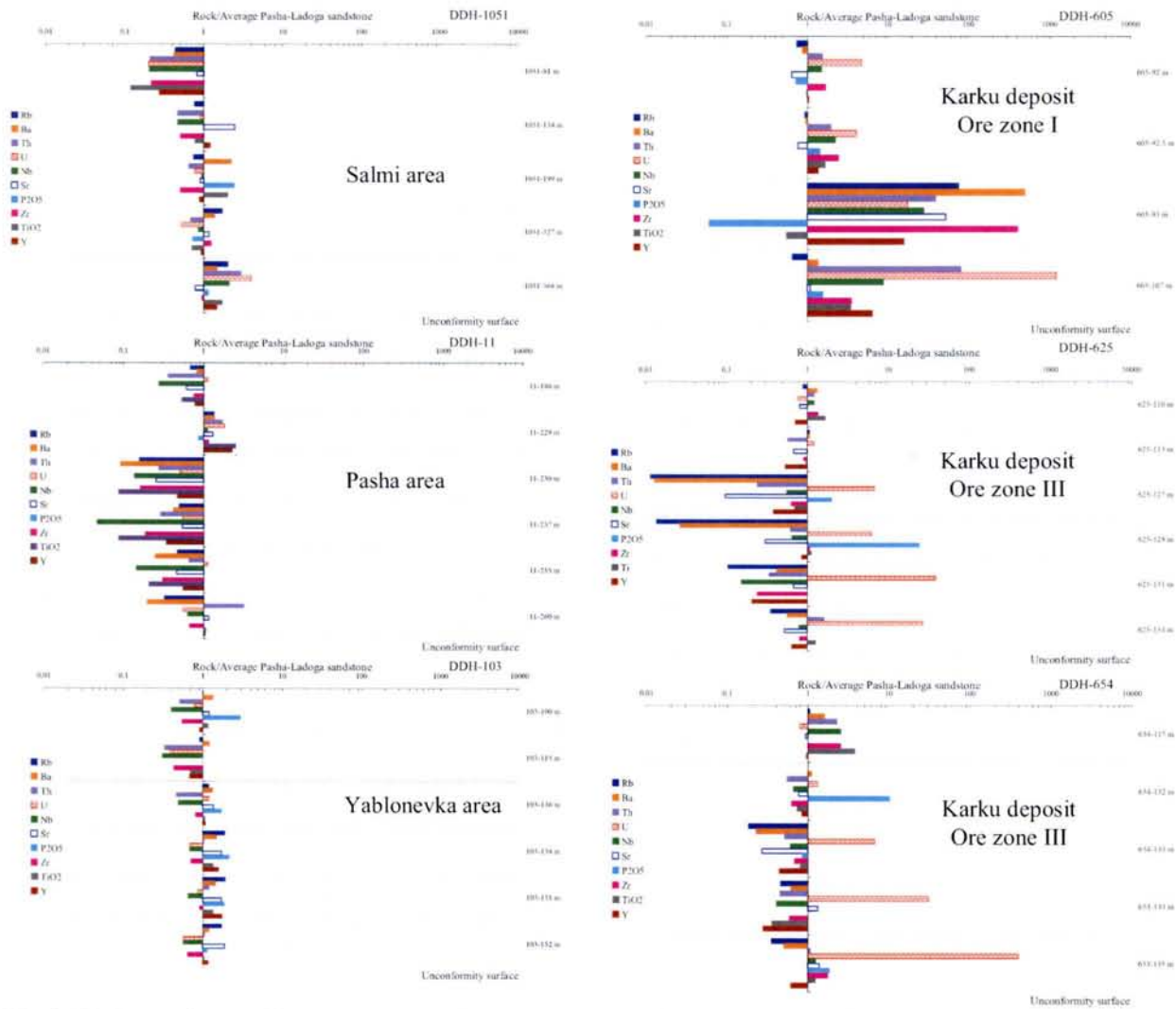

Fig. 3.62. Trace element distribution in the Pasha – Ladoga sandstones in concerning to the DDH position and depth of the samples

For a better understanding of trace elements and REE distribution along the stratigraphic succession and alteration degree the geochemical information has been also examined according to the depth position of the samples in the drill holes with diagram normalized to average "Pasha – Ladoga sandstone"- (Fig. 3.62). An average of the "Pasha – Ladoga sandstone" was calculated (Table 3.8 – 3.9). In the left part of the Figure 3.62 the Pasha – Ladoga non-mineralized sandstones from the Salmi (DDH-1051), Pasha (DDH-11) and Yablonevka (DDH-103) area are considered, in the right part of the Figure 3.62 – mineralized and slightly mineralized sandstones from the Karku deposit area: DDH-605 – ore zone I, DDH-625 and DDH-654 – ore zone III.

Regionally, in the DDH-1051, DDH-11 and DDH-103 (left part of Fig. 3.62) the variations of chemical composition along the profile do not exceed about 30% for most elements relatively to the average Pasha-Ladoga sandstone. No systematic variation is observed along the profiles with depth. In the Salmi area (DDH-1051) the samples mainly present a Rb enrichment, and to a lesser extend in Ba corresponding to the illitic alteration in the 3 samples closer to the unconformity. Most other element are constant or moderately enriched with depth. The upper siltstone of the Pasha suite is depleted in most elements and significantly depleted in U. The lowermost sample (in the vicinity of the unconformity surface) is significantly enriched in uranium but also in thorium.

In the Pasha area (DDH-11) the samples are mainly depleted in all elements with depth compared to average sandstone indicating a higher maturity of the sandstones. A slight Th enrichment is observed only near the unconformity surface. Maximum U content is observed in the upper part of the section in the siltstones of the Pasha suite. In the Yablonevka area (DDH-103) the samples have compositions close to the average sandstone one.

In the Karku deposit area (DDH-605, DDH-625, DDH-654) significant variations in major and trace elements distribution are observed (right part of Fig. 3.62). In the ore zone I (DDH-605) the two upper sandstones near the contact with the Salmi basalts (interval - 92 – 92.5 meters) are similar to the average "Pasha – Ladoga sandstone" for most elements but with significant U enrichment. At the contrary, the sample at -93 m is strongly enriched in most elements including Ba, Rb, Sr, Nb, Zr, Y, Th and U. Such a signature correspond to an initially relatively immature sandstone rich in feldspars and accessory minerals. A depletion in P_2O_5 and surprisingly of TiO_2 is also characteristic of this sample. In the vicinity of the unconformity surface only a strong enrichment in U and Th and moderate enrichments in

most other elements excepted Rb, Ba and Sr are observed. The lower Rb, Sr and Ba content relative to the preceding sample reflect the alteration of the feldspars.

The two drill cores (DDH-625 and 654) from the ore zone III are characterized by specific features. U is strongly enriched with depth in both drill core. In DDH-625, the middle part of the sandstones sequence is strongly depleted in Rb, Ba, Sr, but when approaching the unconformity surface these elements become less depleted up to the average values. In DDH-654 there are no significant variation of Rb, Ba, Sr and other element contents, except U, which is strongly enriched with depth. Significant phosphorus enrichments are sporadically observed in some samples.

3.4.3. REE distribution

The rare-earth elements (REE) distribution of the Mesoproterozoic Pasha – Ladoga sandstones from the different parts of the basin is presented in Fig. 2.105. Total REE content in the non-mineralized sandstones from the Salmi area is strongly variable even within the same drill core. For example, REE abundance varies from 330 ppm (DDH-822-143 m) to 27 ppm (DDH-822-147 m). Average ΣREE in the Salmi area is about 150 ppm. In the Yablonevka area within DDH-103, ΣREE varies from 100 to 200 ppm, in the Pasha area (DDH-11 and DDH-14) – from 40 to 230 ppm.

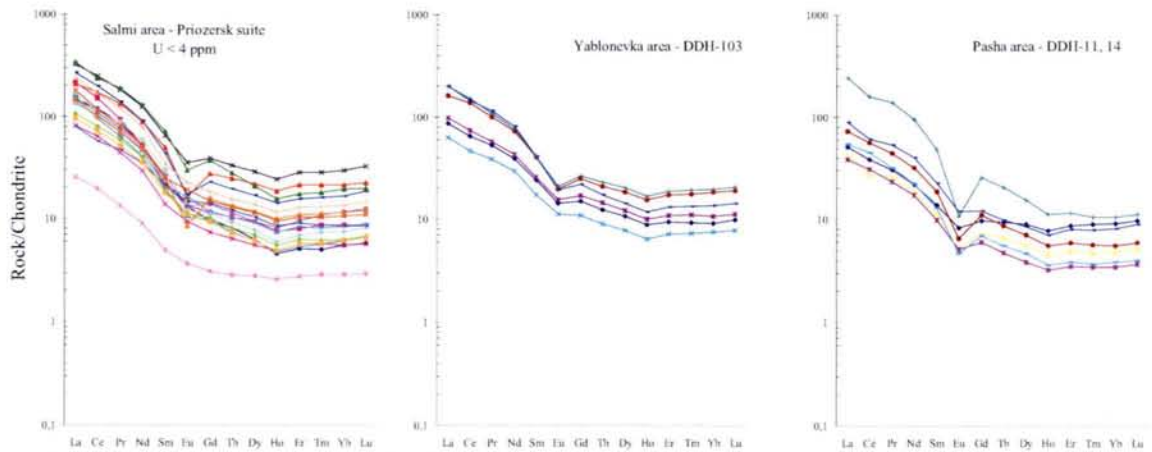

Fig. 3.63. Chondrite-normalized REE distribution patterns of the Pasha – Ladoga sandstones from the different parts of the basin: Salmi, Yablonevka and Pasha areas (chondrite composition after Anders & Grevesse: http://earthref.org/GERM/reservoirs/C1.htm)

REE distribution in the non-mineralized sandstones of the different parts of the Pasha – Ladoga basin is presented in the chondrite-normalized spidergrams (Fig. 3.63). By comparison with other Mesoproterozoic basins (Canada, Australia and Finland) (Fig. 3.64) the REE distribution is quite similar. Most REE patterns are moderately fractionated with a distinct Eu anomaly as classical sediments (shales or greywackes). Some of the Satakunta sandstones present a stronger Eu anomaly. Average characteristics of the REE distribution for all basins are given in Table 3.10.

Mesoproterozoic sedimentary basins, areas, suites	$(Ce/Yb)_N$	Eu/Eu*	$(Gd/Dy)_N$	$(Er/Yb)_N$
Pasha – Ladoga (Salmi area, Priozersk sandstones	12	0.8	1.4	0.95
Satakunta sandstones	12	0.6	1.6	1.05
Shea-Creek (average Erica I - III sandstones)	17	0.5	1.8	1.02
Jabiluka decline sandstones	33	0.7	2.3	0.95

Table 3.10. Average characteristics of the REE distribution in the non-mineralized sandstones of the Pasha – Ladoga (Russia), Satakunta (Finland), Shea-Creek (Canada) and Jabiluka (Australia)

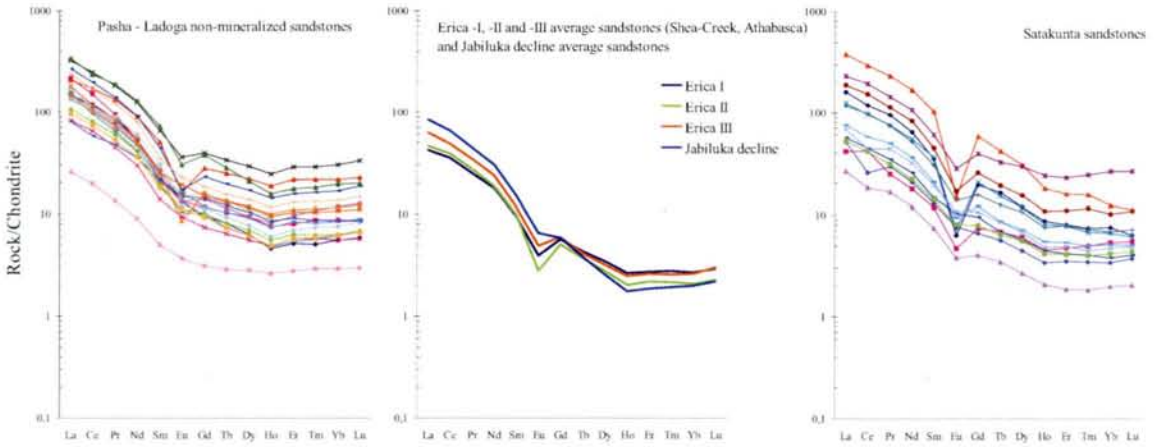

Fig. 3.64. Chondrite-normalized REE distribution patterns of the Pasha – Ladoga (Salmi area), Shea-Creek (Erica) and Satakunta non-mineralized sandstones (chondrite composition after Supplemental data for chondrite (Anders & Grevesse: http://earthref.org/GERM/reservoirs/C1.htm)

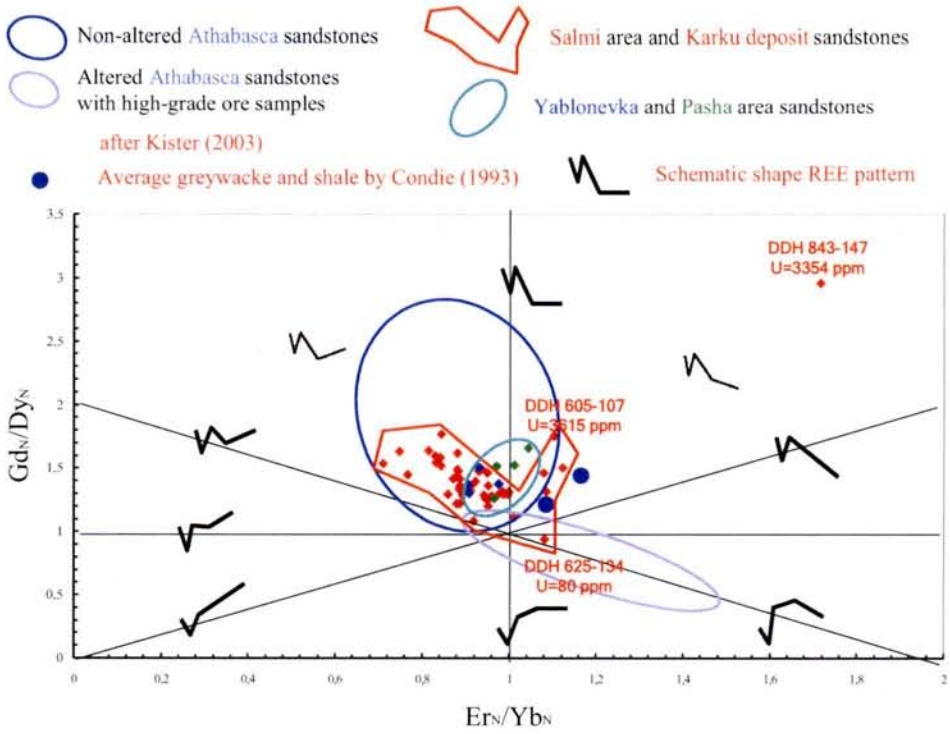

Fig.3.65. Gd_N/Dy_N versus Er_N/Yb_N diagram for Pasha – Ladoga and Athabasca sandstones (after Kister, 2003)

In the Gd_N/Dy_N versus Er_N/Yb_N diagram established by Kister (2003) to evaluate intermediate HREE depletion or enrichment (Fig. 3.65), the representative points of the non-mineralized sandstones from the Athabasca (Erica I-III) (Kister, 2003) and Pasha – Ladoga (Salmi area) (present work) basins plot to the upper left of the average greywacke and shale points. The Athabasca sandstones appear therefore strongly depleted in intermediate HREE (Ho and Er) compared to average greywacke and shale (Condie, 1993). The Pasha – Ladoga sandstones are less depleted and closer to average greywacke and shale compositions.

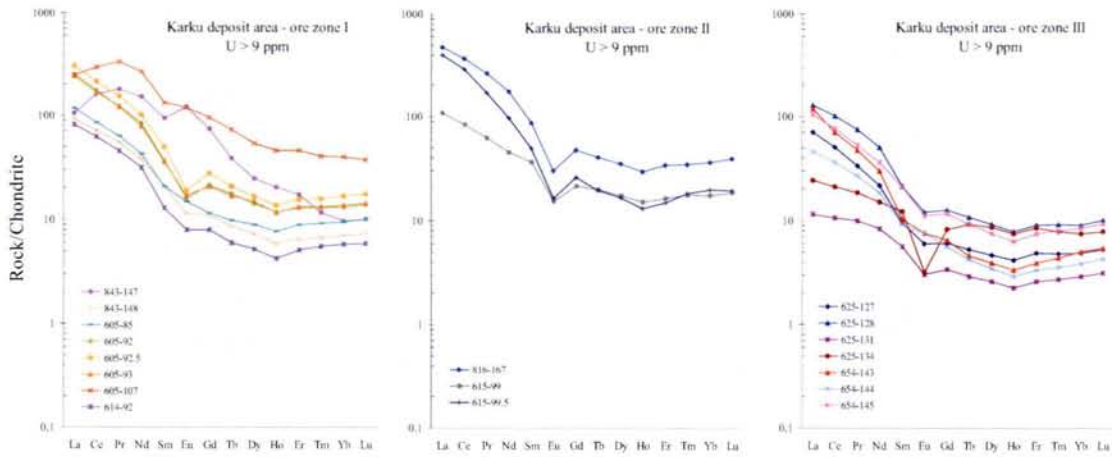

Fig. 3.66. Chondrite-normalized REE distribution patterns of the mineralized sandstones from the different ore zones of the Karku deposit area (Pasha – Ladoga basin) (chondrite composition after Anders & Grevesse: http://earthref.org/GERM/reservoirs/C1.htm)

REE distribution in the mineralized sandstones of the different mineralized zones of the Karku deposit area (Pasha – Ladoga basin) is presented in Fig. 3.66. Some of the REE patterns present enrichments in the intermediate LREE (ore zone I of the Karku deposit). Average characteristics of the REE distribution in the mineralized sandstones from the different ore zones of the Karku deposit are listed in the Table 3.11.

Mesoproterozoic sedimentary basins, areas, suites	$(Ce/Yb)_N$	Eu/Eu*	$(Gd/Dy)_N$	$(Er/Yb)_N$
Ore zone I	11.5	0.8	1.7	1.1
Ore zone II	9.8	0.5	1.4	0.9
Ore zone III	8.6	0.8	1.4	0.9
Outside of the ore zone in the Karku deposit area	10.2	0.7	1.4	1.1

Table 3.11. Average characteristics of the REE distribution in the mineralized sandstones of the different ore zones of the Karku deposit area (Pasha – Ladoga basin, Russia)

For a better understanding of the REE distribution with depth and alteration degree the geochemical data have been also examined according to the depth position of the samples along the drill holes in the vicinity of the Pre-Riphean unconformity surface using diagrams normalized to the average "Pasha – Ladoga sandstone"- (Fig. 3.67).

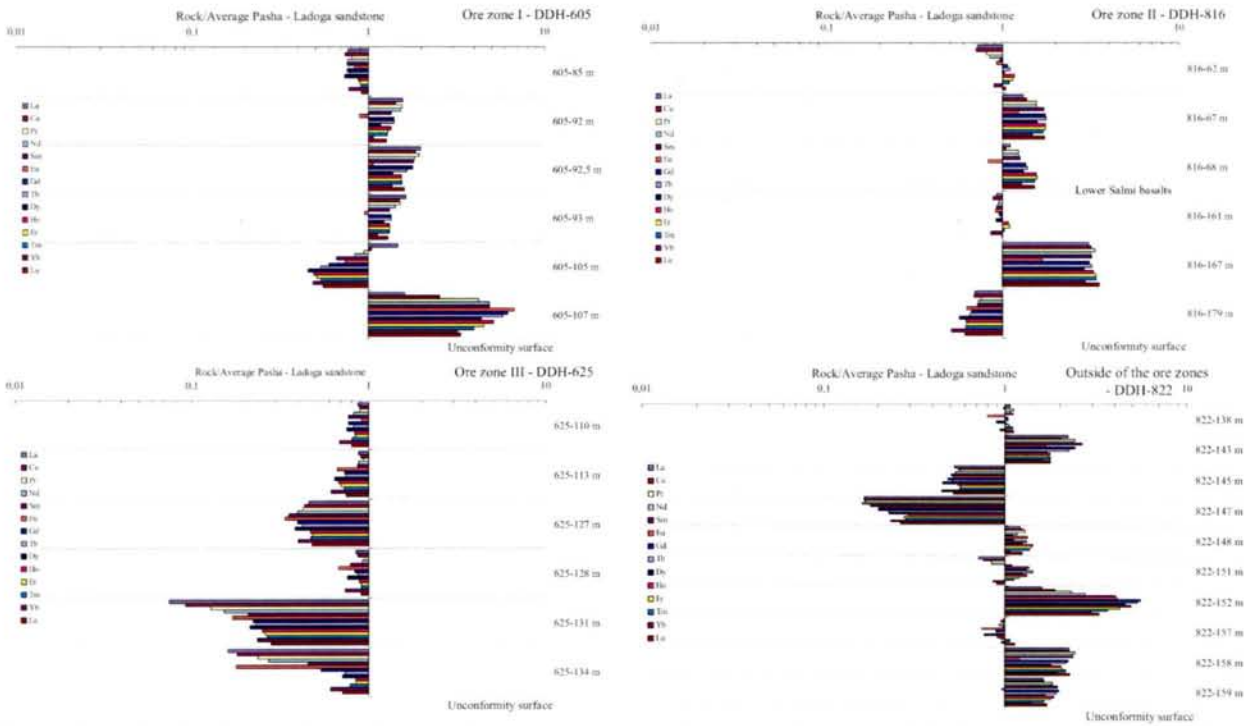

Fig. 3.67. REE distribution in the Pasha – Ladoga sandstones in concerning to the DDH position and depth of the samples

In DDH-605 (ore zone I of the Karku deposit) strong HREE enrichment is observed in the vicinity of the unconformity surface, LREE enrichment in the vicinity of the unconformity surface is also observed, but less significant.

In DDH-816 (ore zone II with two sedimentary suites presented in the section) a strong REE depletion occur in the vicinity of the unconformity, a strong REE enrichment at –167 m (middle part of the Priozersk sandstones). Salmi sandstones are riche in REE in the vicinity of the contact with the Salmi basalts. They are also richer in Th, that mean abundance of the detrital monazite.

In DDH-625 (ore zone III of the Karku deposit) a general depletion in REE with depth is observed, but in the vicinity of the unconformity surface, a slight enrichment in HREE is observed.

In DDH-822 (outside of the ore zones but within the Karku deposit area) strongly variable REE distribution appears. In the middle of the section, all REE (especially HREE) are strongly depleted and some meters below they are strongly enriched (especially HREE). In the vicinity of the unconformity LREE depletion is again observed.

Conclusions for chapter III

The composition of the Pasha – Ladoga sediments from the different parts of the basin varies widely: from subarkoses, arkoses, litharenites, sublitharenites to greywackes. In contrast to the sandstones from the Shea Creek area (Athabasca basin, Canada), which are nearly orthoquartzitic, no true quartz arenites exists in the Pasha – Ladoga basin.

The regional diagenetic features at the scale of the whole Pasha – Ladoga basin are well expressed in selected samples from the Salmi, Yablonevka and Pasha areas, which have not been significantly affected by subsequent alterations. The diagenetic event is multistage and mainly consists of quartz overgrowths over detrital quartz crystals, hematization, transformation of coarse-grained authigenic kaolinite to dickite and authigenic smectite by illite with neoformation of interstratified illite-smectite and illite-chlorite. Quartz overgrowths are generally less well developed than in the Athabasca and Kombolgie basin.

In the Pasha – Ladoga basin the presence of abundant K-feldspar and plagioclase and their stability, except in the vicinity of the mineralized zones, has conferred more alkaline pH conditions to the fluids during the diagenesis, less favourable for uranium solubility. The crystallization of I/S illite-smectite and illite-chlorite and the presence of carbonates during the main mineralization event in these basins is also in favour of relatively alkaline fluids.

Altered and mineralized sandstones from the Karku deposit area are richer in quartz with a relatively constant proportion of clay minerals, feldspars if still present are in much lower proportion. During the uranium mineralization stage the mineralogical assemblage is mainly characterized by the development of Mg-Fe and Fe-rich chlorites and Mn carbonates. Quartz dissolution is much less intense than in the Athabasca basin, providing less open space for the deposition of massive uranium mineralization as in the Athabasca basin in particular.

The characteristic feature of the Pasha – Ladoga sandstones chemical composition is the high abundance of the lithophile element association: U – Th – Ti – Zr – Y – LREE, which can be related to the abundance of detrital accessory minerals composition of such immature sandstones inherited from the basement rocks.

The mineralized sandstones from the Karku deposit area characterized by a chalcophile association: U - Mo - Zn - Pb - Cu, which has to be related to the chlorite - carbonate - sulphide hydrothermal alteration processes. Alteration of detrital monazite grains is exceptional in the mineralized Pasha – Ladoga sandstones with weak neoformation of the

APS minerals on the contrary to the Athabasca basin, where the monazite alteration is the process is regionally developed. Zircon alteration in the Pasha – Ladoga sandstones is a regional feature as the Athabasca basin, where strong alteration of zircon was evidenced.

The barren sandstones of the Pasha Ladoga basin are more enriched in LREE than the barren sandstones of the Athabasca basin. The Pasha – Ladoga mineralized sandstones are less depleted in intermediate HREE (Ho and Er) to the contrary to the Athabasca mineralized sandstones, which are usually strongly depleted in these elements.

Chapter IV

Mesoproterozoic basaltic magmatism of the Pasha – Ladoga basin

Part 4.1. Geological setting

Mesoproterozoic (Riphean or Postjotnian) continental flood basalt (CFB) - type magmatism (1460 – 1265 Ma) on the Baltic Shield commonly accompanied the formation of the Mesoproterozoic (Riphean or Jotnian) sedimentary basins made of continental sandstones and siltstones successions within rift complex zones and faulted-bounded basins (Kohonen & Ramo, 2004). It corresponds to crosscutting (occasionally also concordant) tholeitic dikes in southwestern Finland and adjacent Sweden (Patchett et al, 1994; Amantov et al, 1996), and as extensive alkali basaltic sills in Russian Karelia –Ladoga Lake region (Amantov et al, 1996; Golubev & Svetov, 1983; Kayryak & Khazov, 1967; Khazov & Popov, 1984; Ramo et al., 2004; Tikhomirov & Yanovsky, 1970; Upton et al, 1998).

The ≈ 1265 Ma hypabyssal mafic rocks are well-known in the Satakunta region (southwestern Finland) and some other localities in Finland and Sweden (Kohonen, 1993; Kohonen & Ramo, 2004).

Fig. 4.1. Sketch map of the Lake Ladoga region showing the outlines of two major volcanic sequences (in green) within the Pasha - Ladoga sedimentary basin (in purple) (after Amantov et al., 1996).

In the Ladoga Lake region (Fig. 4.1) similar dolerites and basaltic lavas outcrop along the north-eastern and eastern shore of Ladoga Lake (in the Tulema River bed near Salmi village – Fig. 4.3) and differentiated gabbro – monzonite – syenite Valaam sill outcrops in the Valaam archipelago (Valaam, Mantsinsaari, Lunkkulunsaari islands and skerries in the north-eastern shore of the Ladoga Lake). In the Karku deposit area the Salmi basalts are mainly overlapped by the Quaternary glacial deposits but have been also intersected by exploration drillings (Novikov et al, 2001).

Four phases of magmatic activity have been distinguished during Mesoproterozoic in the Northern Ladoga area. During the first stage the large Salmi rapakivi granitoidic batholith was emplaced (1560-1540 Ma). Two

stages of basaltic lava eruption occur during the sedimentation of the Pasha Ladoga clastic basin corresponding to two main volcanic sheets. The lower sheet (Lower Salmi subsuite) consists of 2 to 9 basalts flows. The most consistent and thick are the first flow (up to 40 meters thick) and the second (15 – 17 meters). The Upper Salmi subsuite consists of 1 to 6 basalts flows and "mandelsteins" rocks (Novikov et al, 2001).

These two eruption stages are separated by a layer of terrigenous sedimentary rocks (Salmi sedimentary subsuite - up to 30 m thick – see in Chapter III), which indicates a pause in the volcanic activities. The last stage of magmatic activity corresponds to the intrusion of the differentiated gabbro – monzonite – syenite Valaam sill (Amantov et al, 1996).

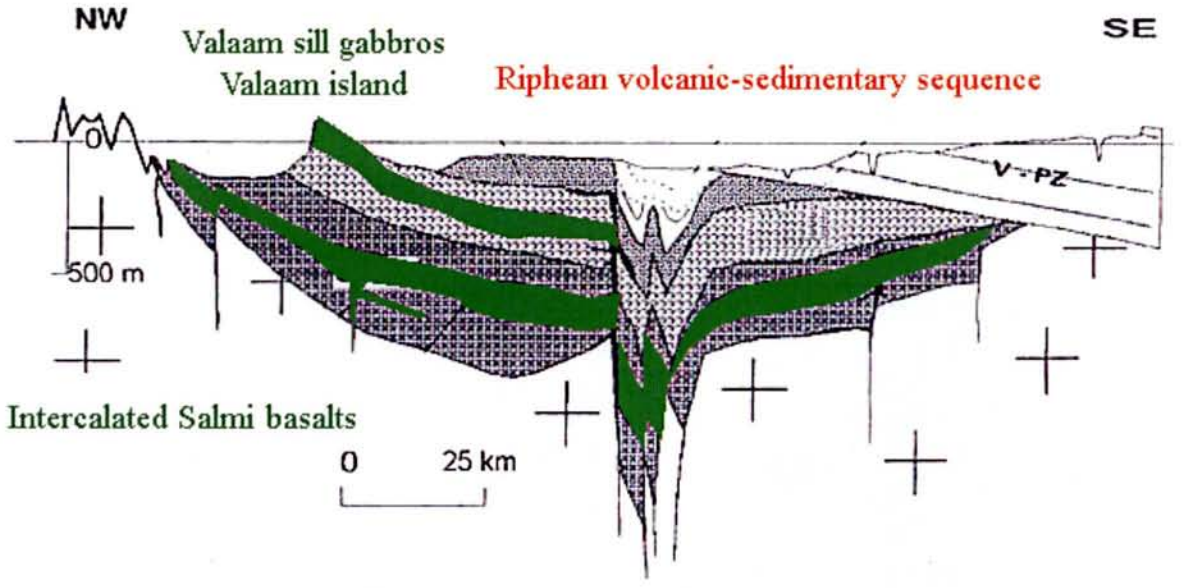

Fig. 4.2. Cross section of the Pasha - Ladoga basin based on seismic reflection studies (Amantov et al., 1996). Two major volcanic sequences in the sedimentary sequence can be discerned.

Comprehensive U-Pb geochronologic data (Suominen, 1991) have defined the age of the tholeitic magmatism in south-western Finland between 1270 and 1260 Ma. It thus also represents a minimum age for the Satakunta sandstones intruded by the mafic dikes. The mafic sills in the Pasha - Ladoga basin were until recently considered to be more or less coeval with the mafic dikes in south-western Finland (Amantov et al, 1996). But two baddeleyite fractions from the Valaam Island in northern part of the Ladoga Lake give a concordia age of 1457.4 ± 2.7 Ma (Ramo et al., 2001), indicating that the mafic magmatism in the Ladoga Lake region is much older that hitherto believed.

According to Amantov et al (1996) and Ramo et al (2001), the Valaam sill consists of two major sill horizons: a lower basic one and an upper potassium rich with intermediate

composition. After joint field investigations of VSEGEI and Helsinki University (summer of 2004) it is possible to conclude, that on the cross section (Fig. 4.2) we can observe Salmi dolerites and basalts intercalated in the Riphean sediments as the lower volcanic unit and the differentiated Valaam sill crosscutting the sediments as the upper member of the Riphean volcanic activity.

Preliminary Nd isotope data on the Salmi basalts cobbles on the coast of the Valaam Island have given ε_{Nd} (at 1460 Ma) values of - 5.8 to - 4.1, whereas the Valaam sill present more negative ε_{Nd} (at 1460 Ma) values of - 9. Therefore, the basalts may have been derived from a different source than the (less radiogenic) subvolcanic mafic rocks of the Valaam sill (Ramo et al., 2004).

Part 4.2. Salmi Suite basalts

4.2.1. Petrography and mineralogy of the Salmi basalts

The Salmi basalts are represented by two main sheets – a Lower one (130 – 140 meters thick) and an Upper one (about 90 meters thick) volcanic Salmi Subsuites. They are composed of a series of separate lava flows. The basalts can be brecciated by calcite veins (lava breccias) and some others may be massive but with brecciated roofs. Detail analysis of the inner structure of both volcanic sheets has not confirmed the presence of porhyroclastic layers (Amantov et al, 1996).

Fig. 4.3. Salmi basalts in the bed of the Tulema river near the Salmi village

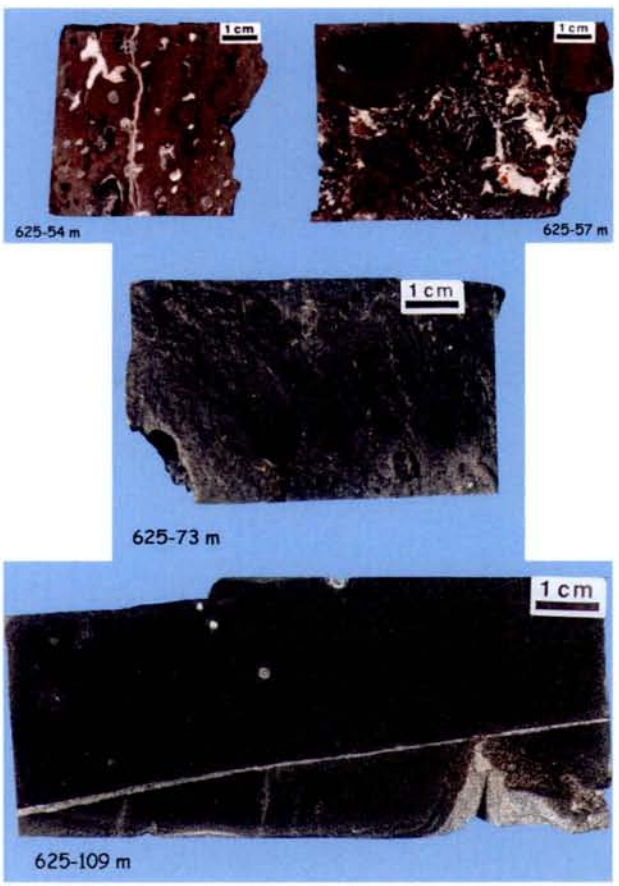

Fig. 4.4. Sequence of basalts from the upper volcanic Salmi subsuite from top to bottom (Karku deposit area, ore zone III, DDH – 625)

The most common rock type is slightly altered (olivine)-plagioclase-clinopyroxene basalt with doleritic and poikilophytic textures. The volcanic rocks are aphyric to microporphyritic with a hyaline to holocrystalline (in the subvolcanic bodies) groundmass texture (Fig. 4.4).

The mineral assemblage, which makes up the Salmi Suite basalts in the Salmi area, includes olivine, clinopyroxene, rare amphibole and plagioclase (An_{60-40}).

Olivine is predominantly ferriferous in composition (Fo_{40-46}), clinopyroxene is represented by a sequence of titanaugite – Fe-titanaugite ($En_{42-34}Wo_{41-38}Hd_{19-28}$) and diopside – Fe augite ($En_{54-37}Wo_{31-26}Hd_{15-37}$) (Amantov et al, 1996).

Ilmenite, titanomagnetite, titanite, apatite (up to 1 wt. %) are the main accessory minerals.

4.2.2. Alteration processes in the Salmi basalts

The first alteration processes in the Salmi basalts start during lava eruption. The high degree of hematization, the great abundance of amygdales in the rocks suggest subaerial solidification of the lavas.

The main basalt-forming minerals (clinopyroxene, olivine and, partially, amphibole) are replaced by chlorite and chlorite-smectite interstratified clay minerals (nontronite and ferriferous saponite). Olivine phenocrysts are replaced with brown aggregate of iddingsite. Albitization processes are very common.

The amygdales are usually filled with chlorite, quartz, and carbonate and, in places, hematite (Fig. 4.4, 4.5). Amygdaloidal basalts and lava breccias from the roofs of lava flows are strongly altered. Quartz, chlorite, calcite are main alteration minerals.

	475-64
SiO_2	31.60
Al_2O_3	15.73
MgO	18.78
FeO	22.41
TiO_2	0.02
MnO	0.37
CaO	0.36
Na_2O	0.05
K_2O	0.029
Total	**89.37**
Si	3.19
Al^{IV}	0.81
Al^{VI}	1.07
Mg	2.83
Fe^{2-}	1.89
Ti	0.00
Mn	0.03
Total VI	5.82
Ca	0.04
Na	0.01
K	0.00
Fe/(Fe + Mg)	**0.40**
n	16

Table. 4.1. Average chlorite composition from Salmi basalts.

The average chemical composition of the chlorites from amygdales of the Salmi basalts is given in Table 4.1.

The structural formula of chlorite from the Salminskaya basalts (DDH – 475 – 64 m) :

$$(Mg_{2.80}Fe_{1.90}Mn_{0.03}Al_{1.06})(Si_{3.19}Al_{0.81})O_{10}(OH)_8,$$

corresponds to a *Mg chamosite*.

The next alteration stage of the basalt is observed in the Karku deposit area in connection with the formation of the uranium mineralization in the vicinity of the Riphean unconformity surface. In the lower Salmi basalt subsuite, vertical quartz-carbonate veins with pitchblende and sulphide mineralization (pyrite, galena) occur, mostly above the high-grade mineralization zones in the sandstones (Fig. 4.6).

a. DDH – 502 – 177 m. Olivine-plagioclase-pyroxene basalt with amygdales

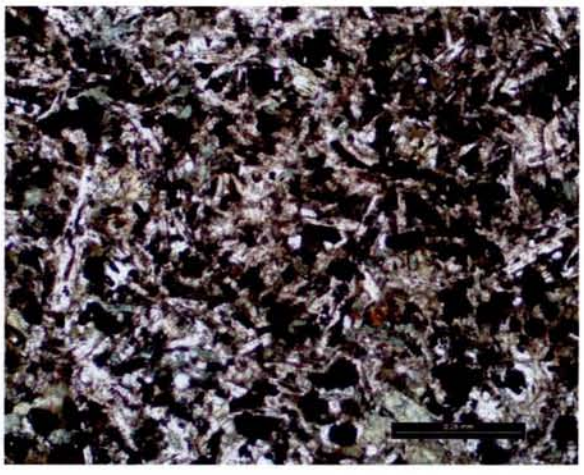

b. DDH – 502 – 177 m. Olivine-plagioclase-pyroxene basalt with amygdales - details of the poikilophytic texture. Parallel nicols, line scale – 0.25 mm

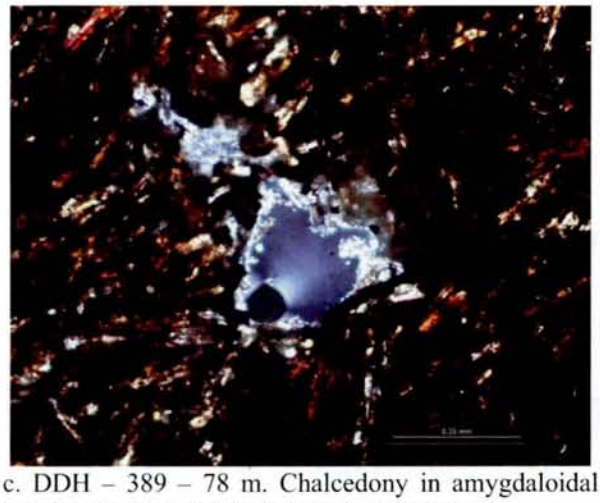

c. DDH – 389 – 78 m. Chalcedony in amygdaloidal basalts. Crossed nicols, line scale 0.25 mm

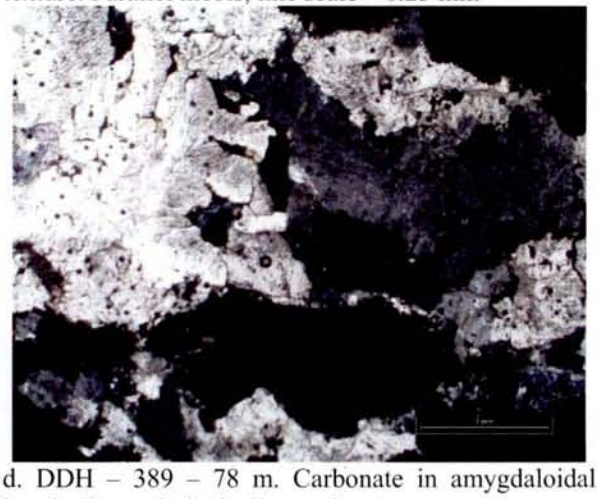

d. DDH – 389 – 78 m. Carbonate in amygdaloidal basalt. Crossed nicols, line scale – 1 mm

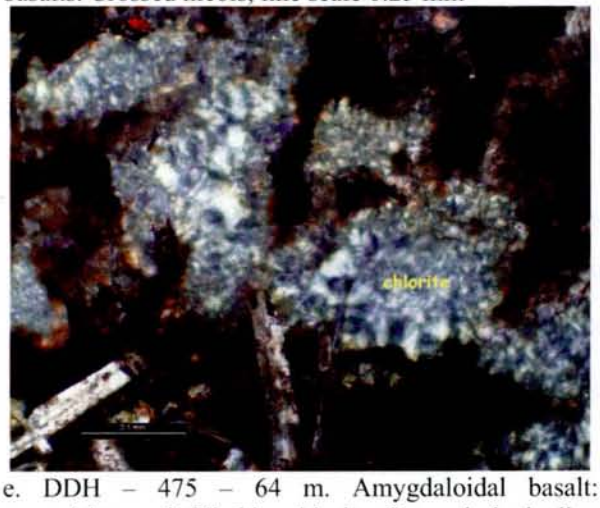

e. DDH – 475 – 64 m. Amygdaloidal basalt: amygdales are infilled by chlorite. Crossed nicols, line scale – 0.1 mm

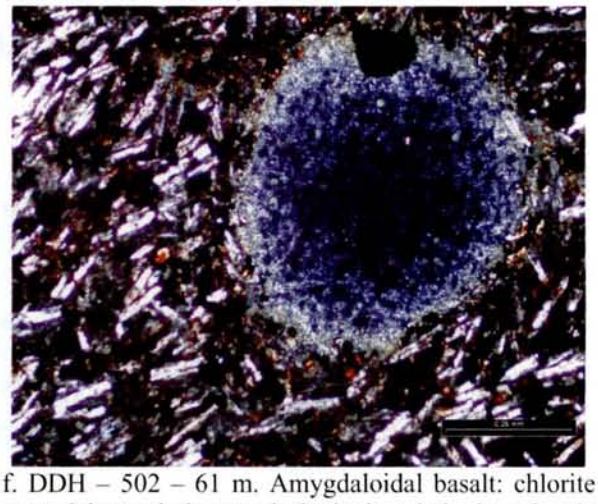

f. DDH – 502 – 61 m. Amygdaloidal basalt: chlorite amygdales and elongated plagioclase laths in volcanic glass. Parallel nicols, line scale – 0.25 mm

Fig. 4.5. Macro and microphotographs of the Salmi basalts

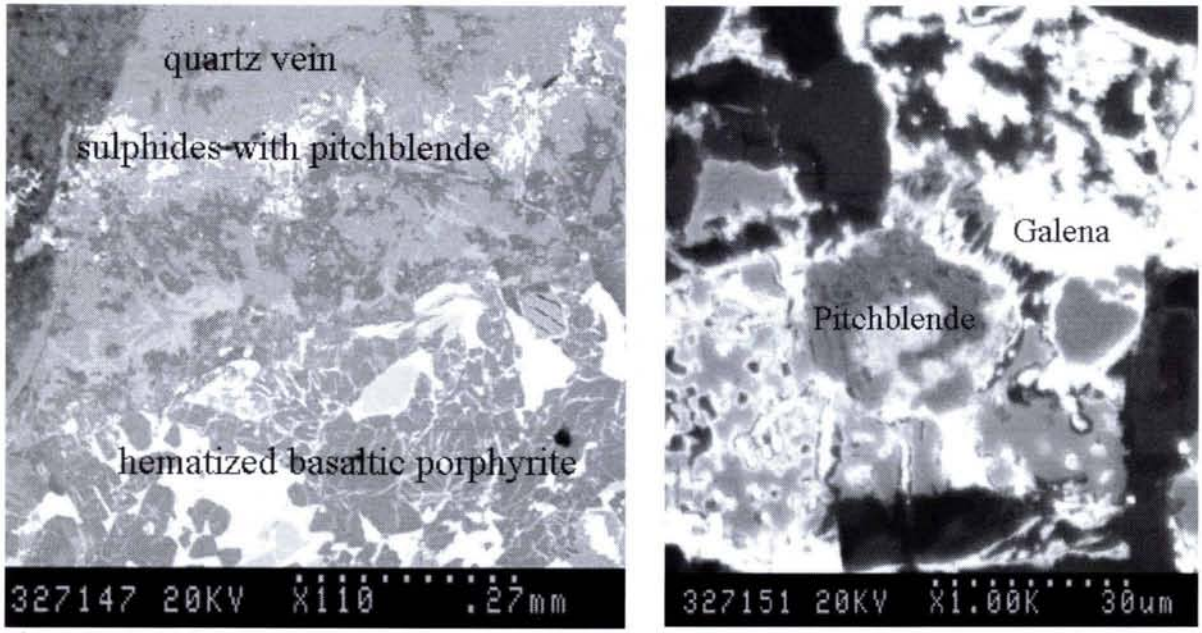

Fig. 4.6. BSEM images of a quartz-carbonate vein with sulphides and pitchblende in the Lower Salmi basalts (Karku deposit area, ore zone III, sample DDH-327-146 m), microphotograph scales: A – 27 mm, B – 30 μm

4.2.3. Petrogeochemistry of the Salmi basalts

Major and trace elements composition of Salmi basalts is listed in the Annex Volcanic. DDH and outcrops samples location is presented in Part 1.4.

Major elements distribution in the basalts

DDH, sample	Fresh Salmi basalts			
	356-310 m	356-441 m	625-50 m	822-66 m
SiO_2	45.26	46.44	46.28	46.77
TiO_2	4.38	3.53	3.79	3.89
Al_2O_3	13.03	13.23	13.86	14.18
Fe_2O_3	16.70	16.43	16.06	14.91
MnO	0.18	0.20	0.22	0.22
MgO	3.54	4.53	4.07	4.48
CaO	7.11	7.62	7.93	7.81
Na_2O	2.66	2.69	2.75	2.71
K_2O	**1.71**	**1.56**	**1.57**	**1.43**
P_2O_5	1.34	1.15	1.05	1.06
IL	2.73	1.18	2.42	2.84
Total	98.62	98.58	100.00	100.30

Table 4.2. Major element composition of the freshest Salmi basalts from the Salmi and Karku deposit areas

Major element compositions of selected fresh varieties of Salmi basalts are listed in table 4.2 and altered ones in table 4.3.

SiO_2 content of the fresh basalts varies from 45 to 47 wt. %. Alkali sum is between 4 – 4.5 wt. %. In the diagram SiO_2 versus $Na_2O + K_2O$, fresh basalts (PF < 4 wt. %) plot in the basalt field.

The fresh Salmi basalts are rich in potassium (1.4 – 1.7 wt. % of K_2O). Sample DDH-625-59 with K_2O contents of 4.88 wt. % corresponds to a strongly illitized sample, leading this sample to plot in the andesite field (Fig. 4.7).

	Altered Salmi basalts					
DDH, sample	625-55 m	625-57 m	625-109 m	822-76 m	822-122 m	822-125.5 m
SiO_2	43,86	45,80	40,27	21,68	30,96	44,50
TiO_2	12,69	7,79	13,20	6,41	1,84	8,68
Al_2O_3	9,62	17,00	16,59	4,19	4,42	10,64
Fe_2O_3	0,28	0,18	0,34	0,26	0,76	0,48
MnO	4,75	2,65	2,97	1,42	1,60	4,10
MgO	9,69	10,00	10,03	**33,72**	**32,90**	12,93
CaO	4,14	1,30	2,18	**1,52**	**0,08**	1,51
Na_2O	**0.49**	**2.20**	**0.47**	**1.25**	**0.06**	**1.03**
K_2O	**3,43**	**2,23**	**3,58**	**1,52**	**0,45**	**2,01**
P_2O_5	1,00	0,66	0,96	0,36	0,00	0,59
IL	**9.91**	**8.04**	**9.32**	**27.32**	**26.70**	**13.46**
Total	99,86	97,85	99,91	99,65	99,77	99,93

Table 4.3. Major element composition of the altered Salmi basalts from the Salmi and Karku deposit areas

At the contrary, sample DDH-389-78 (a relatively fresh basalts, with IL = 3.4 wt. %) has an alkali sum higher than 7 wt. %, including 5 wt.% Na_2O. This sample plot into the tephrite field. Such a composition corresponds to an albitization process in the basalt.

Moderately altered basalts (IL < 8) also range from substantially low-potassic varieties (822 – 122 with K_2O < 1 wt. %) to highly potassic ones 625-59 with K_2O – 4.9 wt. % (Annex volcanic) according to their degree of illitization. In Fig. 4.7, all altered basalts varieties plot into the low-silica field. I.L. value for the strongly altered basalts reach up 27 wt. % and correspond to the development of carbonates including possible magnesite.

Basaltic cobbles from the Valaam island (Ramo data, pers. communication) are characterized by their very high alkali sum (high contents of both - sodium and potassium) and plot in the diagram (Fig. 4.7) into the tephriphonolite field. They are very fresh, their I.L. values does not exceed 1.1 wt.%. Therefore they may not correspond to the same flows as those intersected in the drillings from the Karku area.

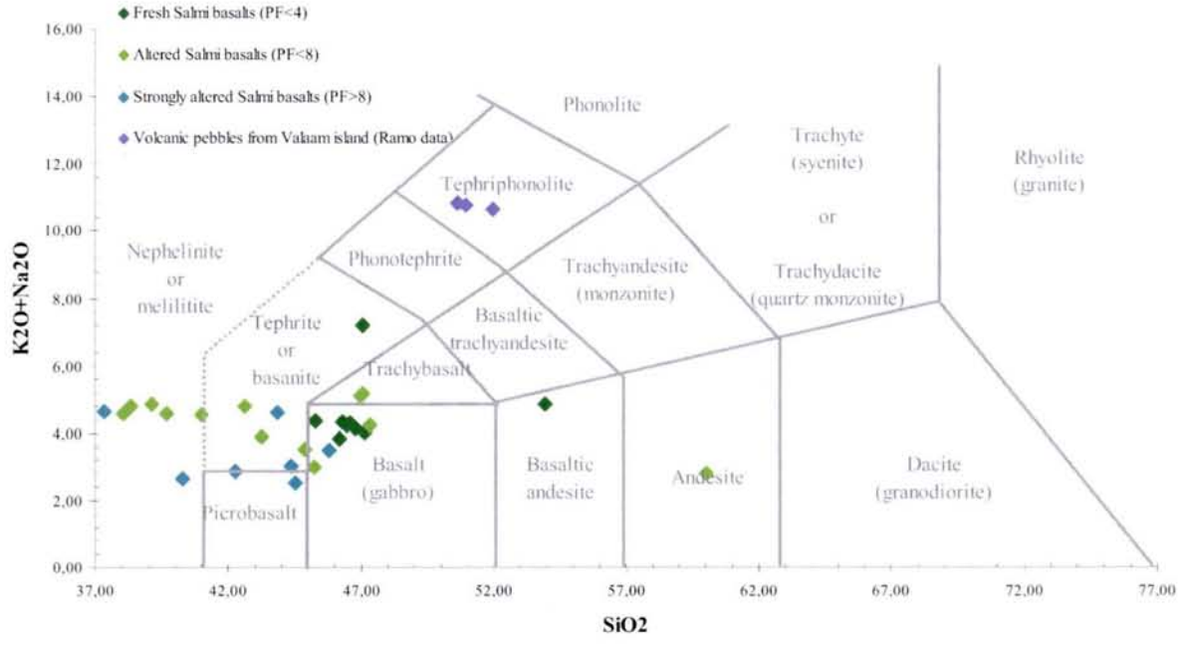

Fig. 4.7. The Salmi basalts in the SiO_2 vs. $K_2O + Na_2O$ classification diagram

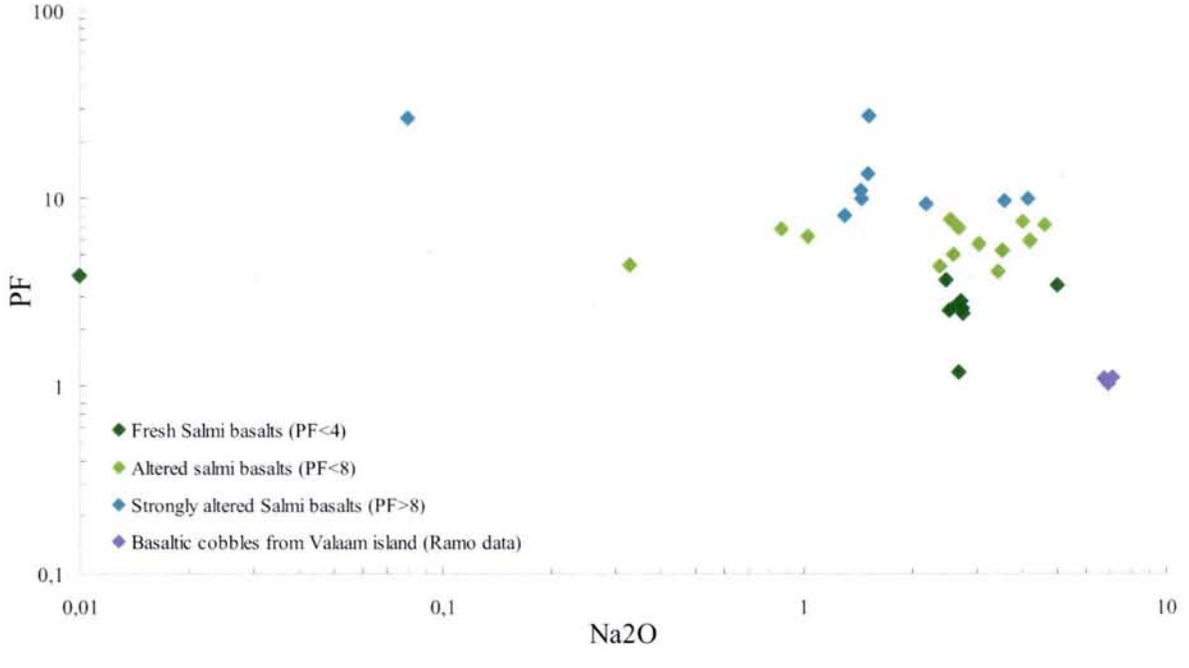

Fig. 4.8. The Salmi basalts in the diagram Na_2O versus PF (loss on ignition)

Among the 34 analysed samples at least seven samples are extremely altered. Ignition Loss (I.L.) varies from 9 to 27 wt. % and hence inhibits the use of many of the standard major

elements plots. In the diagram Na_2O versus PF (loss on ignition) increasing sodium leaching is clearly evidenced with increasing alteration.

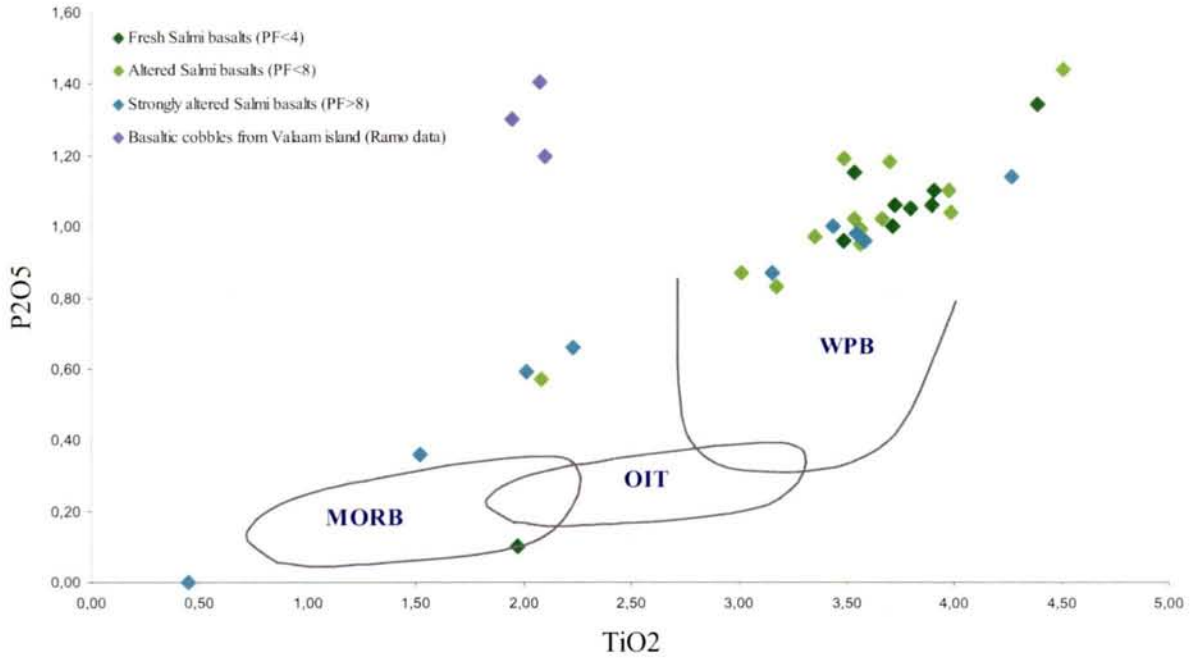

Fig. 4.9. The Salmi basalts in the TiO_2 vs P_2O_5 diagram. Petrotectonic fields of MORB, OIT and WPB are based on Bass et al (1973). Only the freshest basalts have been with IL < 4 wt% or less

The diagram based on TiO_2 and P_2O_5 content, which appear reliable for altered rocks (Volkova & Budanov, 1999), can be used for preliminary discrimination of the investigated basalts. TiO_2 content in the Salmi basalts varies from 3.7 – 4.4 wt. % in fresh varieties and to 2 - 0.5 wt. % in strongly altered basalts. P_2O_5 content is between 1 – 1.3 wt. % in the fresh varieties and less than 1 wt. % in the altered ones. (Fig. 4.9). The fresh Salmi basalts characterized by high TiO_2 and P_2O_5 contents belong to the alkali basalt composition trend, which fall into within-plate basalt field. The basalts cobbles of the Valaam island are also clearly distinguished in this diagram by their high phosphorous contents for intermediate TiO2 values.

In the Q-P diagram of Debon – Le Fort (1983, 1988) different alteration trends can be observed (Fig. 4.10). Fresh Salmi basalts plot near the monzogabbro reference composition, except one point (DDH-389-78), which is extremely sodium-depleted, despite its relatively low I.L. (3.42 wt. %) value. Samples plotting to the right of the monzogabbro reference

composition correspond to samples in which sodium has been leached out and to illitization which correspond to a gain of potassium during alteration, both acting in the same way on the K-(Na + Ca) millication parameter. Samples plotting to the left part of the diagram correspond to samples with albitization (rare) and mainly to carbonate alteration which may led for the Ca-richest ones to their plotting silica undersaturated field (Ca is substracted to silica in the calculation of the Q parameter). However, the fresh basalt cobbles from the Valaam island plot in the silica undersaturated field.

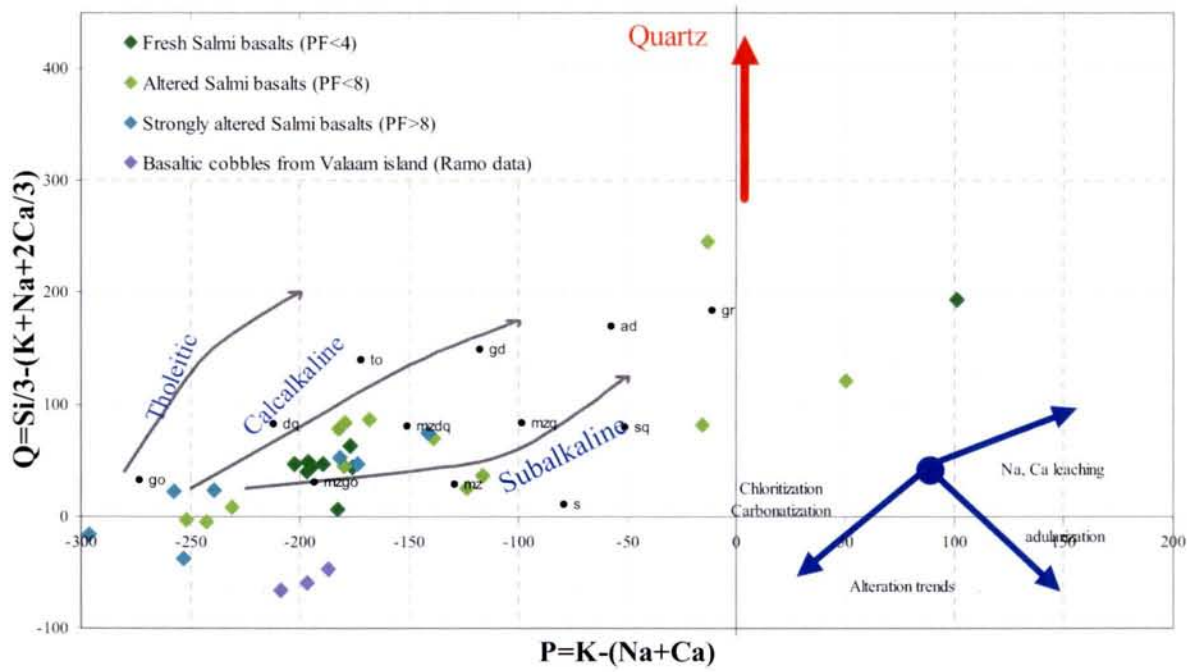

Fig. 4.10. The Salmi basalts in the A vs. Q diagram according to Debon and Le Fort (1983, 1988)

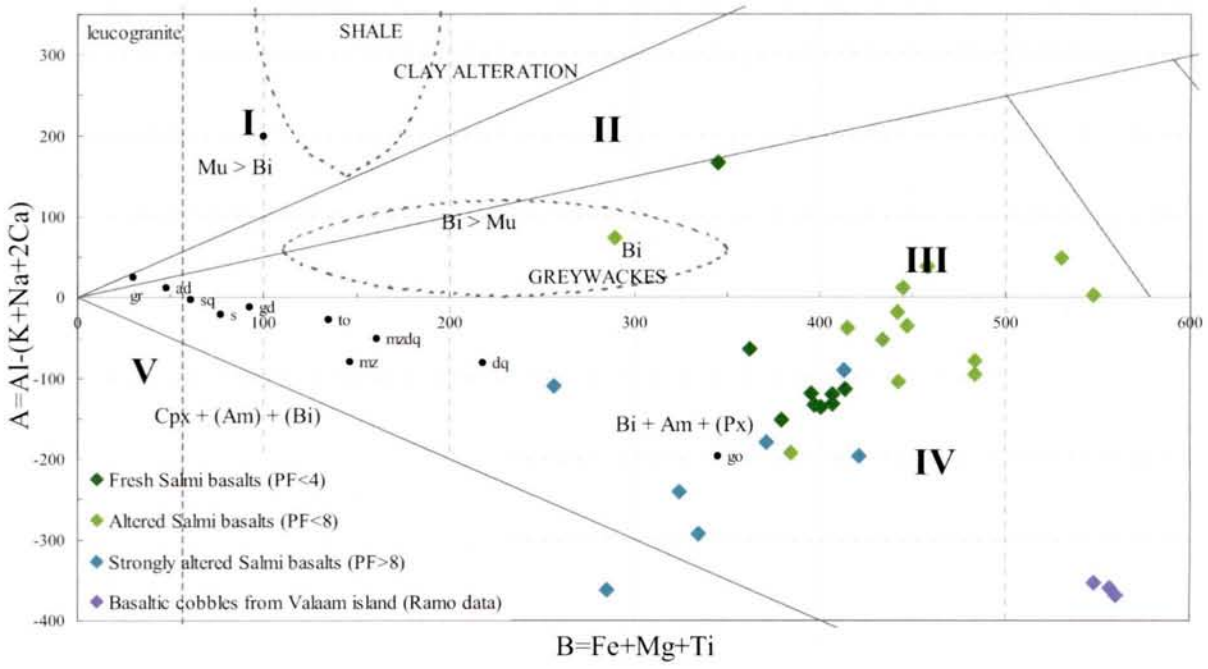

Fig. 4.11. The Salmi basalts in the B vs. A diagram according to Debon and Le Fort (1983, 1988)

The A-B diagram (Fig. 4.11) shows that the freshest basalts (CaO content between 7 – 8 wt. % and lowest IL values) are slightly shifted from the average gabbro composition which means that limited clay alteration occurs in these basalts. Some of the Salmi basalts are dominated by the clay alteration (samples with slightly negative to positive peraluminosity A parameter) with Fe (up to 21 wt. % Fe2O3) and Mg (up to 9 wt. % MgO) enrichment (increasing B parameter with increasing A values), whereas some others are dominated by the carbonate alteration (CaO content up to 34 wt. %) with the most negative A values and I.L. values higher than 8 wt. % because of the CO2 of carbonates.

The basaltic cobbles from Valaam island are characterized by strongly different chemical composition with very high sodium (6 – 7 wt % Na2O) and magnesium (12 to 13 wt % MgO) contents.

Trace elements distribution in the basalts

Because the degree of alteration of some of these rocks is significant, the abundances of all mobile elements are likely to have been strongly modified. Therefore, there is a need to

use for interpretation only the more immobile elements (REE, P, Ti, Zr, Y, Nb, Th), whose abundances in basalts are not to much affected by alteration.

Trace element compositions of the Salmi basalts have been represented in chondrite-normalized spidergram (Fig. 4.12).

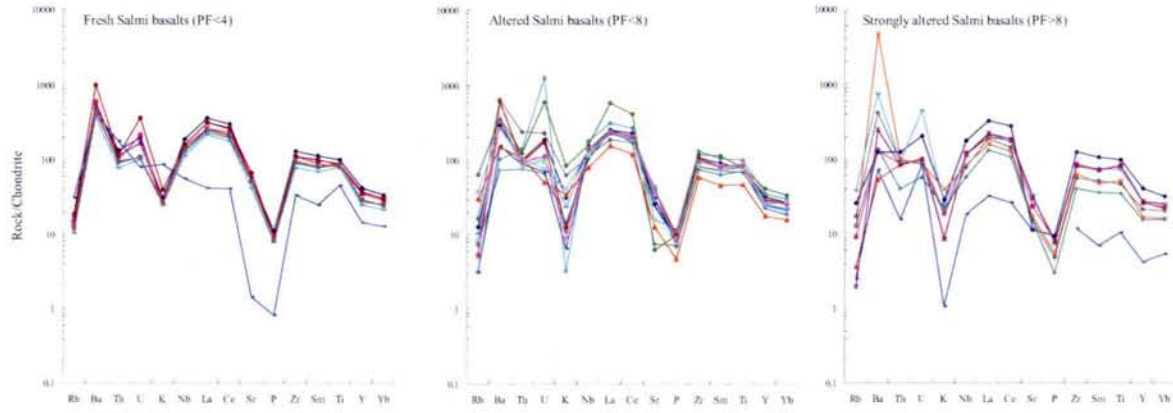

Fig. 4.12. Chondrite-normalized trace element patterns of the Salmi basalts from the Salmi - Karku deposit areas (Northern Ladoga district) (spidergram type after Holm (1979); chondrite composition after E. Anders and N. Grevesse: http://earthref.org/GERM/reservoirs/C1.htm)
The Salmi basalts are plotted into the three spidergrams: fresh (PF<4), altered (PF<8) and strongly altered (PF>8)

In the Fig. 4.12. the Salmi basalts are compared according to their degree of alteration. Some following features have been observed:

(i) fresh varieties present very homogeneous spidergram patterns (except one anomal sample 625-59, which are strongly enriched in K_2O and depleted in Na_2O and P_2O_5);

(ii) strongly altered basalts which are not only occurring in the mineralized zones of the Karku deposit, present more scattered distribution of the elements in the spidergrams compared to the fresh one;

(iii) they are clearly depleted in Rb, Sr and K_2O;

(iv) altered basalts are also relatively enriched in Ba, U, La, Ce.

For a better understanding of the trace elements and REE distribution with depth and alteration degree the geochemical data have been also examined according to the depth position of the samples along the drill holes and normalized with average fresh "Salmi basalt"

(Fig. 4.13). The average fresh "Salmi basalt" was calculated from samples 356-410, 356-440, 502-232, 389-78, 625-50, 625-85, 822-66 and 822-106 (Table 4.4) for normalization:

ppm	Rb	Ba	Th	U	K, %	Nb	Sr	Zr	Ti, %	Y
basalt	33	1266	3	1.4	1.6	36	417	405	4	51

Table 4.4. Trace element values calculated for Average fresh "Salmi basalt" sample

In *DDH-502* (Salmi area – 15 km to NW from the Karku deposit) (Fig. 4.13) trace elements distribution" varies significantly with depth, but mostly in relation with the occurrence of fracture zones in the basalts. Surprisingly, the degree of alteration decrease with depth. Rb, Ba, K and Sr are depleted except in the middle of the section. Other elements do not show strong variations. U is significantly enriched in nearly all the samples despite the location of this drilling away from a mineralized area. U enrichment also decreases from the top (10 ppm) to the bottom (1.4 ppm) of the section in correlation with the decrease of the degree of alteration of the samples. Within a fractured zone U content reaches 4.8 ppm. The weak alteration of the basalts in the lower part of the section is in favour of weak diagenetic and/or hydrothermal fluid circulations in the sandstone in this part of the Salmi area.

In *DDH – 625* (Karku deposit area, ore zone III) all samples present important depletion in most elements but with no significant variation in the trace element distribution with depth except in two cases: at -57 meters strong Ba and K_2O enrichments are observed and at -59 meters Rb, Th and K_2O are significantly enriched with the strongest Sr depletion. No uranium enrichment is noticed in the basalts despite the location of this drilling in a mineralized area (ore zone III).

In *DDH-822* (Karku deposit area but outside of an ore zone), Rb, Ba and K enrichments occur at different depth in relation with the degree of illitization of the samples. (Fig. 4.13). However, the sample located at -122 meters is strongly depleted in all elements, indicating a strong alteration. But, above (at -106m) the basalt is nearly non depleted. U content at the top of the sequence is enriched to 2 ppm, then it is moderately depleted with depth, excepted at -125 meters where U is enriched to 4 ppm, but immediately below at - 125.5 meters, U is down to 0.7 ppm. K depletion is also a characteristic feature of this part of the section.

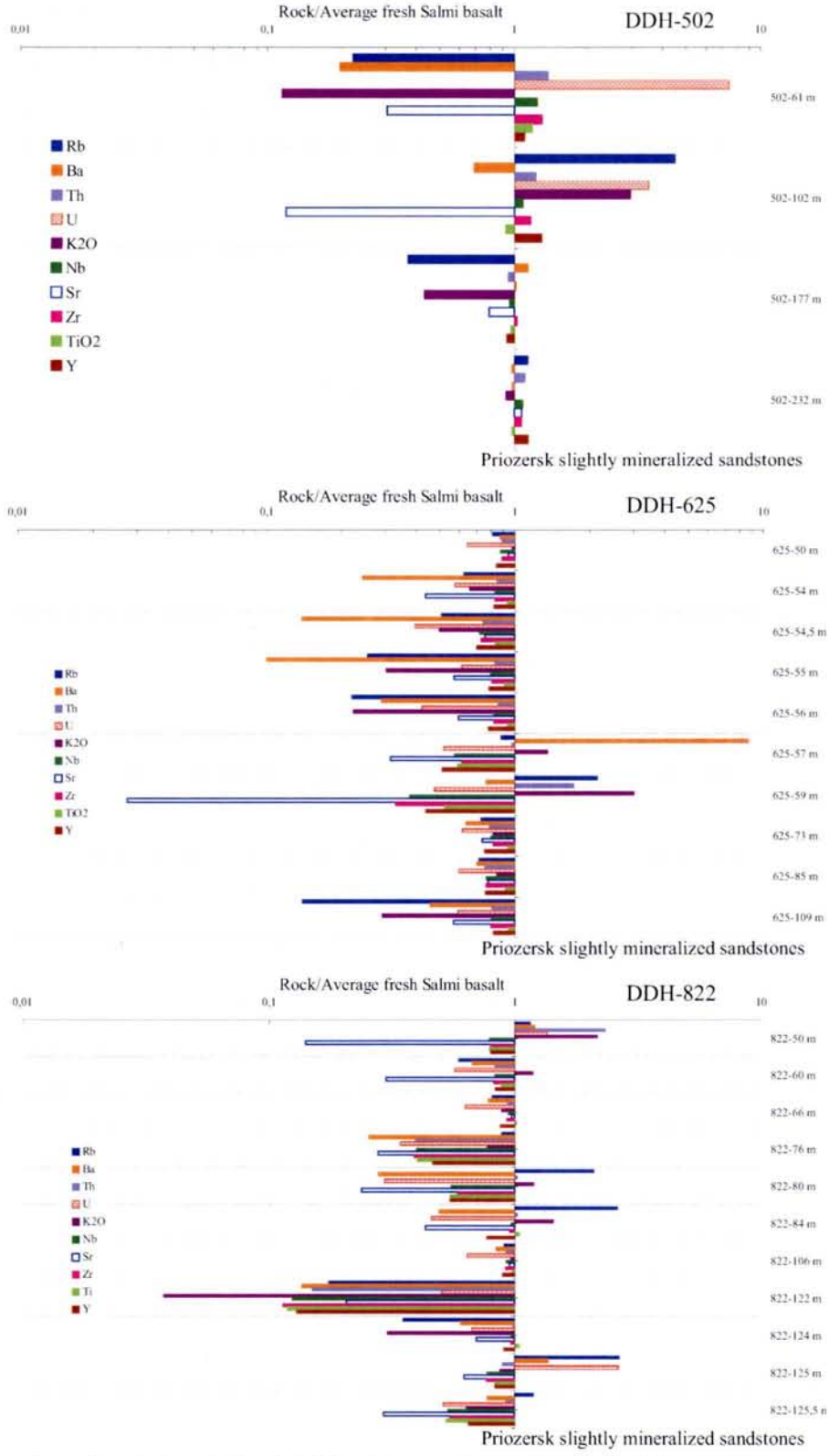

Fig. 4.13. Trace element variations in the Salmi basalts according to the depth of the samples

In general, enrichment or depletion of any of the trace elements is not dependent of its distance to the unconformity surface and mostly depend on the presence of specific tectonic features (fault, fracture) allowing the more or less important development of the alteration.

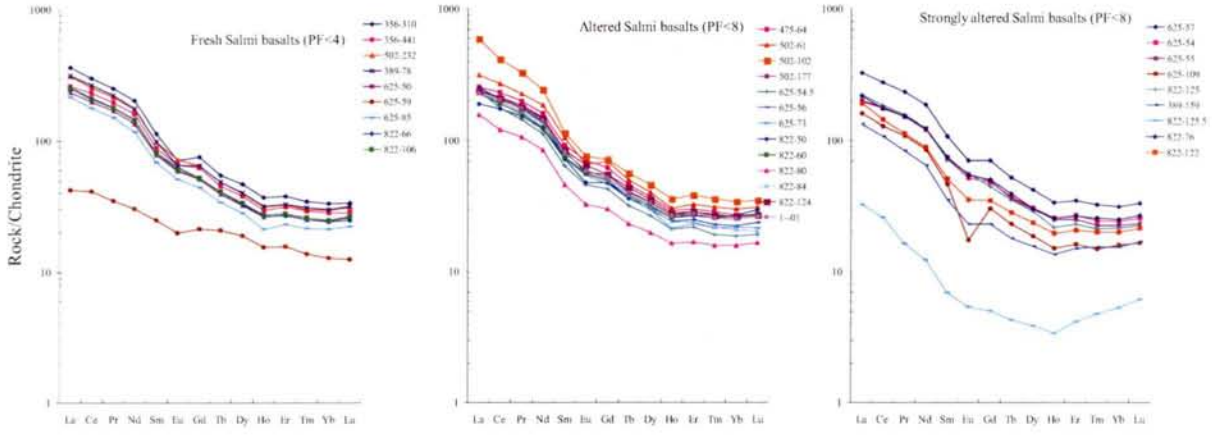

Fig. 4.14. Chondrite-normalized REE patterns of the Salmi basalts from the Karku deposit areas (Northern Ladoga) (chondrite composition after Anders & Grevesse: http://earthref.org/GERM/reservoirs/C1.htm)
Salmi basalts are plotted into the three spidergrams: fresh (PF<4), altered (PF<8) and strongly altered (PF>8)

Salmi basalts are strongly enriched in REE: ΣREE in the fresh varieties (PF<4) is about 313 ppm, and is similar (318 ppm) in moderately altered ones (PF<8). But, strongly altered basalts (PF>8) are depleted in REE (230 ppm in average). They have similar strongly fractionated REE patterns (Ce_N/Yb_N ratio ranging from 8 for fresh basalts, 8.6 for altered, 7.4 for strongly altered) with a weak europium anomaly ($(Eu/Eu^*)_N$ = 0.89 in the fresh and altered basalts, 0.83 in the strongly altered ones). Alteration has mainly an influence on the global REE abundance without strong variation of the global fractionation (Fig. 4.14). Two samples (one non altered : 625-59 and one altered : 822-125.5) show distinctly lower REE abundances with different fractionation of their REE patterns. They probably initially correspond to distinct basalt varieties which would be interesting to characterize more thoroughly.

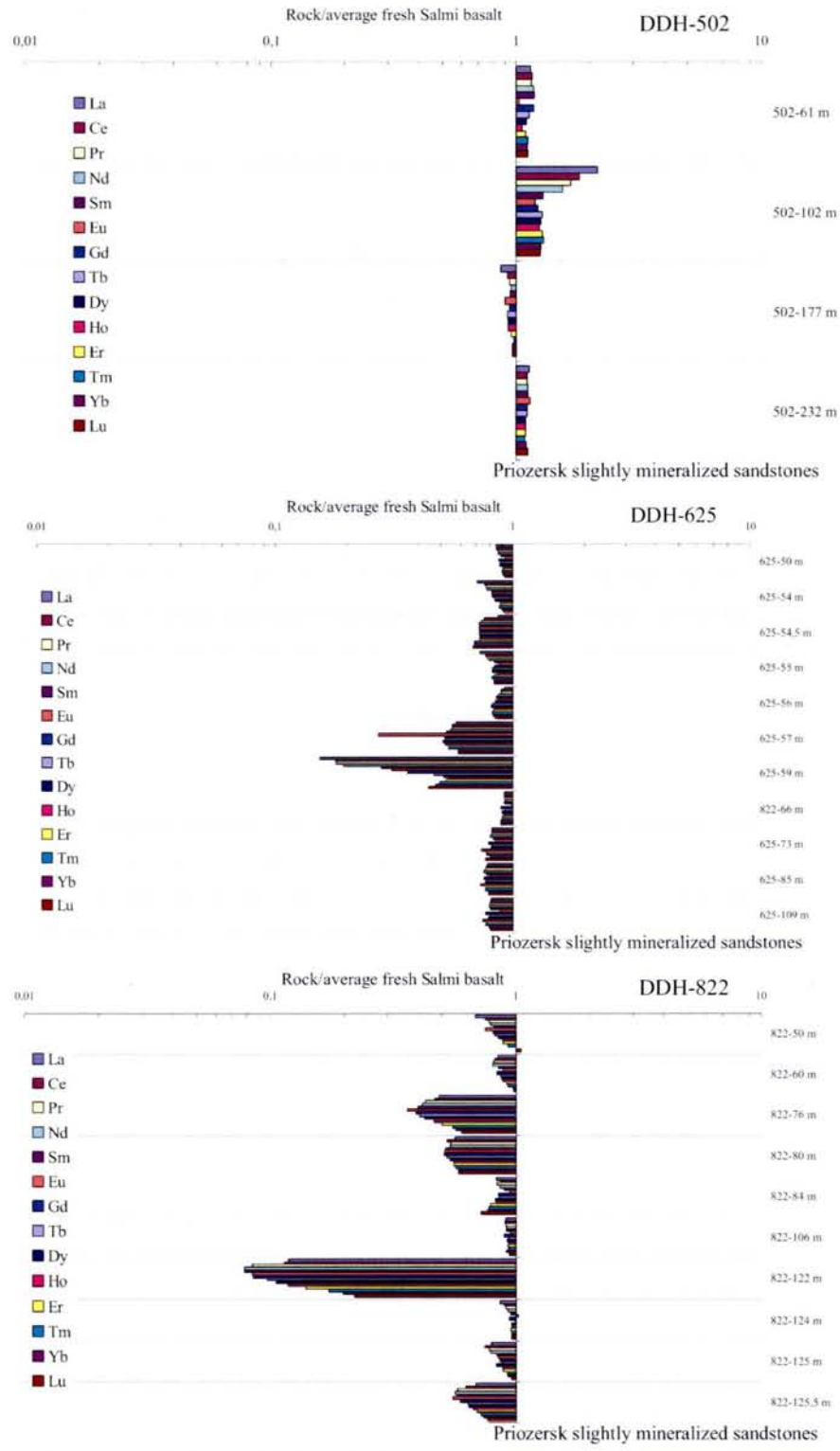

Fig. 4.15. REE distribution in the Salmi basalts in concerning to the DDH position and depth of the samples

An average of the fresh "Salmi basalt" was calculated from samples 356-410, 356-440, 502-232, 389-78, 625-50, 625-85, 822-66 and 822-106 (Table 4.5) for REE normalization:

ppm	La	Ce	Pr	Nd	Sm	Eu	Gd	Tb	Dy	Ho	Er	Tm	Yb	Lu
basalt	65	139	17	71	13	4	12	2	9	2	5	1	4	1

Table 4.5. REE values calculated for Average fresh "Salmi basalt" sample

In *DDH-502* (northern part of the Salmi area – see position in Fig. 1.23) REE distribution varies very slightly (Fig. 4.15), except at -102 meters where a moderate LREE enrichment is observed (La = 140 ppm, Ce = 250 ppm).

In *DDH – 625* (Karku deposit area, ore zone III) there are also no any significant variation in the REE distribution except two samples: at -57 meters a strong Eu and a moderate LREE depletion are observed and at -59 meters strong LREE and moderate HREE depletions are observed.

In *DDH-822* (Karku deposit area – outside of the ore zones) moderate depletion of all REE (mostly LREE) are observed in the interval -76 to - 80 meters and below a strong depletion of all REE is observed in on sample at -122m (Σ REE = 40 ppm).

Part 4.3. Valaam sill

4.3.1. Petrography and mineralogy of the Valaam sill rocks

The ~1460 Ma Valaam sill (Ramo et al., 2001) is intruded along the bedding surface of the Pasha Suite. The lower part of the Valaam differentiated sill is composed mainly of gabbro to monzonite rocks (in the east – Lunkkulunsaari (Fig. 4.16) and Mantsinsaari islands) and the upper part consist of monzonite to quartz syenite (in the west – Valaam and Verkonsaari islands).

Fig. 4.16. Lunkkulunsaari Island shore. Mafic intrusive rocks of the Valaam sill.

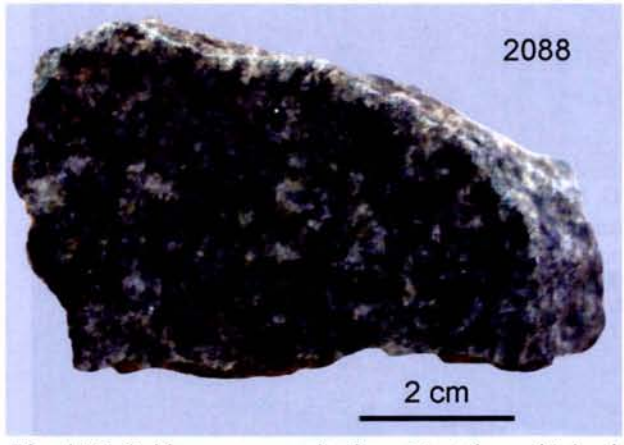

Fig. 4.17. Gabbro – monzonite from Mantsinsaari Island (Sample 2088, Mikhailov collection, VSEGEI, 2003)

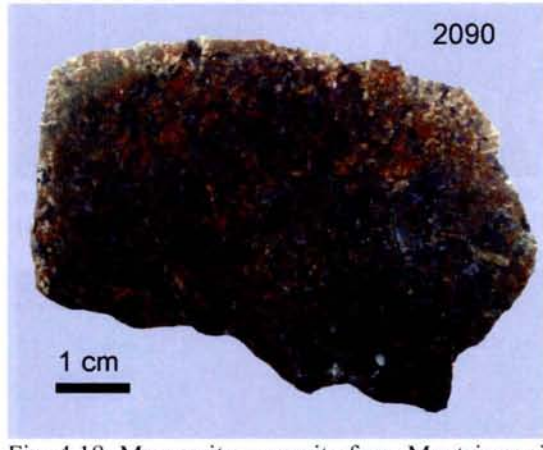

Fig. 4.18. Monzonite – syenite from Mantsinsaari Island (sample 2090, Mikhailov collection, VSEGEI, 2003)

The main rock-forming minerals of the gabbro and gabbro - monzonite rocks from Lunkkulunsaari and Mantsinsaari islands are *clinopyroxene* (diopside – augite), *plagioclase* (oligoclase – andesine) (Fig. 4.17). *Ti amphibole*, biotite, K – Na feldspar (orthoclase – albite) are also very common. Quartz (idiomorphic grains) appears at the final stages of crystallization. Ilmenite, titanomagnetite and apatite are also present (Fig. 4.19 a, c, e).

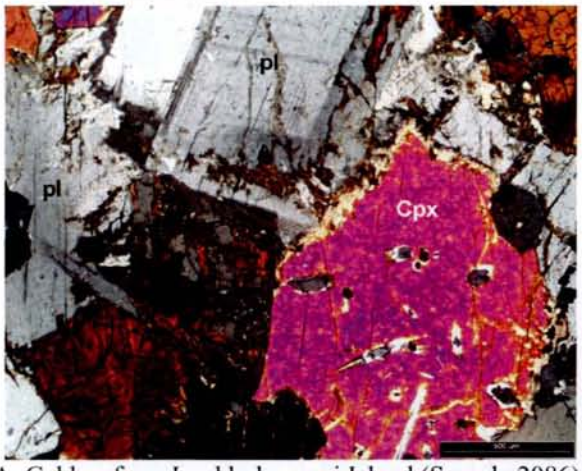

A. Gabbro from Lunkkulunsaari Island (Sample 2086) Crossed nicols, line scale – 0.5 mm

B. Quartz – orthoclase intergrowths in and between plagioclase (sample 2085). Crossed nicols, line scale – 0.5 mm.

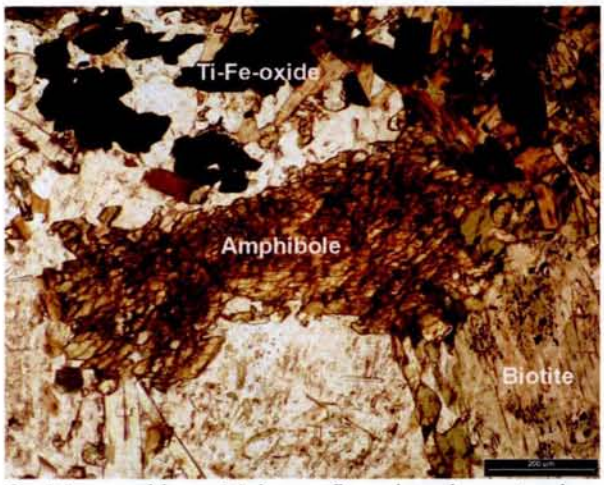

C. Monzogabbro. Main mafic minerals: potassium amphibole, biotite with Fe-Ti-oxides (sample 2088) Parallel nicols, line scale – 0.2 mm.

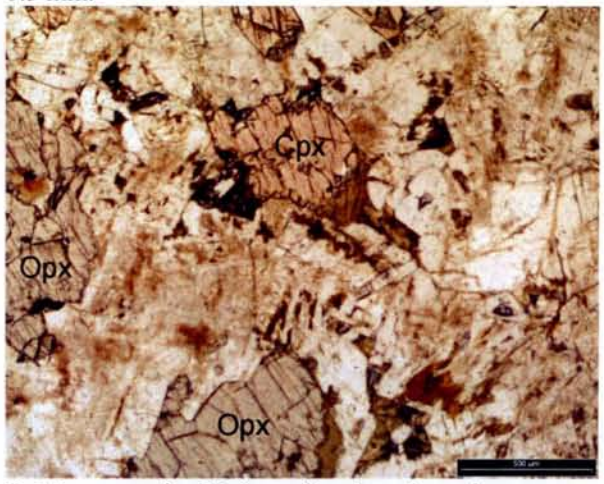

D. Monzosyenite. Main mafic minerals: orthopyroxene and clinopyroxene (sample 2090). Parallel nicols, line scale – 0.5 mm.

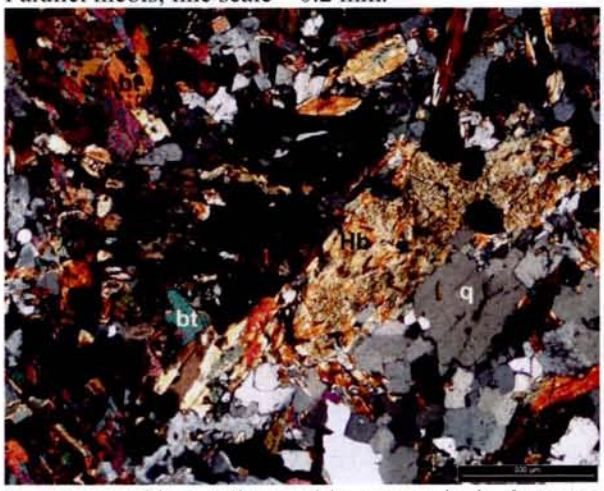

E. Monzogabbro. Idiomorphic quartz is in between hypidiomorphic grains of amphibole and biotite (sample 2088). Crossed nicols, line scale 0.5 mm.

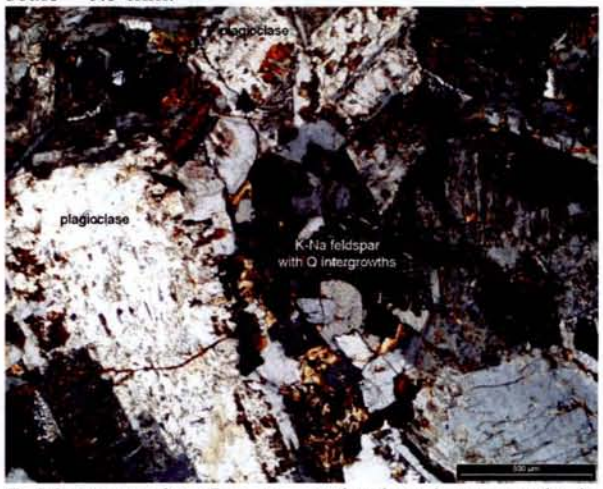

F. Monzosyenite. Quartz – orthoclase intergrowths in plagioclase matrix (sample 2090). Parallel nicols, line scale – 0.5 mm.

Fig. 4.19. Microphotography of the Valaam sill gabbros, gabbro – monzonites and monzosyenites

The mineral assemblage, which make up the intermediate potassium-rich rocks from Mantsinsaari and Valaam islands (syenites – monzosyenites) includes ferriferous orthopyroxene, clinopyroxene, biotite, Ti-amphibole, plagioclase (oligoclase), K – Na feldspar (albite – orthoclase). Quartz – orthoclase intergrowths appear in plagioclase as symplectites. Myrmekitic and symplectitic textures are common, typical of subvolcanic rocks. Granosyenites and potassium granites are the final members of the differentiation and consist of K – Na feldspar (albite and orthoclase) with accessory ilmenite and titanomagnetite (Fig. 4.18, 4.19. b, d, f).

4.3.2. Petrogeochemistry of the Valaam sill rocks

Major and trace elements data of 2 samples are listed in Annex gabbro (present work data). The major element compositions of the Valaam complex rocks are listed in Table 4.6. DDH and outcrops samples location is presented in Part 1.4.

In general the alteration degree of the Valaam sill rocks is very week with I.L. values from 0.50 to 2.91 wt%. The Valaam sill presents an extremely wide range of compositions from gabbros to granites. In the SiO_2 vs. (Na_2O + K_2O) diagram, SiO_2 contents vary from 44.24 up to 48.16 wt. % in the gabbros, from 50.79 to 51.99 wt. % in the monzogabbros, from 57.10 to 64.59 wt. % in the monzonites and quartz monzonites, from 72.83 to 75.85 wt. % in the syenites and potassium granites (Fig. 4.20).

	1	2	3	4	5	6	7	8	9	10	11	12	13	14	15	16
Sample	R4	R5	R6	A12	A13	A20	02-01	A14	A21	A22	A23	A15	A16	11-03	A17	A24
SiO2	44.24	47.31	47.71	48.16	50.79	50.88	51.99	57.10	58.43	61.26	64.59	68.94	72.83	72.4	74.28	75.85
TiO2	1.70	1.56	2.18	3.20	2.76	3.41	2.71	1.70	1.76	1.34	1.27	0.35	0.26	0.29	0.18	0.19
Al2O3	4.65	3.79	4.54	13.70	13.80	13.12	14.14	14.71	13,9	13.90	14.69	12.50	11.49	11.98	12.00	11.57
Fe2O3	13.52	13.53	13.60	14.02	13.85	13.59	13.23	10.69	9.98	9.40	5.79	3.55	2.86	3.55	2.53	2.24
MnO	0.19	0.23	0.10	0.24	0.20	0.20	0.19	0.17	0.15	0.12	0.12	0.04	0.02	0.00	0.07	0.00
MgO	16.55	16.02	16.51	4.12	3.54	3.52	2.76	2.26	2.43	2.61	0.97	1.84	0.86	0.61	0.68	0.59
CaO	4.34	4.34	3.34	7.86	6.94	7.11	6.03	3.74	3.71	1.92	1.59	2.45	1.17	0.81	0.62	0.19
Na2O	5.84	7.91	3.52	3.33	3.38	3.18	3.44	4.29	3.93	3.53	4.01	2.22	2.12	2.43	3.40	2.44
K2O	4.20	2.80	4.02	1.85	2.15	1.92	2.28	2.87	3.48	3.68	5.52	6.86	7.17	5.77	5.70	6.42
P2O5	1.44	1.21	1.43	1.88	1.32	1.52	0.97	0.75	0.53	0.29	0.29	0.97	0.16	0.06	0.06	0.00
PF	2.75	1.00	2.47	2.91	2.49	1.76	1.85	2.71	1.79	1.98	1.47	1.56	1.44	1.41	1.28	0.57
Total	99.43	99.70	99.42	101.27	101.22	100.21	99.59	100.99	100.09	100.03	100.31	101.28	100.38	99.31	100.80	100.06
n					15			2				2	3			

Table 4.6. Major elements composition of the Valaam complex rocks
Sample prefix: R –Tapani Ramo data, A - Alexei Amantov data (1991), n - average on a number of samples is listed
Valaam sill rocks: 1 – 7 = gabbros and monzogabbros; 8 – 10 = monzonites; 11- 12 = monzosyenites; 13 – 16 = syenogranites and potassium granites.

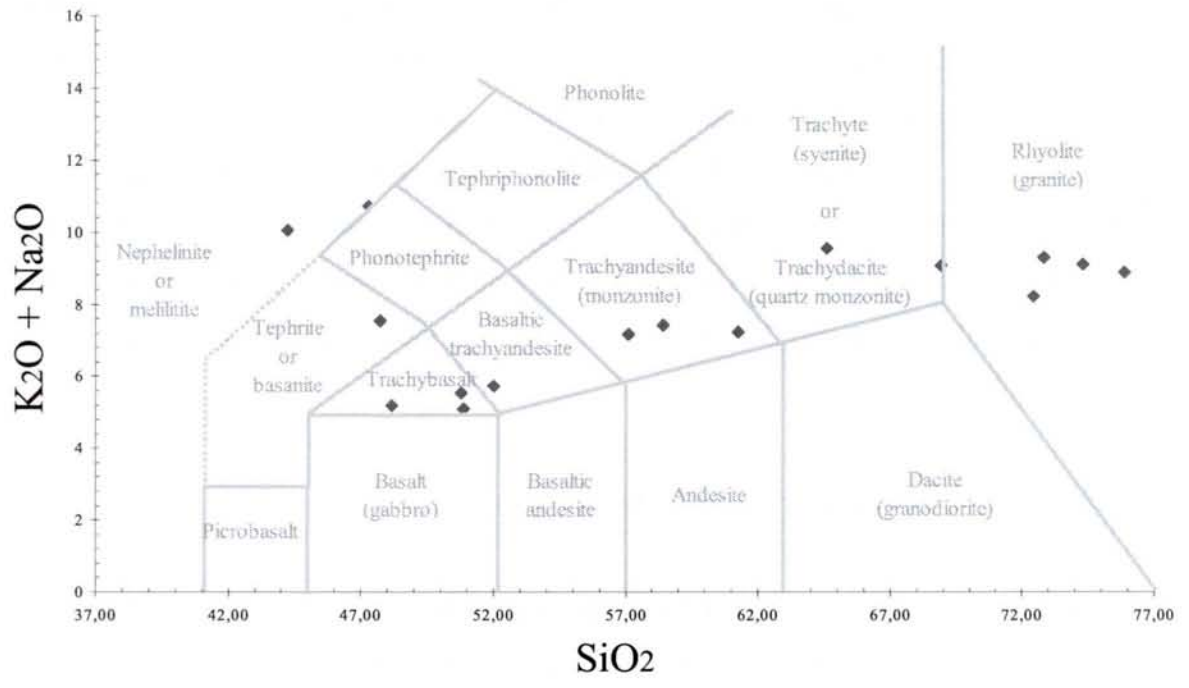

Fig. 4.20. The Valaam complex rocks in the SiO_2 vs. $K_2O + Na_2O$ diagram

TiO_2 content vary from 1.56 to 3.41 wt. % in the gabbros, from 1.70 to 1.27 wt. % in the monzonites, from 0.35 to 0.18 wt. % in the syenites and potassium granites. Maximum MgO content is 16.55 wt. % in the olivine gabbro.

On the spidergram normalized to primitive mantle (Fig. 4.21) the Valaam gabbro (sample 2-01 – green line) is characterized by strong enrichment in Ba (1800 ppm). K_2O (2.3 wt. %) and La (55 ppm), Ce (115 ppm), Rb (40 ppm), P_2O_5 (1 wt. %), and U (0.9 ppm). All these elements are enriched about 70 times with respect to the primitive mantle. Other immobile elements are enriched to a lesser extend (Th = 3 ppm, 40 times; Nb = 20 ppm, 30 times; Zr = 240 ppm and Sr = 490 ppm, 25 times and Y = 40 ppm, 9 times).

The syenite (sample 11-03 – orange line) is relatively enriched in a series of incompatible elements Rb (136 ppm), Th (12.6 ppm), U (2.5 ppm), K_2O (5.8 wt. %), Zr (900 ppm), La (85 ppm), Ce (165 ppm), Yb (52 ppm), typical of high-K calcalkaline granites, but strongly depleted in Nb, Sr, P and Ti indicating titanomagnetite (Nb, Ti), plagioclase (Sr) and apatite (P) fractionation.

The chondrite-normalized REE pattern (Fig. 4.22) of the Valaam gabbro is fractionated (Ce_N/Yb_N ratio = 9.6), with a weak Eu anomaly ($(Eu/Eu^*)_N$ = 1.23) and similar to the average

LREE pattern of the Salmi basalts. The syenite (11-03) present the same global fractionation of its REE pattern (Ce_N/Yb_N = 8.7), but LREE are more fractionated, the Eu anomaly ($(Eu/Eu^*)_N$ = 0.30) is more important, but HREE fractionation is weaker.

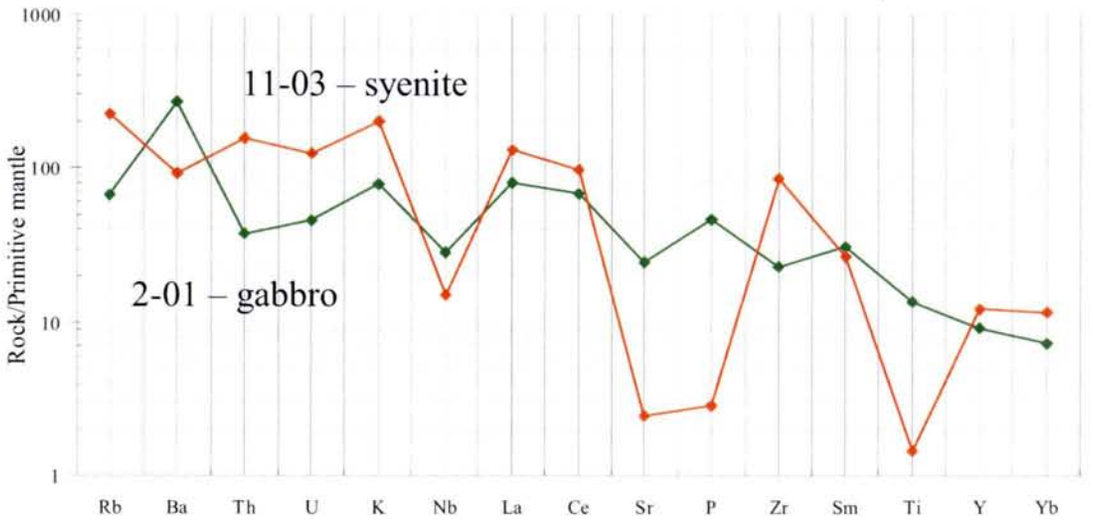

Fig. 4.21. Primitive mantle normalized trace element patterns of the Valaam sill rocks (spidergram type after Holm (1979); primitive mantle composition after Wood et al (1980)

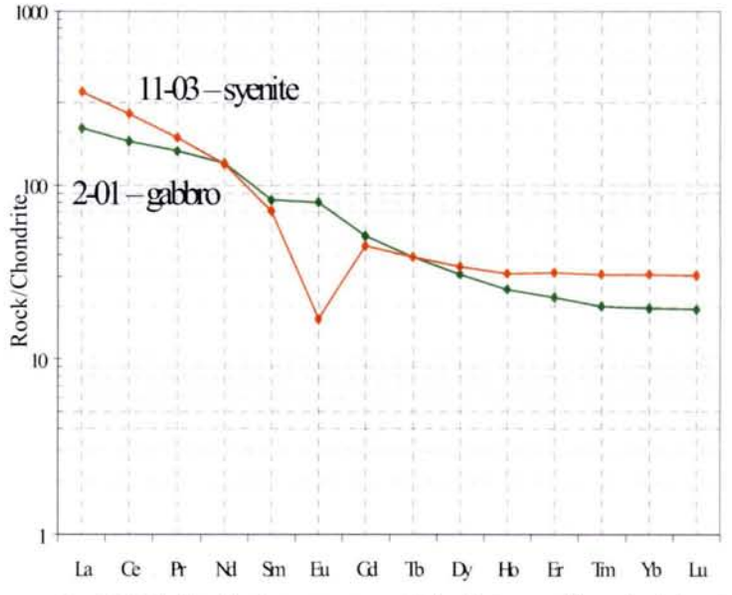

Fig. 4.22. Chondrite-normalized REE distribution patterns of the Valaam sill rocks (chondrite composition after Supplemental data for chondrite (Anders & Grevesse: http://earthref.org/GERM/reservoirs/C1.htm)

Conclusions of Chapter IV

Basaltic magmatism synchronous with the sedimentation is an important characteristic of the Pasha – Ladoga basin. Basaltic magmatism is also present in the Kombolgie basin, represented by the Nungbulgarri volcanics, but the thickness of the deposited sandstone before the basalt emissions is larger. The Salmi intercalated basalts correspond to continental flood basalts type (CFB) of magmatism, but have alkali basalt signature with stronger enrichment in LREE, Th and U, than the typical representatives of this type of magmatism.

The an other episode of basic magmatism occur at least after the deposition of the first clastic sequences preserved in the Pasha Ladoga rift, which is represented by the widely differentiated (potassium-rich gabbro and monzonites in the west up to monzonite and quartz syenites in the east characterized by relative enrichment in LREE, Th and U) Valaam sill (at ca. 1.46 Ga). Basic magmatism occurring at the end of the sedimentation also occur in the Kombolgie basin and is represented by the Oenpelli dolerite sill, but which is essentially basaltic in composition. In the Finnish part of the Fennoscandian Shield basic magmatism occur but as dykes and sill and is much younger (1265 to 1000 Ma) as in the Athabasca basin with the McKenzie dykes at 1260 Ma.

Because of their percolation by the diagenetic and hydrothermal fluids the Salmi basalts underwent strong alteration, mostly characterized by a strong Fe-chlorite development, and redistribution of trace elements. Such an alteration in mostly relation with the occurrence fracture zones in the basalts. Strong alteration of the basalts has been also observed in the Salmi area at the distance more than 10 km to north from the main U mineralization zone of the Karku deposit. This observation represents an interesting indication for the possible development of mineralized processes in that area.

Chapter V

Comparative analysis of the different world Mesoproterozoic sedimentary basins: Athabasca (Canada), Kombolgie (Pine Creek, Australia) and Pasha – Ladoga (Russia)

Interpretation of the results and discussion

Chapter V. Interpretation of the results and general discussion

In this chapter I will interpret the obtained results concerning to the Pasha – Ladoga basin area and compare with the well-known unconformity-type uranium deposits of the Athabasca Uranium Province (Canada) and East Alligator River Uranium Province (Australia).

Part 5.1. Reconstruction of the petrogenetic evolution the basement

5.1.1. Tectonic framework

The Pasha – Ladoga basin is entirely located in the Ladoga mobile zone which represents a part of the larger Raakhe – Ladoga zone (Fig. 1.7). The development of the Ladoga mobile zone takes place in two main stages:

(i) At the beginning of the Paleoproterozoic, two major faults (Ruskeala and Priozersk) control the formation of a rift structure, which have been filled by the Paleoproterozoic metavolcanic and metasedimentary rocks. Then, these Paleoproterozoic rocks have been subjected to high temperature regional metamorphism reaching anatexis and was accompanied by the emplacement of basic plutonic rocks and several generations of potassic, U and Th rich granites mainly in the Western part of the area.

(ii) The Mesoproterozoic begins with the anorogenic emplacement of the huge rapakivi granite batholiths (Vyborg and Salmi) along the main tectonic faults of the Ladoga Lake region, between 1.67 and 1.62 for the Vyborg batholith and then between 1.55 and 1.53 Ga for the Salmi complex, i.e. about 150 Ma after the cessation of the Svecofennian orogeny. After a period of erosion, the Paleoproterozoic rift system was reactivated to lead to the deposition of the Pasha – Ladoga basin Riphean clastic sediments. An important characteristic of the Pasha – Ladoga basin formation is the occurrence of eruptive basaltic magmatism synchronous with the sedimentation of the lower sedimentary units. The deposition of Riphean clastic sediments is followed by the intrusive emplacement of the Valaam mafic sill at ca. 1.46 Ga. Thus, the erosion of the basement leading the rapakivi granites to outcrop, possible paleoweathering (regolith formation), paleovalleys formation and sedimentation of the Riphean formations have to have occurred during a time period of less than 70 Ma.

Therefore, the dating of the basalts interlayered in the Pasha - Ladoga basin sediments will be of outmost importance to further constrain the duration of the sedimentation and the timing between the last magmatic activity related to the emplacement of the Salmi granite complex and the extrusion of the continental flood basalts in the lower clastic formations of the Pasha-Ladoga basin.

5.1.2. Archean intrusive magmatism

The first characteristic feature of the Mesoproterozoic Pasha – Ladoga basin basement is the presence of Archean gneissic orthoderived formations as in the strongly uranium mineralized Athabasca (Canada) and Kombolgie (Australia) areas.

Archean rocks form a series of granite-gneiss oval domes, with size varying from 100 to 150 square kilometers. These domes occur exclusively in the north-eastern part of the Raakhe – Ladoga mobile zone along the Ruskeala master fault (Fig. 1.7). They form a chain of dome structures stretching over more than 100 kilometers in the NW – SE direction. The core of the domes is always represented by Archean granite-gneisses and tonalitic-gneisses. **They also contain abundant pegmatites and potassium-rich leucocratic granites, which are enriched in Th, U, P and REE (Skorospelkin, 1974).** However, such Archean gneiss domes do no exist in the basement to the West of the Ladoga Lake area.

A summary of the characteristics of the Archean lithologies of the Ladoga Lake district is given in Table 5.1 and compared with the similar formations from the Athabasca and Kombolgie basin.

A similar geological situation occurs in the eastern part of the Athabasca basin. The Archean cores of the gneiss domes consist of migmatized granite-gneisses, which are enveloped by Paleoproterozoic metasediments of the Wollaston Group. Most unconformity-related deposits of the eastern part of the Athabasca basin are confined to Wollaston zone and the Eastern part of the Mudjatik zone where these Archean gneiss domes occur (Fig. 1.1).

The Precambrian rocks in the Alligator Rivers Uranium Field comprise two large domains with gneissic granites and migmatites: the Nanambu complex with Archean rocks in the western part of the area and the Nimbuwah complex of Paleoproterozoic age to the East and associated with more massive granitic bodies. There are a lot of different pegmatites confined to the Archean Nanambu complex. The Nanambu complex form gneissic dome structure surrounded by the graphitic and carbonate rocks of the Cahill Formation of

Paleoproterozoic age where the most significant deposits of the area (Koongarra, Ranger, Jabiluka) are localized.

	Canada	Australia	Ladoga Lake district, Russia		
	Athabasca	Kombolgie	Salmi	Western	Pasha
Rock types:					
- tonalites (TTG)...	+		+	-	+
U content, ppm	?		*0.5*		
Th content, ppm	?		*4*		
- K granites...	-	+	+	-	+
U content, ppm		*10*	*2*		
Th content, ppm		*32*	*7*		
Structure types:					
- gneiss dome	+	+	+	-	+
- ...					
- gneissic...	+	+	+		+
- migmatitic...	+	+	+		+
- pegmatite ...	+	+	+		+
Alteration:					
- greisen...	-	+	+		+
- regolith...	+	+	+		+
- ore deposits related to Archean	No	Cu, Au	Sn, Mo		

Table 5.1. Geological and geochemical features of the Archean basement rocks

In the Archean basement of the Pasha - Ladoga basin potassic granitoids slightly enriched in uranium already occurred at this age as observed in the Kombolgie basin area whereas only tonalitic gneisses occur in the Athabasca province. **These Archean potassic granitoids may have represented a source for the uranium enrichment of the Paleoproterozoic epicontinental sediments and an additional uranium source for the unconformity related deposits.**

5.1.3. Paleoproterozoic epicontinental sedimentation, Paleo- and Mesoproterozoic intrusive magmatism

Epicontinental sedimentation during the Paleoproterozoic is also a characteristic feature of the basement of the investigated basin. **In the Northern Ladoga Domain the typical sediments are organic matter rich black shales and carbonate rocks and silicoclastic sediments** (Table 5.2). They are metamorphosed to the upper amphibolite grade and migmatized with formation of skarns and greisens at the contact with the Archean.

	Canada	Australia	Pasha – Ladoga, Russia		
	Athabasca	Kombolgie	Salmi	Western	Pasha
Sediments types:					
- metapelitic…	+		+	+	+
- quartzites…	+		+		
- black shales…	+		+		+
U content, ppm			*5*		
Th content, ppm			*8*		
- metavolcanics…					+
- calc-silicate rocks	+		+		
PR_1 magmatism:					
- K granites…	+	+		+	+
U content, ppm				*3 - 6*	
Th content, ppm				*7 - 28*	
- pegmatites				+	
U content, ppm				*20*	
Th content, ppm				*110*	
- gabbro…	+			+	
U content, ppm				*1*	
Th content, ppm				*5*	
- alkaline rocks	+			+	
U content, ppm				*2*	
Th content, ppm				-	
Metamorphism:					
- granulite				+	
- amphibolite			+	+	+
- retrograde…	+		+	+++	
Migmatization			+	+	+
Tectonic					
- faults orientation	NE		NW	NW	
- faults type	reverse				
Alteration:					
- skarns…			+		
- regolith…			+		
PR_2 magmatism :					
- rapakivi granites			+		+
U content, ppm			*0.5 - 8*		
Th content, ppm			*13 - 35*		
- pegmatites…			+		
Alteration :					
- greisens…			+		
- regolith	+	+	+	+	+

Table 5.2. Geological and geochemical features of the Paleoproterozoic basement rocks

The Paleoproterozoic rocks of the Impilakhti suite in the Northern Ladoga district are also enriched in U and Th (Table 5.2).

The uranium mineralization are clearly at least spatially connected with the carbon-bearing formations which may be the source of the reducing fluid in the fluid mixing model (Kotzer & Kyser, 1995; Derome, 2003; Ledeneva et al., 2000) and of the metals for the complex type (or polymetallic: Ni, As, Co, Cu …) of uranium mineralization (sometimes also with Au, Ag, Pt group elements).

In the South-Western Ladoga area (so-called Southern Domain – Shuldiner et al., 1995) the Paleoproterozoic metasediments belong to Lakhdenpokh and Priozersk zone, which have undergone strong metamorphism up to granulite facies. The calco-sodic metagreywackes and calc-alkaline metavolcanics of the Lakhdenpokh zone are mostly similar to the metamorphic rocks of the Northern Domain (Kitelya or Ladoga series). On the contrary peraluminous metapelites are the most typical rocks of the Priozersk zone. Both zones have undergone retrograde metamorphism, which is stronger than in the Northern Ladoga Domain. **Average U content in the Paleoproterozoic rocks of the Southern Ladoga Domain does not exceeded 2 ppm, Th – about 12 ppm (Petrov et al., 2004) and thus this area does not appear very favorable for the occurrences of uranium mineralization.**

On the contrary in the South-Western Ladoga Lake area syn-orogenic potassium-rich Paleoproterozoic granite complexes are very abundant and enriched in Th, U and REE (Konopelko & Eklund, 2003) and post-orogenic bimodal intrusions, which form shoshonitic (from ultramafic, mafic potassium-rich lamprophyres to peraluminous granites) series, are strongly enriched in P, F, U, Th and LREE (Eklund et al., 1998). **The occurrence of such rocks in the South-Western Ladoga district represents a favorable perspective for the presence of uranium mineralization in the Western Ladoga despite the absence of Archean granite-gneisses.**

An other important event in the south-eastern part of the Baltic shield is the **emplacement of huge anorthosite - rapakivi granite batholiths of Vyborg and Salmi, which are especially rich in U and other trace elements (Sn, Be, W, Mo, F, Li, Th, REE etc).** The most lithophile elements enriched facies are the lithian-fluorine topaz-bearing granites emplaced in the north-western part of the Salmi pluton to the north-eastern part of the Mesoproterozoic Pasha – Ladoga basin. They occur closely to the Ruskeala master fault. In the exocontact of the Salmi pluton abundant Sn-polymetallic deposits in the Archean – Paleoproterozoic rocks. A similar situation is observed in the western part of the Pasha – Ladoga basin, where the Vyborg rapakivi granite batholith was emplaced.

After emplacement of the rapakivi granites and before the deposition of the Pasha Ladoga volcanic-sedimentary sequences, a short period of denudation occurred possibly with intensive weathering of the basement (Novikov et al, 2001). The same process has been proposed for the basement of the Athabasca and Kombolgie basins, where a so-called paleoregolith profile is observed (Hoeve & Sibbald, 1978).

The role of regolith alteration in formation of uranium mineralization is debated. Cuney proposed (2003) that the alteration profile may result from the alteration of the basement by

the percolation of the diagenetic fluids of the overlying basins. But in any case, intensively weathered disintegrated basement rocks (eluvial and alluvial deposits) are characteristic feature within all basins. The burial paleovalleys are very important because some of the high-grade ore deposits are confined to these structures.

In the Athabasca and Kombolgie areas the same type of Paleoproterozoic epicontinental platform sedimentation as in the Pasha - Ladoga basement is observed and respectively correspond to the Wollaston Group sediments and the Cahill formation. The degree of metamorphism of the Wollaston and Mudjatik zones reach upper amphibolite to lower granulite facies conditions with migmatization as in the Pasha - Ladoga area. The degree of metamorphism of the Cahill formation is lower than in the Pasha - Ladoga and Eastern Athabasca basements and reaches only the lower amphibolite facies with no evidence of migmatization.

Part 5.2. Reconstruction of the evolution of the basins

5.2.1. Mineralogical composition of the sediments

In the Ladoga Lake region (Russian Karelia) the Pasha-Ladoga Mesoproterozoic (Riphean) intracontinental clastic volcanic – sedimentary formations are presently preserved in a graben-like basin (approximately 70 000 km^2). Its former extension may have been much larger. In the Athabasca, Canada (350 km West to East) and Northern Territory of Australia (with its huge south-eastern prolongation as the McArthur basin) the clastic basins have presently a much larger extension.

The Athabasca and Kombolgie basins, the clastic sediments are characterized by their extremely mature characteristics (Table 5.3). They mainly consists of nearly orthoquartzitic sandstones with well rounded detrital quartz crystals, a very small proportion of clay minerals in the matrix. On the contrary **in the Pasha – Ladoga basin and adjacent basins in Finland (Satakunta and Muhos) the sediments are very immature sandstones, conglomerates and arkoses with abundant detrital plagioclase, K-feldspar and accessory minerals. They are frequently polymictic and with angular shaped detrital grains.**

	Canada	Australia	Pasha – Ladoga, Russia		
	Athabasca	Kombolgie	Salmi	Western	Pasha
Sediments maturity:	Mature	Mature	Highly immature	Highly immature	Highly immature
- quartz arenites…	+++	+++	+	+	+
- arkoses…	+	+	++	++	++
- Q-KFsp sandstones…			+++	+++	+++
- polymictic…			+	+	+
- greywackes…			+		
- dolomites…				+	
Clays composition:					
- KFsp…	-	-	+	+	+
- plagioclase…	-	-	+	+	+
- illite…	+	+			
- kaolinite…	+	+	+	+	+
- smectite…			+	+	+
Accessory minerals					
- zircon…	+	+	+		
- monazite…	+	+	+		
Accompanying volcanic activity:	+	+	+	-	+

Table 5.3. Composition of the sediments

The primary cement of the Pasha Ladoga clastic sediments is mostly composed of smectite and kaolinite, contrary to the Athabasca and Kombolgie basins where kaolinite was

the main phase together with detrital muscovite and biotite crystals. Small amounts of K-feldspar may have been present but no more exist presently. Illite is rare in the cement of the Pasha – Ladoga basin sandstones but interstratified minerals (illite-smectite varieties) are widespread. The main types of accessory minerals in the different basins are mostly the same: Fe-Ti oxides, zircon and minor amount of monazite, but they are more abundant in the Pasha Ladoga basin sediments.

All these features indicate that the tectonic conditions which have prevailed during the sedimentation in the Pasha - Ladoga basin as well as the Satakunta and Muhos basin should have been much more active than for the Athabasca and Kombolgie basins, and the pedogenetic alteration of the source rock must have been very weak to be able to generate such immature sediments. This tectonic activity is also necessary to generate the deep rift structures in which the Pasha - Ladoga, Muhos and Satakunta sediments have accumulated which still presently reach up to 2 000 meters, but which were probably much thicker, and which are associated with synsedimentary basaltic volcanic activity in the Pasha - Ladoga basin.

Part 5.3. Geochemical remobilization during diagenesis

5.3.1. Diagenetic and hydrothermal alteration

Diagenesis in the Athabasca and Kombolgie basins occurred in similar conditions and have been produced by highly saline, oxidizing fluids (basinal brines) to form formed basin-wide assemblages of clay minerals at temperatures of ca. 200 °C (Kotzer & Kyser, 1995, Derome, 2002). The main diagenetic mineral evolution in both basins corresponds to the development of overgrowths on detrital quartz crystals, the transformation of kaolinite to blocky dickite followed by illitization of the kaolin group minerals with variable intensity in the different part of the basins. Monazite is altered to a variety of (Ca, REE, Sr)Al-phosphate-sulfate minerals (APS) such as goyazite or florencite.

	Canada	Australia	Pasha – Ladoga, Russia		
	Athabasca	Kombolgie	Salmi	Western	Pasha
Regional alteration:					
- dickite…	+++	+++	+++	+++	+++
- illite…	+++	+++	+	+	+
- I/S minerals			+++	+++	+++
- quartz overgrowths….	+++		+	+	+
Ore related alteration:					
- quartz dissolution….	+++		++	+	+
- chlorite:					
- Mg-rich…	++	++			
- Fe-Mg…			++		
- Fe-rich	++		++		
- tourmaline…	++	++			
Fluids' composition					
Early diagenetic…	NaCl	NaCl, CH_4	NaCl, $MgCl_2$		
Mineralization…	$CaCl_2$		$CaCl_2$, CH_4		
Approximate temperature:					
Early diagenetic…	160 - 220°		150 - 260 °		
Mineralization…	140 – 160°				
pH diagenetic	4.5		4-5		
pH mineralization			≈ 7		

Table 5.4. Alteration mineralogy in the different sedimentary basins

In the Pasha – Ladoga basin the presence of abundant K-feldspar and plagioclase and their stability, except in the vicinity of the mineralized zones, have probably conferred more alkaline pH conditions to the fluids during the diagenesis. Quartz overgrowths are generally less well developed than in the Athabasca and Kombolgie basin. Investigation of fluid inclusions in the ore zones of the Karku deposit (Velichkin et al., 2003)

has shown, that the homogenization temperatures of inclusions in quartz and calcite range from 260 to 150 °C and from 240 to 105 °C respectively. It has been shown that the fluids were rich in Na-chloride with concentration of 13 to 0.2 wt. % of NaCl and Mg-chloride with concentration of 19 – 2 wt. % of $MgCl_2$ and some fluids having more complex compositions with predominance of Ca and concentration from 42 – 30 to 16 wt. % $CaCl_2$. Salt concentration in the solutions seems to grow with decrease temperature of mineral formation. Bylinskaya et al (2004), during mineralization stage, is observed two types of inclusions in the quartz overgrowths: (i) early CO_2-bearing and highly saline (mainly chloride) brines with the homogenization temperature 290 – 250 °C and (ii) later highly saline brines with hydrocarbon with homogenization temperature 180 – 170 °C. In the inclusions of the early stage, gypsum and a phosphate phase have been identified (fluelite – $[Al_2(F, OH)_3PO_4]$ $7H_2O$, which is an indicator of near-neutral pH.

Temperatures estimations for the hydrothermal chlorites from the Pasha – Ladoga basin (Salmi area) were calculated using chlorite geothermometer (Cathelineau & Nieva, 1983) and give the same range of values as fluid inclusions. Ripidolite deriving from biotite alteration in the graphite-biotite gneisses away from the mineralized zones gives temperatures of more than 270 °C which may correspond to retrograde stage of metamorphism in the basement. Pycnochlorite is a newly formed chlorite, which developed in the basement close to 3rd ore zone, on biotite flakes, but also in the groundmass which gives temperatures of 270 to 130 °C. This chlorite may correspond to syn-ore hydrothermal alteration in the basement rocks. Chlorite from the Priozersk sandstones (chamosite, which is richer in iron compared to pycnochlorite from the basement) is characterized by the temperature of 250 to 150 °C.

Thus, the early stage is characterized by higher temperatures and pressures with CO_2, H_2O and Na^+, Ca^+, Cl^-, PO_4^{-3}, the late stage is characterized by lower temperature and pressures, mostly water-bearing solutions with SO_4^{-2} and CO_3^-. The hydrocarbons may have represented the reducing medium for the mineralization processes (Bylinskaya et al., 2004).

Most previous investigators (Novikov et al., 2001; Mikhailov, 2001; etc) estimate that the possible total burial depth of the Pasha – Ladoga basin was about 3 – 4 kilometers (Mikhailov, 2001). For a depth of 4 km a temperature of 200°C would mean a geothermal gradient of 50°C/km which is quite elevated for a post-orogenic basin. The high temperatures detected in the Karku area may correspond to the lateral migration of the diagenetic fluids from the deeper part of the basin which may have reached nearly two 2 km more below the Ladoga Lake. For a maximum thickness of 6 km the geothermal gradient would become more normal at about 33°C/km. Another possibility is to connect the temperature peak to a regional

transient thermal anomaly appearing during the intrusion of the Valaam gabbro sill. The dating of the uranium mineralization and associated alteration minerals would be of major interest to support this second hypothesis.

In the Athabasca and Kombolgie the main alteration minerals are Mg-chlorite (sudoite) and Mg-tourmaline (dravite) accompanied by strong quartz dissolution in the immediate vicinity of the mineralized zones. Mg-rich compositions of chlorite and tourmaline in the Athabasca basin reflect the extremely oxidizing conditions prevailing in the Athabasca basin, because trivalent iron is not soluble in hydrothermal solutions. Fe-chlorite only appeared during a late stage after the main mineralization stage (Lorilleux, 2001). The crystallization of illite and the absence of carbonates is in favor of relatively acidic fluids.

In the Pasha – Ladoga basin during the mineralization stage the mineralogical assemblage is quite different: Mg-Fe and Fe-rich chlorites and carbonates is the most widespread mineral assemblage and quartz dissolution is much less intense than in the Athabasca basin. These mineralogical observations mean that the ore forming fluids were:

(i) more reducing to have the crystallization of Fe-rich chlorite, and thus uranium solubility was probably lower,

(ii) more alkaline because of the abundance of carbonates, favored by the occurrence of thick interlayered basalt flows in the sandstones, a factor which also tend to reduce the uranium solubility in the ore forming fluids,

(iii) only weakly silica undersaturated, inducing a much more limited silica dissolution and thus a much smaller creation of open space for massive ore deposition comparatively to the Athabasca uranium deposits.

Late alteration stage in the Athabasca and Pasha – Ladoga basins is characterized by supergene processes with formation of kaolinite, iron oxides and hydroxides and secondary uranium mineralization. Some differences in the bleaching degree are observed: late kaolinization process in the Athabasca basin is more widespread, than in the Pasha – Ladoga basin.

Part 5.4. Nature of the uranium sources and evidence of their leaching

Three major types of uranium minerals have been identified as potential uranium sources for unconformity related uranium deposits, either in the sandstone or in the basement: (i) *uranium oxides*, (ii) *monazite* and (iii) *zircon* (Hecht et al, 2003). Other minerals (allanite, apatite, titanium oxides) may also represent additional uranium sources, but generally for more subordinate amounts. A summary of the uranium source characteristics is given below in Table 5.5.

	Canada	Australia	Pasha – Ladoga, Russia		
	Athabasca	Kombolgie	Salmi	Western	Pasha
Monazite in :				Not studied	Not studied
- Archean rocks…			-		
- Paleoproterozoic rocks…	+++		++		
- Mesoproterozoic rocks…			-		
- Regolith			++		
- in sandstones	+		++	Not studied	Not studied
Monazite alteration in:				Not studied	Not studied
- Archean rocks…	+	+	-		
- Paleoproterozoic rocks…	++	++	-		
- Mesoproterozoic rocks…			-		
- Regolith			+		
- in sandstones	+++	-	+	Not studied	Not studied
Alteration minerals:				Not studied	Not studied
- APS…	+++		+		
- thorite…	+++		+		
Zircon alteration in:				Not studied	Not studied
- Archean rocks…		++	+		
- Paleoproterozoic rocks…		++	+++		
- Mesoproterozoic rocks…			+++		
- regolith			++		
- in sandstones	++	-	++	Not studied	Not studied

Table 5.5. Accessory minerals alteration in the different sedimentary basins

Uranium oxides have never been identified in the Mesoproterozoic sandstones, because of the primary oxidized character of the red-bed sandstones in the absence of reducing traps which have not permitted to uranium to occur as uranium oxide in the sandstones (Hecht et al., 2003).

Monazite, in the sandstone cover and in the altered sections of the basement of the Athabasca area in Canada (Hecht & Cuney, 2000) and in the East Alligator River district in Australia (Cuney et al., 2000) has been submitted to incongruent leaching by highly saline Ca-Na oxidizing diagenetic fluids despite its well known refractory behavior in most geological processes. LREE, P and large proportion of uranium have been leached out. Some uranium was retained in-situ with thorium, which was nearly immobile, within the structure of tiny thorite crystals, which locally still mimic the former monazite crystal shape. An other part of the uranium liberated from monazite alteration has been adsorbed on iron and titanium oxides and substituted in the altered part of zircon, and the residual undetermined part may have been transported by the diagenetic fluid. P and LREE recrystallized together with Al, Ca, LREE and Sr form Al-phosphates of the crandallite-goyazite-florencite group, which are the characteristic feature of the Athabasca and Kombolgie sandstones and are observed regionally (Hecht et al., 2003, Gaboreau et al., 2003).

In the Athabasca sandstones, preserved monazite crystals are exceptional and generally are preserved only where included in detrital quartz grains. In the Priozersk sandstones in the Salmi area of the Pasha – Ladoga basin, monazite alteration is limited and only minor amounts of Al-phosphate are observed. Locally Th also crystallizes as rare newly formed thorite crystals or microcrystalline phase with very low concentrations of U and LREE in the Priozersk sandstones as already observed in the Paleoproterozoic sandstones of the Franceville basin (Mathieu et al., 2001).

In the Athabasca and East-Alligator Rivers basement, the degree of monazite alteration is highly variable according to the degree of alteration of the rocks, but incipient alteration is observed also in the quite fresh rocks. Monazite in the Pasha – Ladoga area has been observed mostly in the Paleoproterozoic graphite-biotite gneisses and schists of the basement. Monazite is a very rare mineral in the Salmi rapakivi granites, but instead there is a lot of different Th-Zr-REE minerals like REE carbonates, allanite etc. There is no evidence of monazite alteration in the Paleoproterozoic graphite-biotite and biotite gneisses and schists of the Salmi area (Pasha – Ladoga basin). In the vicinity of the regolith zone, the Th-rich monazite shows a patchy distribution of domains with varying Th contents, including «intergrowth-like» pattern (as described by Zhu & O'Nions, 1999), but which correspond to primary "high temperature" characteristics of the crystals. The high Th content of the monazites from the regolithized Paleoproterozoic gneisses and schists is a pre-regolithic feature. Such high Th contents are observed in monazite from high grade metamorphic rocks, because the average Th-content in monazite increases with the temperature if Th is available in the rock (Overstreet, 1967). This

rock is particularly enriched in Th (205 ppm). Such Th-rich pegmatoids, rich in monazite are also quite common in the basement of the Athabasca basin (Brouand and Cuney, person. com.).

Zircon is the most common and abundant accessory mineral in the sandstones and in the basement rocks of all investigated basins. In the basal sandstones of the Athabasca basin well rounded zircons show very complex internal structures indicating several magmatic crystallization or alteration stages. Rounded cores are common as one or two zoned rims. In BSEM image, cores are usually bright-light and rims are frequently grey to dark-grey. The grey parts correspond to altered zones with lower average atomic number, where Zr and Si were substituted mainly by Ca, REE, Y, Sr, Al, P. The degree of substitutions may reach up 17 % of the cations (5.5 – 6 atoms of the zircon formula). These elements are characteristic of the Al-phosphates and it means that this type of alteration of zircon should occur synchronously with the monazite alteration and the neoformation of Al-phosphates-sulphates. The uranium content in the zircon grains ranges from a few hundred ppm to several thousands ppm (Hecht et al., 2003).

In the basal sandstones and conglomerates of the Priozersk suite (in the Salmi area) mostly idiomorphic, slightly rounded and, sometimes, elongated were derived from all rock types of the basement: Archean granite-gneisses, Paleoproterozoic gneisses and schists and Salmi rapakivi granites. Most of them (except the ones possibly derived from the Archean gneisses) also show very complex internal structures with strongly irregular or regular zoning. Multiple brighter zones in BSEM images (sometimes it can be crystal core, but it is not necessary) correspond to non-altered parts been of the zircon crystals. The same alteration as been described in the Athabasca basin and altered basement. In the altered zones of the zircons from the Pasha Ladoga area Zr and Si were substituted by the same variety of elements (Al, P, Ca, Fe, Y, U), but distinctly in this area, Th is also enriched (up to 3.5 wt. % ThO_2 and Y contents are generally much higher (up to 5 wt. % Y_2O_3). The degree of substitution in the detrital grains from the Priozersk sandstones (Salmi area, Karku deposit) varies from 0.5 to 8 atoms of the zircon formula, like in the observed granite-gneisses, schists and rapakivi granites (but only up to 5.5 atoms in the sandstones from the Shea-Creek area, Hecht et al., 2003). Exceptionally, in strongly altered zircon grains the substitution may reach up to 12 – 15 atoms of the zircon formula in the Pasha - Ladoga area. Uranium contribution in the substitution is less than 0.2 atoms of the zircon structure, but at the margin of zircon grains from mineralized zones U contents up to 0.2 – 1.2 wt. % of U_2O_3 (values of 6 – 9 wt %

have been measured, but may be related to possible contamination of an adjacent uranium phase).

The alterations observed in the detrital zircon grains of the sandstone are as well observed in zircon crystals from the basement rocks close the unconformity surface below the Pasha - Ladoga basin, but also in the basement rocks besides the basin presently outcropping. **The occurrence of similar zircon alteration below and outside of the basin demonstrates that the Mesoproterozoic Pasha – Ladoga basin was extending over an area much larger that the present one. Such alterations have been detected until 20 to 30 kilometers from the Pasha – Ladoga basin margin, in the western part of the Salmi rapakivi granite batholith and until 5 to 10 kilometers – in the Paleoproterozoic graphitic schists.**

Part 5.5. Model for the Karku unconformity-type uranium deposit

To summarize the previous observations a schematic model of unconformity-related uranium deposit formation specific of the Pasha – Ladoga area is proposed in Fig. 5.1.

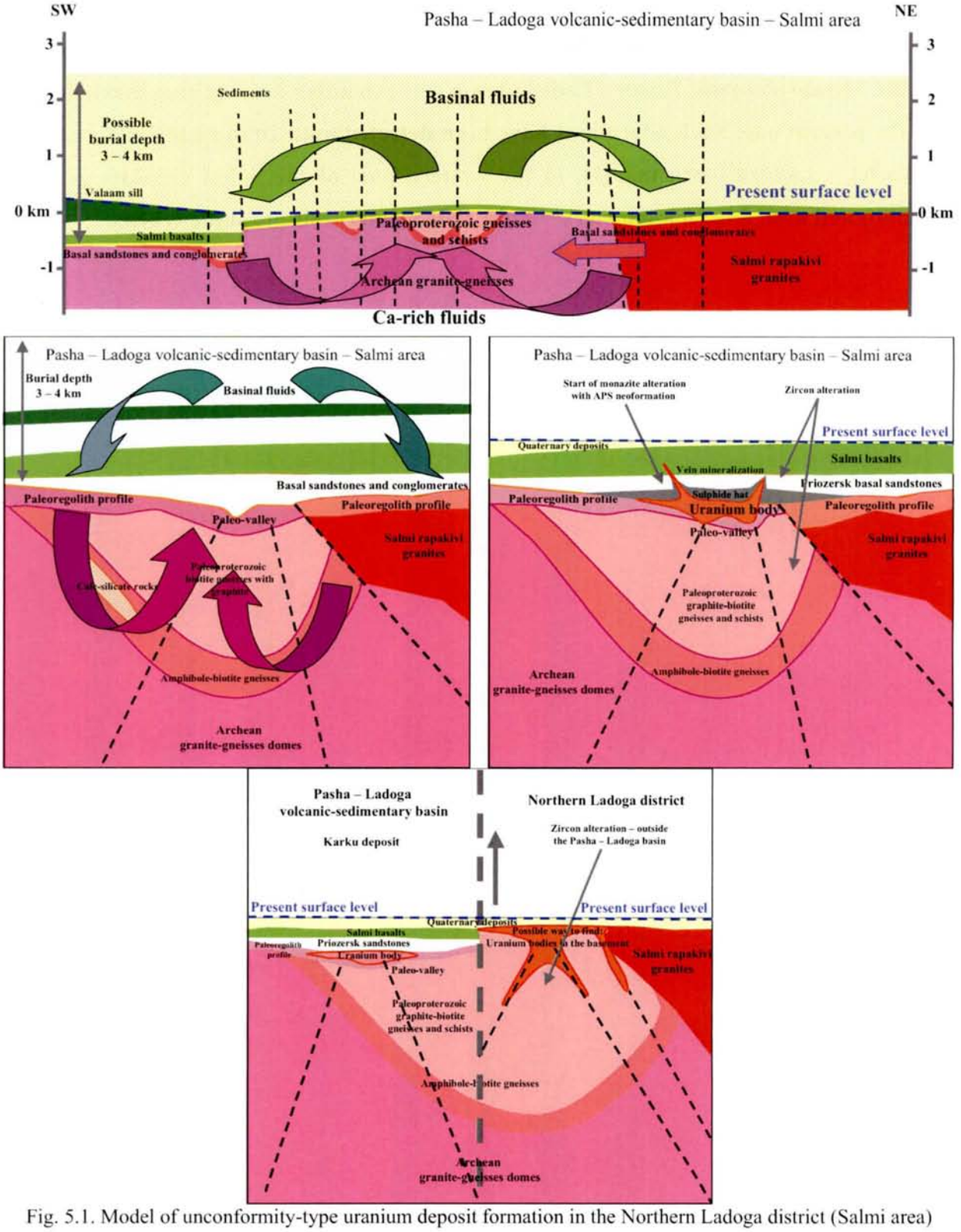

Fig. 5.1. Model of unconformity-type uranium deposit formation in the Northern Ladoga district (Salmi area)

We will now propose a specific model of unconformity related uranium deposits, for the Pasha – Ladoga basin, taking into account the similarities and the differences with the models existing for the unconformity type deposits of the Athabasca and Kombolgie basins (Cuney et al., 2003). A regional section through the Salmi area (from the Lunkkulunsaari island of the Ladoga Lake in the SW to the Salmi rapakivi batholith in the NE part of the section) summarizes the main features of regional geological situation (Fig. 5.1A). The two middle drawings present the evolution of the fluid circulation during the diagenetic-hydrothermal event (Fig. 5.1B), final denudation of the area (5.1C). The last drawing speculates about the possible existence of other uranium deposits in the basement of the Pasha Ladoga area outside the limits of the present extension of the basin (Fig. 5.1D).

The basement appears to be dominantly constituted of Archean rocks in which Paleoproterozoic epicontinental platform clastic and chemical sediments, enriched in uranium and carbonaceous matter are infolded. During Mesoproterozoic the emplacement of the Salmi rapakivi batholith induces the development of skarns and base metal deposits (red arrows) and locally some uranium mineralization. Shortly after the emplacement of the Salmi granite, erosion is rapidly followed by the deposition of up to 4 to 6 km of clastic sediments in tectonically active conditions with synchronous eruption of continental flood basalts at the beginning of basin filling.

The similarities of zircon alteration in the Pasha - Ladoga sediments and altered basement sections comparatively to the Athabasca province suggest that the same types of fluids have percolated in these formations. However, monazite is much less altered in the Pasha - Ladoga basin and basement compared to the Athabasca and East Alligator River Provinces, suggesting a slightly different composition of these fluids in the Pasha - Ladoga area or their lower temperature. During the diagenesis the highly saline basinal Na brines have percolated through the basin and downward below the unconformity surface, where they have interacted with basement lithologies rich in Ca to produce the Ca-rich fluid by comparison with the Athabasca model. The Ca-rich fluid have leached uranium mainly from the Paleoproterozoic U-enriched metasediments and granitoids and deposited it mainly in the most basal part of the sandstones where reducing conditions were created above graphite-sulfide rich schist layers from the basement, a situation similar to that observed in the mineralized Mesoproterozoic basins of Canada and Australia. Compared to Athabasca, the pH conditions were more alkaline because of the abundance of K-feldspar in the basin and of thick interlayered basalts flows near the base of the basin, resulting in calcite precipitation with the uranium mineralization, the fO2 conditions were more reducing as indicated by the

strong development of Fe-rich chlorite at the ore stage and the abundance of pyrrhotite deposited with the uranium oxides, and silica undersaturation was less important as attested by the limited quartz dissolution preventing the creation of large open space for massive ore deposition. The circulation of the diagenetic-hydrothermal fluids may have been induced by the emplacement of the Valaam sill.

The extension of the zircon and monazite alteration, up to 20 km from the present margin of the Pasha - Ladoga basin, let us to propose another way to detection possible uranium mineralization within the Salmi area and whole Pasha – Ladoga basement area (Figure 5.1D) as those observed in the East Alligator field in Australia which may extend down to more than 1000 m below the unconformity.

Moreover, the occurrence of many other clastic continental sediments all over the Fennoscandian basement (Satakunta – Nordingrå – Muhos and many others), presently preserved in small rift structures, may represent the relicts of a huge Mesoproterozoic clastic basin including all these occurrences.

If the Pasha Ladoga area share many similarities with the Athabasca basin, the more alkaline pH and lower fO2 conditions, the less silica undersaturated state of the fluids and the more limited alteration of monazite are characteristics much less favorable for extreme uranium solubility in the diagenetic-hydrothermal fluids and massive uranium deposition.

Part 5.6. Perspectives: complementary work to be performed to improve the knowledge for detection of further uranium mineralization in the Baltic shield

Very high-grade uranium mineralization as those observed in the Athabasca have not been discovered in the Pasha – Ladoga basin. Further research have to be undertaken to improve the geological knowledge of the Pasha – Ladoga area and the genetic and exploration models specific for this area and more generally in the Baltic shield.

The proposed most important directions of research are the followings:

(i) Complementary work on whole rock geochemistry and alteration mineral paragenesis on new drillings in the northern part of the Salmi area where uranium anomalies have detected in the interlayered basalts indicating the circulation of uranium bearing fluids.

(ii) More detailed fluid inclusion studies are necessary to better determine the P-T conditions of the diagenesis and subsequent hydrothermal alteration and the precise composition of the fluid and more especially their uranium content. These determinations are of outmost importance to compare the efficiency of the Pasha - Ladoga brines to transport uranium comparatively with the Athabasca ones.

(iii) More detailed geological and geophysical characterization of the Western and South-Eastern parts of the Pasha – Ladoga basin and basement formations, which already present some favorable characteristics for the detection of unconformity related uranium mineralization. For example, the systematic examination of basement rocks for the detection of the zircon and monazite alterations typical of the large mineralized district of the world with unconformity related uranium deposits has to be undertaken in the areas located to the west and south of the Pasha - Ladoga area until the Finnish border.

(iv) Detailed geological investigation of the surrounding basement rocks in the Northern and Western Ladoga Lake areas, where numerous small uranium occurrences are known to recognized their possible similarities with unconformity related mineralization.

(v) Detailed structural work from satellite images to precise the structural network of the Northern and Western Ladoga Lake areas.

General conclusions

Geological, mineralogical and geochemical studies of the Mesoproterozoic (Riphean) volcanic-sedimentary rocks of the Pasha – Ladoga basin (Karelia, Russia) and its Archean – Paleoproterozoic basement rocks have shown that the area share many similarities with the classical the highly mineralized districts from the Athabasca in Canada and the East Alligator Rivers in Australia hosting unconformity-related uranium deposits.

The Archean potassic granitic gneisses, the Paleoproterozoic epicontinental platform sediments and the Mesoproterozoic Salmi rapakivi granitic complex basement rocks present a primary enrichment in uranium and may have represented sources for the uranium deposits. The alteration of zircon, similar to that observed in the Athabasca basin and basement formations, which has been also observed in all basin and basement formations of the Pasha-Ladoga area, indicates that they all have been percolated by the diagenetic fluids and therefore may have represented uranium sources for the deposits. However, the weaker alteration of monazite indicates that the composition of the diagenetic fluids was different or that their temperature was lower and that the mobilization of uranium by these fluids was less efficient. Such features may explain the lower average grade of the Karku uranium mineralization by comparison with the ones related to the Athabasca basin in Canada.

The search for evidence of accessory mineral alteration (zircon and monazite alteration with formation of Al-phosphates of the crandallite-goyazite-florencite group) in both basement and basinal formations represent an efficient way for estimating the favourability of an area for the presence of unconformity related uranium mineralization.

The clastic sediments of the Pasha Ladoga basin present a low degree of maturity with abundant K-feldspar. The stability of this mineral in the major part of the basin indicate that the fluids were more alkaline than in the Athabasca and Kombolgie Kaolinite-Illite paragenesis of the clastic sediments. This may also have represented an other limiting factor for uranium transport in the diagenetic fluids.

An important conclusion is the much larger extension of the Mesoproterozoic Pasha Ladoga sedimentary basin than its present limits indicating the possible existence of basement hosted unconformity related deposits as those observed in the Athabasca and especially in the East Alligator River district.

It would be interesting to perform further investigations in the Baltic shield to improve our understanding the genesis of the uranium mineralization in such settings and to develop additional criteria for the exploration of such deposits:

(i) geochemical and mineralogical study of the basement rocks especially in the Western and Northern parts of the Pasha – Ladoga basin area;

(ii) study of the geologic formations in the vicinity of the pre-Riphean unconformity surface within other Mesoproterozoic sedimentary basins in Russia (Tersky shore, Kola peninsula), in Finland and in Sweden;

(iii) study of the geologic formations the vicinity of the pre-Jatulian unconformity surface within Onega depression and Tulomozero superimposed structure, where more mature sandstones are observed.

(iv) determination of the ore mineralization events ages in the Karku deposit area and ages of the Salmi intercalated basalts and Valaam sill rocks.

Bibliography

Amantov A., Spiridonov M., 1989. Geology of the Lake Ladoga. Soviet Geology, 4, 83 - 89. In Russian.

Amantov A., 1990. Geology and Cenozoic development of the subaquaeous Fennoscandian margins. Rep. of IX All-Union Marine Geol. School, 6 - 7. In Russian.

Amantov A., 1991. Bedrock basin of the Gulf of Finland as a part of Baltic-White sea form at the boundary of Fennoscandian shield. Abstracts of the II Marine Geological Conference "The Baltic", Rostock – Warnemnde.

Amantov A., 1992. Geological structure of the sedimentary cover of the Northwestern Russia basins. Sedimentary cover of the glacial shelves of the Northwestern seas of Russia. Saint-Petersburg, 25-47. In Russian.

Amantov A., 1993. Stages of the geological evolution of the Lake Ladoga region. 5 – 13. In Russian.

Amantov A., Laitakari I., Poroshin Ye. 1996. Jotnian and Postjotnian: sandstones and diabases in the surroundings of the Gulf of Finland. Geol. Survey of Finland, Special Paper 21, 99 - 113.

Amantov A., 1998 – 2004. Geological history of the Fennoscandia. Internet journal GeoNoRus.

Amantov A., 1998 – 2004. General outline of Baltic shield and Russian platform faulting. Influence on the late Proterozoic and Paleozoic paleogeography. Impact on the Prequaternary erosion. Internet journal GeoNoRus.

Anders E., Grevesse N. Chondrite composition from: http://earthref.org/GERM/reservoirs/C1.htm

Armstrong R., Quirt D., Hoeve J., 1988. Rb-Sr dating of diabase dikes in the Athabasca basin, Northern Saskatchewan: synchroneity with regional hydrothermal alteration and uranium mineralization. Saskatchewan Research Council Publication, R-855-3-A-88.

Beljaev A., Larin A., Amelin Yu. 1991. Salmi batholith and Pitkyaranta ore field in Soviet Karelia: geochemistry. In: Haapala I., Ramo O.T., Salonsaari P.T. (eds). Geol. Survey Finland, Guide 33, pp 11 – 19.

Amelin Yu.A., Larin A.M., Tucker R.D., 1997. Chronology of multiphase emplacement of the Salmi rapakivi granite-anortosite complex, Baltic shield: implications for magmatic evolution. Contrib. Mineral. Petrol., Vol. 127: pp 353 – 368.

Aphanasov, 1999. New data concerning geological structure of the Karelian Isthmus. Svecofennian zone of the Baltic shield. Unpublished. In Russian.

Baltybaev S., Glebovitsky V., Kozyreva I., Shuldiner V., 1996. The Meijeri Thrust: The Main Element of the Suture at the Boundary between the Karelian Craton and the Svecofennian Belt in the Ladoga Region of the Baltic shield. English translation from "Transactions (Doklady) of Russian Academy of Sciences" by MAIK ''Nauka/ Interperiodica'', 348 (4), 581 - 584.

Baltybaev S., Glebovitsky V., Levchenkov O., Berezhnaya N., Levsky L., 2002. Age relations of potassium- and sodium-rich migmatites within Svecofennian rocks (Ladoga Region, Baltic shield). English translation from ''Transactions (Doklady) of Russian Academy of Sciences'' by MAIK ''Nauka/Interperiodica'', 383(4), 1 – 4.

Bantova M., Levkovsky R., Sharkov V., 1975. Geology, mineral composition and age of rocks of the Salmi complex rapakivi granites and gabbro-anorthosites. Soviet geology, 7, pp.74 – 86. In Russian.

Beljaev A., Larin A., Amelin Yu., 1991. Salmi batholith and Pitkyaranta ore field in Soviet Karelia: geochemistry. In: Haapala I., Ramo T., Salonsaari P.T. (eds), Geol. Surv. Finland Guide 33, pp 11 – 19.

Beljaev A., Stepanov K., 1991. Salmi batholith and Pitkyaranta ore field in Soviet Karelia: internal structure and composition of the Salmi batholith. In: Haapala I., Ramo T., Salonsaari P.T. (eds), Geol. Surv. Finland Guide 33, pp 8 – 11.

Brunet R., 2004. Etude des argiles d'une série diagenetique Ripheenne (1.5 Ga) de Karkou (Russie). Unpubl. Mémoire de Maîtrise. Université de Poitiers. 22 p. In French.

Bruneton P., 1993. Geological environment of the Cigar Lake uranium deposit. Can. J. Earth Sci., 30, pp. 653 – 673.

Bruneton P., 2001. Zone de Karkou, Russie. Etude pétrographique de 13 échantillons des sondages carottés 605, 614 et 615. Etude 9002. Cogema, DEX, GST. In French.

Bylinskaya L., Mikhailov V., Tolmacheva E., Demicheva L., 2004. Mineralogy and conditions of the uranium mineralization of the Karku deposit (Ladoga District). Theses of the reports. VIMS, 2004. In Russian.

Card C.D., 2001. Basement rocks in the Western Athabasca Basin in Saskatchewan. Summary of investigations, Saskatchewan Geological Survey, 2: 321-333.

Card C.D., Pana, 2002. New investigations of basement to the western Athabasca Basin. Summary of investigations 2002. Saskatchewan Geological Survey, Saskatchewan Energy and Mines, pp. 17.

Cathelineau, M., et Nieva, D., 1985, A chlorite solid solution geothermometer. The Los-Azufres (Mexico) geothermal system : Contributions to Mineralogy and Petrology, v.91, p. 235-244.

Cumming G.L. and Krstic D., 1992. The age of unconformity-related uranium mineralization in the Athabasca Basin, northern Saskatchewan. Canadian Journal of Earth Sciences, 29: 1623-1639.

Cuney, M. & Mathieu, R., 2000. Extreme Light Rare Earth Element mobilization by diagenetic fluids in the geological environment of the Oklo natural reactor zones, Franceville basin, Gabon. Geology, 28 (8): 743-746.

Cuney M, Brouand M., Cathelineau M., Derome D., Freiberger R., Hecht L., Kister P., Lobaev V., Lorilleux G., Peiffert C., Bastoul A., 2003. What parameters control the high grade – large tonnage of the Proterozoic unconformity related uranium deposits ? Abstracts in the International conference «Uranium Geochemistry – 2003: Uranium deposit, natural analogs, environment». Nancy, France, pp. 123 – 126.

Condie, K.C., 1993. Chemical composition and evolution of the upper continental crust: Contrasting results from surface samples and shales. Chemical Geology, 104: pp. 1-37.

Debon, F. et Le Fort, P., 1983. A chemical - mineralogical classification of common plutonics rocks and associations. Earth Sciences, v. 73, p. 135-149.

Debon, F. et Le Fort, P., 1988, A cationic classification of common plutonic rocks and their magmatic associations : principles, method, applications. Bulletin de minéralogie, v. 111, pp. 493-510.

Derome D., 2002. Evolution et origine des saumures dans les bassins protérozoïques au voisinage de la discordance socle/couverture. L'exemple de l'environnement des gisements d'uranium associés aux bassins Kombolgie (Australie) et Athabasca (Canada). Unpubl. Ph.D. thesis. Université Henri Poincaré, Nancy, 232 pp.

Eklund O., Konopelko D., Rutanen H., Frojdo S., Shebanov A., 1998. 1.8 Ga Svecofennian post-collisional shoshonitic magmatism in the Fennoscandian shield. Lithos, 45, 87–108.

Eskola P., 1930. Rapakiven moroutumisesta. Vanhoja ja uusia tutkimuksia. Terra, 3. 1930. pp. 151-176. Summary in English: On the Disintegration of the Rapakivi.

Eskola P., 1951. Around Pitkäranta. Ann Acad. Sci. Fennicae, Ser. A III, 27, p. 1-90.

Fayek M. and Kyser T.K., 1997. Characterization of multiple fluid-flow events and Rare-Earth-Element mobility associated with formation of unconformity-type uranium deposits in the Athabasca Basin, Saskatchewan. The Canadian Mineralogist, 35: 627-658.

Glebovitsky V., Baltybaev S, Levchenkov O., Berezhnaya N., Levsky, L., 2001. Main Stage of Plutonic Metamorphic Activity in the Ladoga Region: Results of Isotopic Age determination. English translation from ''Transactions (Doklady) of Russian Academy of Sciences'' by MAIK ''Nauka/Interperiodica''. 377A(3), 302 - 306.

Haapala I., Rämö O.T., 1992. Tectonic setting and origin of the Proterozoic rapakivi granites of southern Fennoscandia. Trans. Royal Soc. Edinburgh: Earth Sci. 83, 165–171.

Hecht L. & Cuney M., 2000. Hydrothermal alteration of monazite in the Precambrian basement of the Athabasca basin: implication for the genesis of unconformity related deposits. Mineralium Deposita, 35: pp. 791-795.

Heine T.H., 1986. The geology of the Rabbit Lake uranium deposit, Saskatchewan. In: Uranium deposits of Canada, Evans E. (Ed.). Canadian institute of Mining and Metallurgy. Special vol. 33, pp. 134 – 143.

Heiskanen K.I., 1991. Early Proterozoic sedimentary basin of the Baltic shield. Precambrian geology of the Southern Canadian shield and the Eastern Baltic shield. Ojakangas R.W. (editor). Minnesota Geol. Survey Info Circ. 34, 131 – 137.

Heiskanen K.I., 1992. Lower Proterozoic key events as a basis for geological correlation in the Baltic shield. In Balagansky V., Mitrophanov F. (eds). Correlation of Precambrian formations of the Kola – Karelian region and Finland. Kola sciences center of the Russian academy of sciences. Apatity, Russia. P. 35 – 40.

Hoeve J. and Sibbald T., 1978. On the genesis of Rabbit Lake and other unconformity-type uranium deposit in northern Saskatchewan, Canada. Economic Geology, 73: pp. 1450-1473.

Hoeve J. and Quirt D., 1984. Mineralization and host rock alteration in relation to clay mineral diagenesis and evolution of the middle-Proterozoic Athabasca Basin, Northern Saskatchewan, Canada. Saskatchewan Research Council, Technical Report, pp. 187.

Hoffman P., 1990. Subdivision of the Churchill Province and extent of the Trans-Hudson Orogen. In: Lewry J.F., Stauffer M.R. (Eds.), The Early Proterozoic Trans-Hudson Orogen of North America. Geological Society of Canada, Special paper, 37, pp. 15 – 39.

Holm P., 1979. The geochemical fingerprints of different tectonomagmatic environments using hydromagmatophile element abundances of tholeitic basalts and basaltic andesites. In: Chem. Geol., v. 51, № 3/4, p. 303 - 323.

Holtta P., 1988. Metamorphic zones and the evolution of granulite grade metamorphism in the Early Proterozoic Pielavesi area, Central Finland. Geol. Surv. Finland Bull. 344, 50.

Huhma, H., 1986. Sm-Nd, U-Pb and Pb-Pb isotopic evidence for the origin of the Early Proterozoic Svecokarelian crust in Finland. Geol. Surv. Finland Bull. 337, 48.

Ibrahim A., 2004. Caractérisation minéralogique et géochimique de l'évolution diagenetique des basins gréseux protérozoïque continentaux. L'exemple du Ripheen du bouclier Balte. Implications sur la genèse des gisement métallique. DEA report. UMR-G2R. 37 p. In French.

Ignatov P., 2000. Structure and composition of the Riphean sediments of the Pasha – Ladoga basin in a view of estimation of uranium potential. Unpublished report. MGGA. In Russian.

IUGS, 2000. International Stratigraphic Chart. UNESCO – International Union of Geological Sciences.

Karhu J., 1993. Paleoproterozoic evolution of the carbon isotope ratios of sedimentary carbonates in the Fennoscandian shield. Geol. Surv. Finland Bulletin, 371, 87 p.

Kayryak A., Khazov R., 1967. Jotnian deposits of the Northeastern Ladoga area. Bulletin of the Leningrad State University, 12 pp. 62 – 72. In Russian.

Kayryak A., 1979. To the question of the basis of the Riphean and Karelian border in the southern part of the Baltic shield. In: Collected stories. Stratigraphy of the Upper Proterozoic (USSR). Riphean and Vendian deposits. Leningrad, Nedra, pp. 121 – 125. In Russian.

Khazov R., 1973. Geological features of tin-mineralization in the Northern Ladoga district. Proceeding of the Academy of sciences. Karelian filial. Issue 15. 87 p. In Russian.

Khazov R., Popov M., Biske N., 1993, Riphean potassium alkaline magmatism in South Baltic Shield. St. Petersburg, 216 pp. In Russian .

Kister P., 2003. Mobilité des éléments géochimiques dans un bassin sédimentaire clastique, du Protérozoïque à nos jours : le bassin Athabasca (Saskatchewan, Canada). Unpubl. PhD. thesis, Institut National Polytechnique de Lorraine, Nancy. In French and in English.

Knipping H.D., 1974. The concepts of supergene versus hypogene emplacement of uranium at Rabbit Lake, Saskatchewan, Canada, Formation of Uranium Ore Deposits, Proceedings of a Symposium Athens. IAEA, pp. 531-549.

Kohonen J., Pihlaja P., Kujala H., Marmo J., 1993. Sedimentation of the Jotnian Satakunta sandstone, western Finland. Geol. Surv. Finland, Bull. 369, 1–35.

Kohonen J., Rämö O.T., 2004. Sedimentary rocks, diabases, and late cratonic evolution. In: Lehtinen, M., Nurmi, P.A., Rämö, O.T. (Eds.), Precambrian Geology of Finland – Key to the Evolution of the Fennoscandian Shield. Elsevier Science B.V., Amsterdam, pp. 563–604.

Koistinen T., Klein V., Koppelmaa H., Korsman K., Lahtinen R., Nironen M., Puura V., Saltykova T., Tikhomirov S., Yanovsky A., 1996. Paleoproterozoic Svecofennian orogenic belt in the surroundings of the Gulf of Finland. In: Koistinen, T. J. (ed.) Explanation to the map of Precambrian basement of the Gulf of Finland and surrounding area 1 : 1 mill.. Geological Survey of Finland. Special Paper 21, 21-57.

Koistinen T. & Saltykova T. (Eds.), 1999. Structure-lithology, metamorphism and metallogeny of the Raahe-Ladoga Zone, Map 1: Structure-lithology 1:1 000 000. Geol. Surv. Finland, Espoo, Finland.

Konopelko D., 1997. Postorogenic intrusions of the NW Ladoga Lake region with special references to apatite-bearing potassium ultramafic rocks. Unpubl. PhD thesis. Saint-Petersburg State Univ., p. 200 (In Russian).

Konopelko D., Eklund O., Ivanikov V., 1998. 1.8 Ga phosphorus-rich lamprophyre-granitoid complexes in the Fennoscandian shield: parental magmas and fractionation paths. Proceedings of the International Conference: Genetic significance of phosphorus in fractionated granites. Acta Univ. Carolinae-Geol. 42 (1), 51 -54.

Konopelko D., Eklund O., 2003. Timing and geochemistry of potassium magmatism in the eastern part of the Svecofennian domain, NW Ladoga Lake Region, Russian Karelia. Precambrian Research, 120, 37 – 53.

Konopleva N., 1979. Main questions of the Upper Precambrian stratigraphy of the Baltic shield. In: Collected stories. Stratigraphy of the Upper Proterozoic (USSR). Riphean and Vendian deposits. Leningrad, Nedra, pp. 125 – 129. In Russian.

Konopleva N., Tikhomirova N., 1979. Methods of correlation of the Riphean red-bed sediments by their composition. Stratigraphy of the Upper Proterozoic (USSR). Riphean and Vendian deposits. Leningrad, Nedra, pp. 136 – 139. In Russian.

Kotzer T.G. and Kyser T.K., 1995. Petrogenesis of the Proterozoic Athabasca Basin, northern Saskatchewan, Canada, and its relation to diagenesis, hydrothermal uranium mineralization and paleohydrogeology. Chemical Geology, 120: 45-89.

Kushnerenko V.K., Pichugin V.A., 2000. Karku uranium deposit – the first unconformity type deposit in Russia. Uranium on a boundary of centuries. Abstracts of the reports. VIMS. In Russian.

Kushnerenko V.K., Dolgushina I.S., 2003. Geological and geochemical peculiarities of the Karku deposit: first unconformity-type deposit in Russia. Abstracts in the International conference «Uranium Geochemistry – 2003: Uranium deposit, natural analogs, environment». Nancy, France, pp. 209 – 210.

Laitakari I., Koistinen T., Virransalo, P., 1996. Principles and sources for the basement map, Gulf of Finland and surrounding area. In: T.J. Koistinen (Ed.), Explanation to the map of Precambrian basement of the Gulf of Finland and surrounding area 1:1 mill. Geol. Surv. Finland, Spec. Pap. 21, 9–13.

Ladner G., 1983. Geology of the Oya-Yarvi pluton in the Karelian Isthmus. Bulletin of the Leningrad State University, 12 pp. 23 – 30. In Russian.

Ledeneva N., 1990. Rock alteration and ore composition of the Karku deposit. Unpublished report. VIMS. In Russian.

Ledeneva N., 2000. Mineral content and features of genesis of Karku unconformity type deposit (Baltic shield). Uranium on a boundary of centuries. Theses of the reports. VIMS, 2000. In Russian.

Lobach-Zhuchenko S., Chekulaev V., Sergeev S., Levchenkov O., Krylov, I., 1993. Archean rocks from southeastern Karelia (Karelian granite-greenstone terrain). Precambrian Research. 62, 375–397.

Lobaev V., Cuney M., Terentyev V., 2003. The Karku uranium deposit (Ladoga district, Baltic shield, Russia): mineralogical and geochemical characteristics of the sandstones. Abstracts in the International conference «Uranium Geochemistry – 2003: Uranium deposit, natural analogs, environment». Nancy, France, pp. 223 – 226.

Lorilleux G., 2001. Les brèches associées aux gisements d'uranium de type discordance du bassin Athabasca (Saskatchewan, Canada). Unpubl. Ph. D. thesis, Institut National Polytechnique de Lorraine, Nancy, 319 pp.

Macdonald R., 1980. Mineralogy and Geochemistry of a Precambrian regolith in the Athabasca Basin. M.Sc. Thesis, University of Saskatchewan, Saskatoon, 151 pp.

Mathieu R., Zetterstrom L., Cuney M., Gauthier-Lafaye F. and Hidaka H., 2001. Alteration of monazite and zircon and lead migration as geochemical tracers of fluid paleocirculations around the Oklo-Okélonbondo and Bangombé natural reactor zones (Franceville basin, Gabon). Chemical Geology, 171: 147-171.

Melezhik V., Fallick A.E., Makarikhin V., Lyubtsov V., 1997. Links between Paleoproterozoic paleogeography and rise and decline of stromatolites: Fennoscandian Shield. Precambrian Research, 82, 311-348.

Meunier A., Velde B., 1989. Solid solutions in I/S mixed-layer minerals and illite. Amer. Mineralogist, Volume 74, pp. 1106 - 1112.

Mikhailov V.A., 2001. To the question on genesis of unconformity type ore on Karku deposit (Northern Ladoga). Transactions on geology of uranium, rare and rare-earth metal deposit. Volume 143. VIMS, 2001. In Russian.

Mikhailov V.A., 2003. To the problem of the genesis of the unconformity-type Karku deposit. Abstracts in the International conference «Uranium Geochemistry – 2003: Uranium deposit, natural analogs, environment». Nancy, France, pp. 247 – 248.

Moine B, La Roche (de) H., 1968. Nouvelle approche du problème de l'origine des amphibolites à partir de leur composition chimique. Comptes Rendus de l'Académie des Sciences (Paris), 267, 2084-2087.

Naumov S., Terentyev V., Kharlamov M., Carisey J.-C. (Eds), 2001 Geological map of uranium mineralization of the Baltic shield. Scale 1 : 2 500 000. Saint-Petersburg.

Negroutsa V.Z., 1984. Early Proterozoic stages of evolution of the eastern part of the Baltic Shield. Leningrad: Nauka. 270 p. In Russian.

Neymark L.A., Amelin Yu.V., Larin A.M., 1994. Pb-Nd-Sr isotopic and geochemical constraints on the origin of the 1.54 – 1.56 Ga Salmi rapakivi granite – anorthosite batholith (Karelia, Russia). Mineral. Petrol 50: pp 173 – 193.

Novikov G.I. et al., 2001. Geological-structural position and basic features of Karku uranium deposit (Northern Ladoga). Transactions on geology of uranium, rare and rare-earth metal deposit. Volume 143. VIMS, 2001. In Russian.

Ojakangas R., Marmo J., Heiskanen K., 2001. Basin evolution of the Paleoproterozoic Karelian Supergroup of the Fennoscandian (Baltic) shield. Sedimentary geology, 141 – 142, 255 – 285.

Overstreet W. C. (1967) - The geologic occurrence of monazite. U.S. Geol. Surv. Prof. Pap., 530, 327p.

Pagel M., 1975. Détermination des conditions physico-chimiques de la silicification diagénétique des grès Athabasca (Canada) au moyen des inclusions fluides. Compte Rendu de l'Académie des Sciences de Paris, 280(D): 2301-2304. In French.

Pagel M. and Jaffrezic H., 1977. Analyses chimiques des saumures des inclusions du quartz et de la dolomite du gisement d'uranium de Rabbit Lake (Canada). Aspect méthodologique et importance génétique. Compte Rendu de l'Académie des Sciences de Paris, 284: 113-116.

Pagel M., Poty B., Sheppard S.M.F., 1980. Contribution to some Saskatchewan uranium deposits mainly from fluid inclusion and isotopic data. In: J. Ferguson, A. Goleby (Editors), Uranium in the Pine Creek geosyncline. International Atomic Energy Agency, Vienna, pp. 639-654.

Pagel M., 1991. Lateritization and paleogeomorphology: their role in the genesis of unconformity type uranium deposits in Saskatchewan Canada. In: Source, transport and deposition of metals. Pagel M., Leroy J. (Eds.). 1991. Balkema, Rotterdam.

Pagel M., Ruhlmann F., Bruneton P., 1993. The Cigar Lake uranium deposit, Saskatchewan, Canada. Can. J. Earth Sci., vol. 30, pp. 651 – 762.

Petrov O., Caillat C., Naumov S., Kharlamov M., Kushnerenko V., Mironov Yu., Mikhailov V., 2004. Compilation of a set of uranium-specialized geological-geophysical maps of the Saima – Ladoga region, the Pasha – Ladoga area and the Karku deposit. Unpublished report of COGEMA, VSEGEI, Nevskgeology, Urangeologorazvedka and Novaya Lekhta. Saint-Petersburg.

Pichugin V., 2000. Realization of the prospecting drilling for uranium deposits in the Salmi (with final Karku deposit evaluation) and Svir-Oyat areas (Southern part of the Baltic shield) in 1999 – 2000. Unpubl. Report. Nevskgeology.

Polikarpov V.I., Molchanov A.V., 2000. Karku deposit – the new type of uranium mineralization in Karelia. Transactions on geology of uranium, rare and rare-earth metal deposit. Volume 141. VIMS, 2000. In Russian.

Poutiainen M., Sherbakova T, 1998. Fluid and melt inclusion evidence for the origin of idiomorphic quartz crystals in topaz-bearing granite from the Salmi batholith, Karelia, Russia. Lithos 44, pp. 141–151.

Ramaekers P., 1980. Stratigraphy and tectonic history of the Athabasca group (Helikian) of the Northern Saskatchewan. In: Summary of investigations 1980. Saskatchewan Geological Survey, Miscellaneous Report 80 – 4, pp. 99 – 106.

Ramaekers P., 1990. Geology of Athabasca group (Helikian) in northern Saskatchewan. In: Saskatchewan energy and mines. Saskatchewan Geological Survey, report 195. 49 p.

Ramaekers P., Yeo G. and Jefferson G., 2001. Preliminary overview of regional stratigraphy in the Late Paleoproterozoic Athabasca Basin, Saskatchewan and Alberta. Summary of Investigations, Saskatchewan Geological Survey, Saskatchewan Energy and Mines, pp. 240-251.

Ramo T., 1991. Petrogenesis of the Proterozoic rapakivi granites and related basic rocks of southeastern Fennoscandia: Nd and Pb isotopic and general geochemical constraints. Geol. Survey of Finland Bulletin, 355, 161 p.

Ramo O. T., Mänttäri I., Vaasjoki M., Upton B.G.J., Sviridenko L., 2001. Age and significance of Mesoproterozoic CFB magmatism, Lake Ladoga region, NW Russia. In: 2001 GSA Annual meeting (Boston, Massachusetts) – Igneous Petrology I, Session 57, A-139.

Ramo T., Mänttäri I., Kohonen J., Upton B., Vaasjoki M., Luttinen A., Lindqvist V., Lobaev V., Cuney M., Sviridenko L., 2004. The Lake Ladoga basin; preliminary insights into geochronology, igneous evolution, and tectonic significance. In: Ehlers, C., Eklund, O., Korja, A., Kruuna, A., Lahtinen, R., Pesonen, L.J. (Eds.) Lithosphere 2004 - Third Symposium on the Structure, Composition and Evolution of the Lithosphere in Finland. Institute of Seismology, University of Helsinki, Report S-45, p. 105-106.

Reyx J., 2000. Echantillon № 6 – Sondage 605 – 107 m (grés microconglomeratique gris). Métallographie. Russie (zone de Karkou). Unpubl. COGEMA-GEO-GST report. 6 p. In French.

Ruzicka V., 1993. Unconformity-type uranium deposits. In Mineral deposit modeling: Geological association of Canada, Special paper 40, p. 125 – 149.

Saranchina G., 1972. Granitoid magmatism, metamorphism and metasomatism of Precambrian. Saint-Petersburg, LGU. In Russian.

Sederholm J., 1897. Om indelning af de prekambriska formationerna i Sverige och Finland och om nomenklaturen för dessa äldsta bildningar. Geol. fören. i Stockholm förh. Bd. 19. 1897. S. 20-52.

Sharkov, 1999 Within-plate magmatic Middle Proterozoic systems on example anorthosite – rapakivi granite complexes of the Baltic and Ukrainian shields. Russian journal of Earth science, 1, № 4, pp. 311 – 337. In Russian.

Shergina Yu.P. et al., 1982. Age of the Salmi rapakivi granite massif and the related mineralization. Izv. Akad. Nauk USSR, ser. Geology 12: pp 64-76. In Russian.

Shuldiner V., Kozyreva I., Baltybaev S., 1995. Plutonic-metamorphic evolution of the western Ladoga area: new model. Regional geology and metallogeny, 4, pp. 52 – 62. In Russian.

Shuldiner V., Kozyreva I., Baltybaev S., 1997. Tectonic-metamorphic zoning of the Ladoga Lake area. Bulletin of the Saint-Petersburg State University, series 7, 3 pp. 63 – 70. In Russian.

Shuldiner V., Levchenkov O., Yakovleva S., Makeev A., Komarov A., Konopelko D., Baltybaev S., Kozyreva I., 2000. The Late Karelian in the Stratigraphic Scale of Russia: Determination of Its Lower Boundary and Regional Units in the Stratotype Area. English translation from ''Stratigraphy and Geological Correlation'' by MAIK ''Nauka/Interperiodica''. 8(6), 544 - 556.

Shurilov A., Polekhovsky Yu., Tarasova I., Petrov Yu., 2003. Geology and ore paragenesis of the Karku uranium deposit (North-Eastern Ladoga region). Abstracts in the International conference «Uranium Geochemistry – 2003: Uranium deposit, natural analogs, environment». Nancy, France, pp. 347 – 350.

Shurkin K., 1958. Geological sketch of the ceramic pegmatites of the Pitkyaranta field. Northeastern Ladoga area. Leningrad.

Suominen V., 1991. The chronostratigraphy of SW Finland with special reference to the Postjotnian and Subjotnian diabases. Geol. Surv. Finland Bull. 356, 100 p.

Svetov A., Golubev A., Sviridenko L., 1983. The Tenjarvi intrusion of the plagiogranites (Northern Ladoga district). In: Magmatism and metallogeny of the Precambrian formations of Karelia. Informational reports. Petrozavodsk, pp 3 – 7. In Russian.

Svetov A. & Sviridenko L., 1991. Magmatism of suture zones of the Baltic shield. Leningrad, Nauka. 200 p. In Russian.

Sviridenko L., 1968. Petrology of the Salmi rapakivi granites pluton (Karelia). Proceeding of the Academy of sciences. Karelian filial. Issue 3, 115 p. In Russian.

Sviridenko L., 1994. The evolution of the fluid phase during the crystallization of granite types: Salmi pluton, Karelia, Russia. Mineralogy and petrology, 50, pp. 59 – 67.

Taylor S., McLennan S., 1985. The Continental Crust: its Composition and Evolution. Blackwell Scientific Publications.

Thomas D.J., Matthews R.B., Sopuck V., 2000. Athabasca Basin (Canada) Unconformity-Type Uranium Deposits: Exploration Model, Current Mine Developments and Exploration Directions. Geology and Ore Deposits: The Great Basin and Beyond, GAC-MAC, pp. 1-23.

Trustedt O., 1907. Die Erzlagerstätten von Pitkäranta am Ladoga-See. Bull. comm. geol. Finland, 19, 333 p.

Turekian K., Wedepohl K. Distribution of the elements in some major units of the Earth's crust. Bull. of the Geol. Soc. of America. 196,. 72- 2 : 175 – 192

Upton B.G.J., Rämö O.T., Vaasjoki M., Sviridenko L.P. and Svetov A., 1998. Constraints on petrogenesis of Mesoproterozoic CFBs from the SE Fennoscandian Shield: Trace element and Nd isotopic evidence. Abstracts of ICOG-9, 1998 Beijing. Chinese Sci. Bull. 43, 134.

Vaasjoki M., Ramo O., Sakko, M., 1991. New U-Pb ages from the Wiborg rapakivi area: constraints on the temporal evolution of the rapakivi of the rapakivi granite-anorthosite-diabase dyke association of southeastern Finland. Precambrian Research. 51, 227 - 243.

Vaisanen M., Manttari I., Kriegsman L., Holtta P., 2000. Tectonic setting of post-collisional magmatism in the Paleoproterozoic Svecofennian Orogen, SW Finland. Lithos 54, 63 - 81.

Velichkin V. et al, 2001. Results of the complex geological-mineralogical study of the Karku uranium deposit (Northeastern Ladoga). Comparative analysis of the Ladoga and Athabasca uranium districts. IGEM, Moscow.

Velichkin V.I. et al, 2001. Results of the complex geological – mineralogical study of the Karku uranium deposit in the north-eastern Ladoga and the comparison Ladoga and Athabasca ore districts. Unpublished report. IGEM RAS. In Russian.

Velichkin V.I. et al, 2003. Geology and formation conditions of Karku deposit – the first uranium unconformity deposit in Russia. Abstracts in the International conference «Uranium Geochemistry – 2003: Uranium deposit, natural analogs, environment». Nancy, France, pp. 371 – 374.

Velikoslavinsky D.A. et al. The anortosite-rapakivi granite formation of the East-European platform. Leningrad: Nauka. 1978. In Russian.

Volkova N., Budanov V., 1999. Geochemical discrimination of metabasalt rocks of the Fan–Karategin transitional blue schist/greenschist belt, South Tianshan, Tajikistan: seamount volcanism and accretionary tectonics. Lithos, 47, pp. 201–216.

Wilson M.R. and Kyser T.K., 1987. Stable Isotope geochemistry of Alteration Associated with the Key Lake Uranium Deposit, Canada. Economic Geology, 82: 1540-1557.

Winterhalter B., 1972. On the geology of the Bothnian Sea: an epeiric sea that has undergone Pleistocene glaciation. Geol. Surv. Finland, Bull. 258, 1–66.

Winterhalter B., 1982. The bedrock geology of Lumparn Bay, Åland. Geol. Surv. Finland, Bull. 317, 115–130.

Winterhalter B., 2000. Sedimentary rocks underlying the Gulf of Bothnia. In: Th. Lundqvist, S. Autio (Eds.), Description to the bedrock map of central Fennoscandia (Mid-Norden). Geol. Surv. Finland, Spec. Pap. 28, 76–77, 79.

Zhu X., O'Nions R., 1999. Zonation of monazite in metamorphic rocks and its implications for high temperature thermochronology: a case study from the Lewisian terrain. Earth and Planetary Science Letters, 171, pp. 209–220.

Annexes

Annex I: Archean rocks
Major and trace element analysis of the Archean formations

DDH no.:	10-04-01	DDH-615	5-07-01
Depth (m):	Uuksu dome	109	Koirinoya dome
Rock type:	Granite-gneiss	Altered rock	Amphibolite
SiO_2(wt. %)	65.31	36.42	49.65
Al_2O_3	15.04	6.06	14.58
Fe_2O_3	5.63	8.07	13.63
MnO	0.06	0.44	0.21
MgO	0.91	2.02	7.16
CaO	2.45	23.93	10.73
Na_2O	3.49	0.07	2.20
K_2O	3.02	1.13	0.49
TiO_2	0.96	0.24	1.14
P_2O_5	0.42	0.05	0.08
PF	2.01	21.39	0.63
Total	**99.30**	**99.82**	**100.50**
As (ppm)	0.00	0.83	0.00
Ba	1434.00	110.00	94.56
Be	3.87	3.05	0.57
Bi	0.00	0.28	0.00
Cd	0.41	1.31	0.00
Co	8.07	12.20	50.88
Cr	12.48	60.00	96.40
Cs	3.05	3.95	0.37
Cu	68.63	47.40	10.73
Ga	24.26	10.00	18.81
Ge	1.47	1.15	1.80
Hf	11.26	2.28	2.07
In	0.00	0.00	0.00
Mo	4.03	0.00	0.00
Nb	45.73	3.97	4.69
Ni	6.42	68.70	66.10
Pb total	23.02	12.30	4.72
Rb	119.30	83.90	18.54
Sb	0.00	0.00	0.00
Sn	2.49	1.08	0.86
Sr	444.20	74.30	140.30
Ta	1.50	0.34	0.35
Th	22.33	5.90	1.05
U	5.12	4.64	0.31
V	52.78	248.00	297.80
W	0.39	1.37	0.00
Y	36.60	101.00	20.61
Zn	93.64	68.10	107.50
Zr	553.40	82.00	77.84
La	104.90	53.70	7.98
Ce	208.80	99.30	18.40
Pr	22.55	13.00	2.55
Nd	77.06	52.10	11.33
Sm	11.69	12.50	2.98
Eu	2.43	2.86	0.97
Gd	8.52	14.40	3.28
Tb	1.21	2.39	0.55
Dy	6.76	14.90	3.49
Ho	1.24	3.11	0.73
Er	3.42	9.09	2.04
Tm	0.51	1.48	0.31
Yb	3.42	11.60	2.09
Lu	0.54	2.07	0.33

Annex II Paleoproterozoic formations

Major and trace element analysis of the Paleoproterozoic gneisses and schists

	Bt - Amph - Pitkyaranta Suite			Biotite gneisses and schists of the Impilakhti Suite					
DDH no.:	**DDH-389**	**4-03-01**	**5-02-01**	**327**	**319**	**319**	**614**	**816**	**816**
Depth (m):	**194**			**221**	**142**	**193**	**100**	**185**	**185.5**
Position	II zone	Pitkyaranta	Pitkyaranta	II zone	I zone	I zone	I zone	II zone	II zone
SiO_2(wt. %)	62.37	65.10	46.16	56.07	66.69	52.25	64.16	68.78	88.86
Al_2O_3	13.84	15.14	12.82	14.42	16.36	18.13	17.69	15.23	3.07
Fe_2O_3	6.49	6.53	13.30	7.73	6.68	10.00	3.84	5.13	2.13
MnO	0.08	0.07	0.21	0.30	0.04	0.08	0.00	0.03	0.05
MgO	5.18	2.16	9.15	3.63	2.53	5.44	1.70	0.55	0.49
CaO	0.47	1.67	15.02	4.52	0.27	2.41	0.21	0.16	1.24
Na_2O	0.32	3.34	1.03	0.14	0.07	3.70	0.35	0.19	0.00
K_2O	6.73	2.83	0.40	2.86	0.86	3.78	6.94	1.85	0.27
TiO_2	0.54	0.64	0.68	0.58	0.73	0.85	0.56	0.69	0.10
P_2O_5	0.14	0.14	0.06	0.25	0.17	0.14	0.14	0.21	0.08
PF	3.74	1.76	0.60	7.84	6.43	2.76	4.27	5.99	2.44
Total	**99.90**	**99.38**	**99.43**	**98.34**	**100.82**	**99.53**	**99.88**	**98.81**	**98.73**
As (ppm)	0.00	0.00	5.33	0.00	79.59	0.00	0.00	0.00	0.00
Ba	571.90	371.10	50.40	1020.00	55.15	1157.00	800.00	74.92	81.39
Be	0.00	1.45	0.00	1.52	8.15	1.61	4.65	2.24	0.59
Bi	0.22	0.00	0.00	151.70	0.12	0.47	0.06	3.34	0.77
Cd	0.00	0.00	0.00	97.96	1.62	0.36	0.00	0.42	0.82
Co	51.42	19.37	47.68	33.23	45.76	31.11	11.40	8.61	4.92
Cr	123.90	112.40	267.40	75.28	135.10	189.70	118.00	154.00	25.71
Cs	6.36	7.72	0.37	2.70	2.38	6.29	2.77	4.74	0.74
Cu	98.92	32.62	73.99	1860.00	79.29	83.42	31.00	23.47	11.55
Ga	27.47	19.36	16.12	22.69	40.23	35.21	29.60	23.24	5.39
Ge	1.88	1.55	1.78	1.05	3.45	1.79	2.06	0.97	0.56
Hf	2.43	4.67	1.15	7.37	5.90	4.14	3.57	4.33	0.90
In	0.00	0.00	0.11	0.36	0.00	0.12	0.00	0.34	0.13
Mo	0.00	0.91	0.00	14.24	142.80	4.21	0.57	0.68	1.64
Nb	11.63	9.48	1.61	11.16	11.02	11.62	13.50	9.44	2.12
Ni	96.87	54.63	109.50	93.49	73.11	100.30	39.90	33.19	22.02
Pb	281.37	17.26	6.76	4656.45	80.60	25.53	54.10	48.79	27.72
Rb	225.20	153.30	9.75	148.30	40.90	168.90	167.00	88.78	14.14
Sb	0.00	0.00	0.00	0.15	0.10	0.00	0.00	0.00	0.00
Sn	0.87	1.86	3.72	3.18	1.44	2.21	0.91	5.32	0.96
Sr	87.56	171.10	69.54	108.40	14.20	278.30	93.60	38.66	9.19
Ta	0.89	0.83	0.13	1.40	0.94	1.25	0.96	0.89	0.21
Th	9.42	11.52	0.28	15.99	13.85	11.05	25.70	9.67	2.44
U	2.14	2.99	0.23	8.97	4.23	4.77	6.38	3.89	1.11
V	185.90	108.60	252.50	272.40	138.90	224.60	76.60	93.80	34.14
W	2.50	0.58	0.52	4.22	5.46	1.53	0.81	4.25	0.58
Y	21.66	20.10	15.72	28.26	25.46	19.76	12.50	21.70	7.49
Zn	1038.00	102.80	128.80	21970.00	348.40	169.00	149.00	1405.00	503.90
Zr	82.73	177.40	40.52	280.70	226.90	140.40	109.00	157.90	33.10
La	26.49	38.04	3.06	19.97	39.37	32.68	25.20	54.23	8.87
Ce	52.13	75.14	6.75	40.68	86.73	70.10	51.70	81.18	18.25
Pr	6.48	8.80	1.00	5.66	10.27	8.35	5.97	8.97	2.06
Nd	23.71	32.52	4.86	20.72	37.88	30.27	21.00	32.80	7.81
Sm	4.68	5.89	1.64	4.13	7.15	5.80	4.12	5.92	1.61
Eu	1.07	1.35	0.57	0.79	1.31	1.43	1.03	1.38	0.35
Gd	4.02	4.57	2.15	3.79	5.56	4.79	3.20	4.70	1.39
Tb	0.61	0.67	0.39	0.64	0.84	0.70	0.41	0.69	0.21
Dy	3.59	3.70	2.64	4.21	4.84	3.86	2.21	4.00	1.20
Ho	0.69	0.71	0.57	0.88	0.88	0.71	0.42	0.78	0.22
Er	1.98	1.92	1.64	2.79	2.37	1.93	1.18	2.33	0.61
Tm	0.29	0.29	0.26	0.45	0.34	0.27	0.15	0.35	0.09
Yb	2.01	1.93	1.75	3.27	2.24	1.76	1.12	2.46	0.63
Lu	0.30	0.30	0.28	0.55	0.35	0.27	0.17	0.38	0.10

Annex II Paleoproterozoic formations (Suite)

	Biotite Impilakhti gneisses			Graphite - biotite fresh gneisses and schists					
DDH no.:	**816**	**816**	**816**	**306**	**306**	**605**	**605**	**605**	**625**
Depth (m):	**186**	**196**	**225**	**90**	**100**	**107.5**	**109**	**140**	**140**
Position	II zone	II zone	II zone	I zone	I zone	I zone	I zone	I zone	III zone
SiO_2(wt. %)	66.42	68.50	67.70	68.46	59.05	51.06	62.46	46.05	62.28
Al_2O_3	12.94	10.87	10.45	11.78	15.98	9.83	14.76	11.93	14.24
Fe_2O_3	9.10	7.29	6.37	9.94	7.24	18.99	9.27	12.77	5.24
MnO	0.16	0.08	0.12	0.06	0.09	0.06	0.06	0.09	0.10
MgO	3.18	3.85	2.60	1.89	4.99	0.43	3.90	2.64	3.09
CaO	0.00	0.69	1.49	0.66	2.82	2.53	0.20	9.10	2.81
Na_2O	0.00	0.00	0.91	0.22	3.10	0.09	0.00	3.58	0.29
K_2O	1.29	2.52	2.26	3.01	2.62	1.15	2.13	1.03	5.97
TiO_2	0.61	0.45	0.39	0.12	0.75	0.65	0.63	0.51	0.23
P_2O_5	0.22	0.10	0.06	0.00	0.12	1.35	0.11	0.18	0.16
PF	5.76	4.94	5.88	4.10	3.26	13.77	6.62	11.52	5.80
Total	**99.68**	**99.29**	**98.23**	**100.24**	**100.01**	**99.91**	**100.14**	**99.40**	**100.21**
As (ppm)	0.00	1.26	1.08	14.25	0.00	124.00	0.00	0.00	0.00
Ba	66.17	404.20	568.70	492.50	131.40	193.00	151.90	131.00	903.20
Be	2.64	1.84	0.94	2.73	2.08	4.58	4.57	1.43	1.53
Bi	3.45	0.71	2.20	0.11	0.19	0.21	0.36	0.23	0.20
Cd	0.68	6.98	15.98	0.00	0.50	16.00	0.52	0.00	0.00
Co	33.77	20.78	17.11	15.94	21.47	47.20	13.43	20.10	5.51
Cr	115.20	89.13	73.41	23.54	169.00	81.30	119.90	90.70	33.22
Cs	3.90	5.85	2.70	1.09	3.72	3.64	8.03	2.41	2.45
Cu	39.36	50.66	146.20	60.30	58.77	45.30	46.23	63.90	20.15
Ga	17.97	14.73	13.38	18.26	31.38	11.90	20.45	14.60	19.39
Ge	1.56	1.61	1.24	1.65	1.78	1.14	1.62	1.13	1.33
Hf	3.94	3.02	2.46	1.92	4.15	0.97	3.51	2.72	6.11
In	0.34	0.00	0.00	0.00	0.00	0.00	0.00	0.00	0.00
Mo	0.00	2.60	7.93	1.66	9.00	13.60	0.00	1.82	0.00
Nb	9.29	10.28	12.55	3.58	16.10	9.05	9.87	6.54	9.74
Ni	101.40	111.50	56.54	36.61	75.53	113.00	62.75	67.30	31.17
Pb	68.44	564.34	1471.60	24.02	20.70	181.00	23.79	25.60	52.11
Rb	62.51	115.70	92.04	79.96	202.70	55.60	118.00	52.60	149.50
Sb	0.00	0.00	0.00	0.00	0.00	0.44	0.00	0.14	0.24
Sn	3.38	2.21	2.21	0.00	1.15	2.04	2.14	2.24	1.87
Sr	23.05	36.34	71.54	56.36	110.40	22.10	33.04	66.40	84.86
Ta	0.85	0.77	1.42	0.50	1.56	0.74	0.89	0.66	0.96
Th	8.14	8.16	8.51	8.77	41.44	5.61	8.95	10.60	17.89
U	2.77	6.26	4.23	2.41	8.00	212.00	3.71	11.90	5.19
V	90.59	208.00	127.90	66.46	264.50	112.00	130.00	137.00	70.60
W	3.11	1.80	3.49	0.38	0.50	4.78	1.63	1.58	0.85
Y	16.01	26.02	24.46	8.95	61.08	66.40	15.59	21.00	29.34
Zn	4446.00	3423.00	3392.00	94.65	214.40	994.00	231.90	112.00	65.27
Zr	146.70	108.80	86.48	59.31	148.30	35.00	125.90	96.50	204.70
La	34.85	28.58	26.14	15.30	77.77	15.00	25.96	19.00	73.91
Ce	67.58	54.20	47.48	29.05	158.20	30.80	45.35	37.70	146.50
Pr	8.55	6.76	5.85	3.64	18.52	5.75	5.26	4.53	16.92
Nd	32.59	25.45	21.70	12.68	68.36	28.60	19.00	17.70	62.02
Sm	6.16	4.91	4.16	2.18	13.29	8.54	3.45	3.68	10.75
Eu	1.27	0.83	0.70	0.50	1.26	1.83	0.45	0.80	1.29
Gd	4.53	4.30	3.62	1.53	10.76	11.10	2.94	3.90	8.15
Tb	0.61	0.68	0.58	0.24	1.59	1.74	0.47	0.59	1.12
Dy	3.14	4.04	3.60	1.40	9.51	10.90	2.88	3.64	5.89
Ho	0.57	0.82	0.74	0.27	1.86	2.34	0.58	0.70	1.06
Er	1.64	2.35	2.24	0.81	5.36	6.14	1.72	1.98	2.88
Tm	0.25	0.35	0.35	0.12	0.82	0.86	0.28	0.26	0.43
Yb	1.82	2.40	2.42	0.90	5.55	5.62	2.04	1.89	3.02
Lu	0.30	0.39	0.38	0.14	0.84	0.83	0.33	26.00	0.50

Annex II Paleoproterozoic formations (Suite)

	Graphite - biotite fresh gneisses and schists								
DDH no.:	**625**	**625**	**625**	**654**	**654**	**654**	**654**	**654**	**751**
Depth (m):	**144**	**154**	**157**	**146**	**147**	**151**	**215**	**310**	**74**
Position	III zone	III zone	III zone	III zone	III zone	III zone	III zone	III zone	North from I
SiO_2(wt. %)	59.84	63.70	60.85	64.26	62.60	60.07	76.65	65.66	56.16
Al_2O_3	11.89	15.31	9.32	14.34	13.81	13.13	12.52	14.80	11.30
Fe_2O_3	2.31	1.76	5.66	7.50	6.38	8.73	2.06	5.83	14.68
MnO	0.16	0.03	0.08	0.16	0.12	0.08	0.00	0.04	0.05
MgO	1.64	0.99	2.75	1.05	1.10	3.22	1.11	2.34	7.59
CaO	9.52	4.04	7.77	2.53	3.36	1.41	2.25	2.37	0.92
Na_2O	0.13	0.50	0.12	0.27	0.30	0.33	3.23	4.12	0.00
K_2O	2.91	8.26	1.52	4.92	5.52	2.07	1.05	1.77	2.00
TiO_2	0.10	0.10	0.32	0.00	0.00	0.47	0.14	0.34	0.68
P_2O_5	0.05	0.17	0.10	0.06	0.00	0.14	0.05	0.05	0.13
PF	11.01	4.98	10.82	5.19	5.71	10.82	1.41	2.51	6.30
Total	**99.56**	**99.84**	**99.31**	**100.28**	**98.90**	**100.47**	**100.47**	**99.83**	**99.81**
As (ppm)	11.23	1.77	3.40	4.11	15.23	13.26	0.00	1.90	0.00
Ba	106.10	732.10	63.53	202.10	180.30	272.50	137.80	442.20	121.00
Be	0.00	0.00	1.68	3.44	2.58	2.80	3.14	1.94	4.09
Bi	0.20	0.08	0.31	0.00	0.00	0.94	0.00	0.00	0.30
Cd	0.00	0.00	0.00	0.42	0.00	0.45	0.00	0.00	1.30
Co	7.51	2.89	12.93	0.83	1.74	36.57	1.51	11.51	56.45
Cr	22.85	25.05	54.34	9.51	0.00	91.40	7.28	67.48	390.00
Cs	5.14	5.17	4.82	2.97	6.84	7.06	3.06	4.61	14.81
Cu	17.39	9.05	24.70	9.02	0.00	59.58	10.59	24.51	49.57
Ga	14.67	14.94	11.44	21.44	20.89	18.17	20.88	21.42	16.50
Ge	0.80	1.52	0.98	1.70	1.57	0.82	1.63	1.86	1.98
Hf	1.45	1.90	2.11	1.35	1.93	2.81	4.73	2.68	2.87
In	0.00	0.00	0.00	0.00	0.00	0.00	0.00	0.00	0.00
Mo	5.69	1.51	6.25	3.00	6.83	16.75	1.70	4.21	0.00
Nb	1.41	3.05	7.27	7.15	2.46	7.79	10.10	13.54	10.80
Ni	25.89	17.74	48.51	6.13	10.62	120.30	0.00	42.54	368.70
Pb	20.00	64.91	15.09	69.16	57.05	32.11	21.30	24.39	5.95
Rb	147.60	224.60	82.33	156.20	193.60	105.90	61.04	123.80	140.10
Sb	0.16	0.26	0.26	0.00	0.00	0.22	0.00	0.00	0.00
Sn	0.95	2.05	1.99	1.13	0.98	2.91	1.64	1.32	4.43
Sr	75.04	87.69	53.64	42.80	51.48	40.05	124.90	118.00	25.23
Ta	0.18	0.50	0.76	1.76	0.58	0.91	1.34	1.83	0.80
Th	7.07	3.80	7.60	9.52	14.20	8.58	21.43	13.18	5.64
U	7.45	10.87	5.91	3.63	31.62	76.30	7.89	8.67	1.73
V	39.65	39.01	81.01	24.70	11.49	168.00	8.72	131.40	109.90
W	0.43	0.81	1.16	0.34	0.00	1.89	0.88	0.86	1.42
Y	23.14	18.98	21.88	12.41	24.46	18.70	49.92	30.64	13.12
Zn	30.37	30.73	84.43	58.61	85.41	73.72	50.71	117.30	259.10
Zr	40.30	48.46	69.06	28.34	41.81	103.40	151.70	87.13	105.50
La	14.20	9.48	27.73	10.64	9.30	17.02	61.62	24.61	21.03
Ce	28.71	18.73	57.36	18.56	18.33	32.20	128.40	47.75	38.67
Pr	3.34	2.36	6.75	1.90	2.02	4.09	14.99	5.94	5.56
Nd	12.77	9.50	25.12	5.94	6.74	15.25	54.71	22.01	21.11
Sm	2.62	2.53	4.98	1.22	1.65	3.15	10.74	4.65	3.68
Eu	0.52	0.73	0.69	0.33	0.29	0.47	0.81	0.88	0.82
Gd	2.65	2.82	4.29	1.17	1.84	2.93	8.86	4.22	2.69
Tb	0.49	0.51	0.66	0.24	0.42	0.47	1.43	0.75	0.40
Dy	3.34	3.26	3.79	1.77	3.20	2.96	8.51	4.73	2.37
Ho	0.73	0.67	0.72	0.39	0.72	0.59	1.65	0.97	0.46
Er	2.19	1.88	1.97	1.30	2.45	1.70	4.62	2.91	1.38
Tm	0.36	0.32	0.29	0.25	0.46	0.26	0.71	0.49	0.22
Yb	2.56	2.19	1.88	1.88	3.58	1.72	4.62	3.43	1.50
Lu	0.43	0.34	0.28	0.30	0.55	0.27	0.68	0.54	0.24

Annex II Paleoproterozoic formations (Suite)

	Graphite - biotite fresh gneisses and schists								
DDH no.:	**751-75**	**751-80**	**751-87**	**822-160**	**822-168**	**835-245**	**835-247**	**843-150**	**843-154**
Depth (m):	**75**	**80**	**87**	**160**	**168**	**245**	**247**	**150**	**154**
Position	To north from the ore zone I			To north from zone III		Matala zone		I zone	I zone
SiO_2(wt. %)	27.67	62.72	55.31	72.66	61.90	45.08	57.72	68.69	59.58
Al_2O_3	6.84	10.66	16.88	8.55	10.73	22.55	16.20	14.00	11.89
Fe_2O_3	6.64	10.82	7.87	4.54	4.33	15.33	12.04	8.49	4.77
MnO	0.88	0.08	0.11	0.08	0.15	0.08	0.08	0.05	0.32
MgO	4.73	6.13	5.78	1.03	1.72	2.89	2.71	1.26	2.55
CaO	26.33	0.17	1.38	3.99	5.47	1.41	1.56	0.00	7.46
Na_2O	0.00	0.26	2.52	0.24	0.31	0.19	0.17	0.00	0.16
K_2O	1.17	1.45	2.73	3.32	4.58	4.35	2.05	1.16	2.47
TiO_2	0.47	0.56	0.74	0.46	0.44	1.12	0.64	0.48	0.39
P_2O_5	0.11	0.11	0.03	1.92	0.00	0.72	0.13	0.05	0.03
PF	23.95	7.40	6.76	2.91	9.24	6.19	6.55	4.85	10.32
Total	98.79	100.36	100.11	99.70	98.87	99.91	99.85	99.03	99.94
As (ppm)	1.21	1.47	1.67	9.48	1.40	0.00	24.22	30.11	36.30
Ba	60.89	144.10	214.20	616.10	1099.00	252.40	341.80	61.83	79.49
Be	3.75	4.51	6.17	3.50	0.00	5.35	3.12	4.42	1.53
Bi	0.45	0.55	0.35	0.34	0.44	0.42	0.52	0.00	0.00
Cd	10.28	0.00	0.00	2.58	0.61	0.00	0.00	0.00	0.97
Co	138.00	41.92	24.63	8.60	8.85	27.70	26.89	9.61	18.87
Cr	1270.00	116.60	149.20	32.31	85.30	842.10	137.40	81.57	63.58
Cs	4.42	6.78	12.84	2.79	2.19	8.24	3.77	2.29	3.24
Cu	95.20	89.28	107.90	294.20	34.23	18.28	45.98	32.75	22.73
Ga	10.21	14.43	25.91	15.34	13.34	33.48	23.07	23.73	16.08
Ge	1.69	2.34	1.80	2.05	1.20	2.42	1.93	1.63	0.84
Hf	0.84	3.29	4.18	4.63	2.56	3.62	3.20	5.26	3.65
In	0.00	0.00	0.00	0.30	0.00	0.10	0.00	0.00	0.00
Mo	0.00	3.70	5.92	1.03	5.34	1.19	3.03	4.17	9.49
Nb	6.46	7.53	58.15	14.21	6.90	17.87	6.42	10.56	9.72
Ni	594.70	171.70	95.95	21.76	22.83	271.80	131.70	30.22	73.06
Pb	8.34	11.55	18.99	75.49	39.98	47.97	39.72	21.51	13.74
Rb	75.43	92.12	180.10	107.00	112.20	171.30	66.26	57.19	124.90
Sb	0.00	0.00	0.00	0.31	0.11	0.00	0.00	0.00	0.00
Sn	2.66	1.33	4.05	13.73	1.61	1.87	1.24	0.50	0.53
Sr	59.13	45.75	99.70	83.48	108.10	26.40	40.52	22.57	49.13
Ta	0.46	0.74	10.45	1.16	0.68	1.42	0.57	0.73	0.75
Th	0.45	7.82	9.96	29.82	6.97	10.67	8.06	204.70	45.66
U	2.02	13.48	4.55	29.79	10.00	48.97	10.92	7.92	3.89
V	123.30	173.00	188.70	155.70	169.60	253.40	203.00	116.20	94.38
W	1.26	1.56	1.42	2.98	1.63	4.66	2.25	1.29	0.33
Y	22.19	13.89	19.15	72.51	20.64	41.94	20.66	15.49	18.38
Zn	120.70	178.20	188.30	321.70	112.30	209.10	187.70	57.02	185.30
Zr	31.10	123.50	153.10	170.20	89.17	122.00	117.70	162.70	111.10
La	22.06	5.30	34.74	64.80	33.12	34.10	25.78	126.30	30.02
Ce	40.56	11.19	68.69	136.70	67.95	68.09	50.30	243.40	61.83
Pr	5.73	1.49	8.59	19.80	8.62	9.02	6.07	28.03	7.47
Nd	24.37	6.17	32.43	86.47	31.79	36.50	22.88	103.50	29.09
Sm	5.03	1.85	6.45	18.96	6.31	7.44	4.41	16.33	6.06
Eu	1.44	0.47	0.64	3.64	1.03	2.53	1.07	0.84	1.01
Gd	4.75	2.12	4.87	17.37	4.79	7.28	3.92	9.77	4.71
Tb	0.69	0.35	0.71	2.20	0.74	1.19	0.61	1.06	0.63
Dy	3.71	2.16	3.78	11.06	4.15	7.25	3.55	4.30	3.29
Ho	0.68	0.45	0.66	2.02	0.78	1.45	0.69	0.59	0.58
Er	1.68	1.31	1.93	4.87	2.16	3.92	1.94	1.31	1.48
Tm	0.21	0.20	0.30	0.62	0.34	0.56	0.29	0.15	0.21
Yb	1.30	1.42	2.23	3.78	2.40	3.47	2.02	0.86	1.28
Lu	0.19	0.24	0.35	0.58	0.37	0.53	0.32	0.14	0.21

Annex II Paleoproterozoic formations (Suite)

	Graphite - biotite fresh gneisses and schists	
DDH no.:	**843**	**843**
Depth (m):	**217**	**250**
Position	I zone	I zone
SiO_2(wt. %)	58.23	59.63
Al_2O_3	18.02	13.69
Fe_2O_3	5.35	6.27
MnO	0.04	0.06
MgO	1.83	5.60
CaO	3.36	2.62
Na_2O	0.15	2.63
K_2O	3.41	3.39
TiO_2	0.89	0.68
P_2O_5	0.16	0.10
PF	8.43	4.12
Total	99.87	98.79
As (ppm)	0.00	0.00
Ba	225.10	726.50
Be	1.74	1.51
Bi	0.00	0.27
Cd	0.00	0.78
Co	21.12	21.79
Cr	129.00	131.20
Cs	4.49	5.03
Cu	205.00	41.69
Ga	25.95	17.11
Ge	0.72	1.29
Hf	6.27	4.13
In	0.00	0.00
Mo	5.08	5.86
Nb	19.11	7.48
Ni	69.41	81.84
Pb	19.48	17.93
Rb	178.30	115.10
Sb	0.00	0.00
Sn	5.10	1.10
Sr	46.85	166.60
Ta	1.16	0.61
Th	5.80	9.92
U	4.67	4.40
V	143.80	177.30
W	0.80	0.81
Y	10.70	12.36
Zn	260.50	137.40
Zr	211.90	148.20
La	17.17	29.93
Ce	27.71	47.93
Pr	3.12	5.19
Nd	11.17	18.07
Sm	2.21	2.98
Eu	0.86	0.88
Gd	2.11	2.54
Tb	0.31	0.36
Dy	1.76	2.10
Ho	0.34	0.41
Er	0.94	1.16
Tm	0.14	0.17
Yb	0.96	1.16
Lu	0.16	0.20

Annex III Yablonevka area (DDH-103) – Western part of the Pasha – Ladoga basin
Major and trace element analysis of the Paleoproterozoic gneisses, schists and granites and the Mesoproterozoic (Riphean) sandstones

DDH no.:	**103**	**103**	**103**	**103**	**103**	**103**	**103**	**103**	**103**	**103**
Depth (m):	**100**	**115**	**136**	**138**	**151**	**152**	**156**	**157**	**171**	**176**
Rock type	sandstone	sandstone	sandstone	sandstone	sandstone	sandstone	gneiss	gneiss	gneiss	gneiss
SiO_2(wt. %)	80.98	82.50	74.37	70.84	69.96	75.11	60.24	58.25	61.76	63.63
Al_2O_3	7.72	6.61	9.02	13.33	15.32	11.08	15.83	17.22	17.35	16.87
Fe_2O_3	3.53	2.27	1.63	5.15	4.68	5.45	9.86	8.91	7.26	4.85
MnO	0.00	0.10	0.14	0.00	0.00	0.00	0.03	0.00	0.04	0.09
MgO	0.93	1.07	2.26	1.74	1.08	0.82	2.52	2.85	2.81	2.35
CaO	0.21	0.81	2.15	0.12	0.17	0.00	0.19	0.00	0.46	0.84
Na_2O	0.00	0.00	0.00	0.16	0.00	0.00	0.00	0.24	0.20	0.00
K_2O	3.13	2.90	3.53	3.87	4.13	3.68	4.88	7.29	3.36	5.32
TiO_2	0.40	0.24	0.36	0.46	0.45	0.35	0.89	0.86	0.95	0.55
P_2O_5	0.21	0.07	0.12	0.15	0.13	0.08	0.16	0.08	0.26	0.20
PF	2.61	3.17	6.16	4.03	4.40	3.08	5.16	4.09	5.48	5.09
Total	**99.72**	**99.74**	**99.74**	**99.85**	**100.32**	**99.65**	**99.76**	**99.79**	**99.93**	**99.79**
As (ppm)	1.38	0.00	0.00	3.46	2.95	3.43	1.87	1.07	0.00	0.00
Ba	572.60	516.90	561.40	626.90	613.20	510.40	585.80	841.60	781.60	874.60
Be	1.27	0.95	1.82	3.67	3.37	2.93	3.21	2.66	2.55	1.45
Bi	0.99	0.00	0.00	0.22	0.00	0.20	0.00	0.00	0.00	0.00
Cd	0.00	0.00	0.00	0.00	0.00	0.00	0.41	0.00	0.54	0.00
Co	12.55	3.37	5.17	7.02	5.17	4.26	9.81	14.84	11.25	7.01
Cr	23.55	19.56	33.41	28.81	27.03	25.65	75.75	159.90	44.88	50.07
Cs	1.46	1.28	1.86	6.14	5.32	4.36	9.54	8.57	3.83	5.89
Cu	6.91	13.03	13.81	15.36	23.57	9.72	10.99	6.21	14.91	15.96
Ga	9.72	8.28	12.17	18.04	19.78	15.59	29.73	29.89	25.88	21.05
Ge	1.20	1.08	1.12	1.25	1.17	1.22	2.02	1.78	1.84	1.80
Hf	4.36	3.31	5.91	5.95	7.48	5.57	11.55	6.20	17.86	4.47
In	0.00	0.00	0.00	0.00	0.00	0.00	0.15	0.14	0.10	0.00
Mo	0.00	0.00	0.00	0.00	0.74	0.00	0.94	0.00	0.52	0.58
Nb	6.83	5.28	8.40	11.64	11.13	9.63	36.38	18.26	26.41	11.30
Ni	22.15	9.46	13.49	20.28	17.25	12.90	27.56	51.98	19.06	16.26
Pb	10.61	10.08	8.68	13.67	17.68	14.59	18.41	19.97	13.22	9.00
Rb	83.79	76.66	98.72	158.20	159.00	141.80	251.50	309.30	175.00	136.10
Sb	0.00	0.00	0.00	0.63	0.51	0.40	0.00	0.00	0.00	0.00
Sn	1.09	0.86	1.13	2.99	2.23	1.95	4.16	3.02	1.58	1.63
Sr	70.81	58.79	80.95	100.60	101.90	111.90	54.41	69.53	48.81	31.74
Ta	0.56	0.43	0.60	1.10	1.09	1.01	2.69	1.22	2.27	1.01
Th	6.66	4.28	6.07	13.42	15.53	13.72	41.88	17.37	44.56	11.94
U	2.37	1.17	3.61	2.07	2.60	1.70	6.80	3.74	5.80	3.08
V	30.85	26.17	33.44	30.20	26.64	22.63	59.58	96.83	69.75	66.32
W	0.39	0.37	0.56	2.30	2.34	2.56	2.34	1.04	0.66	2.87
Y	15.56	11.51	18.22	26.63	29.45	19.79	57.96	38.33	85.10	33.94
Zn	35.53	20.46	28.71	73.43	57.03	42.85	195.40	199.80	111.00	123.30
Zr	171.50	135.10	253.00	220.00	280.30	199.00	469.40	230.80	721.50	161.20
La	20.34	14.79	23.07	37.77	46.81	47.27	111.10	55.31	133.60	47.94
Ce	39.08	28.34	44.41	82.72	91.02	86.50	225.10	111.20	268.10	87.68
Pr	4.74	3.43	5.10	8.90	9.69	10.27	26.55	13.11	32.19	10.92
Nd	17.78	13.23	19.44	33.18	34.27	36.59	99.76	50.02	120.80	40.71
Sm	3.50	2.53	3.77	5.91	6.09	6.06	18.67	9.30	21.97	7.30
Eu	0.79	0.62	0.87	1.09	1.16	1.08	1.45	1.41	1.83	1.42
Gd	2.93	2.11	3.31	4.81	5.15	4.23	14.74	7.45	18.26	5.86
Tb	0.45	0.32	0.52	0.75	0.83	0.62	1.95	1.10	2.59	0.91
Dy	2.65	1.93	3.01	4.48	4.93	3.51	10.26	6.43	15.06	5.34
Ho	0.52	0.38	0.58	0.90	0.98	0.69	1.96	1.29	3.02	1.08
Er	1.45	1.11	1.69	2.69	2.90	2.04	5.72	3.84	9.09	3.12
Tm	0.22	0.18	0.27	0.42	0.46	0.32	0.87	0.59	1.39	0.46
Yb	1.48	1.22	1.72	2.95	3.18	2.18	6.08	3.99	9.62	3.12
Lu	0.24	0.19	0.27	0.46	0.50	0.34	0.98	0.64	1.54	0.49

Annex IV Pasha area (DDH-11, DDH-14) – South-Eastern part of the Pasha – Ladoga basin
Major and trace element analysis of the Paleoproterozoic gneisses, schists and granites and the Mesoproterozoic (Riphean) sandstones

DDH no.:	**11**	**11**	**11**	**11**	**11**	**11**	**11**	**11**	**11**
Depth (m):	**180**	**229**	**230**	**237**	**255**	**260**	**269**	**270**	**281**
Rock type	sandstone	sandstone	sandstone	sandstone	sandstone	sandstone	gneiss	gneiss	gneiss
SiO_2(wt. %)	91.94	58.49	93.37	91.17	89.77	90.85	61.55	62.46	64.93
Al_2O_3	4.08	16.26	2.13	5.32	6.49	4.31	16.21	17.13	8.01
Fe_2O_3	0.42	6.26	0.47	0.25	0.41	2.08	10.04	8.34	4.49
MnO	0.00	0.04	0.14	0.00	0.00	0.00	0.04	0.00	0.59
MgO	0.00	1.39	0.44	0.00	0.00	0.00	2.64	2.18	4.80
CaO	0.00	0.16	0.70	0.00	0.00	0.00	0.00	0.16	5.04
Na_2O	0.00	0.00	0.00	0.00	0.00	0.00	0.00	0.00	0.00
K_2O	2.17	3.38	0.38	1.44	1.04	0.73	4.10	2.34	1.99
TiO_2	0.18	0.85	0.03	0.03	0.07	0.36	0.70	0.77	0.56
P_2O_5	0.00	0.06	0.00	0.00	0.00	0.00	0.10	0.18	0.06
PF	0.89	12.91	2.10	1.45	1.98	1.44	4.35	5.70	9.30
Total	**99.68**	**99.80**	**99.76**	**99.66**	**99.76**	**99.77**	**99.73**	**99.26**	**99.77**
As (ppm)	0.00	7.35	1.25	1.12	3.11	4.94	2.59	2.22	0.00
Ba	345.30	579.20	39.42	177.50	104.70	84.52	374.90	167.90	109.10
Be	0.00	1.72	0.00	0.59	0.74	1.19	2.95	4.19	0.93
Bi	0.00	0.29	0.00	0.00	0.00	0.00	0.00	0.00	0.00
Cd	0.00	1.70	0.00	0.00	0.00	0.00	0.00	0.00	0.00
Co	1.50	9.27	1.22	1.18	1.31	1.54	17.13	20.10	10.01
Cr	15.91	79.17	13.27	8.10	11.45	25.12	136.20	130.20	80.20
Cs	0.86	3.38	0.42	0.60	0.93	0.66	9.16	6.84	2.05
Cu	0.00	49.20	0.00	0.00	0.00	5.61	27.36	30.32	5.62
Ga	4.49	20.95	2.62	4.01	6.48	5.32	27.96	27.02	12.32
Ge	1.09	1.35	0.81	0.78	0.83	0.98	2.05	1.50	0.84
Hf	5.99	9.91	1.51	1.78	2.75	5.30	6.85	4.64	2.46
In	0.00	0.00	0.00	0.00	0.00	0.00	0.00	0.00	0.00
Mo	0.00	2.66	0.00	0.00	0.00	0.76	0.00	0.00	0.00
Nb	4.65	19.03	2.34	0.80	2.49	10.68	14.17	11.62	12.32
Ni	7.15	45.57	6.74	6.30	5.70	8.70	44.89	62.77	37.75
Pb	8.19	165.67	6.37	6.10	4.56	9.01	15.16	7.70	6.94
Rb	56.14	112.40	13.24	41.46	39.11	26.84	258.70	156.50	91.64
Sb	0.00	0.39	0.00	0.00	0.00	0.00	0.00	0.00	0.00
Sn	0.65	2.72	0.43	0.65	0.74	26.21	1.05	0.60	0.00
Sr	35.94	77.57	15.06	32.36	27.24	69.09	56.90	17.78	23.78
Ta	0.42	1.64	0.72	0.09	0.35	2.52	1.03	1.22	0.73
Th	4.68	22.33	3.60	3.79	8.51	41.44	20.75	11.05	10.02
U	3.38	5.47	1.53	1.66	3.36	1.66	4.07	3.21	4.10
V	11.84	100.10	5.25	3.11	6.02	21.95	108.60	99.96	92.00
W	0.49	1.32	0.60	0.00	0.00	1.17	0.67	0.85	0.42
Y	13.31	38.48	8.03	5.86	9.42	17.92	55.18	22.43	17.56
Zn	12.48	308.00	10.53	8.51	10.75	12.44	139.00	116.00	94.92
Zr	237.30	360.70	50.86	58.17	95.10	209.00	251.20	174.70	98.86
La	12.07	71.95	9.92	9.06	17.16	57.03	62.08	30.83	32.46
Ce	23.39	142.70	16.47	18.77	34.10	95.23	130.20	64.86	62.55
Pr	2.71	17.38	2.31	2.07	3.97	12.49	14.75	7.66	7.43
Nd	9.85	64.27	8.46	7.73	14.44	42.88	54.61	29.05	26.85
Sm	2.01	11.61	1.66	1.46	2.72	7.12	10.13	5.84	4.85
Eu	0.46	1.87	0.29	0.29	0.37	0.60	1.14	0.75	0.77
Gd	1.91	8.90	1.42	1.17	2.14	5.02	8.49	5.07	3.90
Tb	0.34	1.31	0.24	0.17	0.32	0.75	1.35	0.75	0.56
Dy	2.22	7.30	1.40	0.96	1.75	3.77	8.69	4.20	3.09
Ho	0.45	1.39	0.27	0.19	0.32	0.66	1.86	0.77	0.57
Er	1.35	3.87	0.77	0.55	0.92	1.80	5.51	2.20	1.60
Tm	0.22	0.57	0.12	0.08	0.14	0.26	0.84	0.32	0.23
Yb	1.47	3.82	0.80	0.56	0.90	1.71	5.83	2.29	1.54
Lu	0.24	0.59	0.13	0.09	0.15	0.27	0.91	0.37	0.25

Annex IV (Suite)

DDH no.:	**11**	**11**	**11**	**14**	**14**	**14**	**14**	**14**	**14**
Depth (m):	**283**	**287**	**291**	**259**	**276**	**289**	**301**	**312**	**313**
Rock type	gneiss	gneiss	gneiss	sandstone	sandstone	gneiss	schist	gneiss	granite
SiO_2(wt. %)	61.00	75.06	58.76	88.88	91.55	70.19	67.08	69.93	79.41
Al_2O_3	15.03	14.11	16.84	5.98	5.02	17.22	14.90	15.19	12.63
Fe_2O_3	7.96	0.85	9.28	0.74	0.59	2.71	4.97	2.87	0.00
MnO	0.11	0.00	0.06	0.00	0.00	0.00	0.06	0.00	0.00
MgO	4.10	0.66	4.19	0.00	0.00	0.37	2.49	0.82	0.00
CaO	0.76	0.47	0.34	0.00	0.00	0.00	3.64	1.65	0.00
Na_2O	0.26	0.15	0.18	0.00	0.00	0.16	1.92	3.49	6.66
K_2O	5.69	1.18	4.42	2.42	1.83	4.04	2.05	4.60	0.80
TiO_2	0.67	1.03	0.87	0.13	0.04	0.28	0.55	0.37	0.00
P_2O_5	0.10	0.31	0.11	0.04	0.06	0.20	0.22	0.15	0.06
PF	4.22	6.01	4.81	1.45	1.11	4.63	1.95	0.88	0.15
Total	**99.90**	**99.83**	**99.86**	**99.64**	**100.20**	**99.80**	**99.83**	**99.95**	**99.71**
As (ppm)	0.00	0.00	0.00	1.71	2.54	0.00	0.00	0.00	0.00
Ba	1012.00	52.30	1100.00	266.10	208.90	1270.00	300.40	1438.00	113.80
Be	1.56	1.60	1.92	0.93	0.00	1.62	2.12	1.14	0.00
Bi	0.00	0.00	0.00	0.00	0.00	0.00	0.00	0.00	0.00
Cd	0.00	0.77	0.00	0.00	0.00	0.00	0.00	0.00	0.00
Co	17.08	12.11	21.35	1.51	0.54	4.13	14.18	4.46	0.00
Cr	130.10	157.50	145.40	6.21	4.02	9.95	80.67	23.69	0.00
Cs	2.47	0.71	2.60	1.32	0.97	2.79	1.51	2.24	0.00
Cu	21.32	34.61	0.00	7.32	10.76	8.15	49.10	7.94	0.00
Ga	21.92	14.77	25.98	6.56	4.54	20.38	18.12	18.76	13.50
Ge	1.69	1.61	1.46	0.86	0.88	0.92	1.46	1.26	1.14
Hf	4.49	10.14	6.91	3.63	1.40	4.98	4.63	4.21	0.67
In	0.00	0.00	0.00	0.00	0.00	0.00	0.00	0.00	0.00
Mo	1.03	0.00	0.00	0.00	0.00	0.00	0.00	1.99	0.00
Nb	16.60	16.03	17.58	3.72	2.37	6.63	9.31	9.50	1.34
Ni	49.20	32.81	70.68	0.00	0.00	6.00	34.49	5.66	0.00
Pb	42.35	35.67	16.91	8.14	8.39	11.05	15.26	20.37	4.06
Rb	183.50	33.64	138.10	72.13	52.26	104.70	81.96	97.42	7.28
Sb	0.00	0.00	0.00	0.00	0.21	0.00	0.00	0.00	0.00
Sn	0.57	0.79	0.62	1.33	2.76	0.52	0.46	1.03	1.42
Sr	96.03	33.15	64.09	64.76	45.78	114.00	203.20	346.20	26.29
Ta	1.24	1.34	1.27	0.38	0.81	0.39	0.95	0.71	0.23
Th	16.70	13.69	18.21	7.80	7.98	3.76	11.43	5.57	1.40
U	7.49	5.08	2.91	1.23	0.95	1.23	2.65	5.72	0.50
V	146.80	133.80	138.60	8.24	4.87	18.13	85.42	34.37	0.00
W	0.21	2.73	0.20	0.32	0.32	0.35	0.53	0.86	0.00
Y	45.27	20.63	36.23	13.32	6.26	7.39	18.60	8.61	13.30
Zn	139.60	68.69	155.20	10.20	0.00	50.91	80.06	52.09	0.00
Zr	156.30	444.50	249.70	139.20	48.60	202.50	174.80	167.80	26.76
La	41.87	11.26	52.61	21.07	12.93	23.08	32.76	28.57	21.02
Ce	84.85	23.14	107.00	36.98	27.48	42.25	69.61	52.47	40.69
Pr	10.05	2.96	12.57	4.82	2.84	4.27	8.05	5.57	4.39
Nd	37.06	12.58	47.05	18.19	10.01	15.22	30.05	19.69	14.94
Sm	7.11	3.11	8.51	3.33	1.91	2.56	5.53	3.40	3.06
Eu	1.37	1.03	1.18	0.66	0.26	1.08	0.87	0.99	1.50
Gd	5.90	2.98	6.76	2.37	1.35	1.93	4.14	2.46	2.47
Tb	0.99	0.48	1.03	0.36	0.20	0.24	0.62	0.37	0.41
Dy	6.79	3.05	6.34	2.10	1.15	1.22	3.43	1.78	2.30
Ho	1.51	0.67	1.26	0.42	0.21	0.22	0.66	0.26	0.43
Er	4.67	2.02	3.76	1.25	0.61	0.58	1.89	0.59	1.22
Tm	0.72	0.31	0.57	0.19	0.09	0.08	0.27	0.08	0.18
Yb	5.05	2.09	4.01	1.32	0.62	0.49	1.83	0.47	1.13
Lu	0.79	0.35	0.63	0.22	0.10	0.08	0.29	0.08	0.17

Annex V Salmi Rapakivi Granites
Major and trace element analysis of the Salmi rapakivi granites

DDH no.:	**475**	**475**	**475**	**475**	**389**	**327**	**484**	**484**	**484**
Depth (m):	**110**	**110.5**	**113**	**116**	**189**	**191**	**97**	**103**	**121**
Rock type:	**granite**	**granite**	**granite**	**granite**	**granite**	**granite**	**granite**	**granite**	**granite**
SiO_2(wt. %)	65.80	66.48	71.42	65.60	70.02	48.78	73.30	76.66	79.27
Al_2O_3	15.08	15.30	16.22	14.32	12.79	13.86	15.12	12.49	11.27
Fe_2O_3	7.04	7.20	1.25	6.64	0.55	6.59	1.15	2.20	0.91
MnO	0.00	0.04	0.00	0.12	0.07	0.22	0.00	0.00	0.00
MgO	0.22	0.21	0.22	0.48	0.26	4.42	0.30	0.24	0.17
CaO	0.15	0.16	0.21	2.74	4.22	8.06	0.15	0.26	0.47
Na_2O	0.37	0.41	0.43	2.67	0.30	0.32	0.28	0.33	2.33
K_2O	6.90	7.43	6.97	5.26	5.50	6.59	5.58	6.13	5.09
TiO_2	0.52	0.55	0.54	0.55	0.00	0.56	0.20	0.15	0.10
P_2O_5	0.12	0.12	0.12	0.11	0.05	0.13	0.11	0.00	0.00
PF	2.97	2.87	3.04	0.80	6.04	9.66	3.48	2.43	0.74
Total	**99.16**	**100.77**	**100.43**	**99.30**	**99.80**	**99.20**	**99.66**	**100.88**	**100.34**
As (ppm)	1.85	2.64	0.84	3.11	0.00	0.00	1.23	0.00	1.09
Ba	2718.00	3027.00	2963.00	2457.00	719.80	1744.00	302.00	706.30	750.80
Be	2.88	1.81	1.67	2.89	0.00	1.84	0.00	3.05	2.60
Bi	0.11	0.09	0.14	0.10	0.00	0.47	0.00	0.08	0.00
Cd	0.40	0.41	0.51	1.01	0.57	2.45	0.00	0.00	0.00
Co	2.57	2.33	3.48	3.32	0.83	37.73	1.29	2.12	0.35
Cr	24.09	10.83	15.07	23.87	0.00	122.50	0.00	0.00	0.00
Cs	4.85	4.88	2.46	3.18	8.91	13.02	3.20	5.05	2.40
Cu	6.76	6.47	7.15	12.59	0.00	20.61	5.51	0.00	0.00
Ga	34.23	35.37	37.78	36.91	11.72	23.06	34.69	35.73	28.62
Ge	2.76	2.14	1.44	1.97	1.11	1.70	1.32	1.34	1.60
Hf	26.89	33.93	26.52	26.52	1.23	2.46	13.90	13.37	6.61
In	0.18	0.19	0.11	0.19	0.00	0.00	0.13	0.10	0.00
Mo	0.98	0.81	3.24	3.71	0.00	0.50	0.87	0.47	1.25
Nb	53.39	56.96	55.92	61.69	0.56	9.04	31.55	31.53	17.24
Ni	31.50	0.00	0.00	0.00	0.00	75.41	5.03	0.00	0.00
Pb	29.57	33.01	31.83	29.98	93.91	72.78	15.77	22.38	22.22
Rb	210.90	201.90	175.80	151.50	158.80	243.30	213.70	274.00	225.50
Sb	0.12	0.00	0.00	0.00	0.00	0.00	0.00	0.00	0.00
Sn	2.54	2.50	2.31	2.66	0.00	1.98	2.99	3.28	2.35
Sr	109.70	118.80	108.60	162.60	100.90	143.00	39.58	42.05	56.19
Ta	3.00	3.52	3.00	2.99	0.05	0.97	2.46	3.11	1.50
Th	15.53	11.41	19.99	14.55	12.43	7.39	24.52	37.69	9.55
U	2.45	2.81	6.66	3.32	0.80	4.56	4.38	36.77	8.25
V	44.21	13.56	18.75	20.18	17.87	140.30	5.99	14.93	0.00
W	2.16	2.44	1.93	1.17	0.12	0.98	0.78	1.63	0.43
Y	58.51	65.80	55.63	85.66	11.27	22.59	101.90	84.64	40.40
Zn	128.50	138.10	191.70	309.80	21.43	943.30	65.01	74.54	67.96
Zr	1256.00	1453.00	1226.00	1276.00	35.10	91.83	479.90	460.70	206.40
La	135.80	109.60	161.80	130.20	17.65	22.34	172.60	203.60	49.61
Ce	267.40	233.40	324.30	273.40	34.73	38.05	375.90	423.00	102.40
Pr	32.56	28.12	37.62	33.47	3.95	5.50	43.36	50.70	11.83
Nd	124.80	110.60	146.50	134.50	12.94	20.41	152.00	175.20	43.53
Sm	21.77	20.46	24.58	23.58	2.22	3.98	26.62	31.24	8.33
Eu	5.19	5.38	5.89	5.02	1.08	1.39	1.06	1.13	1.01
Gd	16.73	16.38	18.08	19.90	1.90	3.79	18.26	21.78	7.06
Tb	2.20	2.23	2.37	2.70	0.28	0.60	3.08	3.14	1.13
Dy	11.73	13.06	11.79	15.82	1.50	3.55	18.85	16.47	6.82
Ho	2.13	2.40	1.99	2.92	0.29	0.64	3.65	2.97	1.33
Er	5.99	6.95	5.47	8.06	0.71	1.98	10.71	8.40	3.91
Tm	0.88	1.03	0.75	1.13	0.10	0.29	1.60	1.19	0.60
Yb	5.95	6.78	5.27	7.50	0.57	2.15	11.13	8.06	4.27
Lu	0.96	1.14	0.88	1.26	0.09	0.33	1.67	1.19	0.64

Annex V Rapakivi granite (Suite)

DDH no., sample:	822	3-01	13-02	2097	751	412	412	412	412
Depth (m):	165				69	460.2	427.9	424.6	420.25
Rock type:	granite	granite	granite	granite	granite	granite	granite	granite	granite
SiO_2(wt. %)	62.66	75.01	76.33	74.35	87.21	79.48	74.20	76.54	75.85
Al_2O_3	18.12	12.30	12.73	13.45	6.42	12.53	17.15	13.09	12.83
Fe_2O_3	1.37	2.33	1.13	2.16	0.70	1.13	1.04	1.30	1.29
MnO	0.07	0.00	0.00	0.00	0.00	0.00	0.00	0.00	0.00
MgO	0.00	0.00	0.00	0.00	0.00	0.00	0.00	0.00	0.00
CaO	2.65	0.50	0.35	0.34	0.00	0.57	0.00	0.81	0.66
Na_2O	4.91	2.56	3.76	3.46	0.00	0.00	0.00	3.44	3.66
K_2O	7.57	5.18	4.32	4.72	2.44	3.40	4.71	2.98	4.71
TiO_2	0.00	0.20	0.04	0.15	0.33	0.06	0.00	0.06	0.03
P_2O_5	0.00	0.00	0.00	0.00	0.00	0.00	0.00	0.00	0.03
PF	2.37	0.68	0.62	0.79	1.68	2.55	2.66	1.57	0.74
Total	**99.72**	**98.76**	**99.28**	**99.42**	**98.78**	**99.72**	**99.76**	**99.79**	**99.80**
As (ppm)	0.00	3.02	1.07	1.33	2.77	0.00	0.00	1.04	1.50
Ba	966.60	661.40	23.60	517.00	438.30	13.86	26.40	31.32	36.15
Be	0.00	3.38	8.43	6.94	0.84	5.77	13.15	7.55	9.91
Bi	0.00	0.23	0.00	0.00	0.00	0.00	0.26	0.00	0.00
Cd	0.33	0.00	0.00	0.00	0.41	0.00	0.00	0.00	0.00
Co	1.77	1.16	0.48	1.11	2.49	0.64	0.51	0.64	0.47
Cr	0.00	7.35	4.14	5.02	7.07	152.50	171.30	94.43	147.00
Cs	1.54	4.59	10.03	2.42	0.79	2.38	3.54	3.19	7.68
Cu	0.00	0.00	0.00	0.00	13.84	0.00	0.00	0.00	5.56
Ga	18.50	27.52	47.51	28.97	8.27	40.53	55.57	45.29	46.28
Ge	0.98	2.04	2.85	1.73	0.98	2.04	2.42	2.34	2.54
Hf	5.22	8.17	11.61	6.88	7.62	8.98	13.30	10.32	9.95
In	0.76	0.13	0.00	0.00	0.00	0.00	0.00	0.00	0.00
Mo	0.83	2.89	0.00	0.50	0.67	0.00	2.44	0.00	5.41
Nb	1.50	26.03	74.77	28.33	14.61	122.60	17.32	100.30	89.96
Ni	0.00	0.00	0.00	0.00	7.05	6.74	5.34	5.01	7.56
Pb	38.80	32.65	19.08	27.91	15.99	5.64	5.66	16.74	43.33
Rb	197.10	223.10	535.30	318.20	70.02	352.90	498.90	296.50	483.10
Sb	0.00	0.00	0.00	0.00	0.00	0.00	0.00	0.00	0.00
Sn	11.97	2.59	4.67	4.65	2.18	12.35	13.62	14.46	13.67
Sr	117.00	65.64	6.96	56.21	36.47	11.32	8.40	9.66	7.67
Ta	0.23	1.96	19.05	4.01	1.34	13.15	3.26	10.85	12.27
Th	33.13	22.20	50.61	33.11	12.55	33.52	67.17	40.83	47.05
U	8.16	5.14	4.82	5.92	21.04	15.56	15.97	10.34	16.43
V	17.39	5.86	2.00	6.63	16.50	0.00	1.60	2.31	0.00
W	0.13	1.36	3.25	0.67	1.44	2.58	1.10	2.73	2.36
Y	11.00	66.77	112.60	55.83	13.30	96.80	114.70	144.40	129.40
Zn	95.13	91.51	62.72	50.75	12.01	29.55	19.53	44.87	39.14
Zr	121.00	300.90	137.60	205.80	296.30	140.40	184.70	151.20	141.50
La	13.77	114.20	42.20	70.37	26.64	54.54	33.44	38.15	33.83
Ce	26.16	233.70	104.10	136.80	49.75	127.60	84.39	95.96	86.29
Pr	2.91	27.33	14.39	14.84	5.37	18.47	11.37	13.05	11.31
Nd	10.19	99.47	55.49	50.42	18.19	68.88	45.37	52.78	45.75
Sm	2.14	18.31	15.03	9.18	2.91	15.47	11.44	14.84	12.82
Eu	0.92	1.07	0.14	0.71	0.70	0.22	0.16	0.27	0.21
Gd	2.00	14.23	12.96	7.66	2.17	11.59	10.21	15.07	12.90
Tb	0.30	2.18	2.40	1.29	0.36	2.55	1.85	3.13	2.56
Dy	1.66	12.50	15.91	8.11	2.27	18.47	12.11	21.67	17.69
Ho	0.31	2.31	3.24	1.67	0.46	4.04	2.72	4.69	3.82
Er	0.82	6.27	10.88	5.16	1.37	13.34	9.55	14.76	12.43
Tm	0.11	0.92	2.19	0.87	0.22	2.38	1.86	2.53	2.11
Yb	0.76	5.90	18.28	6.41	1.48	16.98	15.09	17.77	15.34
Lu	0.14	0.88	2.92	1.02	0.23	2.48	2.43	2.56	2.34

Annex V Rapakivi Granites (Suite)

DDH no.. sample:	412	412	1051	139	139	139	139	139	139
Depth (m):	398.2	225.4	379	Sample 9	Sample 8	Sample 5	Sample 7	Sample 3	Sample 2
Rock type:	granite	granite	granite	granite	granite	granite	granite	granite	granite
SiO_2(wt. %)	75.74	76.54	76.03	76.20	75.64	75.88	76.83	75.81	75.95
Al_2O_3	13.52	13.09	12.31	13.34	13.57	13.53	12.56	13.47	13.77
Fe_2O_3	0.96	1.14	1.75	0.97	1.16	0.97	1.16	1.16	1.01
MnO	0.00	0.00	0.00	0.00	0.00	0.00	0.00	0.00	0.00
MgO	0.00	0.00	0.00	0.00	0.00	0.00	0.00	0.00	0.00
CaO	2.69	0.28	0.18	0.00	0.00	0.00	0.00	0.00	0.00
Na_2O	1.21	3.64	2.46	4.32	4.39	4.32	4.14	4.70	4.86
K_2O	3.16	4.16	5.95	4.61	4.72	4.72	4.39	4.30	4.25
TiO_2	0.03	0.00	0.08	0.00	0.00	0.00	0.00	0.00	0.00
P_2O_5	0.03	0.00	0.00	0.00	0.00	0.04	0.05	0.03	0.00
PF	2.66	0.92	1.02	0.34	0.31	0.29	0.33	0.33	0.33
Total	**100.00**	**99.77**	**99.78**	**99.78**	**99.79**	**99.75**	**99.46**	**99.80**	**100.17**
As (ppm)	3.20	0.00	0.00	1.93	1.77	1.85	2.28	3.99	4.14
Ba	577.90	74.96	291.70	7.19	10.05	7.58	8.32	11.34	13.52
Be	7.51	7.99	6.54	9.76	7.76	9.32	6.62	7.91	8.01
Bi	0.37	0.00	0.00	0.00	0.00	0.49	0.00	0.00	0.00
Cd	4.54	0.00	0.00	0.00	0.00	0.00	0.41	0.00	0.00
Co	0.74	0.61	0.28	0.34	0.46	0.21	0.42	0.32	0.48
Cr	235.70	111.50	0.00	94.34	89.16	70.83	96.78	84.86	142.20
Cs	1.75	7.23	4.71	6.89	5.87	6.32	3.70	4.58	4.71
Cu	31.96	0.00	0.00	0.00	0.00	6.03	410.60	0.00	0.00
Ga	38.85	53.23	31.83	53.03	54.83	53.17	49.15	54.98	55.20
Ge	1.74	3.04	2.04	3.37	3.10	3.20	3.04	3.51	3.55
Hf	10.64	10.46	8.72	10.54	12.27	8.84	10.20	10.45	8.77
In	1.17	0.00	0.00	0.00	0.00	0.00	0.00	0.00	0.00
Mo	1.14	0.00	0.00	0.00	0.00	0.00	0.00	0.00	0.00
Nb	61.60	42.40	34.08	51.52	50.83	40.72	36.94	64.40	70.58
Ni	11.84	0.00	0.00	6.43	0.00	0.00	5.39	0.00	7.64
Pb	12.56	28.11	21.82	56.29	42.68	61.51	54.96	42.86	42.03
Rb	277.90	621.30	326.70	714.90	685.10	695.30	605.40	605.50	552.60
Sb	2.45	0.00	0.00	0.00	0.00	0.00	0.00	0.00	0.00
Sn	236.10	16.05	2.97	6.24	4.57	8.09	4.68	2.97	1.77
Sr	5.92	9.83	19.89	0.00	5.74	0.00	1.52	0.00	4.66
Ta	10.17	14.28	2.70	22.55	16.07	18.22	12.31	19.62	24.15
Th	50.38	37.21	22.88	43.53	36.35	26.55	32.99	35.90	27.86
U	10.96	4.59	3.37	6.10	1.92	1.55	2.33	3.74	1.74
V	0.00	1.81	1.70	0.00	0.00	0.00	0.00	0.00	0.00
W	3.57	1.64	1.69	2.05	2.21	1.79	1.61	2.77	2.91
Y	90.64	184.40	87.26	49.09	38.53	32.78	40.83	78.22	60.18
Zn	1630.00	52.19	55.50	38.31	41.89	41.57	332.90	33.65	25.71
Zr	150.00	113.10	242.70	96.90	112.70	79.43	93.02	98.19	78.46
La	12.60	40.57	109.90	16.38	6.87	7.69	11.88	34.06	30.02
Ce	29.13	102.30	222.50	62.35	44.06	32.01	46.27	89.39	79.92
Pr	3.93	14.35	26.34	6.17	2.15	2.31	4.40	13.13	9.73
Nd	16.28	59.25	95.06	22.06	7.52	7.58	16.02	48.78	32.43
Sm	5.18	17.38	19.34	5.94	2.42	2.15	4.45	13.83	8.42
Eu	0.09	0.07	0.45	0.02	0.03	0.01	0.02	0.04	0.03
Gd	5.89	18.41	15.97	4.20	2.19	1.65	3.17	10.14	5.25
Tb	1.37	3.46	2.59	0.95	0.69	0.44	0.74	2.10	1.11
Dy	10.62	22.38	15.42	7.78	7.07	4.30	6.24	13.73	8.12
Ho	2.57	4.49	2.95	1.92	1.92	1.25	1.62	2.85	1.92
Er	9.21	13.79	8.45	8.64	9.16	6.42	7.78	10.48	8.31
Tm	1.72	2.50	1.23	2.23	2.39	1.76	2.03	2.35	2.13
Yb	12.93	19.85	8.06	21.04	22.07	17.02	18.56	21.04	20.38
Lu	2.00	3.10	1.17	3.52	3.56	2.82	3.01	3.39	3.39

Annex VI Mesoproterozoic sandstones of the Salmi and Karku deposit areas
Major and trace element analysis of the mostly arkosic sandstones and conglomerates

	Pasha sandstones				Salmi sandstones				Priozersk
DDH no.:	**1051**	**1051**	**356**	**356**	**1051**	**816**	**816**	**816**	**356**
Depth (m):	**81**	**134**	**160**	**220**	**199**	**62**	**67**	**68**	**475**
Position	Salmi	Salmi	Salmi	Salmi	Salmi	II zone	II zone	II zone	Salmi
SiO_2(wt. %)	91.56	50.72	95.20	86.30	74.14	80.71	71.81	41.25	84.09
Al_2O_3	4.63	5.12	2.96	6.62	9.41	8.77	11.96	4.63	7.92
Fe_2O_3	0.27	1.28	0.39	0.78	2.80	1.37	3.92	1.84	3.06
MnO	0.00	0.18	0.00	0.00	0.04	0.00	0.04	0.45	0.00
MgO	0.00	0.42	0.14	0.12	1.46	0.00	1.12	0.57	0.19
CaO	0.00	21.79	0.00	0.75	1.99	0.89	0.54	27.44	0.10
Na_2O	1.58	1.23	0.94	2.50	1.92	2.37	1.31	0.88	0.17
K_2O	1.22	2.22	0.73	1.37	2.77	2.61	4.16	1.65	2.68
TiO_2	0.04	0.26	0.06	0.00	0.68	0.19	0.59	0.47	0.25
P_2O_5	0.00	0.00	0.00	0.00	0.17	0.05	0.21	0.10	0.00
PF	0.43	16.60	0.41	1.55	4.51	1.64	3.61	21.00	1.94
Total	**99.73**	**99.82**	**100.83**	**99.99**	**99.89**	**98.60**	**99.27**	**100.28**	**100.39**
As (ppm)	0.00	2.54	0.91	43.99	0.00	1.50	1.27	0.00	0.00
Ba	176.20	423.40	170.20	808.20	945.20	431.20	594.10	307.10	271.20
Be	0.65	0.51	0.00	0.00	0.91	1.33	3.69	1.08	0.00
Bi	0.00	0.00	0.00	0.00	0.00	0.00	0.25	0.00	0.00
Cd	0.00	2.29	0.00	0.00	0.00	0.00	0.00	2.20	0.00
Co	0.78	3.56	0.88	2.11	6.58	3.99	9.54	5.16	2.00
Cr	8.53	5.67	7.32	0.00	23.22	17.56	44.93	23.99	0.00
Cs	0.28	0.60	0.00	0.25	18.89	0.74	3.04	0.83	2.27
Cu	6.08	14.72	0.00	10.34	28.99	5.85	9.52	7.54	0.00
Ga	5.35	8.39	3.45	6.54	11.61	12.85	20.86	8.00	11.29
Ge	0.73	0.73	0.75	0.96	0.79	0.96	1.41	0.71	1.10
Hf	2.01	3.93	1.70	1.77	4.38	5.83	7.26	5.93	5.85
In	0.00	0.00	0.00	0.00	0.00	0.00	0.00	0.00	0.00
Mo	0.00	0.00	0.00	1.96	0.00	0.00	0.00	0.51	0.00
Nb	3.45	7.89	2.06	1.36	16.05	10.26	18.22	12.94	10.27
Ni	0.00	0.00	0.00	0.00	9.40	8.42	21.87	11.87	0.00
Pb	4.64	8.82	3.16	22.61	8.17	13.39	11.20	9.20	8.03
Rb	35.84	62.71	22.38	55.86	61.11	74.47	150.70	54.38	80.67
Sb	0.00	0.00	0.00	0.39	0.00	0.00	0.27	0.00	0.00
Sn	0.44	1.83	0.00	0.00	4.16	2.61	4.35	3.41	0.74
Sr	48.37	145.00	33.21	98.36	53.14	70.50	79.82	238.40	25.24
Ta	0.25	0.67	0.17	0.16	1.22	0.80	1.37	0.89	0.80
Th	2.67	5.93	1.94	2.23	8.34	7.57	12.53	8.71	9.85
U	0.59	2.71	0.84	1.09	2.28	3.56	1.77	2.59	2.02
V	6.76	70.82	8.04	4.89	36.91	28.17	58.42	56.27	23.40
W	0.00	0.49	0.13	0.00	0.39	0.56	1.64	0.86	2.42
Y	4.60	20.51	4.75	6.95	14.97	17.76	26.38	24.66	7.90
Zn	0.00	20.46	0.00	0.00	73.25	40.49	75.81	37.49	16.48
Zr	66.86	154.60	62.35	60.51	155.70	195.20	252.80	210.80	231.60
La	14.44	29.03	18.27	26.92	32.84	25.92	47.16	39.71	34.59
Ce	29.09	49.34	33.72	54.47	62.80	49.60	96.11	73.02	72.08
Pr	3.07	6.28	3.85	6.19	6.97	5.68	10.92	8.63	7.68
Nd	10.38	22.78	11.97	19.24	24.25	21.08	39.05	30.81	23.89
Sm	1.60	3.86	1.47	2.61	4.07	3.85	6.88	5.03	3.43
Eu	0.34	0.99	0.27	0.53	0.77	0.92	1.24	0.83	0.73
Gd	1.10	3.12	0.75	1.36	2.98	3.21	5.26	4.05	1.86
Tb	0.15	0.51	0.14	0.22	0.47	0.50	0.81	0.63	0.30
Dy	0.83	3.12	0.78	1.16	2.86	3.05	4.70	3.94	1.56
Ho	0.16	0.67	0.16	0.19	0.56	0.61	0.92	0.81	0.27
Er	0.45	1.96	0.47	0.56	1.70	1.79	2.75	2.46	0.79
Tm	0.07	0.30	0.07	0.08	0.27	0.27	0.42	0.37	0.12
Yb	0.51	2.06	0.49	0.52	1.98	1.79	2.96	2.55	0.90
Lu	0.08	0.31	0.08	0.08	0.30	0.28	0.47	0.41	0.14

Annex VI (Suite)

	Priozersk sandstones								
DDH no.:	**389**	**389**	**475**	**475**	**502**	**502**	**605**	**605**	**605**
Depth (m):	**163**	**174**	**94**	**100**	**252**	**294**	**85**	**92**	**92.5**
Position	II zone	II zone	Salmi	Salmi	Salmi	Salmi	I zone	I zone	I zone
SiO_2(wt. %)	84.22	86.67	84.19	88.26	83.99	81.39	85.53	87.75	83.75
Al_2O_3	7.74	7.28	10.10	7.53	8.77	7.72	7.62	5.45	7.51
Fe_2O_3	2.33	0.83	0.40	0.23	0.76	3.02	1.10	2.22	2.26
MnO	0.00	0.00	0.00	0.00	0.00	0.03	0.00	0.00	0.00
MgO	0.23	0.00	0.13	0.00	0.26	0.56	0.00	0.12	0.00
CaO	0.15	0.21	0.00	0.00	0.10	0.18	0.00	0.00	0.00
Na_2O	0.07	0.09	0.09	0.10	0.12	0.19	0.23	0.09	0.00
K_2O	2.29	2.11	2.10	2.47	3.14	3.62	3.68	2.26	2.64
TiO_2	0.65	0.76	0.27	0.18	0.14	0.87	0.42	0.33	0.56
P_2O_5	0.09	0.09	0.07	0.09	0.05	0.07	0.04	0.05	0.10
PF	2.06	2.23	2.78	1.86	2.47	2.73	1.47	1.52	2.09
Total	99.83	100.27	100.14	100.71	99.80	100.38	100.09	99.83	98.91
As (ppm)	0.92	1.23	0.00	1.14	2.85	0.89	0.00	1.19	0.00
Ba	393.60	328.30	470.40	522.80	224.10	545.70	671.70	364.00	401.90
Be	1.67	0.00	0.00	0.00	3.20	1.55	1.27	0.00	1.26
Bi	0.09	0.00	0.00	0.00	0.00	0.00	0.00	0.11	0.00
Cd	0.34	0.40	0.00	0.00	0.00	0.48	0.46	0.00	0.00
Co	2.33	1.78	1.14	0.67	1.51	2.81	1.56	0.89	2.19
Cr	11.18	10.46	13.11	6.84	7.16	15.71	9.28	0.00	9.81
Cs	0.85	0.64	0.44	0.51	4.13	8.51	1.38	0.86	1.13
Cu	0.00	20.63	5.69	5.26	0.00	0.00	5.27	7.10	5.70
Ga	14.93	13.06	13.69	10.03	17.89	13.62	9.96	9.24	12.51
Ge	1.47	1.20	0.90	1.34	1.28	1.31	1.08	1.28	1.27
Hf	16.68	24.47	5.68	11.97	9.47	32.21	10.03	13.30	18.04
In	0.00	0.00	0.00	0.00	0.00	0.00	0.00	0.00	0.00
Mo	0.44	0.78	0.00	0.00	0.00	0.61	0.00	0.38	0.00
Nb	38.18	51.53	18.06	22.87	23.98	57.36	14.62	25.50	37.72
Ni	0.00	0.00	16.34	20.05	0.00	0.00	5.23	0.00	6.25
Pb	10.19	15.51	7.07	13.41	12.22	16.46	181.06	11.00	13.36
Rb	82.00	64.10	57.16	87.49	160.20	165.40	100.00	61.10	76.71
Sb	0.00	0.21	0.00	0.00	0.00	0.10	0.00	0.24	0.00
Sn	2.40	2.19	3.65	2.31	1.94	5.16	2.04	3.12	3.80
Sr	49.00	44.08	58.41	76.69	31.16	56.16	54.70	37.40	45.19
Ta	2.88	3.83	1.31	2.16	1.92	5.34	1.14	2.43	2.82
Th	27.76	29.66	9.05	27.02	14.13	27.23	14.56	19.80	25.54
U	3.44	5.63	2.12	6.21	2.17	3.84	9.82	13.80	12.15
V	17.51	18.30	22.01	8.25	6.03	23.45	15.84	13.80	18.59
W	3.01	4.94	0.77	1.03	1.50	2.46	2.62	6.10	5.97
Y	22.56	34.60	13.38	31.46	36.23	42.69	12.63	17.50	23.08
Zn	36.46	16.88	10.94	9.77	32.39	29.61	22.40	12.90	20.01
Zr	678.40	1052.00	216.60	451.70	328.00	1425.00	437.20	519.00	752.50
La	62.56	86.04	49.93	81.92	48.38	75.73	27.53	56.30	71.52
Ce	120.30	168.30	91.09	155.80	104.30	149.40	51.81	99.70	129.10
Pr	12.46	17.80	8.35	15.92	11.82	16.27	5.66	10.90	13.60
Nd	41.26	58.52	23.71	49.53	40.57	56.62	19.04	38.00	45.85
Sm	6.45	9.28	3.09	7.27	7.30	9.64	3.03	5.39	7.27
Eu	0.96	1.36	0.75	0.91	0.91	1.98	0.84	0.89	1.07
Gd	4.50	6.11	2.25	5.02	5.44	7.60	2.27	4.21	5.38
Tb	0.71	1.01	0.38	0.84	0.90	1.20	0.36	0.64	0.76
Dy	4.15	5.59	2.30	4.80	5.39	7.15	2.19	3.51	4.13
Ho	0.83	1.15	0.44	0.95	1.09	1.42	0.46	0.70	0.81
Er	2.43	3.44	1.25	2.88	3.33	4.42	1.40	2.02	2.42
Tm	0.39	0.56	0.21	0.44	0.52	0.69	0.22	0.32	0.38
Yb	2.71	3.86	1.42	2.92	3.50	4.83	1.55	2.14	2.73
Lu	0.45	0.63	0.21	0.46	0.54	0.80	0.25	0.34	0.43

Annex VI (Suite)

	Priozersk sandstones								
DDH no.:	**605**	**605**	**605**	**614**	**615**	**615**	**625**	**625**	**625**
Depth (m):	**93**	**105**	**107**	**92**	**99**	**99.5**	**110**	**113**	**127**
Position	I zone	I zone	I zone	I zone	I zone	I zone	III zone	III zone	III zone
SiO_2(wt. %)	81.35	81.75	72.00	94.50	88.21	70.92	70.82	82.89	72.48
Al_2O_3	10.01	8.79	4.60	2.73	6.07	18.78	7.54	7.60	5.37
Fe_2O_3	1.82	2.38	1.62	0.22	0.62	0.91	7.42	2.70	12.36
MnO	0.00	0.03	0.15	0.00	0.00	0.00	0.09	0.03	0.15
MgO	0.22	0.00	0.52	0.00	0.00	0.16	1.12	0.35	1.02
CaO	0.00	0.00	8.88	0.00	0.00	0.10	4.44	0.74	3.92
Na_2O	0.11	0.00	0.13	0.00	0.08	0.14	0.15	0.15	0.00
K_2O	2.71	2.90	2.07	1.56	2.05	1.50	2.78	3.14	0.00
TiO_2	0.55	0.11	1.18	0.12	0.98	0.28	0.57	0.33	0.24
P_2O_5	0.06	0.00	0.11	0.06	0.06	0.08	0.07	0.00	0.14
PF	2.92	2.46	8.68	0.51	1.69	6.93	4.98	2.25	4.26
Total	99.83	98.42	99.94	99.79	99.88	99.80	99.98	100.18	99.94
As (ppm)	0.94	1.41	19.50	10.60	0.94	6.10	3.15	0.00	10.13
Ba	489.00	579.00	577.00	349.00	419.00	317.00	560.60	452.00	5.49
Be	1.56	1.45	5.48	0.00	1.65	5.66	1.72	0.00	1.83
Bi	0.00	0.00	0.00	0.00	0.00	0.07	0.00	0.00	0.00
Cd	0.00	0.00	0.95	1.40	0.00	0.00	0.00	0.00	29.95
Co	1.80	9.00	18.00	2.08	1.72	5.12	11.07	1.38	2.83
Cr	11.70	13.79	6.80	0.00	7.40	8.70	6.53	0.00	0.00
Cs	1.34	1.01	0.93	0.33	0.97	1.42	0.56	1.03	0.00
Cu	8.50	7.30	120.00	8.60	5.00	5.60	0.00	0.00	5.65
Ga	15.60	12.65	8.68	3.47	8.60	28.90	13.26	10.69	10.96
Ge	1.05	1.13	2.59	1.32	1.21	1.28	1.63	0.91	1.41
Hf	10.30	4.25	29.40	4.70	23.20	12.30	10.09	6.98	4.90
In	0.00	0.00	0.00	0.00	0.00	0.00	0.00	0.00	0.00
Mo	0.35	0.00	4.88	0.27	0.40	17.70	0.62	0.41	7.88
Nb	28.00	8.06	150.00	7.85	45.40	54.30	20.83	17.03	9.47
Ni	0.00	10.62	18.30	0.00	0.00	9.70	9.51	9.73	0.00
Pb	13.30	16.44	2616.00	10.70	25.30	48.20	20.26	9.65	60.08
Rb	74.50	82.53	53.40	45.10	60.00	53.60	73.32	89.30	0.95
Sb	0.00	0.00	0.58	0.00	0.00	0.17	0.14	0.24	0.21
Sn	8.44	5.07	739.00	1.12	2.64	7.50	1.60	1.30	0.60
Sr	51.60	54.30	64.30	32.40	37.20	42.30	47.39	40.15	5.71
Ta	2.50	0.74	25.50	0.64	3.57	5.04	1.72	1.31	0.75
Th	38.70	6.40	1040.00	7.59	46.80	32.70	15.80	7.51	3.15
U	17.50	8.45	3615.00	31.20	64.60	215.00	2.28	3.66	20.50
V	23.70	11.43	40.40	4.60	17.40	24.90	20.99	17.23	103.00
W	1.83	1.07	15.80	0.97	7.85	2.22	2.07	1.91	1.65
Y	15.90	7.28	109.00	7.14	24.20	22.90	12.06	9.09	6.47
Zn	25.80	28.80	79.10	30.40	21.80	19.10	52.10	22.40	1814.00
Zr	405.00	147.20	1097.00	181.00	954.00	365.00	425.10	281.60	196.20
La	58.90	52.90	58.10	19.00	25.50	93.70	31.34	31.53	16.50
Ce	105.00	72.84	178.00	37.70	50.50	174.00	62.24	63.13	30.40
Pr	10.70	6.64	29.80	4.02	5.49	15.00	6.26	6.52	2.98
Nd	35.50	20.90	122.00	14.30	20.40	43.50	20.62	21.91	9.92
Sm	5.26	2.65	19.50	1.91	5.36	7.16	3.07	3.45	1.41
Eu	0.95	0.74	6.72	0.45	0.86	0.92	0.91	0.66	0.34
Gd	4.05	1.79	18.60	1.56	4.20	5.08	2.30	2.19	1.19
Tb	0.61	0.24	2.64	0.22	0.72	0.71	0.38	0.34	0.19
Dy	3.68	1.36	13.20	1.28	4.29	4.11	2.26	1.93	1.15
Ho	0.69	0.26	2.68	0.25	0.88	0.77	0.44	0.35	0.25
Er	2.07	0.80	7.13	0.80	2.54	2.31	1.31	1.09	0.76
Tm	0.32	0.13	0.98	0.13	0.43	0.44	0.20	0.18	0.12
Yb	2.25	0.98	6.43	0.95	2.85	3.24	1.36	1.22	0.80
Lu	0.35	0.15	0.91	0.14	0.45	0.47	0.22	0.20	0.13

Annex VI (Suite)

	Priozersk sandstones								
DDH no.:	**625**	**625**	**625**	**654**	**654**	**654**	**654**	**654**	**751**
Depth (m):	**128**	**131**	**134**	**117**	**132**	**143**	**144**	**145**	**50**
Position	III zone	III zone	III zone	III zone	III zone	III zone	III zone	III zone	N to I zone
SiO_2(wt. %)	71.46	61.72	72.73	79.29	82.87	73.32	66.52	58.74	81.67
Al_2O_3	4.56	4.91	3.72	6.50	6.23	4.56	3.79	3.68	7.21
Fe_2O_3	10.71	8.43	4.57	3.63	4.47	8.90	4.29	7.49	3.63
MnO	0.13	0.42	0.21	0.05	0.04	0.10	0.47	0.44	0.00
MgO	0.95	2.89	1.03	0.31	0.28	0.39	0.42	1.10	0.00
CaO	5.50	10.81	7.89	2.04	1.25	5.37	12.41	13.61	0.00
Na_2O	0.00	0.09	0.05	0.17	0.00	0.00	0.00	0.00	0.25
K_2O	0.00	0.34	1.11	3.07	2.82	0.53	1.39	1.02	3.29
TiO_2	0.38	0.00	0.43	1.29	0.25	0.27	0.12	0.42	0.82
P_2O_5	1.70	0.00	0.00	0.07	0.72	0.06	0.00	0.13	0.08
PF	3.67	10.50	7.29	2.54	1.02	5.52	10.47	11.82	1.52
Total	99.06	100.11	99.03	98.96	99.95	99.02	99.88	98.45	98.47
As (ppm)	1.51	81.72	35.85	0.00	0.00	1.49	20.57	96.96	0.00
Ba	11.23	178.20	240.10	689.10	473.70	96.60	260.80	212.80	648.50
Be	2.04	5.47	2.12	1.02	1.39	2.51	2.61	4.16	1.16
Bi	0.00	0.00	0.00	0.00	0.00	0.00	0.00	0.00	0.00
Cd	1.87	19.97	5.37	0.42	0.00	10.64	7.83	21.24	0.81
Co	3.29	5.95	4.13	4.22	2.09	1.79	2.19	6.10	2.73
Cr	0.00	0.00	0.00	10.51	8.96	12.99	5.45	7.45	7.72
Cs	0.00	0.28	0.57	0.72	0.50	0.00	0.37	0.29	1.16
Cu	5.53	11.19	11.53	0.00	37.44	0.00	5.41	0.00	0.00
Ga	12.27	8.44	5.76	10.96	9.97	11.23	6.66	7.27	11.81
Ge	1.47	2.12	1.29	1.38	1.11	1.51	1.44	2.10	1.59
Hf	7.97	2.41	6.57	18.37	5.04	5.63	5.04	13.34	25.04
In	0.00	0.00	0.00	0.00	0.00	0.00	0.00	0.00	0.00
Mo	1.47	125.10	28.41	0.58	0.79	1.32	103.50	314.10	0.65
Nb	10.91	2.61	13.60	43.22	11.31	10.39	6.99	21.30	33.54
Ni	7.29	13.22	14.09	5.73	5.90	6.52	6.21	10.45	0.00
Pb	70.94	1627.20	353.19	12.28	14.90	138.97	93.29	385.72	14.54
Rb	1.14	8.70	29.59	87.24	83.37	15.21	37.91	29.54	93.57
Sb	0.17	0.17	0.15	0.00	0.00	0.00	0.00	0.00	0.00
Sn	0.63	0.57	6.27	1.91	1.05	0.78	0.75	2.23	1.80
Sr	17.79	40.27	31.14	55.82	45.42	15.89	78.58	83.16	57.05
Ta	0.94	0.41	1.95	3.13	0.77	0.82	0.70	1.96	2.53
Th	8.00	4.43	21.14	29.83	7.19	6.63	5.90	14.16	23.39
U	18.51	115.90	79.71	2.40	3.97	20.16	92.99	1210.00	4.82
V	227.00	19.47	23.01	36.51	26.06	25.24	15.06	35.96	18.68
W	2.86	0.49	3.09	3.38	1.46	1.85	1.40	4.43	3.25
Y	14.58	3.53	10.88	16.19	14.39	7.41	4.73	10.55	23.42
Zn	215.50	67.45	296.60	26.10	41.08	528.70	127.40	326.10	27.76
Zr	334.10	75.21	252.50	798.60	193.30	213.10	182.80	553.90	1058.00
La	30.37	2.69	5.76	56.21	18.81	27.94	10.85	24.68	49.08
Ce	61.05	6.45	12.65	102.40	34.50	42.58	21.87	45.79	92.91
Pr	6.67	0.90	1.66	10.80	4.21	4.22	2.40	4.68	10.29
Nd	22.99	3.81	6.81	35.64	15.79	13.48	8.44	16.49	36.21
Sm	3.17	0.84	1.82	5.08	3.11	1.52	1.37	3.12	6.03
Eu	0.68	0.17	0.18	1.25	0.82	0.43	0.43	0.63	1.57
Gd	2.50	0.67	1.61	3.56	2.76	1.27	1.10	2.31	4.80
Tb	0.40	0.11	0.34	0.56	0.44	0.17	0.15	0.34	0.70
Dy	2.28	0.64	2.13	3.37	2.53	0.97	0.85	1.86	4.06
Ho	0.46	0.13	0.44	0.68	0.50	0.20	0.17	0.37	0.81
Er	1.41	0.41	1.32	2.01	1.41	0.62	0.52	1.16	2.44
Tm	0.22	0.07	0.19	0.32	0.21	0.11	0.09	0.19	0.37
Yb	1.48	0.47	1.22	2.20	1.38	0.82	0.63	1.39	2.61
Lu	0.25	0.08	0.19	0.36	0.21	0.13	0.11	0.23	0.44

Annex VI (Suite)

	Priozersk sandstones								
DDH no.:	**751**	**816**	**816**	**816**	**822**	**822**	**822**	**822**	**822**
Depth (m):	**67**	**161**	**167**	**179**	**138**	**143**	**145**	**147**	**148**
Position	N to I zone	II zone	II zone	II zone	N to III zone	N to III zone	N to III zone	N to III zone	N to III zone
SiO_2(wt. %)	87.71	78.20	79.48	88.15	89.95	76.95	89.91	91.51	77.29
Al_2O_3	6.14	7.49	10.03	7.18	4.32	13.06	5.01	3.33	7.05
Fe_2O_3	0.71	5.30	2.54	0.22	1.97	2.45	0.51	1.50	9.61
MnO	0.00	0.06	0.00	0.00	0.00	0.00	0.00	0.00	0.00
MgO	0.00	0.42	0.00	0.00	0.00	0.00	0.00	0.10	0.31
CaO	0.42	1.49	0.00	0.00	0.00	0.14	0.00	0.14	0.24
Na_2O	0.00	0.19	0.00	0.00	0.08	0.18	0.11	0.07	0.16
K_2O	2.59	2.18	2.50	1.21	1.88	4.09	1.99	1.48	2.45
TiO_2	0.06	0.33	1.56	0.23	0.31	0.18	0.19	0.00	0.61
P_2O_5	0.00	0.09	0.11	0.05	0.00	0.00	0.00	0.00	0.06
PF	1.67	3.49	2.89	2.29	1.16	3.02	1.25	0.82	2.05
Total	99.30	99.24	99.11	99.33	99.67	100.07	98.97	98.95	99.83
As (ppm)	0.00	0.00	0.00	0.00	0.00	0.00	0.00	0.00	0.00
Ba	442.50	350.10	209.10	154.60	275.60	289.90	225.10	189.90	312.80
Be	0.70	2.74	2.29	0.67	0.00	1.92	0.00	0.00	2.09
Bi	0.00	0.00	0.00	0.00	0.00	0.00	0.00	0.00	0.00
Cd	0.00	0.00	0.92	0.00	0.00	0.00	0.00	0.00	0.00
Co	4.73	17.25	2.34	0.47	0.94	0.93	0.38	0.43	2.57
Cr	7.58	12.08	17.06	8.07	5.09	5.16	0.00	0.00	8.63
Cs	0.42	1.16	3.93	0.73	2.31	2.45	0.97	0.55	2.23
Cu	0.00	0.00	0.00	5.43	5.28	0.00	0.00	0.00	0.00
Ga	8.09	15.12	16.44	7.96	6.74	17.92	5.95	3.81	10.54
Ge	1.00	1.97	1.41	0.97	1.10	1.26	0.93	0.98	1.80
Hf	2.95	8.23	41.85	5.86	9.03	7.47	4.75	2.48	12.42
In	0.00	0.00	0.00	0.00	0.00	0.00	0.00	0.00	0.00
Mo	0.00	0.00	0.78	1.09	0.42	0.55	0.00	1.11	4.56
Nb	4.07	13.95	80.79	10.76	23.09	30.16	9.29	2.15	22.61
Ni	9.62	20.81	7.91	0.00	0.00	0.00	0.00	0.00	6.54
Pb	8.61	10.10	28.88	7.48	6.22	7.47	4.15	3.45	16.56
Rb	74.28	72.14	96.61	40.39	57.88	110.70	56.55	42.75	75.71
Sb	0.00	0.00	0.00	0.00	0.13	0.18	0.11	0.21	0.29
Sn	1.13	1.71	4.07	1.30	6.53	2.88	0.66	0.00	1.07
Sr	35.27	45.93	48.53	19.84	22.61	40.42	20.70	15.65	31.56
Ta	0.47	1.21	6.17	0.85	1.47	2.42	0.68	0.25	1.68
Th	4.22	14.67	66.62	11.19	22.91	12.08	5.68	1.77	11.14
U	8.58	4.60	10.73	3.76	1.81	2.99	2.73	3.24	11.92
V	15.10	36.59	29.11	12.68	10.96	11.15	9.05	18.74	60.13
W	0.40	0.83	2.76	1.43	2.24	1.30	0.53	3.67	6.34
Y	6.86	16.83	45.27	9.40	13.28	23.71	8.80	4.55	19.83
Zn	17.63	178.20	56.02	26.16	12.41	16.45	6.02	8.56	37.60
Zr	102.70	343.40	1482.00	230.90	354.20	258.30	183.10	83.44	502.80
La	11.46	33.21	110.70	25.04	38.21	79.98	19.00	6.03	43.50
Ce	19.16	61.71	221.50	48.23	68.49	142.10	38.60	11.75	88.20
Pr	2.11	6.72	23.48	5.29	7.82	16.93	3.94	1.19	8.98
Nd	7.44	23.65	78.94	18.18	26.66	58.66	13.30	4.07	29.10
Sm	1.36	3.70	12.73	2.89	4.42	10.57	2.02	0.73	4.38
Eu	0.48	0.91	1.67	0.63	0.80	1.66	0.52	0.21	1.32
Gd	1.14	2.88	9.32	2.00	3.09	7.28	1.45	0.60	3.34
Tb	0.18	0.45	1.47	0.30	0.47	1.02	0.23	0.10	0.60
Dy	1.10	2.76	8.69	1.70	2.69	5.12	1.37	0.69	3.73
Ho	0.22	0.57	1.72	0.33	0.53	0.92	0.29	0.15	0.74
Er	0.65	1.72	5.27	0.98	1.65	2.70	0.89	0.43	2.17
Tm	0.10	0.25	0.83	0.15	0.27	0.44	0.14	0.07	0.33
Yb	0.66	1.71	5.92	1.03	1.87	3.18	0.90	0.47	2.13
Lu	0.10	0.27	0.95	0.17	0.30	0.48	0.14	0.07	0.34

Annex VI (Suite)

	Priozersk sandstones								
DDH no.:	**822**	**822**	**822**	**822**	**822**	**835**	**835**	**835**	**835**
Depth (m):	**151**	**152**	**157**	**158**	**159**	**218**	**230**	**243**	**244**
Position	N to III zone	N to III zone	N to III zone	N to III zone	N to III zone	Matala zone	Matala zone	Matala zone	Matala zone
SiO_2(wt. %)	80.77	73.12	80.43	73.88	81.46	69.92	90.73	82.56	79.89
Al_2O_3	4.93	8.99	9.64	11.51	7.71	14.80	5.00	8.60	6.58
Fe_2O_3	8.07	3.33	2.95	6.32	3.14	3.68	0.64	2.52	3.97
MnO	0.00	0.03	0.00	0.04	0.03	0.00	0.00	0.03	0.05
MgO	0.15	0.40	0.47	0.73	0.49	0.60	0.00	0.00	0.25
CaO	0.91	4.53	0.19	0.26	0.56	0.50	0.00	0.47	2.80
Na_2O	0.12	0.20	0.18	0.18	0.17	0.26	0.00	0.15	0.00
K_2O	1.93	3.25	3.18	3.36	2.70	4.78	1.92	3.29	2.55
TiO_2	0.26	0.61	0.22	0.41	0.53	1.18	0.15	0.28	0.23
P_2O_5	0.35	2.58	0.05	0.10	0.29	0.20	0.00	0.05	0.04
PF	1.58	2.78	2.34	3.08	2.07	3.99	1.10	2.25	3.37
Total	99.07	99.82	99.65	99.87	99.15	99.91	99.54	100.20	99.73
As (ppm)	0.00	0.00	2.20	0.00	1.42	2.16	0.00	0.00	0.00
Ba	275.10	353.90	534.20	606.30	534.20	460.40	209.10	449.50	473.00
Be	1.52	4.35	1.67	2.85	2.17	4.28	0.60	1.40	1.07
Bi	0.00	0.00	0.14	0.11	0.20	0.21	0.00	0.00	0.00
Cd	0.00	0.00	0.00	0.57	0.41	0.50	0.00	0.00	0.00
Co	1.93	2.26	3.82	4.56	3.74	4.43	0.80	2.30	7.50
Cr	6.28	71.14	13.71	22.51	18.42	60.68	9.65	13.04	10.86
Cs	1.95	3.69	1.37	2.64	2.76	5.94	0.87	3.34	1.80
Cu	0.00	0.00	6.39	12.55	8.24	21.22	0.00	12.57	0.00
Ga	7.02	17.80	15.01	19.80	12.99	37.44	7.38	12.68	9.44
Ge	1.49	1.68	1.31	1.76	1.49	1.82	1.06	1.35	1.30
Hf	5.79	9.23	5.45	14.06	16.66	24.97	5.00	9.81	6.05
In	0.00	0.00	0.00	0.00	0.15	0.00	0.00	0.00	0.00
Mo	3.86	1.16	2.95	12.98	0.49	0.80	0.00	0.66	5.29
Nb	9.78	30.72	14.51	28.53	31.38	74.68	8.90	32.00	19.63
Ni	0.00	0.00	6.55	10.53	6.32	14.12	0.00	13.27	31.71
Pb	12.55	12.38	19.41	29.30	22.19	15.10	3.91	10.31	81.05
Rb	57.00	118.40	100.90	99.06	80.67	169.40	58.96	105.60	67.07
Sb	0.25	0.17	0.11	0.30	0.18	0.31	0.00	0.00	0.00
Sn	0.73	2.46	1.84	4.74	8.40	10.34	0.76	1.98	1.51
Sr	27.52	68.50	64.92	72.42	64.64	78.93	19.04	49.37	58.33
Ta	1.07	2.69	1.02	2.57	3.17	4.76	0.70	1.74	1.06
Th	7.57	22.29	9.10	25.95	46.77	57.88	5.10	21.49	30.74
U	9.89	11.13	3.22	16.56	23.01	7.96	3.64	2.94	17.05
V	45.25	33.53	36.10	68.71	37.34	297.00	30.33	23.99	54.97
W	4.81	4.81	1.07	3.12	2.12	3.30	0.37	2.62	1.34
Y	19.62	79.51	12.90	28.25	26.55	43.40	8.10	16.25	16.54
Zn	24.34	37.31	43.48	97.58	57.24	76.14	11.25	32.68	53.64
Zr	233.60	335.80	185.70	488.00	583.20	1034.00	198.20	349.30	198.70
La	25.90	57.17	35.44	81.10	58.47	151.40	22.38	34.42	42.21
Ce	53.42	131.10	66.76	156.90	114.80	202.00	43.65	60.31	82.98
Pr	5.90	16.13	6.83	16.95	12.83	20.79	4.64	6.33	8.99
Nd	21.11	68.74	23.12	58.45	45.17	66.81	16.03	21.70	31.12
Sm	4.32	16.12	3.88	9.40	7.77	10.38	2.60	3.70	5.05
Eu	1.35	4.10	0.75	1.20	0.96	1.56	0.62	0.48	0.62
Gd	3.93	16.58	2.69	6.64	5.92	8.02	1.80	3.07	3.70
Tb	0.65	2.44	0.41	0.98	0.87	1.29	0.26	0.48	0.53
Dy	3.72	13.70	2.31	5.36	4.99	8.09	1.51	2.91	3.06
Ho	0.69	2.57	0.47	1.06	0.97	1.65	0.29	0.58	0.58
Er	1.87	6.66	1.48	3.21	2.78	5.13	0.89	1.72	1.64
Tm	0.27	0.90	0.26	0.53	0.40	0.84	0.14	0.27	0.24
Yb	1.71	5.90	1.91	3.84	2.80	5.93	1.01	1.88	1.52
Lu	0.24	0.89	0.30	0.61	0.46	0.90	0.16	0.29	0.25

Annex VI (Suite)

	Priozersk sandstones					
DDH no.:	**843**	**843**	**843**	**843**	**1051**	**1051**
Depth (m):	**141**	**146**	**147**	**148**	**327**	**368**
Position	I zone	I zone	I zone	I zone	Salmi	Salmi
SiO_2(wt. %)	89.12	84.15	80.09	66.24	81.60	79.78
Al_2O_3	4.54	4.70	6.48	5.01	10.42	6.52
Fe_2O_3	1.98	0.74	2.62	4.78	0.62	1.86
MnO	0.00	0.07	0.05	0.32	0.00	0.10
MgO	0.00	0.00	0.40	0.73	0.27	0.27
CaO	0.00	3.47	2.07	9.61	0.10	3.32
Na_2O	0.00	0.00	0.19	0.21	0.20	0.00
K_2O	2.12	2.57	3.09	2.64	4.10	3.73
TiO_2	0.09	0.34	0.17	0.21	0.24	0.58
P_2O_5	0.00	0.03	0.31	0.04	0.05	0.08
PF	0.88	3.45	4.67	9.20	2.25	3.50
Total	98.73	99.52	100.14	98.99	99.85	99.74
As (ppm)	0.00	8.12	24.09	52.93	1.20	3.42
Ba	385.40	599.20	722.50	819.40	578.90	622.70
Be	1.03	0.00	2.77	2.71	2.84	2.64
Bi	0.00	0.00	0.00	0.00	0.00	0.00
Cd	0.00	0.00	7.72	10.37	0.00	0.00
Co	1.87	0.95	9.26	8.13	2.09	3.42
Cr	5.86	5.38	8.96	18.43	11.13	6.73
Cs	0.33	0.39	4.24	1.75	3.18	2.97
Cu	0.00	0.00	13.91	11.00	6.56	29.22
Ga	9.57	6.31	11.90	8.53	20.95	12.54
Ge	1.04	0.82	1.72	0.95	0.84	1.00
Hf	3.66	6.62	4.51	6.54	8.77	7.52
In	0.00	0.00	0.00	0.00	0.00	0.00
Mo	0.00	0.85	81.67	240.70	0.00	3.87
Nb	6.81	21.21	9.57	13.98	14.55	35.44
Ni	0.00	0.00	8.40	22.14	6.29	0.00
Pb	8.62	101.81	1378.83	442.53	9.53	16.28
Rb	59.11	69.23	89.70	73.51	141.60	165.60
Sb	0.00	0.00	0.40	0.00	0.00	0.00
Sn	1.28	8.62	0.93	3.83	2.04	11.52
Sr	31.51	48.59	69.00	113.60	68.77	46.08
Ta	0.47	2.24	0.80	1.44	1.08	2.50
Th	5.60	31.02	7.07	18.57	8.83	38.29
U	6.34	2.65	3354.00	1259.00	1.54	11.78
V	22.05	15.46	46.36	24.31	19.19	20.25
W	0.81	2.24	3.10	4.43	0.61	3.31
Y	5.61	7.57	107.20	9.04	15.76	25.01
Zn	17.65	9.52	684.00	1050.00	23.73	38.65
Zr	142.50	247.20	159.40	238.50	381.50	293.00
La	18.87	36.90	24.56	21.61	42.50	51.39
Ce	33.86	57.28	97.56	43.41	70.39	87.83
Pr	3.54	5.73	15.99	4.86	7.25	8.74
Nd	11.78	18.67	68.89	17.14	23.98	29.32
Sm	1.64	2.76	13.82	3.05	3.66	5.28
Eu	0.45	0.58	6.81	0.63	1.07	0.66
Gd	1.15	1.91	14.55	2.15	2.89	4.41
Tb	0.18	0.27	1.39	0.32	0.47	0.72
Dy	1.06	1.50	6.12	1.81	2.85	4.31
Ho	0.21	0.28	1.20	0.35	0.56	0.85
Er	0.64	0.84	2.71	1.01	1.61	2.47
Tm	0.11	0.14	0.28	0.16	0.25	0.38
Yb	0.72	0.99	1.57	1.14	1.74	2.64
Lu	0.11	0.16	0.25	0.18	0.27	0.40

Annex VII Salmi basalts
Major and trace element analysis of the Salmi basalts

DDH no.:	356	356	475	502	502	502	502	389	389
Depth (m):	310	441	64	61	102	177	232	78	159
Rock type:	volcanic	volcanic	volcanic	volcanic	volcanic	volcanic	volcanic	volcanic	volcanic
SiO_2(wt. %)	45.26	46.44	47.05	38.35	46.96	47.33	47.13	47.05	44.36
Al_2O_3	13.03	13.23	13.30	13.70	11.80	13.12	13.59	14.33	15.78
Fe_2O_3	16.70	16.43	15.72	16.29	18.67	14.03	15.34	17.03	9.18
MnO	0.18	0.20	0.18	0.18	0.16	0.18	0.22	0.15	0.23
MgO	3.54	4.53	6.30	6.74	5.51	5.92	3.79	2.06	1.41
CaO	7.11	7.62	3.68	5.43	2.26	4.67	8.57	3.84	9.49
Na_2O	2.66	2.69	3.43	4.64	0.33	3.54	2.52	5.00	1.44
K_2O	1.71	1.56	1.75	0.18	4.77	0.70	1.49	2.22	1.59
TiO_2	4.38	3.53	3.53	4.50	3.48	3.69	3.72	3.90	4.26
P_2O_5	1.34	1.15	1.02	1.44	1.19	1.18	1.06	1.10	1.14
PF	2.73	1.18	4.09	7.19	4.39	5.23	2.53	3.42	10.96
Total	**98.62**	**98.58**	**100.03**	**98.63**	**99.51**	**99.60**	**99.96**	**100.10**	**99.84**
As (ppm)	2.34	0.00	0.00	6.18	6.05	2.65	0.00	3.72	11.11
Ba	1157.00	1390.00	686.70	245.70	866.10	1437.00	1236.00	2303.00	291.00
Be	3.02	0.00	0.00	2.58	2.15	1.82	1.84	2.08	3.87
Bi	0.00	0.00	0.00	0.00	0.00	0.00	0.00	0.00	0.00
Cd	0.00	0.38	0.00	0.34	0.00	0.00	0.00	0.00	0.45
Co	29.37	45.12	44.70	30.99	43.05	42.32	48.53	42.13	39.10
Cr	59.48	54.48	48.12	55.87	63.99	53.42	62.69	62.76	72.00
Cs	0.22	0.98	0.00	0.28	2.30	0.86	0.73	0.76	3.36
Cu	38.63	38.07	87.54	25.25	21.99	49.99	54.04	19.00	48.78
Ga	25.43	25.79	25.82	25.83	29.11	24.82	29.23	26.68	25.01
Ge	1.71	1.57	1.26	1.37	1.53	1.47	1.97	1.38	1.61
Hf	10.29	9.09	8.83	10.90	9.57	8.69	9.22	9.41	10.48
In	0.12	0.11	0.14	0.13	0.18	0.12	0.12	0.14	0.14
Mo	3.66	2.64	1.38	5.23	2.12	1.53	3.05	3.00	4.48
Nb	45.92	37.21	35.12	44.61	39.15	34.43	39.18	39.43	43.77
Ni	20.71	25.57	28.60	51.96	68.29	61.74	30.36	26.65	29.12
Pb total	11.76	8.91	11.98	14.72	11.67	9.82	10.89	18.23	43.87
Rb	42.52	34.27	29.24	7.30	147.70	12.20	37.46	42.78	59.78
Sb	0.00	0.00	0.00	0.29	0.14	0.11	0.00	0.12	0.11
Sn	1.60	1.38	2.09	2.11	4.05	1.51	1.40	1.43	1.60
Sr	421.40	425.40	201.30	126.70	49.00	330.40	446.10	520.10	88.49
Ta	2.99	2.46	2.46	3.04	2.70	2.39	2.39	2.46	2.72
Th	3.91	2.97	3.00	4.16	3.71	2.86	3.35	3.41	3.72
U	1.60	1.71	1.54	10.16	4.81	1.40	1.35	2.90	1.67
V	170.40	264.80	244.20	139.60	193.20	225.90	296.70	299.80	326.30
W	0.81	0.51	0.60	0.84	1.72	0.55	0.61	0.69	3.31
Y	66.15	54.18	51.89	55.93	65.52	47.25	57.71	57.41	62.98
Zn	215.70	237.80	222.00	197.40	286.10	215.70	275.40	240.70	339.90
Zr	509.80	436.50	430.30	524.50	472.70	416.90	433.90	437.70	497.30
La	85.30	61.24	59.83	73.92	138.30	55.88	72.98	73.98	76.42
Ce	180.50	139.30	138.60	162.00	251.10	128.40	154.10	159.90	166.70
Pr	22.39	17.42	17.62	20.04	29.06	16.37	19.27	19.83	20.90
Nd	91.53	72.22	72.18	83.58	109.80	67.61	78.76	79.34	84.51
Sm	16.75	13.15	13.54	15.58	16.87	12.38	14.63	14.56	15.77
Eu	4.02	3.72	3.98	3.69	4.27	3.22	4.08	3.69	3.98
Gd	14.99	12.37	12.26	13.63	14.15	10.87	12.76	12.84	13.96
Tb	2.02	1.66	1.67	1.82	2.06	1.49	1.79	1.77	1.91
Dy	11.76	9.42	9.25	9.96	11.46	8.42	9.92	9.98	10.49
Ho	2.18	1.75	1.72	1.79	2.12	1.58	1.86	1.87	1.99
Er	5.96	4.90	4.71	5.14	6.01	4.47	5.11	5.20	5.50
Tm	0.84	0.71	0.69	0.75	0.87	0.66	0.73	0.76	0.79
Yb	5.46	4.61	4.39	4.89	5.56	4.26	4.83	4.91	5.15
Lu	0.83	0.69	0.67	0.76	0.85	0.66	0.76	0.78	0.81

Annex VII Volcanic (Suite)

DDH no.:	625	625	625	625	625	625	625	625	625	625
Depth (m):	50	54	54,5	55	56	57	59	73	85	109
Rock type:	volcanic	volcanic	volcanic	volcanic	volcanic	volcanic	volcanic	volcanic	volcanic	volcanic
SiO_2(wt. %)	46.28	37.37	42.63	43.86	39.71	45.80	53.94	43.24	46.16	40.27
Al_2O_3	13.86	13.33	11.89	12.69	12.94	7.79	14.05	13.09	12.65	13.20
Fe_2O_3	16.06	15.79	17.68	9.62	21.45	17.00	17.73	17.52	17.60	16.59
MnO	0.22	0.22	0.20	0.28	0.17	0.18	0.04	0.29	0.15	0.34
MgO	4.07	5.43	3.36	4.75	5.07	2.65	2.97	5.39	4.28	2.97
CaO	7.93	8.96	7.81	9.69	5.76	10.00	0.13	6.98	7.10	10.03
Na_2O	2.75	3.59	4.01	4.14	4.22	1.30	0.00	2.59	2.47	2.18
K_2O	1.57	1.06	0.80	0.49	0.36	2.20	4.88	1.32	1.37	0.47
TiO_2	3.79	3.54	3.17	3.43	3.56	2.23	1.97	3.56	3.48	3.58
P_2O_5	1.05	0.98	0.83	1.00	0.95	0.66	0.10	0.99	0.96	0.96
PF	2.42	9.61	7.48	9.91	5.90	8.04	3.88	5.00	3.65	9.32
Total	**100.00**	**99.88**	**99.86**	**99.86**	**100.09**	**97.85**	**99.69**	**99.97**	**99.87**	**99.91**
As (ppm)	0.91	0.00	0.83	0.00	1.22	1.82	0.00	1.67	0.00	1.67
Ba	1099.00	304.60	173.90	125.80	366.50	11010.00	972.40	804.00	886.20	576.50
Be	1.50	0.00	0.00	0.00	1.70	0.00	1.51	1.51	0.00	2.93
Bi	0.00	0.00	0.00	0.00	0.00	0.00	0.00	0.00	0.00	0.00
Cd	0.00	0.00	0.00	0.00	0.00	0.00	0.00	0.00	0.35	0.00
Co	42.63	47.19	30.36	52.79	37.33	25.98	33.23	39.63	29.44	40.59
Cr	50.46	49.88	42.29	46.16	44.81	29.51	260.40	47.35	45.08	49.76
Cs	0.35	0.31	0.36	0.48	0.25	0.27	1.04	0.00	0.24	0.40
Cu	35.83	35.89	37.19	51.07	48.28	44.19	31.37	37.52	33.09	38.41
Ga	23.96	21.48	16.68	18.87	23.60	13.74	16.75	22.83	20.87	22.64
Ge	1.46	0.81	0.99	0.74	2.72	1.51	2.34	1.34	1.54	1.51
Hf	7.81	7.42	6.52	7.15	7.41	5.33	3.17	6.95	6.46	6.62
In	0.12	0.11	0.10	0.12	0.13	0.12	0.00	0.11	0.00	0.12
Mo	2.27	1.19	1.54	0.62	2.47	0.95	0.00	2.07	1.92	1.80
Nb	31.57	29.83	25.98	28.70	29.39	20.51	13.59	28.79	27.64	28.89
Ni	28.26	36.50	21.94	32.58	26.42	23.14	120.70	26.65	27.12	30.90
Pb total	9.41	6.49	9.36	4.54	9.83	6.45	2.17	6.16	7.42	6.06
Rb	26.77	20.51	16.67	8.38	7.24	28.99	70.93	24.03	23.70	4.57
Sb	0.14	0.14	0.17	0.15	0.13	0.16	0.28	0.12	0.15	0.17
Sn	2.17	1.40	1.27	1.46	1.70	1.33	2.20	1.23	1.19	1.38
Sr	391.40	182.50	316.90	237.10	246.90	131.00	11.38	307.90	325.00	236.30
Ta	2.14	2.03	1.80	2.00	2.07	1.40	1.08	1.91	1.81	1.86
Th	2.68	2.56	2.27	2.52	2.61	2.95	5.25	2.40	2.30	2.44
U	0.89	0.79	0.54	0.84	0.58	0.71	0.65	0.85	0.82	0.81
V	245.10	197.80	203.40	197.00	243.90	135.00	200.30	236.20	223.80	235.60
W	0.54	0.75	1.15	1.77	1.82	0.77	0.34	0.55	0.57	0.59
Y	42.76	41.79	35.56	40.00	39.58	25.84	22.20	38.50	38.71	41.51
Zn	218.70	154.40	143.40	160.40	142.30	105.70	129.70	337.60	184.20	94.49
Zr	359.80	336.40	295.20	326.70	333.50	247.10	133.60	330.30	309.70	325.10
La	54.67	45.80	55.94	47.06	59.32	37.37	9.95	52.79	50.57	52.44
Ce	119.40	106.20	105.80	106.90	124.10	77.55	25.00	113.80	107.80	111.70
Pr	15.11	13.45	12.79	13.52	15.51	9.68	3.14	14.22	13.35	13.90
Nd	61.30	55.04	51.37	56.20	61.60	38.73	13.80	57.20	53.35	56.23
Sm	11.67	10.68	9.55	10.98	11.15	6.91	3.67	10.86	10.18	10.54
Eu	3.34	2.92	2.60	3.13	3.14	0.97	1.11	3.05	2.90	3.18
Gd	10.12	9.50	8.42	9.67	9.75	5.94	4.16	9.13	8.78	8.85
Tb	1.44	1.36	1.16	1.32	1.33	0.85	0.75	1.33	1.25	1.30
Dy	8.03	7.64	6.60	7.48	7.37	4.63	4.65	7.37	6.99	7.17
Ho	1.55	1.51	1.24	1.48	1.42	0.89	0.91	1.26	1.25	1.27
Er	4.27	4.21	3.40	3.92	3.89	2.52	2.45	3.63	3.60	3.64
Tm	0.61	0.59	0.47	0.55	0.55	0.36	0.33	0.52	0.52	0.52
Yb	4.01	3.97	3.04	3.67	3.64	2.60	2.08	3.55	3.48	3.49
Lu	0.64	0.63	0.47	0.57	0.58	0.40	0.30	0.53	0.54	0.55

Annex VII Volcanic (Suite)

DDH no.:	822	822	822	822	822	822	822
Depth (m):	50	60	66	76	80	84	106
Rock type:	volcanic	volcanic	volcanic	volcanic	volcanic	volcanic	volcanic
SiO_2(wt. %)	41.01	38.08	46.77	21.68	60.01	39.15	46.57
Al_2O_3	13.79	13.83	14.18	6.41	9.98	14.18	13.57
Fe_2O_3	17.75	18.81	14.91	4.19	12.99	18.35	16.03
MnO	0.26	0.25	0.22	0.26	0.12	0.21	0.23
MgO	9.38	9.19	4.48	1.42	3.00	4.74	4.31
CaO	3.18	3.95	7.81	33.72	1.47	5.11	7.88
Na_2O	1.03	2.68	2.71	1.52	0.87	2.54	2.73
K_2O	3.51	1.92	1.43	1.25	1.94	2.33	1.56
TiO_2	3.01	3.35	3.89	1.52	2.08	3.98	3.71
P_2O_5	0.87	0.97	1.06	0.36	0.57	1.04	1.00
PF	6.20	6.92	2.84	27.32	6.81	7.70	2.58
Total	**99.99**	**99.95**	**100.30**	**99.65**	**99.84**	**99.33**	**100.17**
As (ppm)	1.53	1.30	0.00	0.00	1.40	0.85	0.00
Ba	1528.00	849.50	989.60	322.00	352.00	624.00	1065.00
Be	2.08	1.63	0.00	0.00	0.00	1.88	1.63
Bi	0.08	0.00	0.00	0.00	0.00	0.00	0.00
Cd	0.00	0.00	0.00	0.53	0.00	0.00	0.00
Co	45.58	51.55	37.35	13.33	29.32	50.42	43.03
Cr	43.31	46.52	55.00	22.60	29.49	55.28	51.94
Cs	0.46	0.00	0.00	0.56	2.20	1.49	0.25
Cu	30.26	10.92	30.16	82.77	18.56	26.10	36.87
Ga	27.95	27.87	24.37	9.66	16.86	25.57	24.38
Ge	1.56	1.00	1.52	0.37	1.14	1.19	1.60
Hf	7.59	7.02	8.22	3.37	5.12	8.50	7.92
In	0.13	0.12	0.13	0.00	0.00	0.12	0.12
Mo	0.94	1.49	2.36	0.69	1.22	1.55	2.41
Nb	28.42	29.79	33.78	14.27	19.77	34.71	33.18
Ni	30.98	31.97	25.08	7.57	19.54	27.52	24.65
Pb total	9.09	11.08	8.01	4.50	8.77	9.92	7.66
Rb	38.14	19.47	26.72	29.28	69.24	86.60	29.73
Sb	0.13	0.15	0.11	0.12	0.15	0.00	0.10
Sn	2.30	1.38	1.59	0.62	0.95	1.63	1.32
Sr	58.91	124.80	404.40	115.70	99.37	181.30	398.50
Ta	2.07	1.97	2.25	0.93	1.33	2.36	2.17
Th	7.09	2.52	2.84	1.19	3.12	3.10	2.80
U	1.87	0.79	0.86	0.47	0.41	0.63	0.88
V	200.20	213.70	259.80	92.77	128.90	234.20	254.60
W	0.41	0.43	0.58	0.27	0.38	0.36	0.56
Y	40.75	42.47	44.43	23.59	27.77	39.02	45.19
Zn	245.70	248.30	238.90	44.44	182.30	279.10	214.00
Zr	324.60	333.30	376.50	157.60	235.30	386.30	371.80
La	44.16	54.40	59.49	31.50	36.46	53.68	58.73
Ce	104.60	114.70	128.00	65.24	73.03	121.10	125.60
Pr	13.52	14.11	16.03	7.45	9.47	14.63	15.88
Nd	55.93	57.20	65.95	29.54	38.22	61.21	64.86
Sm	10.71	11.15	12.13	5.24	6.79	11.75	12.07
Eu	2.70	3.19	3.56	1.29	1.84	3.41	3.41
Gd	9.37	9.72	10.32	4.54	5.90	9.86	10.36
Tb	1.33	1.40	1.49	0.66	0.85	1.39	1.51
Dy	7.70	7.94	8.22	3.86	4.89	7.54	8.39
Ho	1.51	1.51	1.57	0.79	0.96	1.42	1.61
Er	4.17	4.31	4.23	2.35	2.62	3.70	4.35
Tm	0.63	0.63	0.61	0.37	0.39	0.53	0.63
Yb	4.41	4.29	3.93	2.51	2.58	3.38	4.05
Lu	0.72	0.67	0.61	0.41	0.40	0.50	0.65

Annex VII Volcanic (Suite)

DDH no.:	822	822	822	822	1-01	V 1	V 2	V 3
Depth (m):	122	124	125	125.5		Valaam - Ramo, Upton data		
Rock type:	volcanic	volcanic	volcanic	volcanic	volcanic	volcanic	volcanic	volcanic
SiO_2(wt. %)	30.96	44.87	42.26	44.50	45.22	50.62	51.95	50.91
Al_2O_3	1.84	14.36	12.05	8.68	13.78	2.85	2.67	2.94
Fe_2O_3	4.42	15.75	17.00	10.64	18.15	13.55	14.24	13.59
MnO	0.76	0.18	0.21	0.48	0.14	13.78	12.79	13.49
MgO	1.60	5.96	4.88	4.10	4.62	0.18	0.16	0.18
CaO	32.90	4.52	6.99	12.93	6.51	3.24	2.94	3.17
Na_2O	0.08	3.04	1.45	1.51	2.38	7.12	6.74	6.89
K_2O	0.06	0.49	1.41	1.03	0.62	3.71	3.90	3.87
TiO_2	0.45	3.97	3.15	2.01	3.66	1.94	2.09	2.07
P_2O_5	0.00	1.10	0.87	0.59	1.02	1.30	1.20	1.40
PF	26.70	5.70	9.92	13.46	4.32	1.10	1.09	1.02
Total	**99.77**	**99.94**	**100.19**	**99.93**	**100.42**	**99.40**	**99.77**	**99.53**
As (ppm)	0.00	0.80	0.00	0.00	0.00			
Ba	171.60	764.80	1738.00	977.60	801.30	1695.90	1764.90	1716.50
Be	0.00	1.52	1.86	0.00	1.78			
Bi	0.00	0.00	0.00	0.00	0.00			
Cd	0.00	0.00	0.00	0.00	0.00			
Co	5.34	45.05	24.59	17.85	43.69			
Cr	7.59	53.91	49.41	28.47	50.52	3.9	5.4	3.5
Cs	0.00	1.04	2.84	0.82	2.10			
Cu	0.00	40.43	26.08	20.81	12.00	18.6	12.4	21.4
Ga	4.88	26.01	20.77	14.87	24.13			
Ge	0.70	2.08	1.62	1.14	1.90			
Hf	1.02	8.62	6.87	5.04	7.93			
In	0.00	0.11	0.10	0.00	0.12			
Mo	1.76	1.31	1.34	0.76	1.56			
Nb	4.47	34.71	27.91	19.19	34.17	20.3	20.6	21.1
Ni	0.00	34.16	26.96	10.81	29.85	2.9	3	5.4
Pb total	1.28	13.68	5.99	4.27	12.67	9.6	10.9	8.2
Rb	5.76	11.60	87.95	39.47	17.44	33.1	34.7	35.1
Sb	0.00	0.22	0.22	0.11	0.00			
Sn	0.00	1.49	1.33	1.09	1.51			
Sr	86.10	291.10	259.90	122.10	341.90	521.2	535.8	516.4
Ta	0.29	2.39	1.88	1.31	2.14			
Th	0.45	3.00	2.70	2.79	2.77	3.2	3.1	3
U	0.70	0.92	3.65	0.71	0.92			
V	15.43	252.40	167.60	148.40	241.90	98.2	91	115.8
W	0.20	0.40	0.50	0.29	0.53			
Y	6.56	45.90	42.41	33.12	45.78	45.7	44	47.4
Zn	22.81	207.80	143.70	101.40	167.00	152.3	150.6	149
Zr	46.11	389.80	311.30	220.60	388.20	230.2	240.9	242.5
La	7.65	55.82	51.26	44.61	53.53	49.2	46.5	49.2
Ce	15.84	125.30	104.30	86.97	121.60	112.3	110.7	115.2
Pr	1.47	15.81	13.51	10.07	15.59			
Nd	5.57	65.79	55.83	40.09	63.54	62.5	59.2	63.8
Sm	1.03	12.57	11.04	7.57	12.02			
Eu	0.30	3.67	3.05	1.98	3.32	230.2	240.9	242.5
Gd	0.98	10.86	9.98	6.87	10.20	5.04	5.48	5.12
Tb	0.16	1.61	1.43	1.03	1.46			
Dy	0.96	8.75	7.57	5.85	8.29			
Ho	0.20	1.65	1.51	1.14	1.57			
Er	0.65	4.49	4.16	3.27	4.30			
Tm	0.12	0.65	0.63	0.49	0.62			
Yb	0.87	4.27	4.10	3.28	4.11			
Lu	0.15	0.66	0.66	0.53	0.65			

Annex VIII: Valaam sill rocks
Major and trace element analysis of the Valaam sill rocks

Sample no.:	2-01	11-03
Rock type:	**Gabbro**	**Syenite-granite**
Position	**Lunkkulunsaari**	**Mantsinsaari**
SiO_2(wt. %)	51.99	72.40
Al_2O_3	14.14	11.98
Fe_2O_3	13.23	3.55
MnO	0.19	0.00
MgO	2.76	0.61
CaO	6.03	0.81
Na_2O	3.44	2.43
K_2O	2.28	5.77
TiO_2	2.71	0.29
P_2O_5	0.97	0.06
PF	1.85	1.41
Total	99.59	99.31
As (ppm)	0.00	0.00
Ba	1786.00	615.50
Be	1.51	4.21
Bi	0.00	0.00
Cd	0.00	0.58
Co	22.95	3.24
Cr	0.00	5.12
Cs	0.44	0.63
Cu	14.30	0.00
Ga	25.31	27.56
Ge	1.48	1.47
Hf	5.87	19.97
In	0.11	0.00
Mo	1.70	1.11
Nb	18.90	9.87
Ni	5.07	0.00
Pb total	9.24	14.70
Rb	39.81	135.70
Sb	0.00	0.00
Sn	1.67	3.09
Sr	486.60	49.01
Ta	1.29	1.28
Th	2.99	12.60
U	0.91	2.49
V	103.40	6.27
W	0.27	0.33
Y	39.56	51.81
Zn	160.20	23.23
Zr	242.70	889.30
La	52.05	84.62
Ce	114.00	163.70
Pr	15.00	18.14
Nd	63.02	62.83
Sm	12.57	10.96
Eu	4.64	0.98
Gd	10.37	9.14
Tb	1.43	1.44
Dy	7.82	8.63
Ho	1.40	1.73
Er	3.61	5.04
Tm	0.50	0.76
Yb	3.21	5.07
Lu	0.48	0.75

université HENRI POINCARÉ
NANCY 1

Rue du Doyen Roubault - BP 11
54601 VILLERS-LES-NANCY Cedex

Monsieur **LOBAEV Vladimir**

DOCTORAT de l'UNIVERSITE HENRI POINCARE, NANCY 1

en SCIENCES DE LA TERRE & DE L'UNIVERS

VU, APPROUVÉ ET PERMIS D'IMPRIMER N° 1056

Nancy, le 31 mai 2005

Le Président de l'Université

UNIVERSITÉ HENRI POINCARÉ, NANCY 1 ★ LE PRÉSIDENT

T.P. FINANCE

Université Henri Poincaré, Nancy I
24-30 rue Lionnois - B.P. 3069 - 54013 NANCY Cédex
Tél. : 03 83 68 20 00 - Fax : 03 83 68 21 00

Résumé

Une étude minéralogique et géochimique du bassin volcano-sédimentaire clastique intracontinental mésoprotérozoique (Ripheen) de Pasha – Ladoga (Carélie, Russie) ainsi que des minéralisations uranifères associées et des lithologies du socle sous-jacent a été réalisée. Une comparaison avec d'autres districts fortement minéralises d'age et de lithologie comparables indique qui les sediments clastiques du bassin de Pasha – Ladoga sont nettement moins matures que ces de bassins fortement minéralises de l'Athabasca (Canada) et de Kombolgie (Australie). Toutefois, de circulations importantes de fluides ont été mises en evidence dans les roches métamorphiques de l'Archéen et du Paléoprotérozoique et les granites rapakivi, ainsi que dans les sediments clastiques sous-jacent de la région de Pasha – Ladoga ou le gisement d'uranium de type discordance de Karku ont été découverts. Ces circulations de fluides ont conduit a une alteration a l'échelle régional de zircon et, dans une moins de mesure, de monazite, ainsi qu'a la formation de chlorites ferrifères et de carbonates dans les zones minéralisées.

Mots clés : Uranium, Discordance, Grès, Bassin Mésoprotérozoique, Altérations hydrothermales, Zircon, Monazite

Abstract

The mineralogy and the geochemistry of the Mesoproterozoic (Riphean) Pasha-Ladoga volcanic - sedimentary intracontinental clastic basin (Russian Karelia), associated uranium mineralization and underlying basement lithologies have been characterized and compared with those of highly mineralized districts having similar age and lithologic associations. The clastic sediments appear much more immature than highly mineralized basins of the Athabasca (Canada) and Kombolgie (Northern Australia). However, large-scale fluid circulation has been evidenced in the Archean to Paleoproterozoic metamorphic rocks and Mesoproterozoic rapakivi granites of the basement and in the overlying clastic sediments of the Pasha - Ladoga area, where the Karku unconformity related uranium deposit has been discovered. These fluid circulations are related to zircon alteration and to a lesser degree to monazite at the regional scale and essentially with a Fe-chlorite and carbonate alteration assemblage produced in the mineralized districts.

Key words : Uranium, Unconformity related deposits, Sandstones, Mesoproterozoic basin, Hydrothermal alteration, Zircon, Monazite.